

AN ABSTRACT OF THE THESIS OF

Kristopher Walker for the degree of Master of Science in Civil Engineering and Wood Science presented on June 18, 2015.

Title: Use of Virtual Visual Sensors in the Determination of Natural Frequencies of Timber Structures for Structural Health Monitoring

Abstract approved:

Rakesh Gupta

Thomas H. Miller

Many nondestructive techniques for structural health monitoring are subjective and based on visual observations of degradation. In addition, dynamic properties of structures are already used to obtain quantitative structural health data. However, most current data collection is limited to localized damage on the structure, rather than global response. Recent research involves the use of commercially available digital video cameras, or virtual visual sensors, to observe structural dynamic behavior. This project focuses on the determination of natural vibration frequencies by monitoring the intensity value of a single pixel coordinate over the course of a few seconds of a video of structural vibration, and then applying a fast Fourier transform to extract signal frequencies. Natural frequencies can be used to observe changes in stiffness properties of materials and structural systems that may relate to deterioration. The focus here is primarily on the development and application of the virtual visual sensor technique to wood structures to obtain information relevant to objective structural health monitoring. The experiments focus on verification of the method to extract natural frequencies in various scenarios, using the natural color gradients in wood structures to observe the motion. Additionally, effects of moisture content and simulated damage on natural frequencies are observed on simply-supported beams of dimensional lumber. Applications are also made to an in-place US Forest Service pedestrian bridge. Results show comparable accuracy in determining vibrational frequencies with virtual visual sensors and accelerometer measurements, successful observation of vibrational frequencies in a timber bridge, and good use of naturally occurring color gradients in both laboratory and field tests. Moisture content and simulated damage had measureable effects on

natural frequencies using conventional accelerometers and virtual visual sensors. Digital video cameras show potential to be a promising tool for structural health monitoring of timber structures.

©Copyright by Kristopher Walker
June 18, 2015
All Rights Reserved

Use of Virtual Visual Sensors in the Determination of Natural Frequencies of Timber Structures
for Structural Health Monitoring

by
Kristopher Walker

A THESIS

submitted to

Oregon State University

in partial fulfillment of
the requirements for the
degree of

Master of Science

Presented: June 18, 2015
Commencement: June 2016

Master of Science thesis of Kristopher Walker presented on June 18, 2015

APPROVED:

Co-Major Professor representing Wood Science

Co-Major Professor representing Civil Engineering

Head of the Department of Wood Science and Engineering

Head of the School of Civil and Construction Engineering

Dean of the Graduate School

I understand that my thesis will become part of the permanent collection of Oregon State University libraries. My signature below authorizes release of my thesis to any reader upon request.

Kristopher Walker, Author

ACKNOWLEDGMENTS

I would like to thank the following individuals and organizations for their support. Their guidance, laboratory help, and encouragement have made this work possible.

I would like to acknowledge Oregon State University's College of Forestry and College of Engineering for providing financial support, Dr. Thomas Schumacher and Ali Shariati, of the University of Delaware for providing key elements of the methodology and software and for reviewing the results of our research, Cole Smith, USDA Forest Service engineer, for giving us access and design information on the bridge examined in this study, and Jeff Mintz for his consulting work regarding statistics.

- Dr. Rakesh Gupta – Professor, Oregon State University
- Dr. Thomas H. Miller – Associate Professor, Oregon State University
- Dr. Thomas Schumacher – Assistant Professor, University of Delaware
- James Batti – Civil and Construction Engineering Lab/Research Manager
- Milo Clauson – Wood Science and Engineering Lab/Research Manager
- Cole Smith – USDA Forest Service Civil Engineer
- Jeff Mintz – Graduate Student, Oregon State University
- Faculty and staff in the School of Civil and Construction Engineering, OSU
- Faculty and staff in the Department of Wood Science and Engineering, OSU

CONTRIBUTION OF AUTHORS

Dr. Rakesh Gupta and Dr. Thomas H. Miller have provided much needed guidance for writing and preparing the manuscript for publication.

TABLE OF CONTENTS

INTRODUCTION	1
BACKGROUND/JUSTIFICATION	1
RESEARCH OBJECTIVES	5
MANUSCRIPT: USE OF VIRTUAL VISUAL SENSORS IN THE DETERMINATION OF NATURAL FREQUENCIES OF TIMBER STRUCTURES FOR STRUCTURAL HEALTH MONITORING.....	6
Abstract	6
Introduction.....	6
Objectives	10
Materials and Methods.....	11
Experimental Approach	11
Cameras and Specifications	11
Video Recording and Analysis	12
Experiments Conducted	13
Results and Discussion	20
Covered Bridges.....	20
Shake Table.....	21
Nominal 2x4 Boards (Tested Flatwise)	28
US Forest Service Pedestrian Bridge.....	35

TABLE OF CONTENTS (Continued)

Conclusions.....	38
Challenges and Future Work	39
Practical Applications	40
References.....	40
CONCLUSIONS AND RECOMMENDATIONS	42
BIBLIOGRAPHY.....	43
APPENDICES	44

LIST OF FIGURES

<u>Figure</u>	<u>Page</u>
Figure 1 - Example Signal and Frequency Spectra from Small Shake Table Experiment	13
Figure 2 – Thomas Creek (Gilkey) Covered Bridge Located East of Jefferson, OR	14
Figure 3 - Underside of Shimanek Covered Bridge Located East of Jefferson, OR	15
Figure 4 - Shake Table Model	16
Figure 5 - Hole Pattern Applied to Region near Mid-Span	18
Figure 6 - USDA Forest Service Pedestrian Bridge	20
Figure 7 - Shake Table Distribution of Measured Frequency Values (Mode 1)	23
Figure 8 - Shake Table Distribution of Measured Frequency Values (Mode 2)	24
Figure 9 - Shake Table Distribution of Measured Frequency Values (Mode 3)	25
Figure 10 – 2x4 Distribution of Measured Values (all experiments)	33
Figure 11 - VVS Time-Intensity and Fourier Transform for USFS Pedestrian Bridge (October 2014)	36
Figure 12 - VVS Time-Intensity and Fourier Transform for USFS Pedestrian Bridge (February 2015)	37

LIST OF TABLES

<u>Table</u>	<u>Page</u>
Table 1 - Shake Table Results (Canon)	22
Table 2 - Shake Table Results (GoPro)	22
Table 3 - Difference in Measured Frequency across All Shake Table Modes	27
Table 4 - Results from Moisture Content Experiments	30
Table 5 - Results from Simulated Damage Experiments.....	31

LIST OF APPENDICES

<u>Appendix</u>	<u>Page</u>
Appendix A – Comprehensive Literature Review	45
Appendix B – Profiles of 2x4 Wood Specimens	50
Appendix C – Results of 2x4 Experiments.....	54
Appendix D – Example Calculation of 2x4 E	70
Appendix E – Time and Frequency Figures from Hot-Wet 2x4 Experiments	72
Appendix F – VVS Figures from Hot-Dry 2x4 Experiments	115
Appendix G – VVS Figures from ASTM Standard 2x4 Experiments.....	157
Appendix H – Canon VVS Figures from Simulated Damage 2x4 Experiments.....	202
Appendix I – GoPro VVS Figures from Simulated Damage 2x4 Experiments	235
Appendix J – Shake Table Accelerometer Test Results	267
Appendix K – Shake Table Accelerometer Figures (Canon)	269
Appendix L – Shake Table VVS Figures (Canon)	280
Appendix M – Shake Table Accelerometer Figures (GoPro).....	291
Appendix N – Shake Table VVS Figures (GoPro).....	302
Appendix O – Forest Service Pedestrian Bridge VVS Figures (Preliminary).....	313
Appendix P – Forest Service Pedestrian Bridge VVS Figures (Oct 27, 2014).....	319
Appendix Q – Forest Service Pedestrian Bridge VVS Figures (Feb 12, 2015).....	324
Appendix R – Results from Shake Table Statistical Analysis	328
Appendix S – Results from 2x4 Statistical Analysis	331
Appendix T – Theoretical Estimations for Natural Frequencies	334
Appendix U - House Rock Camp Trail Bridge Drawings	339

LIST OF APPENDICES (Continued)

<u>Appendix</u>	<u>Page</u>
Appendix V - MATLAB Code Used for Analysis	348
Appendix W – Analysis Step-by-Step Guide	351
Appendix X – R Software Bootstrap Analysis Code.....	358

LIST OF APPENDIX TABLES

<u>Table</u>	<u>Page</u>
Table C1 - 2x4 Frequency Data after Hot-Wet Room Equilibrium.....	55
Table C2 - 2x4 Specimen Dimensions after Hot-Wet Room Equilibrium	56
Table C3 - Calculated Moduli of Elasticity: MC (Hot-Wet Room)	57
Table C4 - 2x4 Frequency Data after Hot-Dry Room Equilibrium.....	58
Table C5 - 2x4 Specimen Dimensions after Hot-Dry Room Equilibrium.....	59
Table C6 - Calculated Moduli of Elasticity: MC (Hot-Dry Room).....	60
Table C7 - 2x4 Frequency Data after ASTM Standard Room Equilibrium	61
Table C8 - 2x4 Specimen Dimensions after ASTM Standard Room Equilibrium.....	62
Table C9 - Calculated Moduli of Elasticity: MC (ASTM Standard Room)	63
Table C10 - 2x4 Frequency Data from Simulated Damage (Planing).....	64
Table C11 - 2x4 Specimen Dimensions for Damage Simulation (Planing)	64
Table C12 - Calculated Moduli of Elasticity: Planing.....	65
Table C13 - 2x4 Frequency Data from Simulated Damage (Knot Removal).....	66
Table C14 - 2x4 Specimen Dimensions for Damage Simulation (Knot Removal).....	66
Table C15 - Calculated Moduli of Elasticity: Knot Removal.....	67
Table C16 - 2x4 Frequency Data from Simulated Damage (Hole Pattern)	68
Table C17 - 2x4 Specimen Dimensions for Damage Simulation (Hole Pattern)	68
Table C18 - Calculated Moduli of Elasticity: Hole Pattern	69
Table J1 - Shake Table Accelerometer Results (Canon)	268
Table J2 - Shake Table Accelerometer Results (GoPro)	268

LIST OF APPENDIX TABLES (Continued)

<u>Table</u>	<u>Page</u>
Table R1 - Bootstrap Estimate of Frequency (Mode 1).....	329
Table R2 - Bootstrap Estimate of Frequency (Mode 2).....	329
Table R3 - Bootstrap Estimate of Frequency (Mode 3).....	329
Table R4 - Difference in Measured Fundamental Frequencies between Methods (Mode 1).....	329
Table R5 - Difference in Measured Fundamental Frequencies between Methods (Mode 2).....	330
Table R6 - Difference in Measured Fundamental Frequencies between Methods (Mode 3).....	330
Table R7 - Difference in Measured Frequency Overall (Combining all Mode Measurements)	330
Table S1 - 2x4 T-test Results.....	332
Table S2 - Bootstrap Estimate of Frequency per Moisture Treatment	332
Table S3 - Bootstrap Estimate of difference in Frequency per Moisture Treatment.....	332
Table S4 - Bootstrap Estimates of Frequency before and after Planing	332
Table S5 - Bootstrap Estimates for Difference in Frequency due to Planing	333
Table S6 - Bootstrap Estimates of Frequency before and after Hole Pattern	333
Table S7 - Bootstrap Estimates for Difference in Frequency due to Hole Pattern	333
Table S8 - Bootstrap Estimates of Frequency before and after Knot Removal.....	333
Table S9 - Bootstrap Estimates for Difference in Frequency due to Knot Removal.....	333

LIST OF APPENDIX FIGURES

<u>Figure</u>	<u>Page</u>
Figure B1 - Profile Images for 2x4 Specimen 1	51
Figure B2 - Profile Images for 2x4 Specimen 2	51
Figure B3 - Profile Images for 2x4 Specimen 3	51
Figure B4 - Profile Images for 2x4 Specimen 4	52
Figure B5 - Profile Images for 2x4 Specimen 5	52
Figure B6 - Profile Images for 2x4 Specimen 6	52
Figure B7 - Profile Images for 2x4 Specimen 7	53
Figure B8 - Profile Images for 2x4 Specimen 8	53
Figure B9 - Profile Images for 2x4 Specimen 9	53
Figure D1 - Key for 2x4 Hot-Wet Figures.....	73
Figure E1 - Key for 2x4 Hot-Dry Figures	116
Figure F1 - Key for 2x4 ASTM Standard Figures	158
Figure G1 - Key for (Canon) 2x4 Simulated Damage Figures	203
Figure H1 - Key for (GoPro) Simulated Damage Figures	236

INTRODUCTION

BACKGROUND/JUSTIFICATION

It is becoming increasingly important to use materials in the most responsible and sustainable manner; however, global population increase and economic growth demand more and more infrastructure. Wood, when compared to other materials common to structures, is unique in that it is renewable. It is organic in origin and has non-homogeneous and anisotropic properties that are less predictable than manufactured materials such as concrete or steel. Wood also has durability issues specific to the organic nature of the material that make the inspection and health evaluation of timber structures a unique challenge.

Kasal (2014) suggests several categories in which structural health monitoring techniques can be placed. Suggested categories include: direct and indirect, local and global, qualitative and quantitative, and the level of destructivity. Destructive tests are conducted to accurately assess the condition of a structure by loading the structure to failure or removing members and testing them until failure in a lab setting. Kasal (2014) suggests destructive testing produces more complete information about the investigated member or structure, but the value of this information is limited as the member is permanently lost, making the gathered information practically useless in the maintenance of the structure. Semi-destructive tests aim to reduce the persistent effects of introduced damage to the structure. An example of this type of health evaluation applied to a timber structure is resistance drilling (Ross et al. 2004). Resistance drilling can give an evaluator a good idea of the distribution of degradation in a wood member, but this information is limited to isolated points of entry and is not necessarily representative of the entire structure. Completely nondestructive evaluation methods aim to leave no lasting effect

on the structure. Nondestructive structural health evaluation of timber structures is largely based on visual observations which are subjective in nature and it can be difficult to convert the data collected to useful information for considering the overall health of structures (Ross et al. 2004 and Kasal 2014).

Video-based methods of observation are an emerging nondestructive technology in the field of structural health monitoring. One common application of video-based methods is the use of digital image correlation (DIC) to map displacements and strains on the surfaces of materials subjected to stress (Choi et al. 1997, Sutton et al. 1983, and Sinha 2007). DIC uses multiple cameras to produce images from multiple perspectives at set intervals during loading. In the same manner, digital video cameras can be used to take continuous observations of motion. An example of this type of observation can be seen in a study done by Wu et al. (2012), in which Eulerian based magnification are applied to videos in order to make subtle changes more visible to the naked eye. During Wu et al.'s (2012) study the method was successfully used to amplify color changes in an individual's face and subtle movements of blood vessels in an individual's wrist to observe heart rates (Wu et al. 2012).

In a similar manner, Song et al. (2015) proposed that virtual visual sensors (VVS) could be used in place of current physical methods of data collection, with many advantages due to the non-contact nature of the VVS. Contemporary means of structural dynamic behavior data collection are done by means of a network of small sensors. They proposed advantages of using VVS in place of conventional sensor networks to include simpler installation, cost effectiveness, and ease of management. Song et al.'s (2015) study investigates the potential of using a series of images, or videos, to observe and measure structural behavior. During the study, Hough Transform based algorithms were employed to extract markers from videos and VVS were used

to acquire modal shapes of structures, used to detect structural damage. By Song et al.'s (2015) proposed method any one of potentially millions of pixels in the image series or videos can be analyzed as virtual visual sensors.

Schumacher and Shariati (2013) investigated a method in which a pixel coordinate in a digital video can be used to observe and measure fundamental vibrational frequencies of structural systems by combining aspects of the work by Song et al. (2015) and Wu et al. (2012). In Schumacher and Shariati's (2013) study, the grey scale intensity value of a set pixel coordinate was tracked with time and Fourier transforms were used to extract signal frequencies (Schumacher and Shariati 2013). Schumacher and Shariati's (2013) study investigated the theoretical feasibility of the VVS method and included a small scale experimental test for verification as well as an application to video data taken of an existing bridge. This study builds on this work by studying the applications of the method to wooden structures.

Fundamental natural frequencies are objective and quantitative data related to the mass and stiffness characteristics of structural systems. The potential use of vibrational characteristics of structures in determination of structural health has been widely examined and discussed in literature reviews such as Doebling et al. (1996). The literature review in question discusses the potential use for changes in frequency and mode shape in the determination of structural health. The study focused on data collection through conventional network sensors as VVS were not yet introduced. While vibrational characteristics can be a powerful tool in evaluating structural health, Doebling et al. (1996) concluded that conventional means of data collection were lacking. One of the critical issues for damage identification and localization discussed in Doebling et al.'s (1996) study was the limitation on the number and locations of measurement sensors. One

potential advantage of the VVS method is the alleviation of this key disadvantage to conventional sensor systems.

Wang et al. (2005) investigated the use of fundamental frequencies in determination of structural health of timber bridges, with promising results. Wang et al. (2005) was successfully able to observe natural frequencies of several bridges using accelerometers and used this data to estimate material properties such as the stiffness, or EI product. This study focuses on a similar approach to that of Wang et al. (2005) in investigating the usefulness of using fundamental frequencies to examine mechanical properties and their changes.

Equation (1) determines the natural frequencies of a uniform simply-supported beam as a function of mass, stiffness and length (Chopra 2012).

$$f = \frac{1}{2\pi} \left(\frac{n\pi}{L} \right)^2 \sqrt{\frac{EI}{\rho}} \quad (1)$$

where: f = natural frequency for vibrational mode n , L = span length, E = modulus of elasticity, I = area moment of inertia, and ρ = mass per unit length.

The fundamental frequency (with $n=1$ and the lowest and generally dominant frequency in terms of structural behavior) is affected by changes in these parameters. Wood structures can degrade in a multitude of ways. Rot and wood-boring insects can remove material as well as decrease the stiffness of the wood, with damage remaining mostly invisible from the outside. Fire damage can reduce the effective cross sectional area of members by removing exterior material. In addition to these, wood's natural tendency to absorb moisture can have significant effects on mechanical properties including its linear mass, modulus of elasticity, and cross

sectional area due to shrinkage and swelling. Moisture content of a wood structure can be measured relatively easily, but the potential effects still need to be considered.

RESEARCH OBJECTIVES

The objective of this study is to verify the accuracy and precision of using virtual visual sensors to obtain natural frequencies and the application of the method with regards to timber structures. This study focuses on the verification of the accuracy and precision of the VVS method compared to accelerometers, testing camera and perspective limitations, and applying the method to dimensional lumber beams and a bridge. During experimentation, the effects of moisture content and simulated damage on fundamental frequencies will be investigated as well as the usefulness of naturally occurring color gradients in the data analysis process.

MANUSCRIPT: USE OF VIRTUAL VISUAL SENSORS IN THE DETERMINATION OF NATURAL FREQUENCIES OF TIMBER STRUCTURES FOR STRUCTURAL HEALTH MONITORING

Abstract

Dynamic properties of structures have been used to obtain quantitative structural health data; however, most data collection is limited to localized damage rather than global response. Recent research involves the use of commercially available digital video cameras, or virtual visual sensors, to measure structural dynamic response on a more global scale. The focus here is primarily on application of virtual visual sensors to wood structures in an attempt to obtain objective data relevant to structural health evaluation. Analysis is performed by monitoring the intensity of a single pixel coordinate over time in recorded videos, and then applying a fast Fourier transform to extract vibration frequencies. In this study, the VVS method was first compared to accelerometer measurements. Effects unique to wood were investigated including moisture content and simulated damage, and an application was made to an existing pedestrian bridge. Virtual visual sensors are found to be an accurate and promising tool for collecting quantitative data for structural health monitoring.

Introduction

It is becoming increasingly important to use materials in the most responsible and sustainable manner; however, global population increase and economic growth demand more and more infrastructure. Wood, when compared to other materials common to structures, is unique in that it is renewable. It is organic in origin and has non-homogeneous and anisotropic properties that are less predictable than manufactured materials such as concrete or steel. Wood

also has durability issues specific to the organic nature of the material that make the inspection and health evaluation of timber structures a unique challenge.

Kasal (2014) suggests several categories in which structural health monitoring techniques can be placed. These include: direct and indirect, local and global, qualitative and quantitative, and the level of destructivity. Destructive tests are conducted to accurately assess the condition of a structure by loading the structure to failure or removing members and testing them until failure in a lab setting. Kasal (2014) suggests destructive testing produces more complete information about the investigated member or structure, but the value of this information is limited as the member is permanently lost, making the gathered information practically useless in the maintenance of the structure. Semi-destructive tests aim to reduce the persistent effects of introduced damage to the structure. An example of this type of health evaluation applied to a timber structure is resistance drilling (Ross et al. 2004). Resistance drilling can give an evaluator a good idea of the distribution of degradation in a wood member, but this information is limited to isolated points of entry and is not necessarily representative of the entire structure. Completely nondestructive evaluation methods aim to leave no lasting effect on the structure. Nondestructive structural health evaluation of timber structures is largely based on visual observations which are subjective in nature and it can be difficult to convert the data collected to useful information for considering the overall health of structures (Ross et al. 2004 and Kasal 2014).

Video-based methods of observation are an emerging nondestructive technology in the field of structural health monitoring. One common application of video-based methods is the use of digital image correlation (DIC) to map displacements and strains on the surfaces of materials subjected to stress (Choi et al. 1997, Sutton et al. 1983, and Sinha 2007). DIC uses multiple cameras to produce images from multiple perspectives at set intervals during loading. In the

same manner, digital video cameras can be used to take continuous observations of motion. An example of this type of observation can be seen in a study done by Wu et al. (2012), in which Eulerian based magnification is applied to videos in order to make subtle changes more visible to the naked eye. During Wu et al.'s (2012) study the method was successfully used to amplify color changes in an individual's face and subtle movements of blood vessels in an individual's wrist to observe heart rates (Wu et al. 2012).

In a similar manner, Song et al. (2015) proposed that virtual visual sensors (VVS) could be used in place of current physical methods of data collection, with many advantages due to the non-contact nature of the VVS. Contemporary structural dynamic behavior data collection is done by means of a network of small sensors (Song et al. 2015). Song et al. (2015) proposed advantages of using VVS in place of conventional sensor networks to include simpler installation, cost effectiveness, and ease of management. Their study investigates the potential of using a series of images, or videos, to observe and measure structural behavior. Hough Transform-based algorithms were employed to extract markers from videos, and VVS were used to acquire modal shapes of structures, used to detect structural damage (Song et al. 2015). By the proposed method any one of potentially millions of pixels in the image series or videos can be analyzed as virtual visual sensors.

Schumacher and Shariati (2013) investigated a method in which a pixel coordinate in a digital video can be used to observe and measure fundamental vibrational frequencies of structural systems by combining aspects of the previous two studies. In Schumacher and Shariati's (2013) study, the grey scale intensity value of a set pixel coordinate was tracked with time and Fourier transforms were used to extract signal frequencies. The study investigated the theoretical feasibility of the VVS method and included a small scale experimental test for

verification as well as an application to video data taken of an existing bridge. The current research effort builds on this work by studying the applications of the method to wooden structures.

Fundamental natural frequencies are objective and quantitative data related to the mass and stiffness characteristics of structural systems. The potential use of vibrational characteristics of structures in determination of structural health has been widely examined and discussed in literature reviews such as Doebling et al. (1996). They discuss the potential use of observed changes in frequency and mode shape in the determination of structural health. Doebling et al.'s study focused on data collection through conventional network sensors as VVS were not yet introduced. While vibrational characteristics can be a powerful tool in evaluating structural health, Doebling et al. (1996) conclude that conventional means of data collection is lacking. One of the critical issues for damage identification and localization discussed was the limitation on the number and locations of measurement sensors (Doebling et al. 1996). One potential advantage of the VVS method is the alleviation of this key disadvantage to conventional sensor systems.

Wang et al. (2005) investigated the use of fundamental frequencies in determination of structural health of timber bridges, with promising results. They were successfully able to observe natural frequencies of several bridges using accelerometers and used this data to estimate material properties such as the stiffness, or EI product. This study focuses on a similar approach to that of Wang et al. (2005) in investigating the usefulness of using fundamental frequencies to examine mechanical properties and their changes.

Equation (1) determines the natural frequencies of a uniform simply-supported beam as a function of mass, stiffness and length (Chopra 2012).

$$f = \frac{1}{2\pi} \left(\frac{n\pi}{L} \right)^2 \sqrt{\frac{EI}{\rho}} \quad (1)$$

where: f = natural frequency for vibrational mode n , L = span length, E = modulus of elasticity, I = area moment of inertia, and ρ = mass per unit length.

The fundamental frequency (with $n=1$ and the lowest and generally dominant frequency in terms of structural behavior) is affected by changes in these parameters. Wood structures can degrade in a multitude of ways. Rot and wood-boring insects can remove material as well as decrease the stiffness of the wood, with damage remaining mostly invisible from the outside. Fire damage can reduce the effective cross sectional area of members by removing exterior material. In addition to these, wood's natural tendency to absorb moisture can have significant effects on mechanical properties including its linear mass, modulus of elasticity, and cross sectional area due to shrinkage and swelling. Moisture content of a wood structure can be measured relatively easily, but the potential effects still need to be considered.

Objectives

The objective of this study is to investigate, through proof of concept, the use of virtual visual sensors to obtain natural frequencies and the application of this method to timber structures. This study focuses on the investigation of accuracy and precision of the VVS method compared to accelerometers, testing camera and perspective limitations, and applying the method to dimensional lumber beams and a bridge. During experimentation, the effects of moisture content and simulated damage on fundamental frequencies will be investigated as well as the usefulness of naturally occurring color gradients in the data analysis process.

Materials and Methods

Experimental Approach

A small shake table and piezoelectric accelerometer was used to test the accuracy and precision of the virtual visual sensor method of observing natural frequencies of vibration. Further verification of the accuracy and precision of the method were tested in a series of simply-supported nominal 2x4 beam experiments by comparing the VVS method to an accelerometer built into a METRIGUARD E-Computer. The nominal 2x4 beam experiments were also aimed at examining the effects moisture content and simulated damage has on a specimen's natural frequency as well as the usefulness of naturally occurring color gradients in applying VVS to wood members. Several in-situ bridges were used to further test the usefulness of naturally occurring color gradients in wood structures for analysis as well as to test camera limitations and perspective.

Cameras and Specifications

Two commercially available digital video cameras were used during the experiments; a Canon Rebel T3i and a GoPro Hero 3+ Black. The Canon camera was used to record video at 1280x720 pixels and 60 frames per second for most experiments. To change the effective zoom range on the Canon, two different lenses were used: an EF-S 18-55mm and EF-S 55-250. The GoPro camera was used to record video at 1280x720 pixels and 120 frames per second. For the majority of experimentation the cameras were mounted on a tripod and activated remotely to avoid additional movement in the video caused by camera motion. A simple lightweight Vivitar tripod was used for camera stabilization. Remote control of the GoPro camera was done through use of the GoPro Android app. A Canon RC-6 remote control was used for the Canon camera.

Video Recording and Analysis

The digital video cameras/virtual visual sensors were used to record a few seconds of structural vibration. This video was then analyzed using MATLAB to track the intensity values of a pixel coordinate over each frame of the video. Digital representation of color is done by combining red, blue and, green color values. Intensity is the greyscale equivalent of presented colors, which can be calculated as shown in equation (2). Intensity ranges from pure black at a value of 0 and pure white at a value of 255.

$$I = 0.2989R + 0.5870G + 0.1140B \quad (2)$$

where I = intensity value, R = red color value, G = green color value, B = blue color value.

Videos are recorded by taking a series of images at a set frame rate. By knowing the frame rate of the video it is possible to determine how much time elapses between each image and then use that in calculations. Knowing the recording frame-rate of the video, the intensity values from each frame can be mapped versus time and normalized about a zero by subtracting the average value of the signal. This is done by subtracting the average intensity value from a set of data points, giving positive and negative values about a zero axis. An example pixel intensity time history done in this fashion, taken from a shake table experiments, is shown in Figure 1(a). Once the time-intensity values are determined, a fast Fourier transform is applied to the signal. This transforms the data from the time domain into the frequency domain. An example of this transformation, taken from a shake table experiment, is shown in Figure 1(b). Relatively tall spikes in these plots correlate to significant, measurable natural frequencies of the signal. If the frequency spectrum of the signal does not have clearly defined spikes or has too much noise, another pixel coordinate is selected and the process repeated. Analysis was repeated with different pixel coordinates until several transforms were produced with clear spikes. A transform

with the least amount of noise was then saved for comparison. Pixel coordinates which lay on a color gradient in the direction of motion on the structure give the clearest results. A color gradient is defined as a range of position-dependent colors.

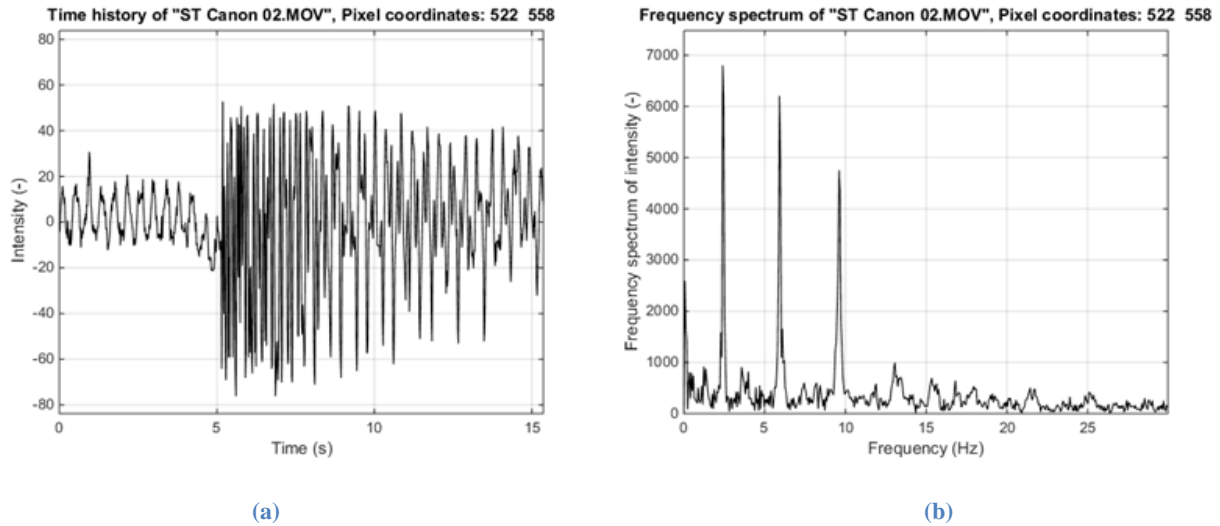


Figure 1 - Example Signal and Frequency Spectra from Small Shake Table Experiment

Experiments Conducted

Covered Bridges

The virtual visual sensor method was applied to several historical covered bridges East of Albany, OR during typical traffic loads. This was done during the early stages of the project to become more familiar with the analysis process and to examine the usefulness of vehicle traffic in inducing vibrational response. Figure 2 depicts one of the covered bridges examined.



Figure 2 – Thomas Creek (Gilkey) Covered Bridge Located East of Jefferson, OR

For these experiments, only the Canon camera was available and it was set to record 1280x720 video at 60 frames per second. Perspectives included looking at the sides of the structures similar to the view seen in Figure 2, as well as some videos recorded from underneath the structure when it was accessible. The dynamic properties of the structures were unknown so various levels of zoom were also utilized in an attempt to observe any vibration. Views ranged from as far as depicted in Figure 2 to as close as depicted in Figure 3.



Figure 3 - Underside of Shimanek Covered Bridge Located East of Jefferson, OR

Small Shake Table

The purpose of this experiment was to investigate the accuracy and precision of the VVS method in observing relatively complex vibrations with both digital video cameras. The VVS approach was applied to a small shake table and a 2-D model with three degrees of freedom and three significant natural frequencies and compared to accelerometer data. For these experiments, the entire structure was kept in view of the cameras and the cameras were not moved across all videos. This relatively far perspective was used to allow the widest range of locations on the model to be used for pixel coordinate analysis. The Canon was used to record 1280x720 video at 60 frames per second, and the GoPro was used to record 1280x720 video at 120 frames per second. Ten repetitions of experimentation were performed with each camera. The accelerometer used for this experiment was a Crossbow CXL02LF1 fixed to the bottom “story” mass and used to record at a rate of 100 times per second. Data acquisition was done with LabVIEW Signal Express software. MATLAB was then used to apply a Fourier transform to the accelerometer

data, transforming the signal into the frequency domain. The MATLAB script used to perform this can be found in Appendix V.

For these tests, the accelerometer was used to record vibration at the same time video was being taken by the digital video cameras. Excitation of the structure was in the form of a light pull and release of the middle story mass. This produces free vibration, with some small damping, after an initial displacement. Figure 4 depicts the setup used for this experiment as well as an example video pixel coordinate used during analysis.

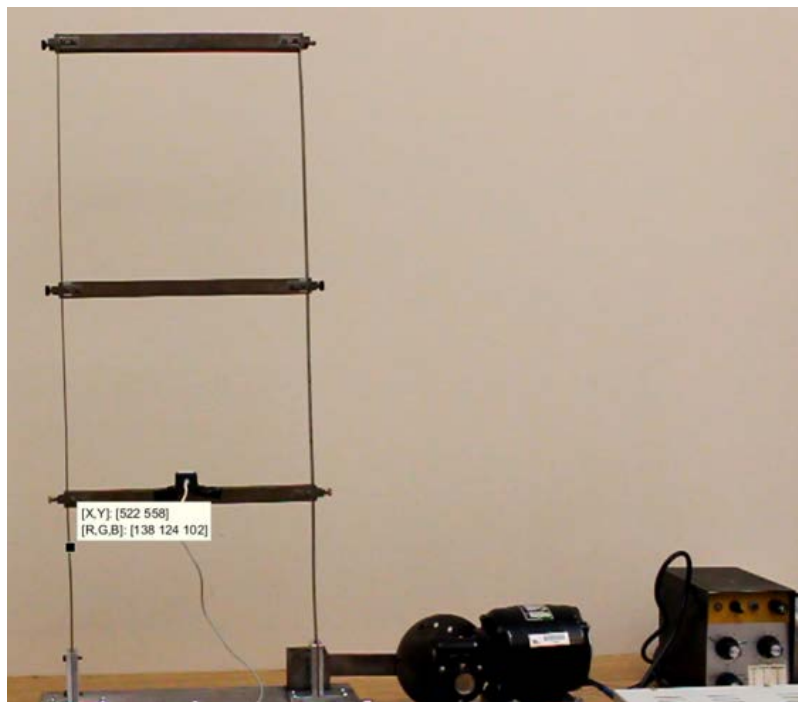


Figure 4 - Shake Table Model

Nominal 2 x 4 Wood Boards (Tested Flatwise)

The purpose of these experiments was to examine the potential effects moisture content and various types of simulated damage can have on the natural frequency of wood structures.

Ten nominal 2x4 *Pseudotsuga menziesii* (Douglas-fir) boards were used for the moisture content experiments. Additionally three boards were used for each of three types of damage

simulation. The boards were of unknown grade and had a range of properties with variances in cross-sectional dimensions, length, and specific gravity. Measurements of breadth, height, length, and weight were recorded at each stage before vibrational experiments were conducted.

The 2.44 m long *Pseudotsuga menziesii* (Douglas-fir) specimens were allowed to reach moisture content equilibrium in various climate-controlled chambers. The first chamber was kept at 30°C and a relative humidity of 30%. Equilibrium moisture content for wood under these conditions is about 6%. The specimens were allowed to reach equilibrium at relatively low moisture contents in this chamber for several weeks before testing. The second climate chamber used was kept at a constant temperature of 30°C and relative humidity of 90%, and the specimens allowed to equilibrate to relatively high moisture contents. Equilibrium moisture content for wood under these conditions is about 19%. Finally the specimens were placed in an ASTM standard climate chamber which is kept at a temperature of 20°C and a relative humidity of 65%. Equilibrium moisture content for wood in these conditions is about 12%. Specimen dimensions, weight, and moisture content were recorded just prior to conducting the experiments. Moisture content of each board was measured using a DELMHORST RDM-3 handheld meter by averaging results from three points along each board.

Nine of these specimens were also subjected to simulated damage of varying degrees. For these experiments three methods of simulated damage were used. The first method was to decrease the cross section by removing depth of the specimens, when laid flatwise, in 6.35 mm intervals. This test was designed to simulate the removal of material from sources such as rot, wood borers, or even fire. The second form of damage simulation was the introduction of a 50.8 mm diameter hole. One of the specimens had an existing knot this size 109 cm from one end and

slightly off center when laid flatwise. It was decided to drill a hole this size and in this same location for this board and two others, to simulate the effects of a knot that had been removed. The third method was to apply a pattern of holes as depicted in Figure 5 at intervals along the length of the beam in the region near mid-span. The hole pattern used for these specimens consisted of 12.7 mm diameter holes drilled at 38.1 mm intervals at the centerline, when laid flatwise, and additional 12.7 mm diameter holes offset from the centerline between the previous holes. The hole pattern was another simulation of the removal of material from sources such as rot and wood borers. Again VVS results were compared to those from accelerometers to further investigate the accuracy of the method.



Figure 5 - Hole Pattern Applied to Region near Mid-Span

In the experiments, the beams were supported flatwise at a span of 238 cm. A Metriguard Model 340 E-Computer was used during these experiments including the tripod supports. Under these conditions the boards were assumed to be simply supported. A single tap near mid-span was used to excite the boards into free vibration. The Metriguard was then used to record the natural frequency of each board, which was immediately available on a laptop display, and later comparisons were made to the results from the VVS method. For these experiments, the cameras were set and adjusted on the tripod so the sensors were roughly level with the boards, orientated perpendicularly to the span of the boards, and focused roughly at mid-span. This was done to allow for the greatest amplitude of motion observed within the videos. Additionally, two perspectives were used for each camera; one closer and one further away. Two videos were

recorded of each board at these two perspectives with each camera. The multiple perspectives were used to increase the likelihood of successful observation with the cameras and also allow for different amplitudes to be used in conjunction with color gradients. This experimentation was done to the boards for each moisture content equilibrium and level of simulated damage. To ensure fair comparisons, each board was marked to allow for the same span and orientation across all experimentation.

Forest Service Pedestrian Bridge

The VVS method was applied to a USDA Forest Service pedestrian bridge to examine an actual full-scale structure. The bridge examined was the Rock Camp trail bridge, located off of FS road 2044. This bridge is depicted in Figure 6. The bridge was 21 m long with a deck clear width of 0.91 m and supported by two 171 mm width x 1070 mm depth pressure-treated, *Pseudotsuga menziesii* (Douglas-fir) glue-laminated timber stringers.

For these experiments, the bridge was excited by a single person jumping once near mid-span. It should be noted that the mass of the person does introduce a small mass to the bridge and discontinuity in the linear mass of the structure; however, this was considered to have minimal effect in this case. The VVS method was applied to this bridge in October 2014 and February 2015 and moisture content was measured each time. Moisture content of the glulam beams, deck, and rails were measured using a DELMHORST RDM-3 handheld wood moisture meter. Video of the structure was taken at varying distances and perspectives. Again, cameras were focused near mid-span of the structure to allow for the greatest amplitude of vibration to be observed. Contrary to previous experiments, an attempt was made at recording video holding the cameras by hand in addition to mounted on a tripod.



Figure 6 - USDA Forest Service Pedestrian Bridge

Results and Discussion

Covered Bridges

Observed traffic across the covered bridges was discovered to be quite low. Pixel coordinates which lie on a color gradient were abundant in these videos. The general approach was to begin with a coordinate located on the corner or edge of a member. Additional pixel coordinates involved the use of the color gradients caused by naturally occurring stains on both the steel members and wood members. Coordinates which lay on rounded bolt ends, as seen in Figure 3, were also utilized to try and observe vibration. The VVS analysis was unable to show observation of structural vibration during any observed vehicle passing events. A single video

captured while a pickup truck went over one of the bridges towing a relatively large camper trailer did show some signs of deflection, but again no structural vibration measured.

The deep truss bridges were assumed to be very stiff and highly damped. The remote locations of the bridges combined with low speed limits and traffic consisting mostly of small passenger cars limited opportunities for vibration measurements. Traffic was relatively slow so the impact as the vehicle crossed the bridge was lessened and the velocity of the cars in crossing dominated the response. From these experiments it became clear that structural vibrations may not always be so easily observed under typical service conditions. Some form of forced excitation may be helpful in creating a response in some structures.

Shake Table

Table 1 summarizes the results from the series of shake table tests comparing vibrational frequencies observed with the Canon camera and an accelerometer, and Table 2 summarizes the results from those involving the GoPro camera. All videos were successfully used to observe the first two modes of vibration, but the third mode was only clearly defined for 80% of the tests performed. The pixel intensity time history diagrams and corresponding Fourier transforms for the shake tables experiments are found in Appendices K, L, M, and N.

Table 1 - Shake Table Results (Canon)

Test	Accelerometer Frequencies (Hz)			Test	Canon Frequencies (Hz)		
	Mode 1	Mode 2	Mode 3		Mode 1	Mode 2	Mode 3
1	2.385	5.923	9.615	1	2.43	5.915	9.634
2	2.417	5.917	9.583	2	2.402	5.918	9.609
3	2.385	5.923	9.615	3	2.402	5.918	9.375
4	2.429	5.929	9.571	4	2.461	5.918	9.375
5	2.455	5.909	9.636	5	2.402	5.918	-
6	2.417	5.917	9.583	6	2.402	5.918	9.609
7	2.462	5.923	9.615	7	2.43	5.915	9.604
8	2.455	5.909	9.545	8	2.402	5.918	-
9	2.417	5.917	9.583	9	2.43	5.915	9.604
10	2.385	5.923	9.615	10	2.401	5.915	9.399
Mean	2.421	5.919	9.596		2.416	5.917	9.526
STDEV	0.030	0.006	0.027		0.021	0.002	0.119

Table 2 - Shake Table Results (GoPro)

Test	Accelerometer Frequencies (Hz)			Test	GoPro Frequencies (Hz)		
	Mode 1	Mode 2	Mode 3		Mode 1	Mode 2	Mode 3
1	2.444	5.889	9.611	1	2.43	5.914	-
2	2.438	5.938	9.625	2	2.43	5.914	9.690
3	2.438	5.938	9.625	3	2.43	5.914	9.602
4	2.462	5.923	9.615	4	2.401	5.914	9.631
5	2.438	5.875	9.625	5	2.43	5.914	9.368
6	2.417	5.917	9.583	6	2.46	5.915	9.605
7	2.455	5.909	9.636	7	2.401	5.915	9.605
8	2.438	5.938	9.625	8	2.459	5.914	9.631
9	2.417	5.917	9.667	9	2.46	5.915	9.605
10	2.455	5.909	9.636	10	2.46	5.915	-
Mean	2.440	5.915	9.625		2.436	5.914	9.592
STDEV	0.015	0.021	0.021		0.023	0.001	0.095

Inferential statistical analysis was done to determine trends of the underlying distribution of the data. This type of analysis is made from samples that are collected from individuals to make inferences about the entire population. In order to estimate the approximate distribution of each measurement type, bootstrap resampling was applied. Bootstrap resampling is a statistical method for estimating the distribution of a set of samples by sampling with replacement from the original values. This method allows assigning measures of accuracy to sample estimates. 10,000 simulations were run for each mode and method. R software was used for these simulations, the code for which can be found in Appendix X. With the data generated by the bootstrapping it became possible to see expected mean values and 95% confidence intervals. The details of this analysis can be seen in Appendix R.

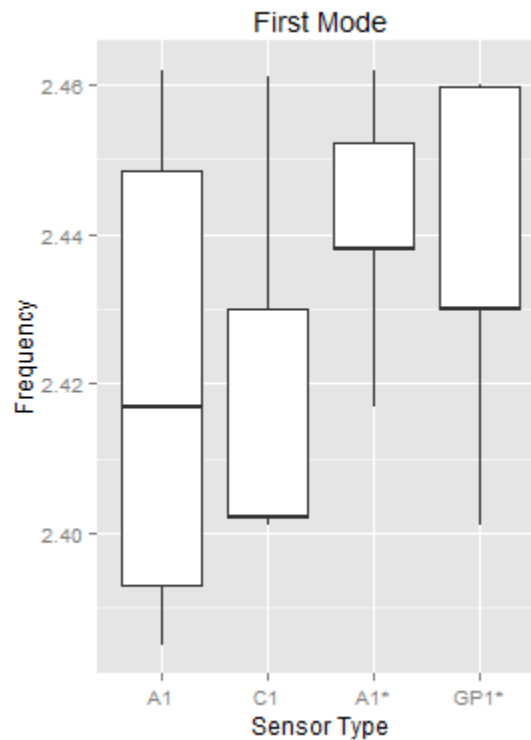


Figure 7 - Shake Table Distribution of Measured Frequency Values (Mode 1)

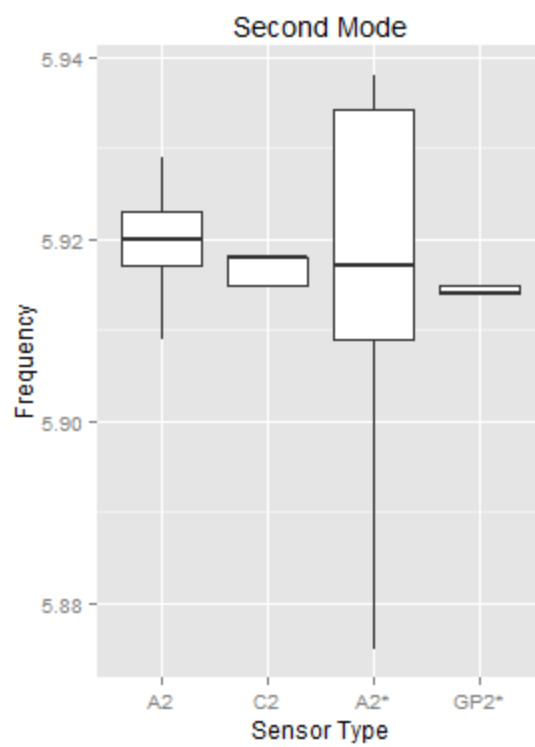


Figure 8 - Shake Table Distribution of Measured Frequency Values (Mode 2)

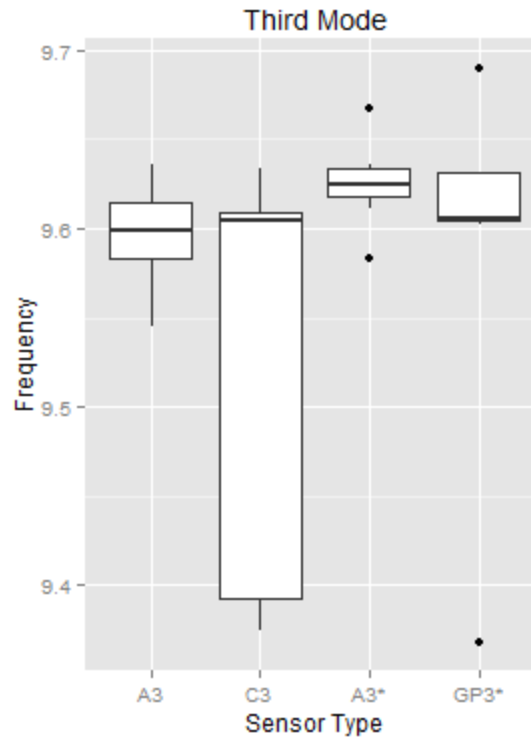


Figure 9 - Shake Table Distribution of Measured Frequency Values (Mode 3)

Three boxplots were created to show the distribution of the dataset generated by resampling, one for each mode of vibration in the shake table experiments. In a boxplot, the bold line represents the median of the data set. 50% of the data points are above this and 50% of the data points are below this. The bottom of the box is the first quartile, the median is the second quartile, and the top of the box is the third quartile. Data points are separated into four equal parts each represented as a quartile. 50% of data points are contained within the box while the remaining 50% of data points are represented in the whiskers. The upper whisker extends from the top of the box to the highest value within 1.5x the interquartile range (IQR). The lower whisker extends from the bottom of the box to the lowest value within 1.5x the IQR. The IQR is defined as the distance between the top and bottom of the box. If outliers are present these are

represented by points. Depending on the data set, it is possible that the median value lies on or very close to one end of the box.

Figure 7 visualizes the distributions for the first mode of vibration, Figure 8 for the second mode, and Figure 9 for the third. A1, A2, and A3 represent the resampled Accelerometer data from the Cannon experiments for modes 1, 2, and 3 respectively. C1, C2, and C3 represent the resampled Cannon data from the Cannon experiments for modes 1, 2, and 3 respectively. A1*, A2*, and A3* represent the resampled Accelerometer data from the GoPro experiments for modes 1, 2, and 3 respectively. GP1*, GP2*, and GP3* represent the resampled GoPro data from the GoPro experiments for modes 1, 2, and 3 respectively.

Comparing the mean values from the accelerometer and Canon samples for the first two modes, found in Figure 7 and Figure 8, shows a very close relationship, while the mean values for the third mode, shown in Figure 9, are further apart. The distribution for the values was also more tightly grouped for the Canon values relative to the accelerometer for the first two modes, shown in Figure 7 and Figure 8, and much larger for the third, shown in Figure 9. Mean values for the accelerometer and GoPro experiments were close across all three modes as shown in Figure 7, Figure 8, and Figure 9. The distribution of the GoPro data points was much tighter than that of the accelerometer for the second mode of vibration and wider spread for the first and third modes as found in Figure 7 and Figure 9.

Table 3 - Difference in Measured Frequency across All Shake Table Modes

	95% Lower bound	Est. of Mean Difference	95% Upper bound	Est. of Std. Dev.
Accelerometer - Canon	-0.0007	0.0227	0.0511	0.0134
Accelerometer - GoPro	-0.0065	0.0112	0.0344	0.0106

Table 3 depicts the combined results of the three modes when comparing overall performance across all three fundamental frequencies. The estimated difference in frequency measured by the accelerometer and the Canon is 0.0227 Hz which was determined from the data generated from the bootstrap resampling. With 95% confidence, the accelerometer measures the frequency to be between 0.0007 Hz lower and 0.0511 Hz higher than measurements made by the Canon. When comparing the accelerometer and the GoPro, the estimated difference in means was 0.112 Hz. With 95% confidence, the accelerometer measures the frequency between 0.0065 Hz lower and 0.0344 Hz higher than the GoPro as determined using bootstrapping. These low differences in frequencies observed with 95% confidence interval testing show a small margin between the accelerometer and the VVS methods used. This statistical analysis shows promise for the use of virtual visual sensors in detecting structural vibrations with similar results to that obtained by use of traditional accelerometers.

The structural frame specimen allowed for a wide range of amplitudes to choose from when doing the video analysis, with smaller displacement amplitudes being near the bottom and larger amplitudes near the top. This range of amplitudes was advantageous because excitation amplitudes were not consistent between each experiment. Various locations along legs beneath the bottom mass were successfully used to extract clear frequency spikes after applying the Fourier transform. This was most likely due to the relatively thin nature of the legs, causing an equally small color gradient. In addition to this, success was met when analyzing locations on the

bottom mass, utilizing color gradients created by the round surface fastening screws and stains existing on the metallic mass. During the analysis of these videos, it was found that several different pixel coordinates were successful in leading to the same three spikes in the Fourier transform. The pixel intensity time- history diagrams and their corresponding Fourier transforms for different pixel coordinates yielded similar results with varying levels of noise.

Since only 80% of the videos were successfully used to observe the third mode of vibration, it can be determined that the chosen perspective may not have been the most appropriate for observing these vibrations. The use of videos from additional perspectives might have allowed more successful observation of the third mode and enhanced the data collection process. In order to avoid being limited in this manner, multiple perspectives were utilized in the following experiments.

Nominal 2x4 Boards (Tested Flatwise)

After equilibrium in the ASTM standard room, average specimen breadth, depth, length, and weight were 38.6 mm, 91.1 mm, 2.44 m, and 46.6 N, respectively. Breadth, depth, and length had coefficients of variation of 3.2%, 2.1%, and 0.03%, respectively. Weight of the boards, and thus their specific gravity, had much greater variation with a coefficient of variation of the weight of the boards was 15.2% leading to a coefficient of variation for their specific gravity to be 14.2%.

Moisture contents and fundamental vibration frequencies of the ten nominal 2x4 specimens after reaching moisture content equilibrium in the three different chambers are given in Table 4. Equation (3) shows the relationship used to estimate the modulus of elasticity of the

samples based on measured material properties. This relationship was derived by solving for E in Equation (1).

$$E = (2\pi f (\frac{L}{n\pi})^2)^2 \frac{\rho}{I} \quad (3)$$

where: f = natural frequency for vibrational mode n , L = span length, E = modulus of elasticity, I = area moment of inertia, and ρ = mass per unit length.

Entering measured values for the natural frequency, calculated values for I based on measured geometric properties, and calculated values for ρ based on the specimens' measured weights and lengths it becomes possible to calculate E . An example of this calculation can be seen in Appendix D. The E was calculated for each experiment using the frequencies observed through the VVS method. Two frequencies were observed with the Canon and two frequencies were observed with the GoPro for each specimen and each experiment. These groups of four natural frequencies, one group for each board and experiment, were separately used to find E with Equation (3). These calculated E values were averaged to find the mean E for each specimen. These calculated means for E for the moisture content experiments are summarized in Table 4. The average value for moisture content, frequency, and mean E are included as the bottom row in Table 4.

Table 4 - Results from Moisture Content Experiments

Specimen	Hot-Dry			ASTM Standard			Hot-Wet		
	MC (%)	Mean Frequency (Hz)	Mean E (MPa)	MC (%)	Mean Frequency (Hz)	Mean E (MPa)	MC (%)	Mean Frequency (Hz)	Mean E (MPa)
1	6.1	16.38	19167	10.7	16.05	17201	11.0	15.65	16607
2	6.8	13.94	10957	11.8	13.48	10197	13.0	13.15	10441
3	6.2	14.59	9994	12.1	14.10	9939	14.0	13.77	10469
4	5.8	16.11	15647	11.0	15.76	14620	14.0	15.44	16622
5	6.3	14.25	10474	11.5	13.80	9849	12.0	13.49	9309
6	6.2	16.58	21744	10.5	16.23	20333	13.0	15.84	18138
7	6.7	15.41	12940	11.5	15.06	12561	13.0	14.78	12299
8	6.3	14.12	13589	11.7	13.80	12885	12.0	13.42	12324
9	5.5	14.71	11787	11.2	14.33	10976	14.0	13.99	10499
10	6.0	14.53	11070	12.0	14.09	10398	13.5	13.59	10065
Mean	6.19	15.06	13737	11.4	14.67	12896	13.0	14.31	12677

Changes in moisture content have effects on all three material properties this study is interested in. As moisture content increases, below the fiber saturation point, the modulus of elasticity is expected to decrease, area moment of inertia is expected to increase, and the linear mass should increase. The swelling with moisture content increase and additional weight were both observed and the data for this can be found in Appendix C. When the area moment of inertia and linear mass effects were taken into account, the modulus of elasticity decreased as expected.

As seen In Table 4, the moisture content had a measureable effect on the natural frequencies of the specimens. The decrease in natural frequency from 15.06 Hz to 14.31 Hz is a 5% reduction. The specimen's calculated mean modulus of elasticity also decreased by about 7.7%. There are many commonly available tools designed to measure the moisture content of wood in the field. Because of the measureable change in natural frequency from differences in moisture content, it is recommended to note the moisture content of observed wood structures

when using vibrational data in structural health monitoring. It is possible that these relatively small effects may skew data collected, which may lead an evaluator to incorrectly estimate the health of a structure.

Results from the experiments in which the specimens were subjected to various types of damage simulation are summarized in Table 5. The effective E was again calculated with Equation (3) taking into account the measured changes to ρ . For the experiments involving the uniform removal of material, the actual E was calculated. For the experiments involving the introduction of the hole pattern and the simulated knot removal an effective E was calculated. The effective E was calculated assuming no changes in the uniformity of the boards' mass and cross-sectional area, as if from the perspective of an evaluator whom had not seen the damage. The results of these calculations can be found in Appendix C.

Table 5 - Results from Simulated Damage Experiments

Specimen Designation	1,2,3		4,5,6	7,8,9	
Simulated damage applied	6.35 mm removed	12.7 mm removed	Knot removed	30.5 cm of hole pattern	61 cm of hole pattern
Mean Reduction in Frequency (Hz)	3.20	5.06	0.47	0.88	1.43
Mean Reduction in Effective E (MPa)	246.8	1,188.3	1,470.5	1,851.8	980.2

For statistical analysis of these experiments, bootstrapping resampling was again utilized. Details on the parameters of this analysis can be found in Appendix X. Figure 10 depicts the distribution of data collected for all nominal 2x4 experiments. In this figure the ASTM standard room experiments are designated with ASTM, hot-dry experiments are designated with HD, hot-wet experiments are designated with HW, planed once and planed twice are designated as P1 and

P2, respectively, the introduction of the hole pattern for 30.5cm and 61cm are designated as H1 and H2, respectively, and the knot removal experiments are designated with K.

As seen in Figure 10, data collected from the accelerometers and by use of virtual visual sensors using video from the Canon and GoPro cameras are nearly indistinguishable. Means and distributions across the experiments were very close for most cases, the hot-dry being the exception. For one of the specimens in this condition the METRIGUARD measured a mean value of 15.43 Hz while the VVS method resulted in a mean of 16.58 Hz which is likely where this discrepancy originates. Also visualized in this figure is the relationship between the different experiments. By looking at the groups of accelerometer, Canon, and GoPro data the relative means and distributions for each experiment are shown. For example: when comparing P1 and P2 there was a very clear separation in the data.

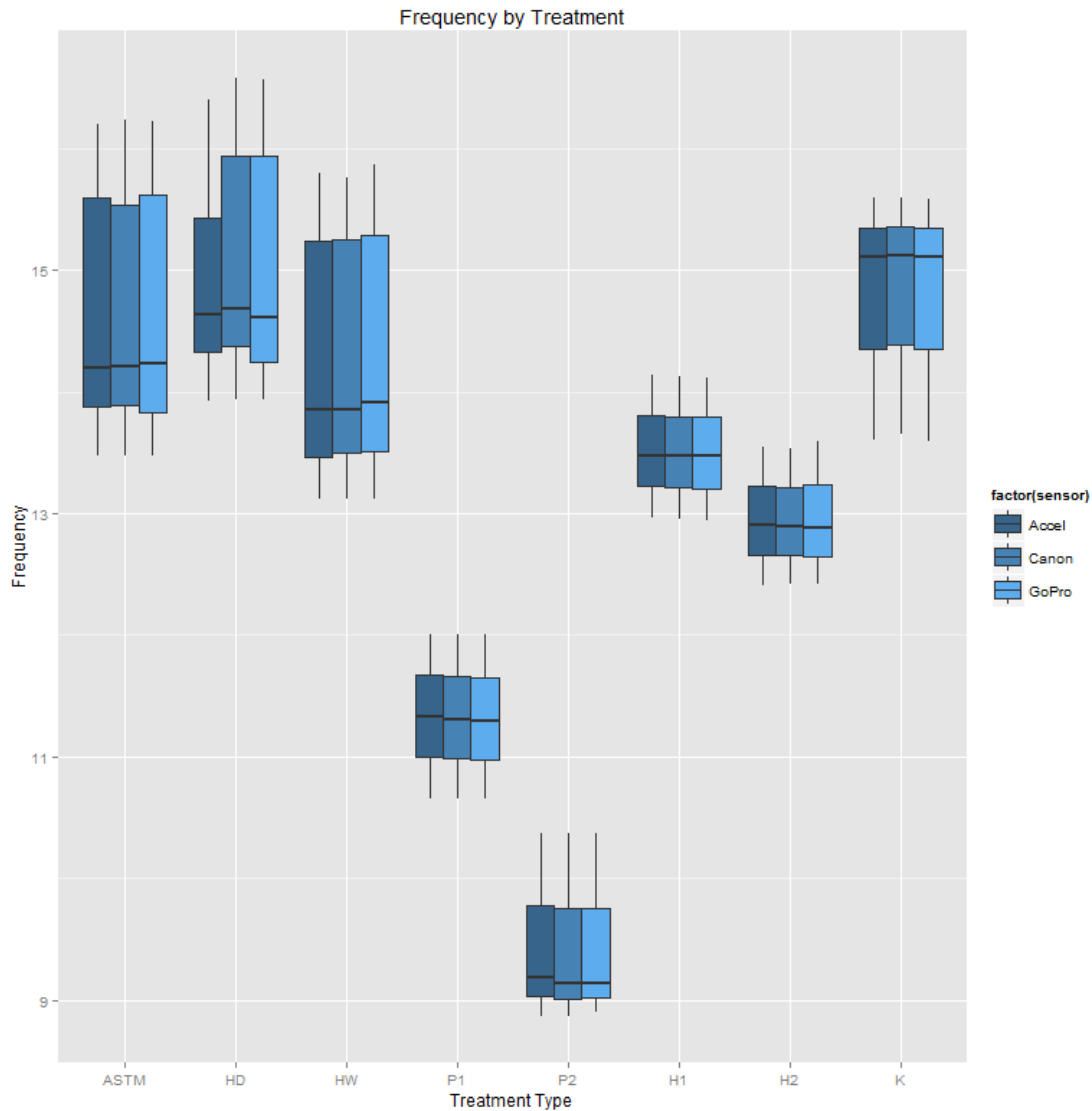


Figure 10 – 2x4 Distribution of Measured Values (all experiments)

For the three moisture content levels the 95% confidence interval for difference in frequencies shows evidence that frequency differs by moisture level as seen in Figure 10. The details are found in Appendix S. Relative to the ASTM standard room conditions, the hot-dry experiments showed a difference in frequency 0.29 Hz higher with 95% confidence to be within 0.02 to 0.57 Hz higher. The hot-wet experiments showed a difference relative to the ASTM standard to be 0.39 Hz lower with 95% confidence to be within 0.34 and 0.43 Hz lower. When

comparing the hot-dry to the hot-wet experiments the difference was estimated to be 0.68 Hz with 95% confidence to be between 0.41 and 0.96 Hz.

Differences in frequencies between conditions from the ASTM standard room and the various levels of damage simulation also shows evidence of statistical difference. This difference is represented in Figure 10, the details of which can be found in Appendix S. Planing the boards once reduced the frequency by 3.20 Hz with 95% confidence to be between 2.74 and 4.04 Hz. The second application of planing was estimated to reduce the frequency by an additional 1.86 Hz with 95% confidence to be between 1.64 and 2.14 Hz. As expected there is a fair amount of confidence that a statistically significant difference was introduced by planing the members. The decrease in frequency due to the introduction of 30.5 cm of the hole pattern was estimated to be 0.863 Hz with 95% confidence to be between 0.81 and 0.92 Hz. The introduction of the additional 30.5 cm of the hole pattern was estimated to decrease the frequency by an additional 0.57 Hz with 95% confidence to be 0.56 to 0.59 Hz. The hole pattern was estimated to introduce statistically significant differences to the natural frequency with confidence. The estimation for the decrease in natural frequency by the simulated knot removal was found to be 0.495 Hz with 95% confidence to be 0.21 to 0.66 Hz. Again, as expected the introduction of this type of simulated damage was shown to decrease the natural frequencies of the boards with some confidence.

Using the data generated from the bootstrap method it was possible to apply a series of T-tests to investigate evidence of statistical difference between the experiments. The T-tests show statistically significant differences were present for moisture content, planing, and introduction of the hole pattern. The T-Tests for the introduction of the knot was not quite able to conclude a statistically significant difference. These results can be found in Appendix S.

Similar to the results from the shake table experiments, the virtual visual sensor method of vibration observation proved to be highly comparable to that from the accelerometer. Naturally occurring color gradients also proved to be very beneficial during these experiments. Wood members naturally have patterns on them from sources such as growth rings, stains, presence of knots, and even heartwood to sapwood transitions. These naturally occurring color gradients made it possible to use any one of a vast array of pixel coordinates located on the member for successful frequency observation and extraction. The abundance of these color gradients was found to be much more useful than in the previous shake table experiments. The VVS method was able to observe vibrations in all tests, including some videos that were out of focus. The reduction in natural frequencies caused by the removal of material clearly shows the potential for virtual visual sensors to be used for overall structural health monitoring in wood structures subject to invisible effects such as decay.

Preliminary estimation of the natural frequency of a nominal 2x4 board was calculated using tabulated values. The estimation was made for *Pseudotsuga menziesii* (Douglas-fir) at 12% moisture content and resulted in a natural frequency of 13.05 Hz. Values used for this estimation were taken from the Wood Handbook (2010). This calculation and primary assumptions used can be found in Appendix T. The difference between this calculated value and those observed during the experimentation can be attributed to the use of values from the Wood Handbook rather than the specimen's true values.

US Forest Service Pedestrian Bridge

The VVS were successfully able to observe structural vibration of the pedestrian bridge in all visits to the bridge. The observed fundamental natural frequency of the bridge was determined to be about 6.22 Hz in October, 2014 and 6.17 Hz in February, 2015. Time-intensity

and Fourier transforms for these experiments can be found in Appendix O, P, and Q. Shown in Figure 11(a) is a pixel intensity time history of a video taken of the bridge in October and in Figure 11(b) is the corresponding Fourier transform. A time-intensity of video taken from the bridge in February is depicted in Figure 12(a) with its corresponding Fourier transform shown in Figure 12(b). The pixel intensity time histories and corresponding Fourier transforms appeared to have much noise. This may be attributed to the distance at which the cameras were used to record video, which was much greater than in the shake table and nominal 2x4 experiments. Increased distance effectively decreases the amplitude of vibration which limits the potential for appropriate color gradients to be used, eventually reaching a point where the motion is contained within very few pixels or even one.

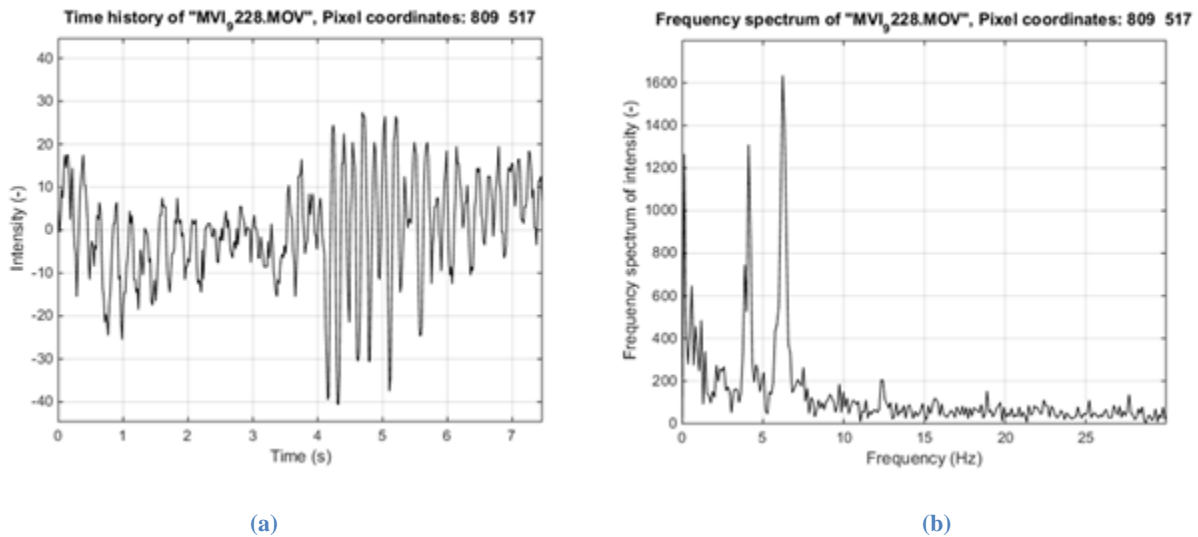


Figure 11 - VVS Time-Intensity and Fourier Transform for USFS Pedestrian Bridge (October 2014)

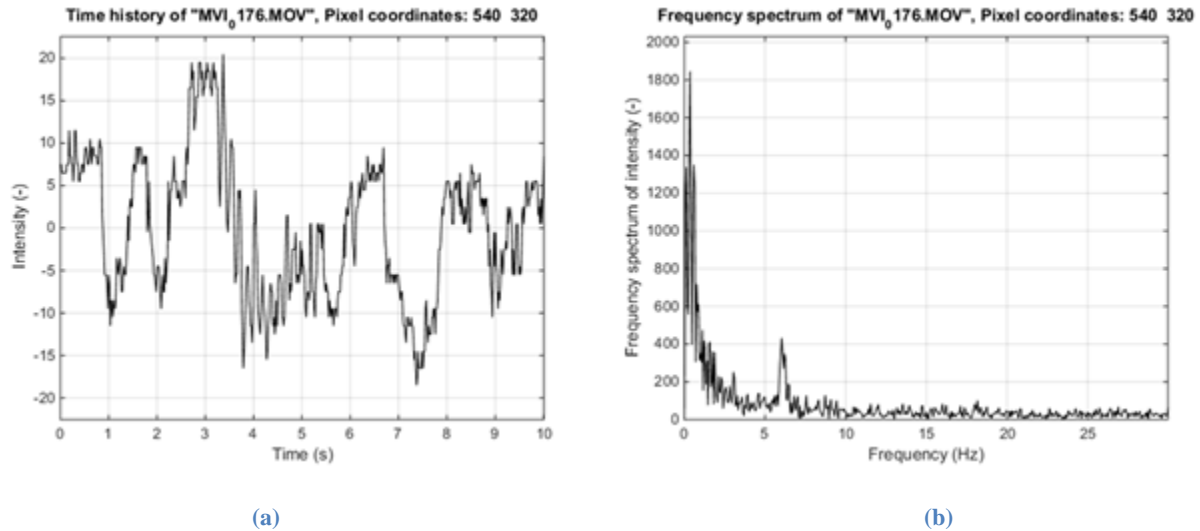


Figure 12 - VVS Time-Intensity and Fourier Transform for USFS Pedestrian Bridge (February 2015)

The moisture content recorded in October was an average of 15.8% in the glulam girders, 22% in the deck boards, and 30% in the side rails. In February, the average moisture content was 18.8% for the girders, 25% for the deck boards, and 33% in the rails. It should be noted that the bridge is treated with a copper compound which may have interfered with the moisture content measurements.

It was also discovered that the distance at which the video was taken was a major factor in successful observation of the vibration as many perspectives from a larger distance were unsuccessful. Videos were taken at a range of distances and perspectives. During these experiments, videos taken at one end of the bridge looking down the span at the deck were successfully used for frequency observation and extraction. The video used to create the pixel intensity time history diagram in Figure 11(a) is an example created from this perspective. Other perspectives included looking at a more perpendicular viewpoint along the river bank, which was easily accessible. Additionally, using lenses with a further focal point on the Canon cameras was beneficial by allowing closer perspectives from further distances. Utilizing the different lenses, successful observation of structural vibration was possible from a wide range of distances. The

GoPro was less useful in this regard as it had a set focal point. Generally speaking, the further perspectives led to smaller spikes in the Fourier transform, such as the example depicted in Figure 12 Figure 12(b), and the closer perspectives resulted in more distinct and clear spikes. Naturally occurring color patterns and stains on the glued laminated timber members proved to be beneficial during the analysis stage.

Preliminary estimates of the natural frequency for the pedestrian bridge were made based on the bridge's design provided by the Forest Service. This calculation and primary assumptions used can be found in Appendix T. The four sets of assumptions used resulted in estimations for the natural frequency of the bridge to be between 4.18 Hz and 4.78 Hz. The difference between these calculated values and those observed during the experimentation can be attributed primarily to the assumptions of perfectly pinned supports and no contribution from the deck and rails to the area moment of inertia.

Conclusions

The use of virtual visual sensors to observe vibrations under various conditions was successful. The natural frequencies extracted from the virtual visual sensor analysis were found to be comparable to the accelerometers used. Naturally occurring color gradients proved to be very beneficial when applying the method to wood beams and wood structures. The successful observation of natural frequencies was observed to be affected by factors such as distance from the structure at which the video was recorded, frame rate of the recorded video, perspective, and motion of the cameras. The VVS method shows promise as a viable method of observing structures with objective results, with ease of data collection in the field, and relatively inexpensive cost. The method requires good line of sight to the observed structure, but is non-contact in nature and allows for application to structures that are difficult to reach. Additional

benefits of the virtual visual sensors include the ability to use multiple data points and not be constrained to a single plane of motion. Commercially available digital video cameras prove to be a promising tool for structural health monitoring of timber structures.

Challenges and Future Work

While the VVS method is a promising tool in the field of structural health monitoring, there remains much that needs to be studied. Wind can sometimes affect the collection of useful data and stabilization attempts were not yet successful. In addition, the applied method of analysis produces signal amplitudes that are not immediately relatable to real deflections. It is recommended that the VVS method be applied to more complex structures to examine the effects individual members can have on the overall structure's fundamental frequency. Correlations between vibration frequencies and type, location, and degree of damage present the greatest challenge and much future work is required.

Recommendations for future research would be to further study the effects of moisture content and wood degradation on natural frequencies, and application of some external loading system for excitation of structures. Several boards could be placed in a water bath and periodically tested. This would provide insight on the effects of moisture content beyond the fiber saturation point. Also, it would be beneficial to subject several wooden boards to actual degradation such as exposure to rot or wood borers for an extended period in order to eliminate the need to simulate damage. This would create a closer to real- life example of the effects of degradation on wood structures and its effect on observed natural frequencies. This study encountered difficulty in observing vibrations in larger bridges under normal traffic conditions. An oscillating mass attached to an electric motor or some similar device could possibly be used to excite larger bridges or even other types of structure to vibrate at an observable level using

VVS. Finally, it would be useful to create a finite element analysis of a real structure and compare theoretical results to observed vibrations over an extended period and to model the effects of observed changes in natural frequency on overall health of the structure. These studies would help to further enhance and bring this method closer to be used in the field.

Practical Applications

The results of the research show promise for virtual visual sensors to be used in determination of natural frequencies of structures which can be used to calculate changes in material properties. Observation of changes in natural frequency of a structure with time can be very useful in determining overall structural health. Using commercially available digital video cameras, as discussed in this report, can be a powerful addition to current health monitoring methods by introducing a relatively simple means of gathering useful quantitative data.

References

- Choi, S. and Shah, S. P. (1997). "Measurement of deformations on concrete subjected to compression using image correlation." *Experimental Mechanics*, 37(3), 307–313.
- Chopra, A. (2012) *Dynamics of Structures: Theory and Applications to Earthquake Engineering*, Pearson Education, Inc., publishing as Prentice Hall, New Jersey.
- Doebeling, S., Farrar, C., Prime, M., and Shevitz, D. (1996) *Damage Identification and Health Monitoring of Structural and Mechanical Systems from Changes in Their Vibration Characteristics: A Literature Review*. Los Alamos National Lab: Los Alamos, NM.
- Forest Products Laboratory (2010) "Wood Handbook: Wood as an Engineering Material." Madison, WI.
- Kasal, B. (2014) "Structural health assessment of in situ timber: An interface between service life planning and timber engineering." *Wood Material Science & Engineering*, 9:3, 134-138; DOI: 10.1080/17480272.2014.903298
- Ross R., Brashaw B., Wang X., White R., and Pellerin R. (2004) *Wood and Timber Condition Assessment Manual*. Forest Products Society, USA.

- Schumacher T., and Shariati A. (2013) “Monitoring of Structures and Mechanical Systems Using Virtual Visual Sensors for Video Analysis: Fundamental Concept and Proof of Feasibility.” *Sensors* 13(12): 16551-16564
- Sinha, A. (2007). “Strain Distribution in OSB and GWB in Wood Frame Shear Walls.” MS thesis, Oregon State University, Corvallis, OR.
- Song, Y., Bowen C., Kim H., Nassehi A., Padget J., and Gathercole N. “Virtual Visual Sensors and Their Application in Structural Health Monitoring.” Available online at: http://urmassn11.iids.org/papers/urmassn11_submission_7.pdf (accessed April 2015)
- Sutton, M.A., Wolters, W.J., Peters, W.H., Rawson, W.F., and McNeill, S.R. (1983). “Determination of displacements using an improved digital image correlation method.” *Image and Vision Computing*, 1(3), 133-139
- Wang, X., Wacker, J., Ross, J., and Brashaw, B. (2005) “Nondestructive Assessment of Timber Bridges Using a Vibration-Based Method.” *Structures Congress*, 10.1061/40753(171)39
- Wu, H., Rubinstein, M., Shih, E., Guttag, J., and Durand, F. (2012) “Eulerian video magnification for revealing subtle changes in the world.” *ACM Trans. Graph.* 31 4, Article 65; DOI: 10.1145/2185520.2185561

CONCLUSIONS AND RECOMMENDATIONS

The use of virtual visual sensors to observe vibrations under various conditions was successful. The natural frequencies extracted from the analysis were highly accurate when compared to accelerometers. In addition, frequencies observed by the VVS method were very precise and repeatable. Naturally occurring color gradients proved to be very beneficial when applying the method to wood beams and wood structures. The successful observation of natural frequencies was observed to be affected by factors such as distance from the structure at which the video was recorded, frame rate of the recorded video, perspective, and motion of the cameras. The VVS method is a promising method of observing structures with objective results, with ease of data collection in the field, and relatively inexpensive cost. The method requires good line of sight to the observed structure, but is non-contact in nature and allows for application to structures that are difficult to reach. Additional benefits of the virtual visual sensors include the ability to use multiple data points and not be constrained to a single plane of motion. Commercially available digital video cameras prove to be a promising tool for structural health monitoring of timber structures.

BIBLIOGRAPHY

- Choi, S. and Shah, S. P. (1997). "Measurement of deformations on concrete subjected to compression using image correlation." *Experimental Mechanics*, 37(3), 307–313.
- Chopra, A. (2012) *Dynamics of Structures: Theory and Applications to Earthquake Engineering*, Pearson Education, Inc., publishing as Prentice Hall, New Jersey.
- Doebling, S., Farrar, C., Prime, M., and Shevitz, D. (1996) *Damage Identification and Health Monitoring of Structural and Mechanical Systems from Changes in Their Vibration Characteristics: A Literature Review*. Los Alamos National Lab: Los Alamos, NM.
- Forest Products Laboratory (2010) "Wood Handbook: Wood as an Engineering Material." Madison, WI.
- Kasal, B. (2014) "Structural health assessment of in situ timber: An interface between service life planning and timber engineering." *Wood Material Science & Engineering*, 9:3, 134-138; DOI: 10.1080/17480272.2014.903298
- Ross R., Brashaw B., Wang X., White R., and Pellerin R. (2004) *Wood and Timber Condition Assessment Manual*. Forest Products Society, USA.
- Schumacher T., and Shariati A. (2013) "Monitoring of Structures and Mechanical Systems Using Virtual Visual Sensors for Video Analysis: Fundamental Concept and Proof of Feasibility." *Sensors* 13(12): 16551-16564
- Sinha, A. (2007). "Strain Distribution in OSB and GWB in Wood Frame Shear Walls." MS thesis, Oregon State University, Corvallis, OR.
- Song, Y., Bowen C., Kim H., Nassehi A., Padget J., and Gathercole N. "Virtual Visual Sensors and Their Application in Structural Health Monitoring." Available online at: http://urmassn11.iids.org/papers/urmassn11_submission_7.pdf (accessed April 2015)
- Sutton, M.A., Wolters, W.J., Peters, W.H., Rawson, W.F., and McNeill, S.R. (1983). "Determination of displacements using an improved digital image correlation method." *Image and Vision Computing*, 1(3), 133-139
- Wang, X., Wacker, J., Ross, J., and Brashaw, B. (2005) "Nondestructive Assessment of Timber Bridges Using a Vibration-Based Method." *Structures Congress*, 10.1061/40753(171)39
- Wu, H., Rubinstein, M., Shih, E., Guttag, J., and Durand, F. (2012) "Eulerian video magnification for revealing subtle changes in the world." *ACM Trans. Graph.* 31 4, Article 65; DOI: 10.1145/2185520.2185561

APPENDICES

Appendix A – Comprehensive Literature Review

Doebeling et al. discussed the wide range of applications in which vibrational behavior characteristics can be used in structural health evaluation and monitoring. The study investigates damage identification methods including changes in natural frequency, mode shape and curvatures, and dynamically measured flexibility. They also consider the application of damage identification and health monitoring to off-shore structures and bridges. The report highlights some difficulties of collecting and using vibrational data including the limitations imposed by using single-point sensors such as accelerometers. The use of virtual visual sensors may alleviate this particular concern.

Kasal discusses the three categories of structural health evaluation in great detail and describes their potential for usefulness. The three categories are destructive, semi-destructive, and nondestructive. Destructive health evaluation is described as a direct method for in-situ determination of health while nondestructive is categorized as indirect. Semi-destructive tests are considered a mixture of both direct and indirect. Destructive tests generally remove an entire member from a structural system which is then tested to failure. This type of testing can give a complete understanding of the member's health state, but the usefulness of the information for structural health monitoring is nearly useless as the member is left permanently damaged. Semi-destructive tests usually involve the extraction of a small piece of a member or members which is then investigated destructively. These types of test yield similar levels of information as destructive tests, but the information gathered is typically localized and some damage is done to the structure in the process. Nondestructive methods of structural health evaluation typically involve the measuring of some physical property which is then used to estimate a property of interest. This study also categorizes several commonly used methods of structural health

evaluation into qualitative and quantitative results, which was useful in understanding structural health monitoring as a whole.

Ross et al.'s Wood and Timber Condition Assessment Manual consolidates many currently used methods of evaluating the health of timber structures and explains their use. This manual explains nondestructive evaluation methods such as visual inspection and stress wave timing in detail. Visual inspection is described as the simplest method for locating deterioration on timber structures, but should never be the sole source of information. Additionally, visual inspection can be subjective in nature as the level of deterioration is left up to the evaluator's judgement. This document was also helpful in describing semi-destructive methods such as drilling, coring, and probing techniques.

Schumacher and Shariati discuss the use of virtual visual sensors in monitoring structures and mechanical systems. Virtual visual sensors can be used as an alternative to more conventional sensors used in the observation of structural vibration such as accelerometers. The study goes into detail of the mathematics of how digital videos are analyzed to extract structure frequencies and also discusses the limiting factors. Pixel intensity values are mapped versus time and a Fourier transform is applied to the signal, creating a frequency spectra. Virtual visual sensors offer advantages such as eliminating the need for wiring, very easily expanding data collection to multiple data points, and offering additional flexibility in that it only requires a good line of sight to the structure observed. The study concludes that virtual visual sensors are accurate when compared to other methods.

Song et al. propose the virtual visual sensor system as a convenient substitute to conventional physical sensor devices used to measure structural vibrations. The paper discusses

the use of virtual visual sensors in observing modal shapes as well as frequencies. Deploying, maintaining, and managing physical sensors can be a complex and expensive process. Instead of using such devices, the paper suggests the use of virtual visual sensors as a relatively simple and inexpensive alternative. Commonly complex networks of piezoelectric accelerometers are deployed at set locations on a structure and data is transmitted wirelessly to some computer. Data collection of this type can be very complex and collected data is limited by the number of points on which sensors are installed. Instead of this complex system of sensors, Song et al. propose the use of virtual visual sensors for data collection. Using virtual visual sensors, data can potentially be collected from any number of potentially millions of video pixel coordinates. In this study circular Hough transforms are used to extract markers. These markers are then used to observe dynamic structural behaviors. By plotting the paths of the individual markers it is possible to see wave shapes and relative amplitudes of motion. Using these mode shapes it is possible to employ a wavelet transform in an attempt to detect where damage has occurred. Damage is located by finding peaks in the wavelet coefficients. Modal frequencies are also extracted through use of Fourier transforms.

Wang et al. discuss the use of vibration-based behavior in the assessment of timber bridges. The paper goes into detail describing the material properties affecting natural frequencies with regards to wood and wood structures, including consideration for effects from moisture content. The main focus of the article is in the determination of stiffness properties, the product EI , based on vibrational data. Experiments were conducted on a range of timber bridges including dynamic and static loading. Results from the dynamic testing were compared to those calculated under static loading conditions. For dynamic motion detection, Wang et al. used a single piezoelectric accelerometer located at mid-span, and all vibrations were assumed to be in

the fundamental mode. Findings in the study conclude forced vibration methods have the potential to be used in the field as a quick method of assessing timber bridge stiffness, but understanding the bridge's weight is critical in the determination of a bridge's stiffness. The study recommends the use of more data points for collection as the single accelerometer limited their observations in some cases.

Wu et al. discussed the potential uses for digital videos to be used to observe physical changes in the world. The study introduces method in which Eulerian magnifications to subtle changes in videos could be used to show minute changes that are invisible to the naked eye. One example of this discussed in the study was the magnification of changes in the Red value of pixels in a video taken of an individual's face. Exaggerating these changes in pixel Red values led to a video in which the flow of blood through the person's face was visible and the individual's heartrate measured based on this. Similarly subtle movements in an individual's wrists were exaggerated and observed versus time to calculate a person's heartrate. This study may have been the first done considering the use of video cameras to observe and measure dynamic physical properties.

Appendix B – Profiles of 2x4 Wood Specimens



Figure B1 - Profile Images for 2x4 Specimen 1



Figure B2 - Profile Images for 2x4 Specimen 2

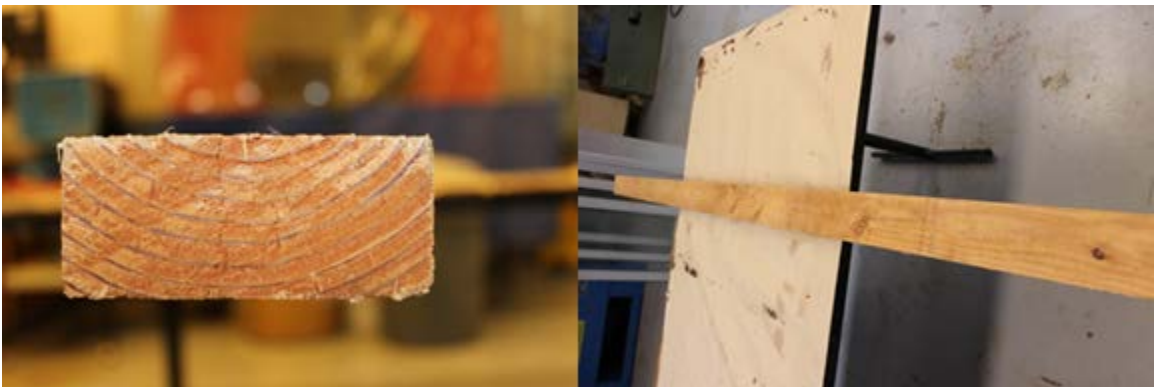


Figure B3 - Profile Images for 2x4 Specimen 3



Figure B4 - Profile Images for 2x4 Specimen 4



Figure B5 - Profile Images for 2x4 Specimen 5

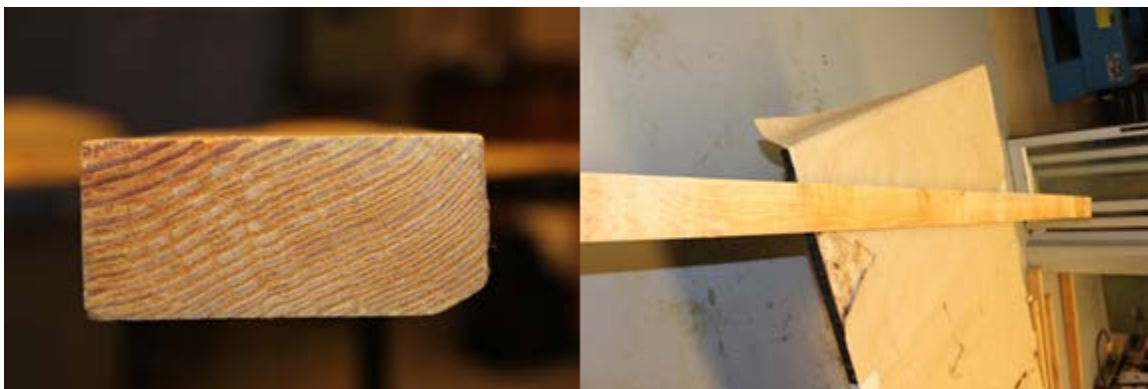


Figure B6 - Profile Images for 2x4 Specimen 6



Figure B7 - Profile Images for 2x4 Specimen 7



Figure B8 - Profile Images for 2x4 Specimen 8



Figure B9 - Profile Images for 2x4 Specimen 9

Appendix C – Results of 2x4 Experiments

Table C1 - 2x4 Frequency Data after Hot-Wet Room Equilibrium

		Metriguard frequency (Hz)			VVS frequency (Hz)					
Specimen	MC	1	2	Mean	Canon 1	Canon 2	GoPro 1	GoPro 2	Mean	St dev
1	6.1%	16.40	16.40	16.40	16.29	16.41	16.40	16.40	16.38	0.0569
2	6.8%	13.93	13.93	13.93	13.94	13.94	13.94	13.94	13.94	0.0000
3	6.2%	14.60	14.60	14.60	14.59	14.59	14.58	14.58	14.59	0.0058
4	5.8%	16.12	16.07	16.10	16.11	16.11	16.11	16.11	16.11	0.0000
5	6.3%	14.24	14.24	14.24	14.30	14.24	14.23	14.23	14.25	0.0337
6	6.2%	15.43	15.43	15.43	16.58	16.58	16.57	16.57	16.58	0.0058
7	6.7%	15.43	15.43	15.43	15.41	15.41	15.40	15.40	15.41	0.0058
8	6.3%	14.14	14.14	14.14	14.12	14.12	14.11	14.11	14.12	0.0058
9	5.5%	14.64	14.68	14.66	14.71	14.71	14.64	14.76	14.71	0.0493
10	6.0%	14.62	14.59	14.61	14.65	14.59	14.29	14.58	14.53	0.1613

Table C2 - 2x4 Specimen Dimensions after Hot-Wet Room Equilibrium

Specimen	Depth, d (in)	Breadth, b (in)	Weight (lb)
1	3.61	1.55	12.90
2	3.56	1.50	10.26
3	3.35	1.50	9.31
4	3.66	1.45	11.01
5	3.53	1.55	9.51
6	3.68	1.55	14.02
7	3.65	1.53	10.41
8	3.66	1.39	9.52
9	3.75	1.58	11.23
10	3.53	1.49	9.00
Mean	3.60	1.51	10.72
STDEV	0.11	0.06	1.64
CV	3.1%	3.7%	15.3%

Table C3 - Calculated Moduli of Elasticity: MC (Hot-Wet Room)

Specimen	MC	E Canon 1 (MPa)	E Canon 2 (MPa)	E GoPro 1 (MPa)	E GoPro 2 (MPa)	E Mean (MPa)
1	11.0	16490	16490	16724	16724	16607
2	13.0	10393	10488	10393	10488	10441
3	14.0	10386	10396	10553	10553	10469
4	14.0	16568	16568	16675	16675	16622
5	12.0	9295	9295	9281	9364	9309
6	13.0	17967	18150	18219	18219	18138
7	13.0	12283	12283	12266	12366	12299
8	12.0	12333	12333	12315	12315	12324
9	14.0	10522	10522	10522	10432	10499
10	13.5	9976	9976	10154	10154	10065
Mean	13.0					12677

Table C4 - 2x4 Frequency Data after Hot-Dry Room Equilibrium

		Metriguard frequency (Hz)			VVS frequency (Hz)					
Specimen	MC	1	2	Mean	Canon 1	Canon 2	GoPro 1	GoPro 2	Mean	Stdev
1	11.0%	15.57	15.65	15.61	15.59	15.59	15.70	15.70	15.65	0.0635
2	13.0%	13.11	13.13	13.12	13.12	13.18	13.12	13.18	13.15	0.0346
3	14.0%	13.71	13.81	13.76	13.71	13.71	13.82	13.82	13.77	0.0635
4	14.0%	15.39	15.41	15.40	15.41	15.41	15.46	15.46	15.44	0.0289
5	12.0%	13.43	13.43	13.43	13.48	13.48	13.47	13.53	13.49	0.0271
6	13.0%	15.75	15.85	15.80	15.76	15.84	15.87	15.87	15.84	0.0520
7	13.0%	14.71	14.81	14.76	14.77	14.77	14.76	14.82	14.78	0.0271
8	12.0%	13.37	13.34	13.36	13.42	13.42	13.41	13.41	13.42	0.0058
9	14.0%	13.93	13.96	13.95	14.00	14.00	14.00	13.94	13.99	0.0300
10	13.5%	13.44	13.64	13.54	13.53	13.53	13.65	13.65	13.59	0.0693

Table C5 - 2x4 Specimen Dimensions after Hot-Dry Room Equilibrium

Specimen	Depth, d (in)	Breadth, b (in)	Weight (lb)
1	3.52	1.50	12.01
2	3.50	1.51	9.61
3	3.50	1.55	8.66
4	3.60	1.50	10.36
5	3.47	1.52	8.89
6	3.61	1.48	13.10
7	3.60	1.52	9.75
8	3.58	1.37	8.88
9	3.69	1.54	10.39
10	3.46	1.48	8.32
Mean	3.55	1.50	10.00
STDEV	0.07	0.05	1.54
CV	2.1%	3.3%	15.4%

Table C6 - Calculated Moduli of Elasticity: MC (Hot-Dry Room)

Specimen	MC	E Canon 1 (Mpa)	E Canon 2 (Mpa)	E GoPro 1 (Mpa)	E GoPro 2 (Mpa)	E Mean (MPa)
1	6.1	18968	19249	19225	19225	19167
2	6.8	10957	10957	10957	10957	10957
3	6.2	10000	10000	9987	9987	9994
4	5.8	15647	15647	15647	15647	15647
5	6.3	10548	10460	10445	10445	10474
6	6.2	21757	21757	21731	21731	21744
7	6.7	12949	12949	12932	12932	12940
8	6.3	13599	13599	13579	13579	13589
9	5.5	11795	11795	11683	11876	11787
10	6.0	11256	11164	10710	11149	11070
Mean	6.2					13737

Table C7 - 2x4 Frequency Data after ASTM Standard Room Equilibrium

		Metriguard frequency (Hz)			VVS frequency (Hz)					
Specimen	MC	1	2	Mean	Canon 1	Canon 2	GoPro 1	GoPro 2	Mean	Stdev
1	10.7%	16.05	16.04	16.05	16.05	16.05	16.05	16.05	16.05	0.0000
2	11.8%	13.47	13.48	13.48	13.48	13.48	13.47	13.47	13.48	0.0058
3	12.1%	14.10	14.04	14.07	14.06	14.12	14.11	14.11	14.10	0.0271
4	11.0%	15.83	15.70	15.77	15.70	15.70	15.81	15.81	15.76	0.0635
5	11.5%	13.80	13.81	13.81	13.83	13.83	13.76	13.76	13.80	0.0404
6	10.5%	16.19	16.20	16.20	16.23	16.23	16.22	16.22	16.23	0.0058
7	11.5%	15.06	15.06	15.06	15.06	15.06	15.05	15.05	15.06	0.0058
8	11.7%	13.75	13.81	13.78	13.83	13.83	13.76	13.76	13.80	0.0404
9	11.2%	14.35	14.30	14.33	14.30	14.30	14.35	14.35	14.33	0.0289
10	12.0%	14.03	14.09	14.06	14.12	14.12	14.06	14.06	14.09	0.0346

Table C8 - 2x4 Specimen Dimensions after ASTM Standard Room Equilibrium

Specimen	Depth, d (in)	Breadth, b (in)	Weight (lb)
1	3.58	1.55	12.59
2	3.54	1.53	10.07
3	3.52	1.54	9.09
4	3.63	1.53	10.83
5	3.49	1.54	9.33
6	3.64	1.51	13.69
7	3.63	1.53	10.19
8	3.62	1.39	9.31
9	3.73	1.57	10.92
10	3.50	1.50	8.75
Mean	3.59	1.52	10.48
STDEV	0.076	0.049	1.597
CV	2.1%	3.2%	15.2%

Table C9 - Calculated Moduli of Elasticity: MC (ASTM Standard Room)

Specimen	MC	E Canon 1 (Mpa)	E Canon 2 (Mpa)	E GoPro 1 (Mpa)	E GoPro 2 (Mpa)	E Mean (MPa)
1	10.7	17201	17201	17201	17201	17201
2	11.8	10204	10204	10189	10189	10197
3	12.1	9883	9967	9953	9953	9939
4	11.0	14518	14518	14722	14722	14620
5	11.5	9899	9899	9799	9799	9849
6	10.5	20345	20345	20320	20320	20333
7	11.5	12569	12569	12552	12552	12561
8	11.7	12951	12951	12820	12820	12885
9	11.2	10938	10938	11015	11015	10976
10	12.0	10442	10442	10354	10354	10398
Mean	11.4					12896

Table C10 - 2x4 Frequency Data from Simulated Damage (Planing)

	Metriguard Frequency (Hz)				VVS Frequency (Hz)					
Specimen	1	2	3	Mean	Canon 1	Canon 2	GoPro 1	GoPro 2	Mean	St dev
1 Planed	12.01	12.01	12.00	12.01	12.01	12.01	12.01	12.01	12.01	0.0000
2 Planed	10.66	10.65	10.65	10.66	10.66	10.66	10.66	10.66	10.66	0.0000
3 Planed	11.33	11.33	11.33	11.33	11.31	11.31	11.30	11.30	11.31	0.0058
1 Planed Twice	10.36	10.37	10.37	10.37	10.37	10.37	10.37	10.37	10.37	0.0000
2 Planed Twice	8.88	8.86	8.88	8.87	8.87	8.91	8.90	8.90	8.90	0.0158
3 Planed Twice	9.16	9.21	9.17	9.19	9.14	9.14	9.14	9.14	9.14	0.0023

Table C11 - 2x4 Specimen Dimensions for Damage Simulation (Planing)

Specimen	MC	Depth, d (in)	Breadth, b (in)	Weight (lb)
1 Planed	9.5%	3.60	1.15	9.49
2 Planed	10.3%	3.56	1.21	7.53
3 Planed	9.2%	3.56	1.23	-
1 Planed Twice	9.5%	3.60	1.03	8.05
2 Planed Twice	10.3%	3.56	1.02	6.23
3 Planed Twice	9.2%	3.56	1.01	5.58
	Mean	3.57	1.11	7.38
	STDEV	0.02	0.10	1.54
	CV	0.6%	9.1%	20.9%

Table C12 - Calculated Moduli of Elasticity: Planing

Specimen	MC	E Canon 1 (Mpa)	E Canon 2 (Mpa)	E GoPro 1 (Mpa)	E GoPro 2 (Mpa)	E Mean (MPa)
1	10.7	17201	17201	17201	17201	17201
2	11.8	10204	10204	10189	10189	10197
3	12.1	9883	9967	9953	9953	9939
Mean	11.5	12429	12458	12448	12448	12446
1 Planed	9.5	17677	17677	17677	17677	17677
2 Planed	10.3	9593	9593	9593	9593	9593
3 Planed	9.2	9278	9278	9261	9261	9269
Mean	9.7	12183	12183	12177	12177	12180
1 Planed Twice	9.5	15559	15559	15559	15559	15559
2 Planed Twice	10.3	9178	9248	9240	9240	9226
3 Planed Twice	9.2	8986	8986	8978	8978	8982
Mean	9.7	11241	11265	11259	11259	11256

Table C13 - 2x4 Frequency Data from Simulated Damage (Knot Removal)

	Metriguard Frequency (Hz)				VVS Frequency (Hz)					
Specimen	1	2	3	Mean	Canon 1	Canon 2	GoPro 1	GoPro 2	Mean	Stdev
4 knot	15.11	15.10	15.10	15.11	15.12	15.12	15.11	15.11	15.12	0.0058
5 knot	13.60	13.60	13.68	13.60	13.65	13.65	13.59	13.59	13.62	0.0346
6 knot	15.58	15.59	15.57	15.59	15.59	15.59	15.58	15.58	15.59	0.0058

Table C14 - 2x4 Specimen Dimensions for Damage Simulation (Knot Removal)

Specimen	MC	Depth, d (in)	Breadth, b (in)	Weight (lb)
4 knot	9.5%	3.63	1.53	10.33
5 knot	10.3%	3.51	1.54	8.86
6 knot	9.2%	3.64	1.51	13.42
	Mean	3.59	1.53	10.87
	STDEV	0.07	0.02	2.33
	CV	2.0%	1.0%	21.4%

Table C15 - Calculated Moduli of Elasticity: Knot Removal

Specimen	MC (%)	E Canon 1 (Mpa)	E Canon 2 (Mpa)	E GoPro 1 (Mpa)	E GoPro 2 (Mpa)	E Mean (MPa)
4	11.0	14518	14518	14722	14722	14620
5	11.5	9899	9899	9799	9799	9849
6	10.8	20345	20345	20320	20320	20333
Mean	11.1	14921	14921	14947	14947	14934
4 knot	9.5	12843	12843	12826	12826	12835
5 knot	10.3	9105	9105	9025	9025	9065
6 knot	9.2	18402	18402	18378	18378	18390
Mean	9.7	13450	13450	13410	13410	13430

Table C16 - 2x4 Frequency Data from Simulated Damage (Hole Pattern)

	Metriguard Frequency (Hz)				VVS Frequency (Hz)					
Specimen	1	2	3	Mean	Canon 1	Canon 2	GoPro 1	GoPro 2	Mean	Stdev
7-1ft	14.13	14.14	14.12	14.14	14.12	14.12	14.11	14.11	14.12	0.0058
7-2ft	13.56	13.54	13.56	13.55	13.53	13.59	13.59	13.53	13.56	0.0346
8-1ft	12.94	12.99	12.95	12.97	12.95	12.95	12.94	12.94	12.95	0.0058
8-2ft	12.41	12.40	12.41	12.41	12.42	12.42	12.42	12.42	12.42	0.0000
9-1ft	13.48	13.46	13.45	13.47	13.48	13.48	13.47	13.47	13.48	0.0058
9-2ft	12.90	12.91	12.91	12.91	12.89	12.95	12.88	12.88	12.90	0.0337

Table C17 - 2x4 Specimen Dimensions for Damage Simulation (Hole Pattern)

Specimen	MC	Depth, d (in)	Breadth, b (in)	Weight (lb)
7-1ft	10.6%	3.63	1.52	9.77
7-2ft	10.6%	3.63	1.52	9.65
8-1ft	9.9%	3.62	1.38	8.67
8-2ft	9.9%	3.62	1.38	8.56
9-1ft	10.5%	3.73	1.57	10.44
9-2ft	10.5%	3.73	1.57	10.26
	Mean	3.66	1.49	9.56
	STDEV	0.05	0.09	0.79
	CV	1.5%	5.9%	8.2%

Table C18 - Calculated Moduli of Elasticity: Hole Pattern

Specimen	MC (%)	E Canon 1 (Mpa)	E Canon 2 (Mpa)	E GoPro 1 (Mpa)	E GoPro 2 (Mpa)	E Mean (MPa)
7	11.5	12569	12569	12552	12552	12561
8	11.7	12951	12951	12820	12820	12885
9	11.2	10938	10938	11015	11015	10976
Mean	11.5	12153	12153	12129	12129	12141
7-1ft	10.6	10804	10804	10789	10789	10796
8-1ft	9.9	10806	10806	10789	10789	10798
9-1ft	10.5	9292	9292	9279	9279	9285
Mean	10.3	10301	10301	10286	10286	10293
7-2ft	10.6	9798	9885	9885	9798	9842
8-2ft	9.9	9814	9814	9814	9814	9814
9-2ft	10.5	8350	8428	8337	8337	8363
Mean	10.3	9321	9376	9345	9316	9339

Appendix D – Example Calculation of 2x4 E

$$E = (2\pi f(\frac{L}{n\pi})^2)^2 \frac{\rho}{I}$$

Assumptions:

1. Perfectly pinned supports
2. Uniform material properties
3. Mode 1 vibration

Specimen 01, hot-dry, Canon sample #1:

$$f = 16.29\text{Hz}$$

$$L = 96\text{in} = 2.438\text{m}$$

$$n = 1$$

$$\rho = \frac{\text{mass}}{\text{length}}$$

$$\text{mass} = \frac{\text{wt}}{g}$$

$$\text{wt} = 12.01\text{lb} = 5.448\text{N}$$

$$I = \frac{bh^3}{12}$$

$$b = 3.5\text{in} = 0.08941\text{m}$$

$$h = 1.5\text{in} = 0.03810\text{m}$$

$$(2\pi(16.29\text{Hz})(\frac{2.438\text{m}}{\pi})^2)^2 \frac{\frac{5.448\text{N}}{9.81 \frac{\text{m}}{\text{s}^2}}}{\frac{2.438\text{m}}{(0.08941\text{m})(0.03810\text{m})^3} \frac{1}{12}} = 18,968 \text{ MPa}$$

Appendix E – Time and Frequency Figures from Hot-Wet 2x4 Experiments

- The first highlighted section contains the specimen designation followed by the test number.
 - In this example: Specimen 1, Test 1
- The second highlighted section contains the camera which was used.
 - In this example: Canon

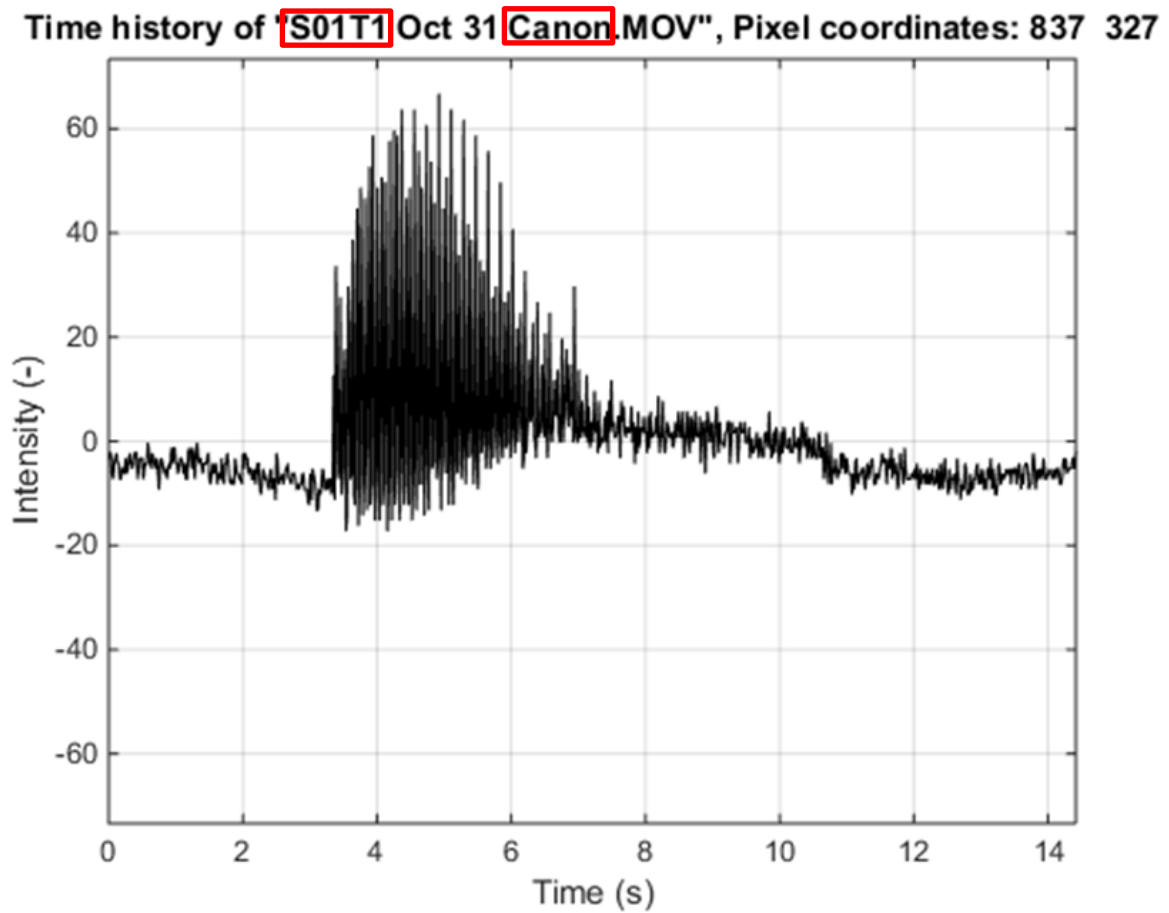
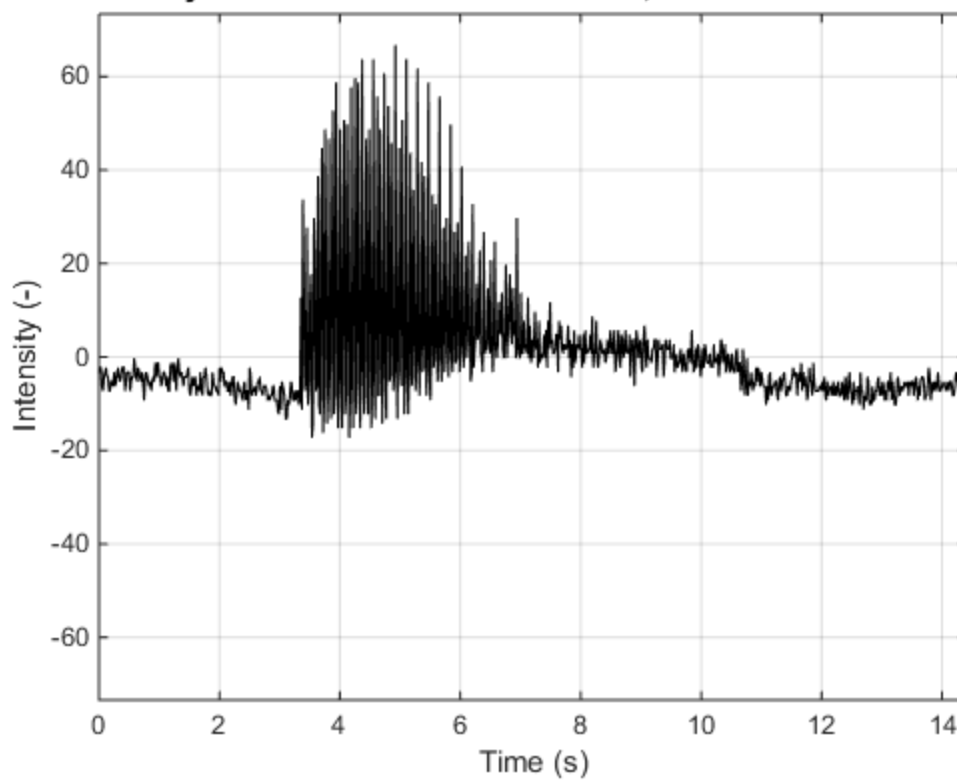
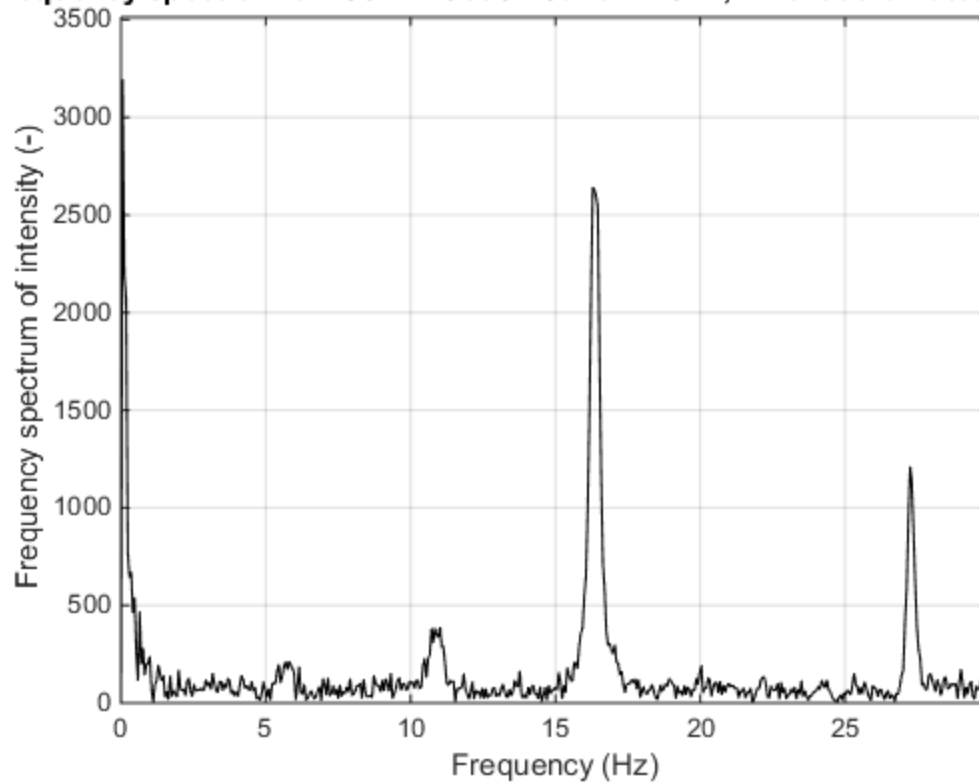


Figure D10 - Key for 2x4 Hot-Wet Figures

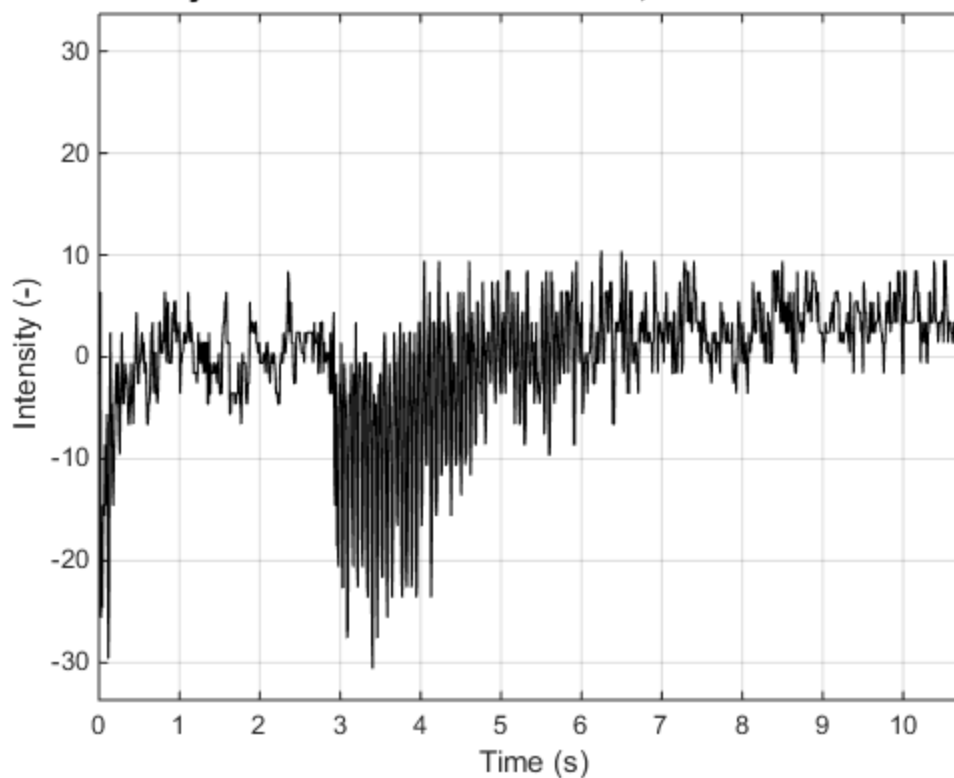
Time history of "S01T1 Oct 31 Canon.MOV", Pixel coordinates: 837 327



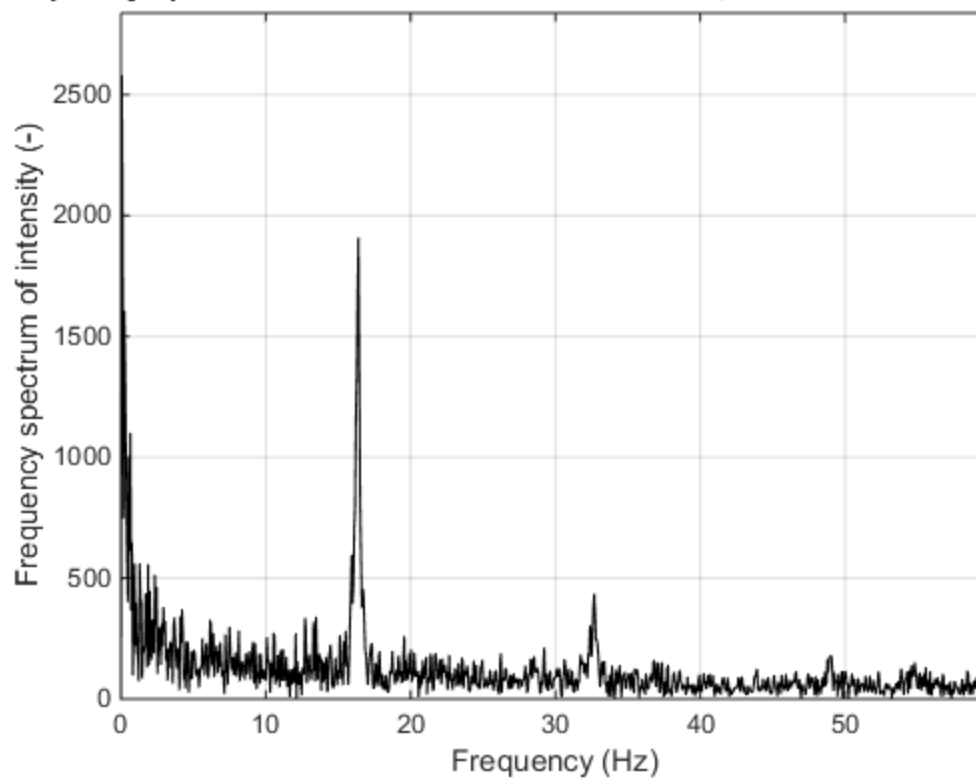
Frequency spectrum of "S01T1 Oct 31 Canon.MOV", Pixel coordinates: 837 327



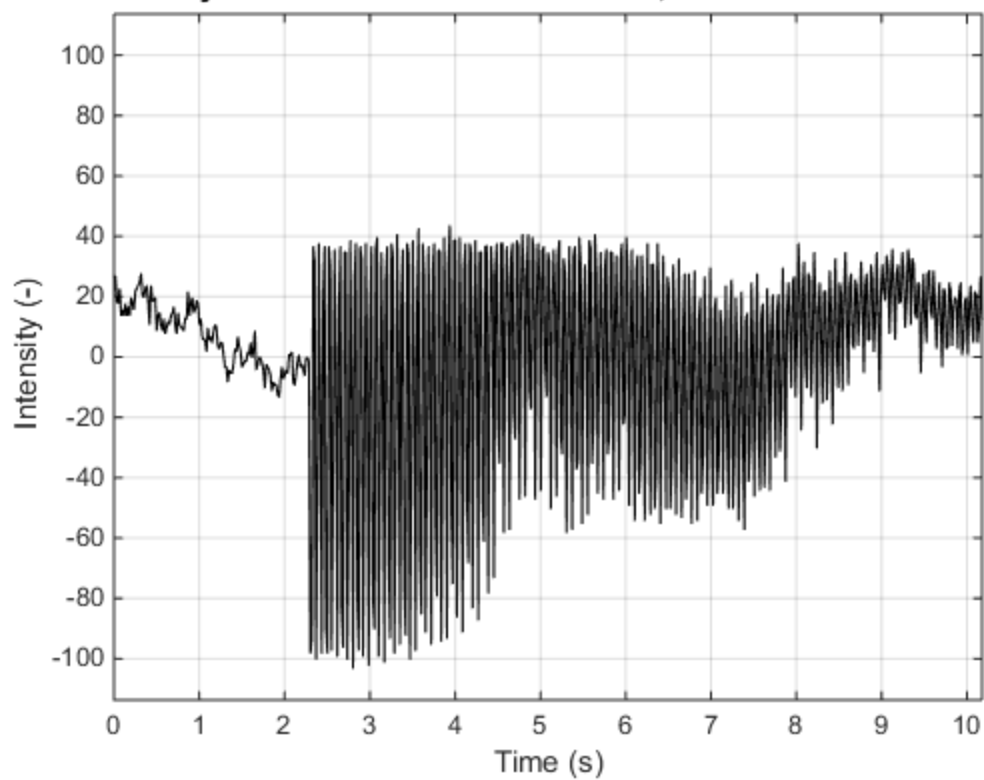
Time history of "S01T1 Oct 31 GoPro.MP4", Pixel coordinates: 271 367



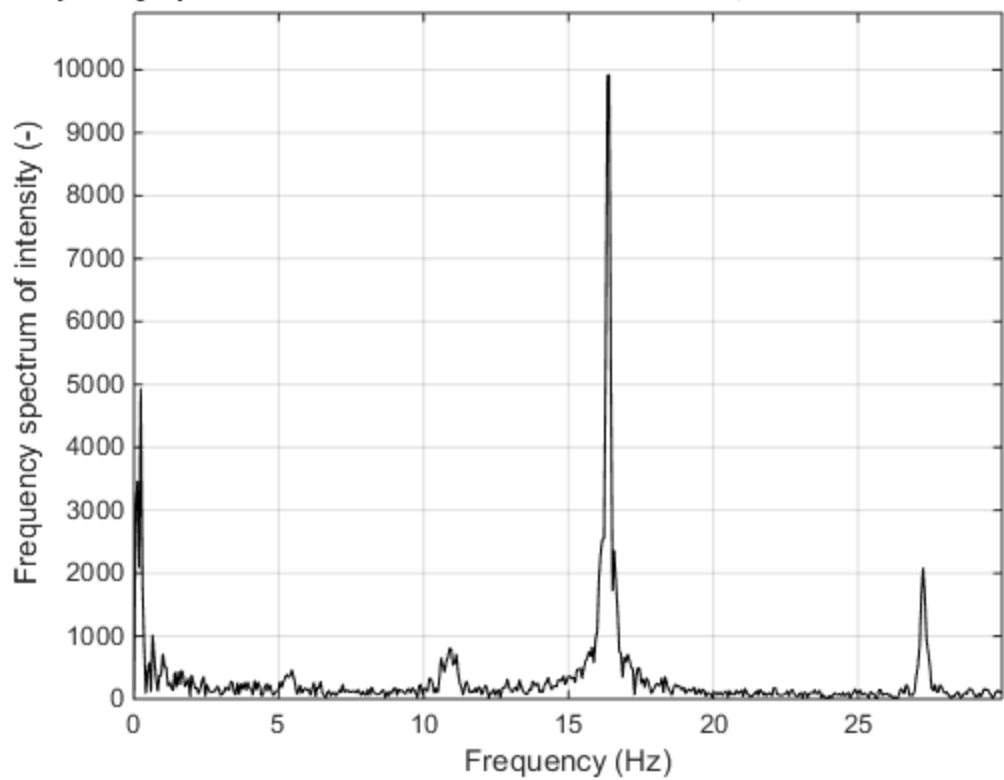
Frequency spectrum of "S01T1 Oct 31 GoPro.MP4", Pixel coordinates: 271 367



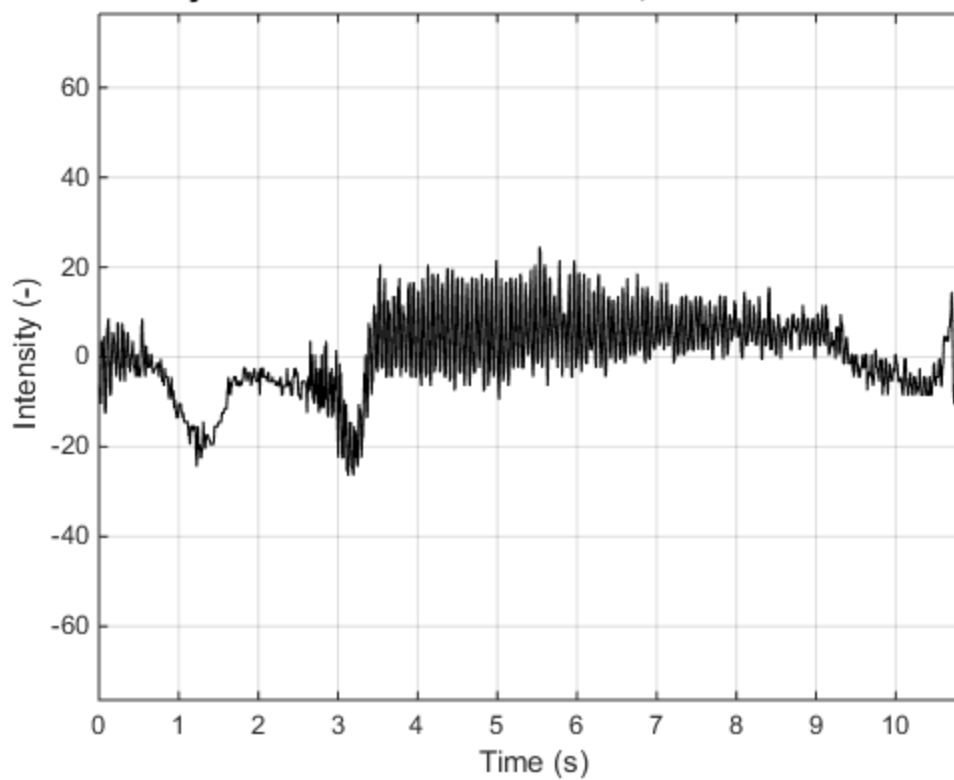
Time history of "S01T2 Oct 31 Canon.MOV", Pixel coordinates: 629 398



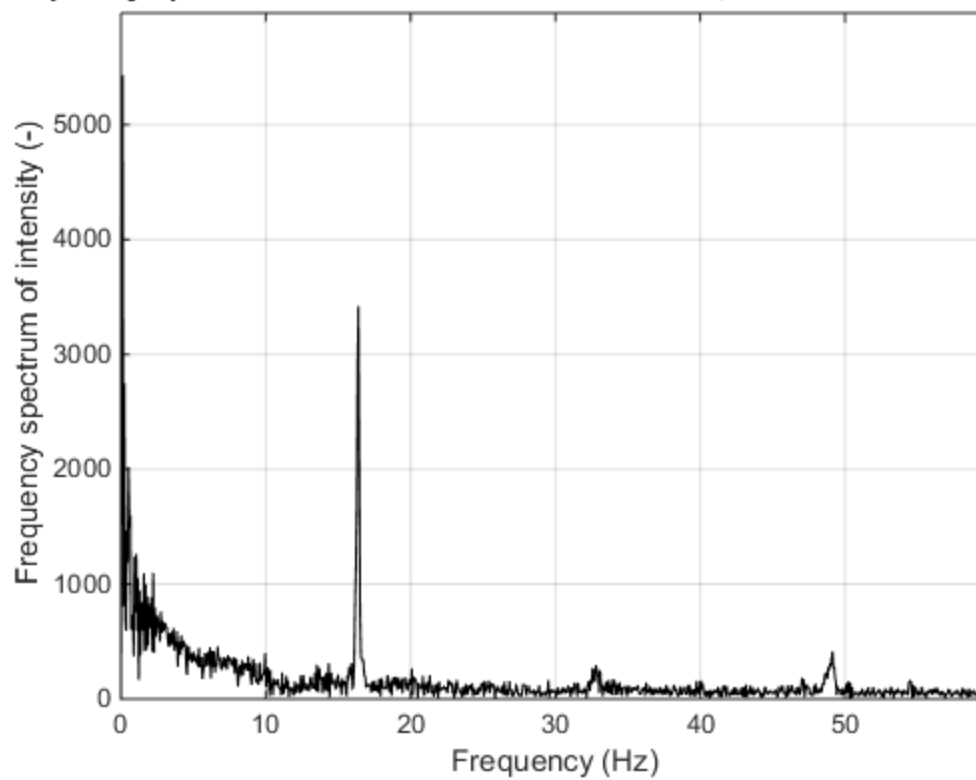
Frequency spectrum of "S01T2 Oct 31 Canon.MOV", Pixel coordinates: 629 398



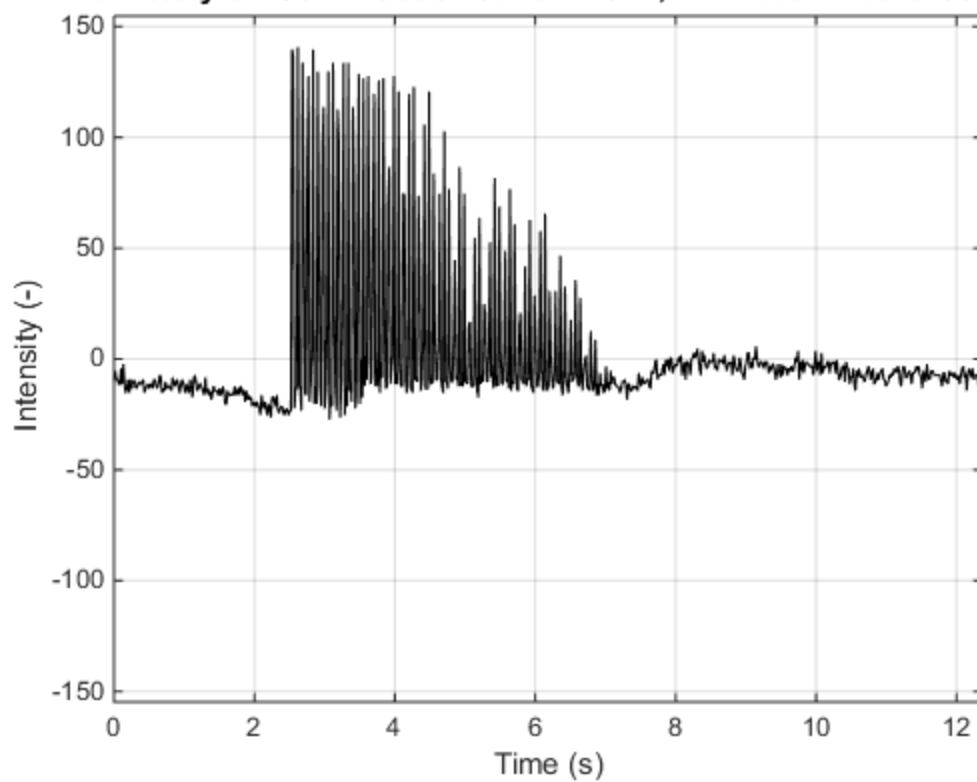
Time history of "S01T2 Oct 31 GoPro.MP4", Pixel coordinates: 591 329



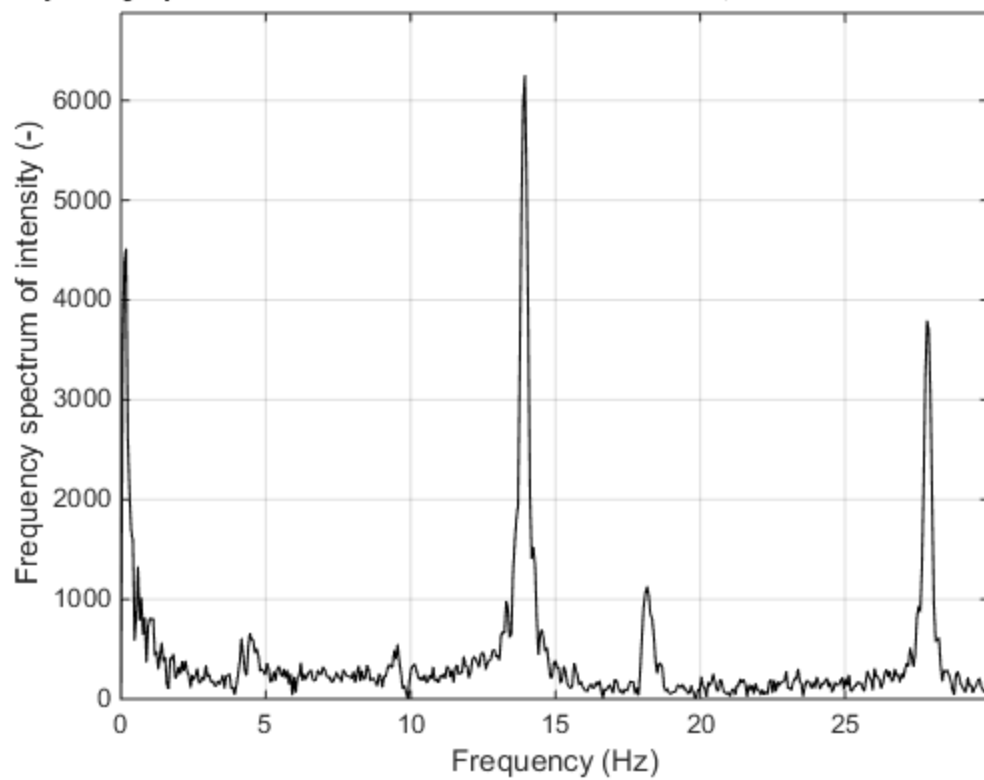
Frequency spectrum of "S01T2 Oct 31 GoPro.MP4", Pixel coordinates: 591 329



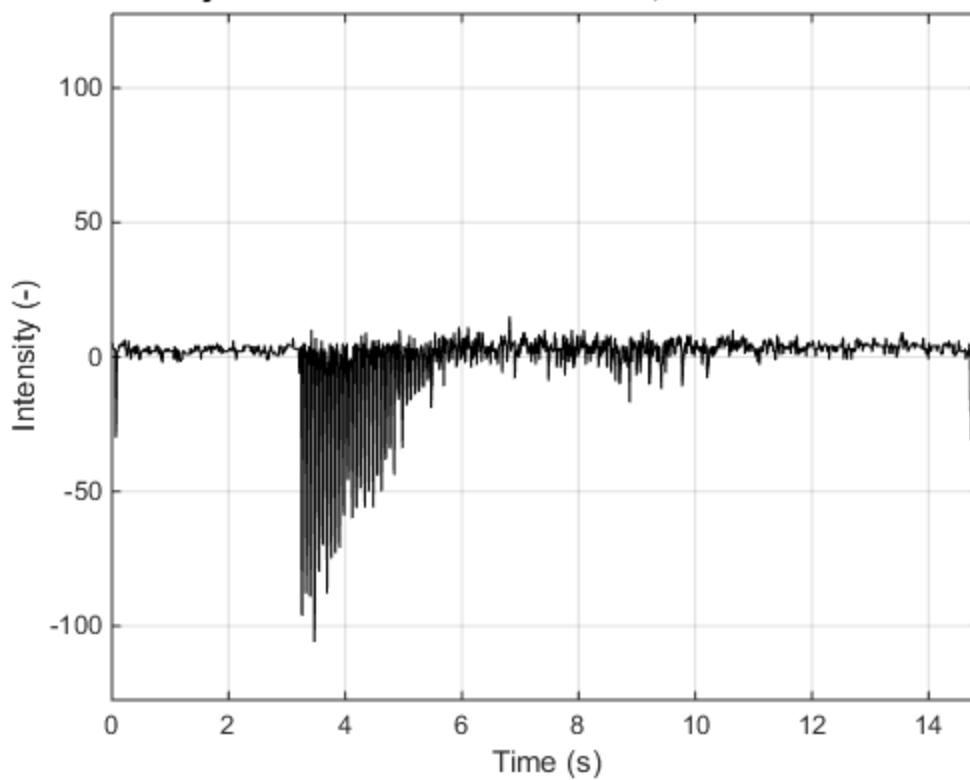
Time history of "S02T1 Oct 31 Canon.MOV", Pixel coordinates: 833 316



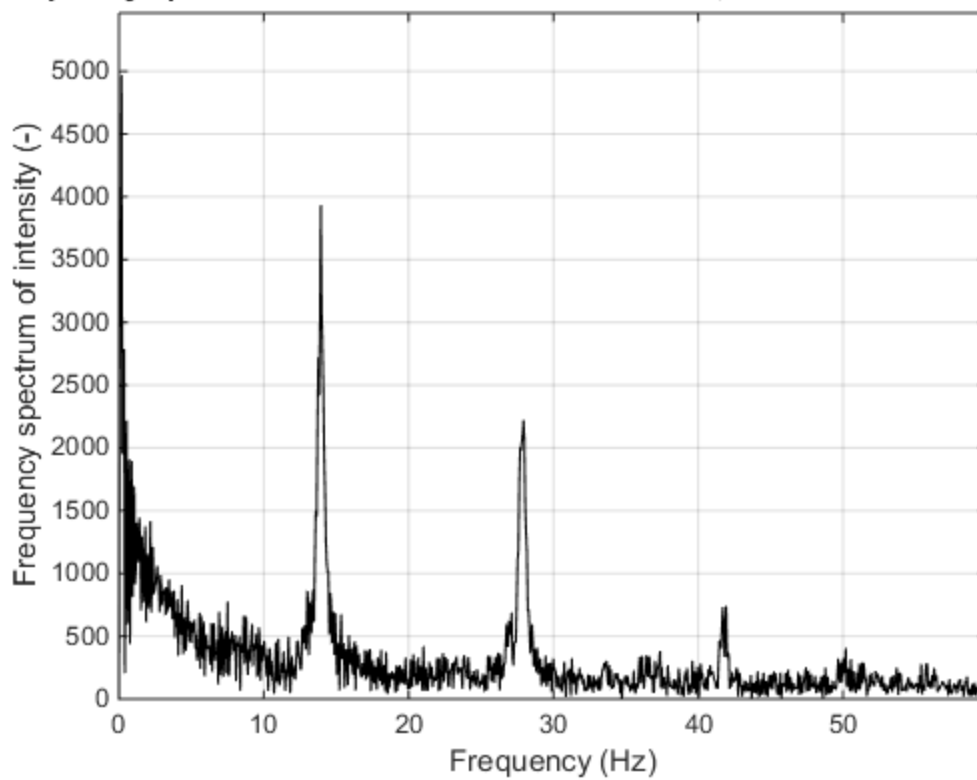
Frequency spectrum of "S02T1 Oct 31 Canon.MOV", Pixel coordinates: 833 316



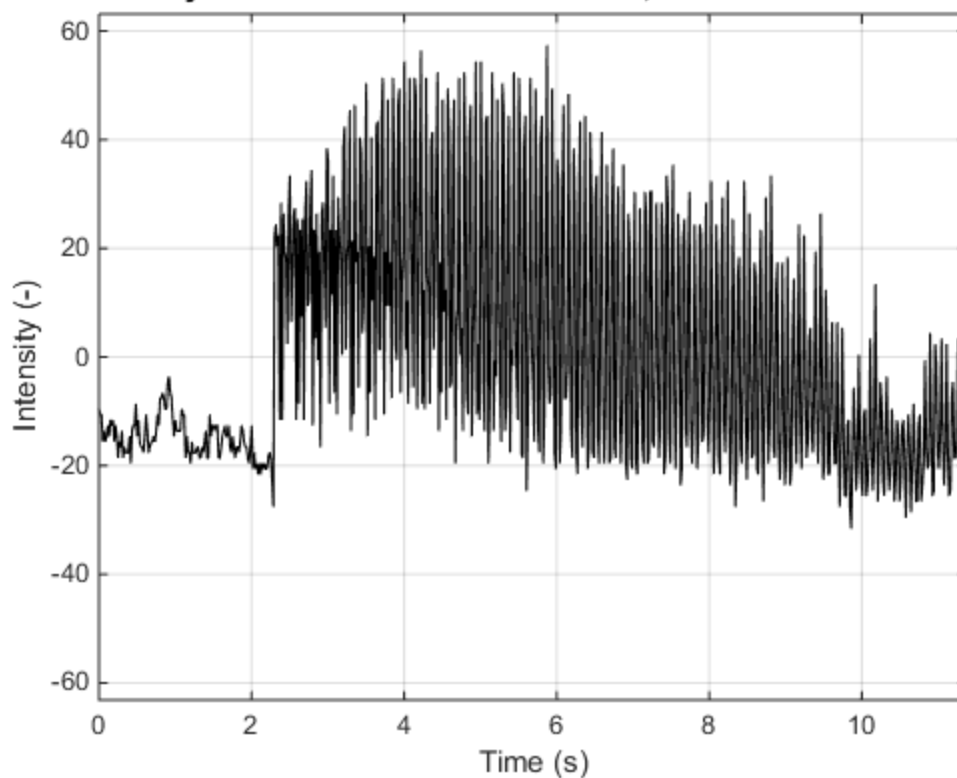
Time history of "S02T1 Oct 31 GoPro.MP4", Pixel coordinates: 445 355



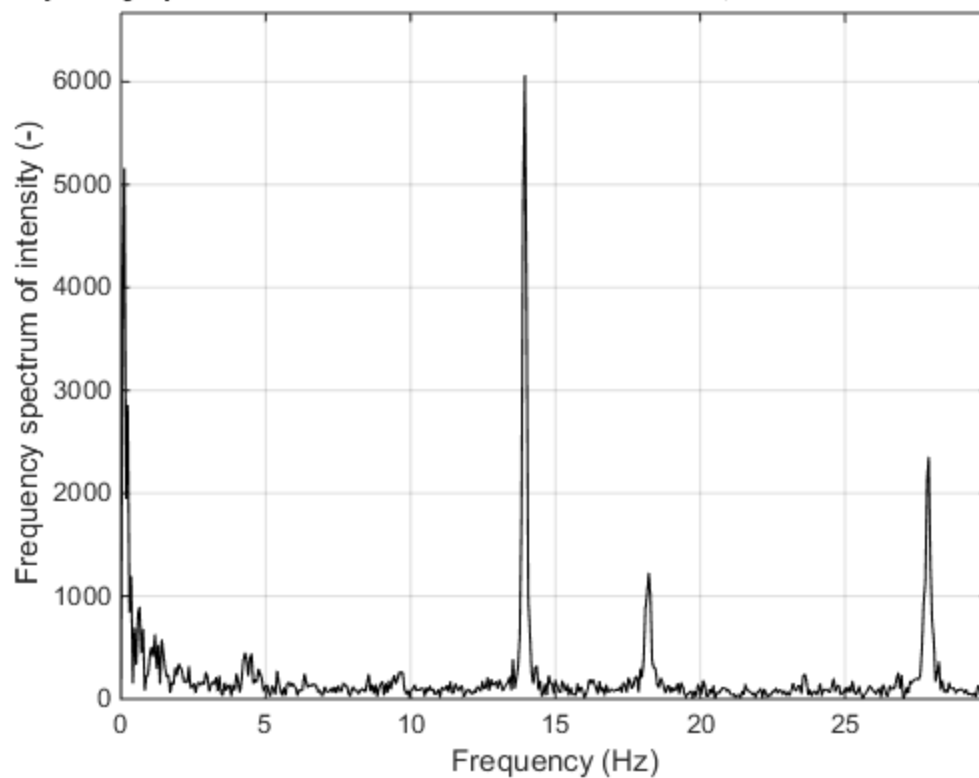
Frequency spectrum of "S02T1 Oct 31 GoPro.MP4", Pixel coordinates: 445 355



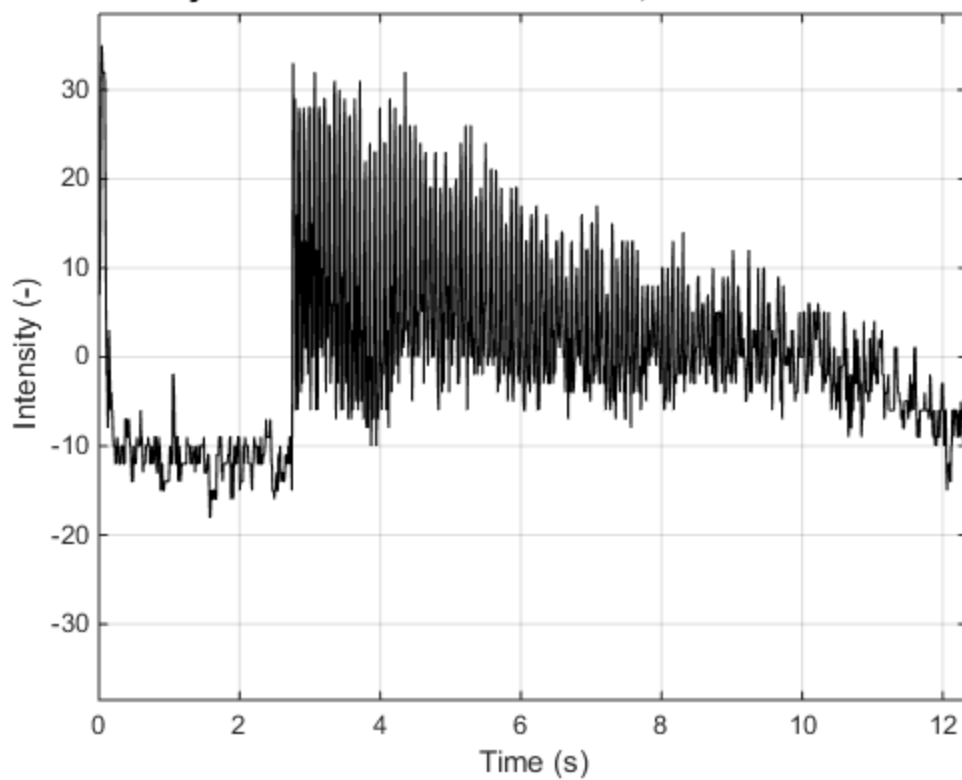
Time history of "S02T2 Oct 31 Canon.MOV", Pixel coordinates: 501 286



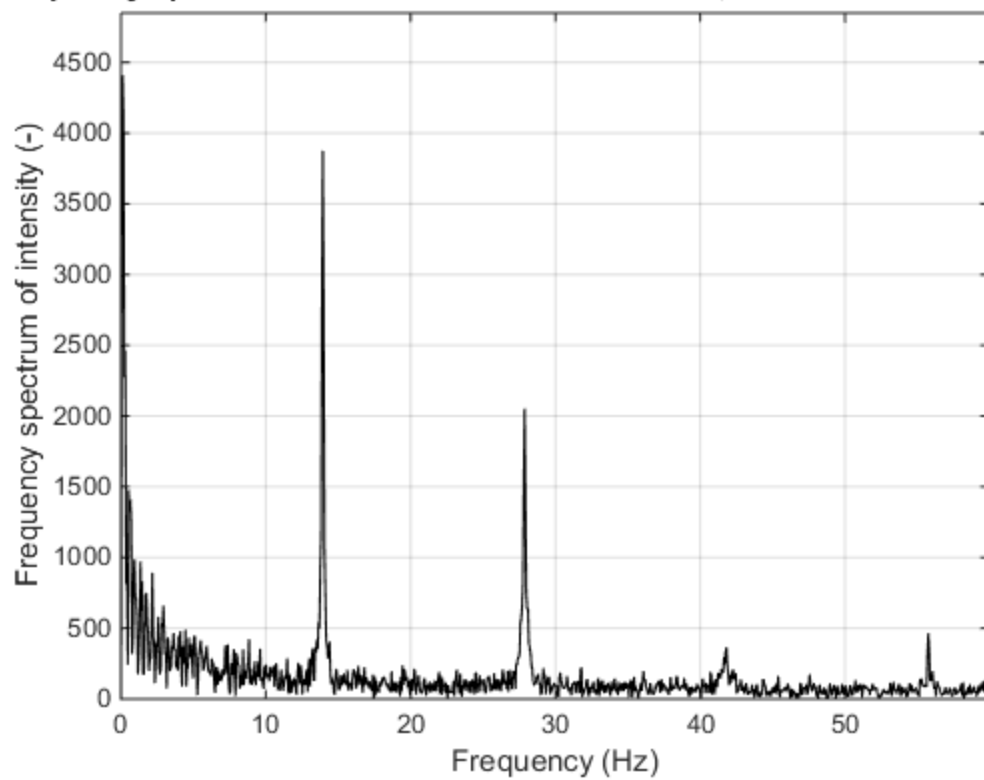
Frequency spectrum of "S02T2 Oct 31 Canon.MOV", Pixel coordinates: 501 21



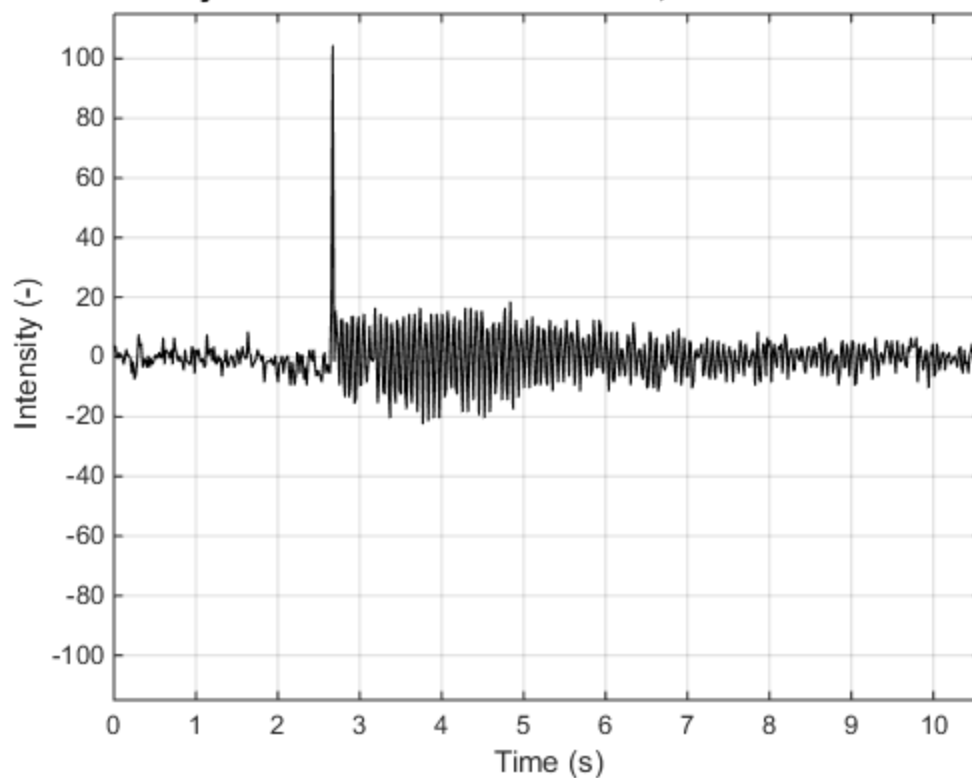
Time history of "S02T2 Oct 31 GoPro.MP4", Pixel coordinates: 482 376



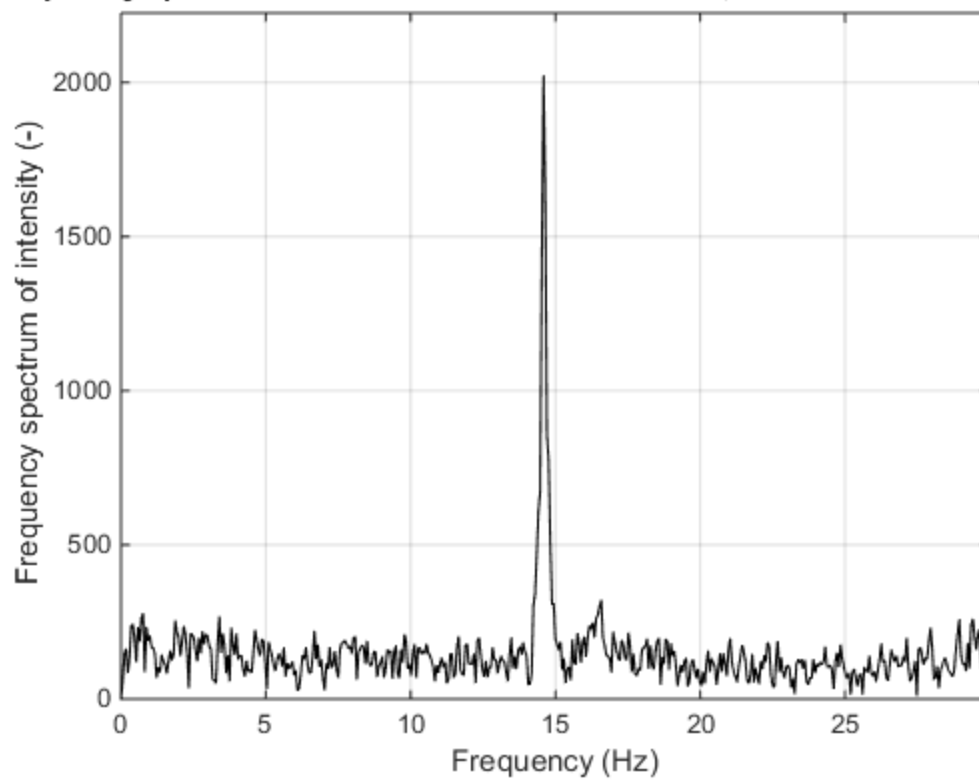
Frequency spectrum of "S02T2 Oct 31 GoPro.MP4", Pixel coordinates: 482 37



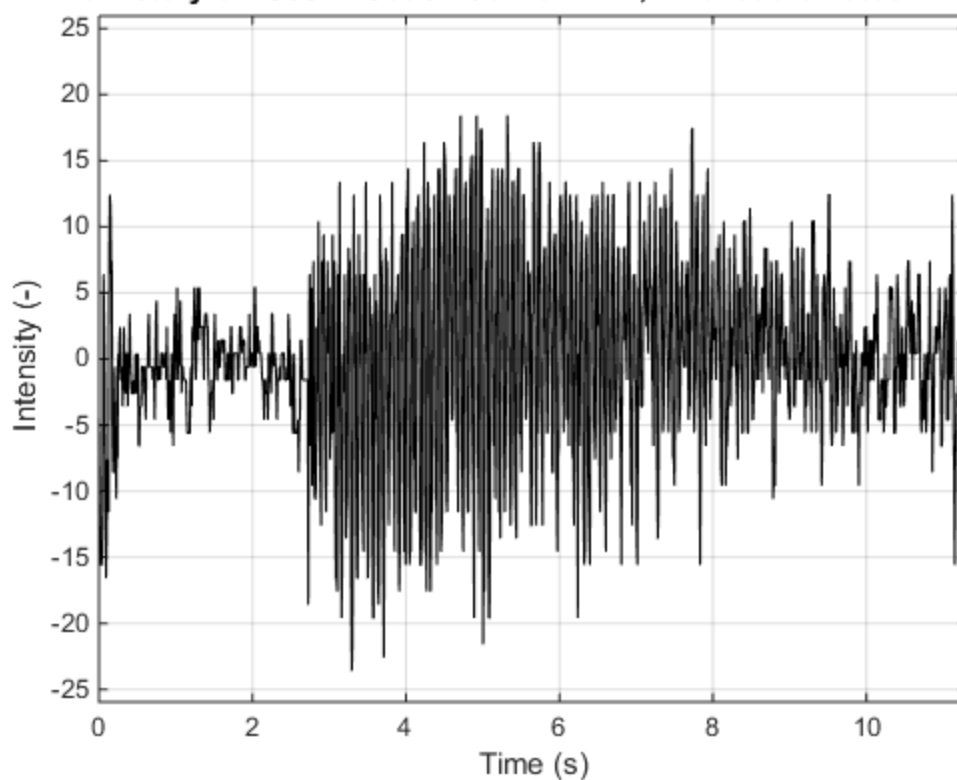
Time history of "S03T1 Oct 31 Canon.MOV", Pixel coordinates: 432 317



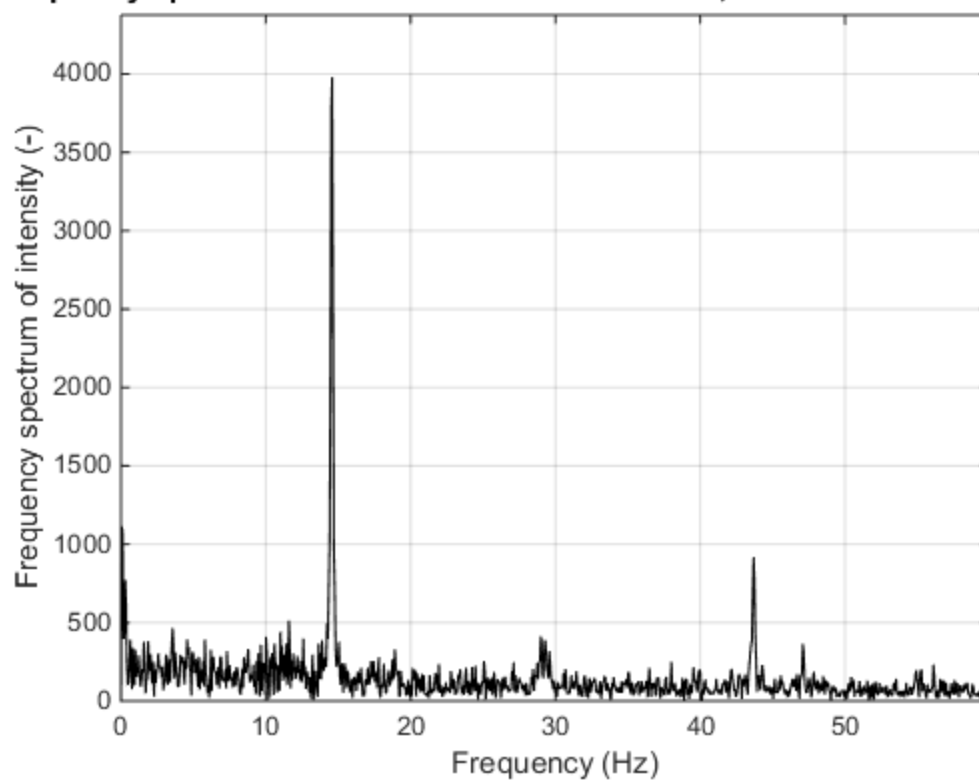
Frequency spectrum of "S03T1 Oct 31 Canon.MOV", Pixel coordinates: 432 317



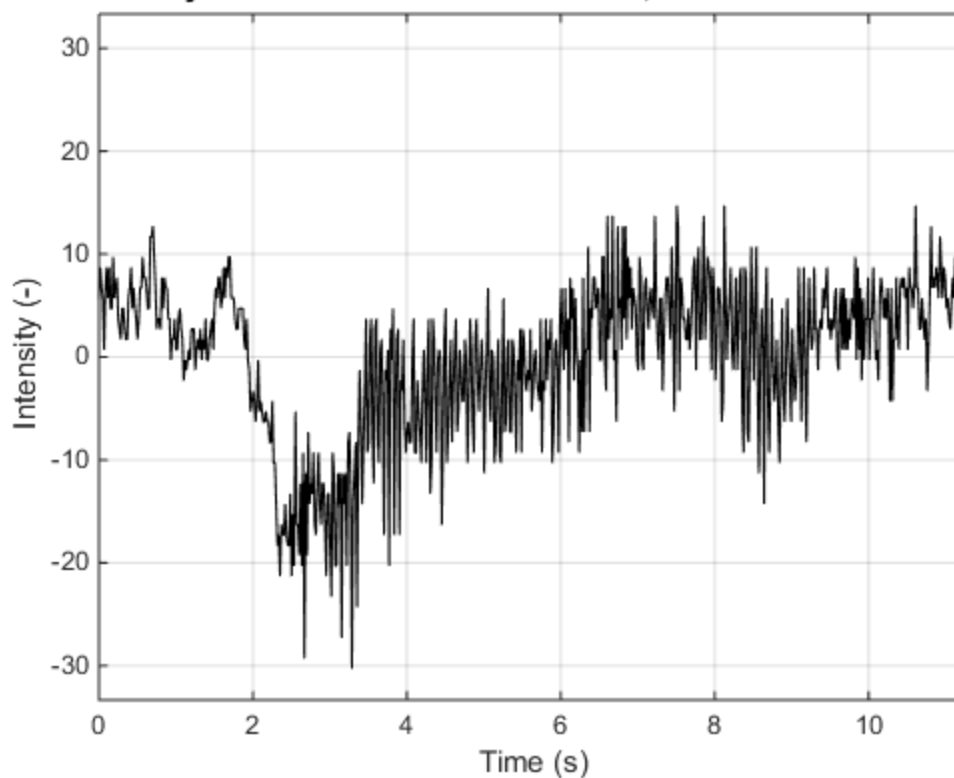
Time history of "S03T1 Oct 31 GoPro.MP4", Pixel coordinates: 445 355



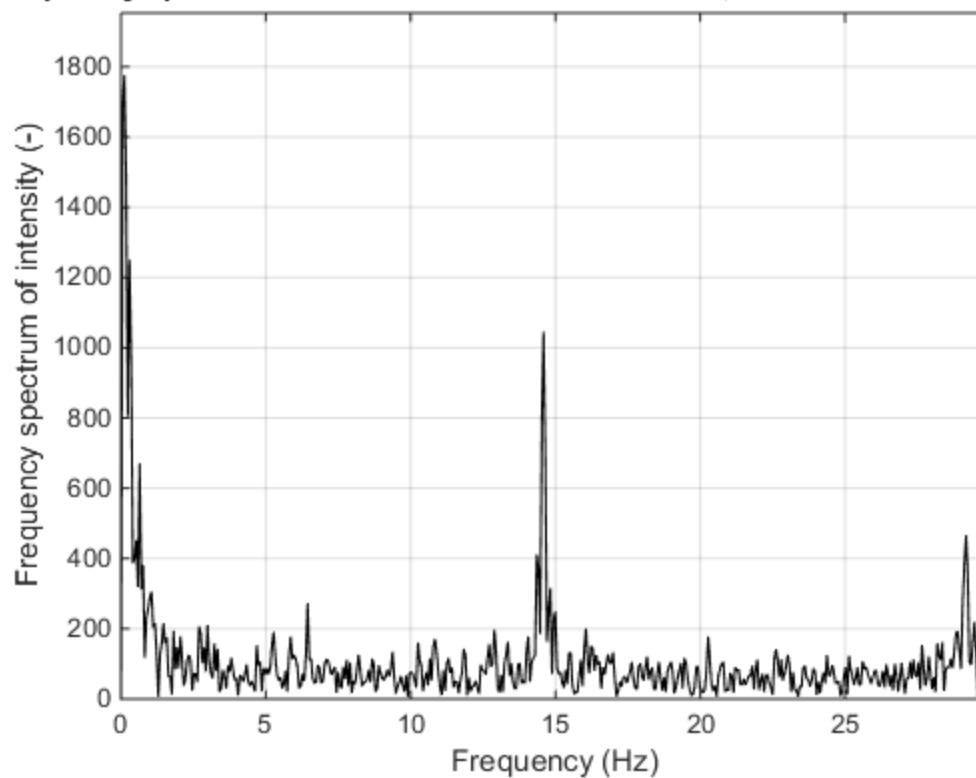
Frequency spectrum of "S03T1 Oct 31 GoPro.MP4", Pixel coordinates: 445 355



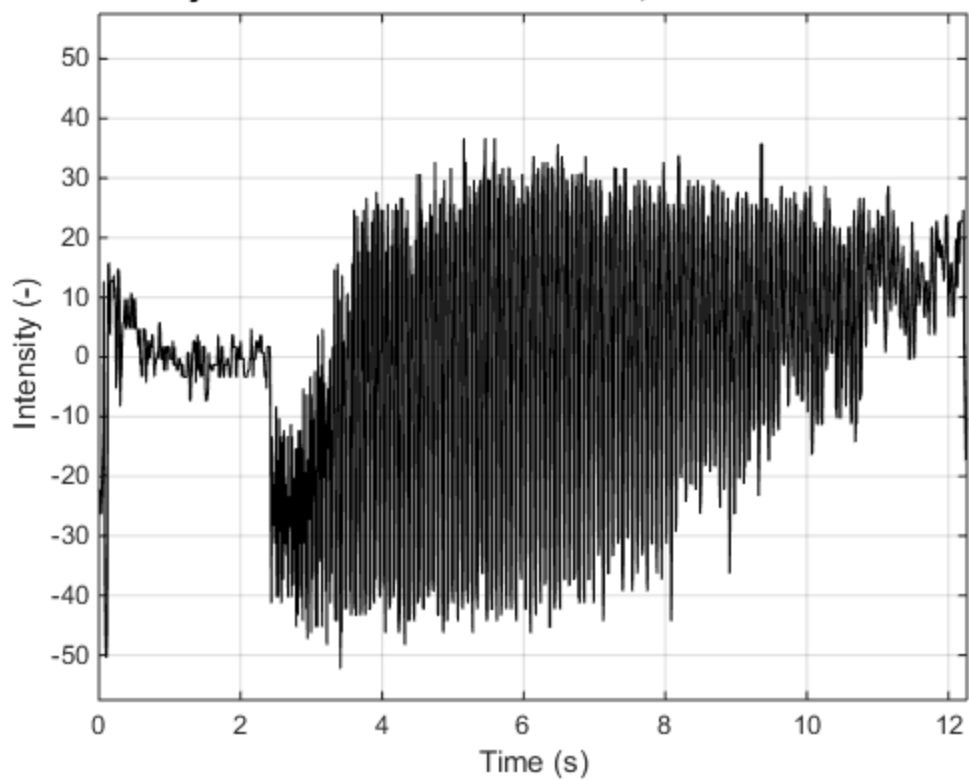
Time history of "S03T2 Oct 31 Canon.MOV", Pixel coordinates: 501 286



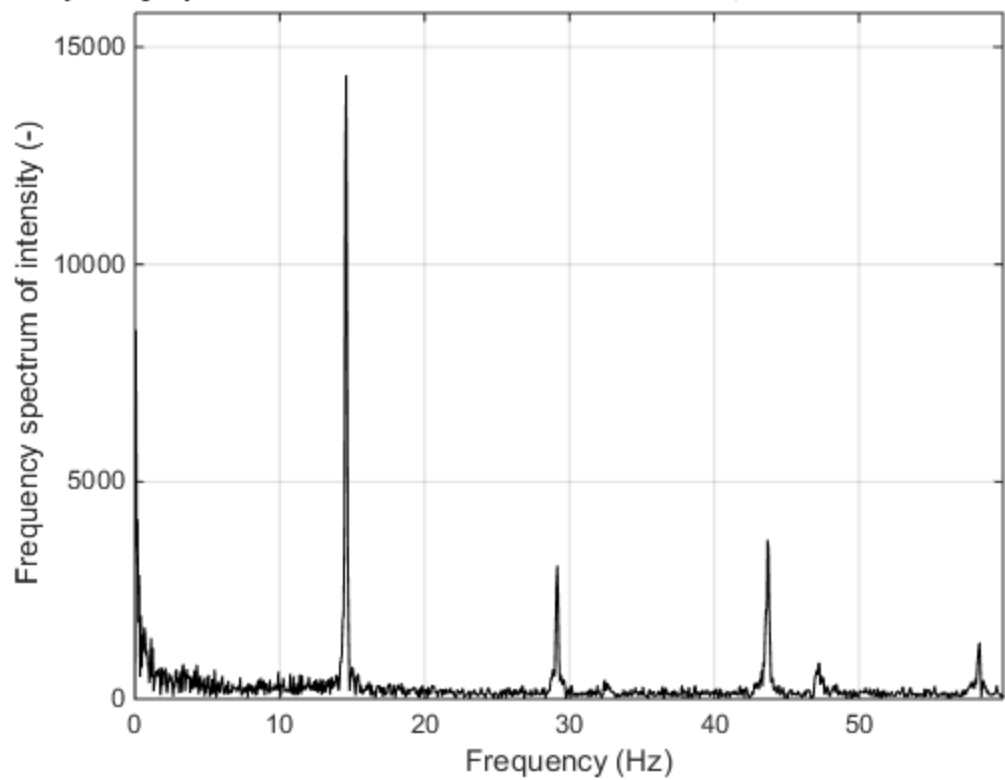
Frequency spectrum of "S03T2 Oct 31 Canon.MOV", Pixel coordinates: 501 21



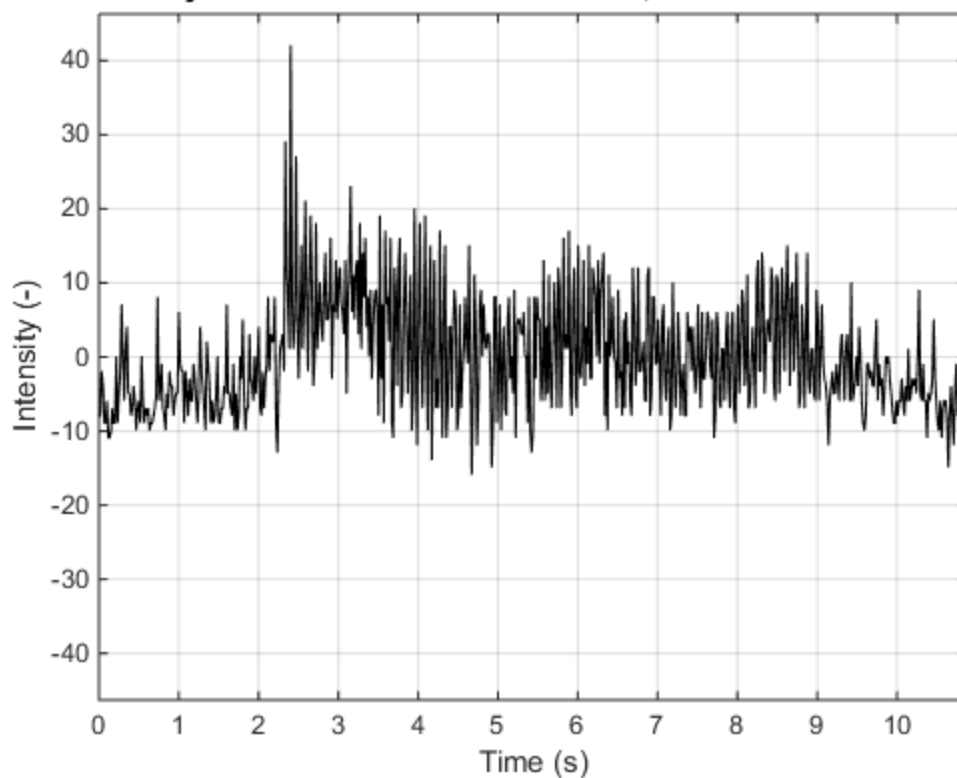
Time history of "S03T2 Oct 31 GoPro.MP4", Pixel coordinates: 482 376



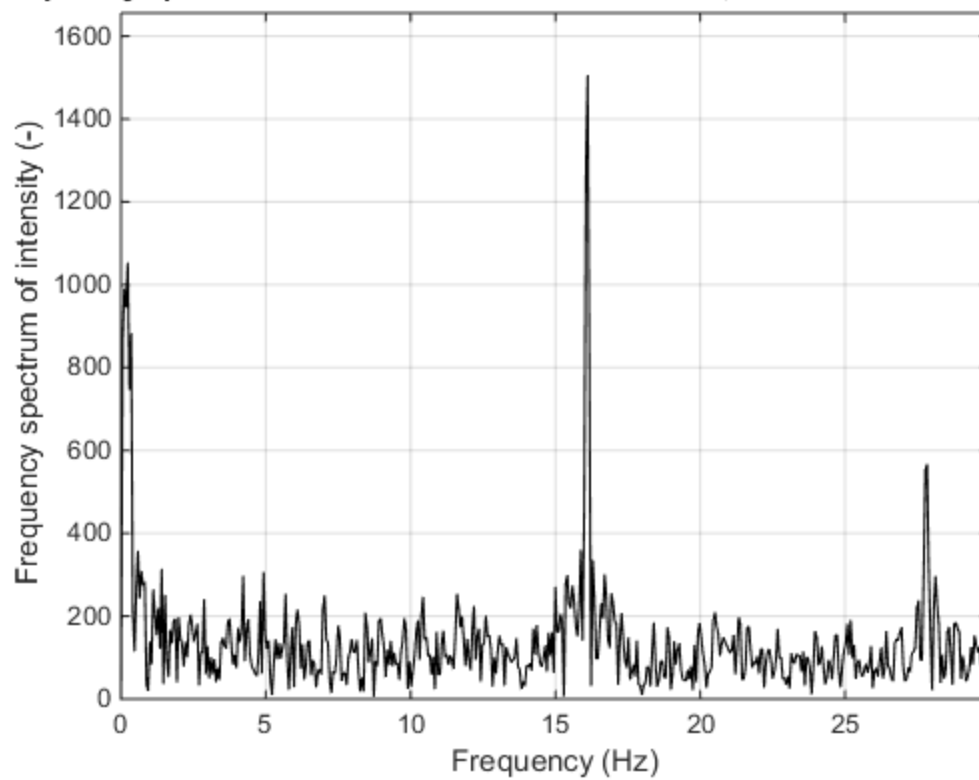
Frequency spectrum of "S03T2 Oct 31 GoPro.MP4", Pixel coordinates: 482 37



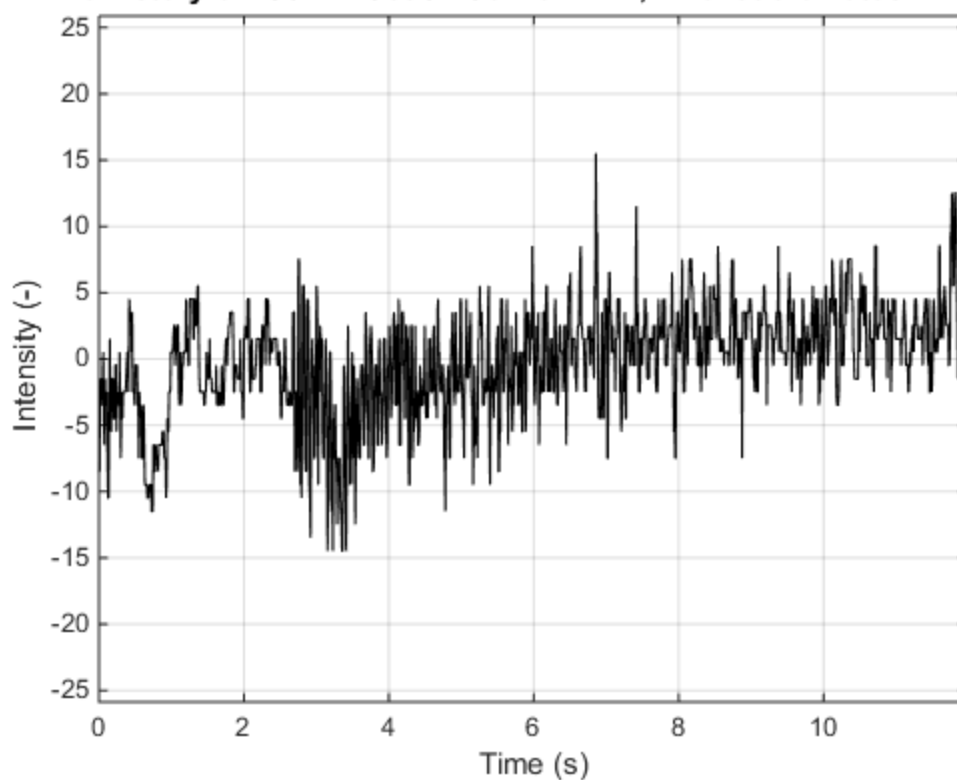
Time history of "S04T1 Oct 31 Canon.MOV", Pixel coordinates: 433 317



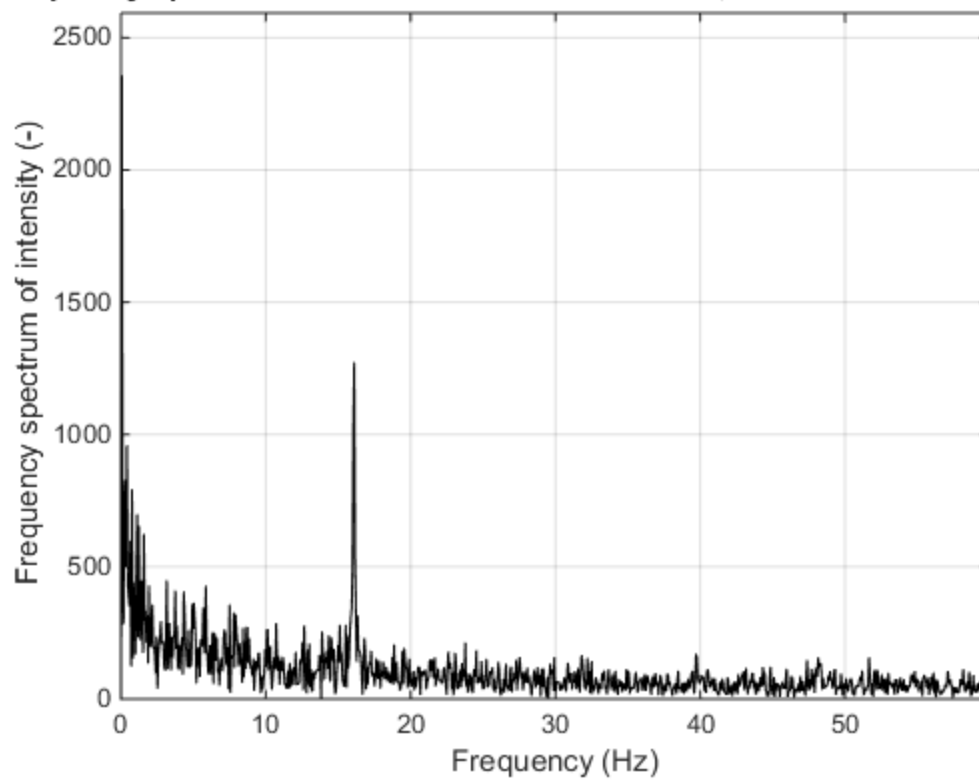
Frequency spectrum of "S04T1 Oct 31 Canon.MOV", Pixel coordinates: 433 317



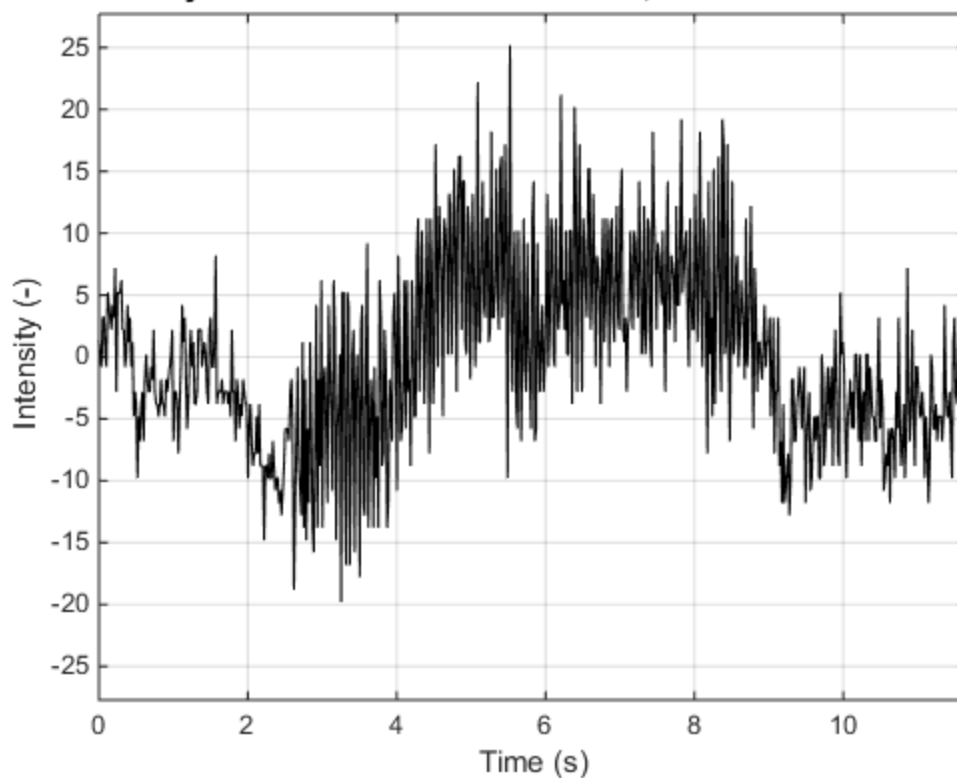
Time history of "S04T1 Oct 31 GoPro.MP4", Pixel coordinates: 445 355



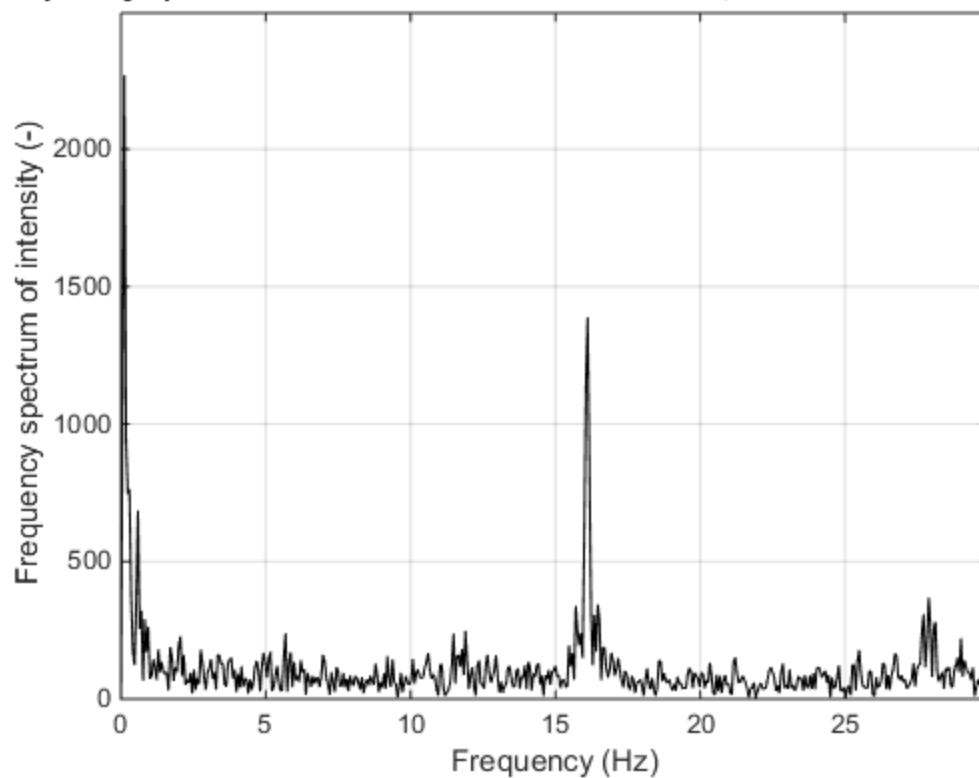
Frequency spectrum of "S04T1 Oct 31 GoPro.MP4", Pixel coordinates: 445 355



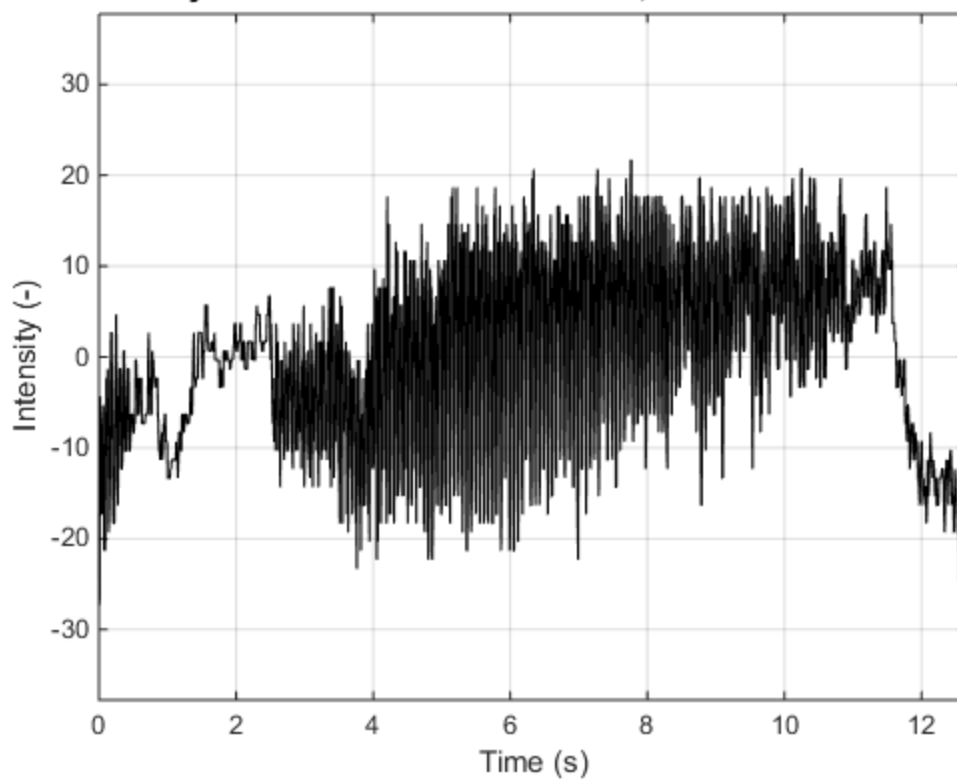
Time history of "S04T2 Oct 31 Canon.MOV", Pixel coordinates: 501 286



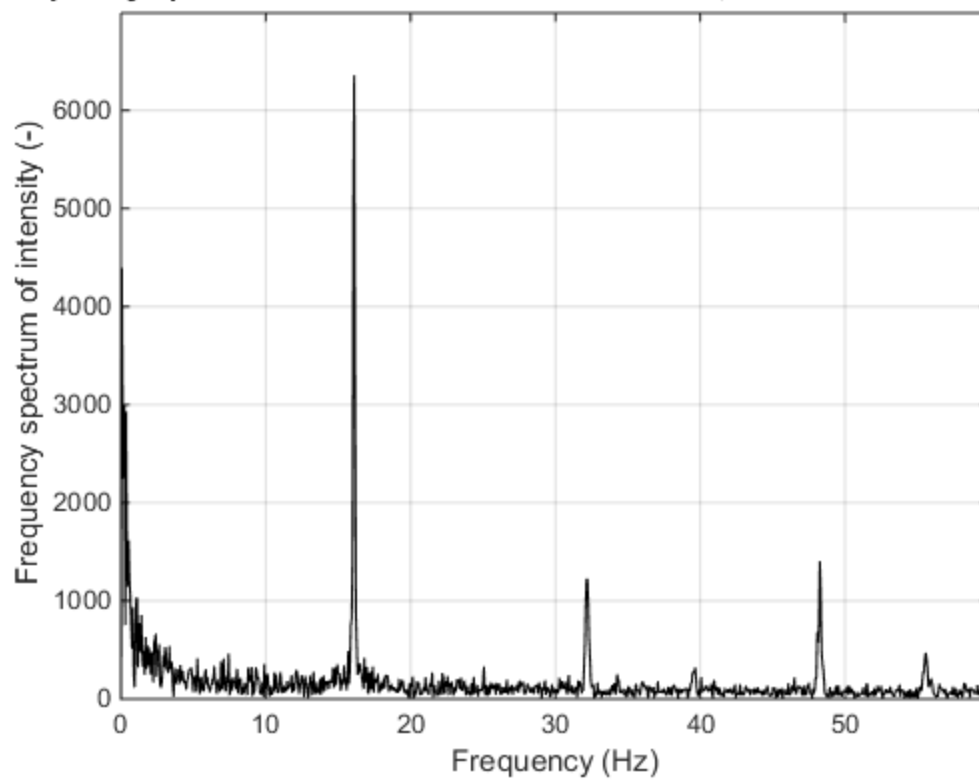
Frequency spectrum of "S04T2 Oct 31 Canon.MOV", Pixel coordinates: 501 21



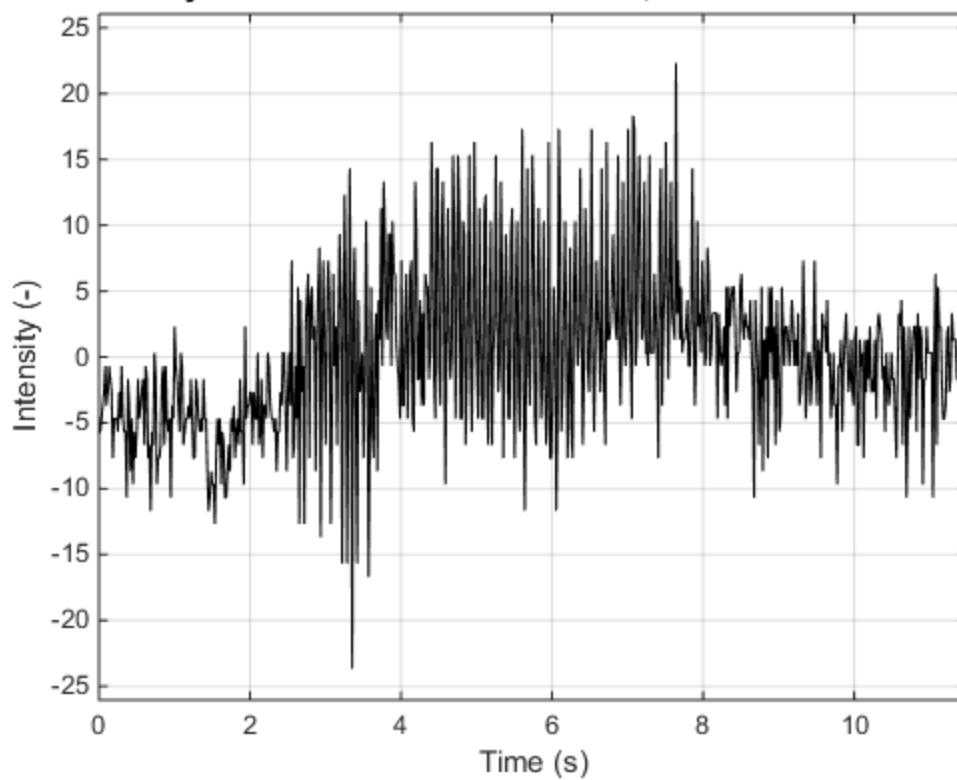
Time history of "S04T2 Oct 31 GoPro.MP4", Pixel coordinates: 482 376



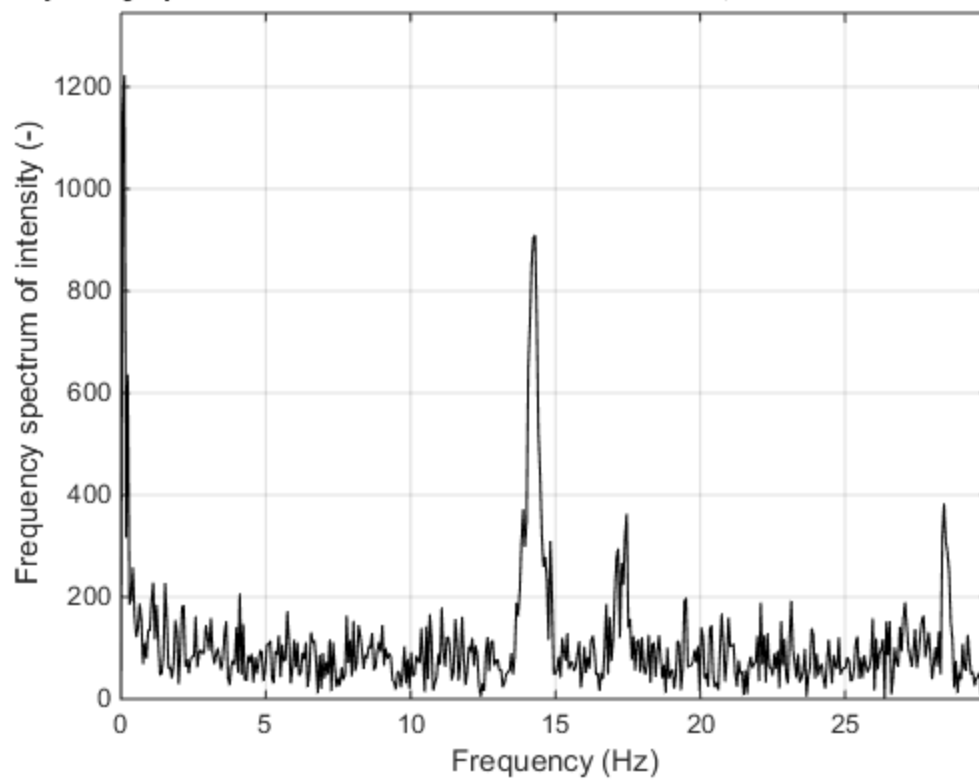
Frequency spectrum of "S04T2 Oct 31 GoPro.MP4", Pixel coordinates: 482 37



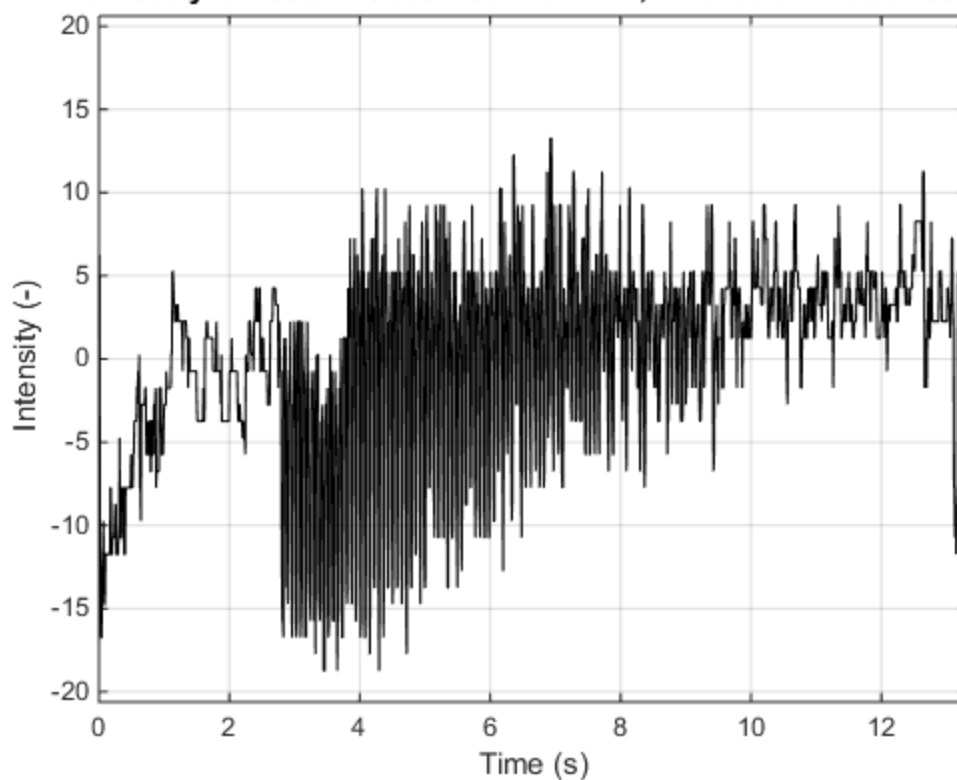
Time history of "S05T1 Oct 31 Canon.MOV", Pixel coordinates: 433 316



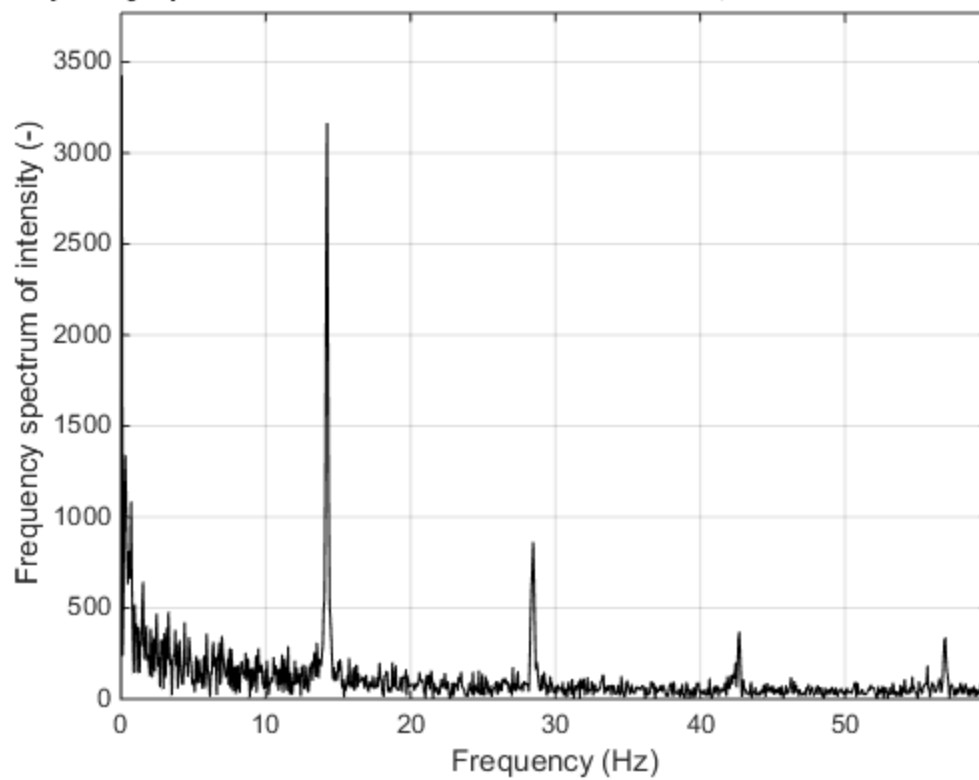
Frequency spectrum of "S05T1 Oct 31 Canon.MOV", Pixel coordinates: 433 316



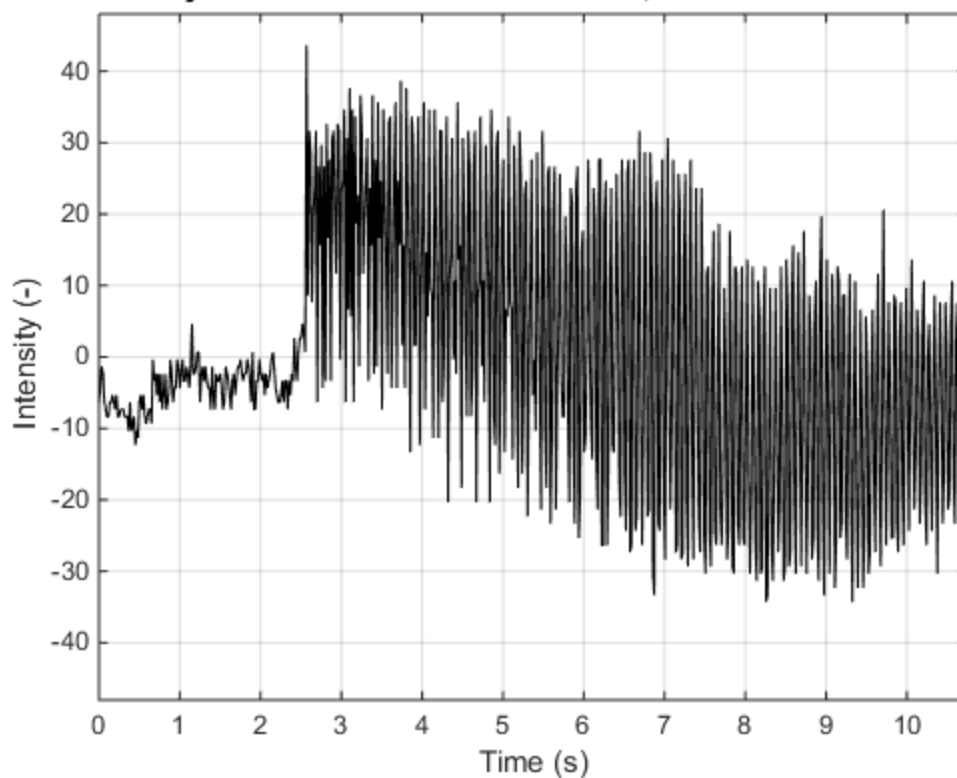
Time history of "S05T1 Oct 31 GoPro.MP4", Pixel coordinates: 558 370



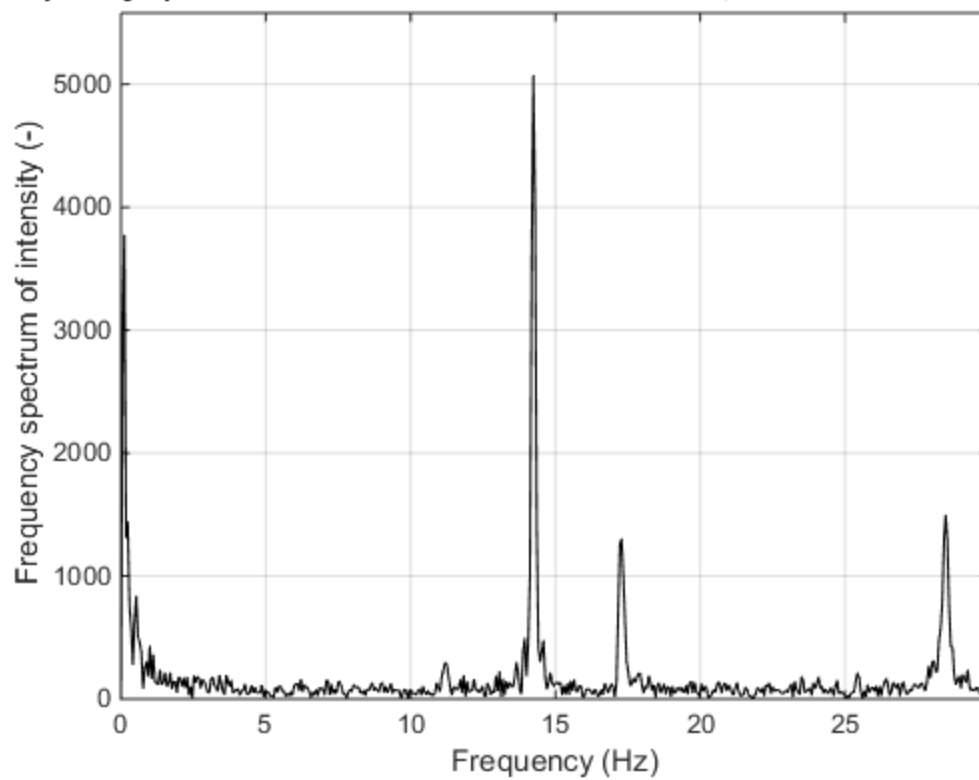
Frequency spectrum of "S05T1 Oct 31 GoPro.MP4", Pixel coordinates: 558 37



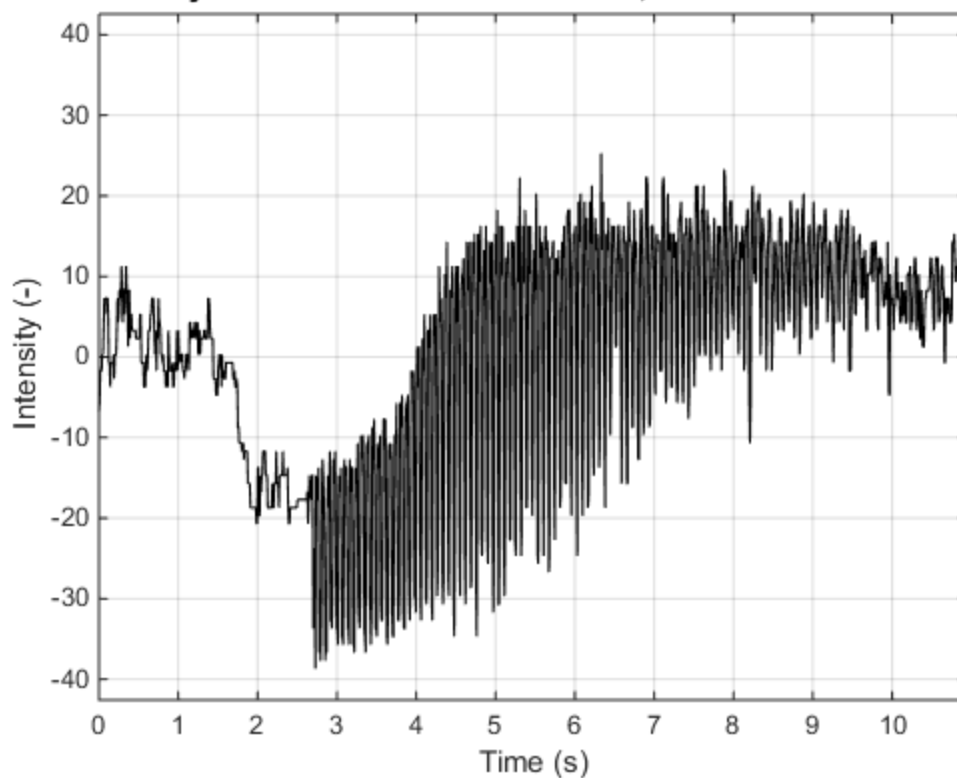
Time history of "S05T2 Oct 31 Canon.MOV", Pixel coordinates: 706 301



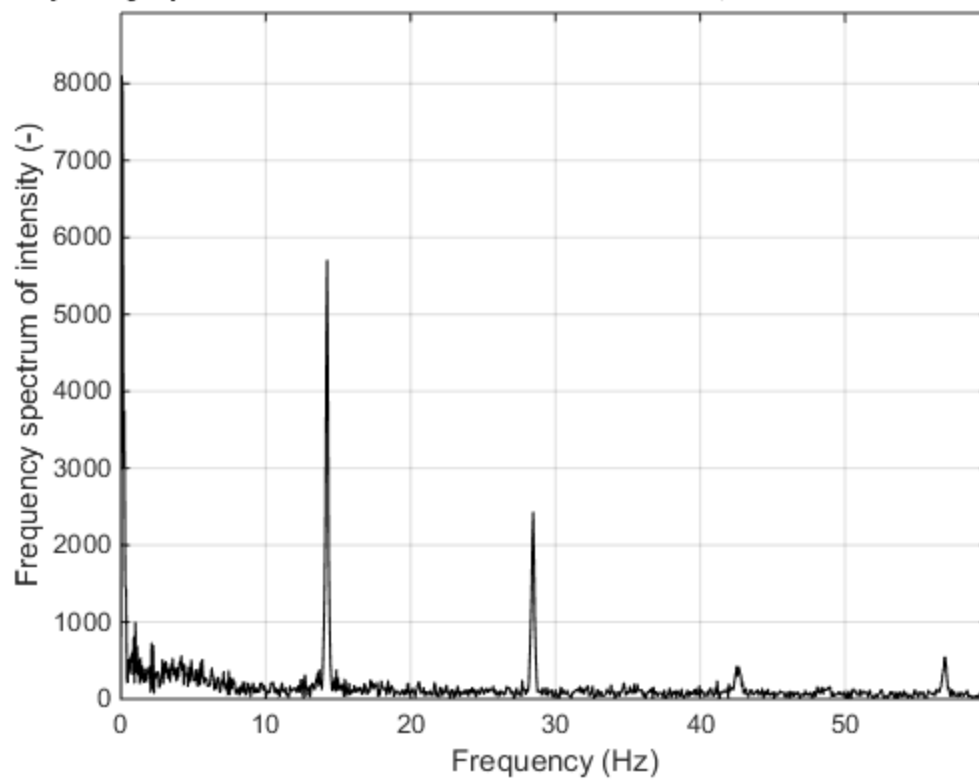
Frequency spectrum of "S05T2 Oct 31 Canon.MOV", Pixel coordinates: 706 301



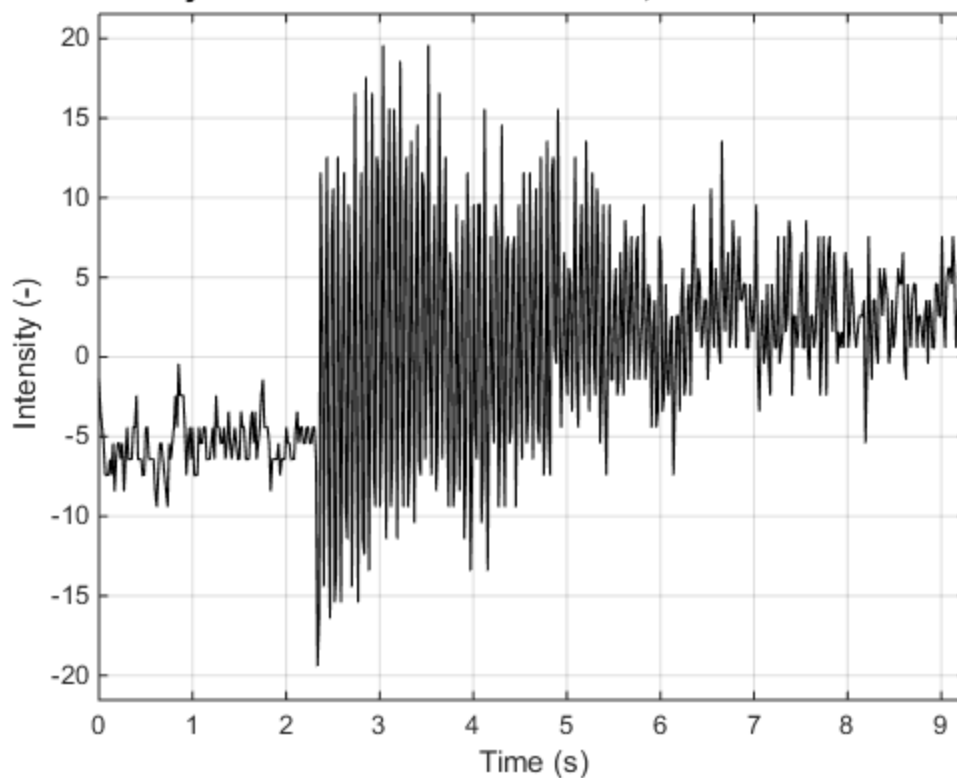
Time history of "S05T2 Oct 31 GoPro.MP4", Pixel coordinates: 356 363



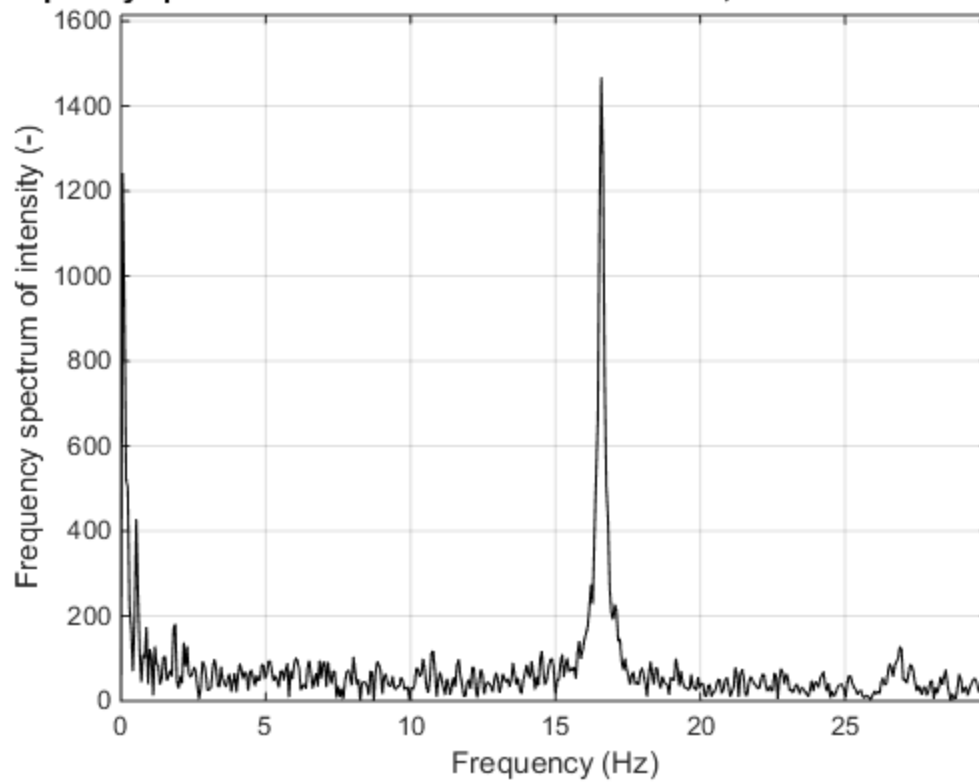
Frequency spectrum of "S05T2 Oct 31 GoPro.MP4", Pixel coordinates: 356 363



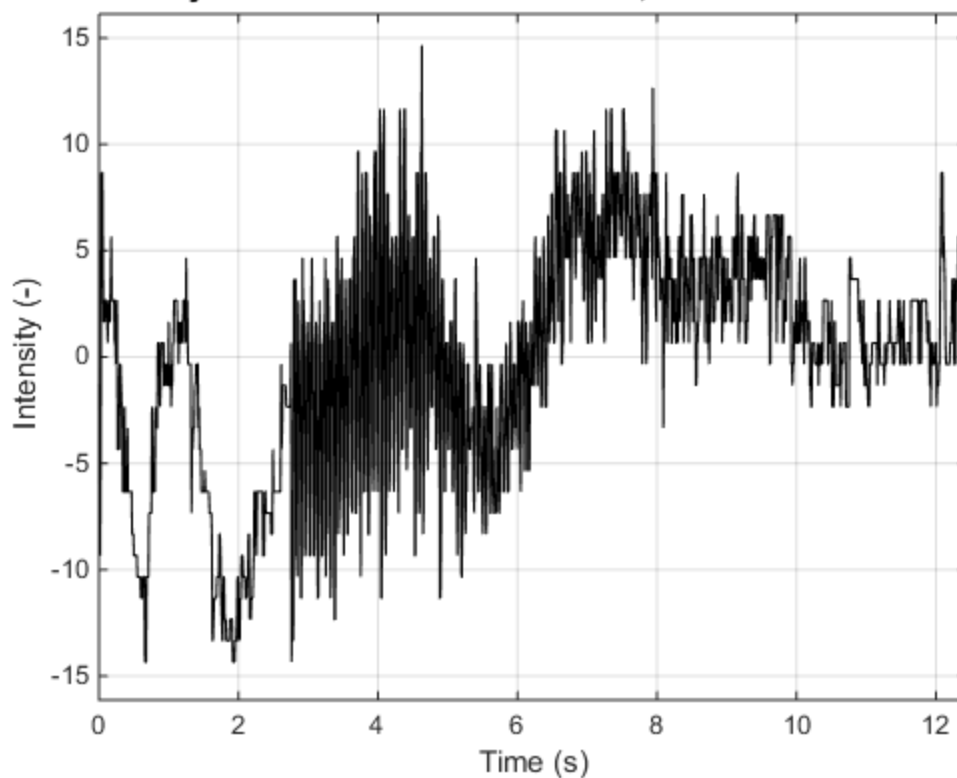
Time history of "S06T1 Oct 31 Canon.MOV", Pixel coordinates: 610 335



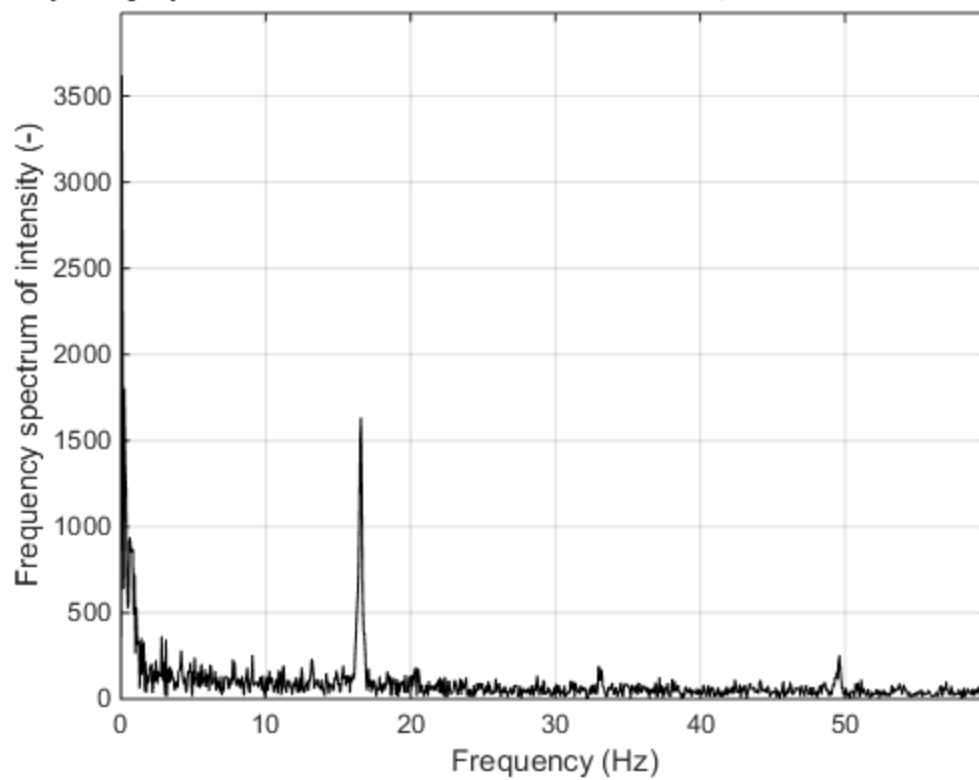
Frequency spectrum of "S06T1 Oct 31 Canon.MOV", Pixel coordinates: 610 335



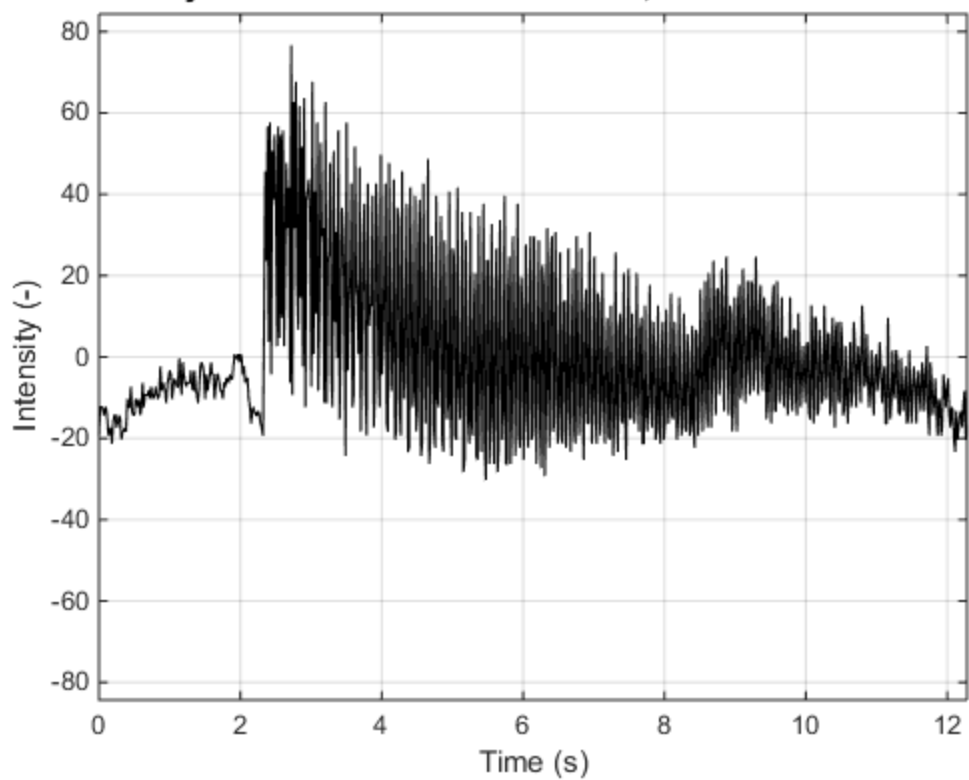
Time history of "S06T1 Oct 31 GoPro.MP4", Pixel coordinates: 558 370



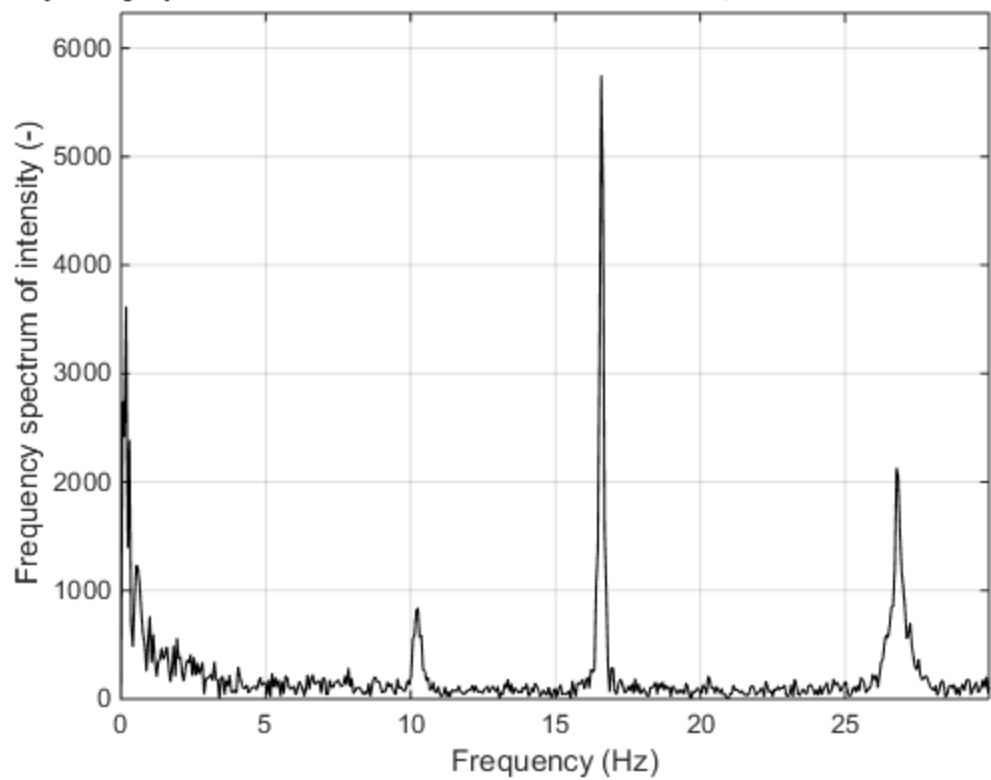
Frequency spectrum of "S06T1 Oct 31 GoPro.MP4", Pixel coordinates: 558 37



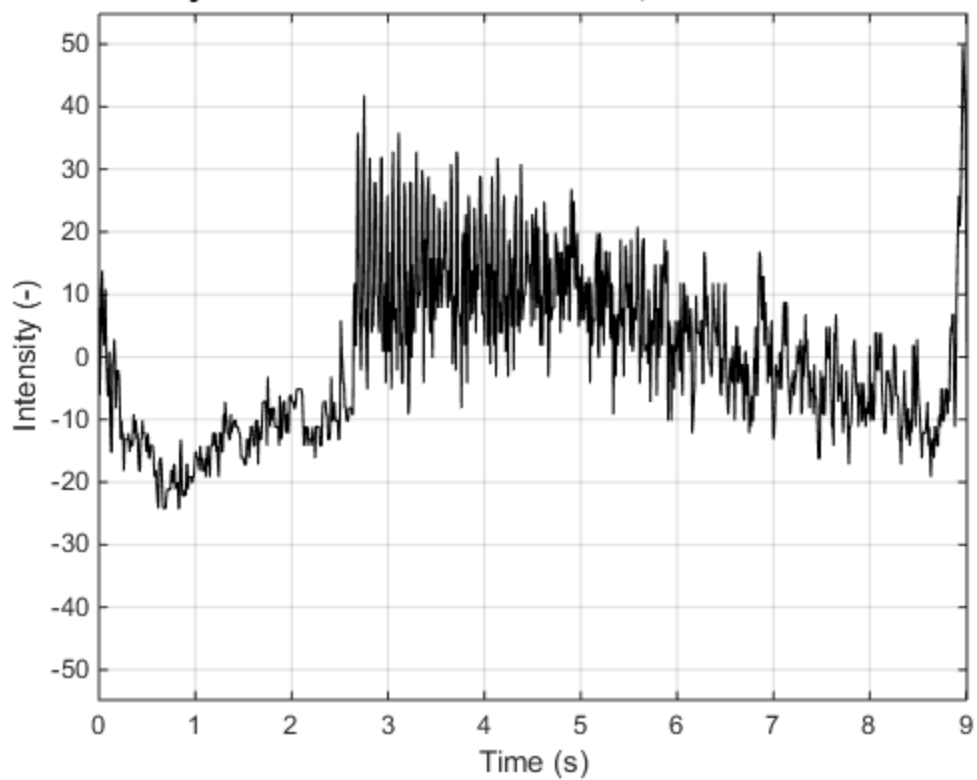
Time history of "S06T2 Oct 31 Canon.MOV", Pixel coordinates: 480 242



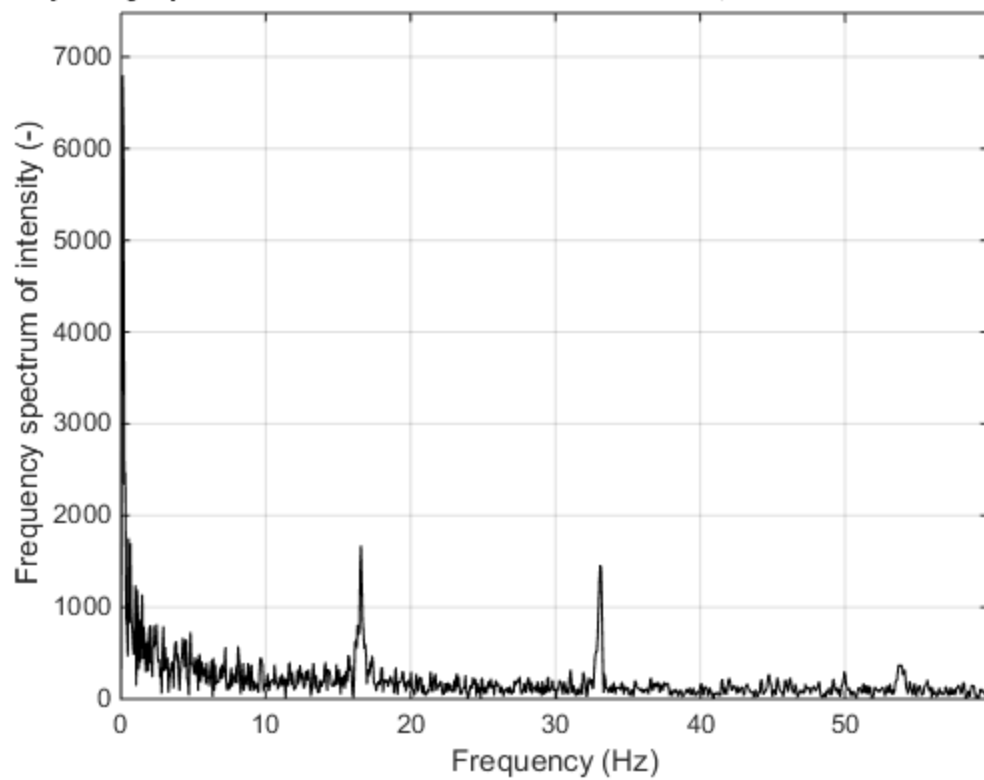
Frequency spectrum of "S06T2 Oct 31 Canon.MOV", Pixel coordinates: 480 242



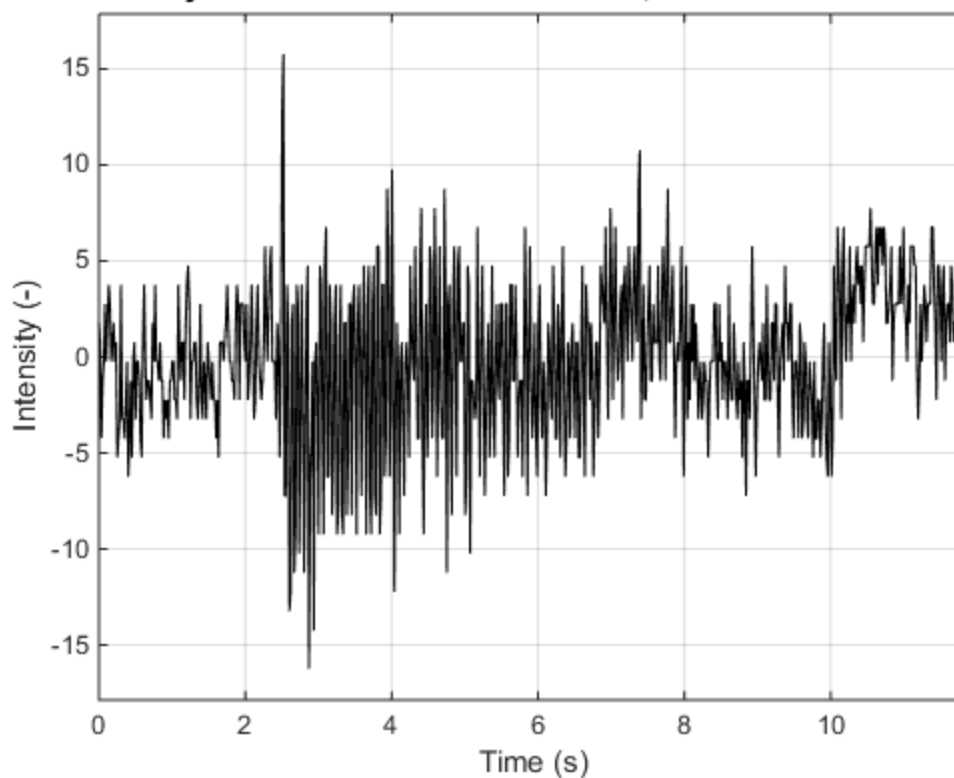
Time history of "S06T2 Oct 31 GoPro.MP4", Pixel coordinates: 250 341



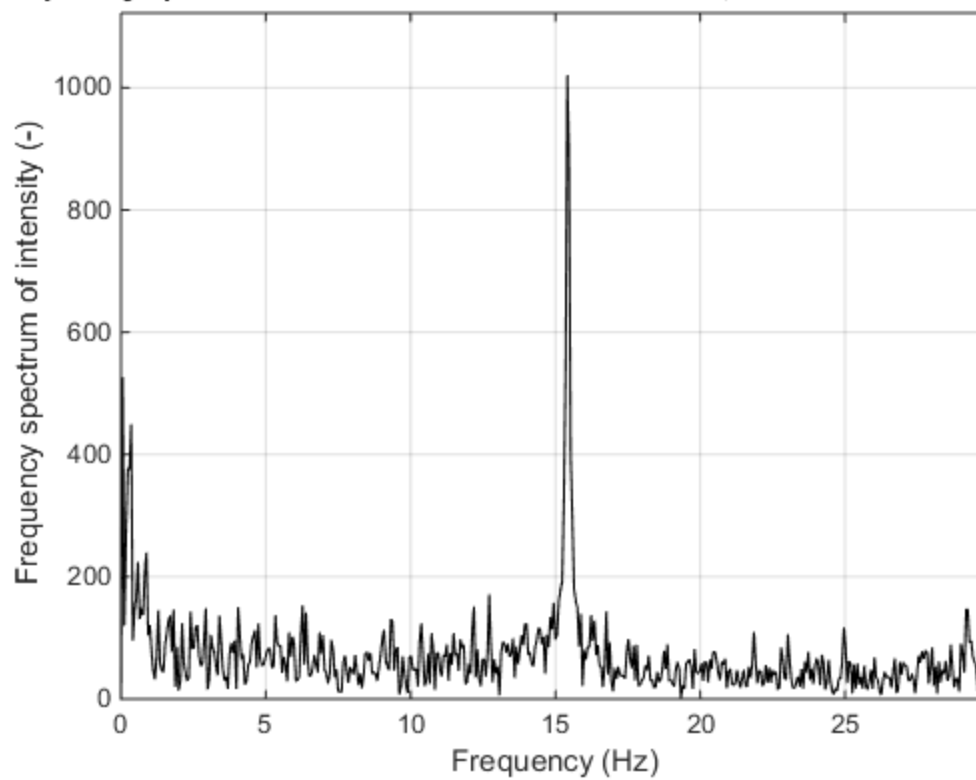
Frequency spectrum of "S06T2 Oct 31 GoPro.MP4", Pixel coordinates: 250 341



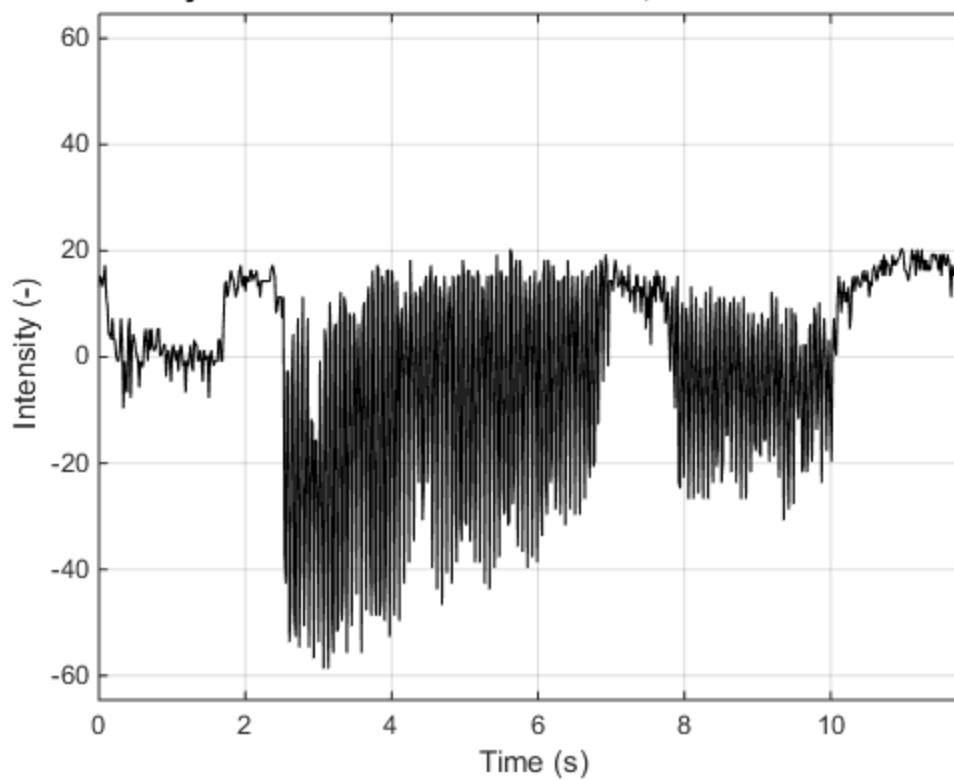
Time history of "S07T1 Oct 31 Canon.MOV", Pixel coordinates: 271 368



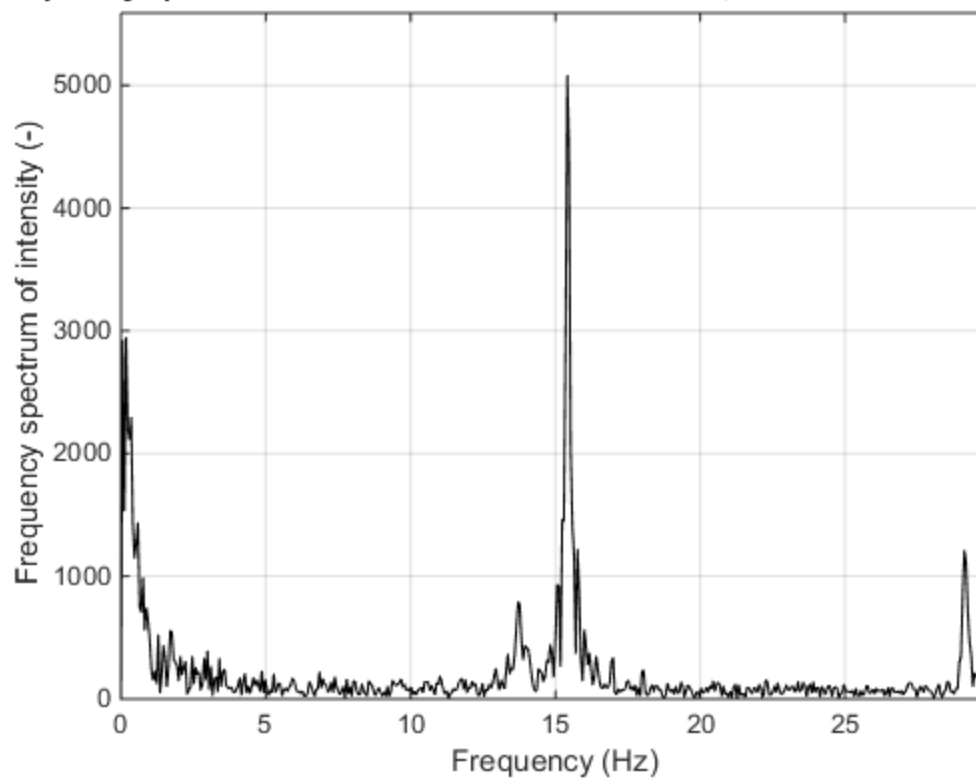
Frequency spectrum of "S07T1 Oct 31 Canon.MOV", Pixel coordinates: 271 368



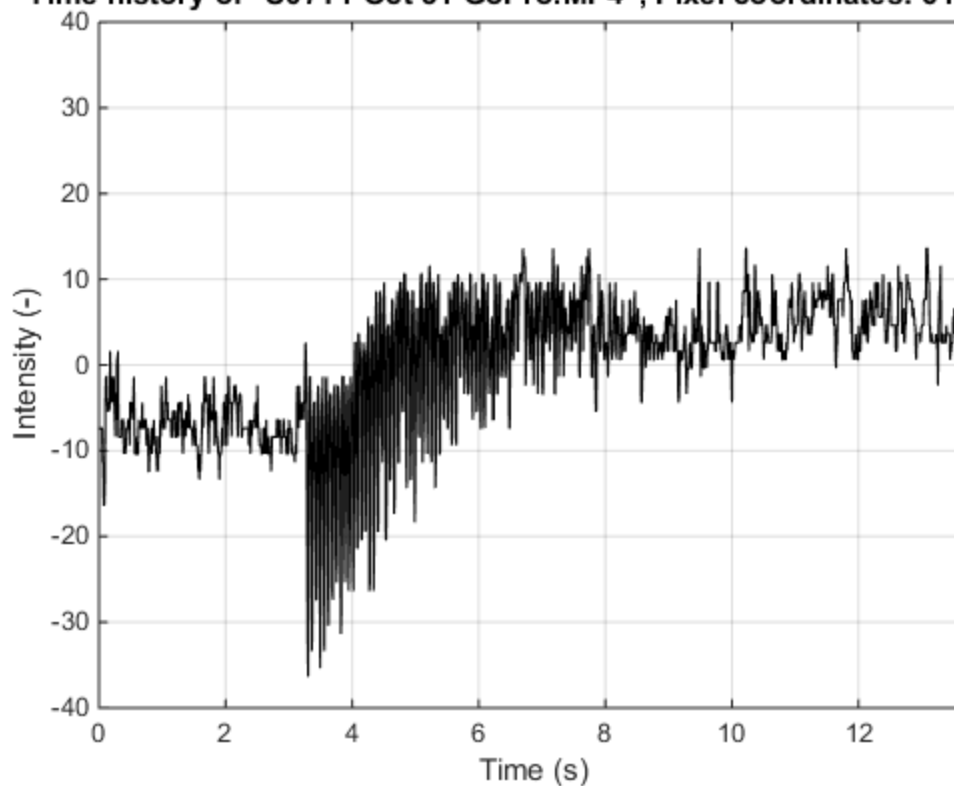
Time history of "S07T1 Oct 31 Canon.MOV", Pixel coordinates: 642 312



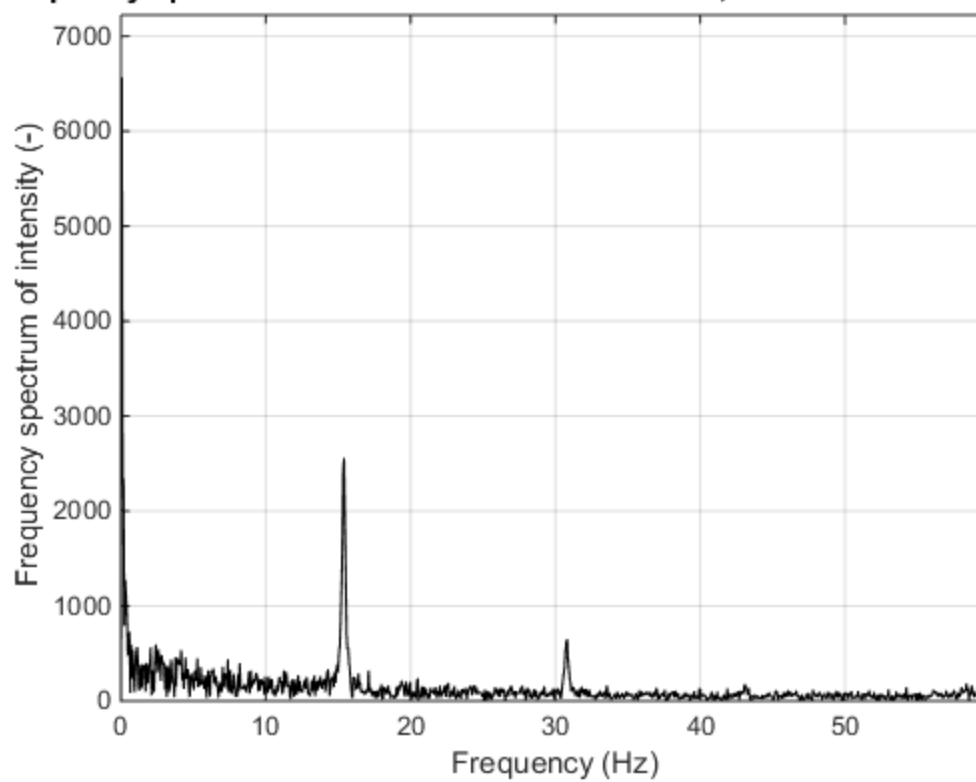
Frequency spectrum of "S07T1 Oct 31 Canon.MOV", Pixel coordinates: 642 312



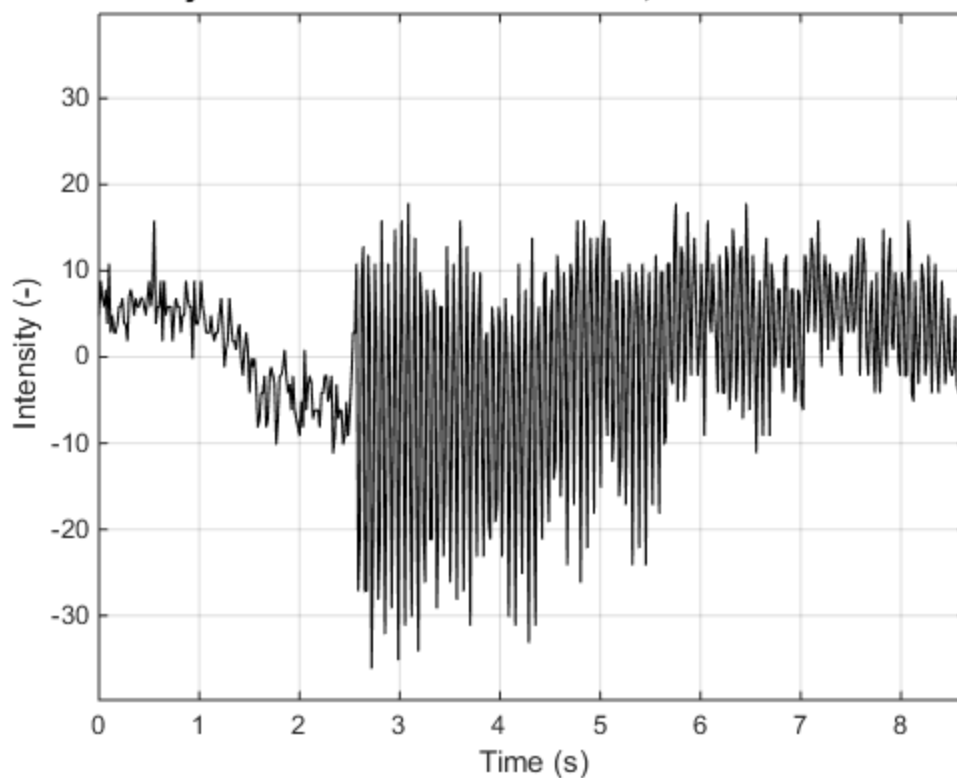
Time history of "S07T1 Oct 31 GoPro.MP4", Pixel coordinates: 616 367



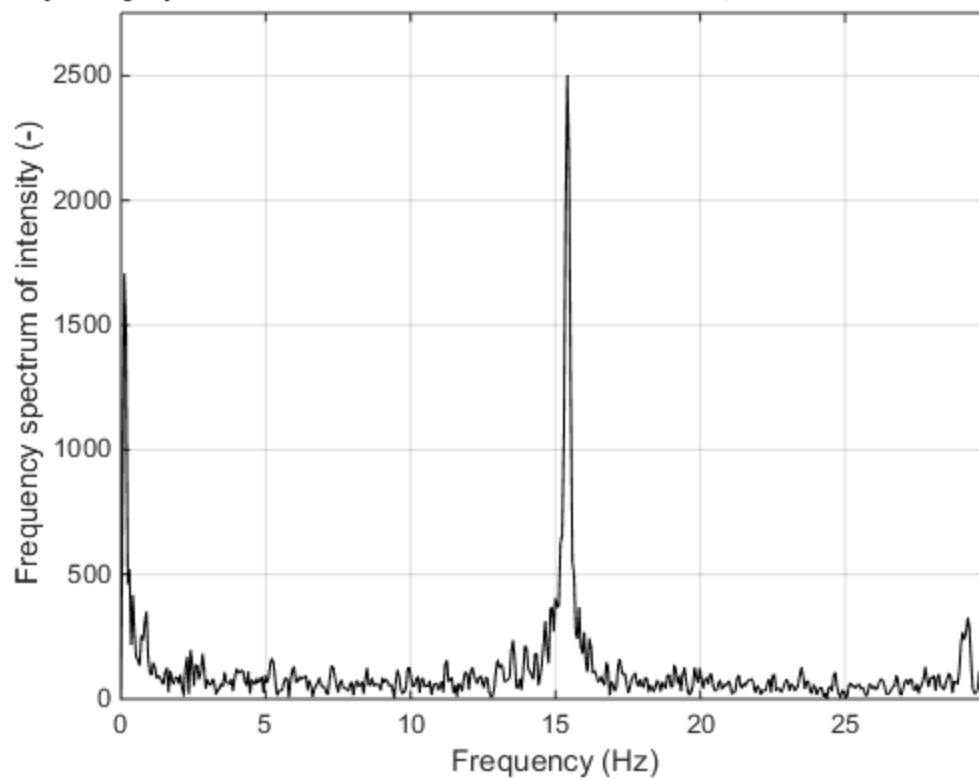
Frequency spectrum of "S07T1 Oct 31 GoPro.MP4", Pixel coordinates: 616 367



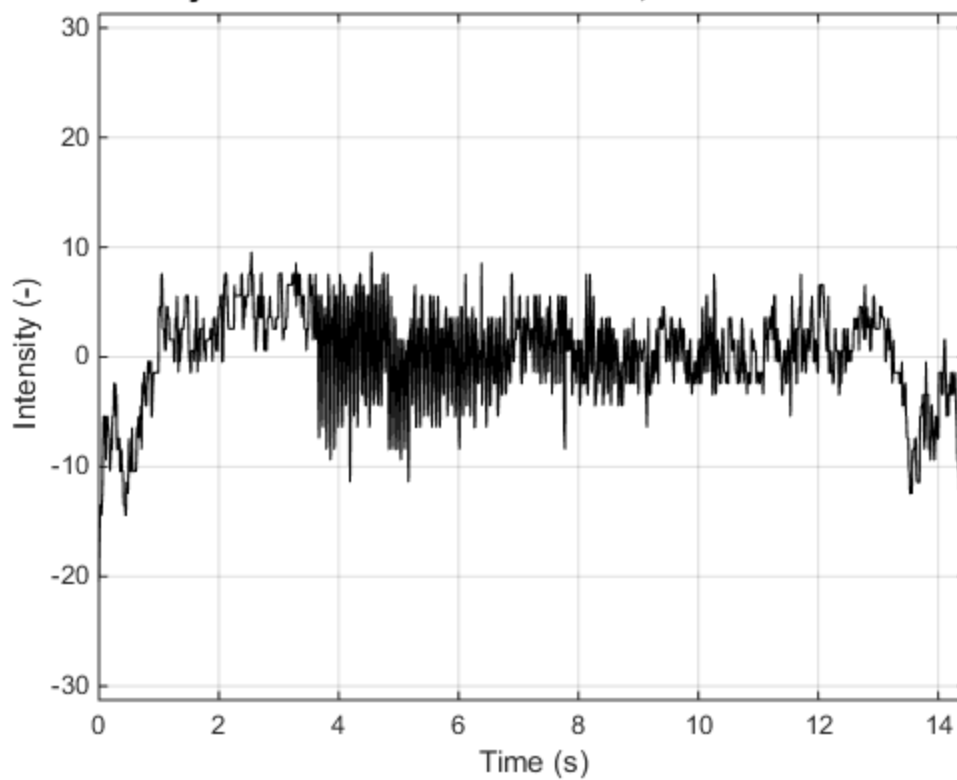
Time history of "S07T2 Oct 31 Canon.MOV", Pixel coordinates: 480 242



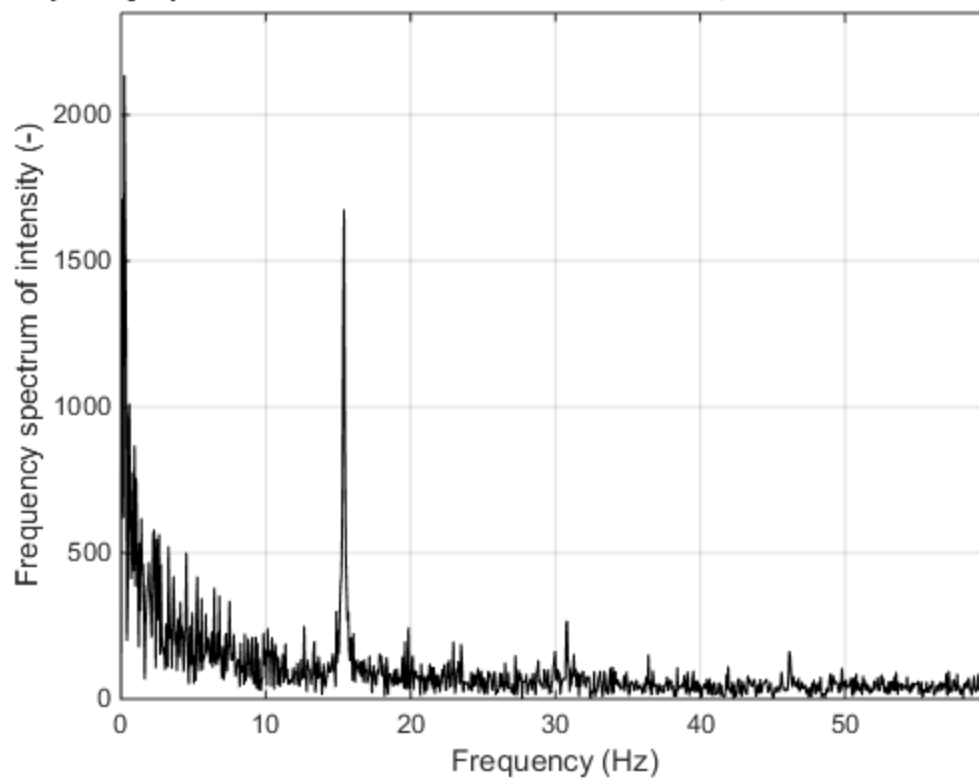
Frequency spectrum of "S07T2 Oct 31 Canon.MOV", Pixel coordinates: 480 242



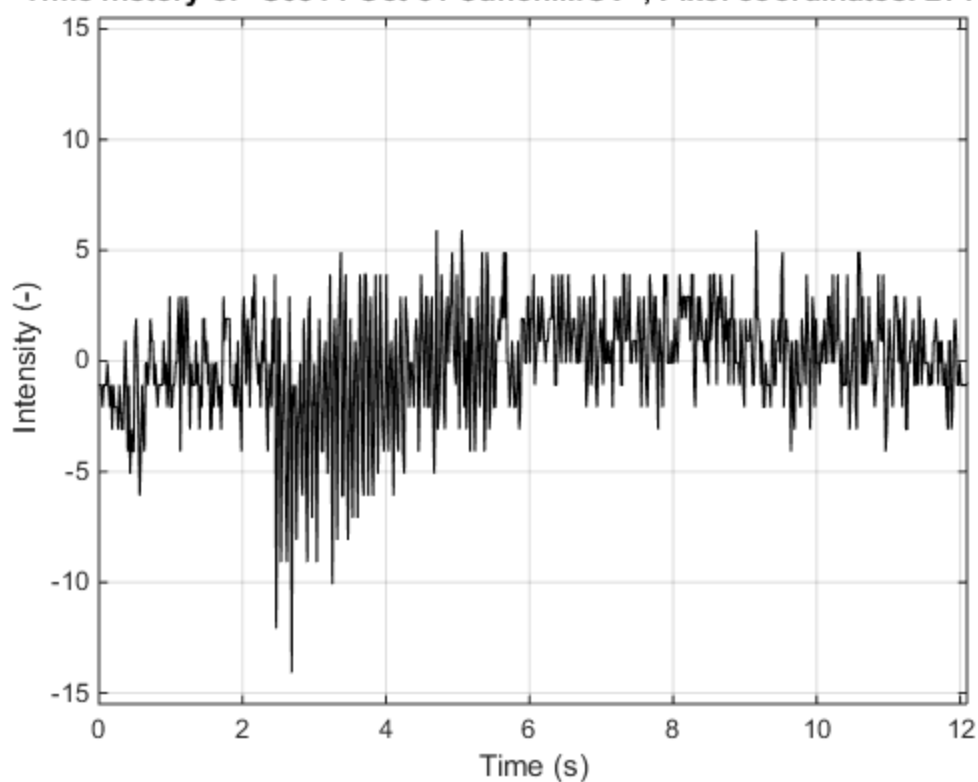
Time history of "S07T2 Oct 31 GoPro.MP4", Pixel coordinates: 250 341



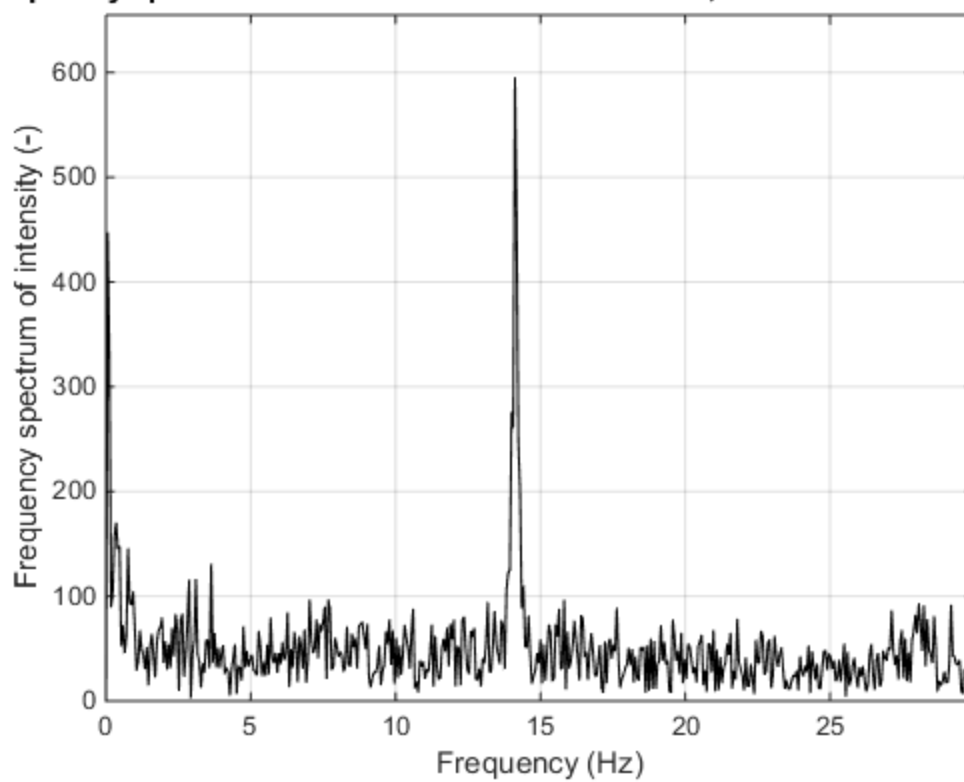
Frequency spectrum of "S07T2 Oct 31 GoPro.MP4", Pixel coordinates: 250 341



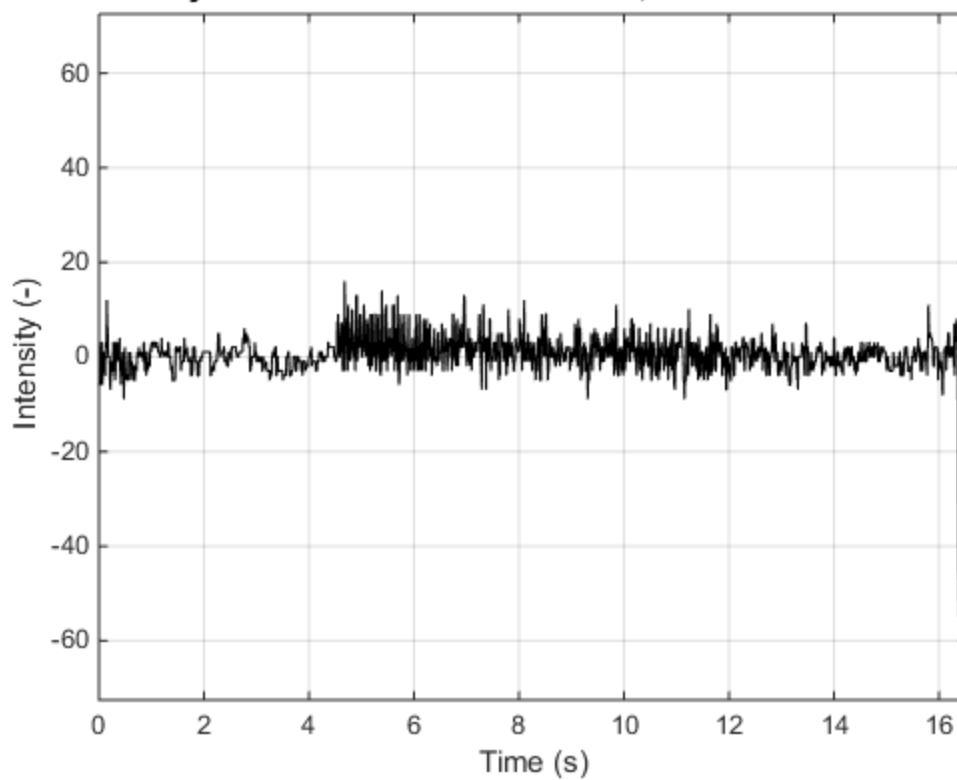
Time history of "S08T1 Oct 31 Canon.MOV", Pixel coordinates: 271 368



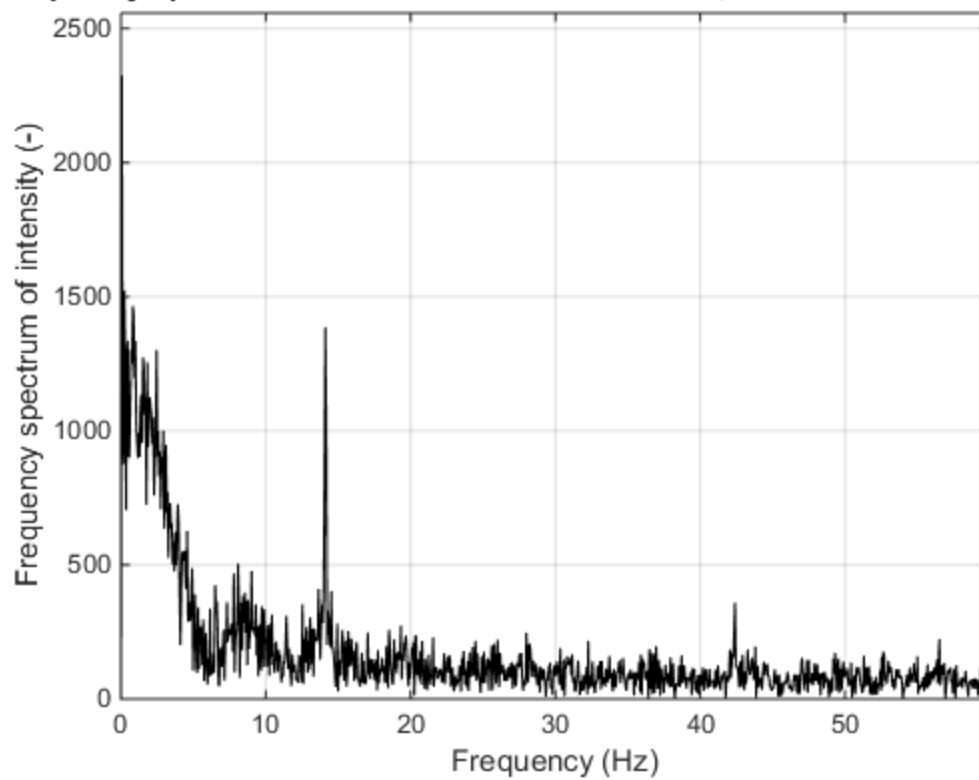
Frequency spectrum of "S08T1 Oct 31 Canon.MOV", Pixel coordinates: 271 368



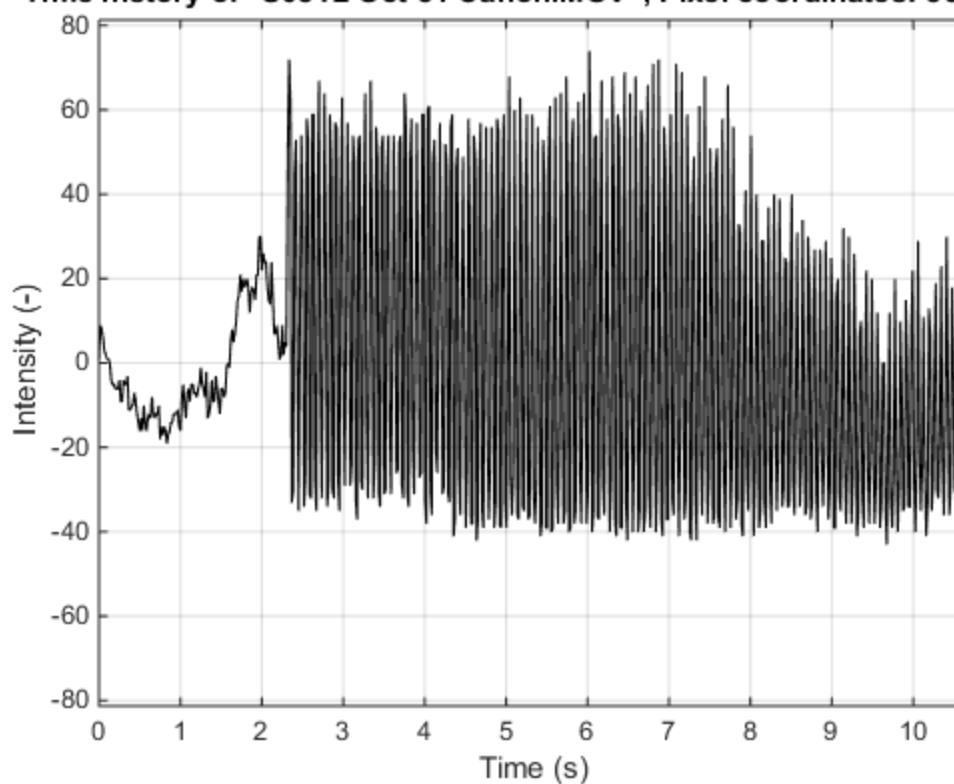
Time history of "S08T1 Oct 31 GoPro.MP4", Pixel coordinates: 372 357



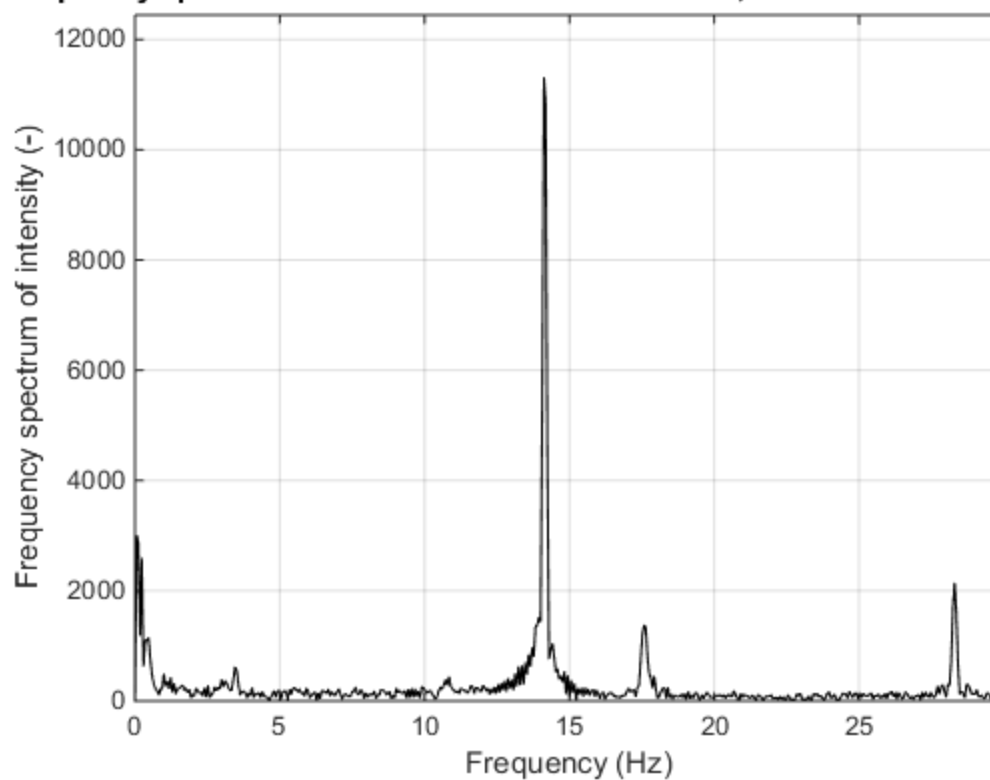
Frequency spectrum of "S08T1 Oct 31 GoPro.MP4", Pixel coordinates: 372 357



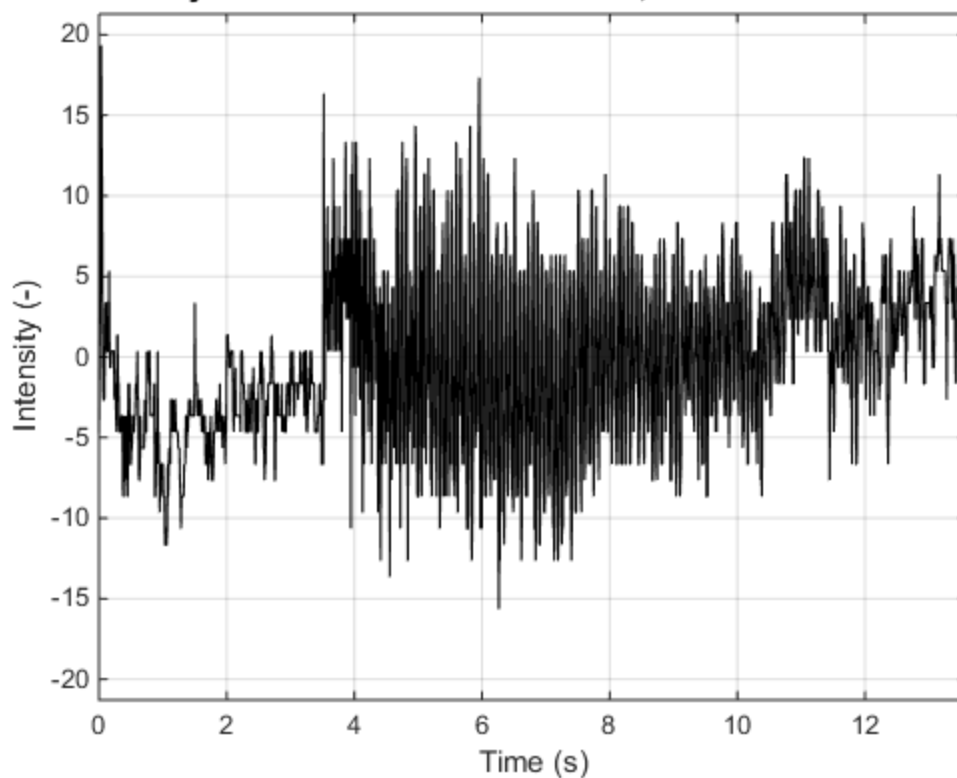
Time history of "S08T2 Oct 31 Canon.MOV", Pixel coordinates: 561 338



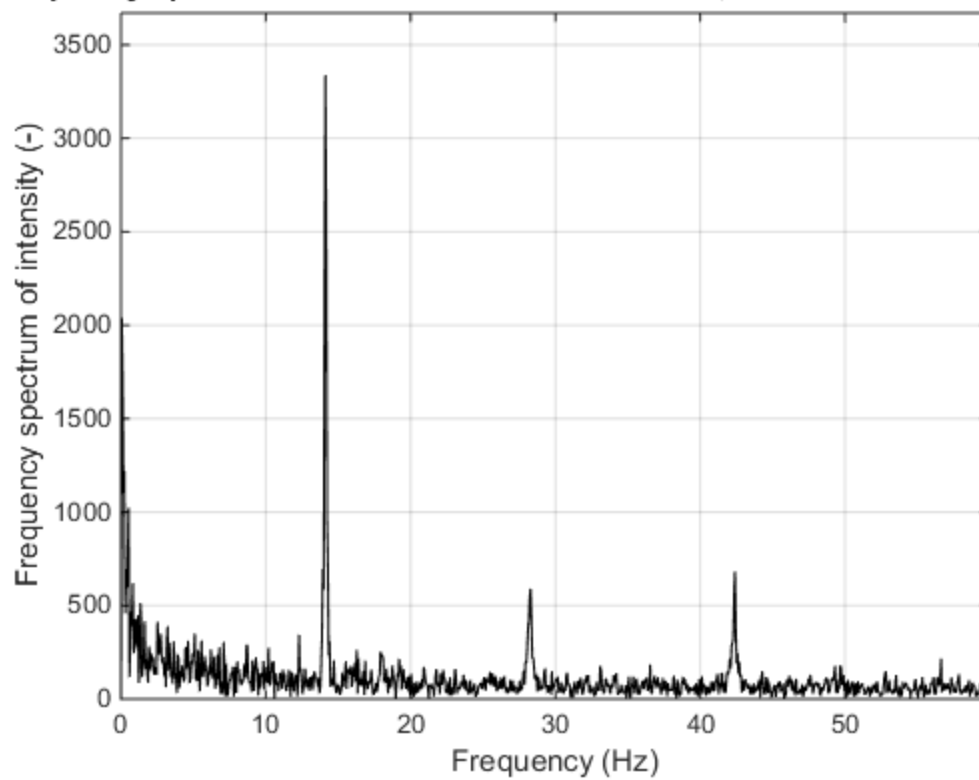
Frequency spectrum of "S08T2 Oct 31 Canon.MOV", Pixel coordinates: 561 338



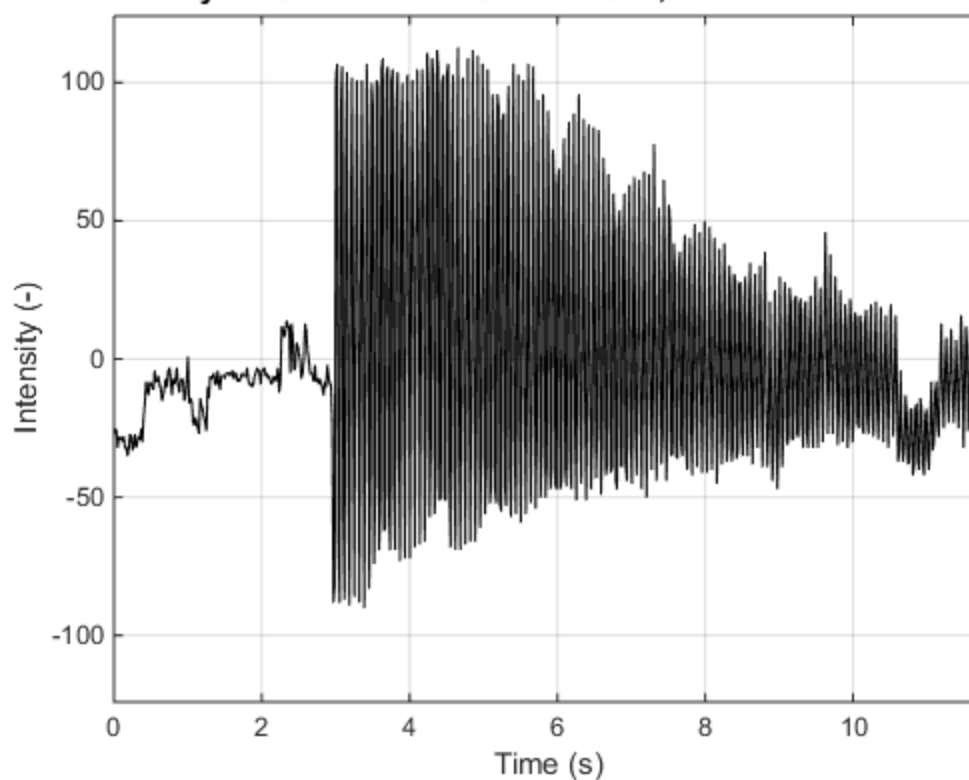
Time history of "S08T2 Oct 31 GoPro.MP4", Pixel coordinates: 250 341



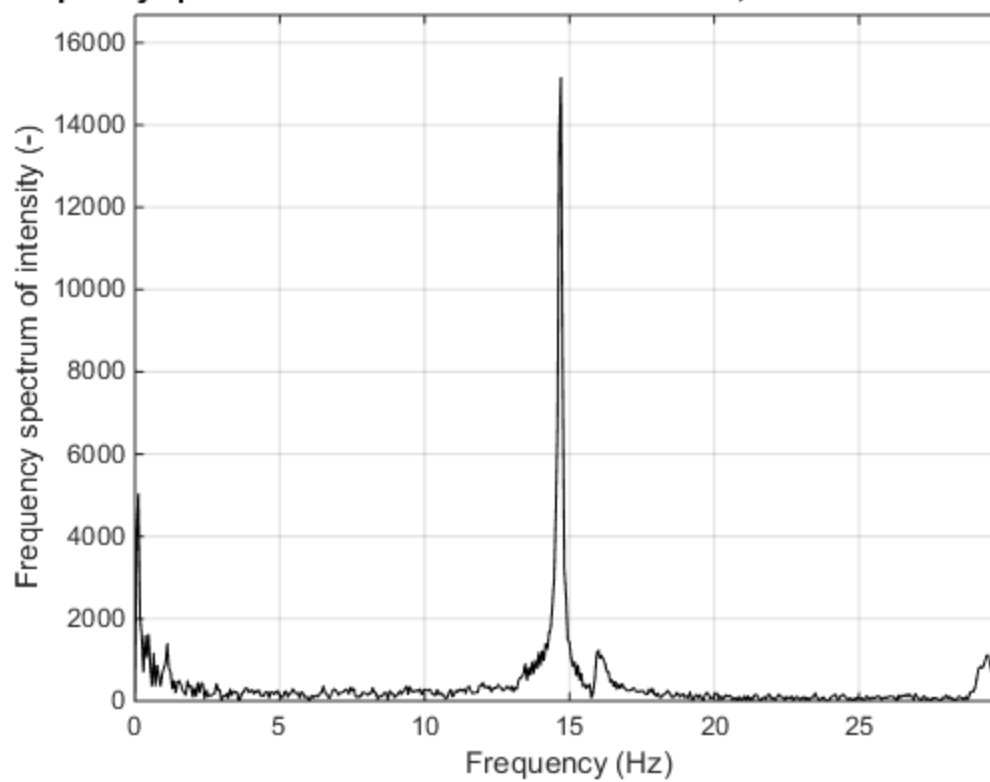
Frequency spectrum of "S08T2 Oct 31 GoPro.MP4", Pixel coordinates: 250 34



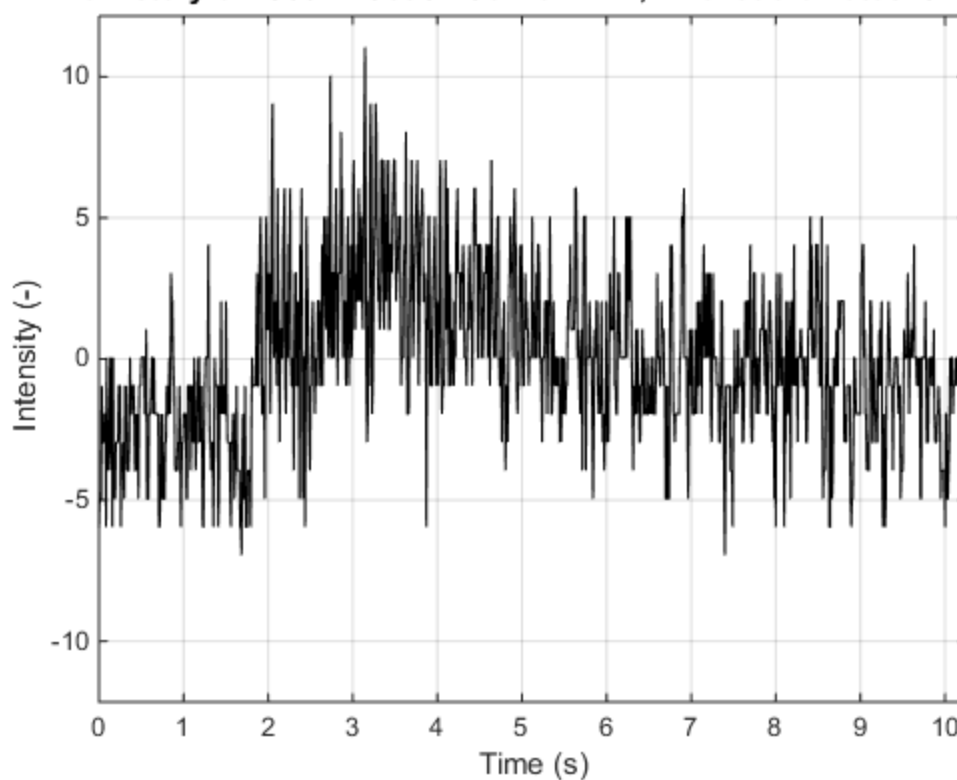
Time history of "S09T1 Oct 31 Canon.MOV", Pixel coordinates: 271 367



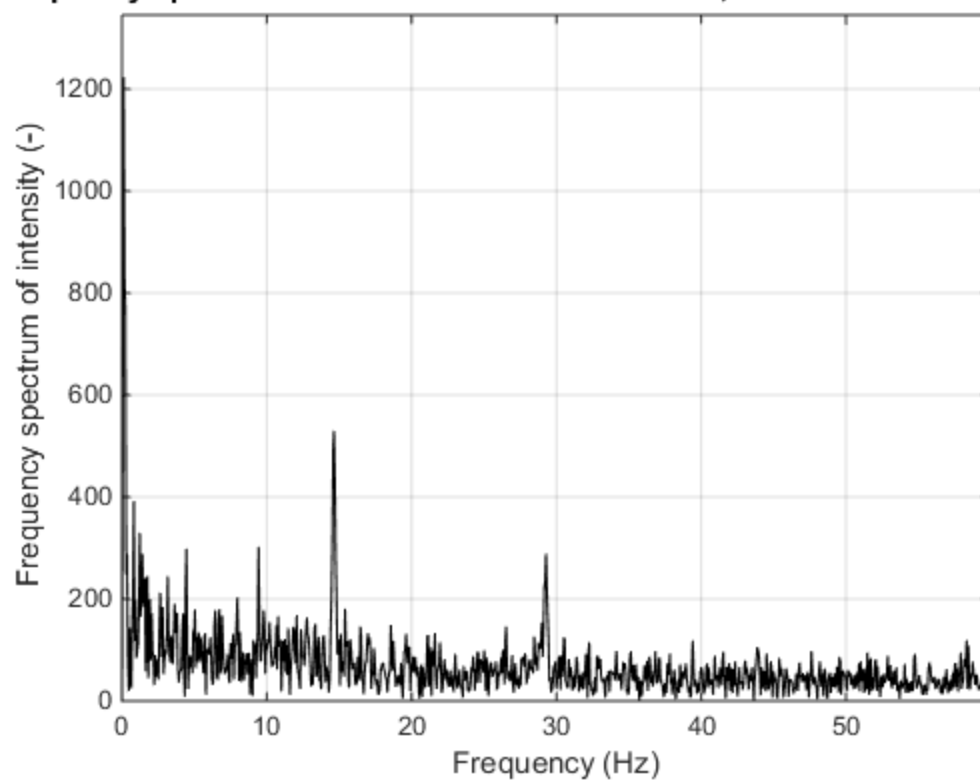
Frequency spectrum of "S09T1 Oct 31 Canon.MOV", Pixel coordinates: 271 367



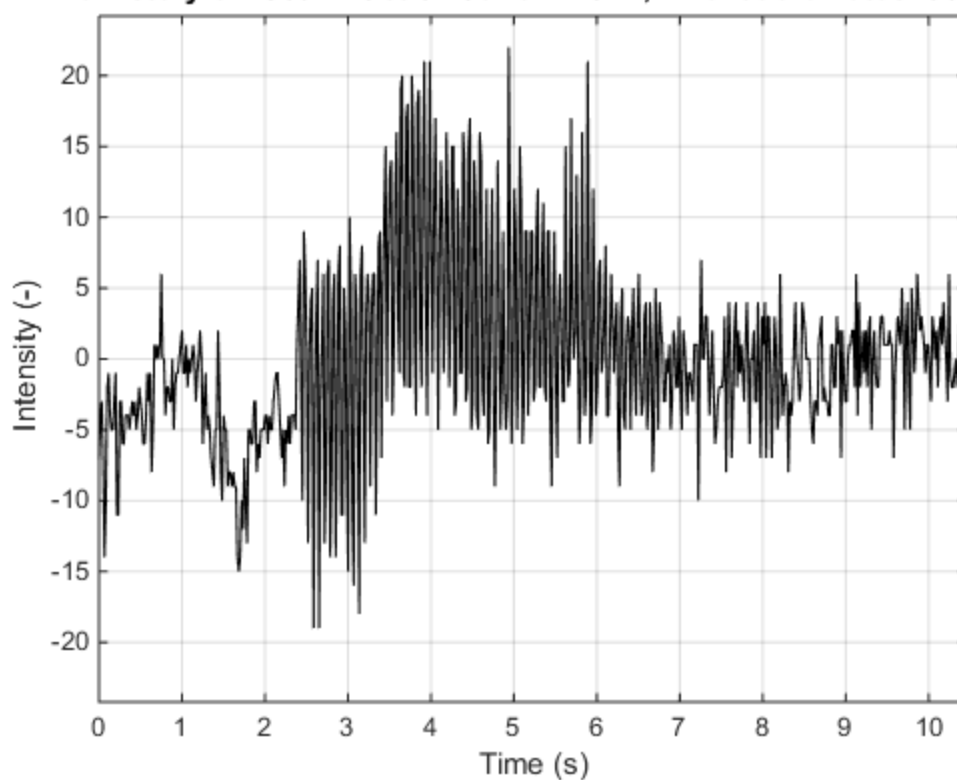
Time history of "S09T1 Oct 31 GoPro.MP4", Pixel coordinates: 372 357



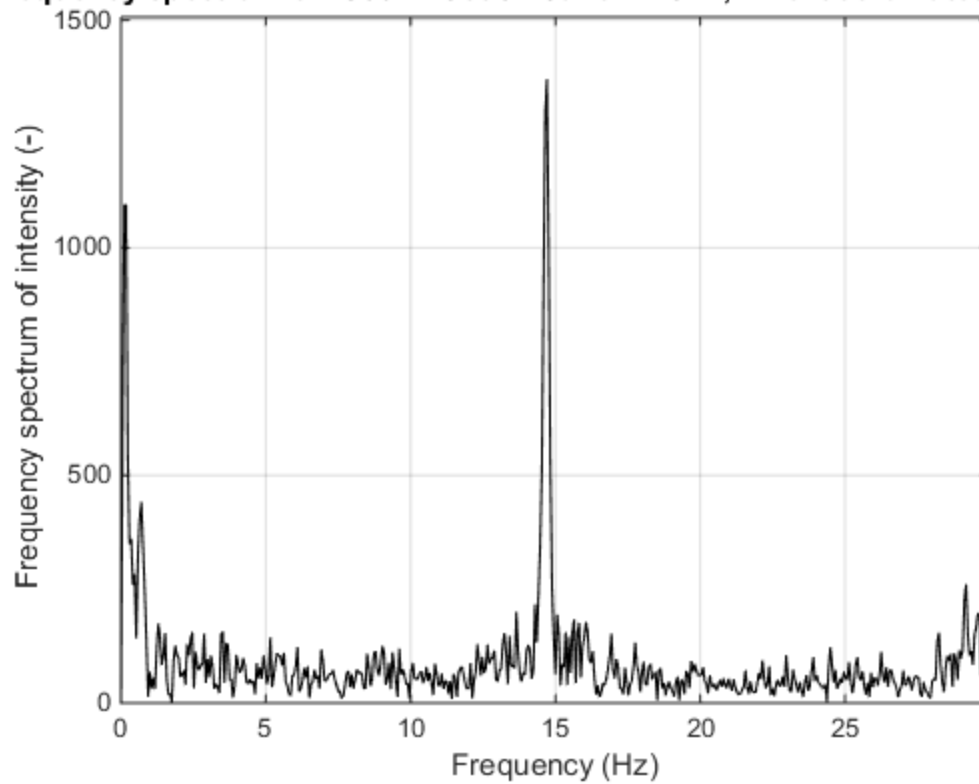
Frequency spectrum of "S09T1 Oct 31 GoPro.MP4", Pixel coordinates: 372 357



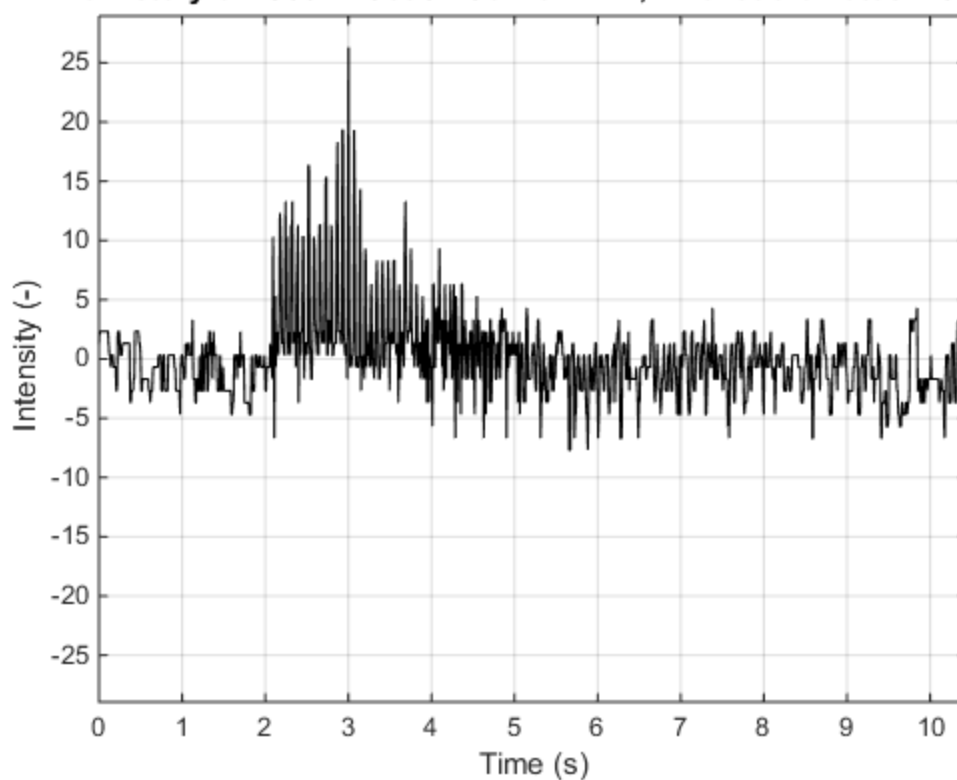
Time history of "S09T2 Oct 31 Canon.MOV", Pixel coordinates: 561 338



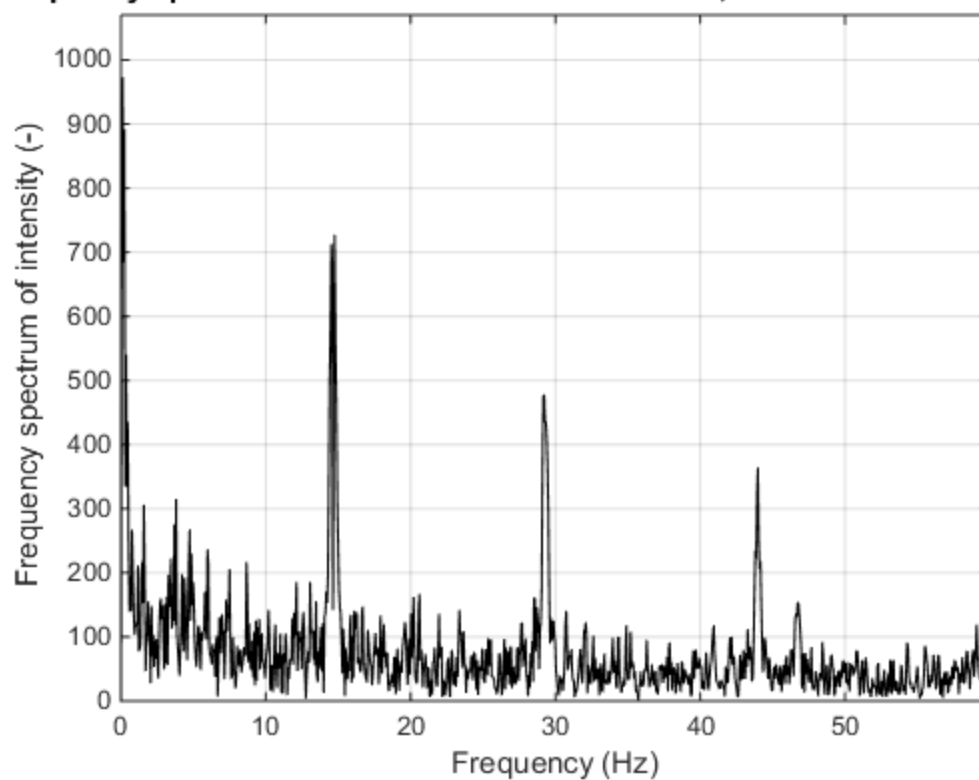
Frequency spectrum of "S09T2 Oct 31 Canon.MOV", Pixel coordinates: 561 338



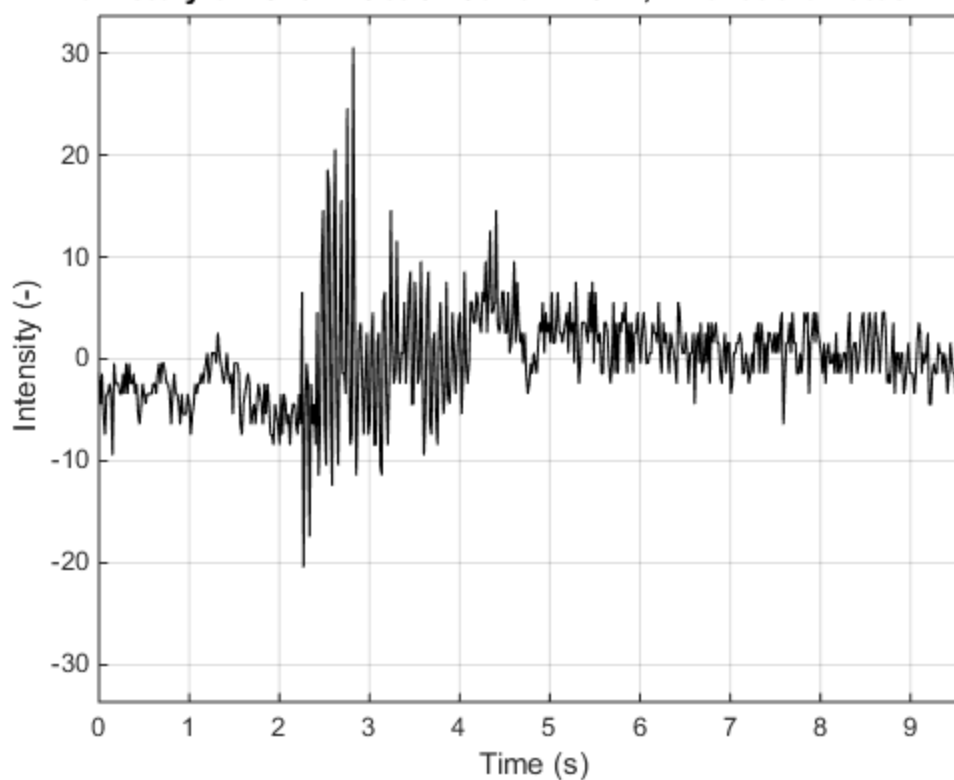
Time history of "S09T2 Oct 31 GoPro.MP4", Pixel coordinates: 250 341



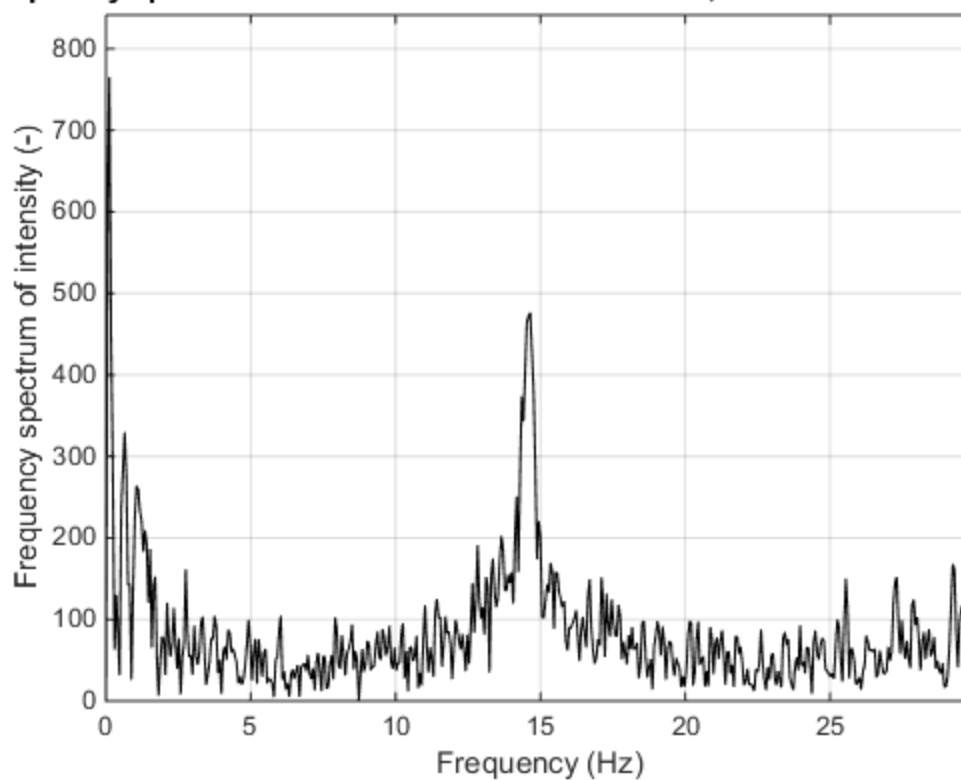
Frequency spectrum of "S09T2 Oct 31 GoPro.MP4", Pixel coordinates: 250 34



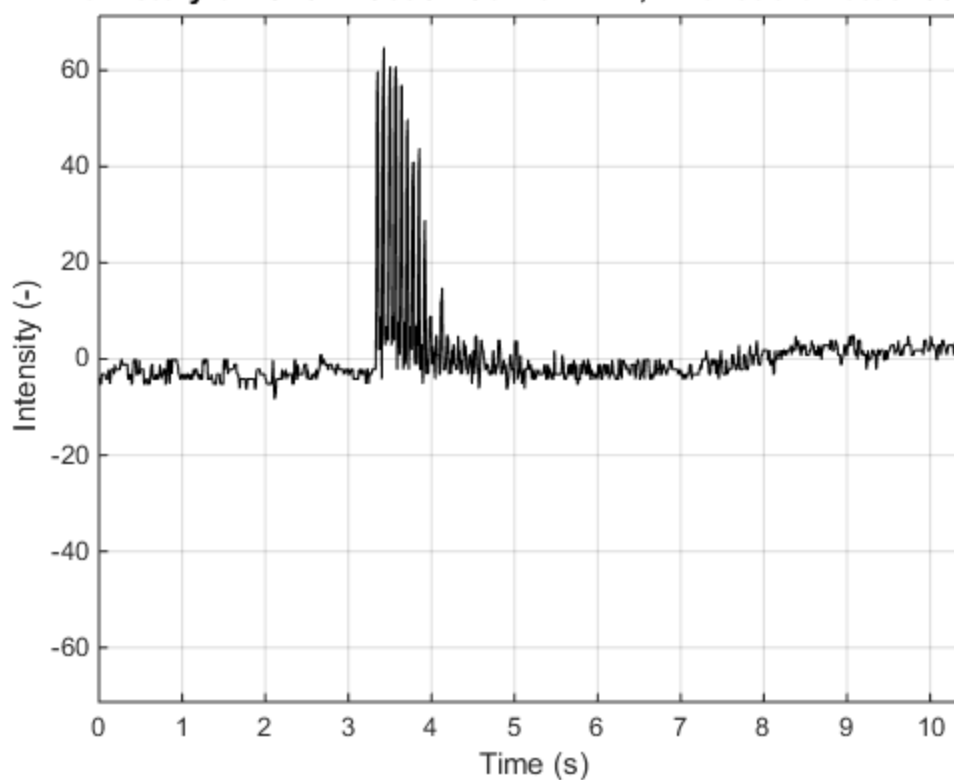
Time history of "S10T1 Oct 31 Canon.MOV", Pixel coordinates: 271 367



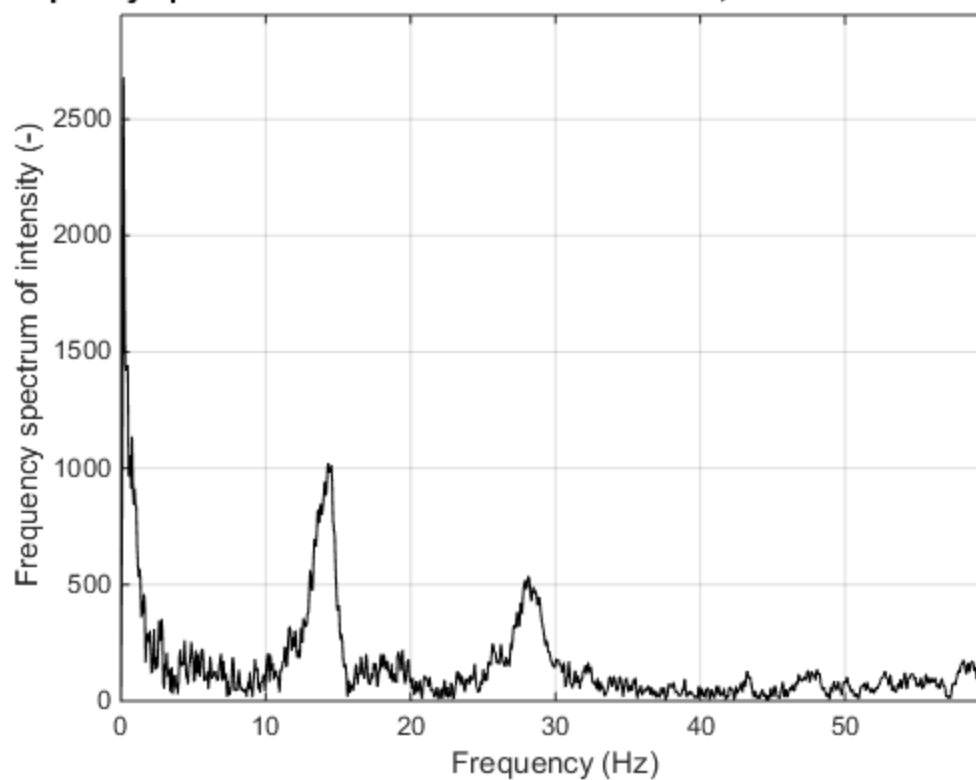
Frequency spectrum of "S10T1 Oct 31 Canon.MOV", Pixel coordinates: 271 367



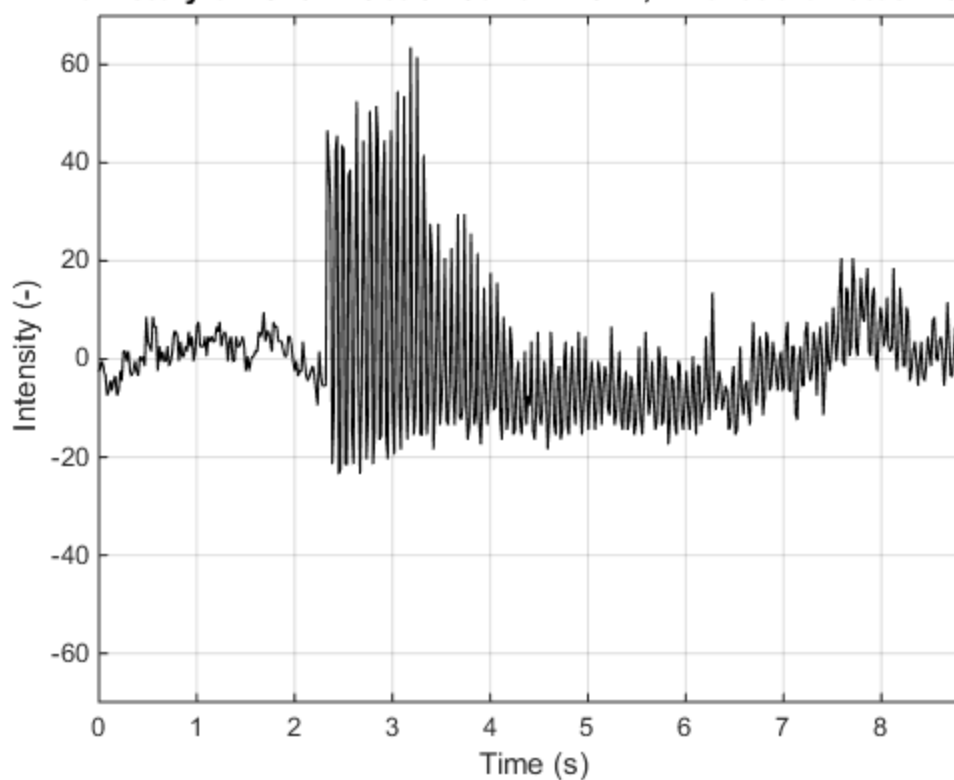
Time history of "S10T1 Oct 31 GoPro.MP4", Pixel coordinates: 607 351



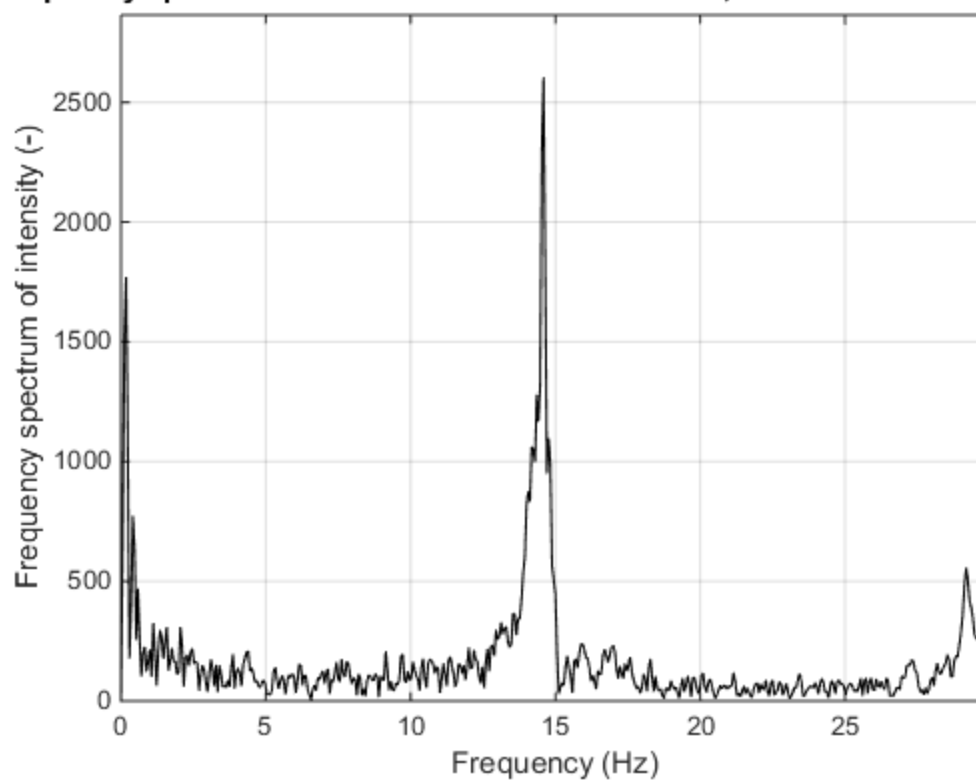
Frequency spectrum of "S10T1 Oct 31 GoPro.MP4", Pixel coordinates: 607 351



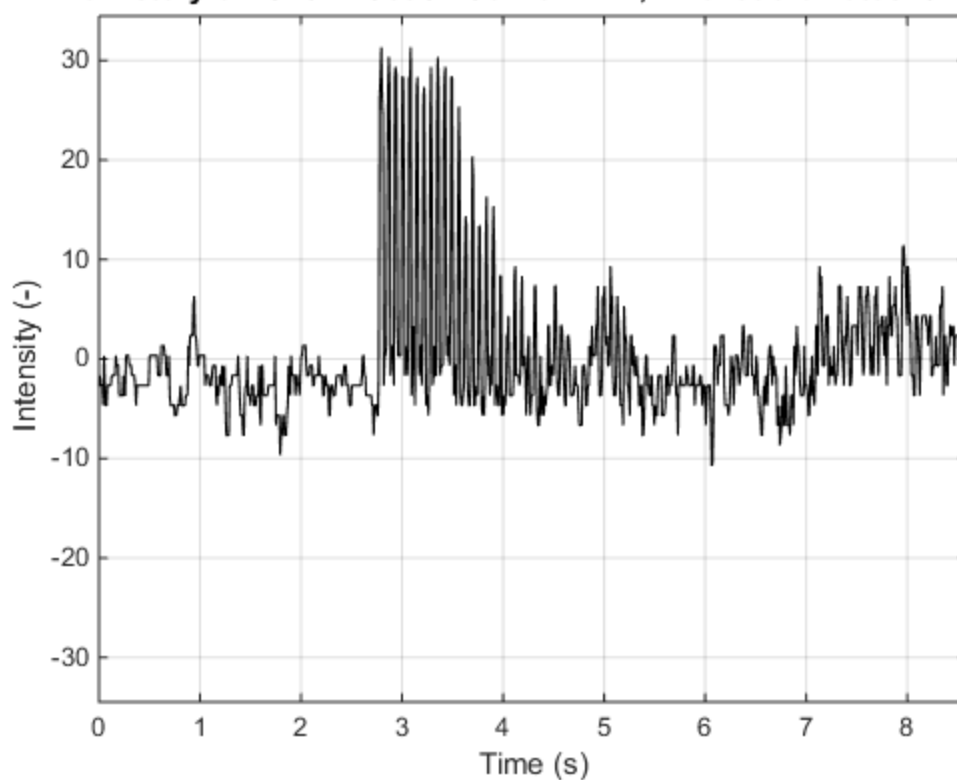
Time history of "S10T2 Oct 31 Canon.MOV", Pixel coordinates: 708 357



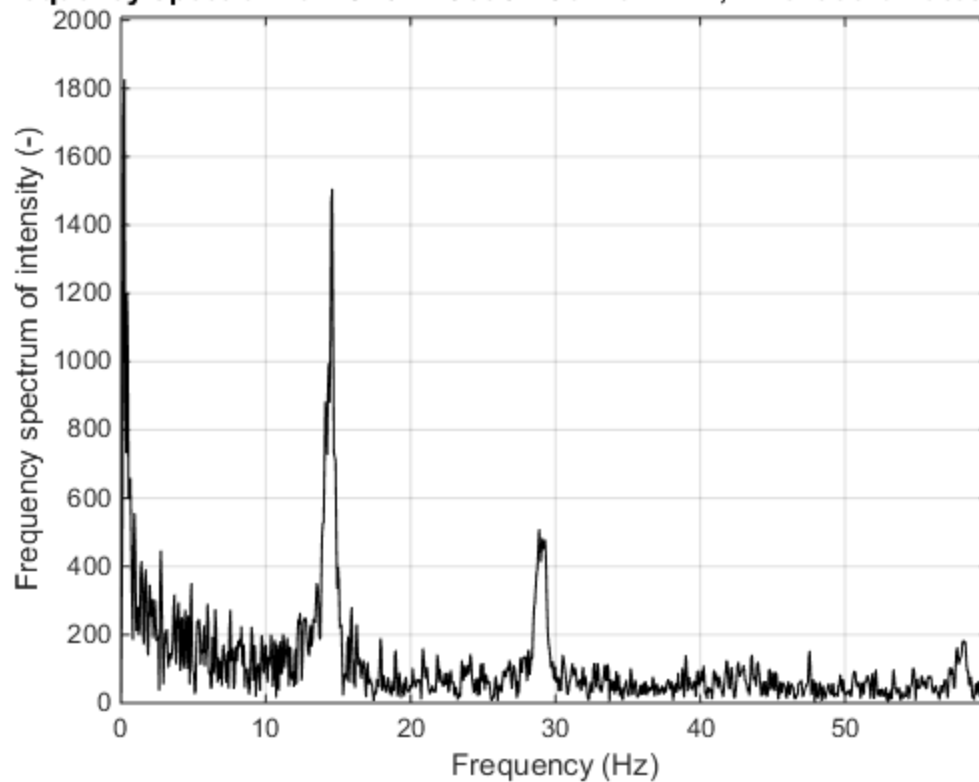
Frequency spectrum of "S10T2 Oct 31 Canon.MOV", Pixel coordinates: 708 357



Time history of "S10T2 Oct 31 GoPro.MP4", Pixel coordinates: 629 398



Frequency spectrum of "S10T2 Oct 31 GoPro.MP4", Pixel coordinates: 629 398



Appendix F – VVS Figures from Hot-Dry 2x4 Experiments

- The first highlighted section contains the specimen designation followed by the test number.
 - In this example: Specimen 1, Test 1
- The second highlighted section contains the camera which was used.
 - In this example: Canon

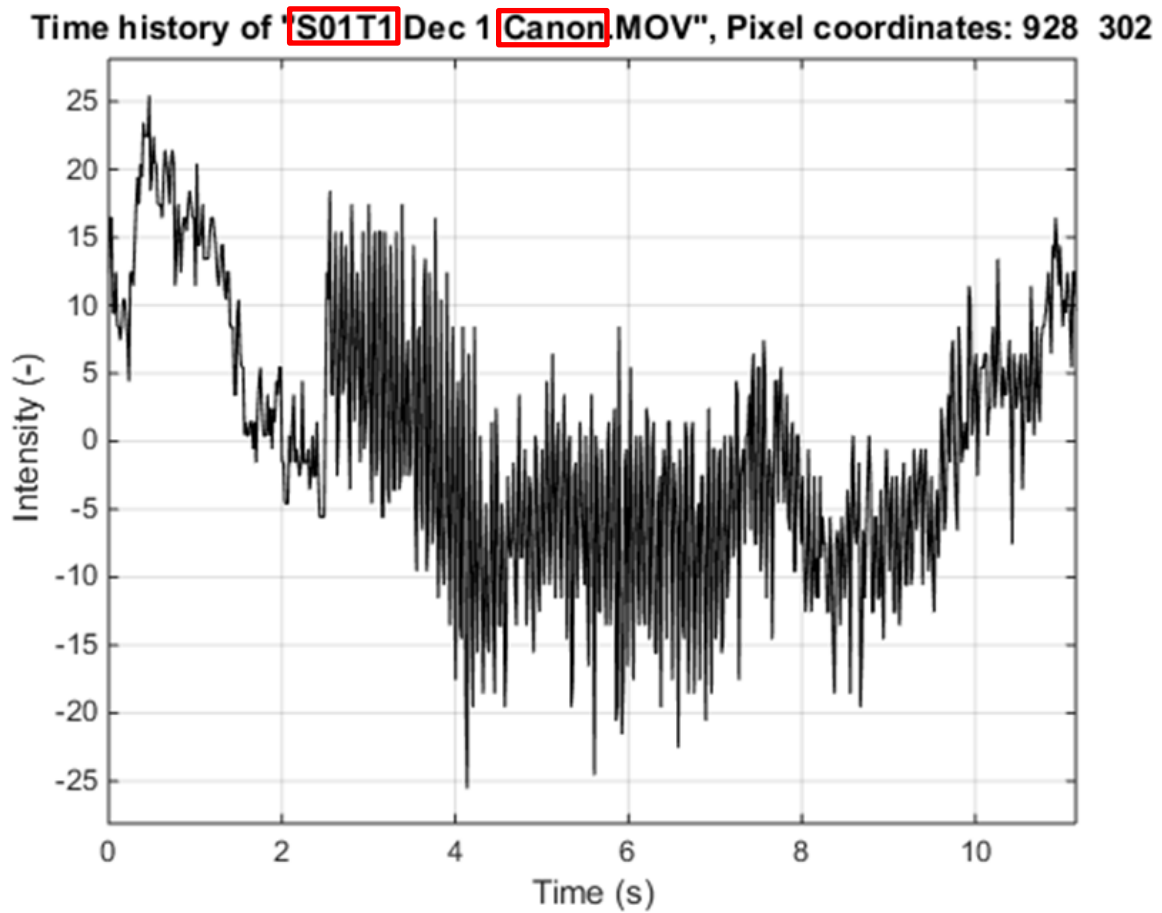
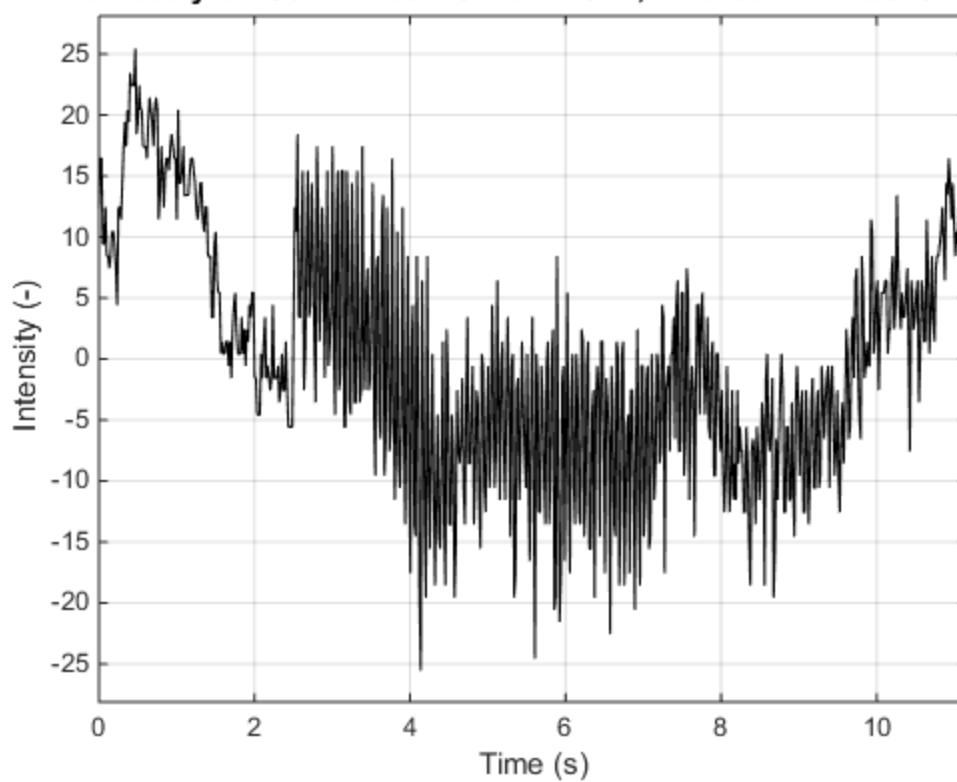
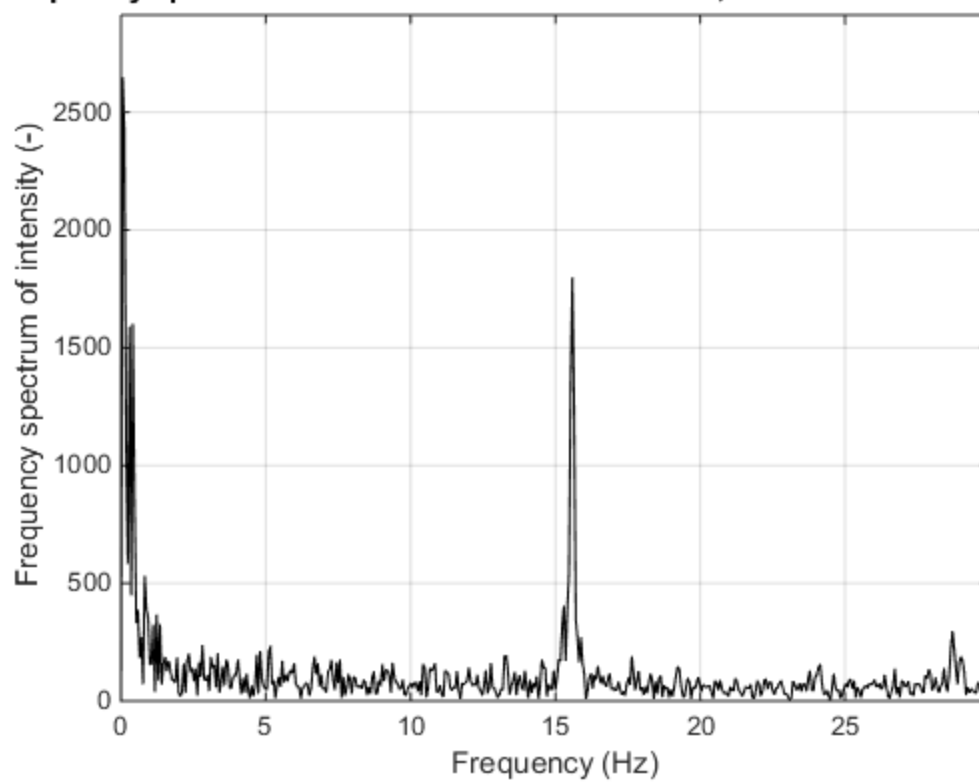


Figure E11 - Key for 2x4 Hot-Dry Figures

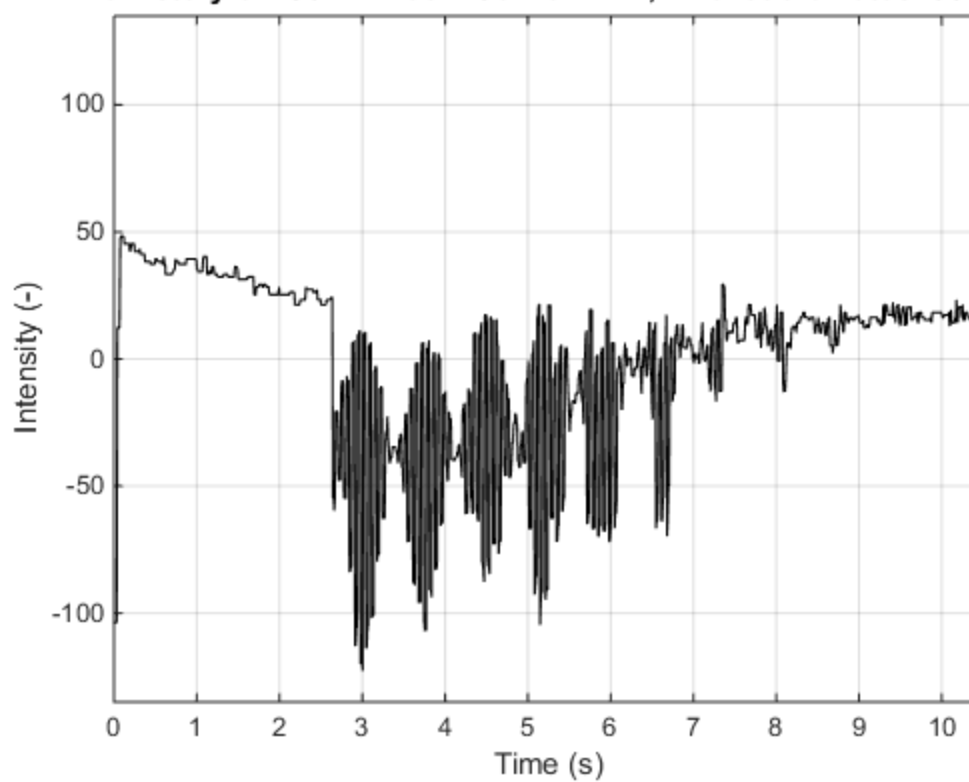
Time history of "S01T1 Dec 1 Canon.MOV", Pixel coordinates: 928 302



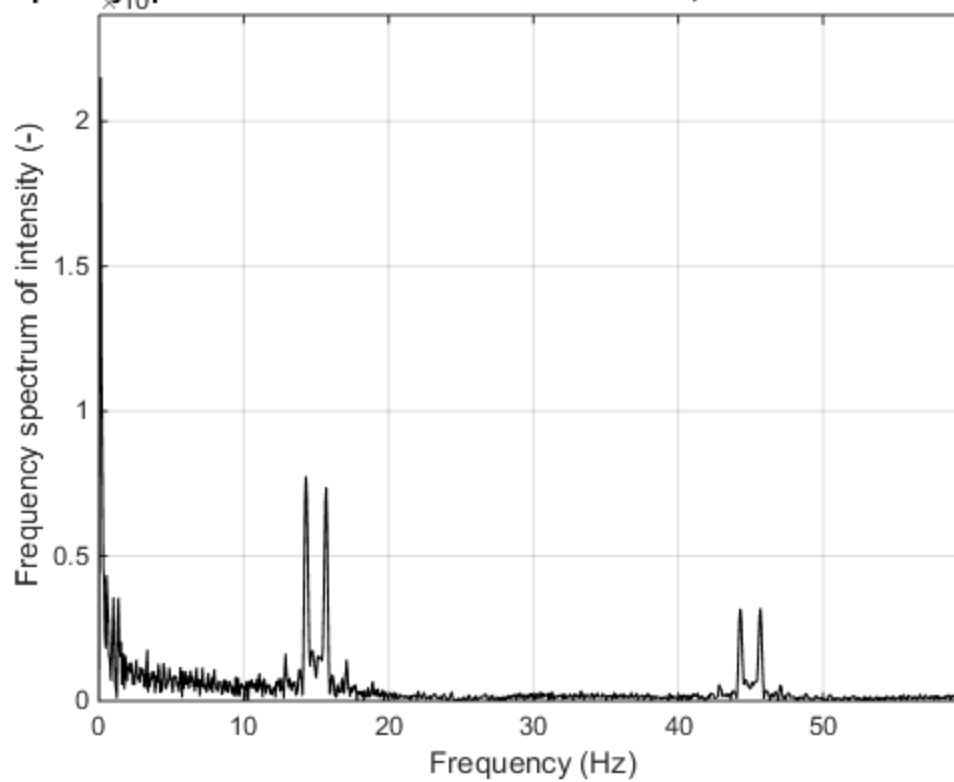
Frequency spectrum of "S01T1 Dec 1 Canon.MOV", Pixel coordinates: 928 302



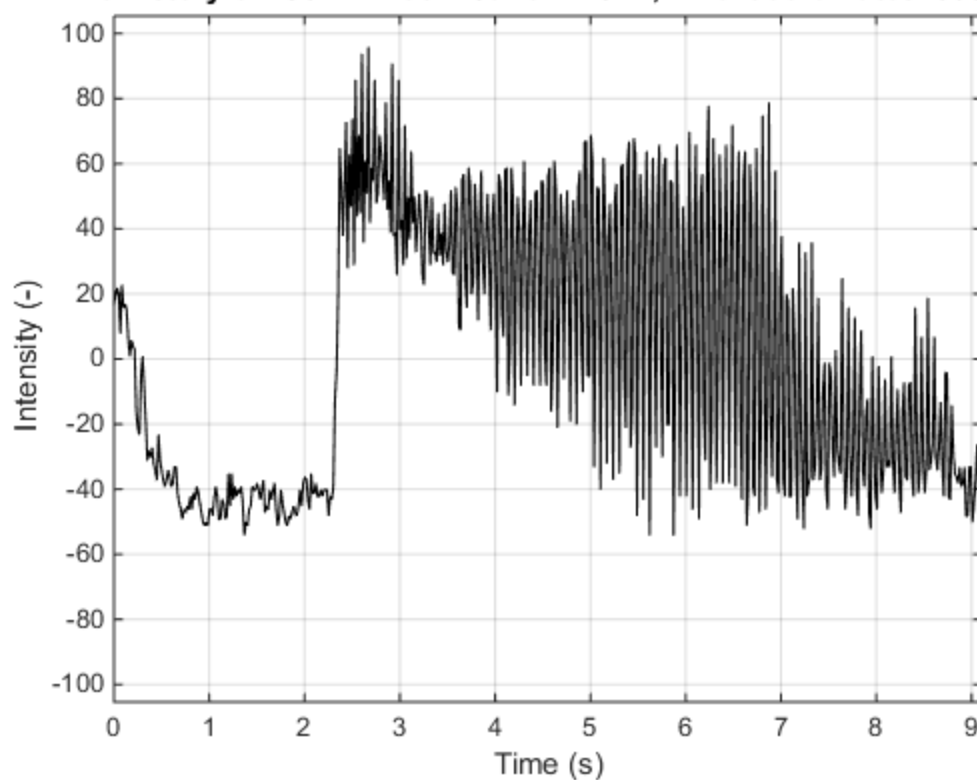
Time history of "S01T1 Dec 1 GoPro.MP4", Pixel coordinates: 588 319



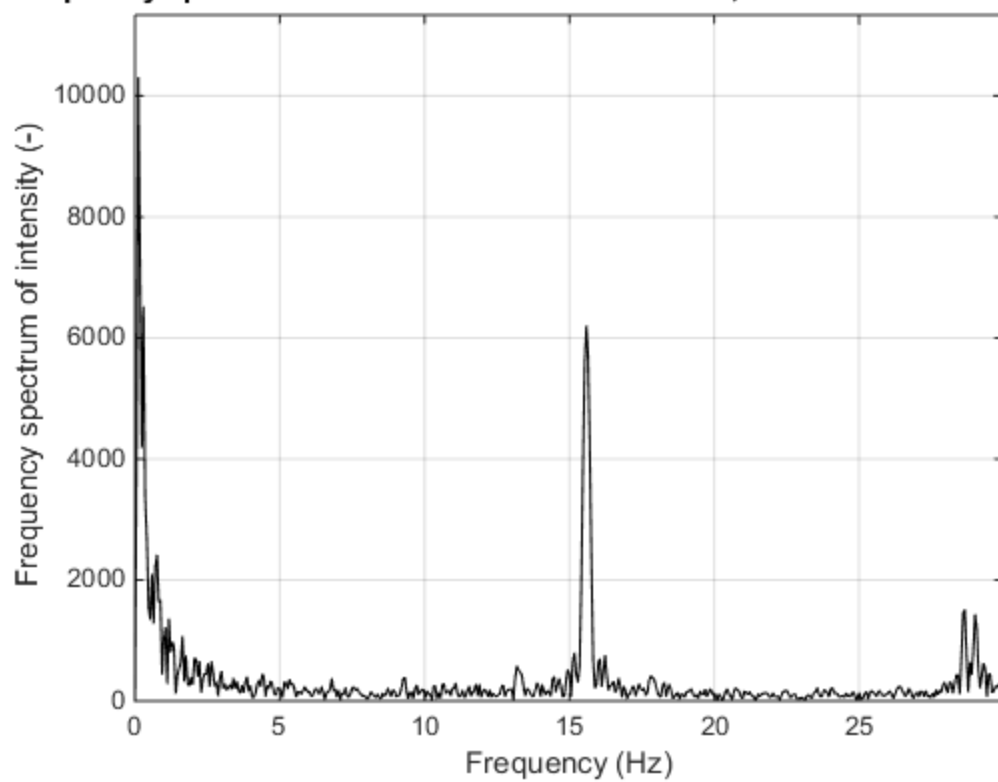
Frequency spectrum of "S01T1 Dec 1 GoPro.MP4", Pixel coordinates: 588 31



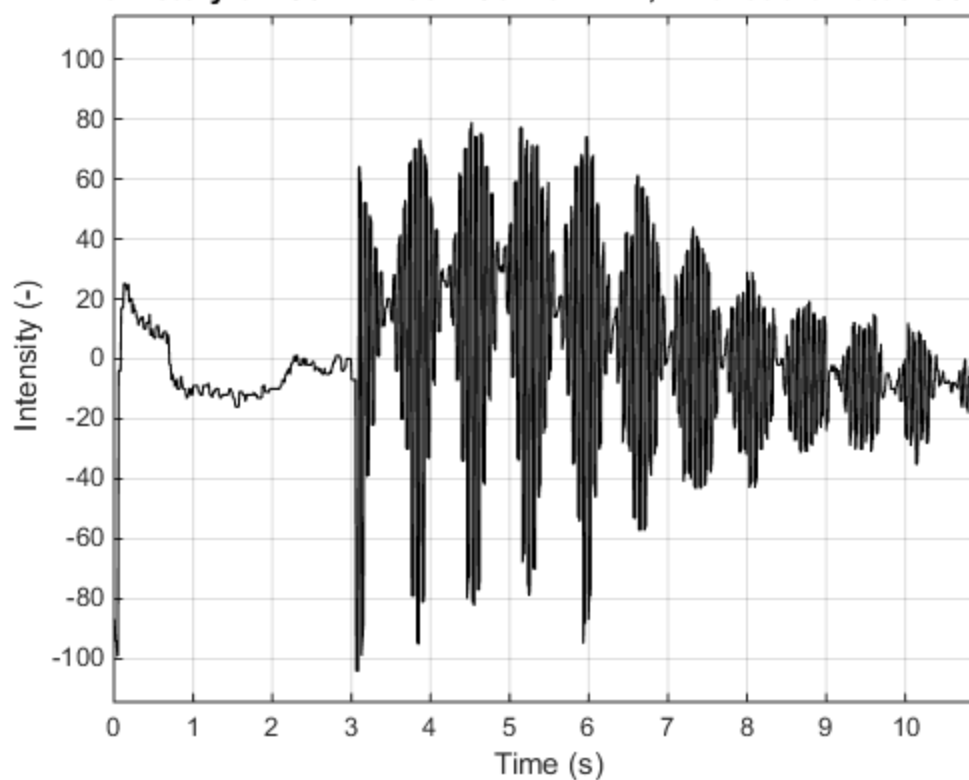
Time history of "S01T2 Dec 1 Canon.MOV", Pixel coordinates: 595 237



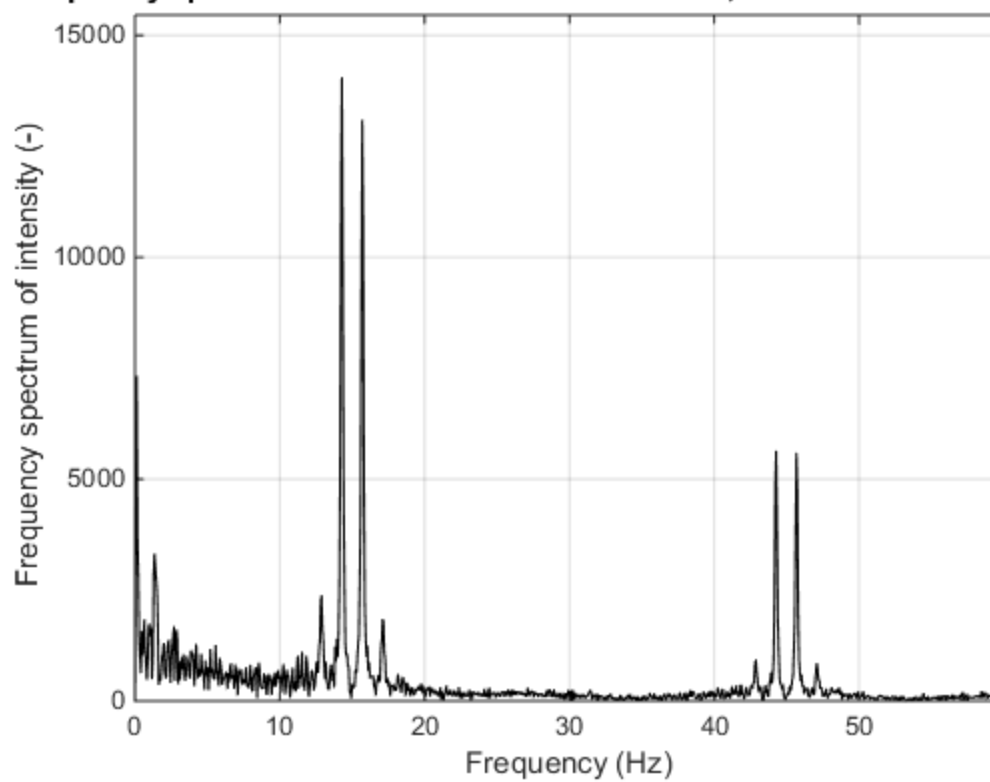
Frequency spectrum of "S01T2 Dec 1 Canon.MOV", Pixel coordinates: 595 23



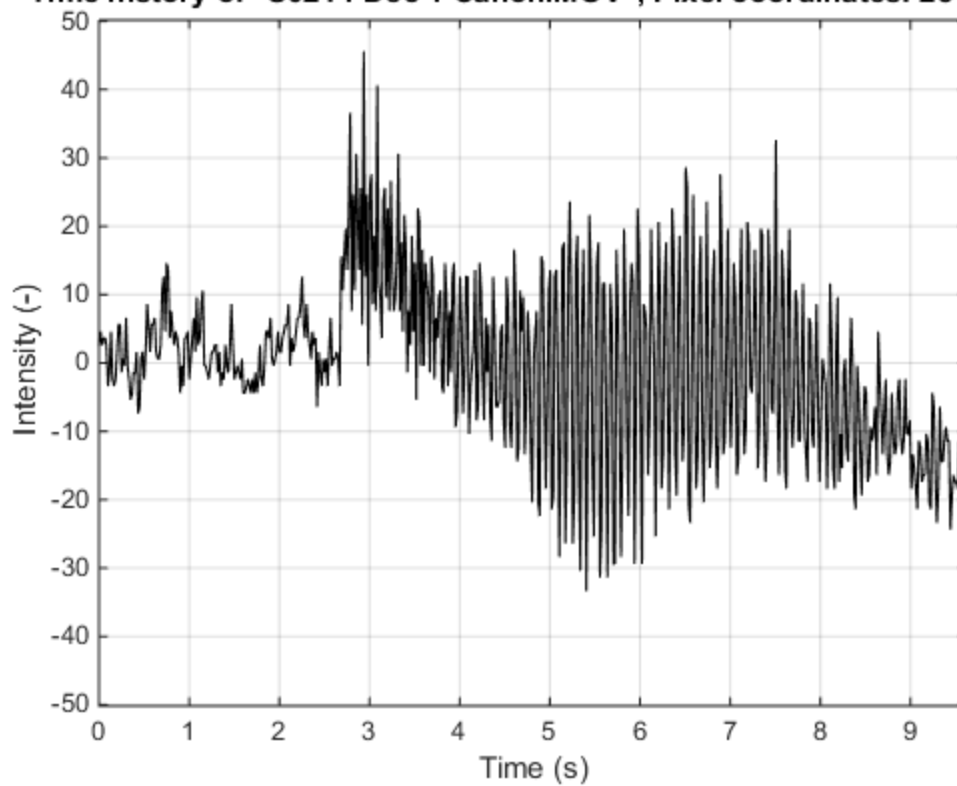
Time history of "S01T2 Dec 1 GoPro.MP4", Pixel coordinates: 833 259



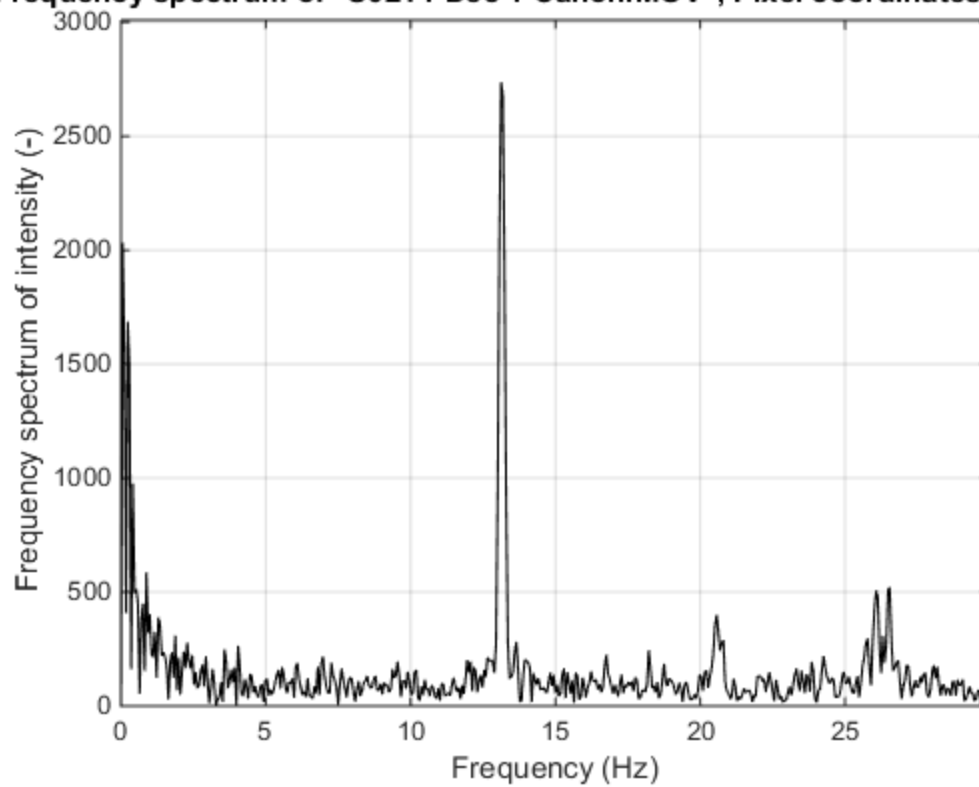
Frequency spectrum of "S01T2 Dec 1 GoPro.MP4", Pixel coordinates: 833 25



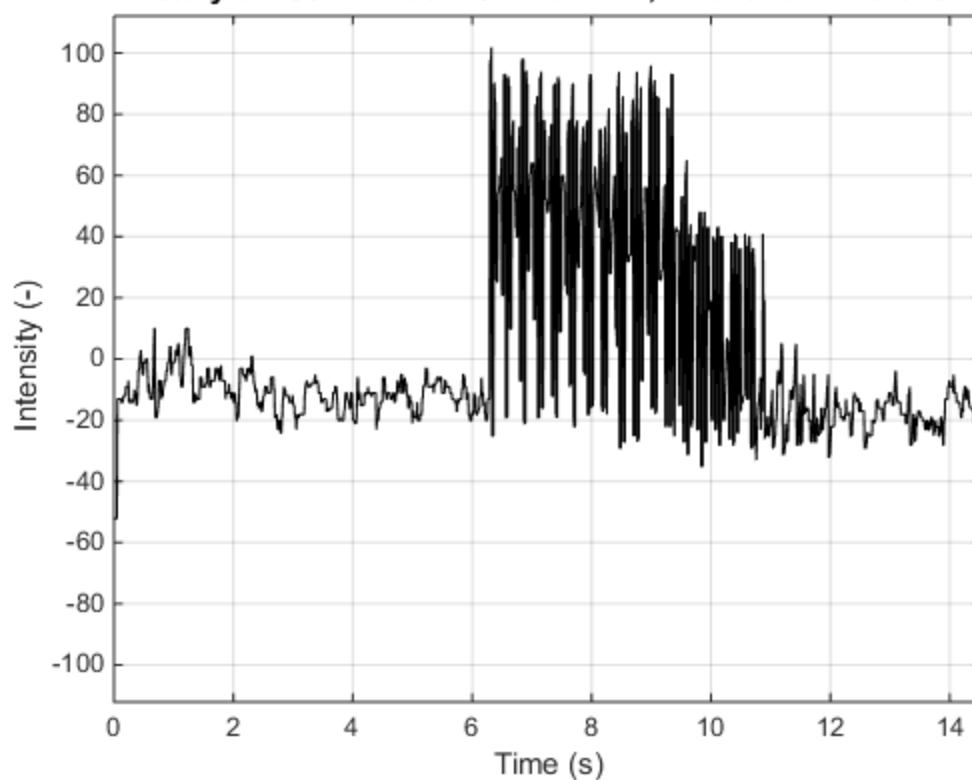
Time history of "S02T1 Dec 1 Canon.MOV", Pixel coordinates: 254 371



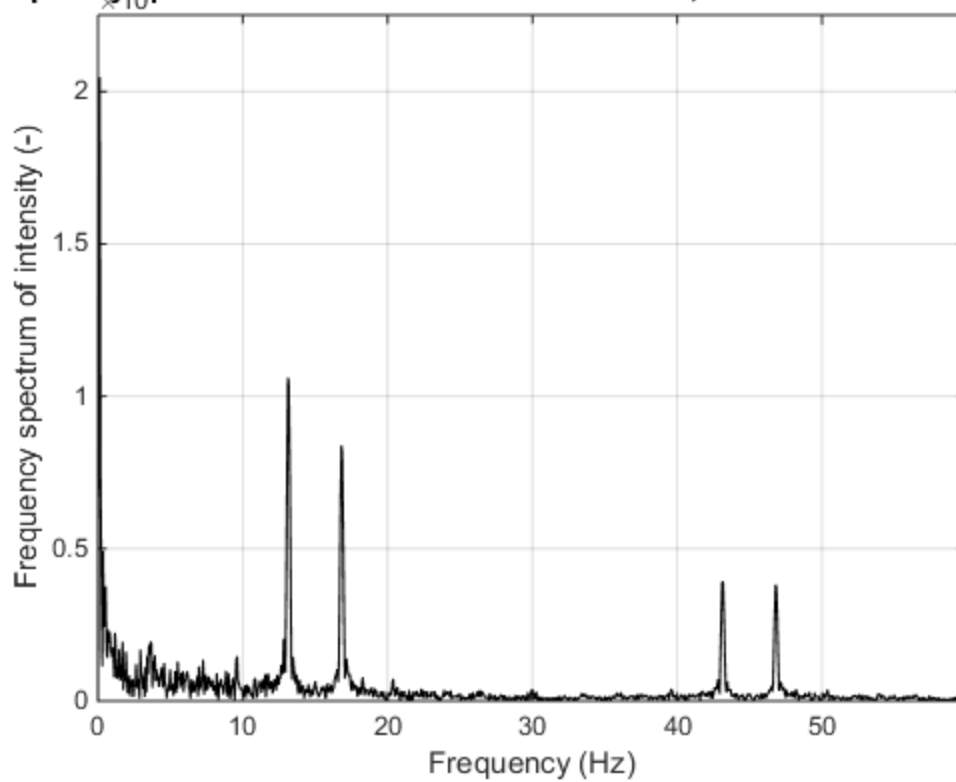
Frequency spectrum of "S02T1 Dec 1 Canon.MOV", Pixel coordinates: 254 37



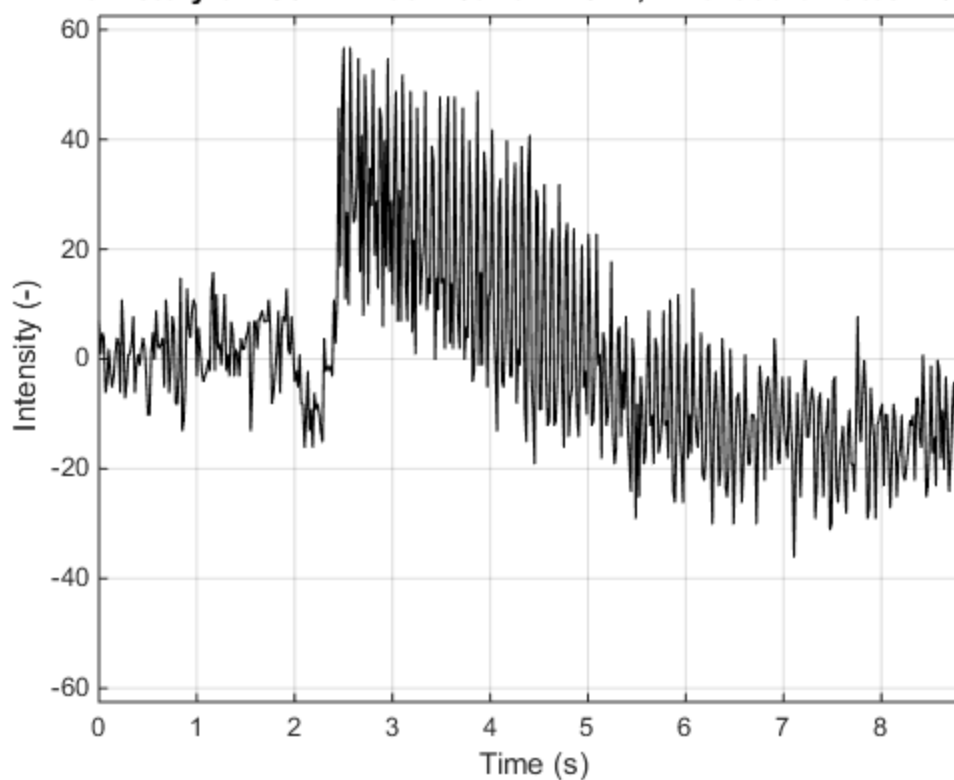
Time history of "S02T1 Dec 1 GoPro.MP4", Pixel coordinates: 644 312



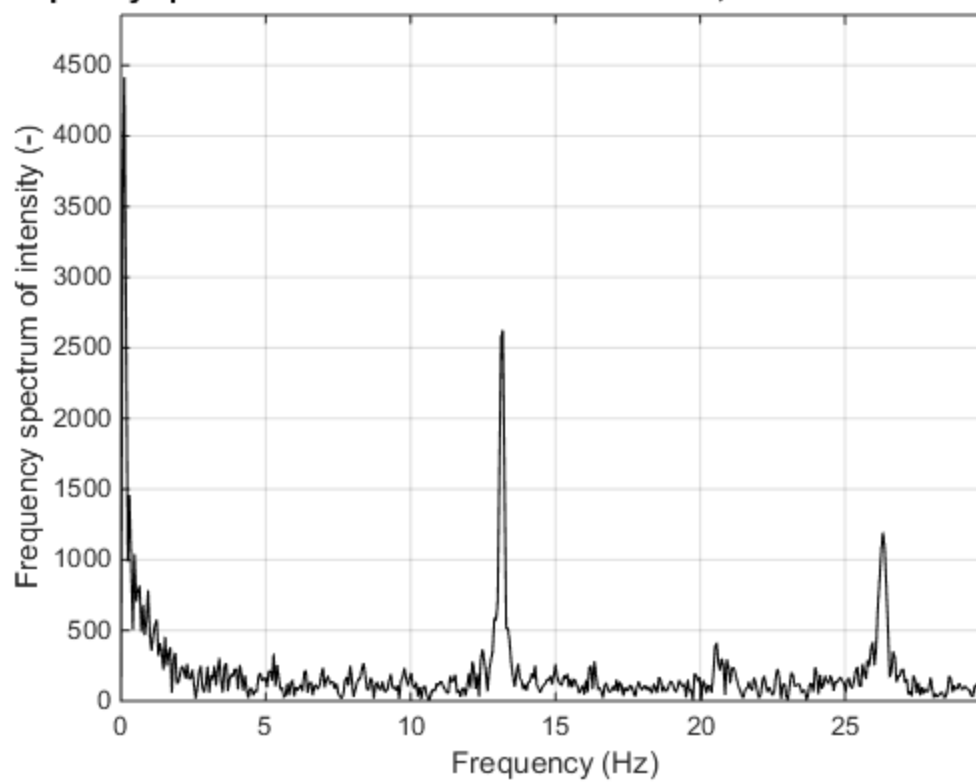
Frequency spectrum of "S02T1 Dec 1 GoPro.MP4", Pixel coordinates: 644 31



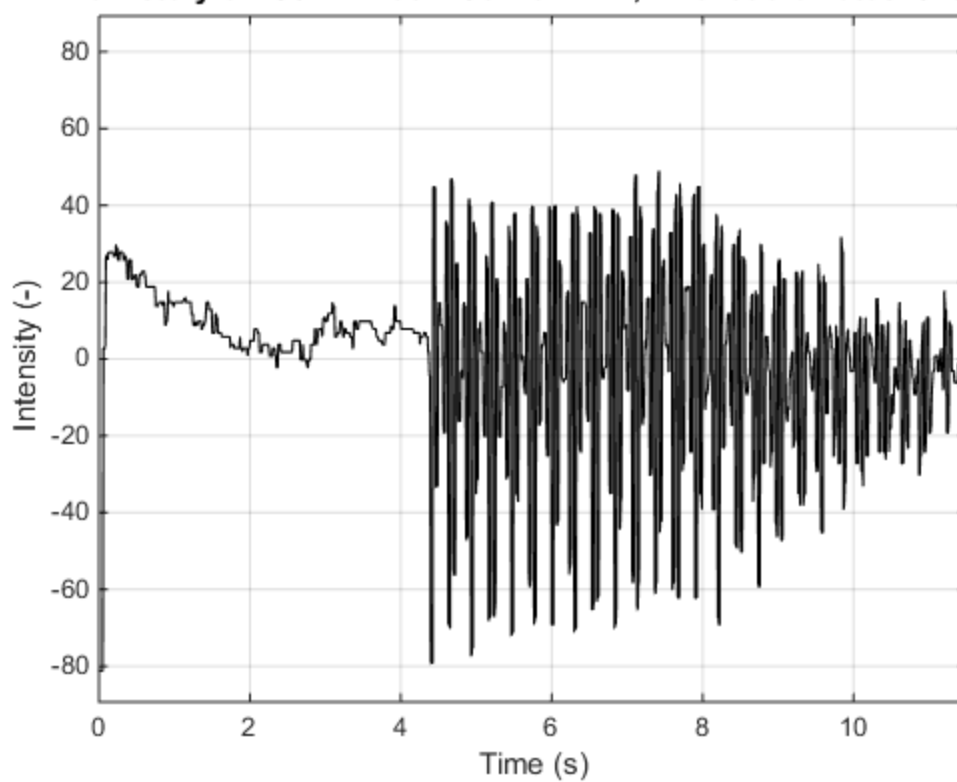
Time history of "S02T2 Dec 1 Canon.MOV", Pixel coordinates: 269 264



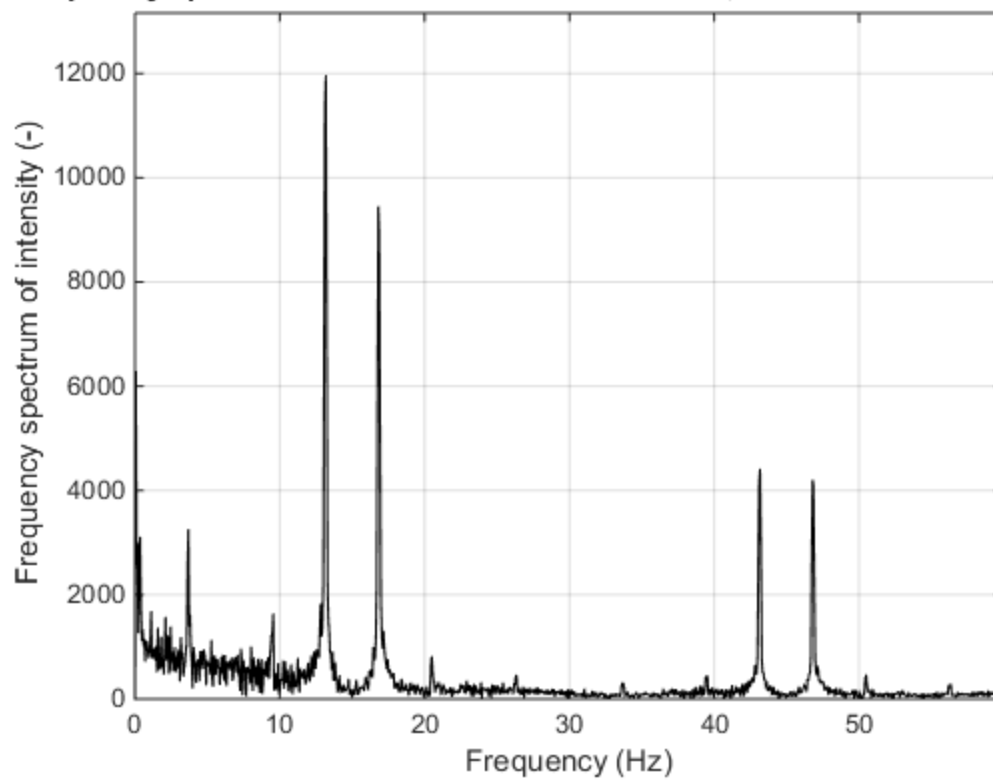
Frequency spectrum of "S02T2 Dec 1 Canon.MOV", Pixel coordinates: 269 264



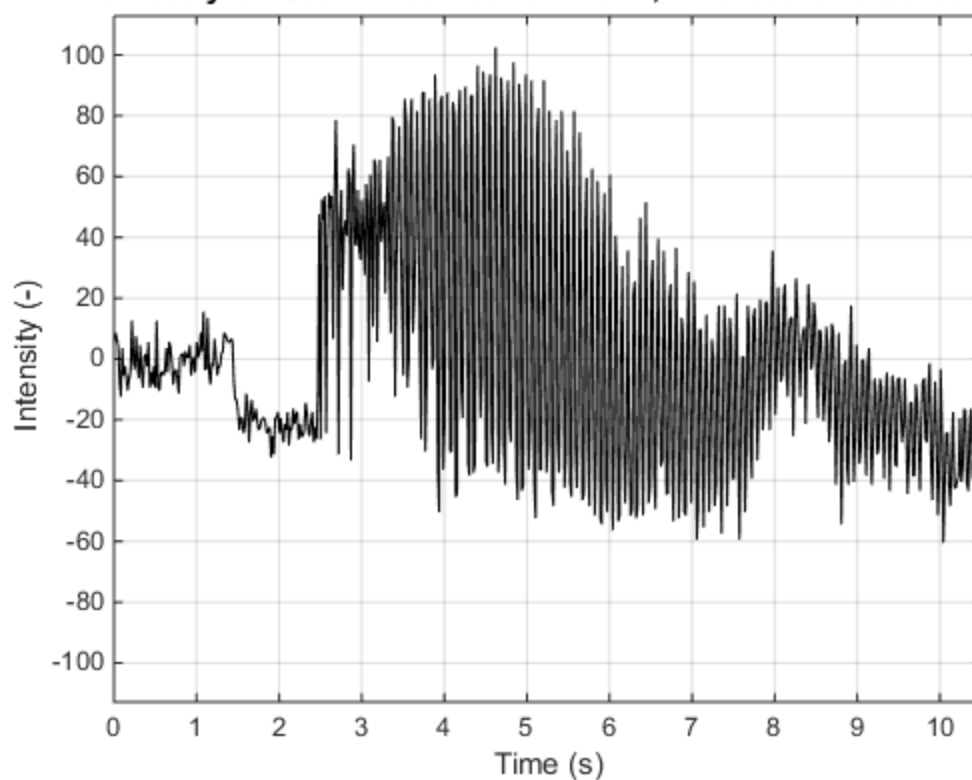
Time history of "S02T2 Dec 1 GoPro.MP4", Pixel coordinates: 816 258



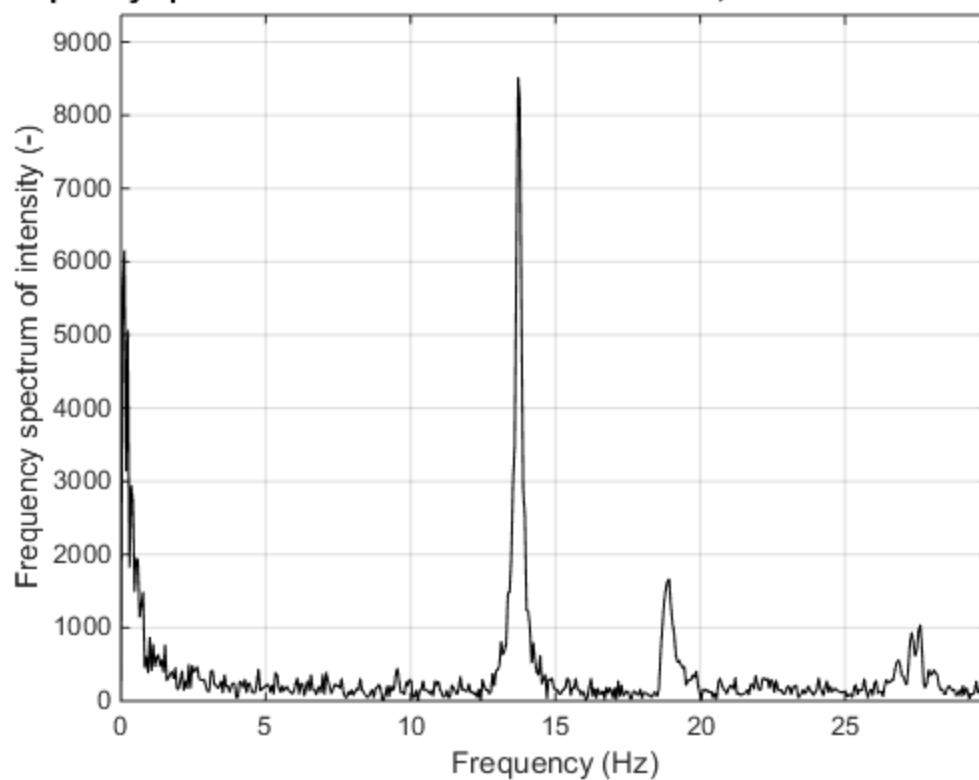
Frequency spectrum of "S02T2 Dec 1 GoPro.MP4", Pixel coordinates: 816 25



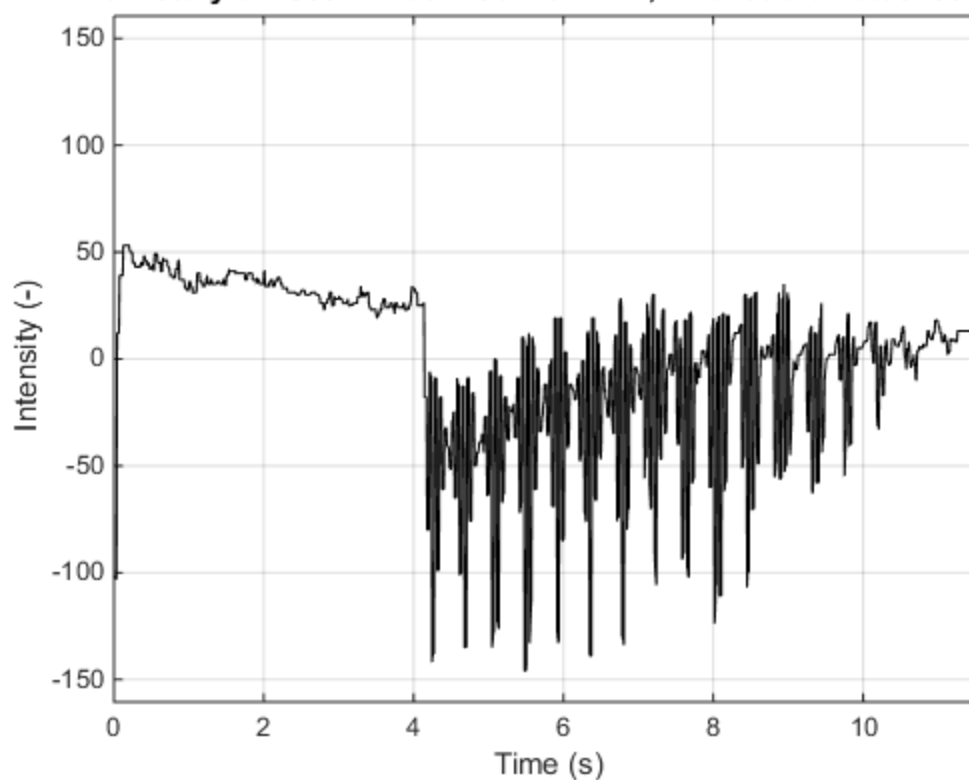
Time history of "S03T1 Dec 1 Canon.MOV", Pixel coordinates: 699 288



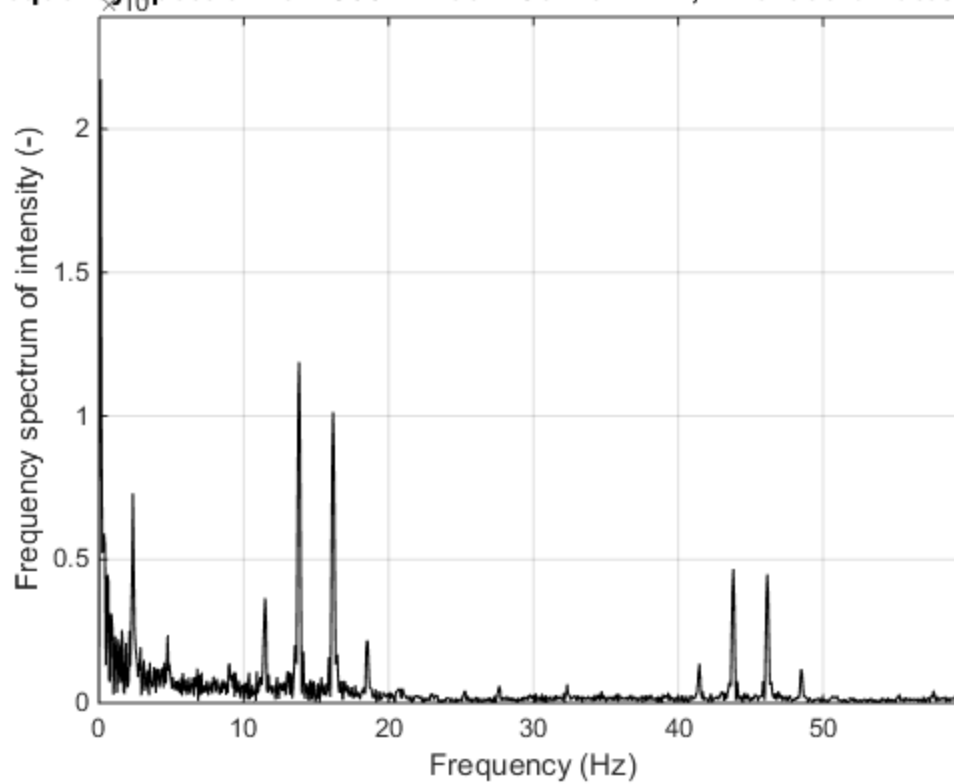
Frequency spectrum of "S03T1 Dec 1 Canon.MOV", Pixel coordinates: 699 28



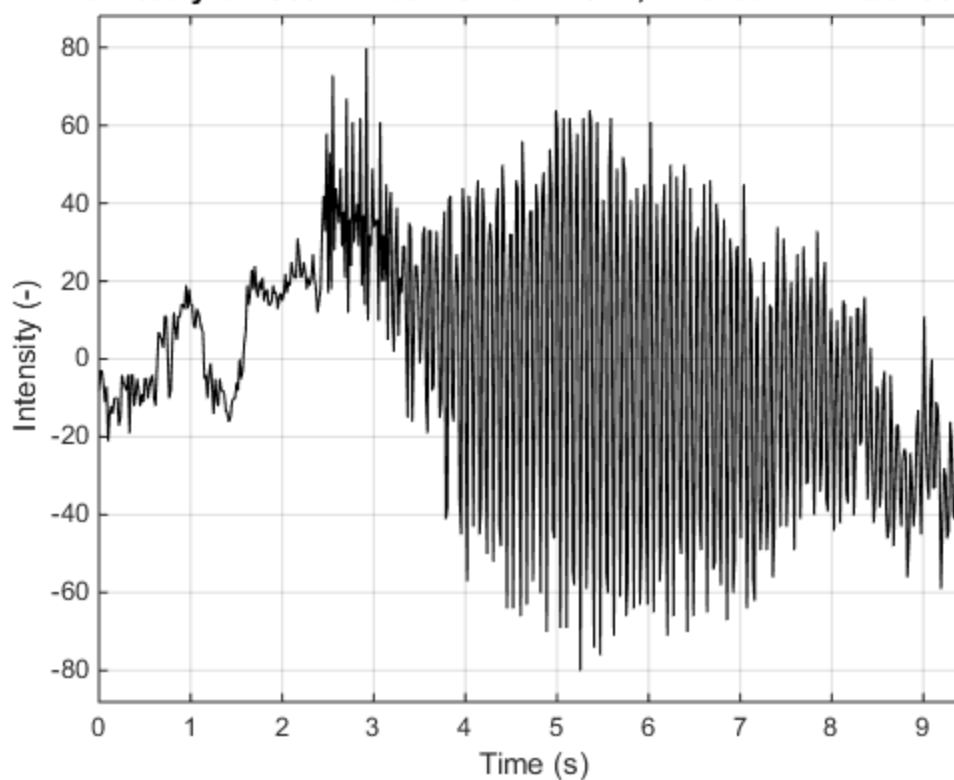
Time history of "S03T1 Dec 1 GoPro.MP4", Pixel coordinates: 693 307



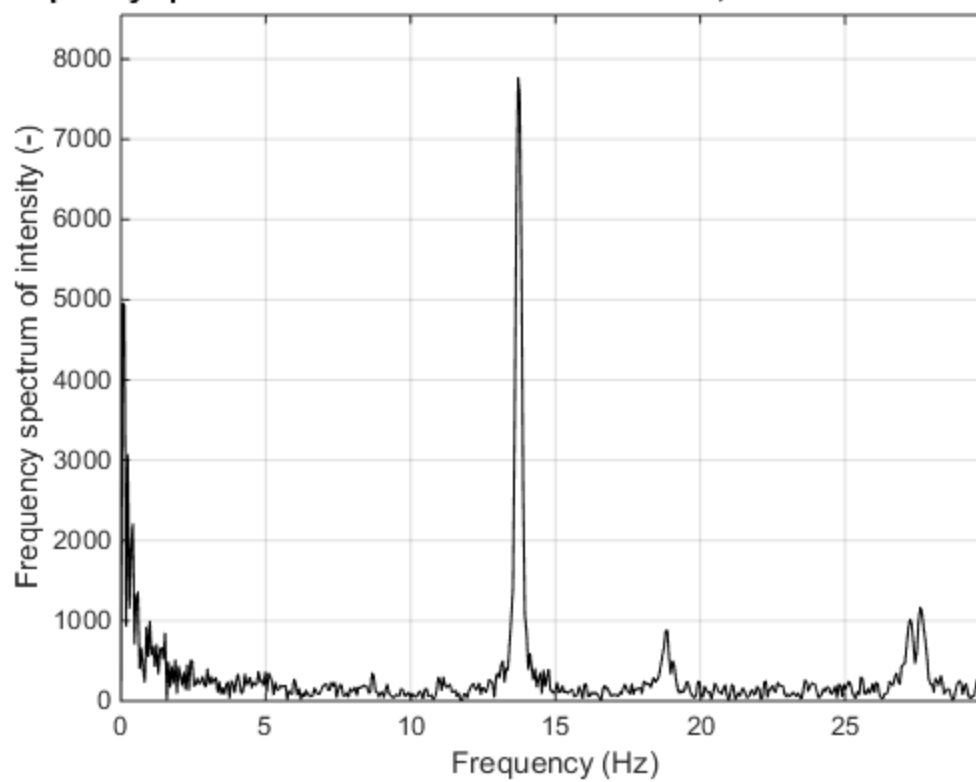
Frequency spectrum of "S03T1 Dec 1 GoPro.MP4", Pixel coordinates: 693 30



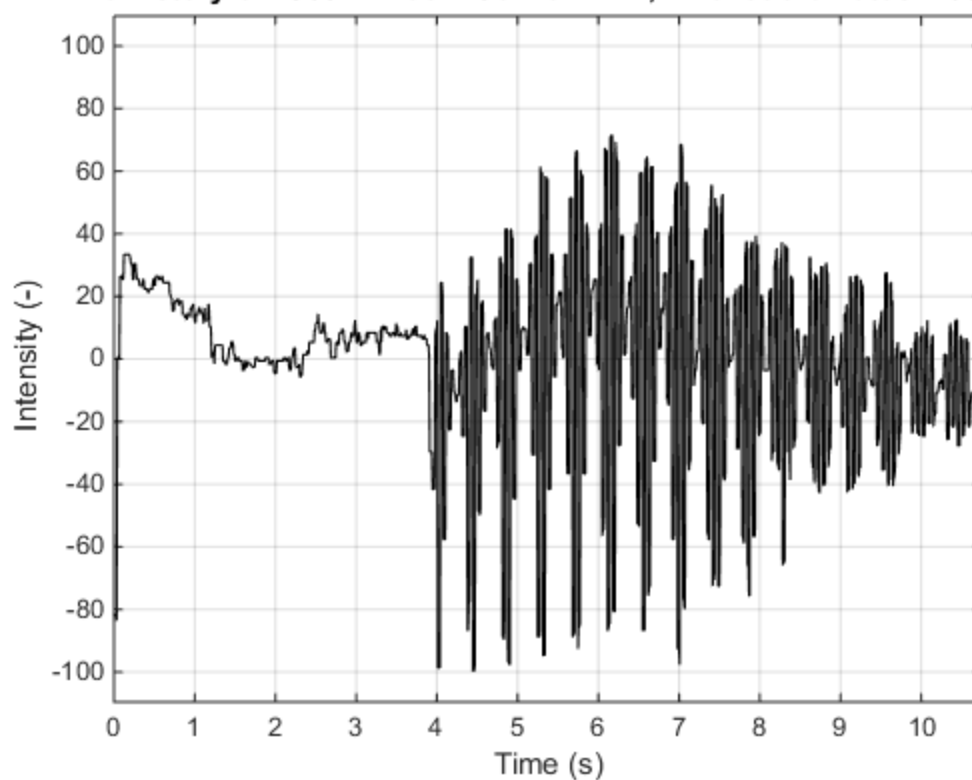
Time history of "S03T2 Dec 1 Canon.MOV", Pixel coordinates: 663 250



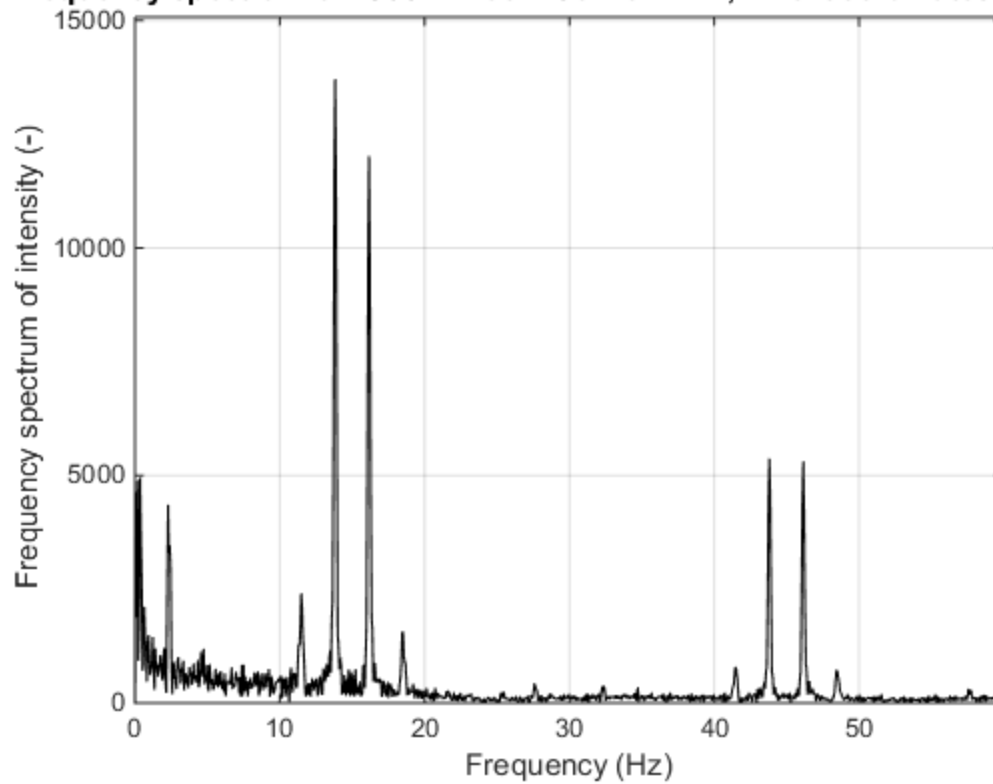
Frequency spectrum of "S03T2 Dec 1 Canon.MOV", Pixel coordinates: 663 25



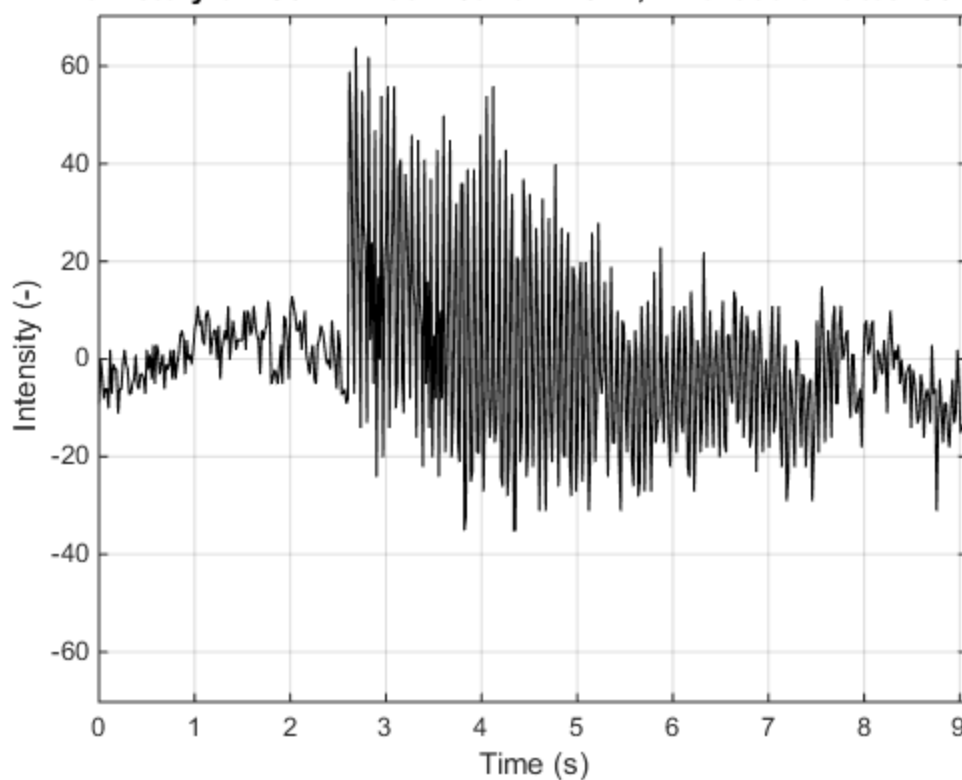
Time history of "S03T2 Dec 1 GoPro.MP4", Pixel coordinates: 793 237



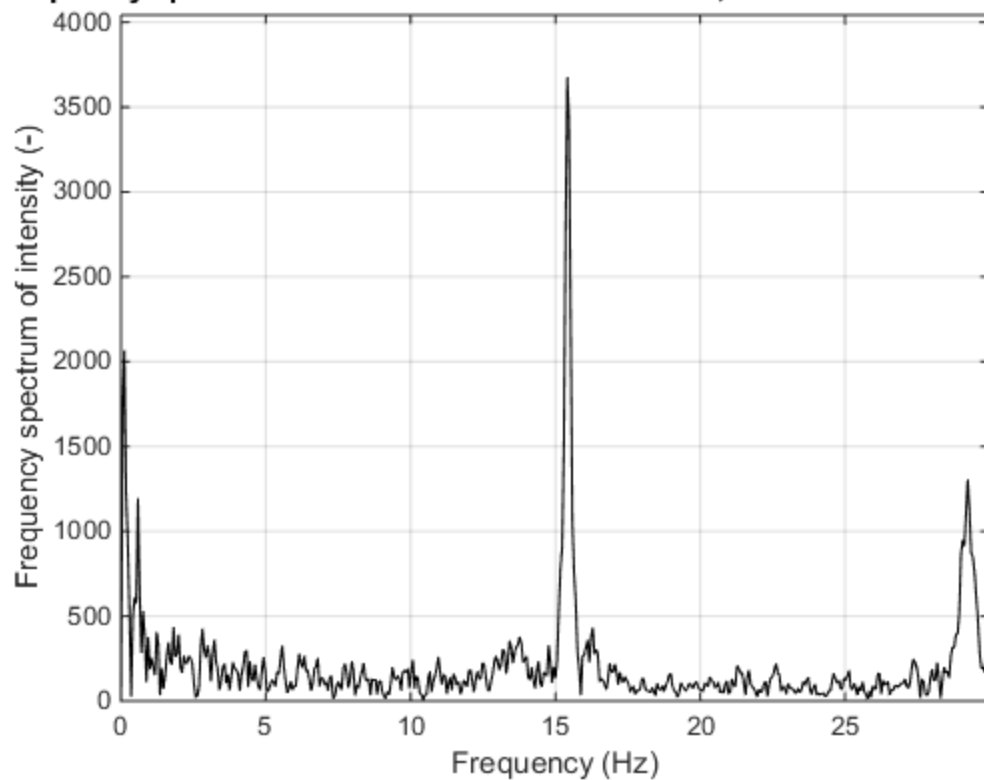
Frequency spectrum of "S03T2 Dec 1 GoPro.MP4", Pixel coordinates: 793 23



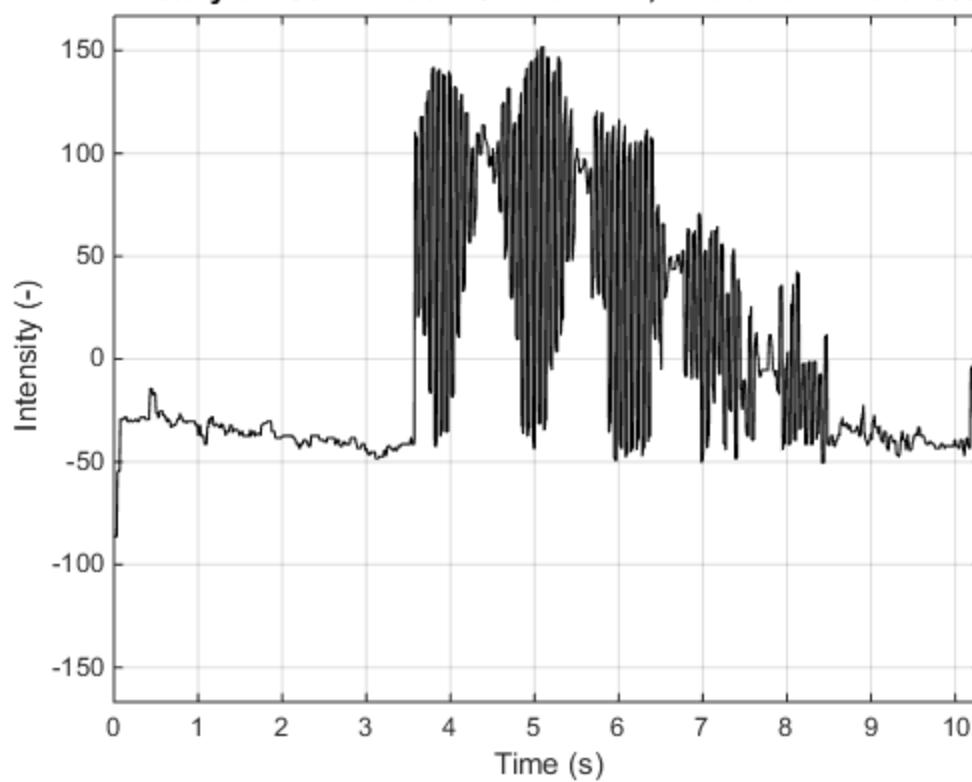
Time history of "S04T1 Dec 1 Canon.MOV", Pixel coordinates: 387 300



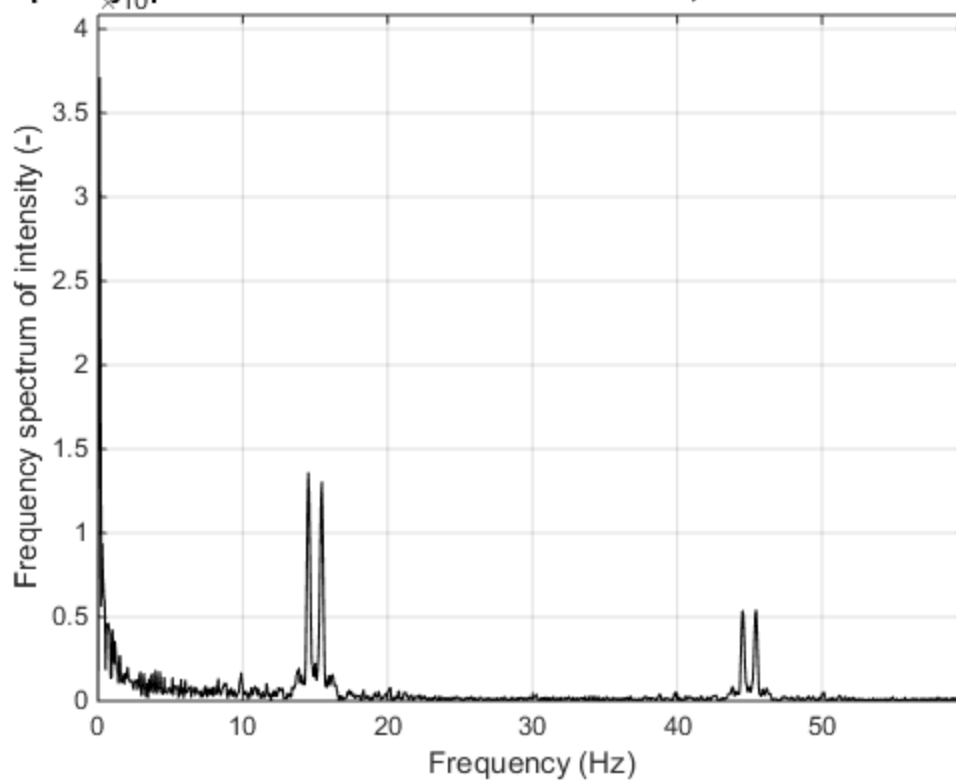
Frequency spectrum of "S04T1 Dec 1 Canon.MOV", Pixel coordinates: 387 300



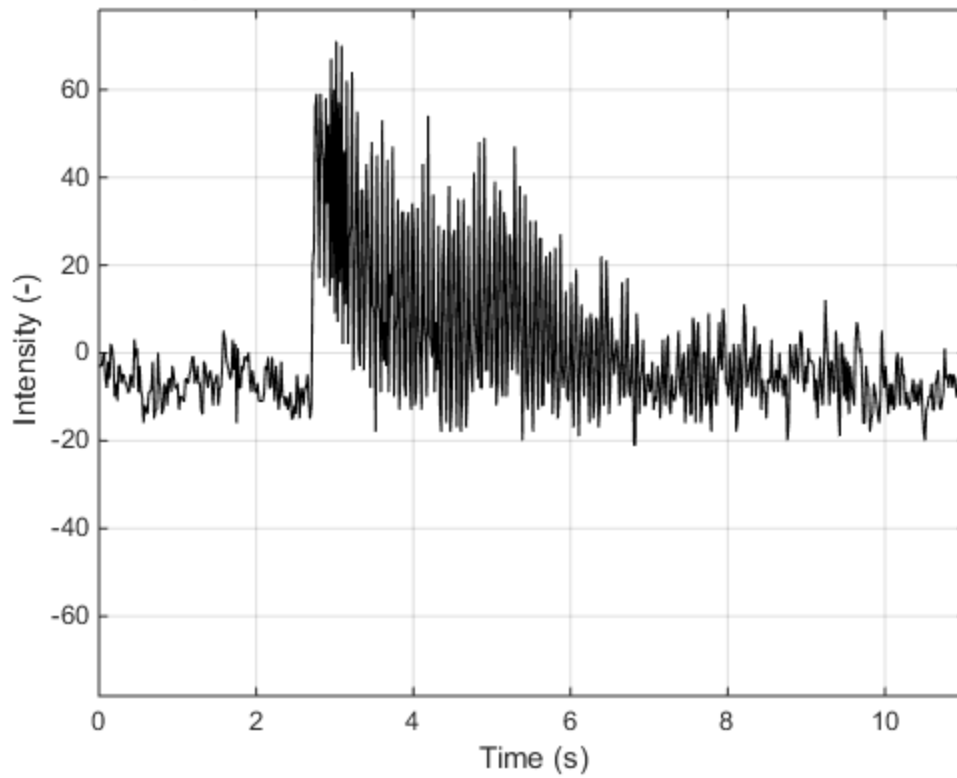
Time history of "S04T1 Dec 1 GoPro.MP4", Pixel coordinates: 635 302



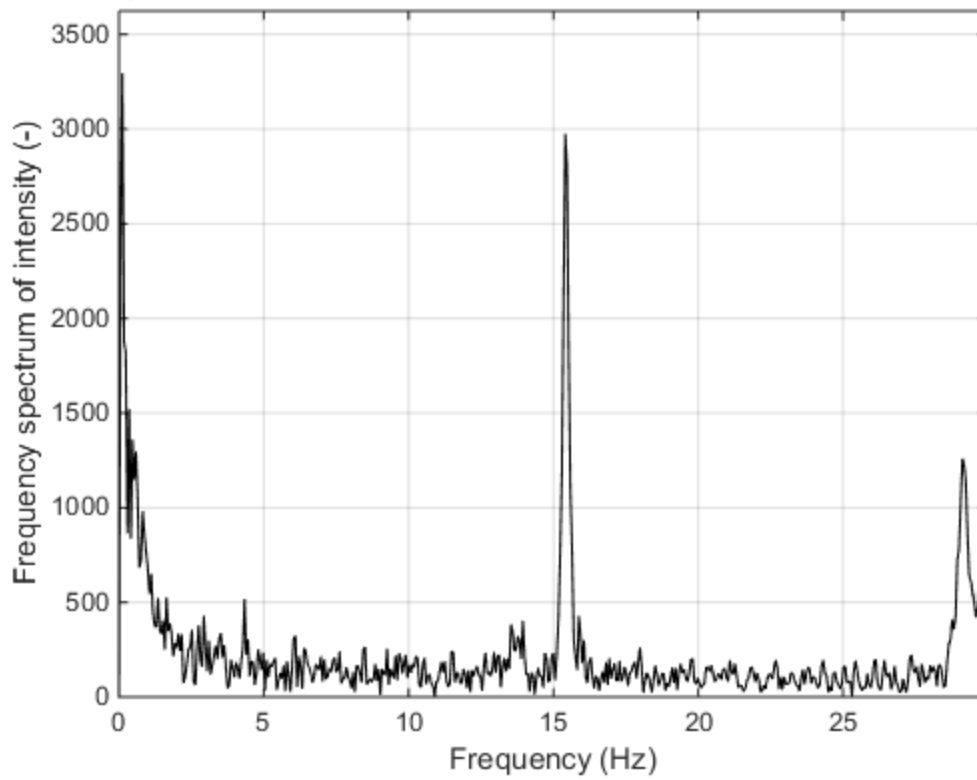
Frequency spectrum of "S04T1 Dec 1 GoPro.MP4", Pixel coordinates: 635 30



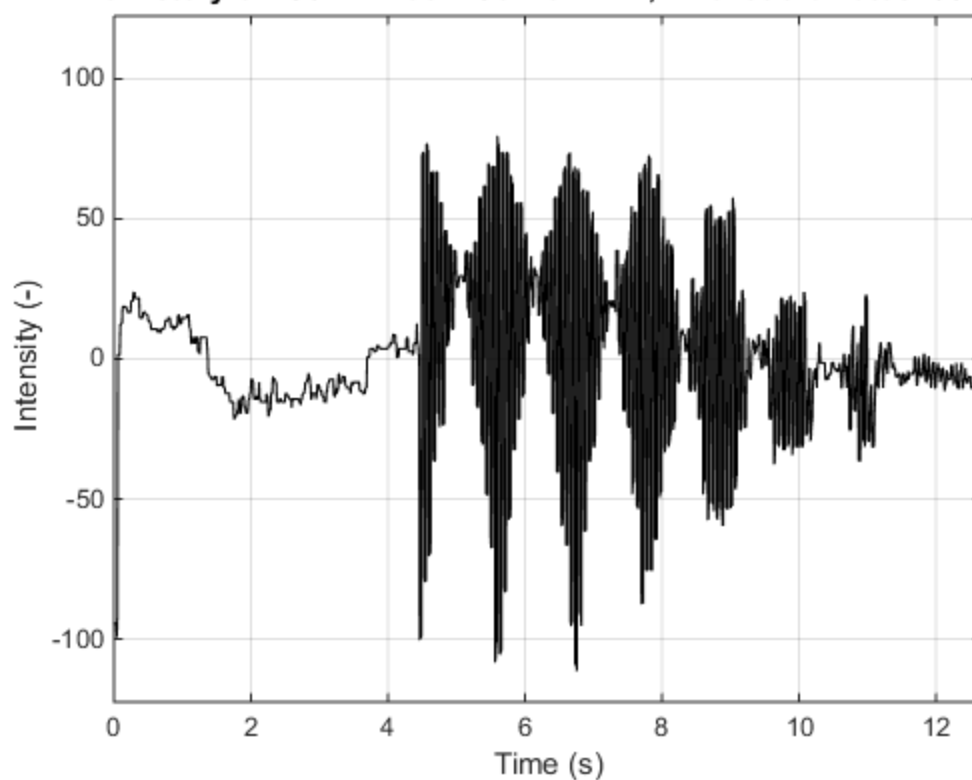
Time history of "S04T2 Dec 1 Canon.MOV", Pixel coordinates: 267 272



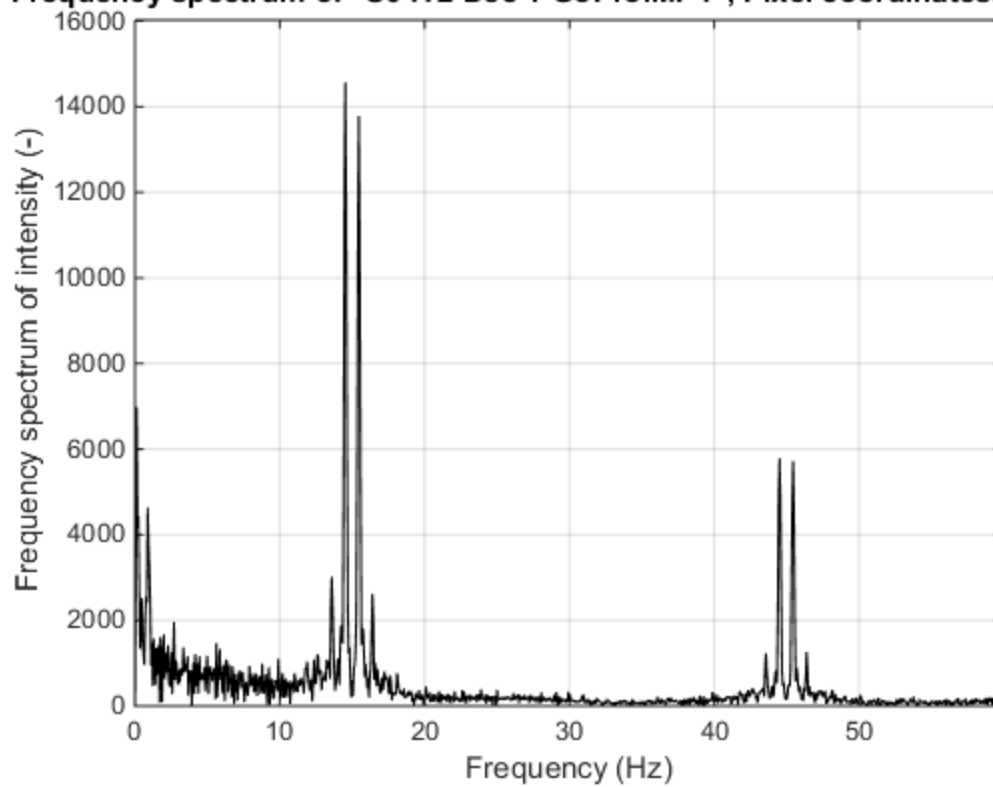
Frequency spectrum of "S04T2 Dec 1 Canon.MOV", Pixel coordinates: 267 27



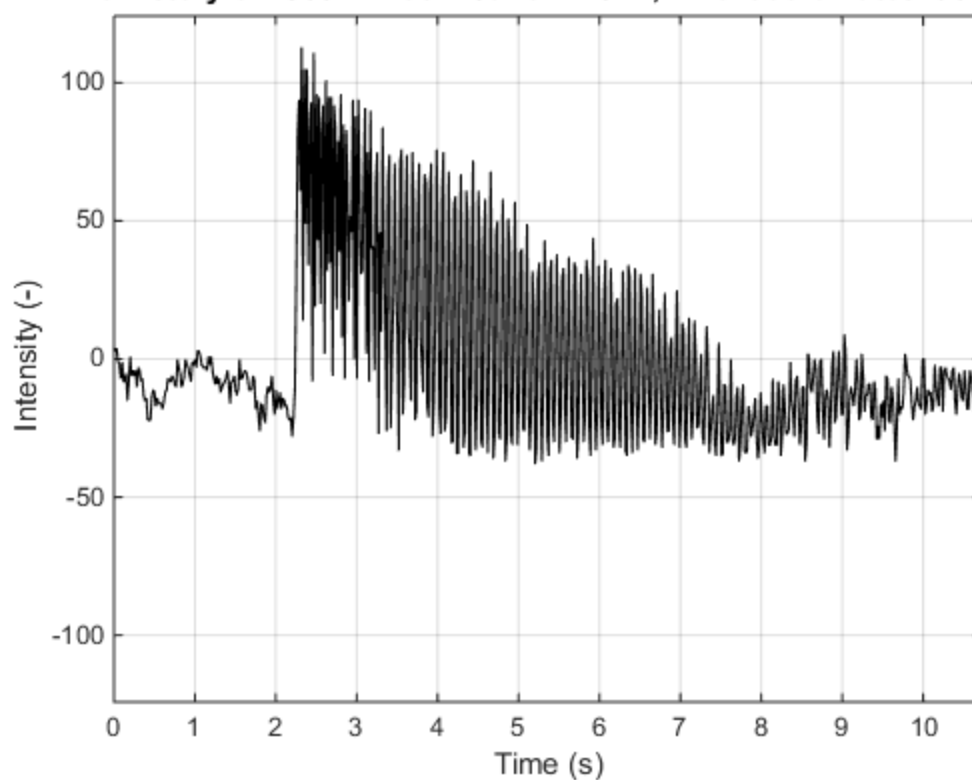
Time history of "S04T2 Dec 1 GoPro.MP4", Pixel coordinates: 632 256



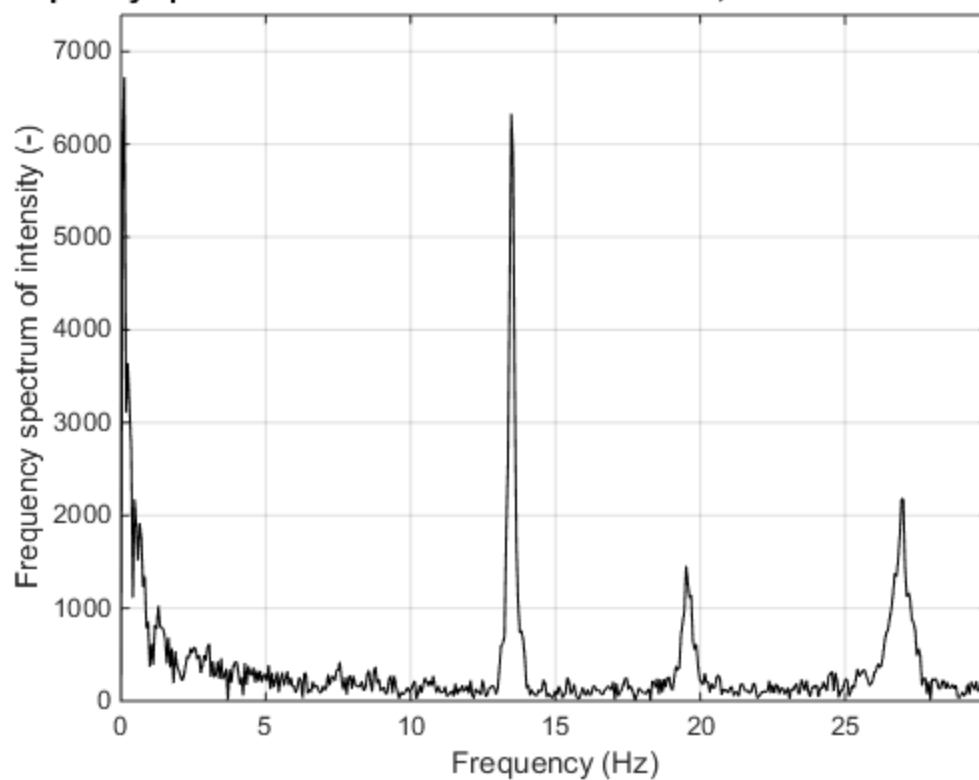
Frequency spectrum of "S04T2 Dec 1 GoPro.MP4", Pixel coordinates: 632 25



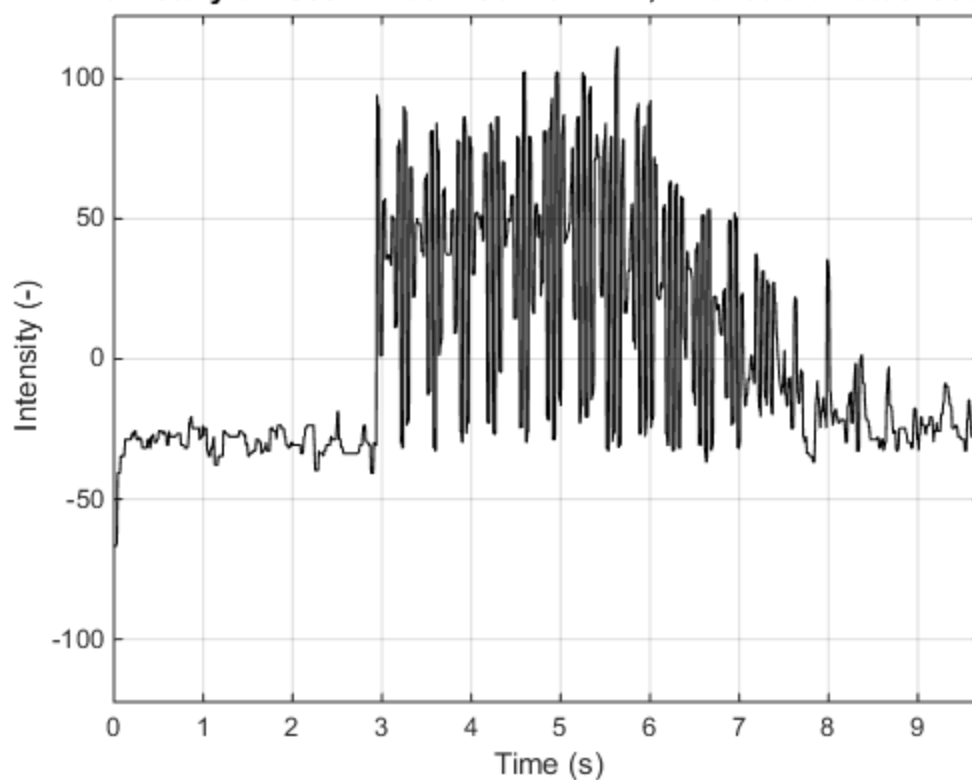
Time history of "S05T1 Dec 1 Canon.MOV", Pixel coordinates: 903 317



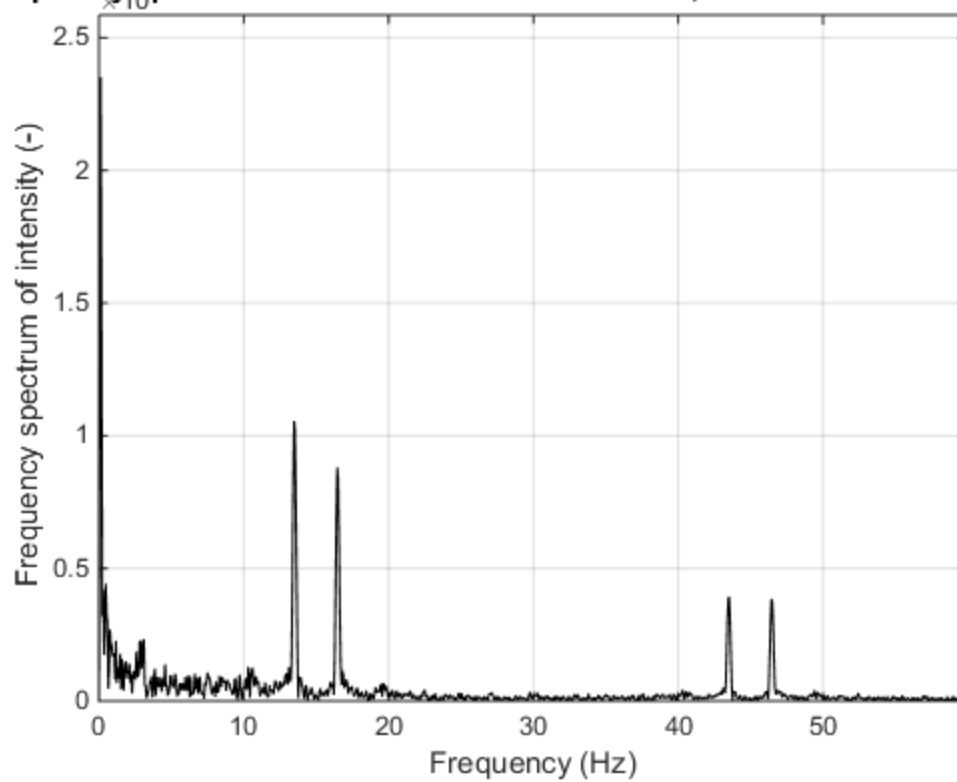
Frequency spectrum of "S05T1 Dec 1 Canon.MOV", Pixel coordinates: 903 31



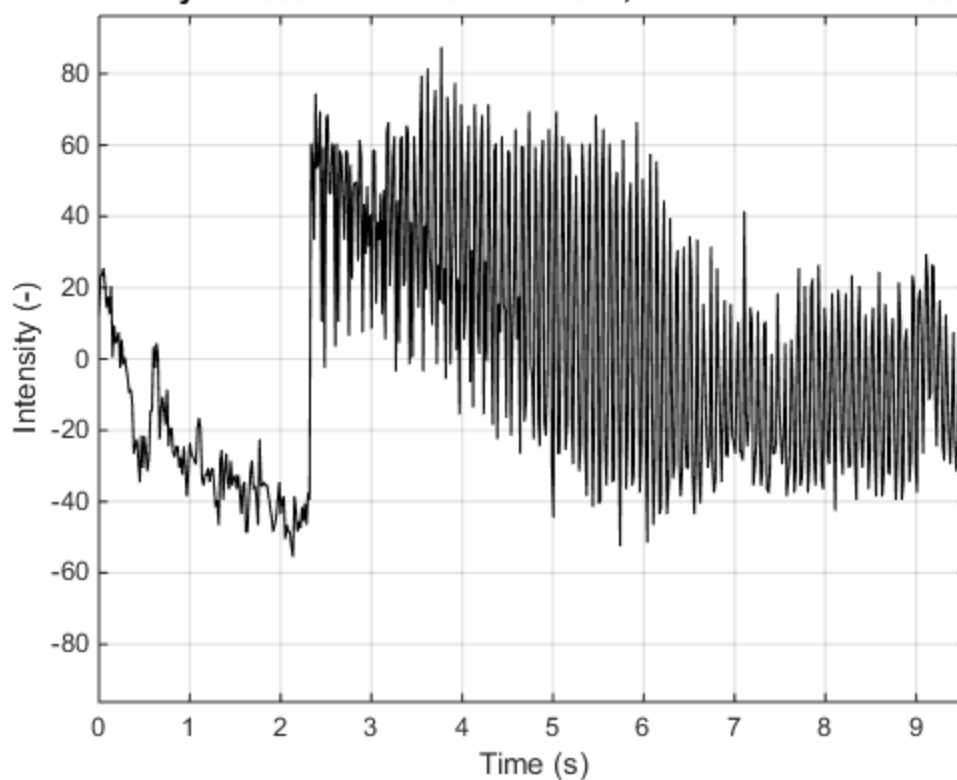
Time history of "S05T1 Dec 1 GoPro.MP4", Pixel coordinates: 595 306



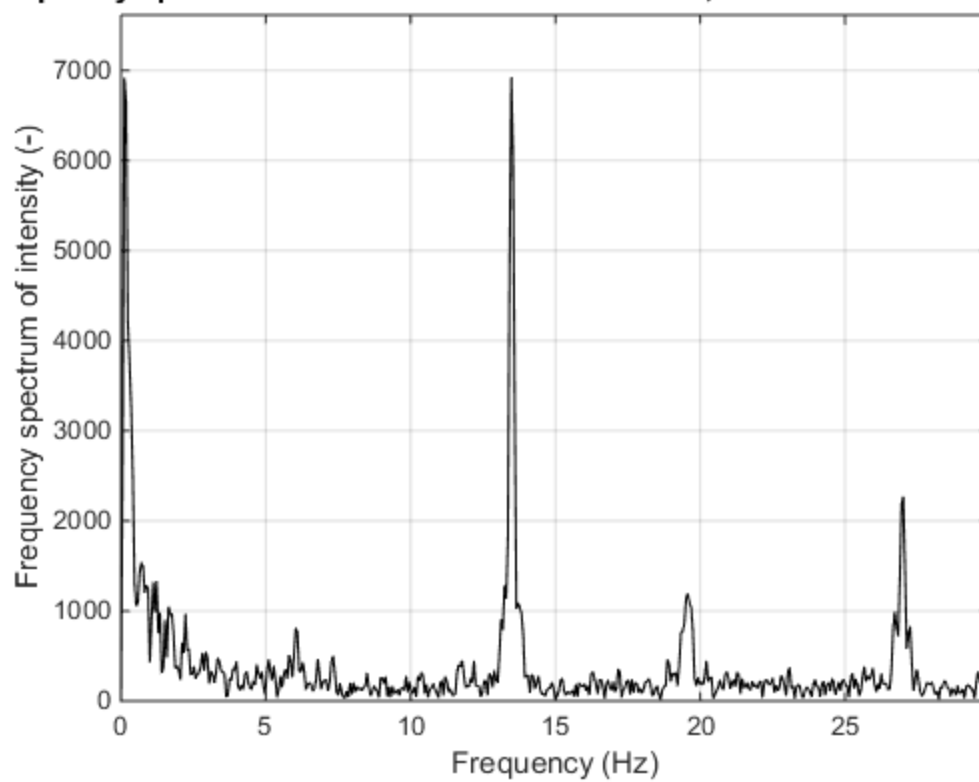
Frequency spectrum of "S05T1 Dec 1 GoPro.MP4", Pixel coordinates: 595 30



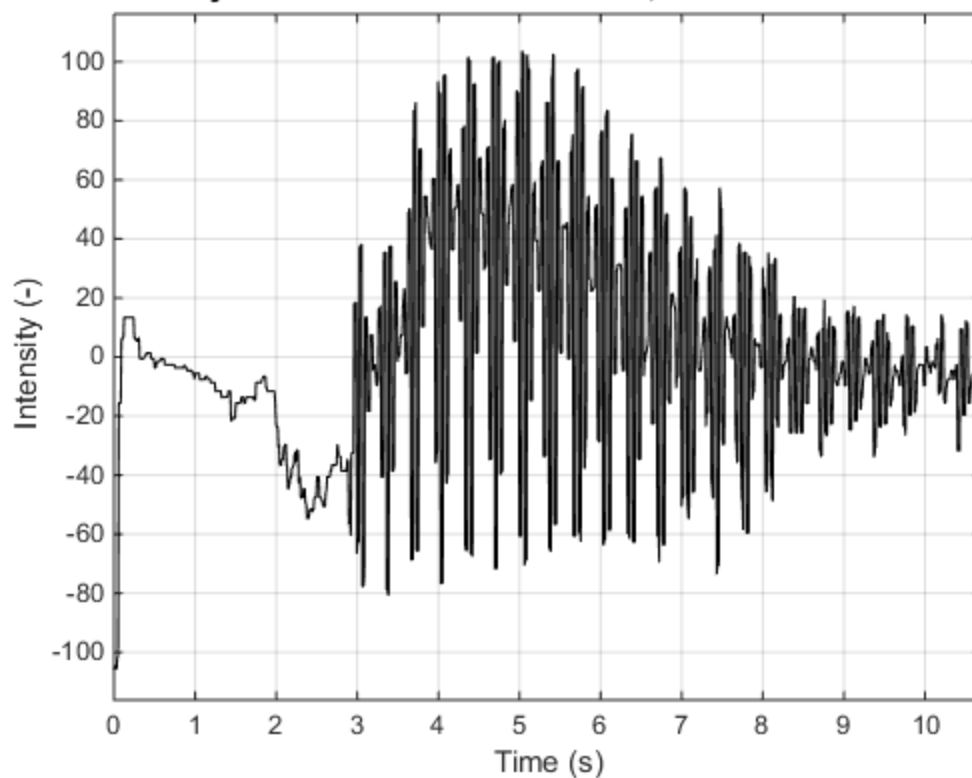
Time history of "S05T2 Dec 1 Canon.MOV", Pixel coordinates: 1031 298



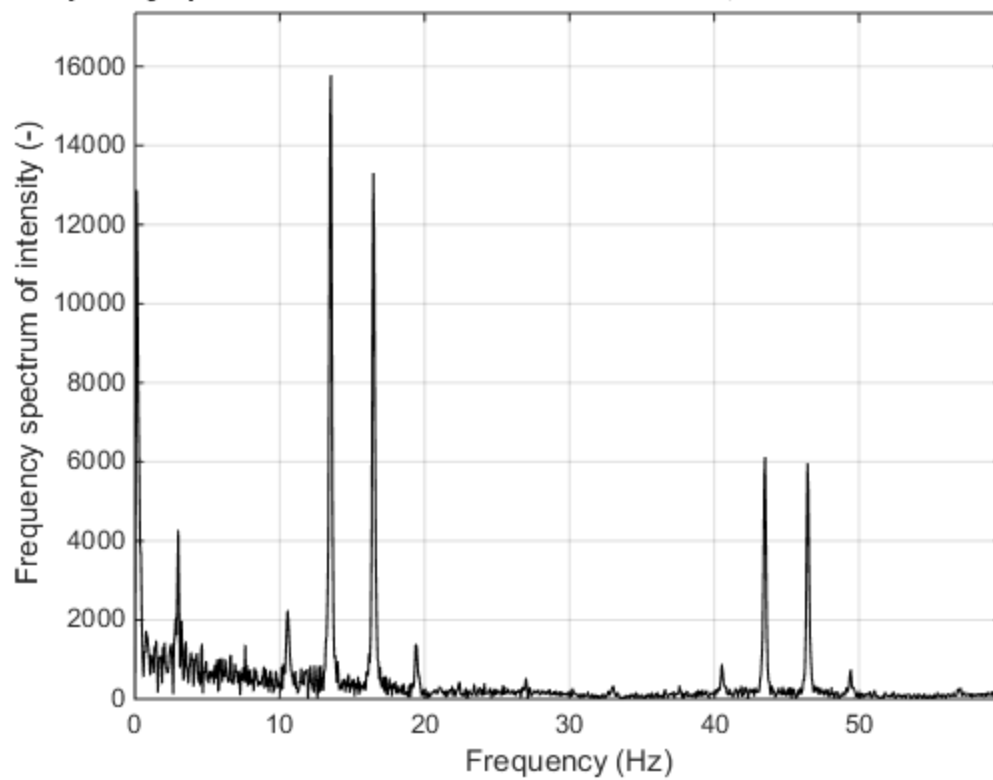
Frequency spectrum of "S05T2 Dec 1 Canon.MOV", Pixel coordinates: 1031 2



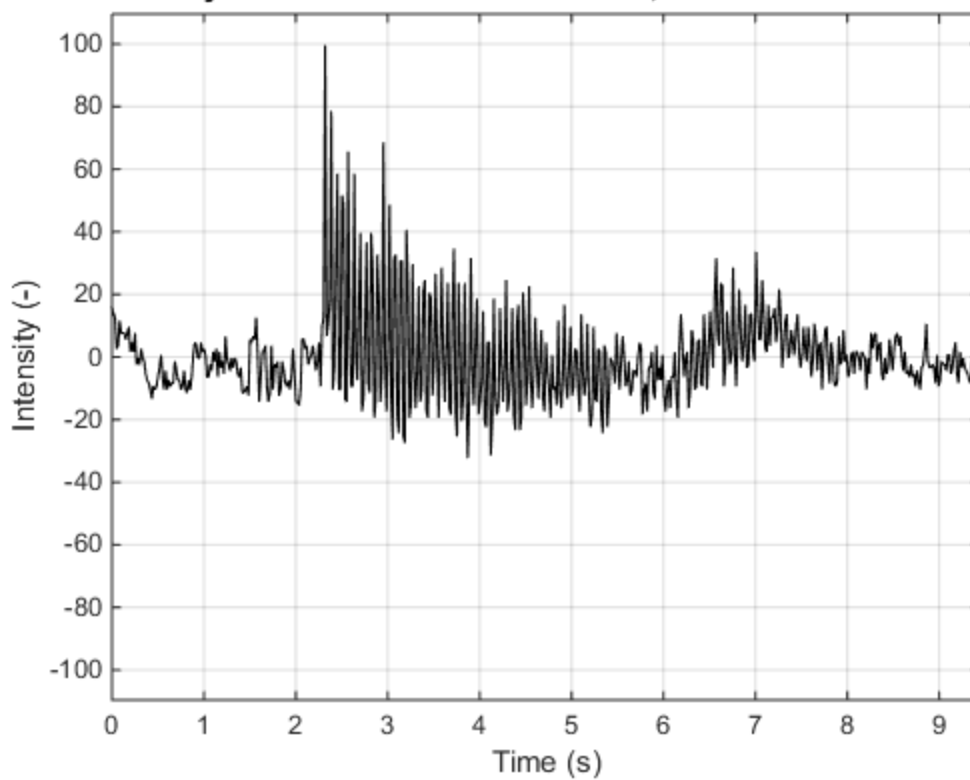
Time history of "S05T2 Dec 1 GoPro.MP4", Pixel coordinates: 564 247



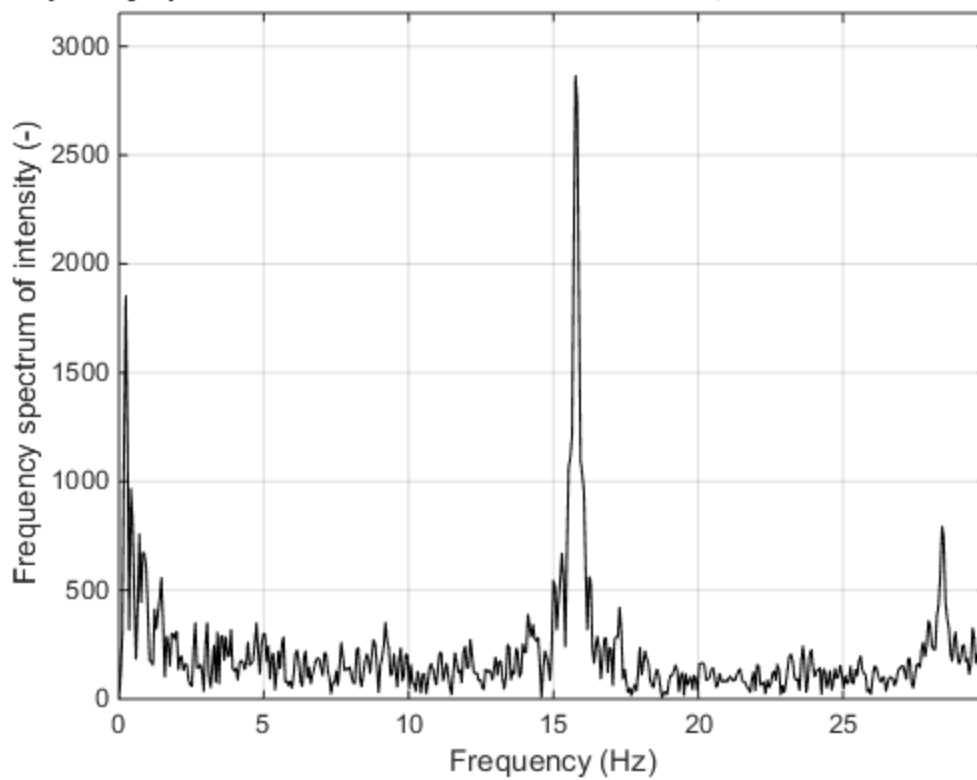
Frequency spectrum of "S05T2 Dec 1 GoPro.MP4", Pixel coordinates: 564 24

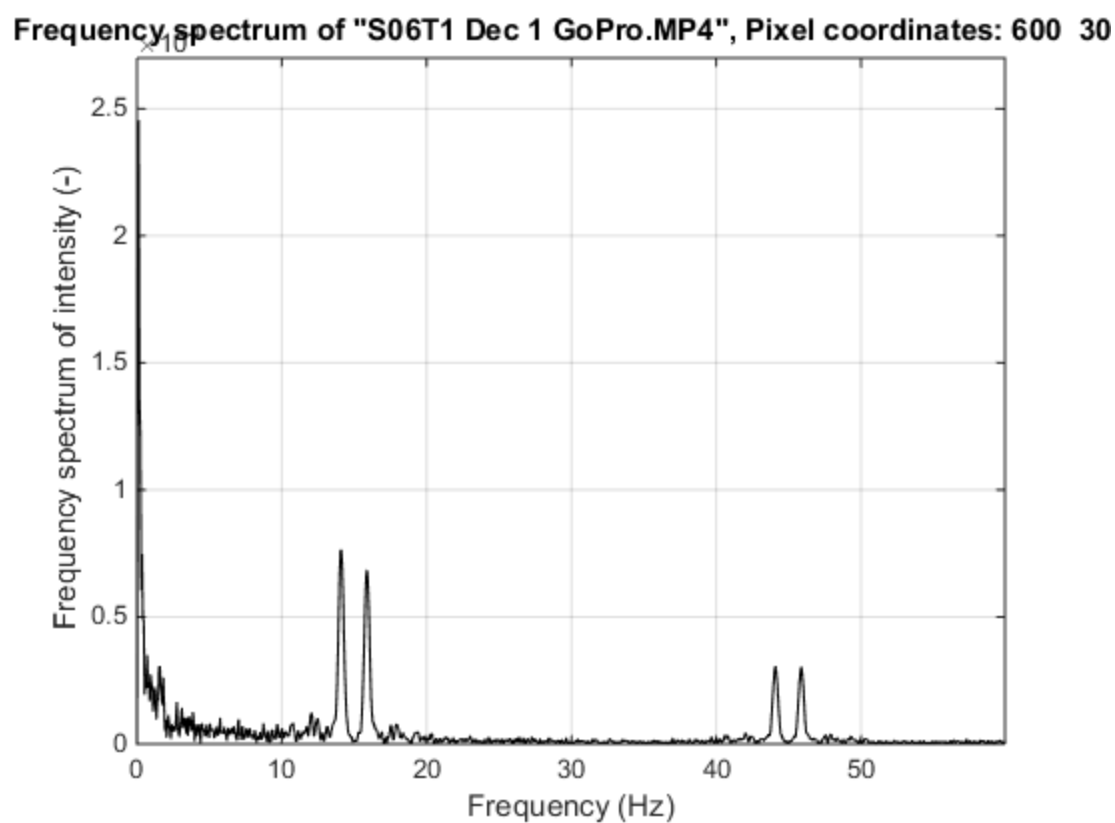
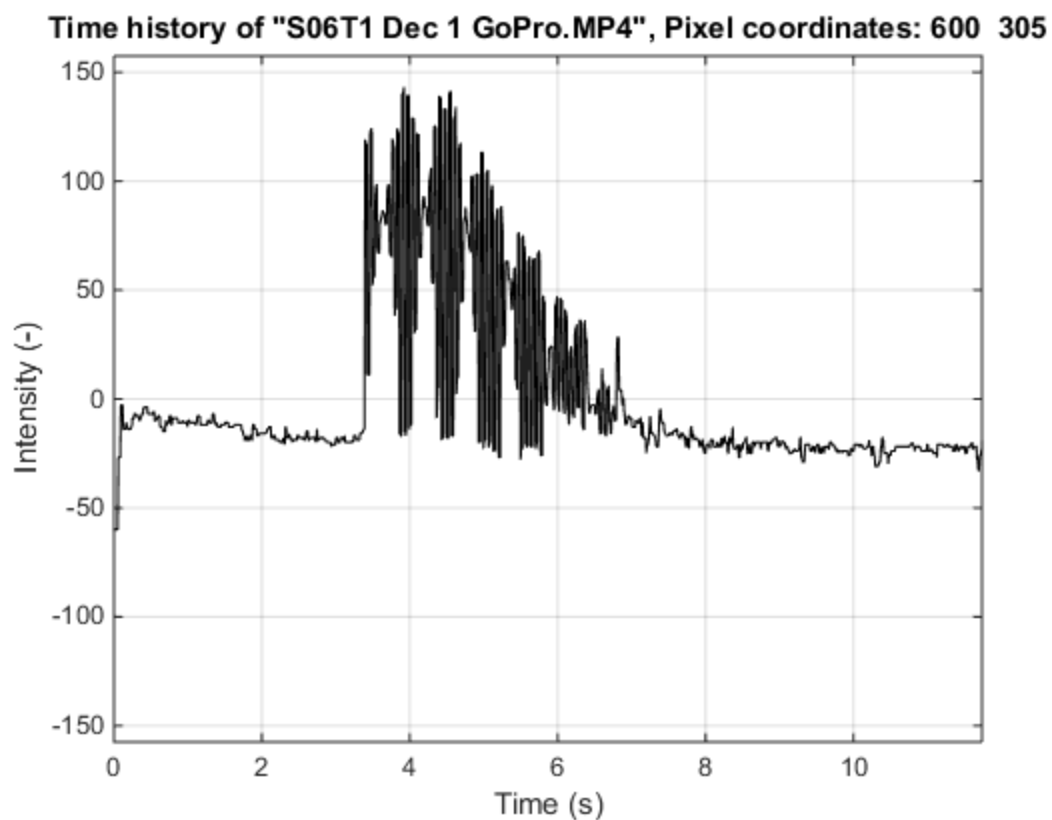


Time history of "S06T1 Dec 1 Canon.MOV", Pixel coordinates: 688 331

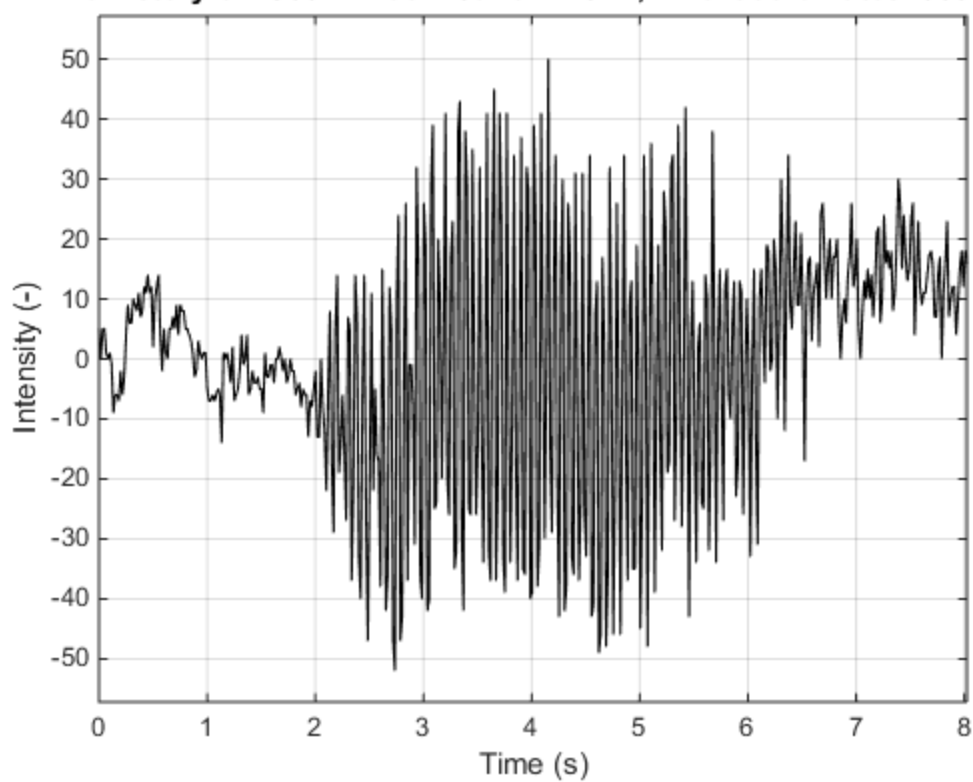


Frequency spectrum of "S06T1 Dec 1 Canon.MOV", Pixel coordinates: 688 33

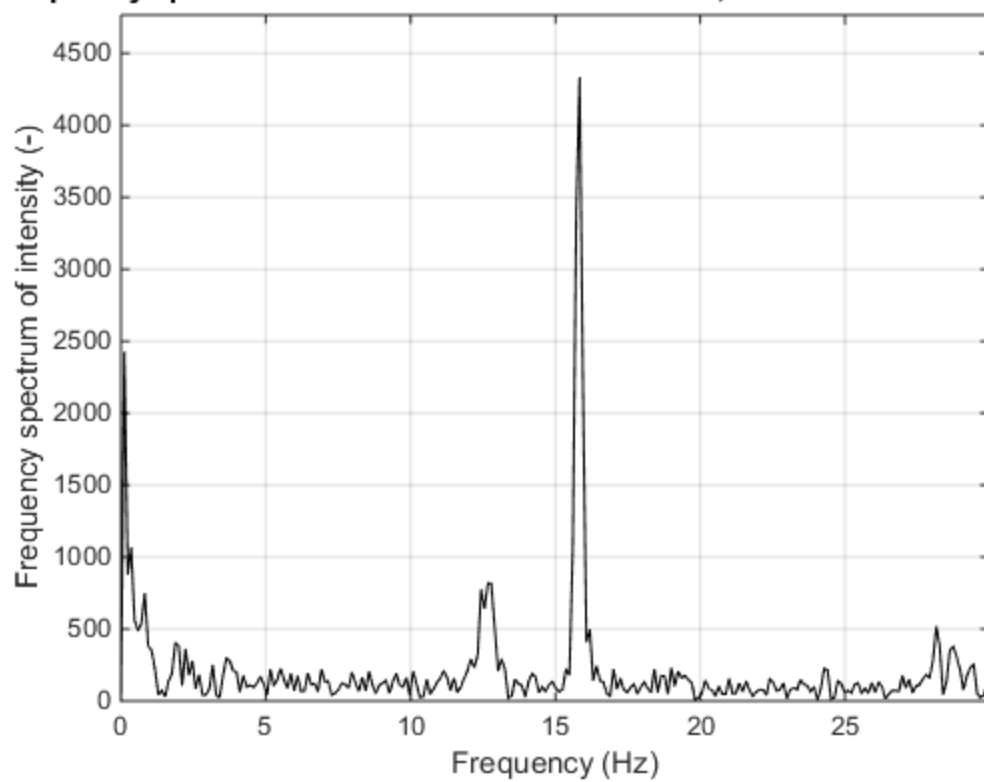




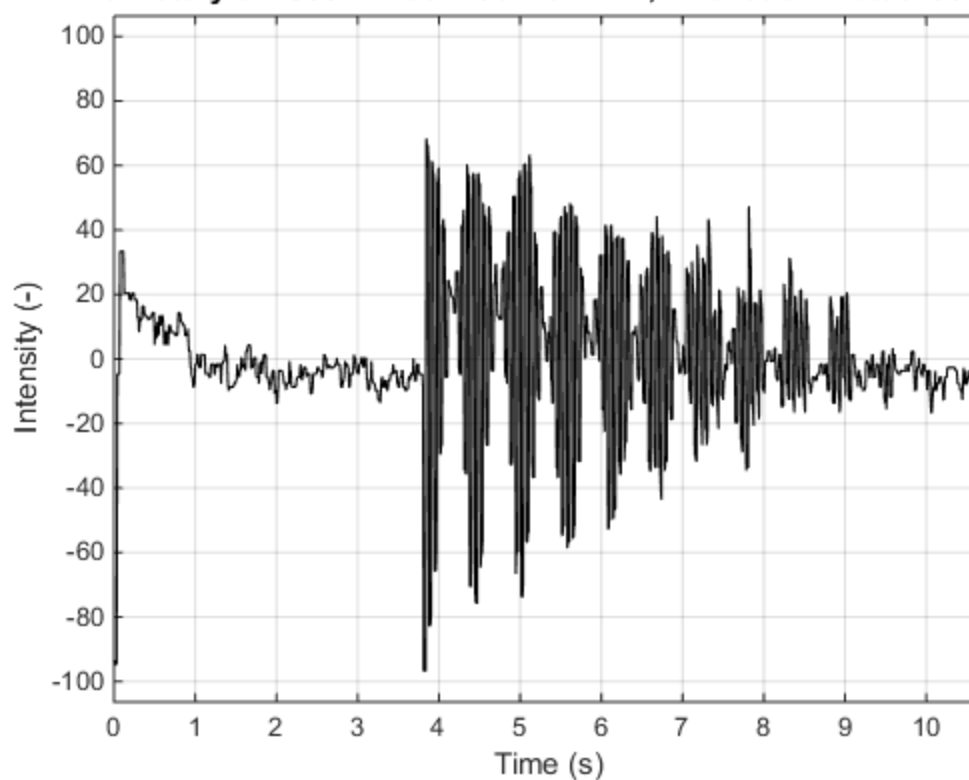
Time history of "S06T2 Dec 1 Canon.MOV", Pixel coordinates: 688 331



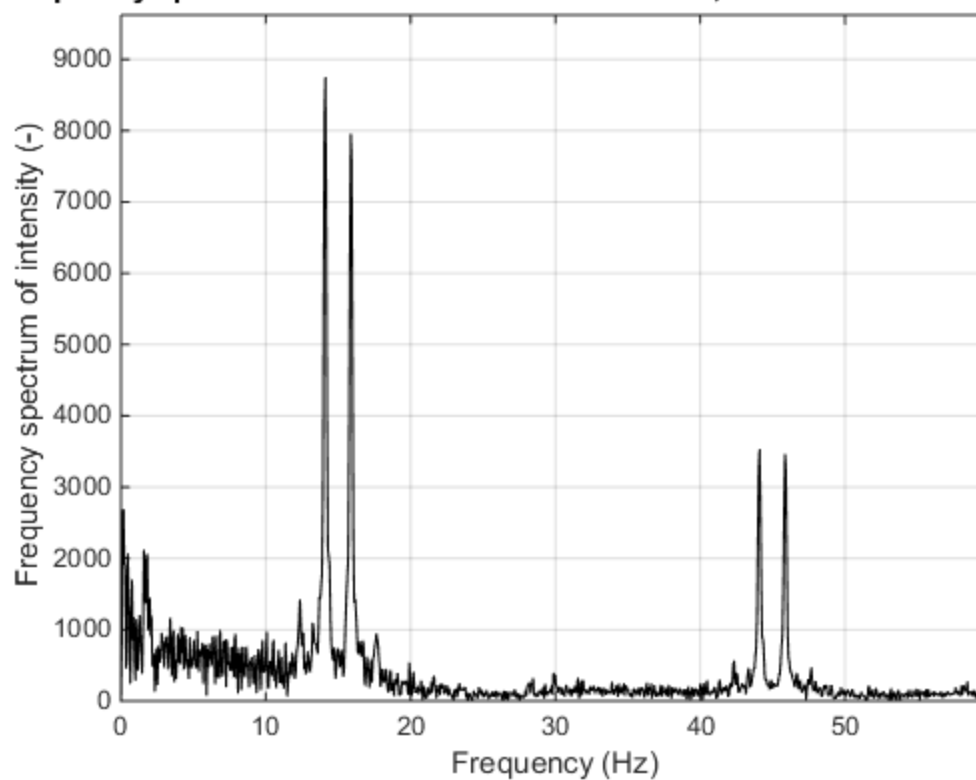
Frequency spectrum of "S06T2 Dec 1 Canon.MOV", Pixel coordinates: 688 33



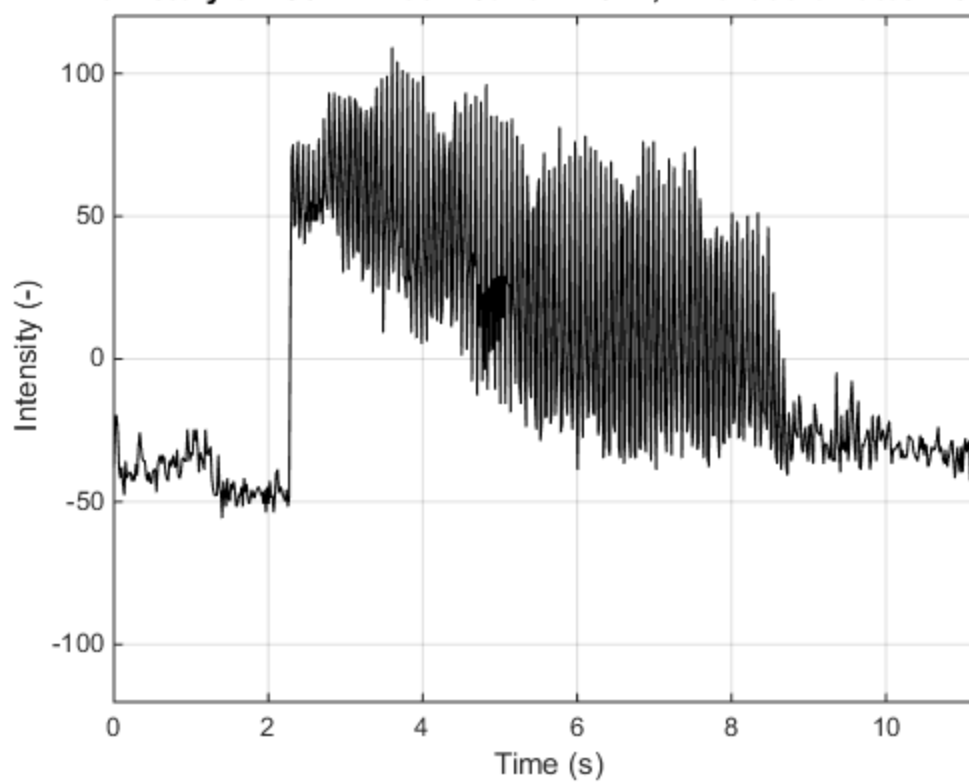
Time history of "S06T2 Dec 1 GoPro.MP4", Pixel coordinates: 560 244



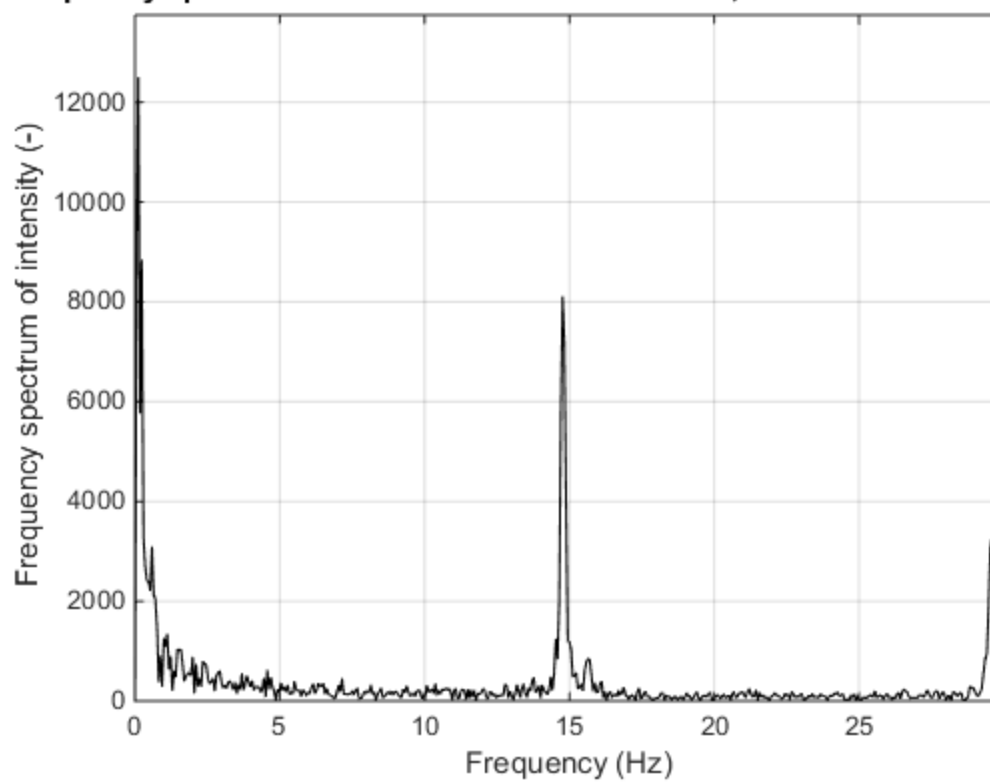
Frequency spectrum of "S06T2 Dec 1 GoPro.MP4", Pixel coordinates: 560 24



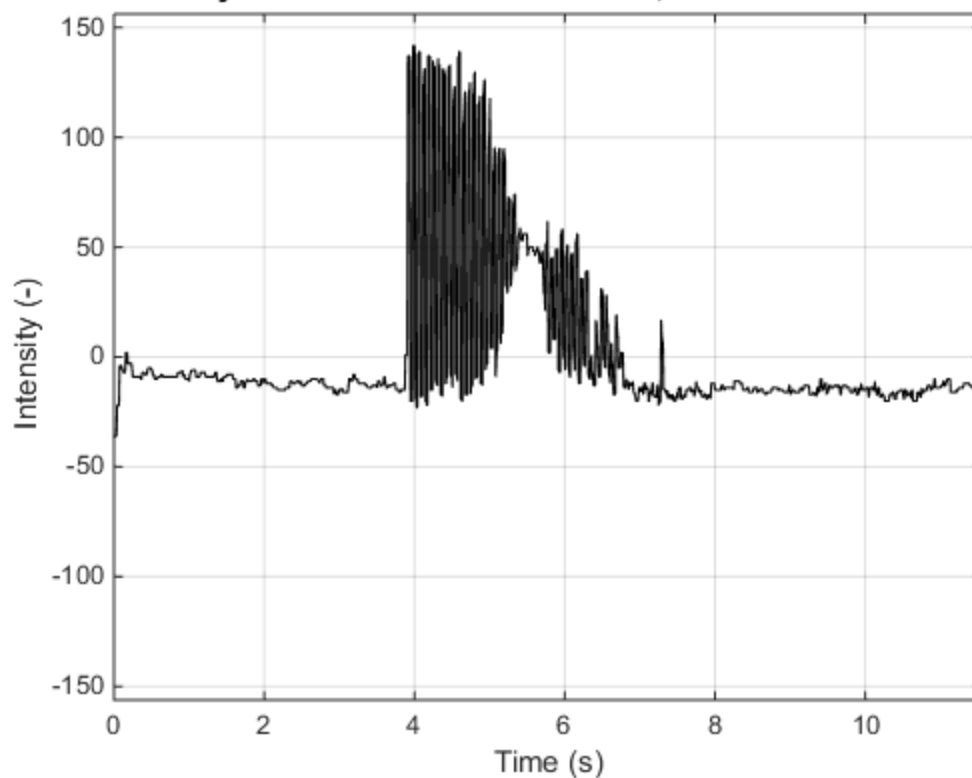
Time history of "S07T1 Dec 1 Canon.MOV", Pixel coordinates: 753 293



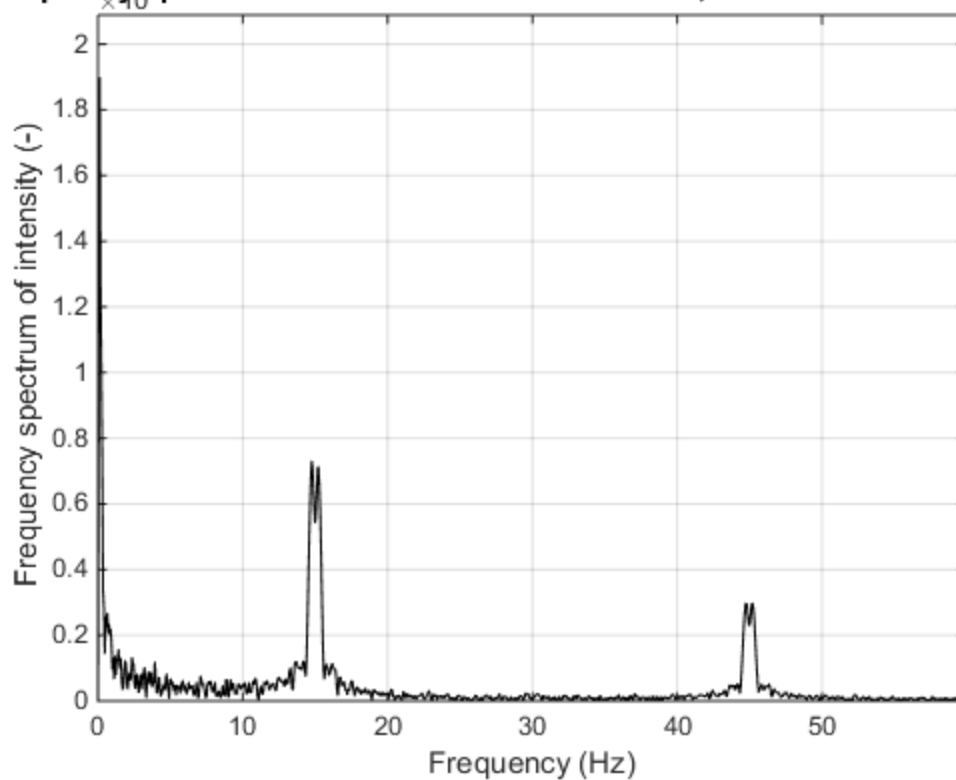
Frequency spectrum of "S07T1 Dec 1 Canon.MOV", Pixel coordinates: 753 29



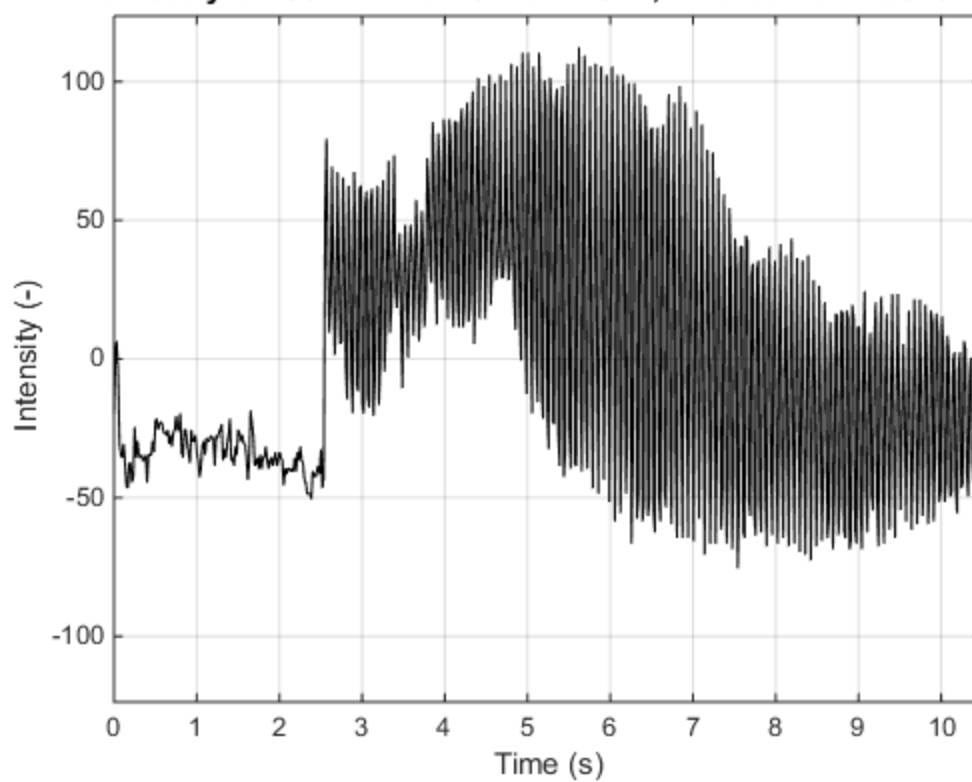
Time history of "S07T1 Dec 1 GoPro.MP4", Pixel coordinates: 52 327



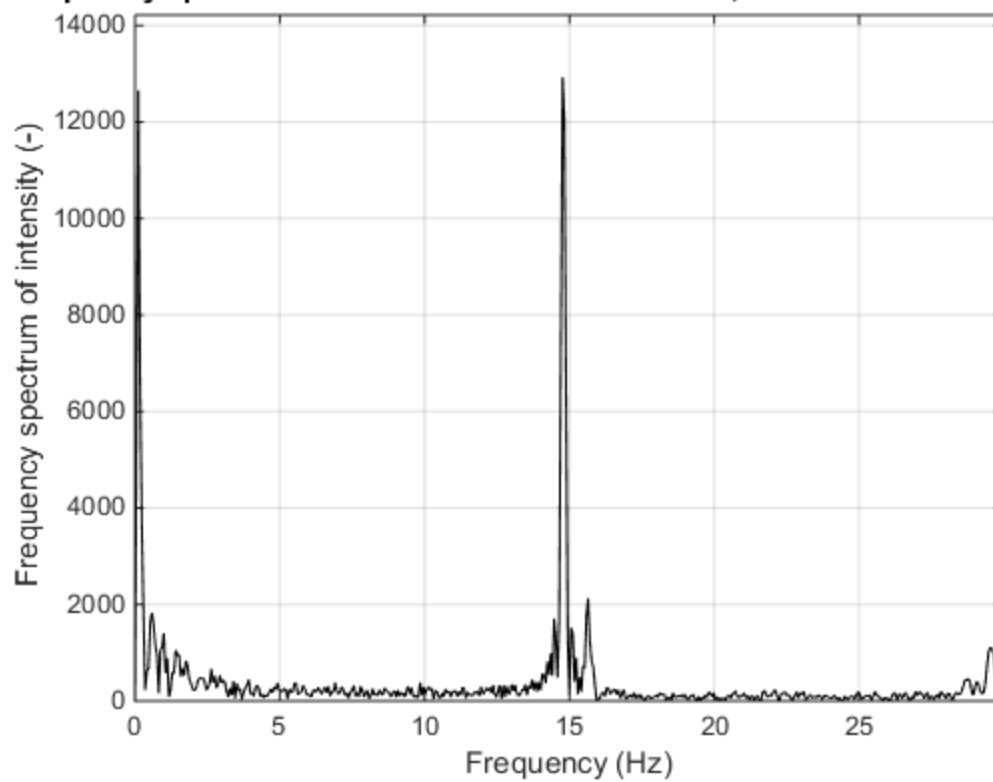
Frequency spectrum of "S07T1 Dec 1 GoPro.MP4", Pixel coordinates: 52 327



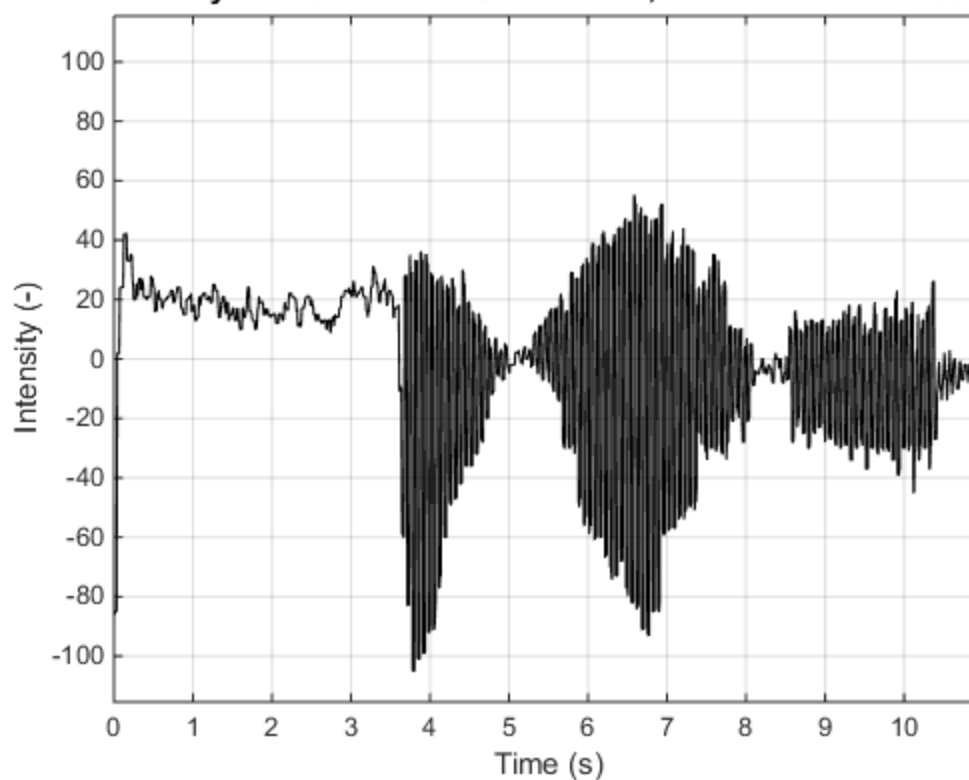
Time history of "S07T2 Dec 1 Canon.MOV", Pixel coordinates: 520 193



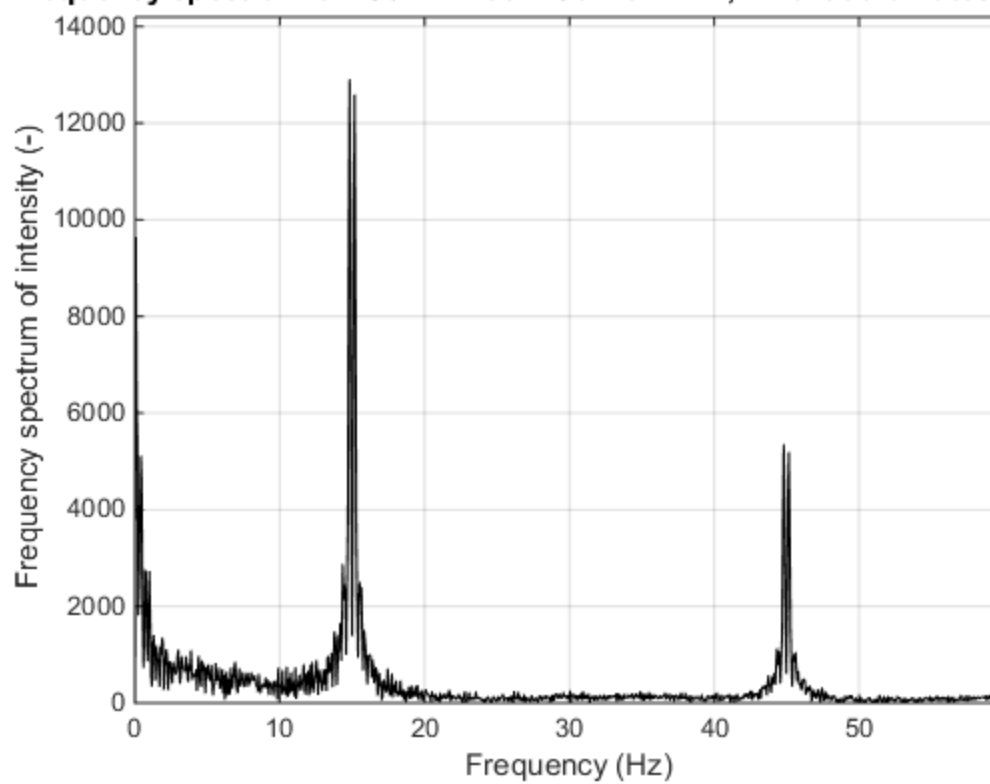
Frequency spectrum of "S07T2 Dec 1 Canon.MOV", Pixel coordinates: 520 19



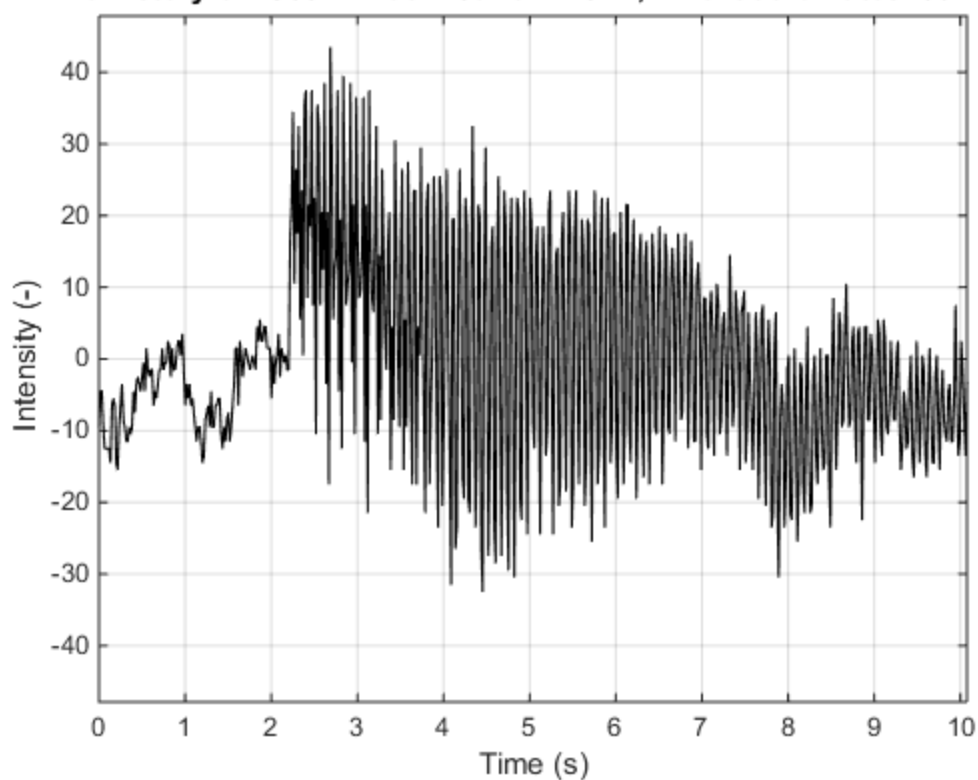
Time history of "S07T2 Dec 1 GoPro.MP4", Pixel coordinates: 800 244



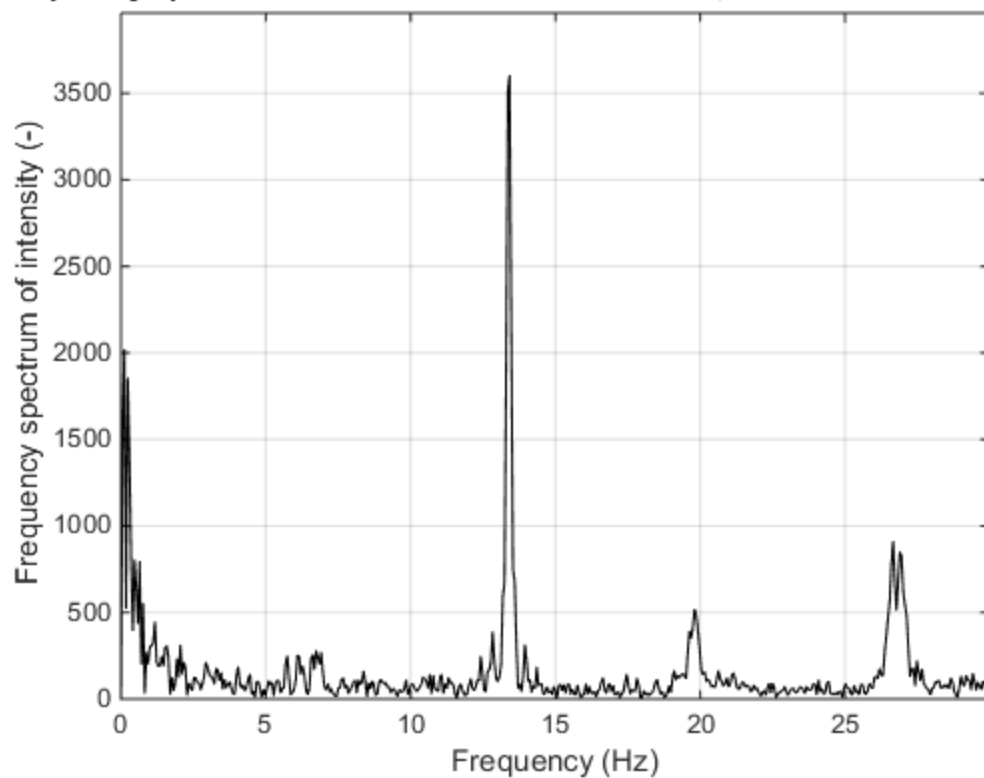
Frequency spectrum of "S07T2 Dec 1 GoPro.MP4", Pixel coordinates: 800 24



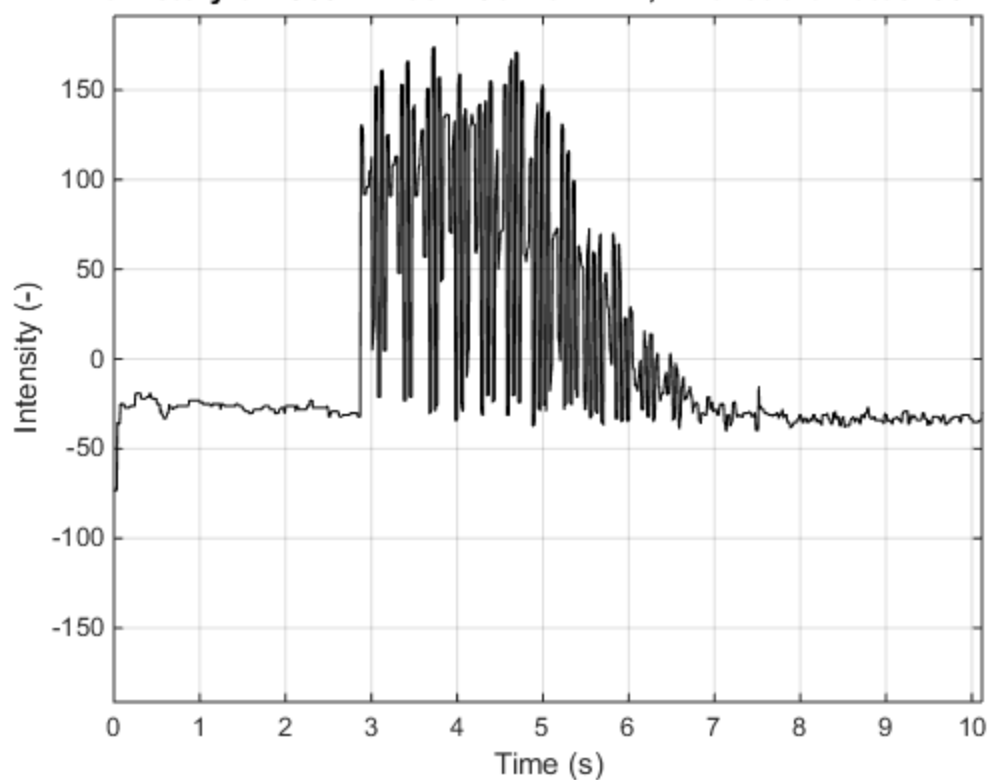
Time history of "S08T1 Dec 1 Canon.MOV", Pixel coordinates: 691 315



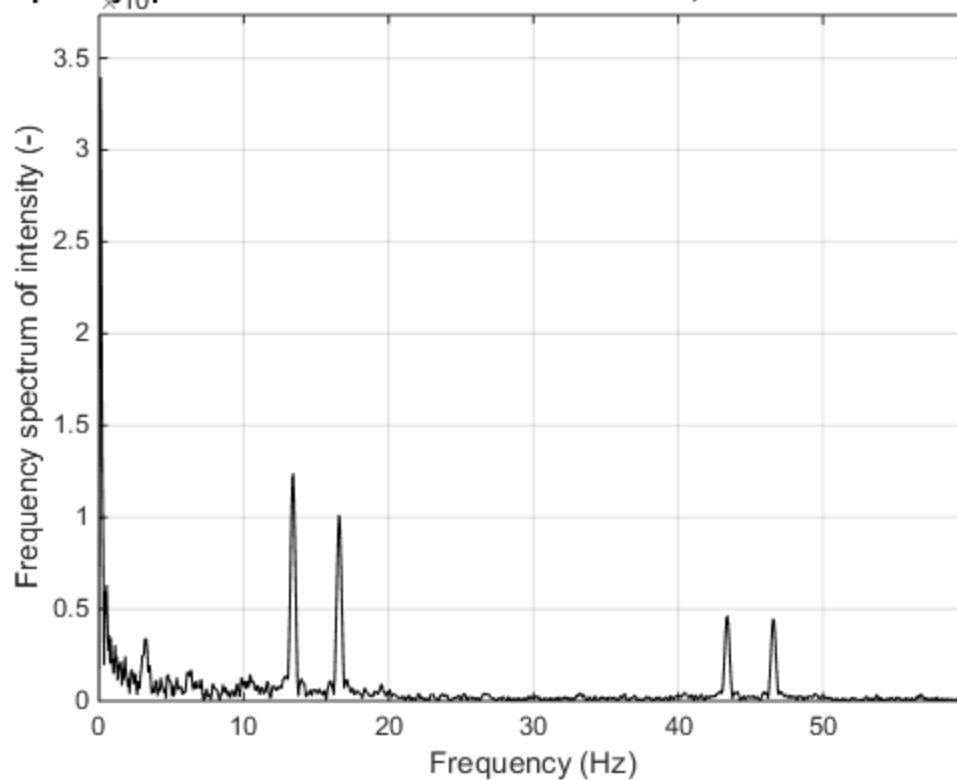
Frequency spectrum of "S08T1 Dec 1 Canon.MOV", Pixel coordinates: 691 31



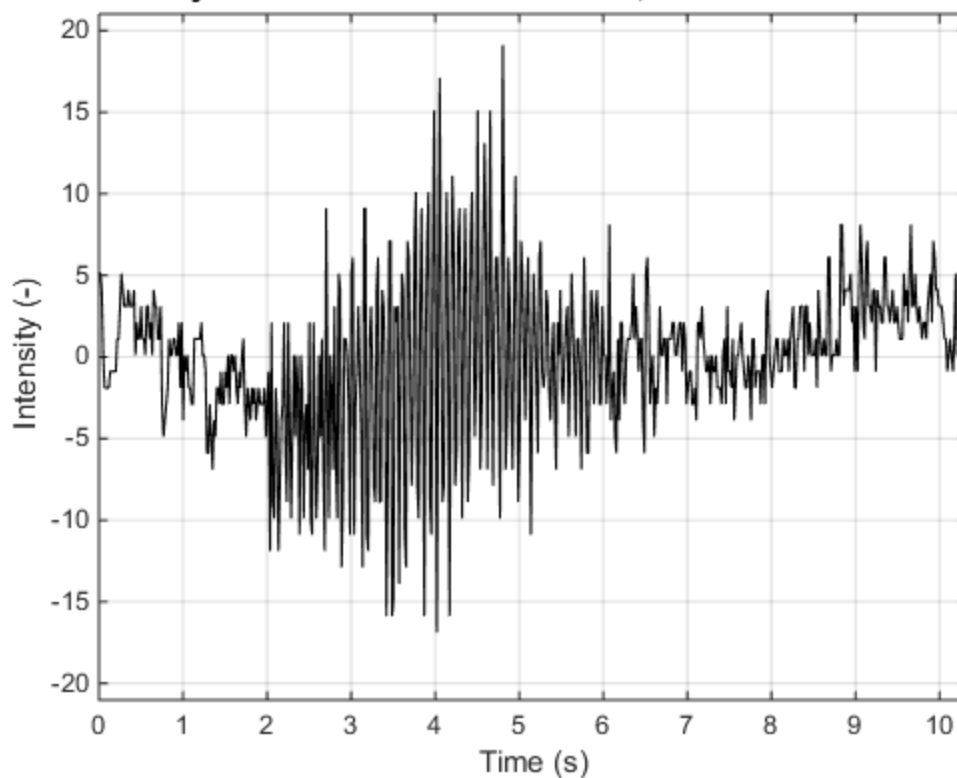
Time history of "S08T1 Dec 1 GoPro.MP4", Pixel coordinates: 587 315



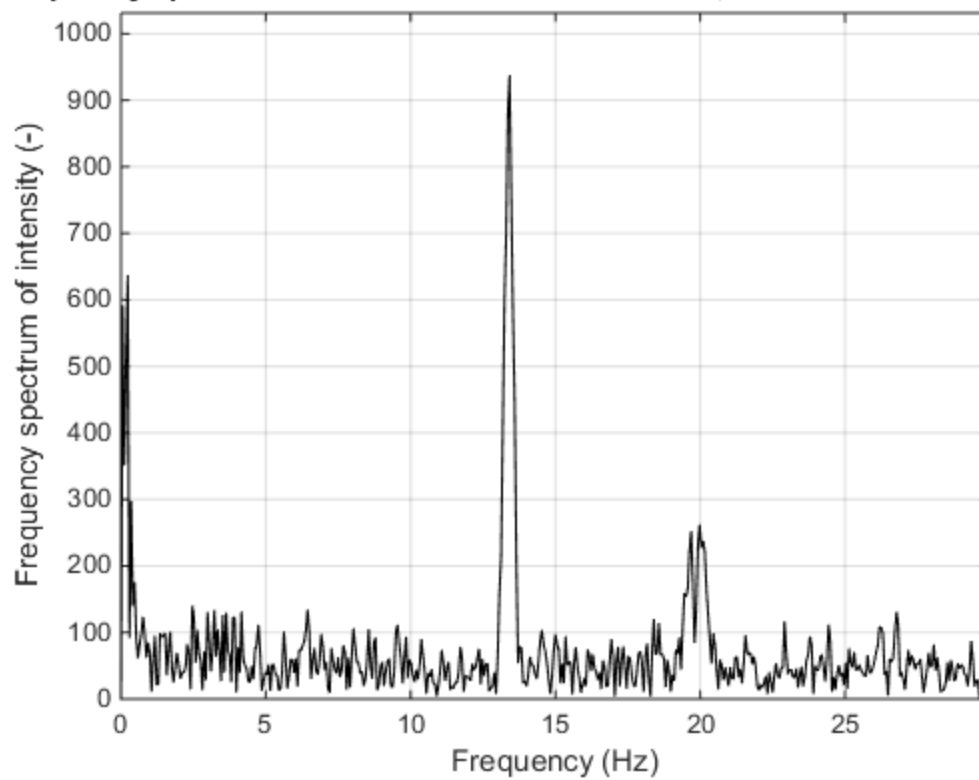
Frequency spectrum of "S08T1 Dec 1 GoPro.MP4", Pixel coordinates: 587 31



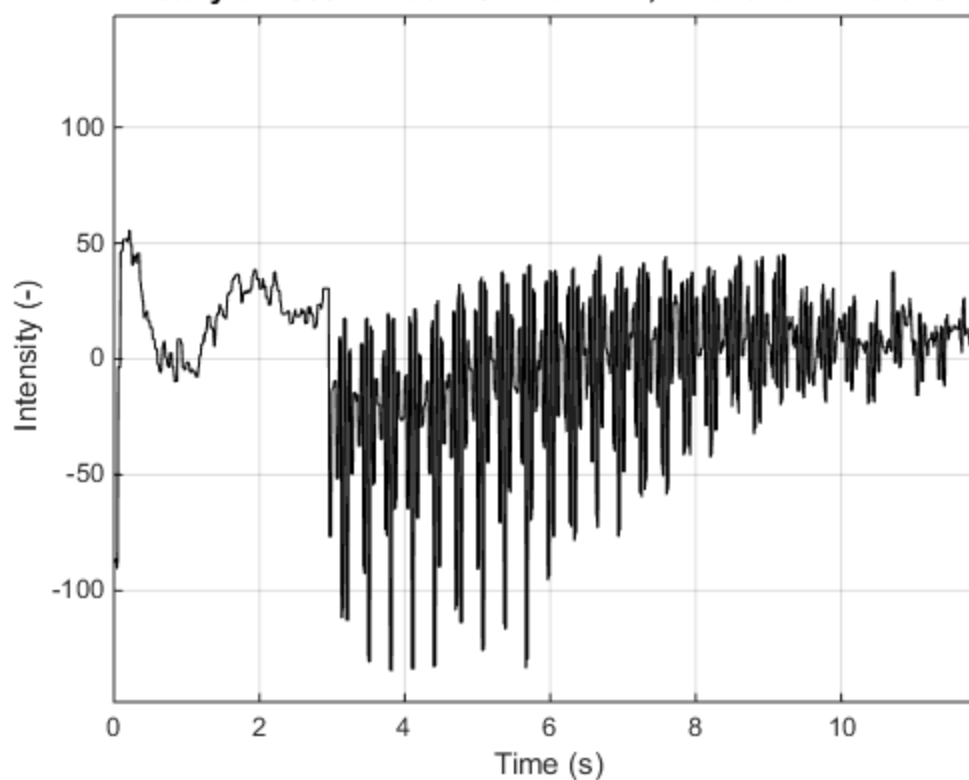
Time history of "S08T2 Dec 1 Canon.MOV", Pixel coordinates: 691 315



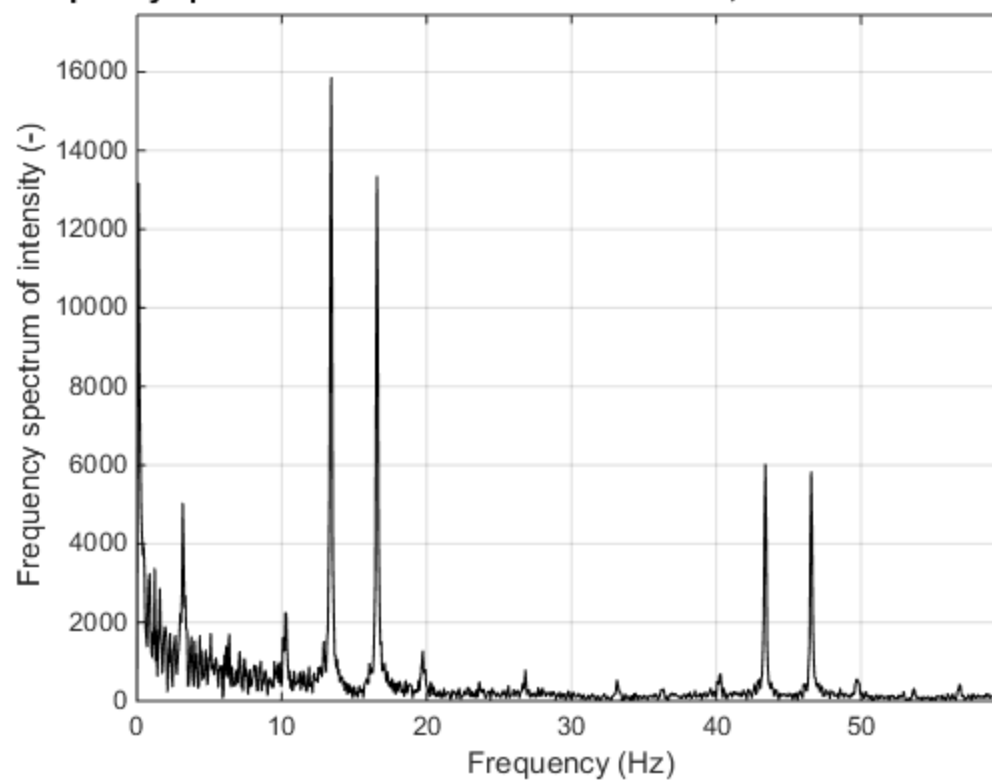
Frequency spectrum of "S08T2 Dec 1 Canon.MOV", Pixel coordinates: 691 31



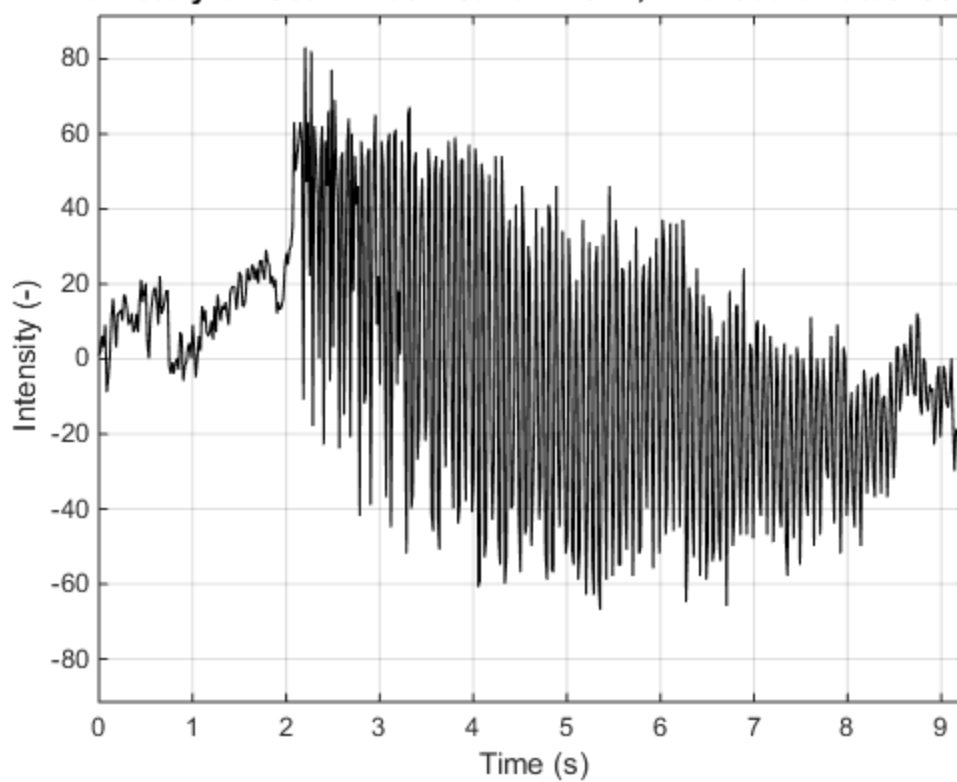
Time history of "S08T2 Dec 1 GoPro.MP4", Pixel coordinates: 611 244



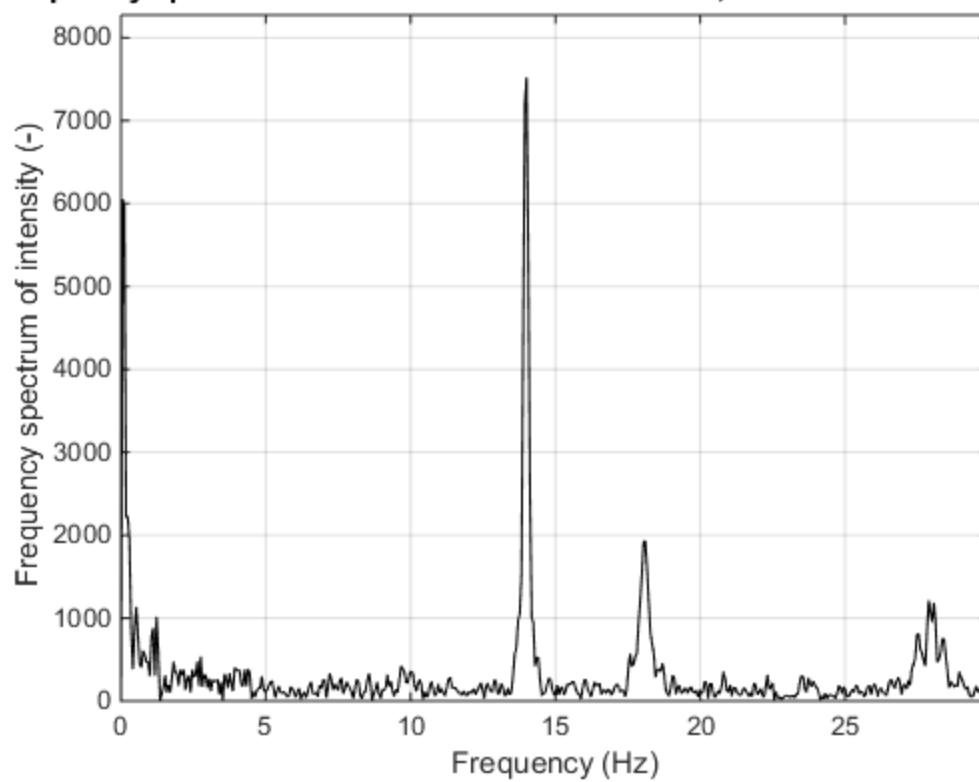
Frequency spectrum of "S08T2 Dec 1 GoPro.MP4", Pixel coordinates: 611 24



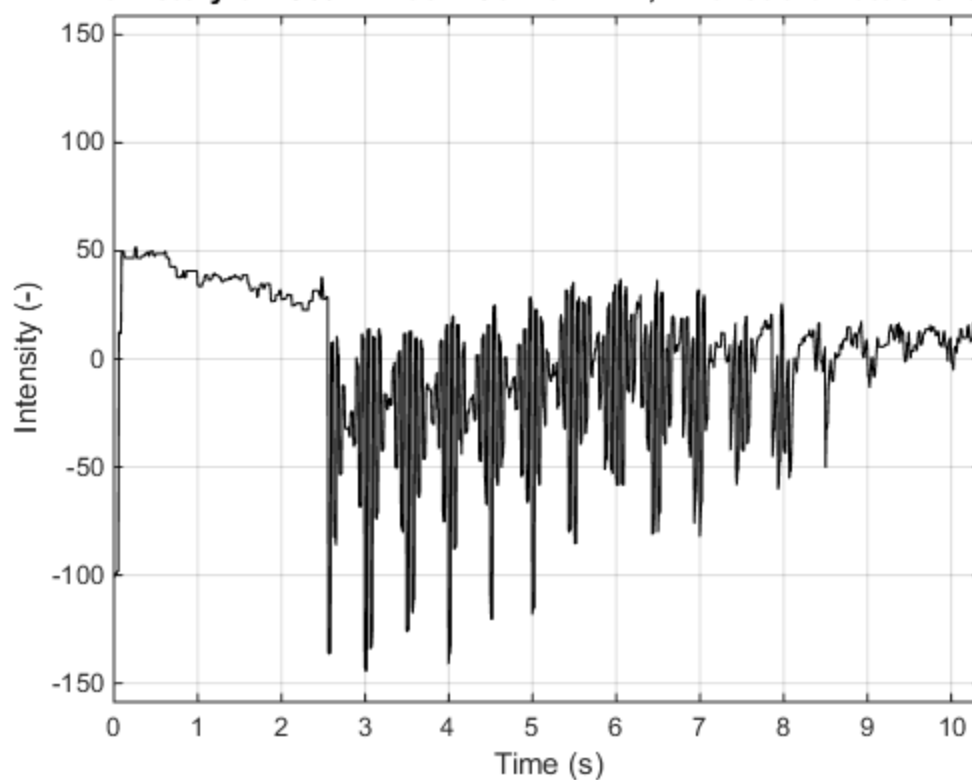
Time history of "S09T1 Dec 1 Canon.MOV", Pixel coordinates: 882 376



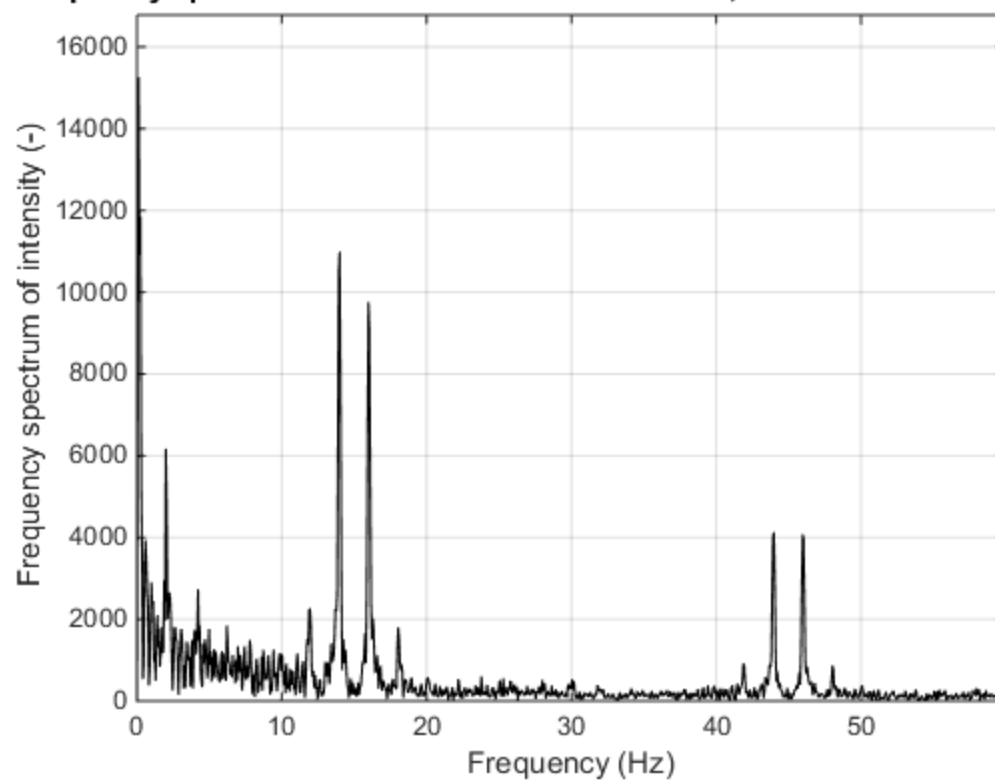
Frequency spectrum of "S09T1 Dec 1 Canon.MOV", Pixel coordinates: 882 37



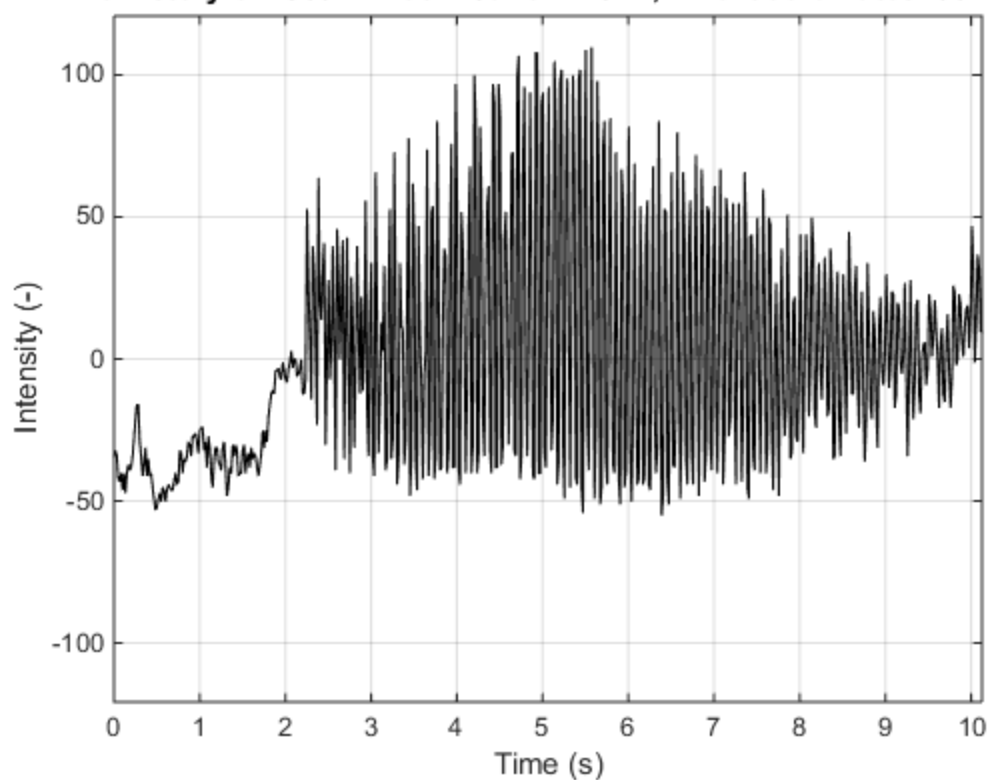
Time history of "S09T1 Dec 1 GoPro.MP4", Pixel coordinates: 640 291



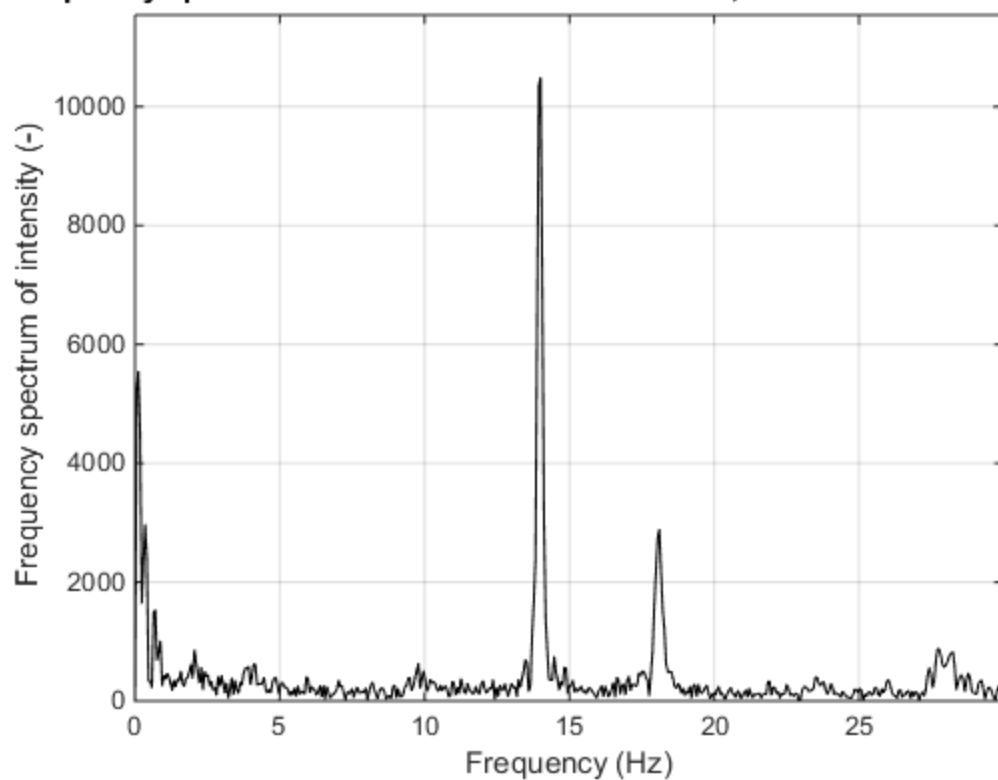
Frequency spectrum of "S09T1 Dec 1 GoPro.MP4", Pixel coordinates: 640 29



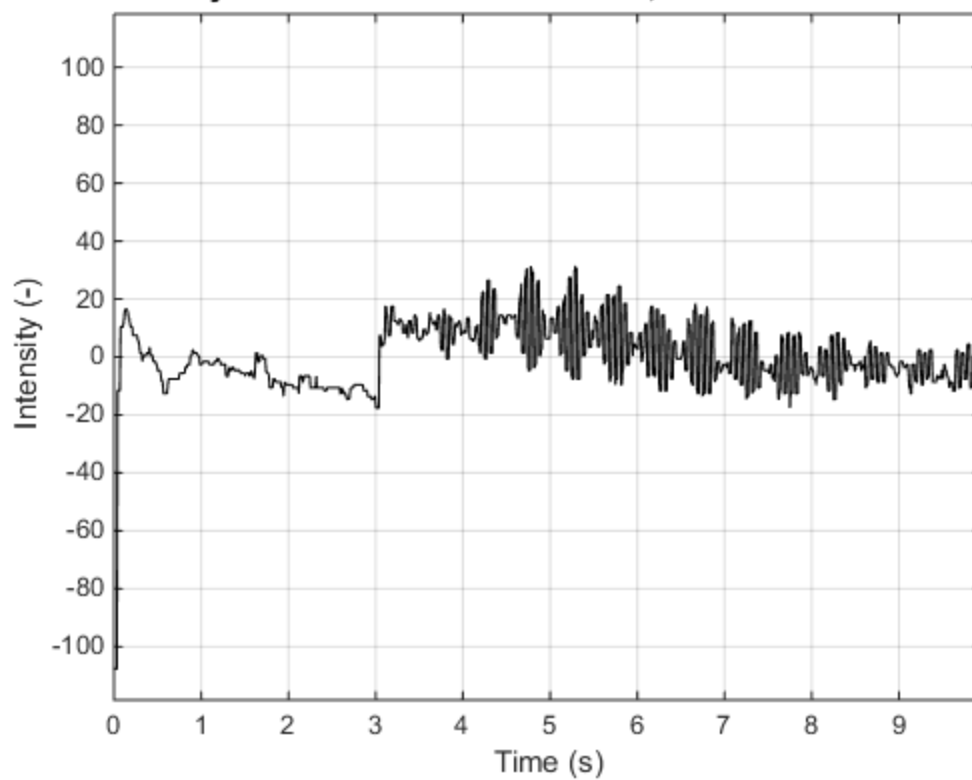
Time history of "S09T2 Dec 1 Canon.MOV", Pixel coordinates: 604 429



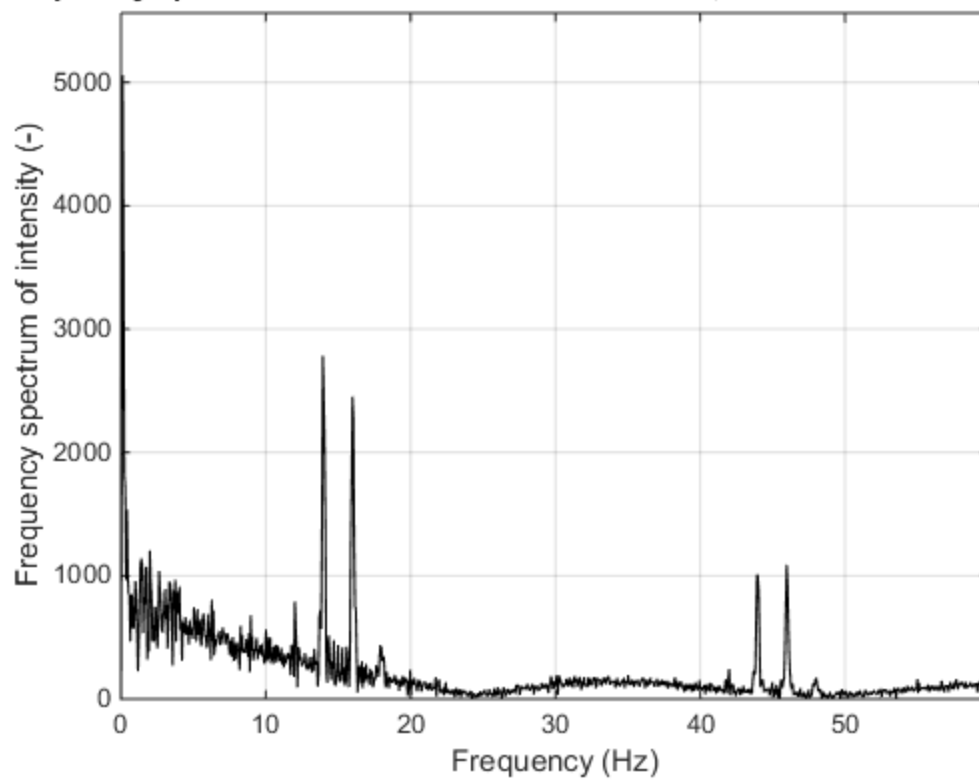
Frequency spectrum of "S09T2 Dec 1 Canon.MOV", Pixel coordinates: 604 42



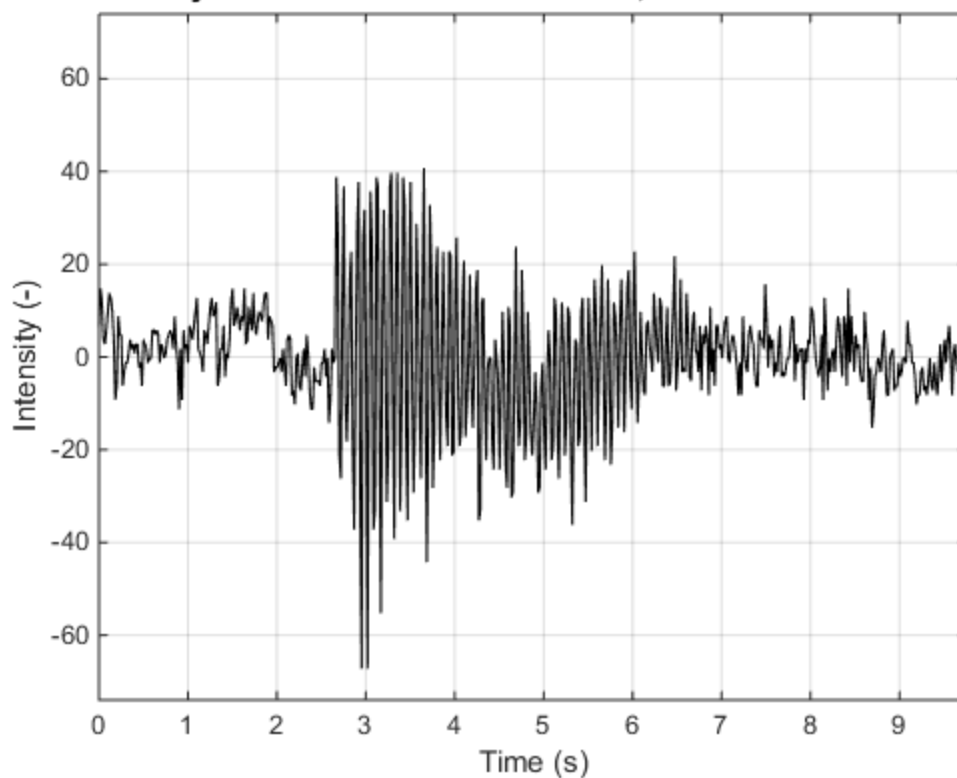
Time history of "S09T2 Dec 1 GoPro.MP4", Pixel coordinates: 640 291



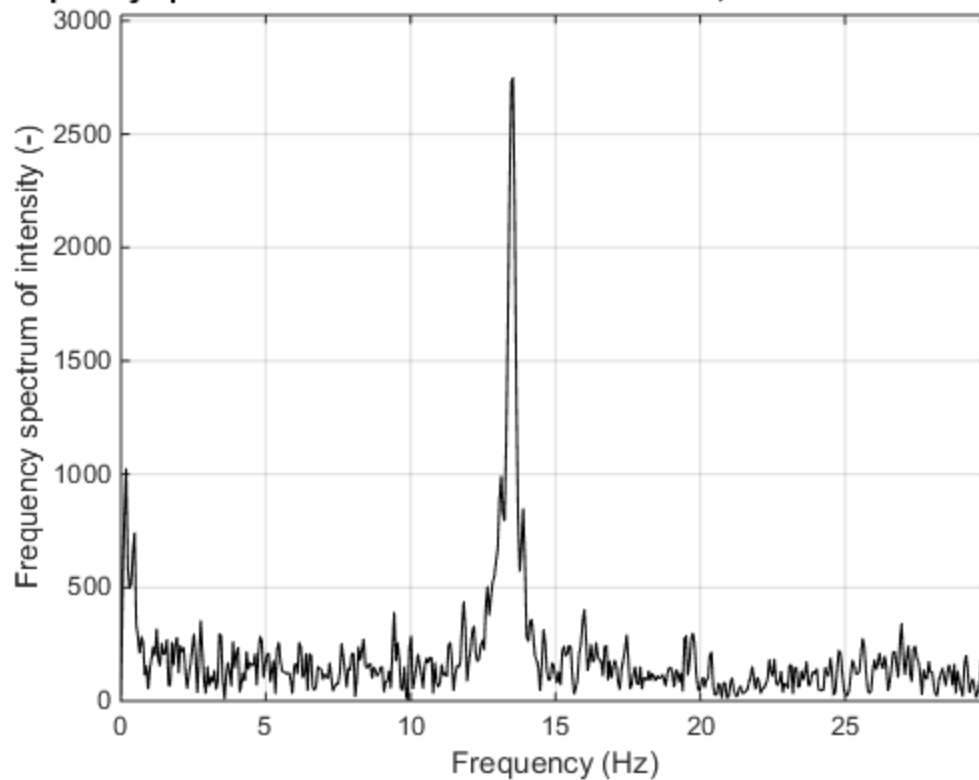
Frequency spectrum of "S09T2 Dec 1 GoPro.MP4", Pixel coordinates: 640 29



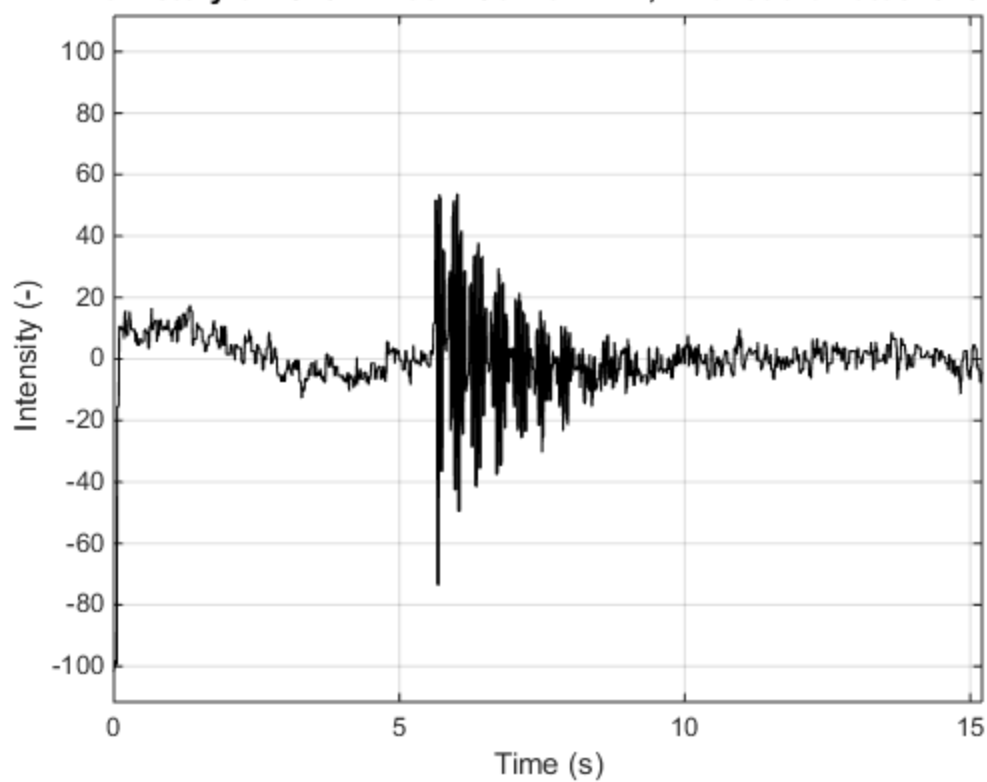
Time history of "S10T1 Dec 1 Canon.MOV", Pixel coordinates: 285 380



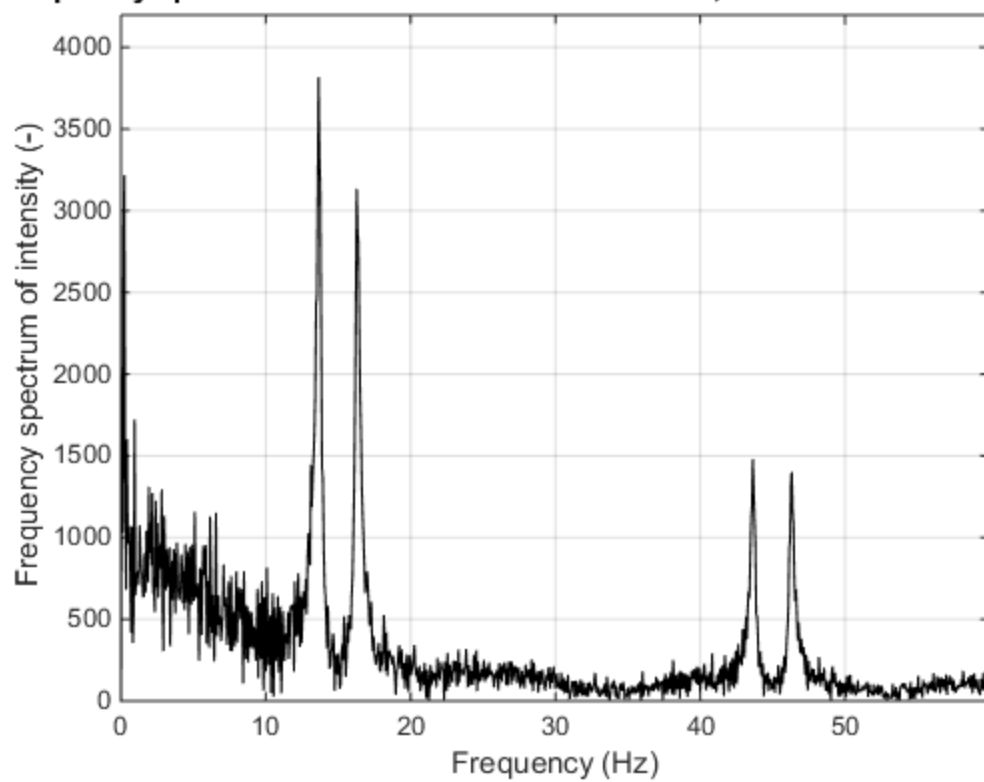
Frequency spectrum of "S10T1 Dec 1 Canon.MOV", Pixel coordinates: 285 38



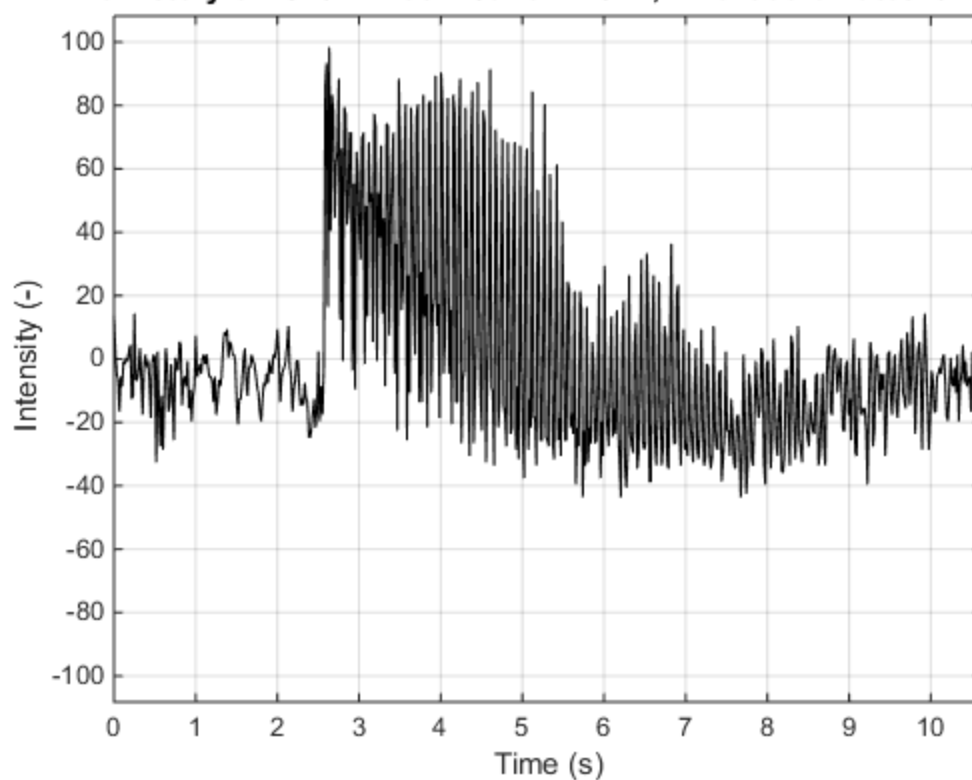
Time history of "S10T1 Dec 1 GoPro.MP4", Pixel coordinates: 548 370



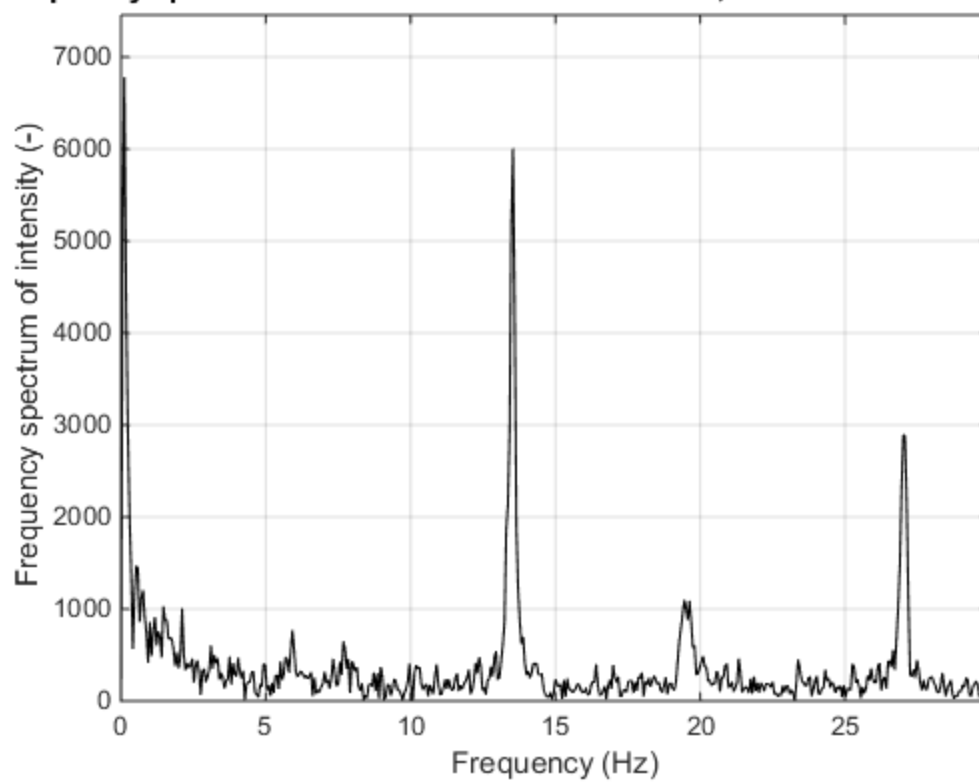
Frequency spectrum of "S10T1 Dec 1 GoPro.MP4", Pixel coordinates: 548 37



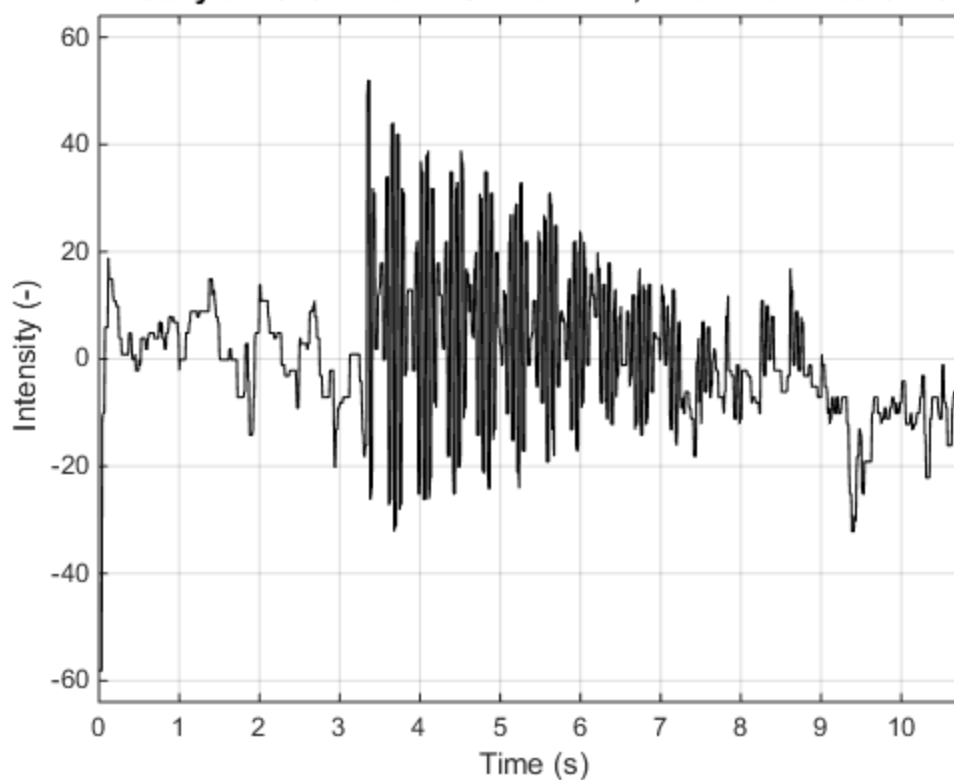
Time history of "S10T2 Dec 1 Canon.MOV", Pixel coordinates: 928 302



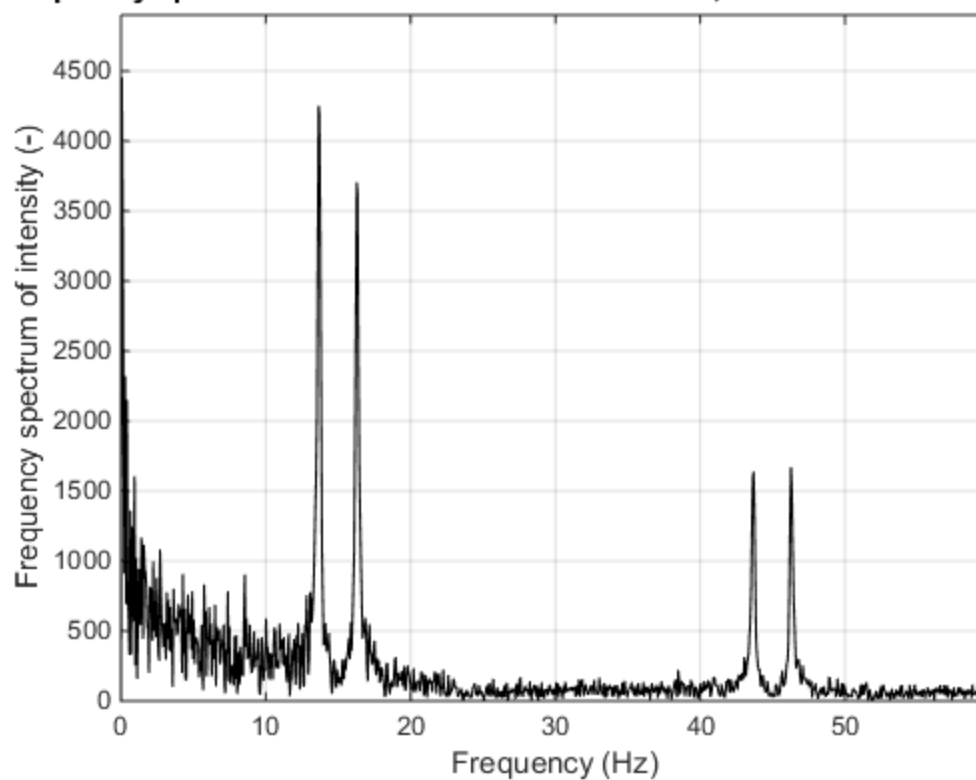
Frequency spectrum of "S10T2 Dec 1 Canon.MOV", Pixel coordinates: 928 302



Time history of "S10T2 Dec 1 GoPro.MP4", Pixel coordinates: 407 394



Frequency spectrum of "S10T2 Dec 1 GoPro.MP4", Pixel coordinates: 407 39



Appendix G – VVS Figures from ASTM Standard 2x4 Experiments

- The first highlighted section contains the specimen designation followed by the test number.
 - In this example: Specimen 1, Test 1
- The second highlighted section contains the camera which was used.
 - In this example: Canon

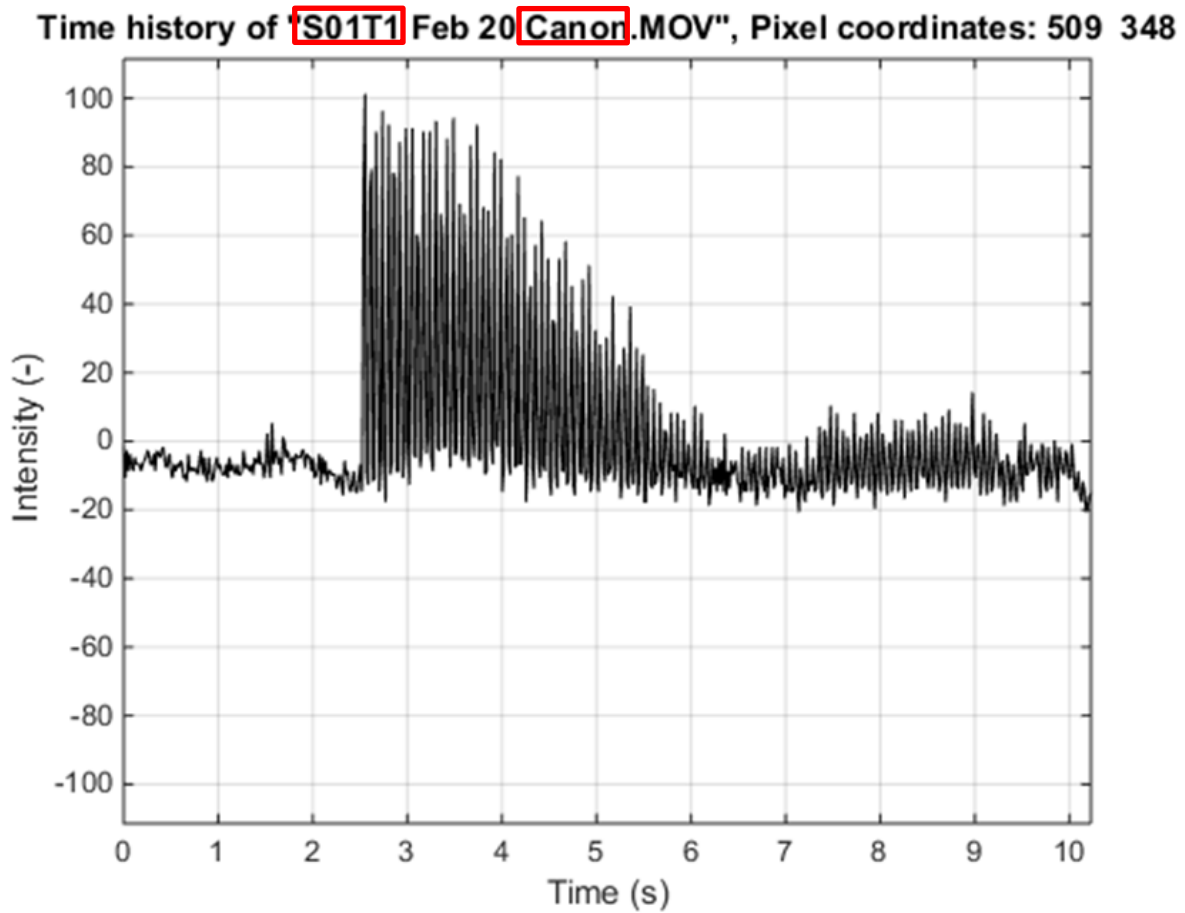
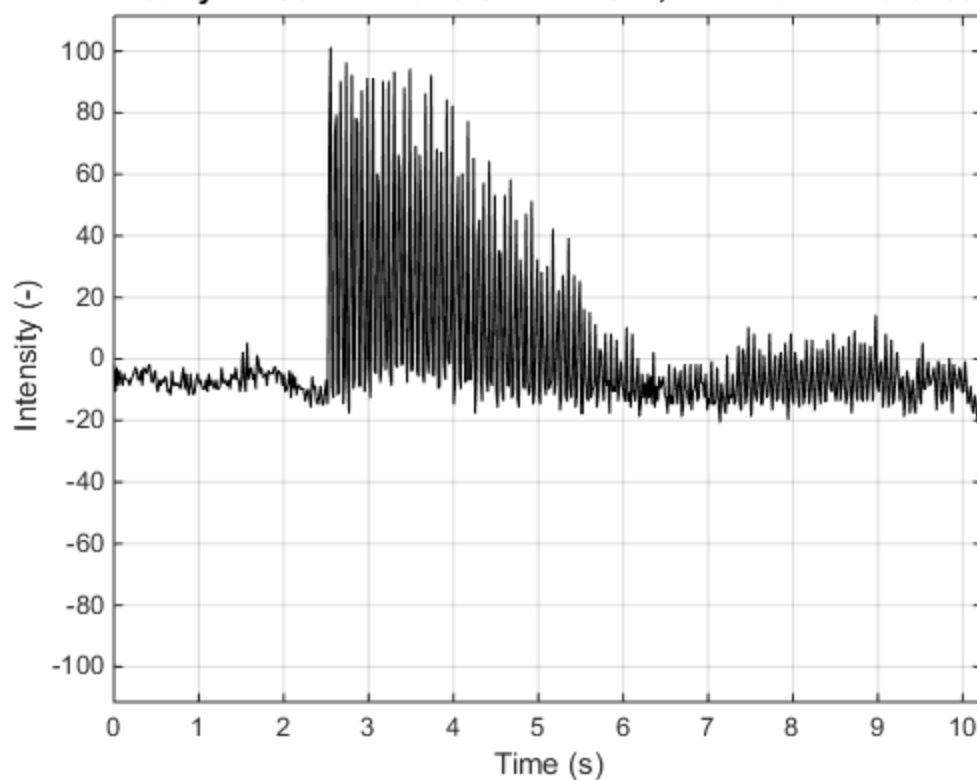
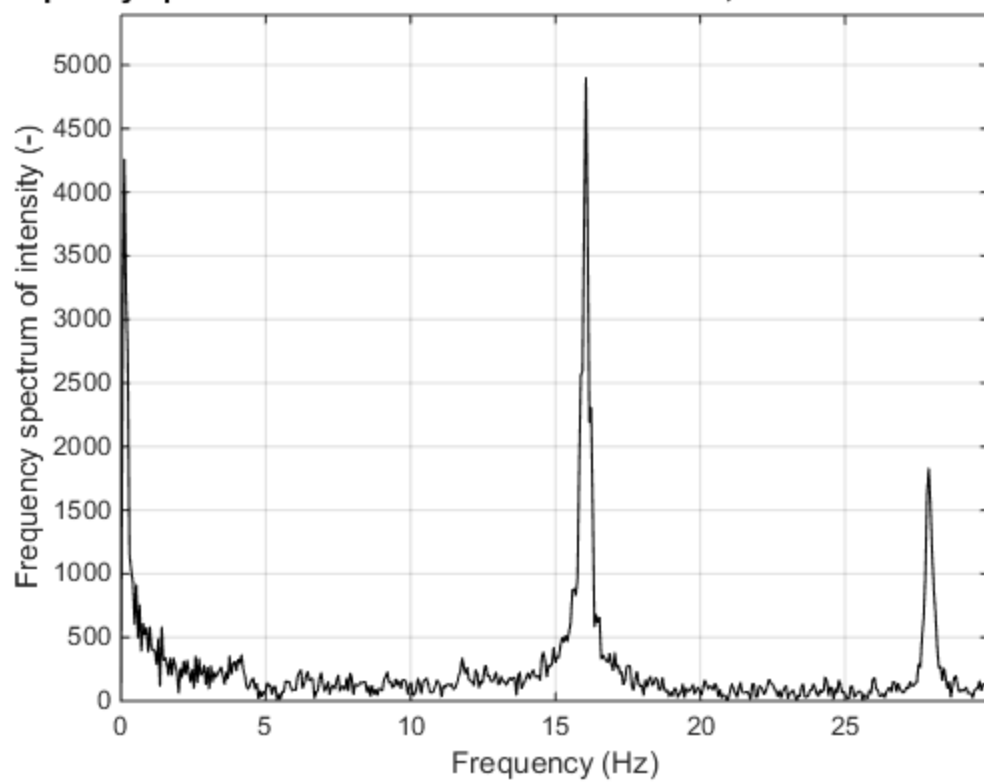


Figure F12 - Key for 2x4 ASTM Standard Figures

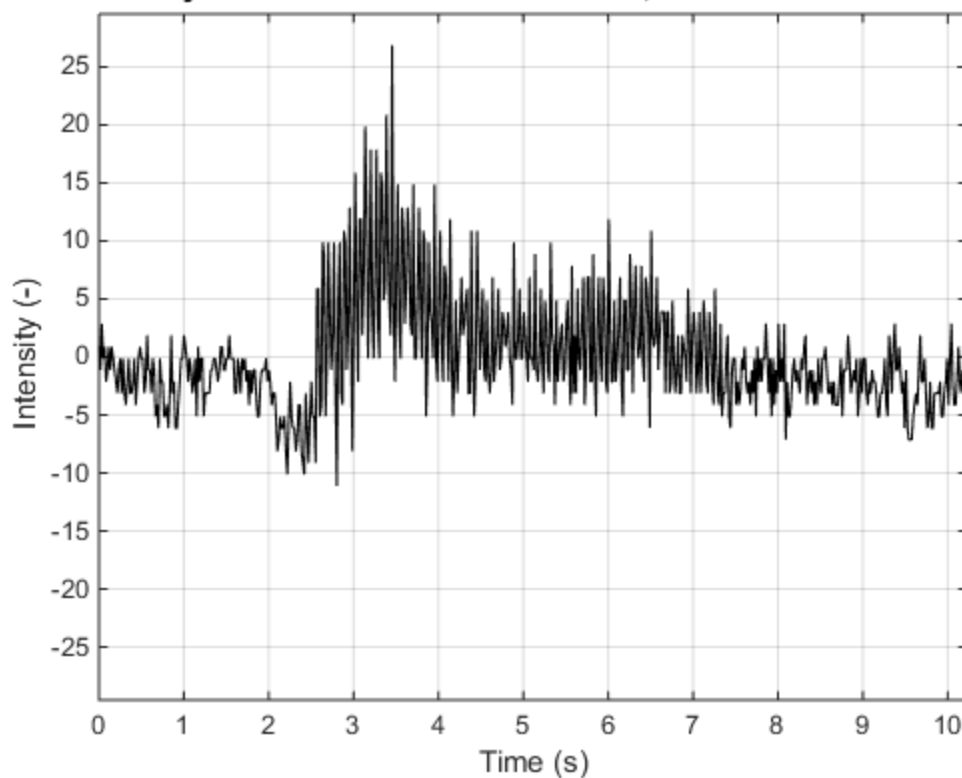
Time history of "S01T1 Feb 20 Canon.MOV", Pixel coordinates: 509 348



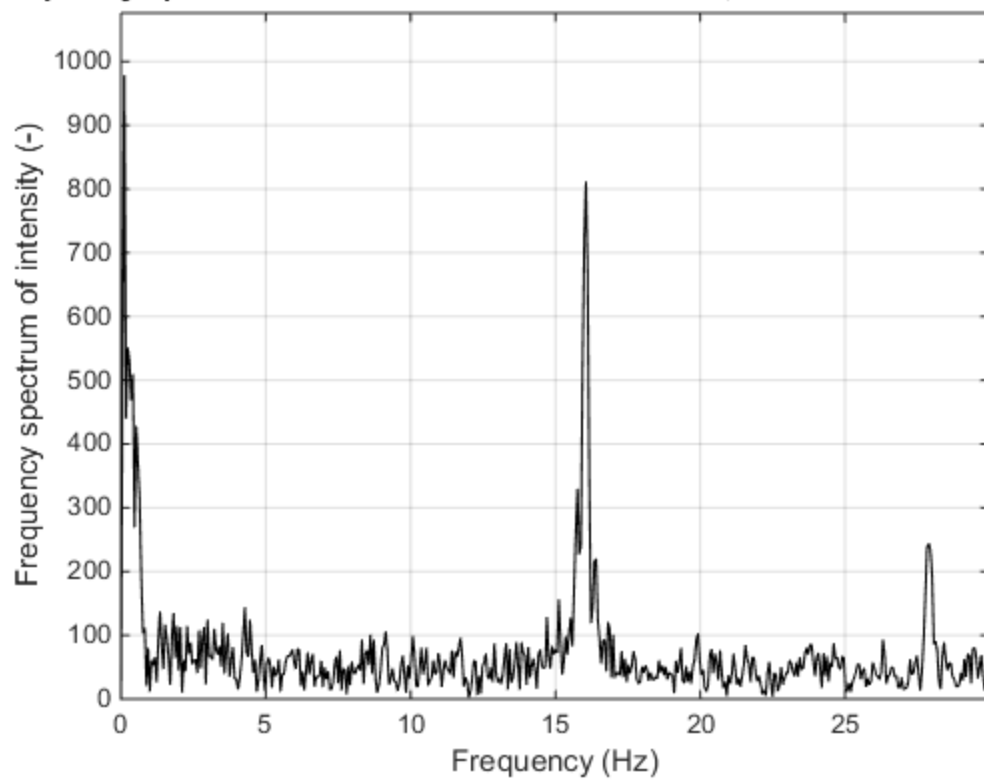
Frequency spectrum of "S01T1 Feb 20 Canon.MOV", Pixel coordinates: 509 348



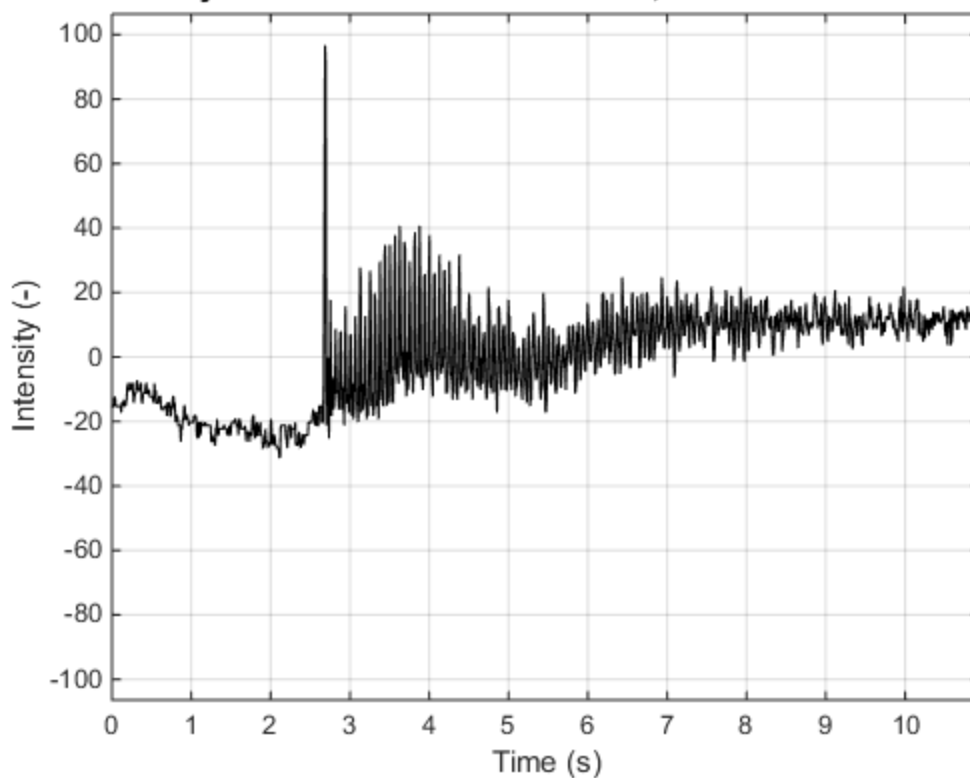
Time history of "S01T1 Feb 20 Canon.MOV", Pixel coordinates: 518 370



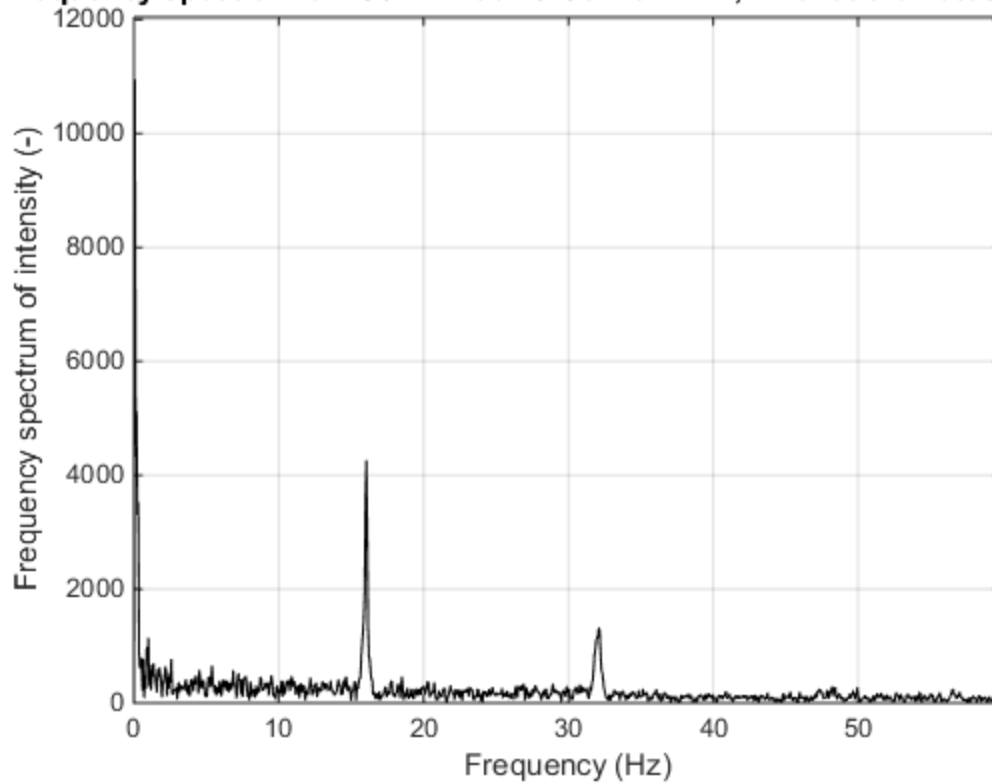
Frequency spectrum of "S01T1 Feb 20 Canon.MOV", Pixel coordinates: 518 3'



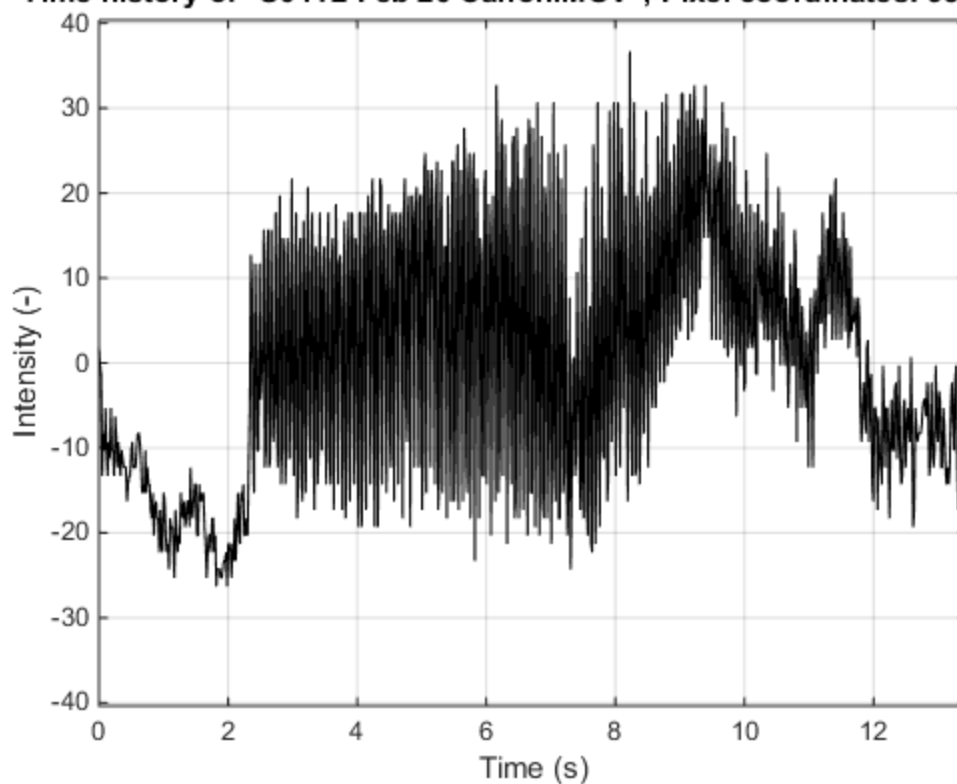
Time history of "S01T1 Feb 20 GoPro.MP4", Pixel coordinates: 550 319



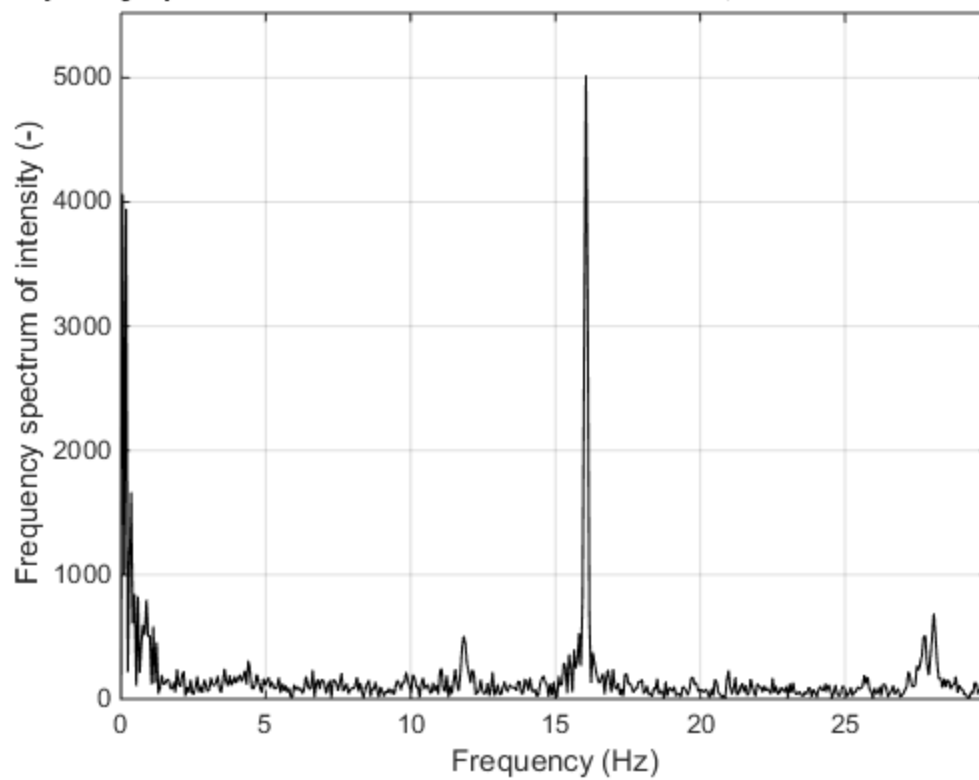
Frequency spectrum of "S01T1 Feb 20 GoPro.MP4", Pixel coordinates: 550 319



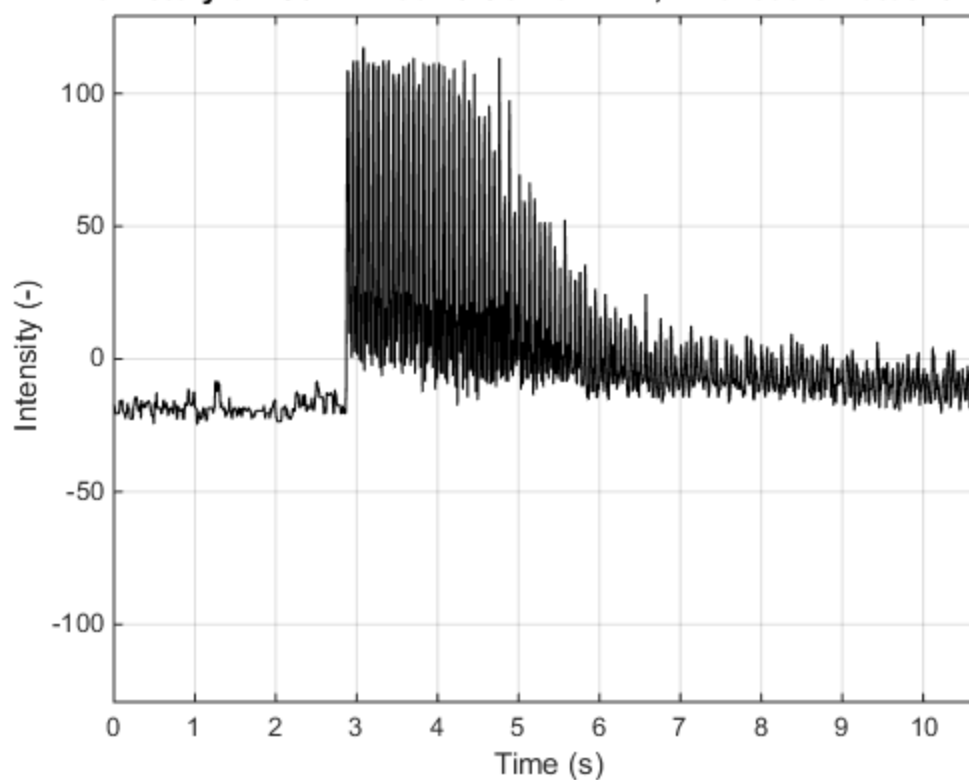
Time history of "S01T2 Feb 20 Canon.MOV", Pixel coordinates: 932 344



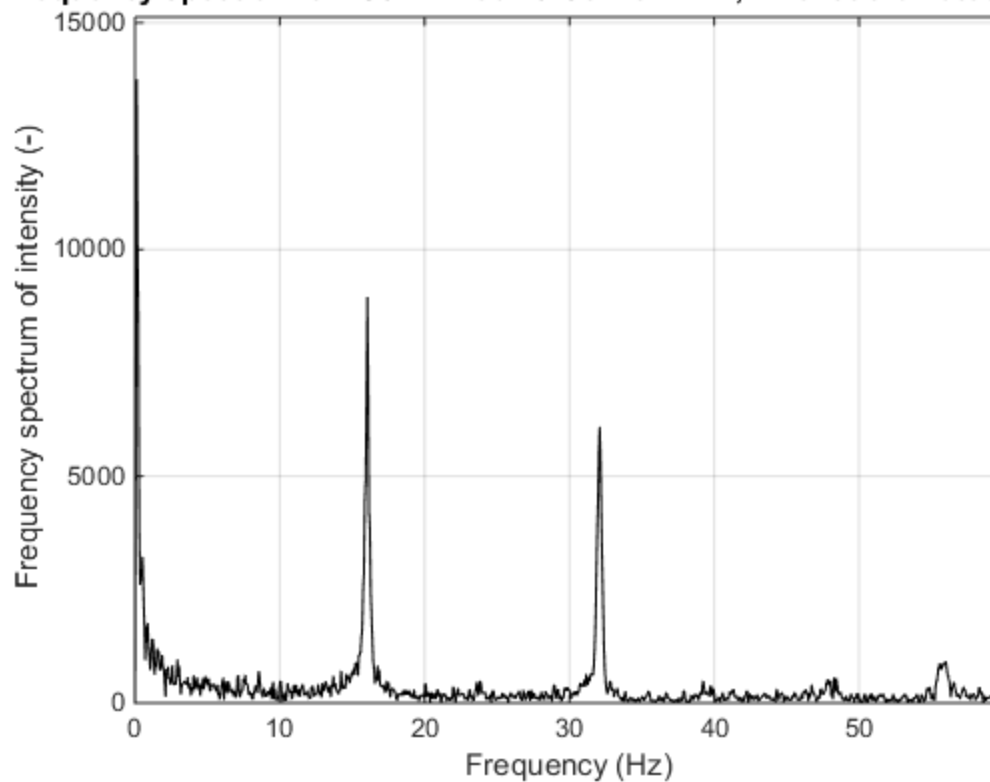
Frequency spectrum of "S01T2 Feb 20 Canon.MOV", Pixel coordinates: 932 344



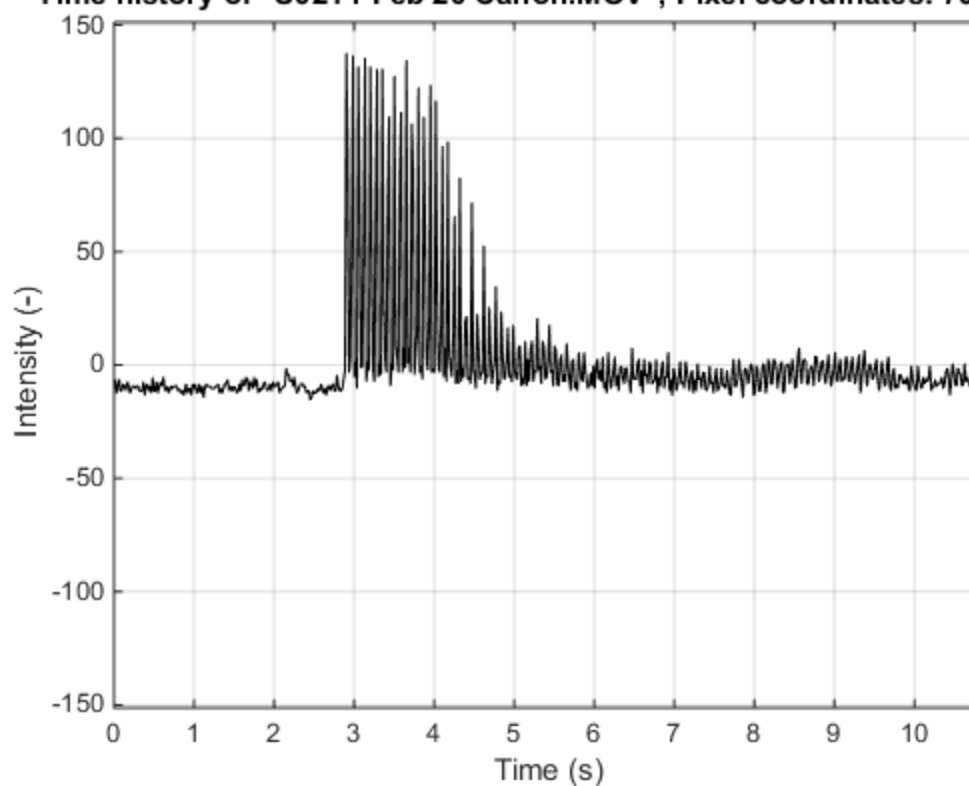
Time history of "S01T2 Feb 20 GoPro.MP4", Pixel coordinates: 527 286



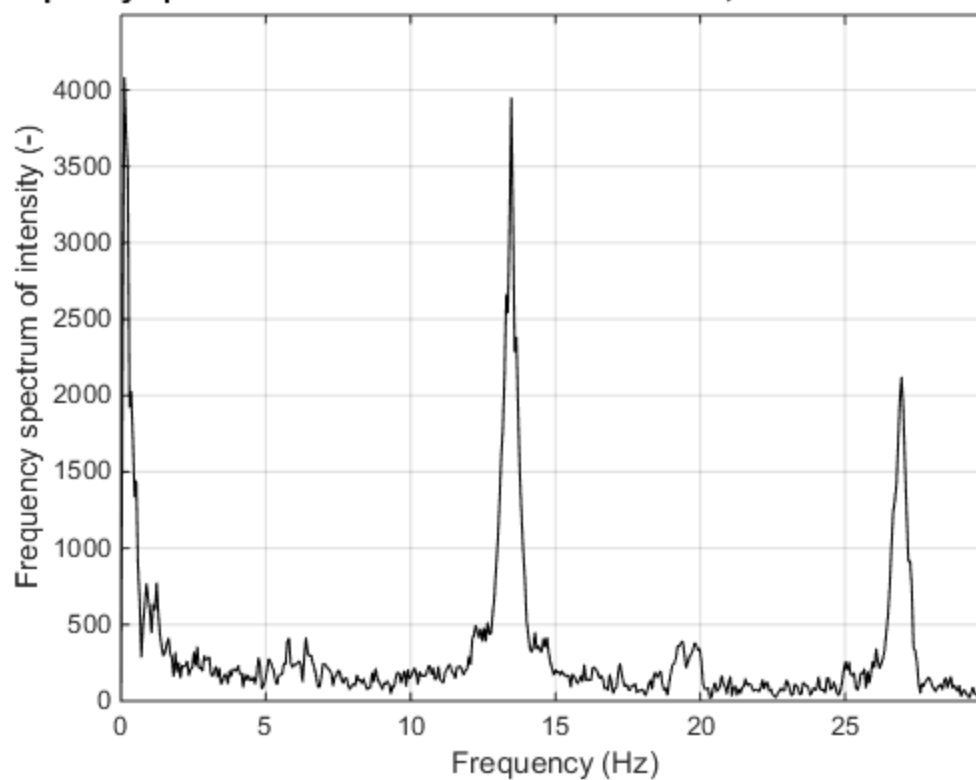
Frequency spectrum of "S01T2 Feb 20 GoPro.MP4", Pixel coordinates: 527 286



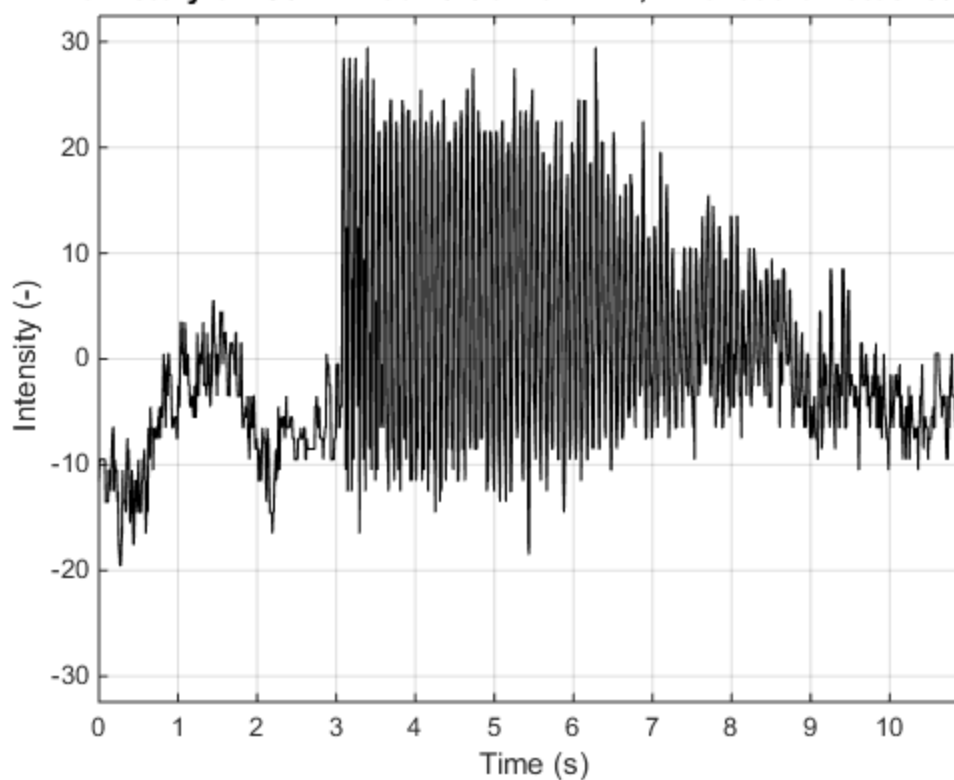
Time history of "S02T1 Feb 20 Canon.MOV", Pixel coordinates: 703 349



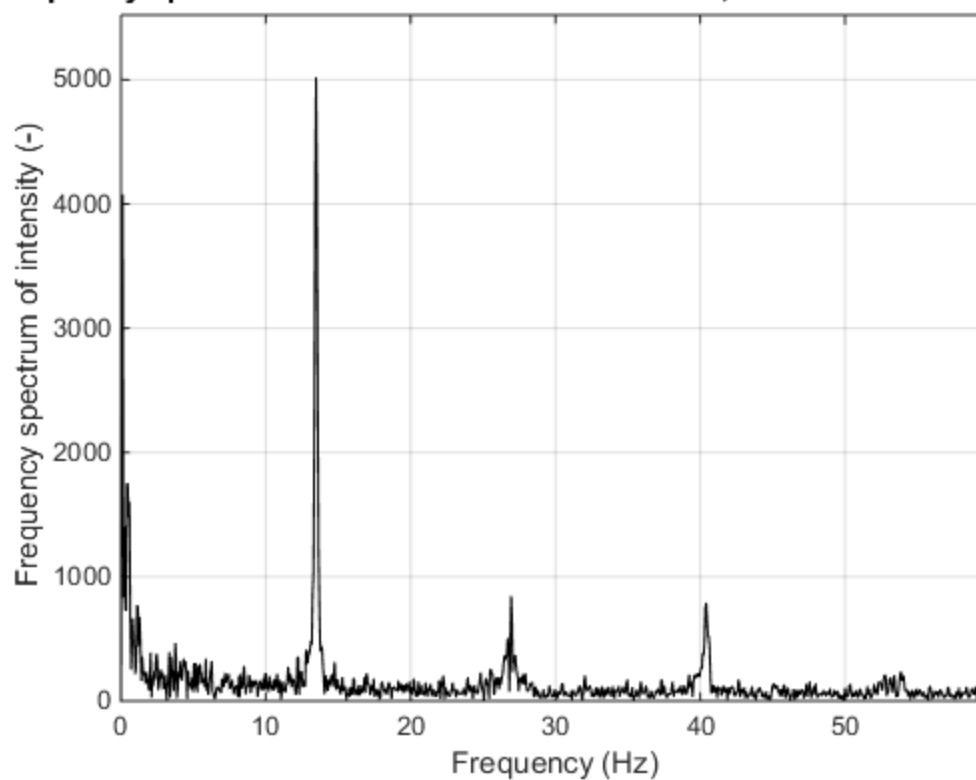
Frequency spectrum of "S02T1 Feb 20 Canon.MOV", Pixel coordinates: 703 349



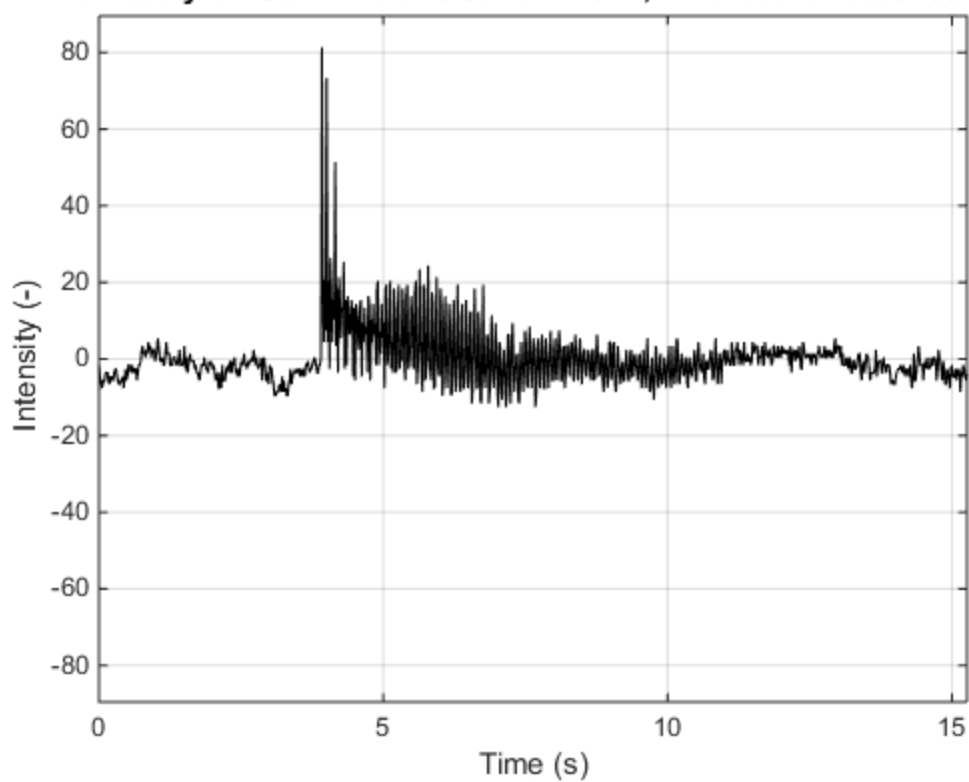
Time history of "S02T1 Feb 20 GoPro.MP4", Pixel coordinates: 595 347



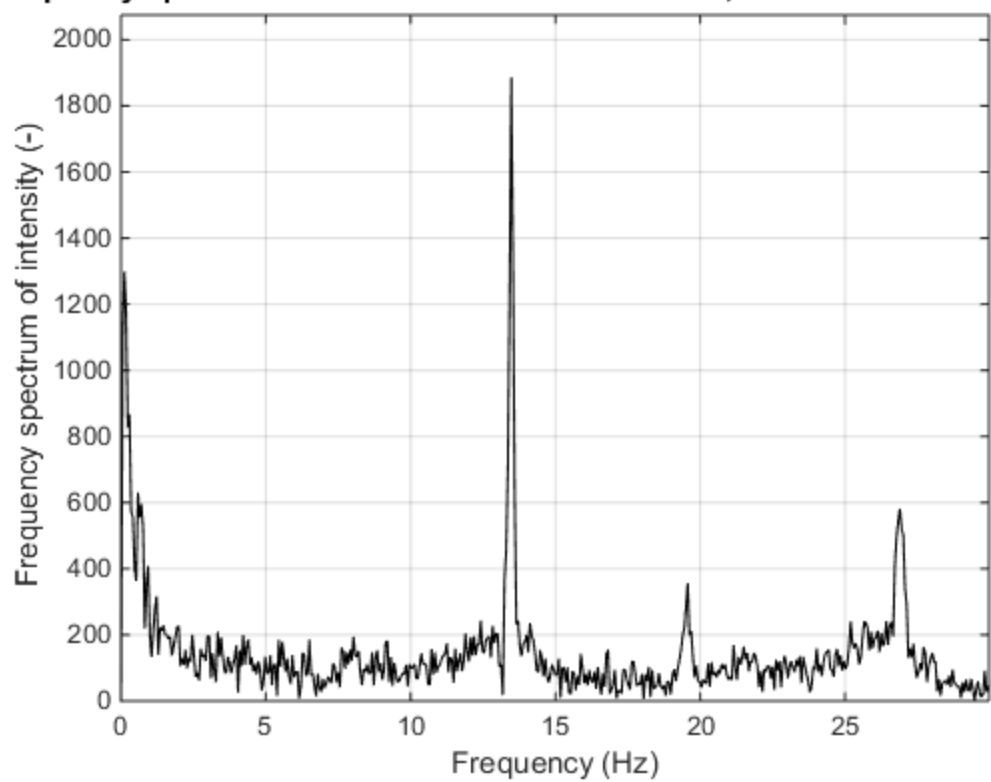
Frequency spectrum of "S02T1 Feb 20 GoPro.MP4", Pixel coordinates: 595 347



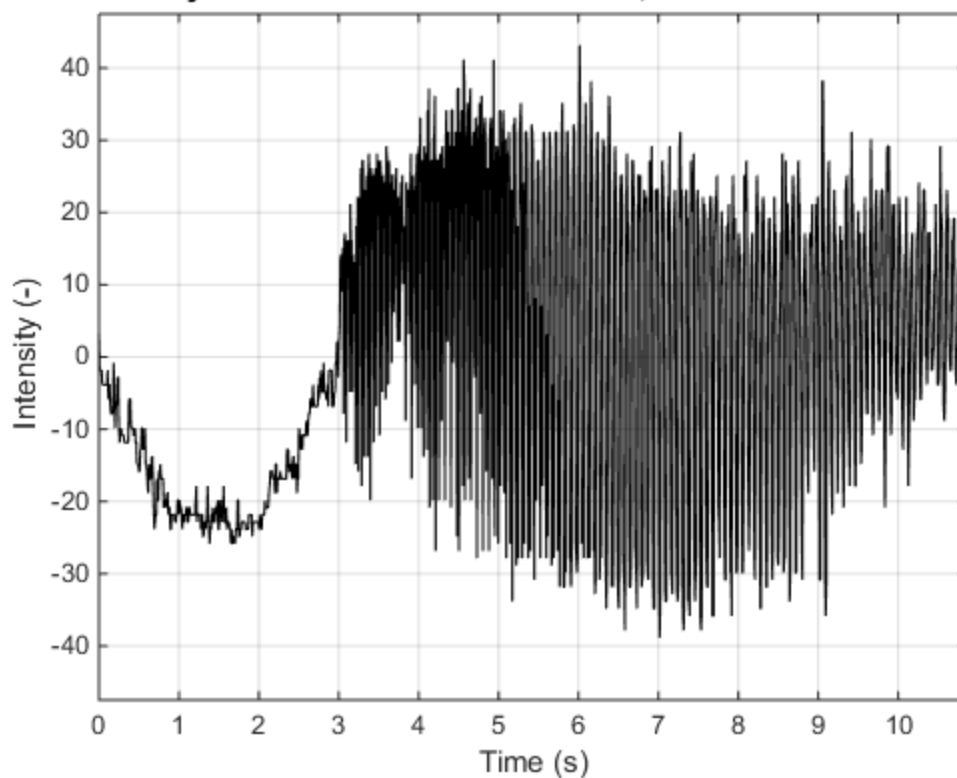
Time history of "S02T2 Feb 20 Canon.MOV", Pixel coordinates: 332 329



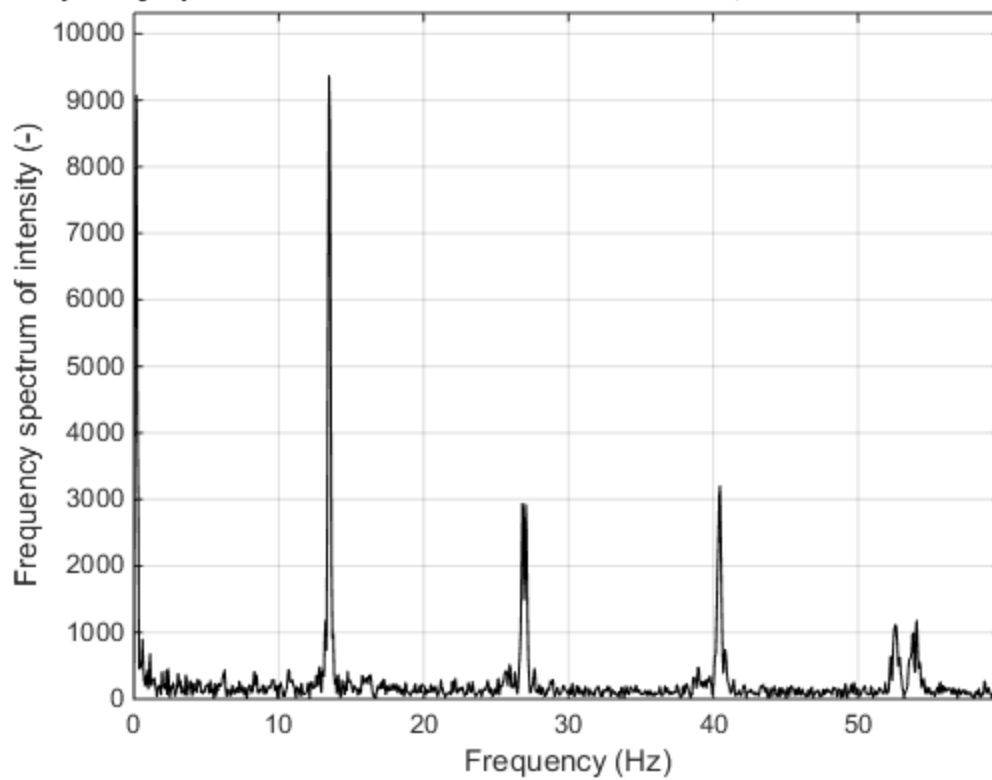
Frequency spectrum of "S02T2 Feb 20 Canon.MOV", Pixel coordinates: 332 329



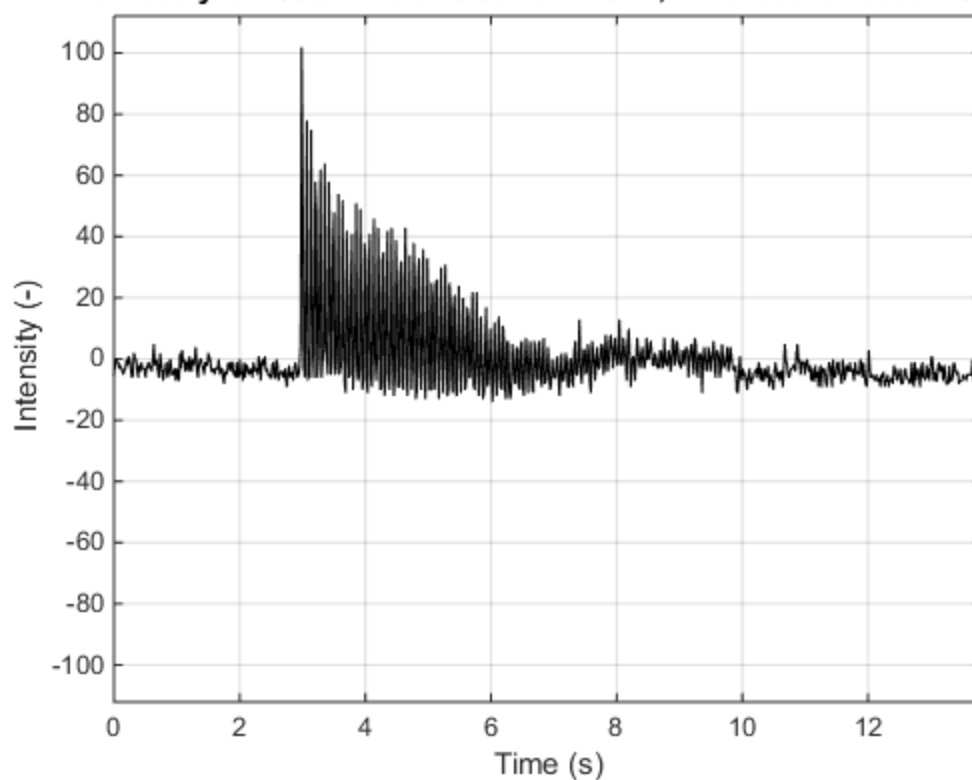
Time history of "S02T2 Feb 20 GoPro.MP4", Pixel coordinates: 918 370



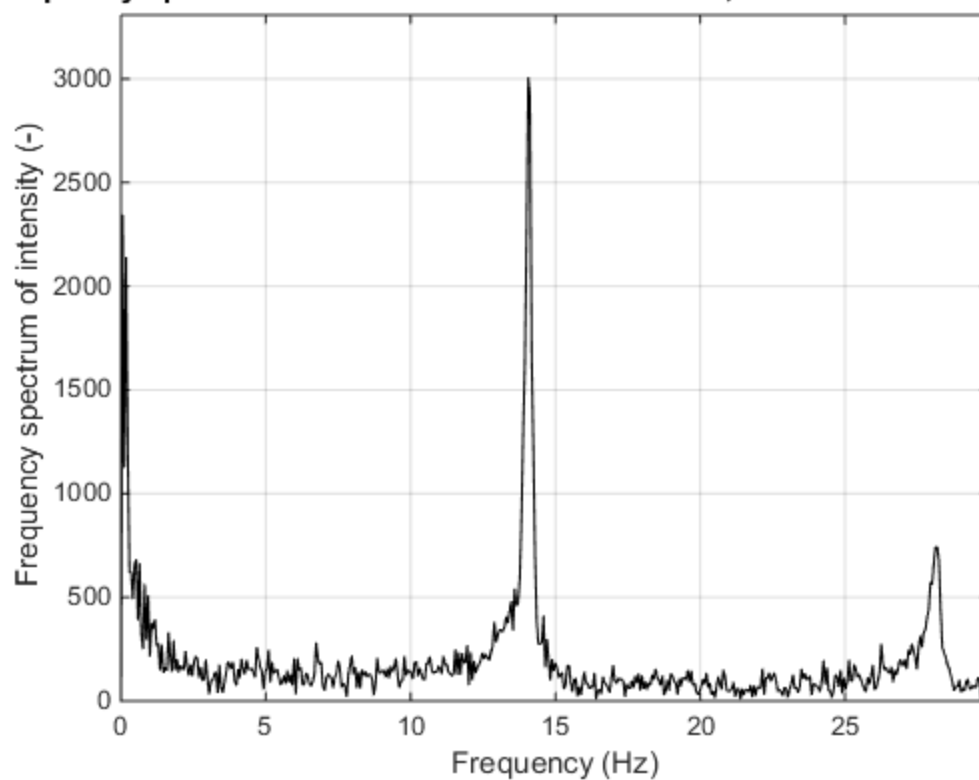
Frequency spectrum of "S02T2 Feb 20 GoPro.MP4", Pixel coordinates: 918 370



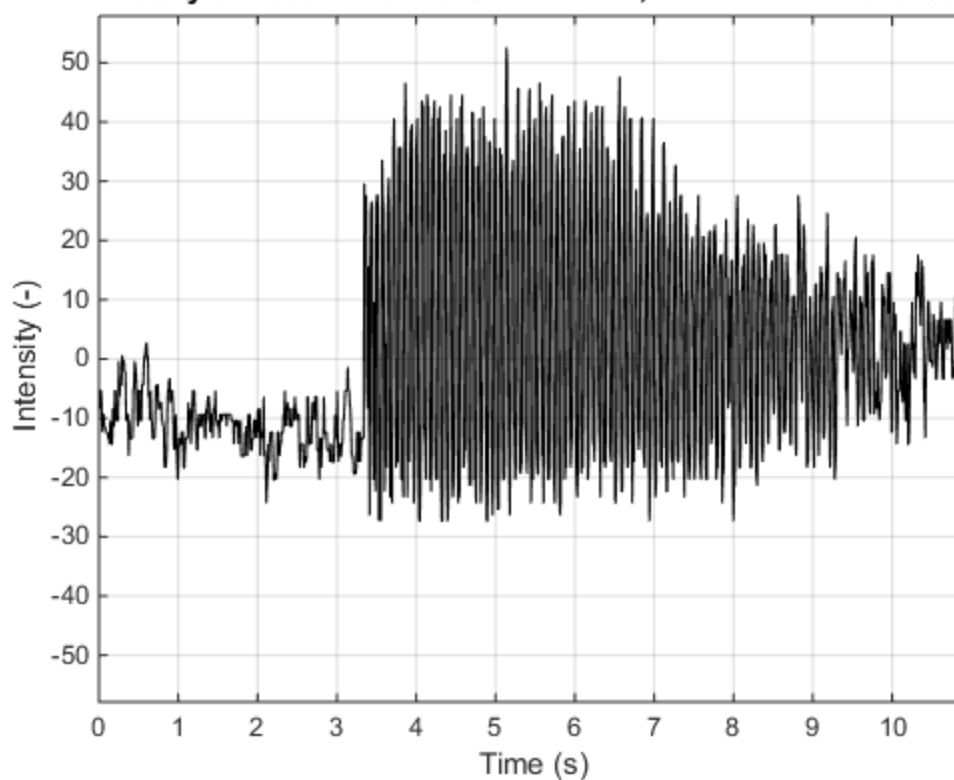
Time history of "S03T1 Feb 20 Canon.MOV", Pixel coordinates: 486 348



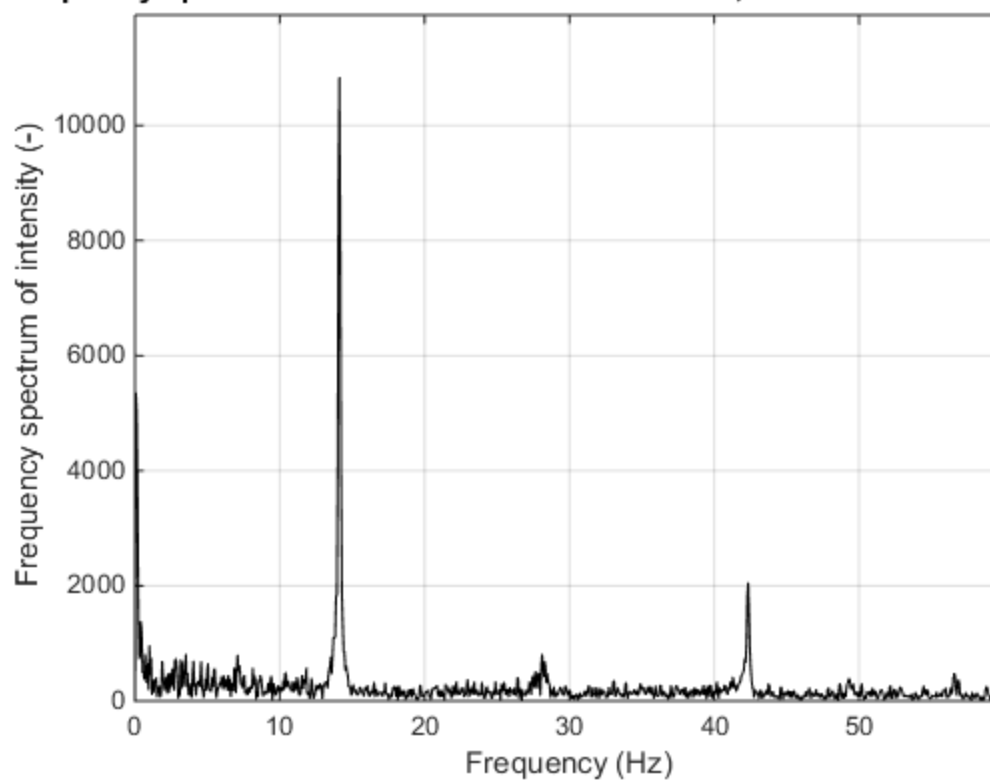
Frequency spectrum of "S03T1 Feb 20 Canon.MOV", Pixel coordinates: 486 348



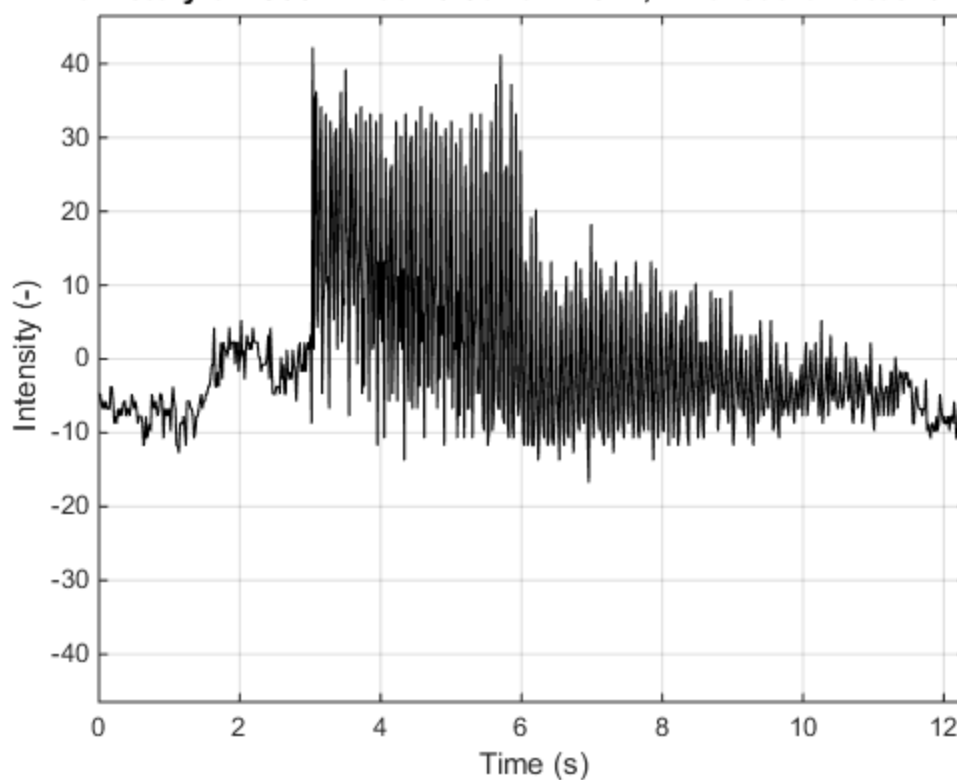
Time history of "S03T1 Feb 20 GoPro.MP4", Pixel coordinates: 831 334



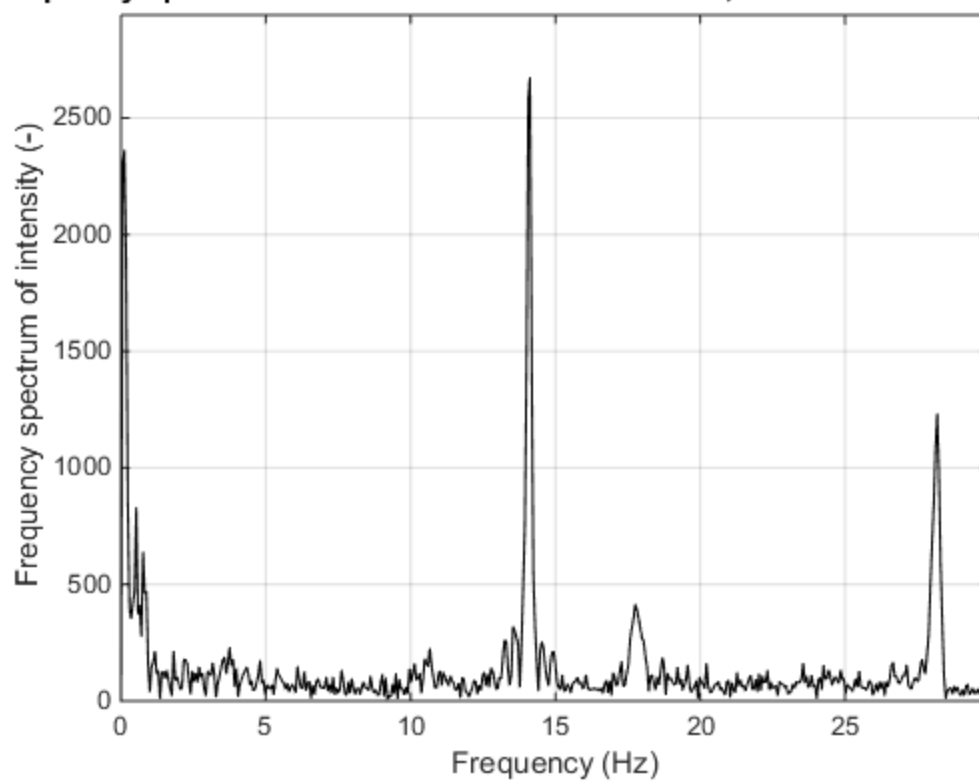
Frequency spectrum of "S03T1 Feb 20 GoPro.MP4", Pixel coordinates: 831 334



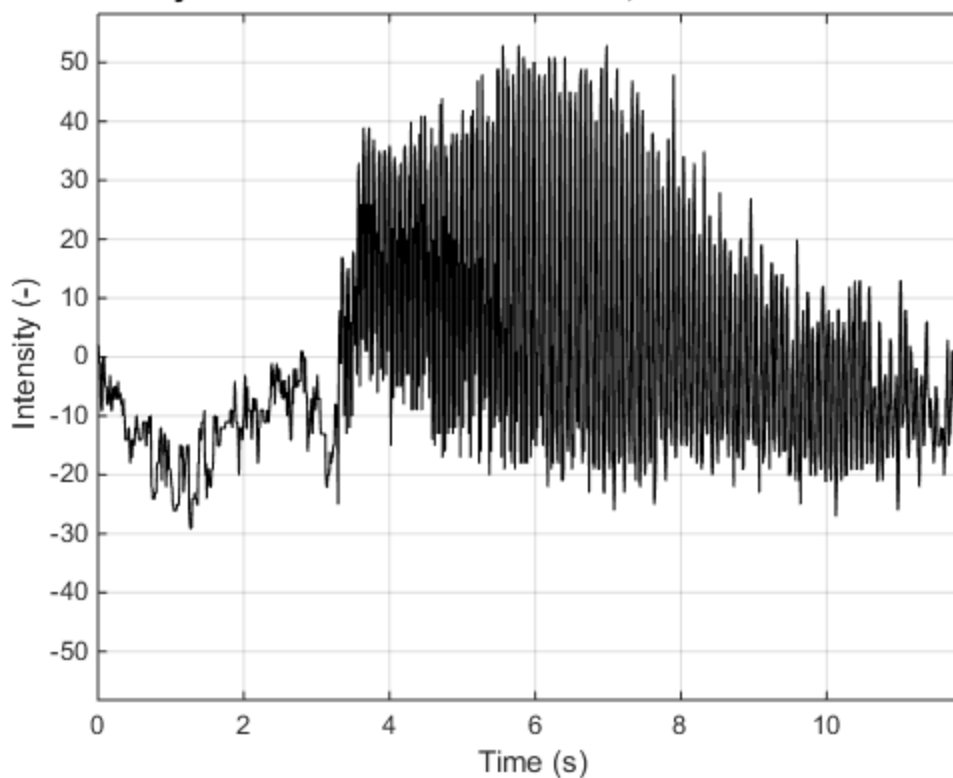
Time history of "S03T2 Feb 20 Canon.MOV", Pixel coordinates: 942 306



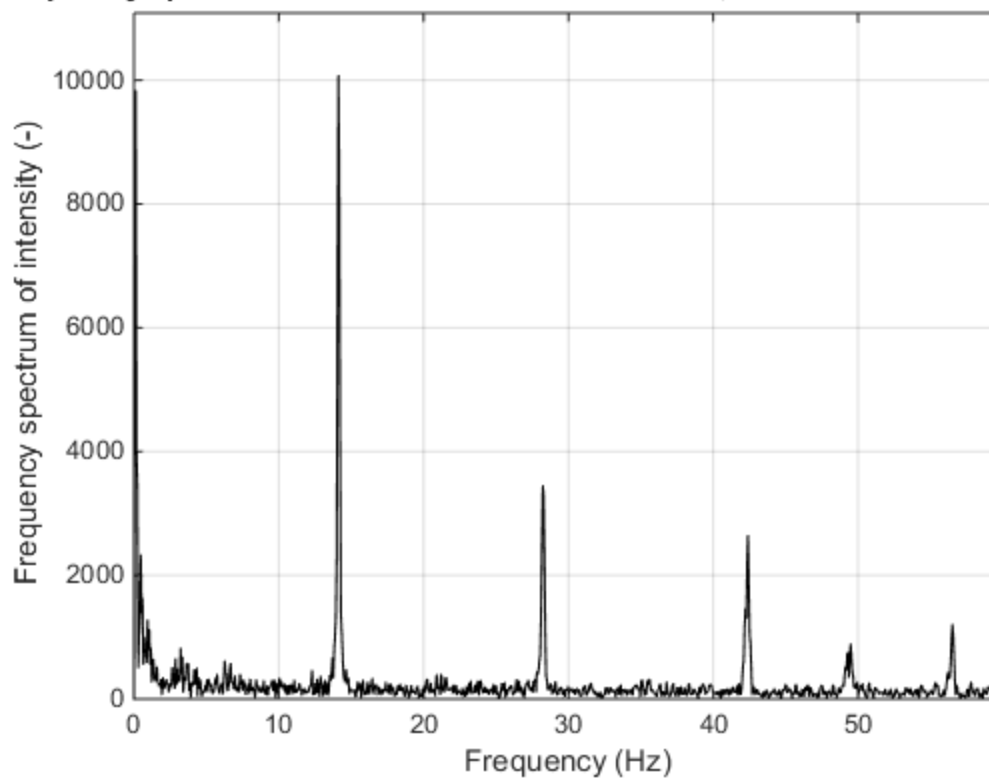
Frequency spectrum of "S03T2 Feb 20 Canon.MOV", Pixel coordinates: 942 306



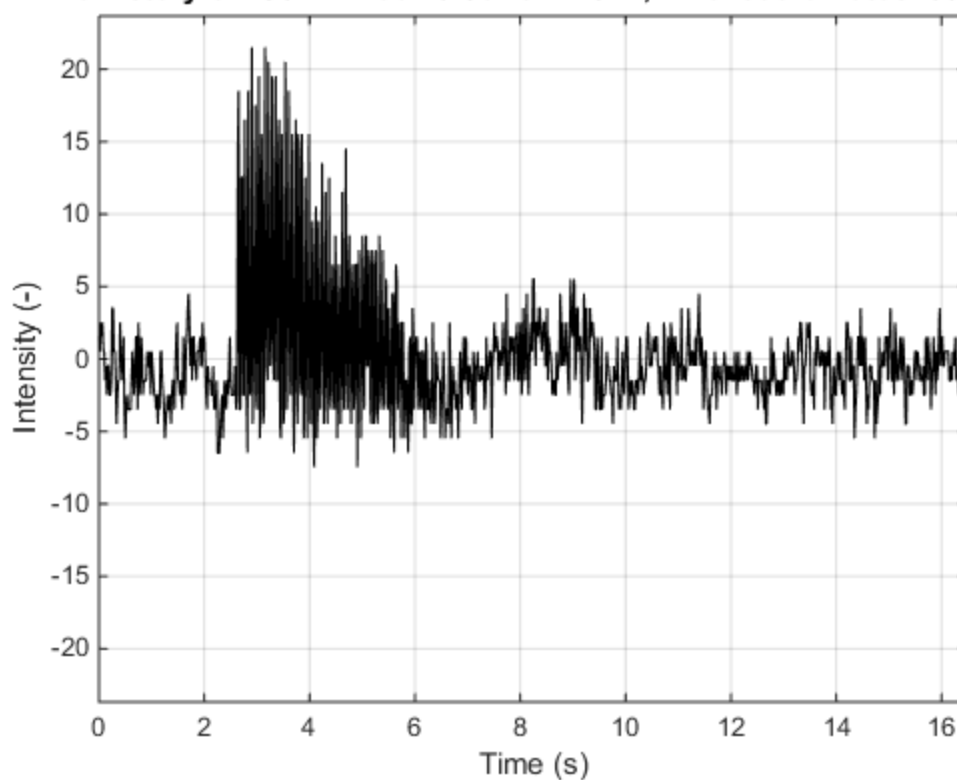
Time history of "S03T2 Feb 20 GoPro.MP4", Pixel coordinates: 1037 302



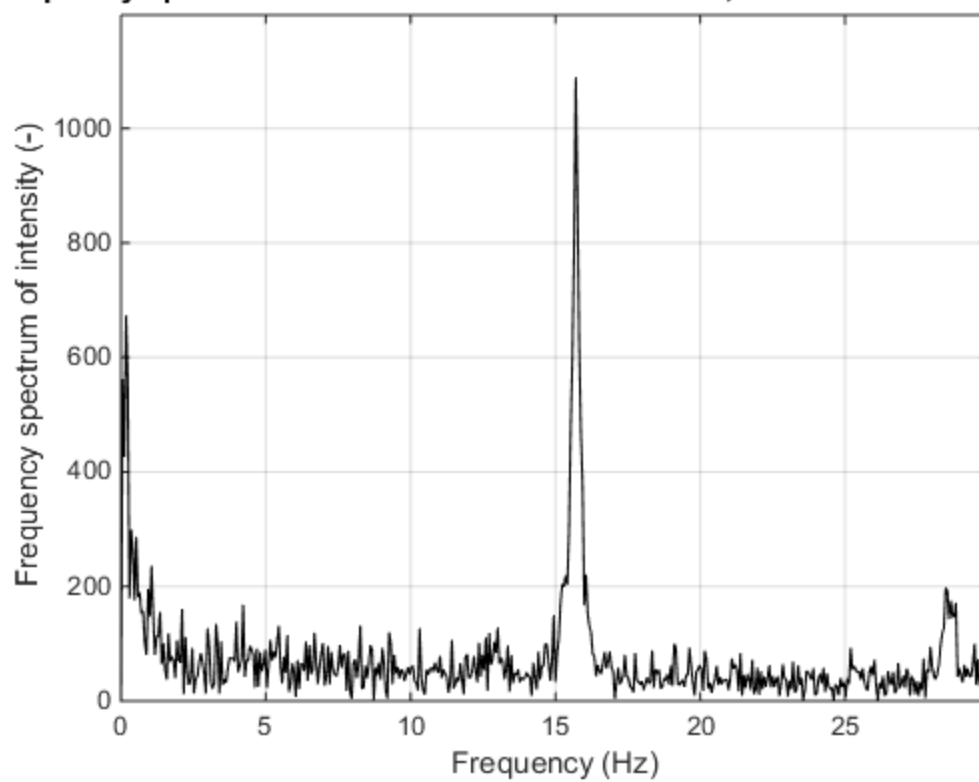
Frequency spectrum of "S03T2 Feb 20 GoPro.MP4", Pixel coordinates: 1037 3



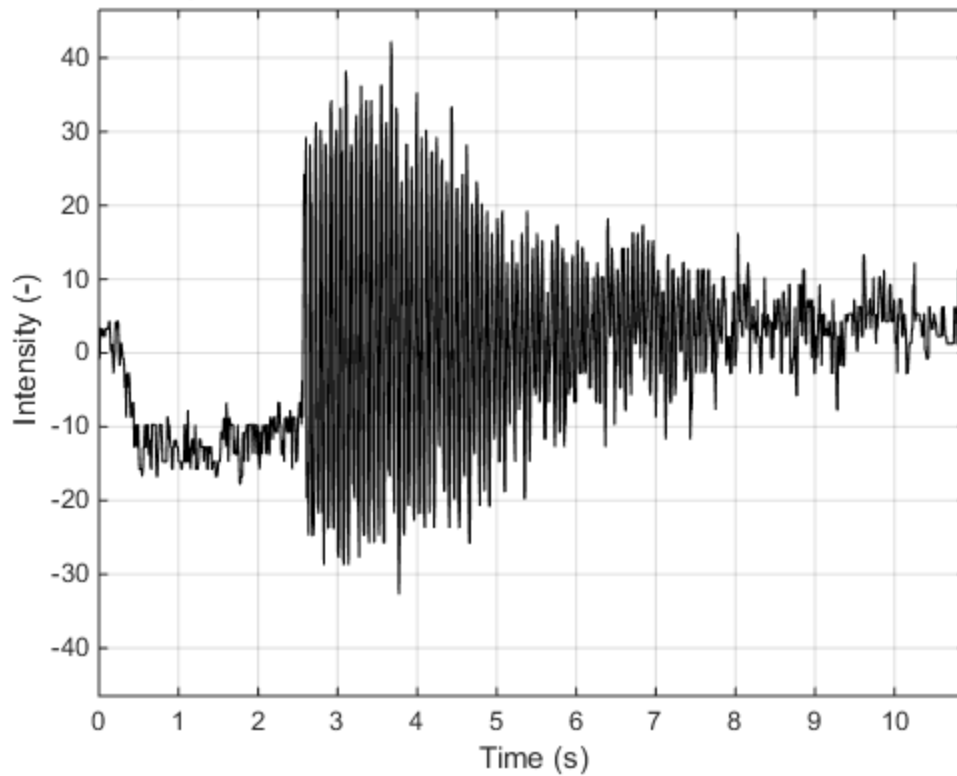
Time history of "S04T1 Feb 20 Canon.MOV", Pixel coordinates: 560 362



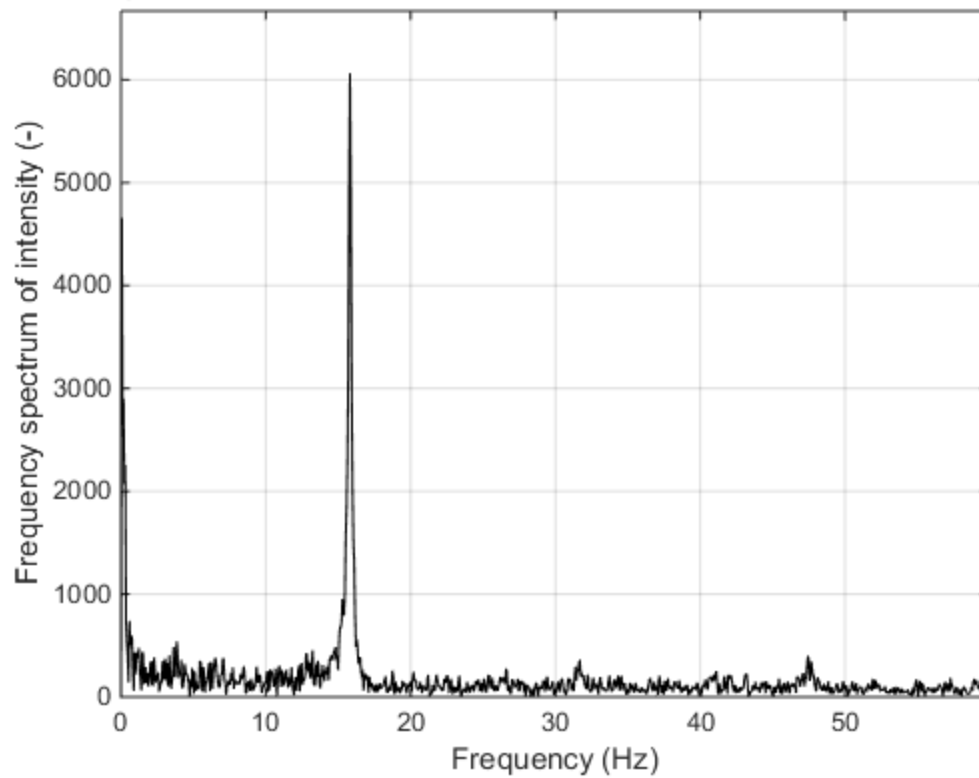
Frequency spectrum of "S04T1 Feb 20 Canon.MOV", Pixel coordinates: 560 362



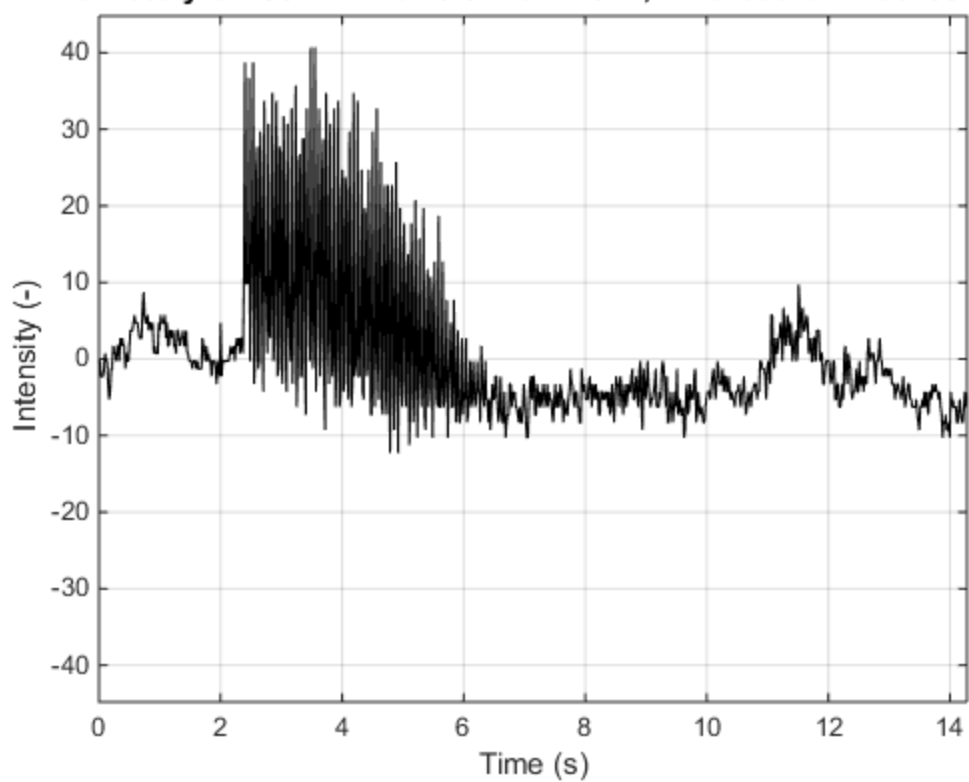
Time history of "S04T1 Feb 20 GoPro.MP4", Pixel coordinates: 623 329



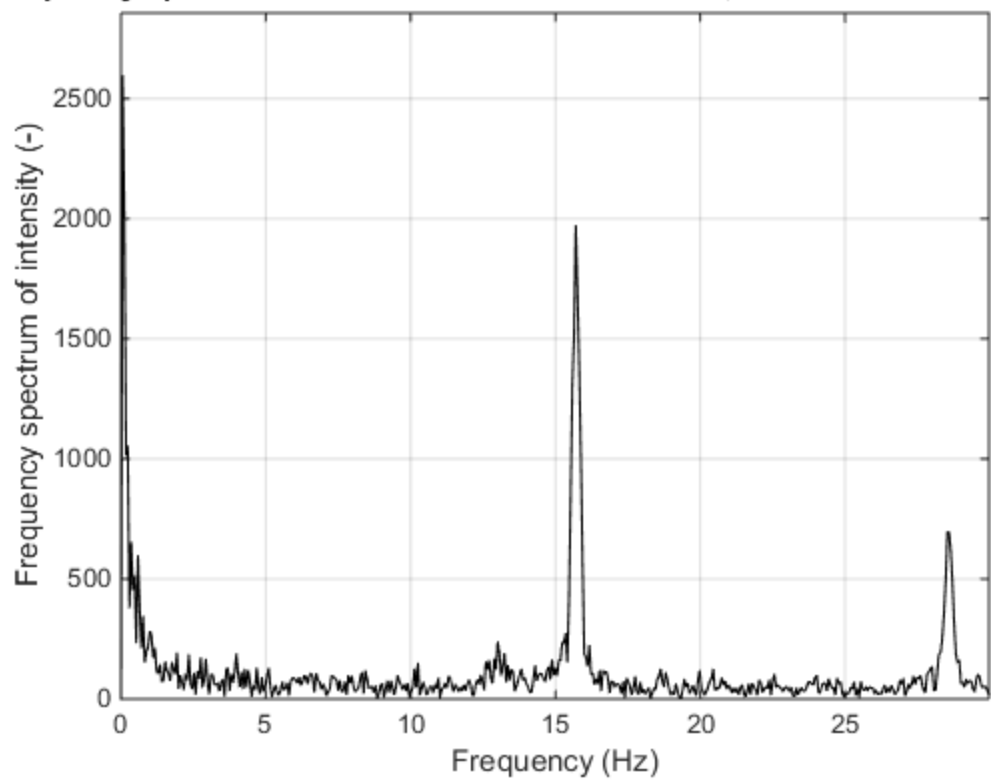
Frequency spectrum of "S04T1 Feb 20 GoPro.MP4", Pixel coordinates: 623 329



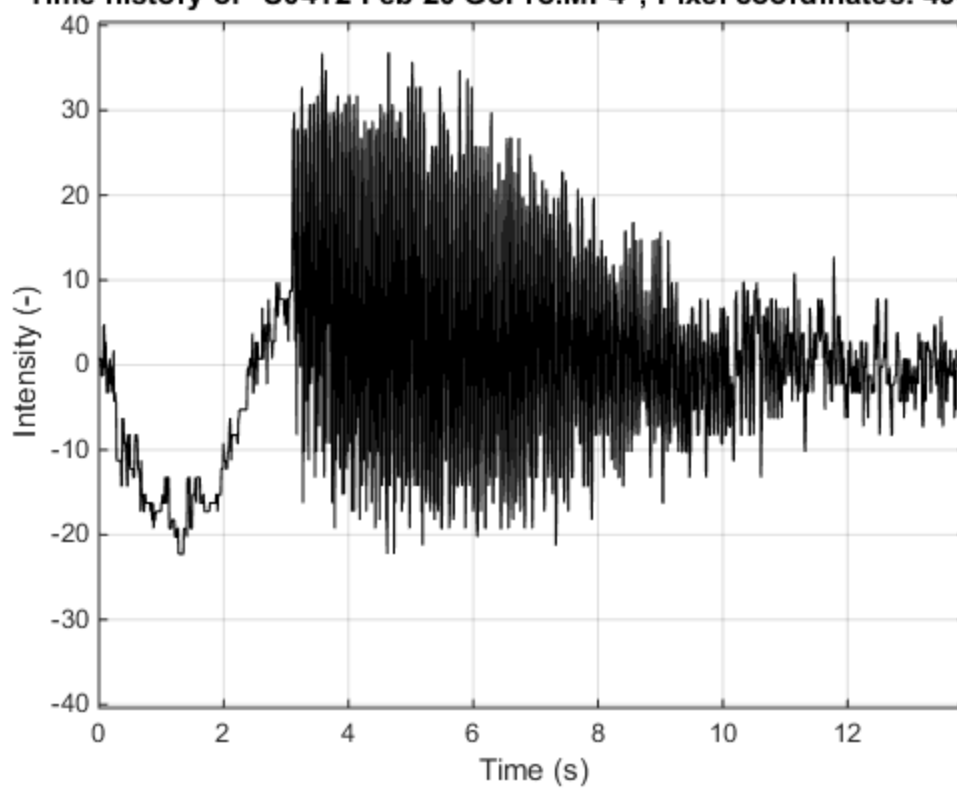
Time history of "S04T2 Feb 20 Canon.MOV", Pixel coordinates: 364 342



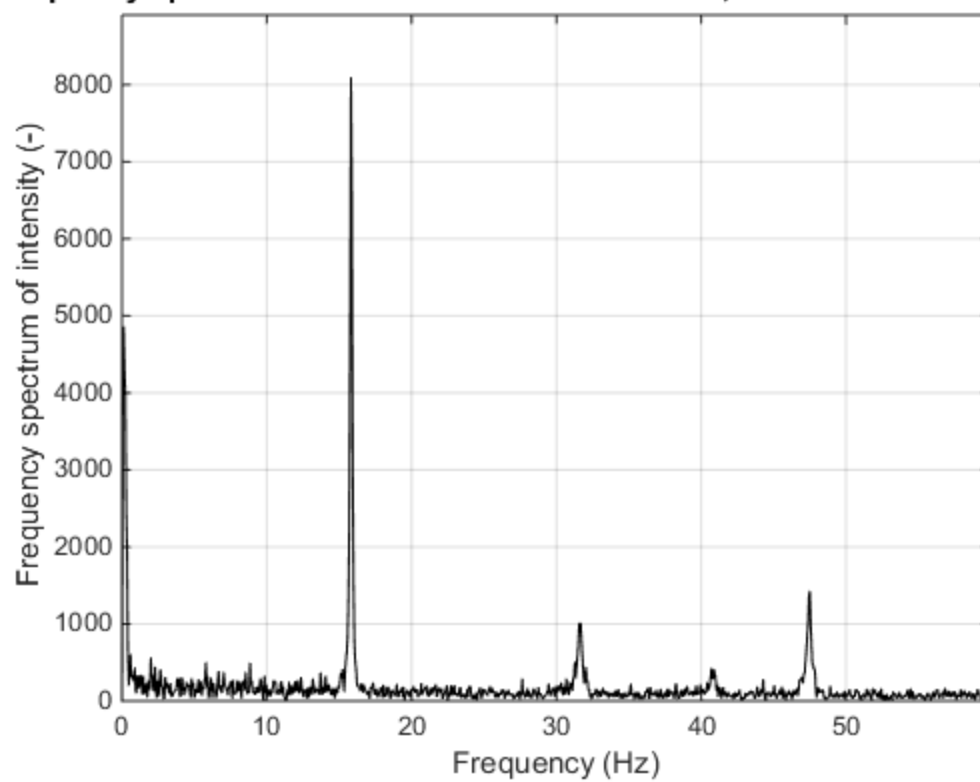
Frequency spectrum of "S04T2 Feb 20 Canon.MOV", Pixel coordinates: 364 342



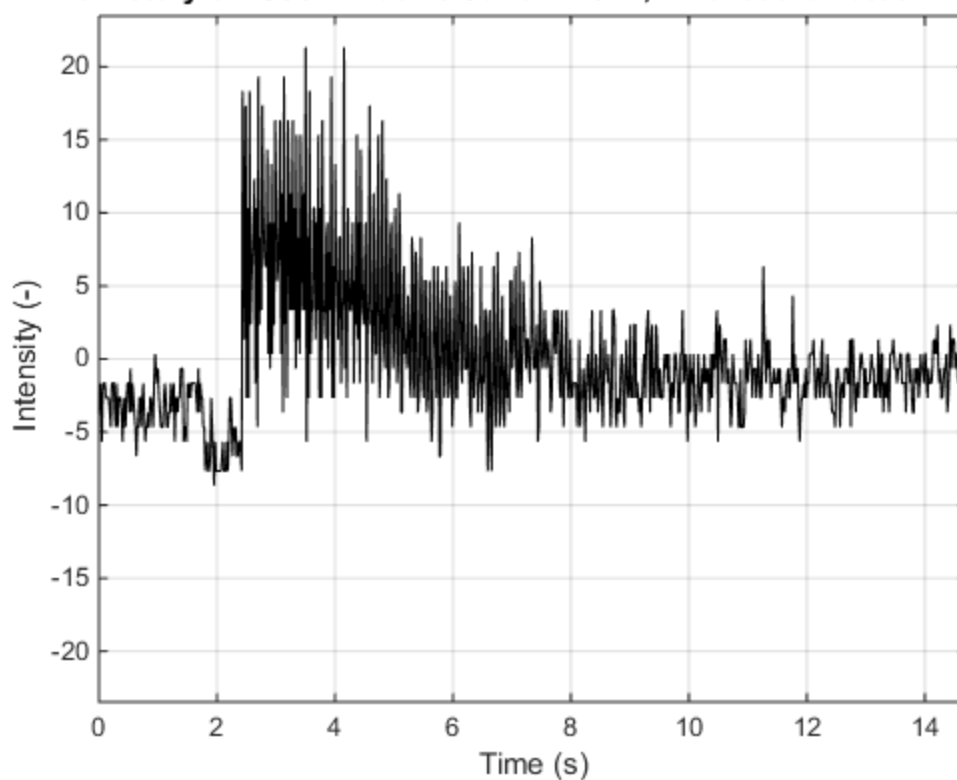
Time history of "S04T2 Feb 20 GoPro.MP4", Pixel coordinates: 494 282



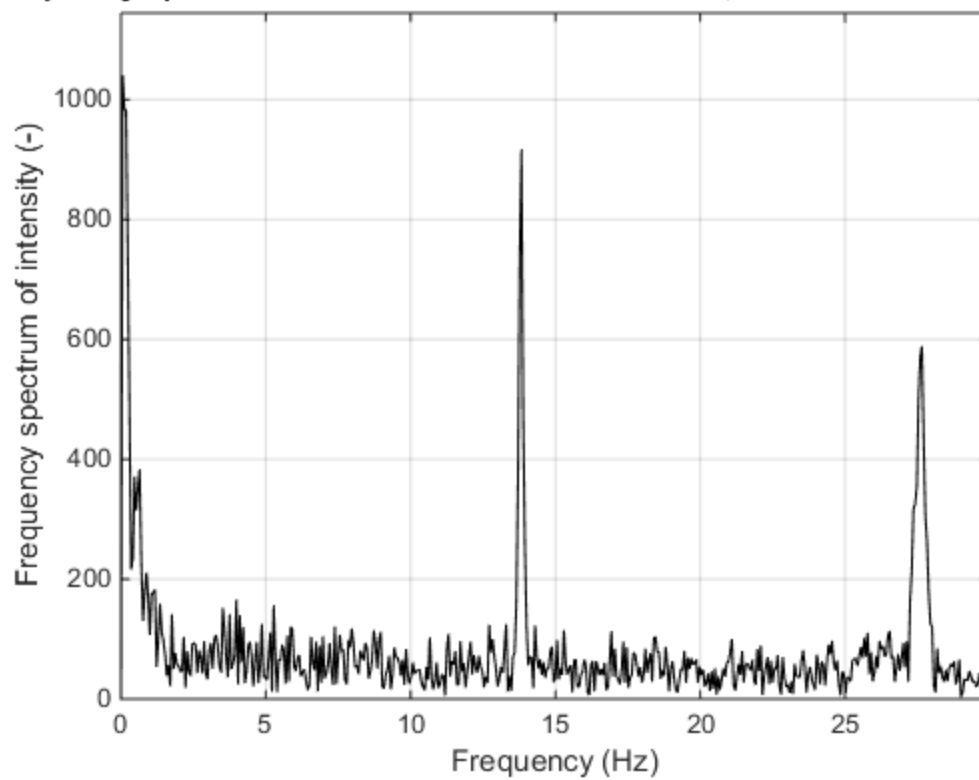
Frequency spectrum of "S04T2 Feb 20 GoPro.MP4", Pixel coordinates: 494 282



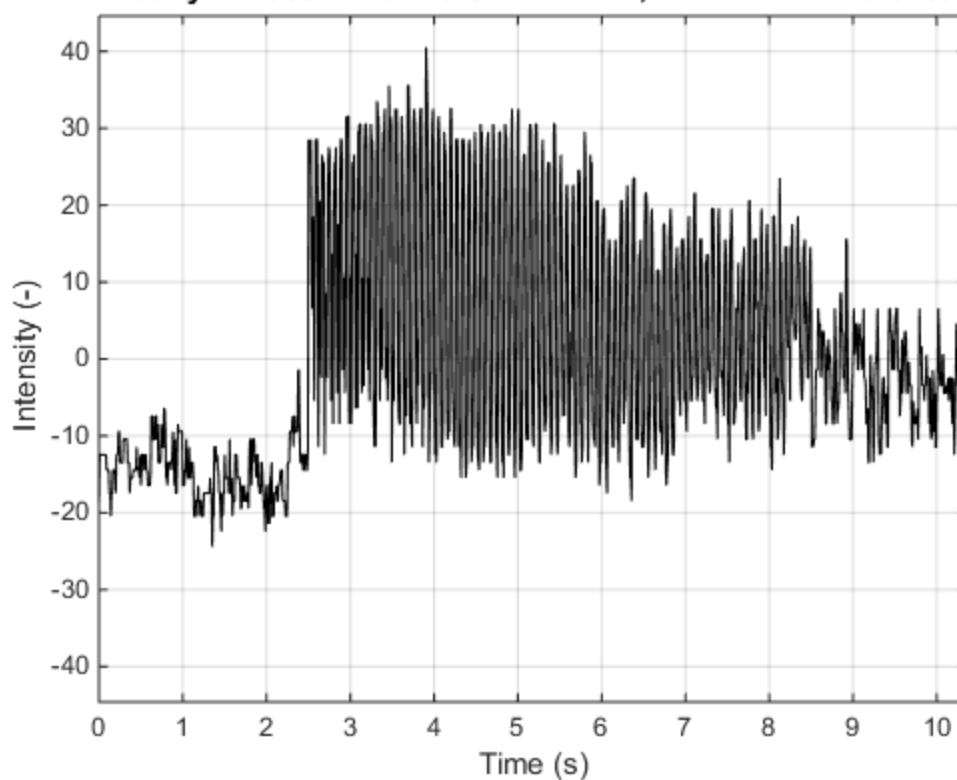
Time history of "S05T1 Feb 20 Canon.MOV", Pixel coordinates: 711 360



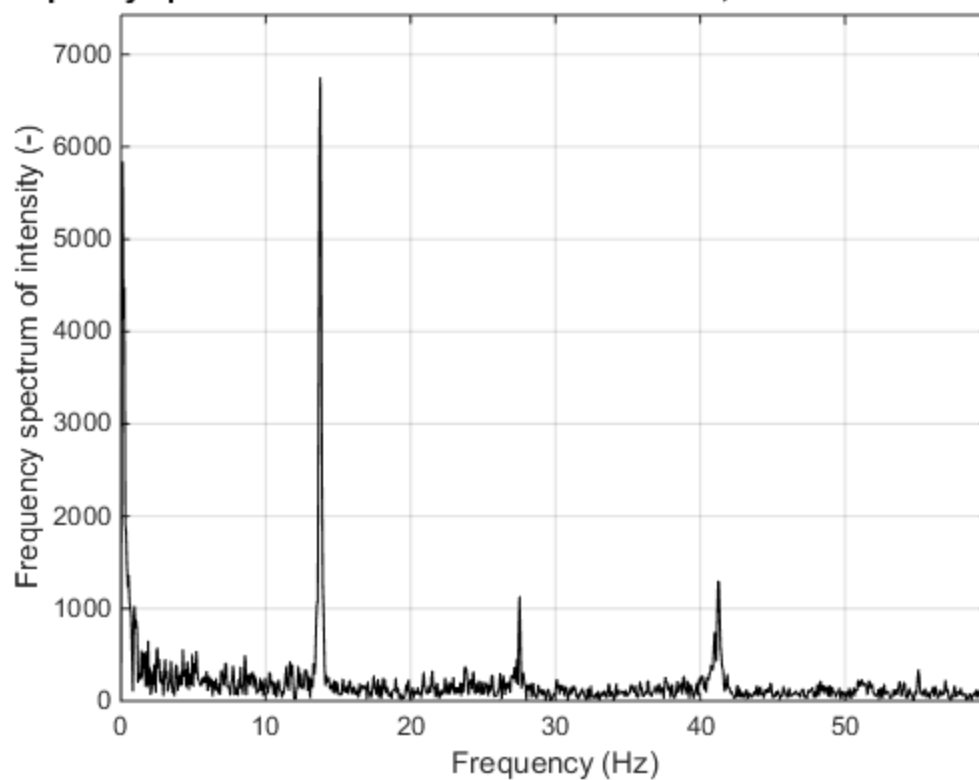
Frequency spectrum of "S05T1 Feb 20 Canon.MOV", Pixel coordinates: 711 360



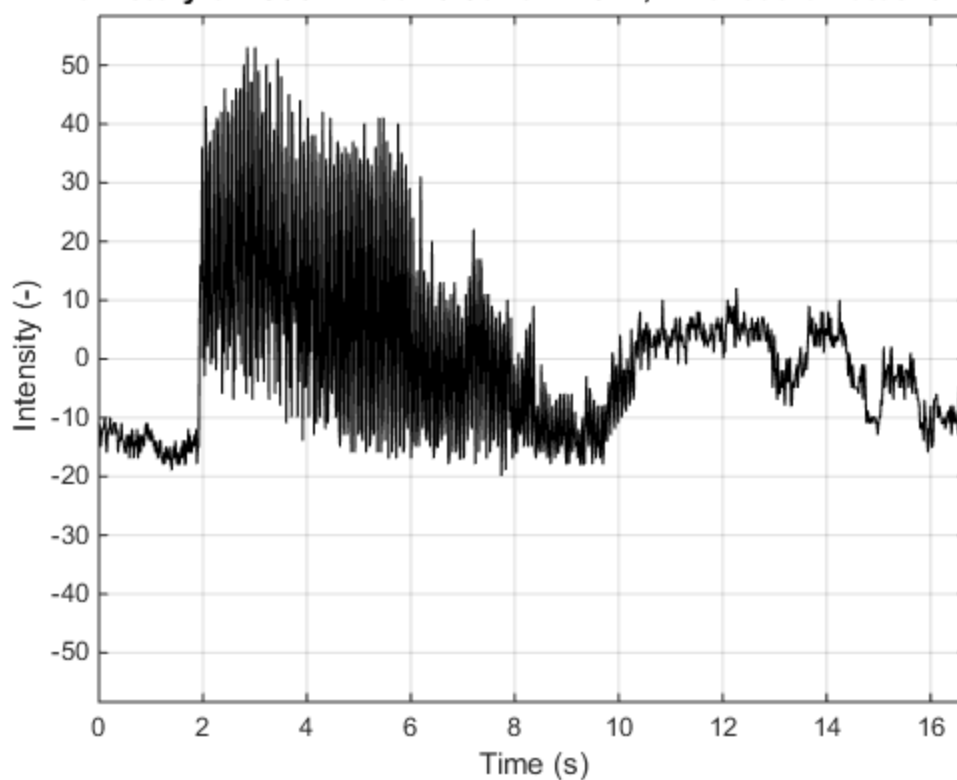
Time history of "S05T1 Feb 20 GoPro.MP4", Pixel coordinates: 693 348



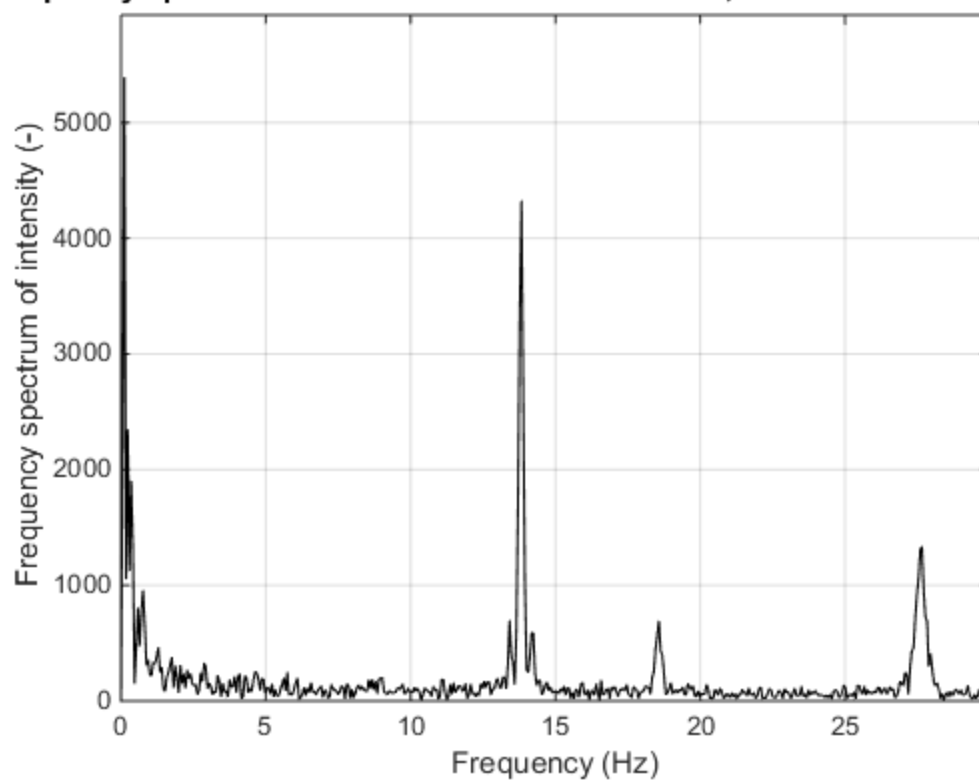
Frequency spectrum of "S05T1 Feb 20 GoPro.MP4", Pixel coordinates: 693 34



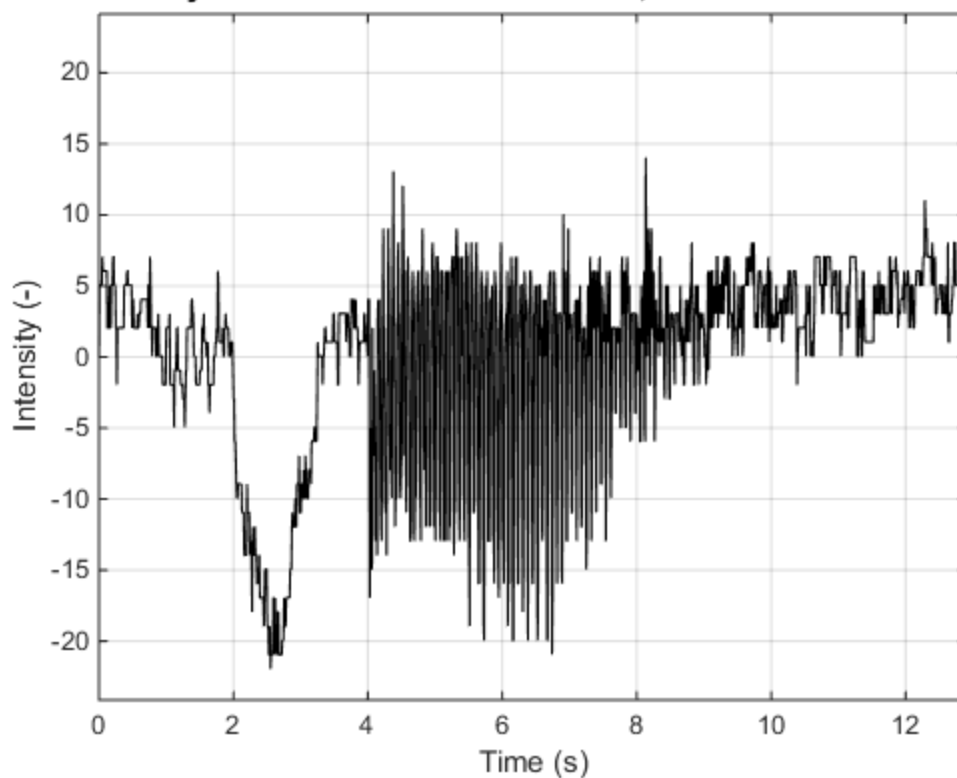
Time history of "S05T2 Feb 20 Canon.MOV", Pixel coordinates: 828 348



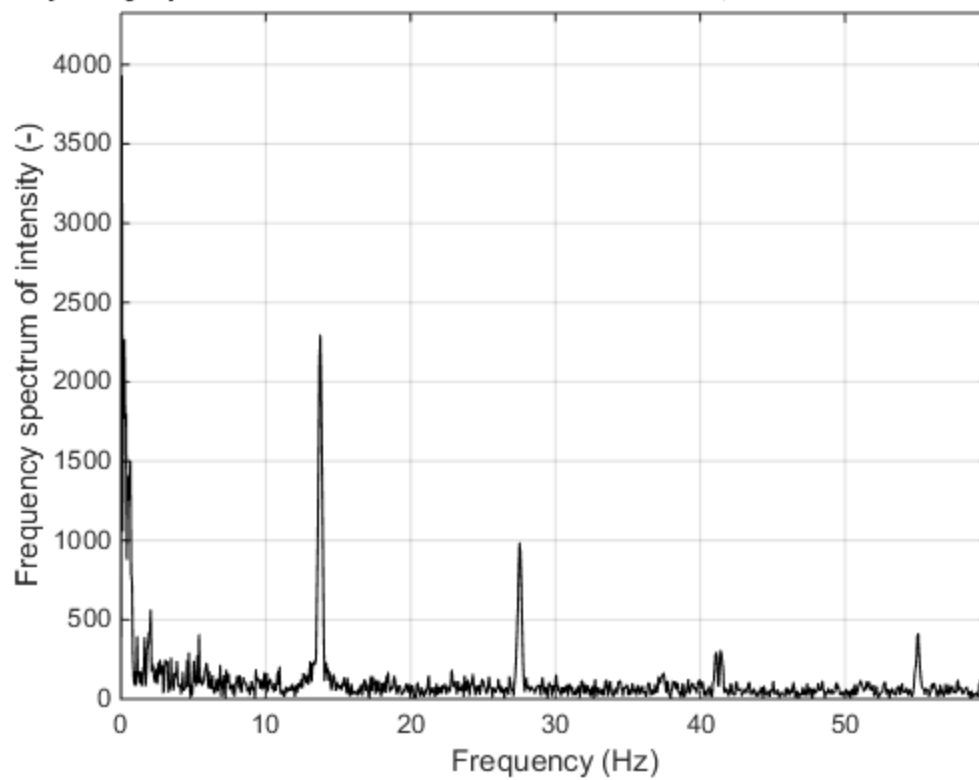
Frequency spectrum of "S05T2 Feb 20 Canon.MOV", Pixel coordinates: 828 348



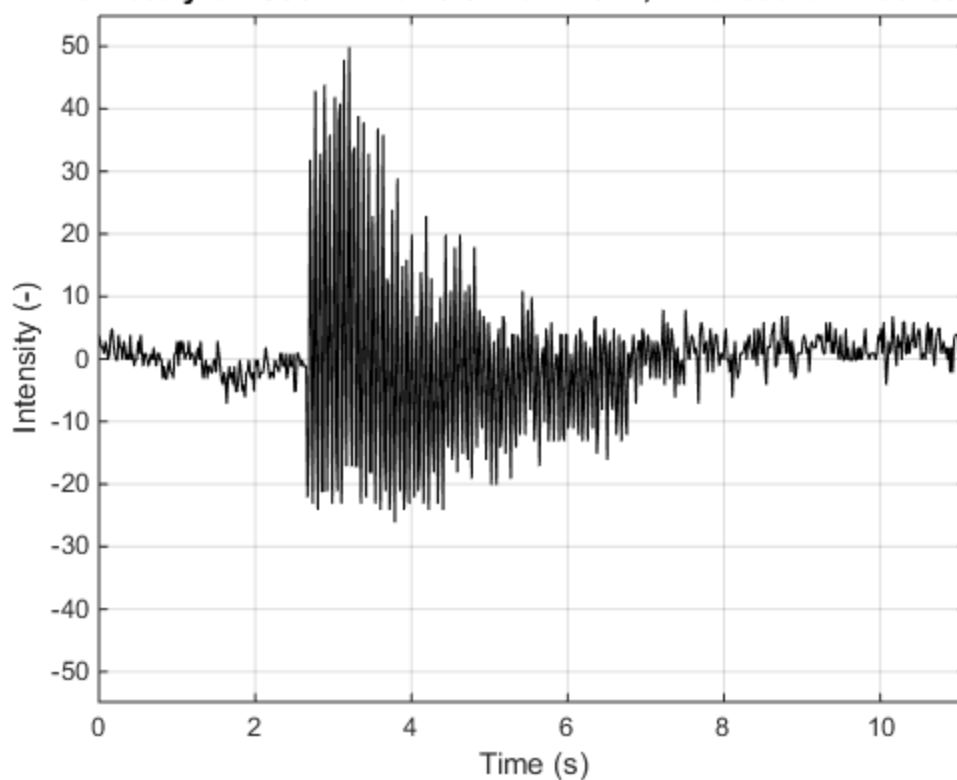
Time history of "S05T2 Feb 20 GoPro.MP4", Pixel coordinates: 693 346



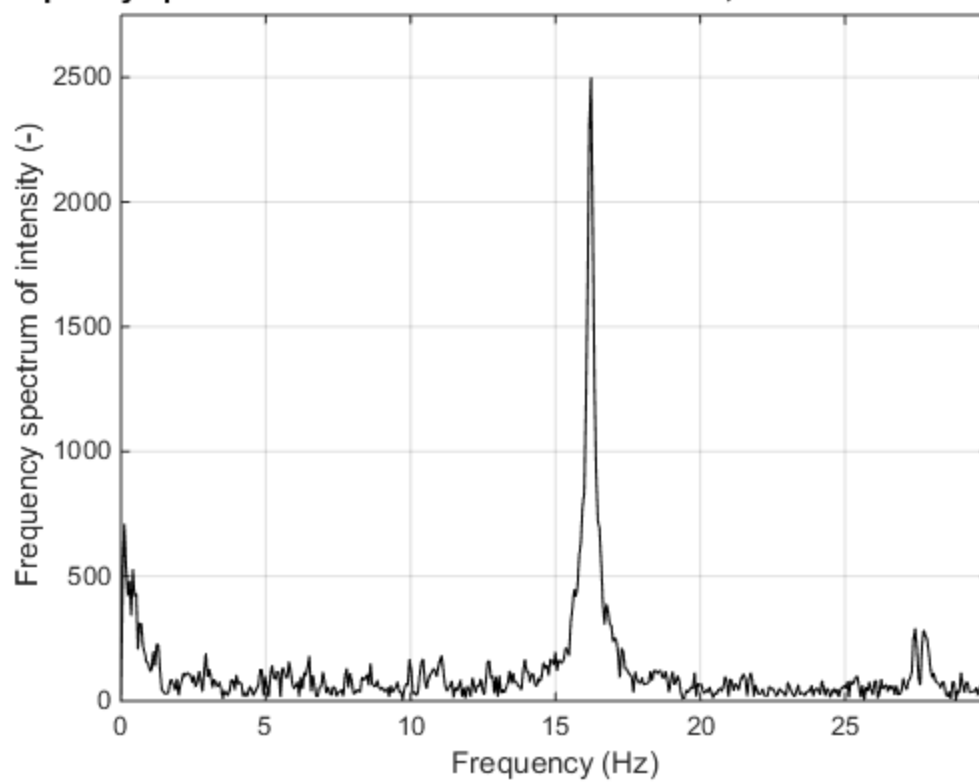
Frequency spectrum of "S05T2 Feb 20 GoPro.MP4", Pixel coordinates: 693 346



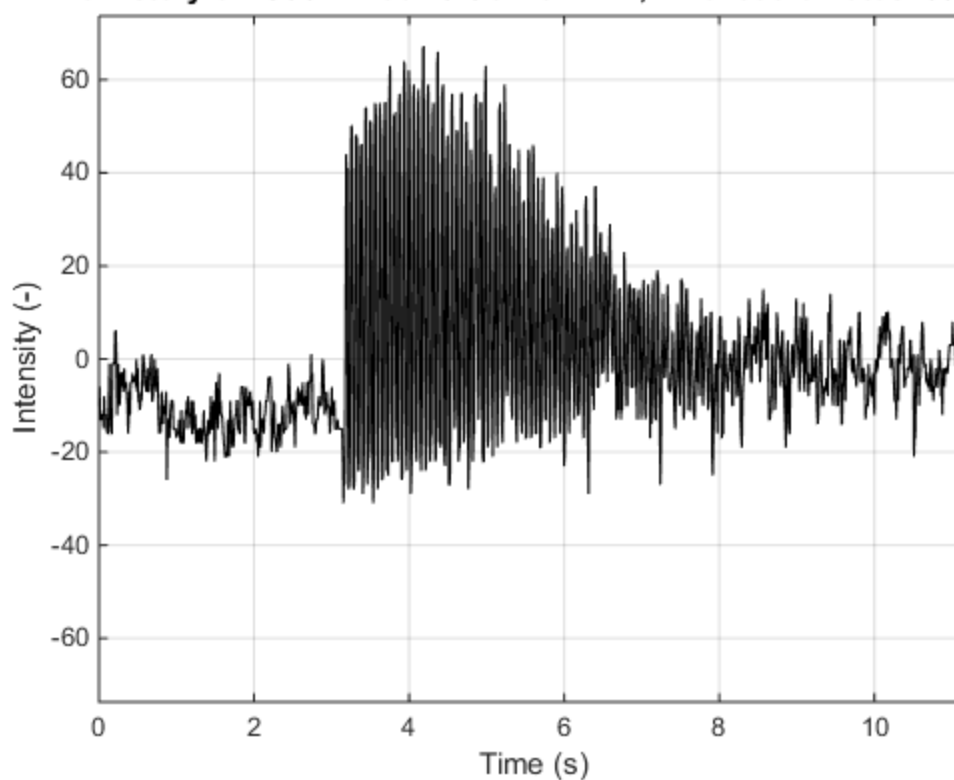
Time history of "S06T1 Feb 20 Canon.MOV", Pixel coordinates: 652 378



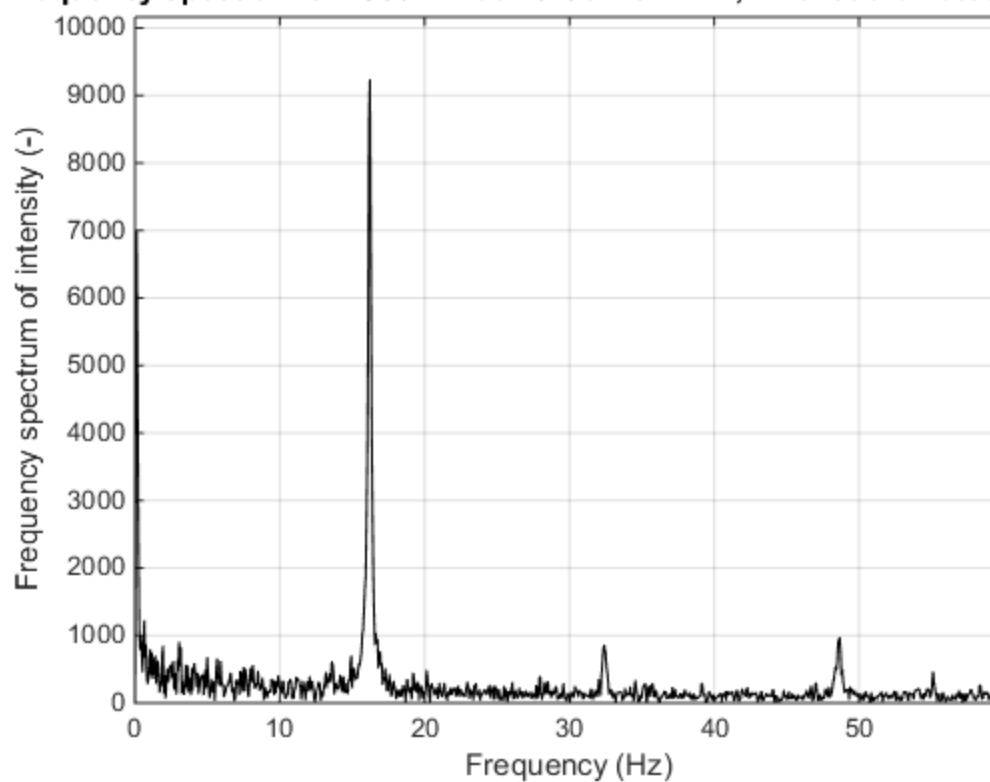
Frequency spectrum of "S06T1 Feb 20 Canon.MOV", Pixel coordinates: 652 3'



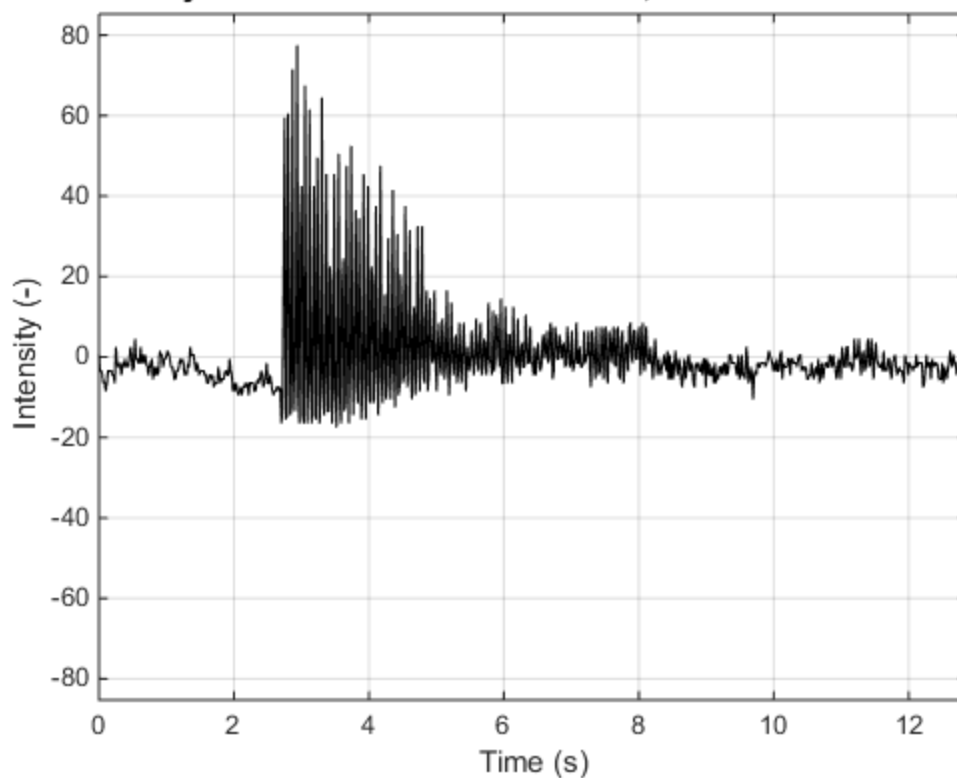
Time history of "S06T1 Feb 20 GoPro.MP4", Pixel coordinates: 664 333



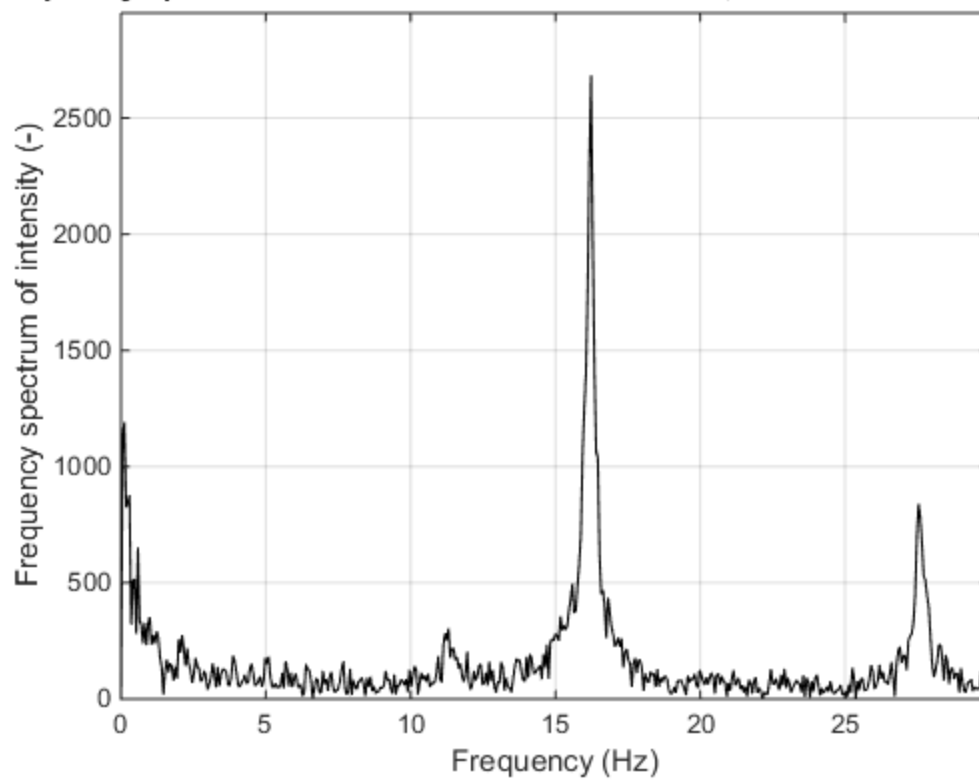
Frequency spectrum of "S06T1 Feb 20 GoPro.MP4", Pixel coordinates: 664 333



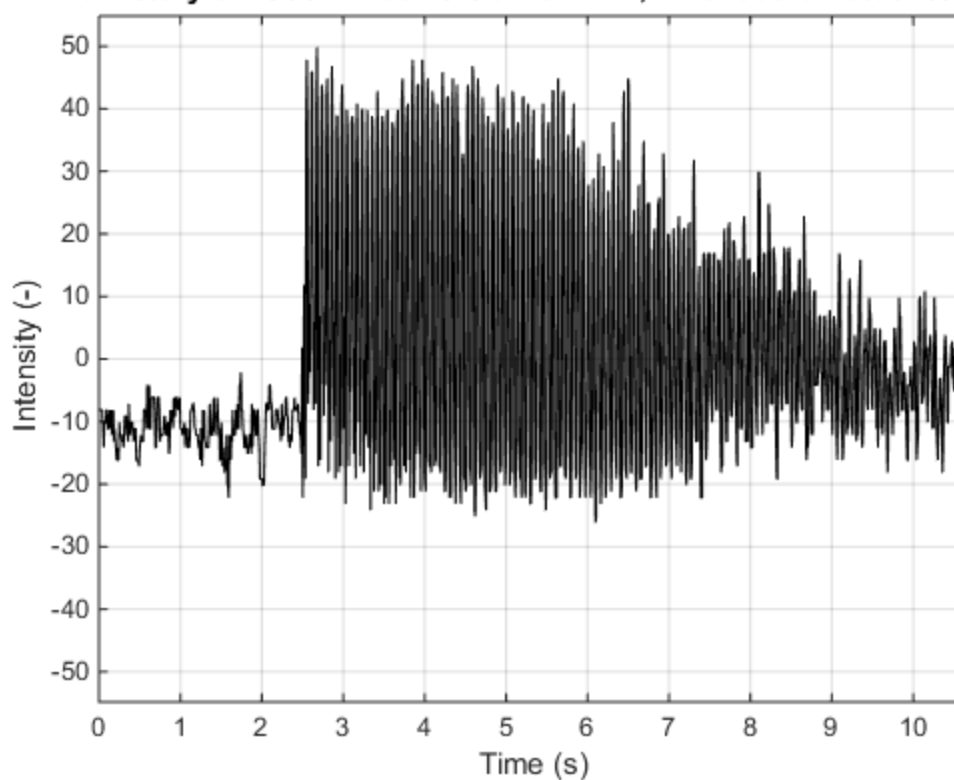
Time history of "S06T2 Feb 20 Canon.MOV", Pixel coordinates: 625 354



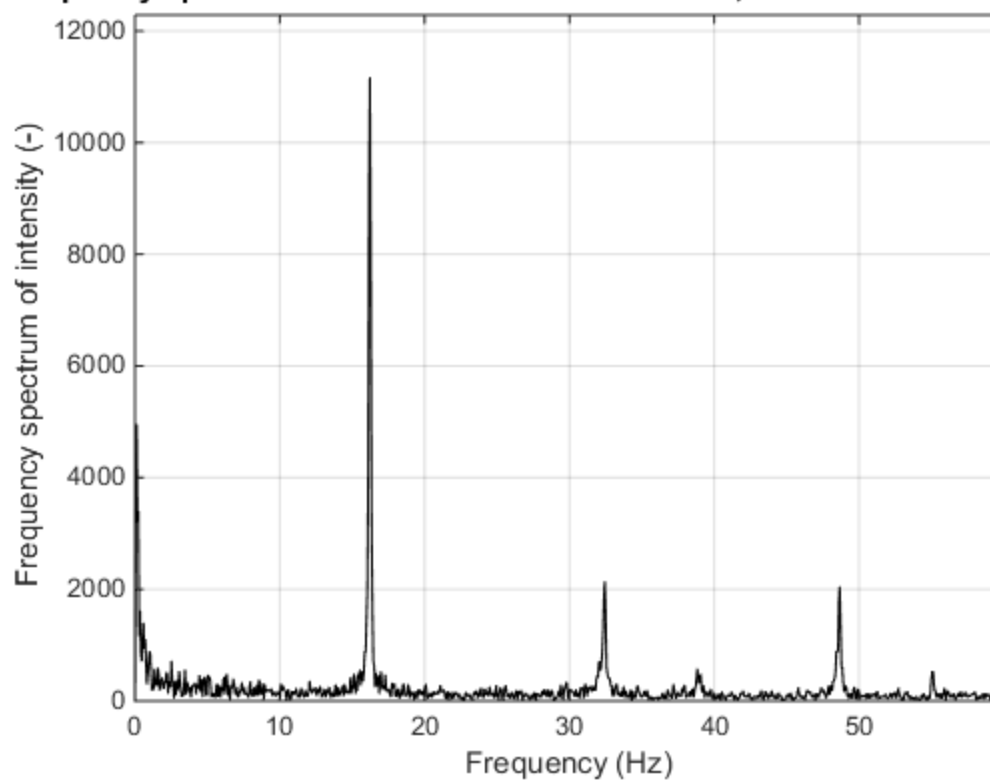
Frequency spectrum of "S06T2 Feb 20 Canon.MOV", Pixel coordinates: 625 354



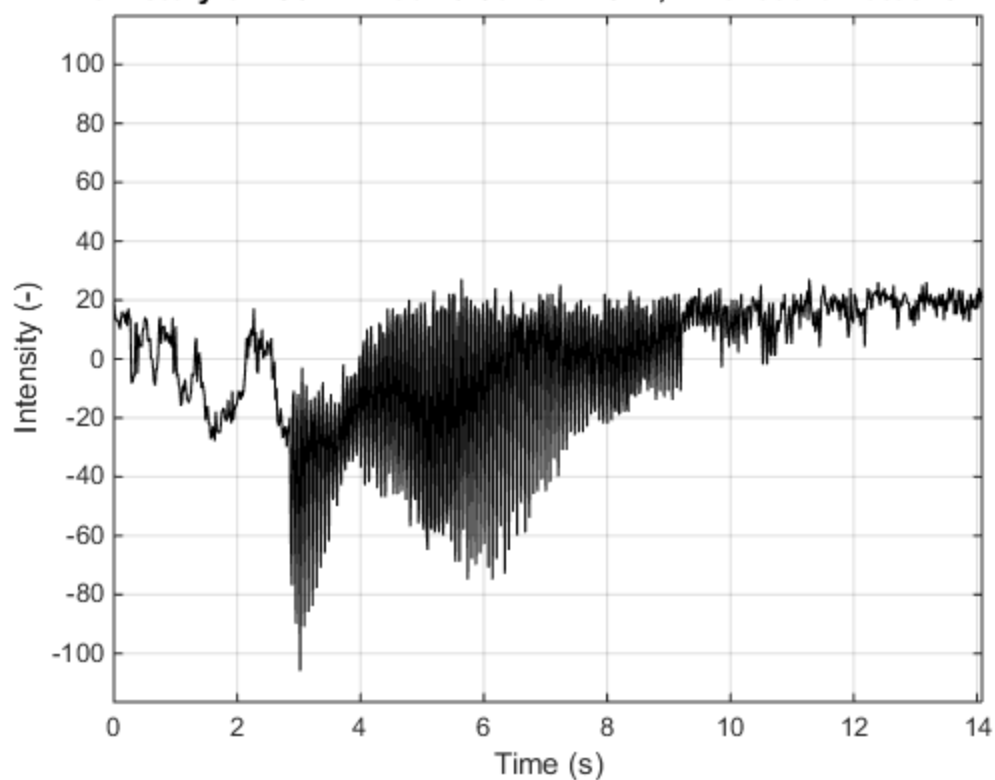
Time history of "S06T2 Feb 20 GoPro.MP4", Pixel coordinates: 599 359



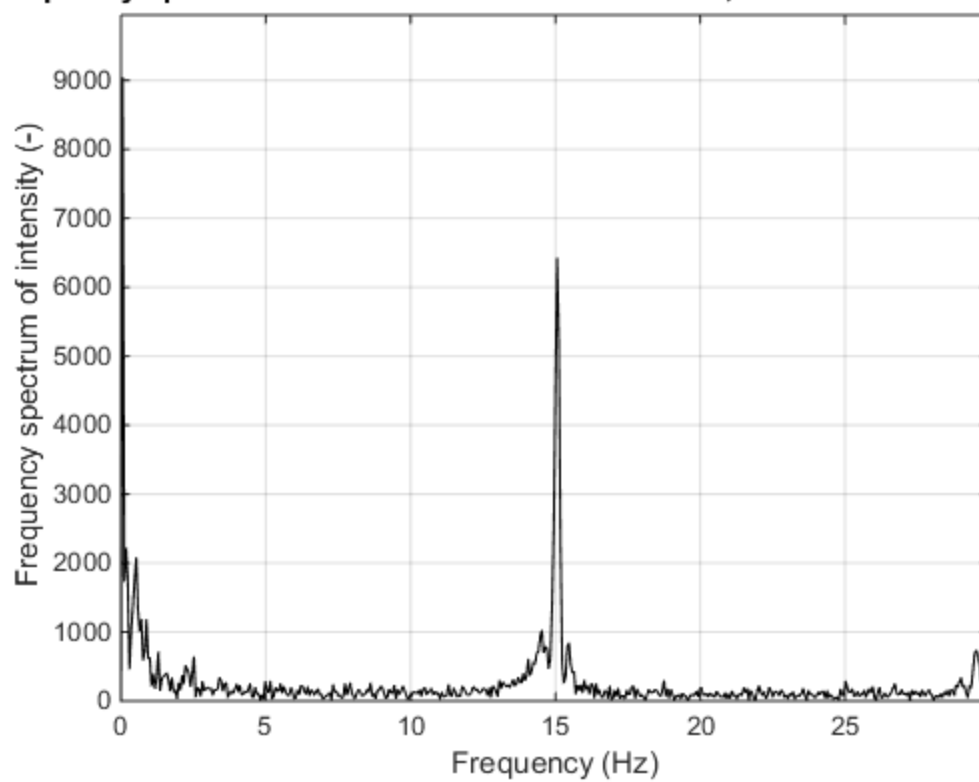
Frequency spectrum of "S06T2 Feb 20 GoPro.MP4", Pixel coordinates: 599 359



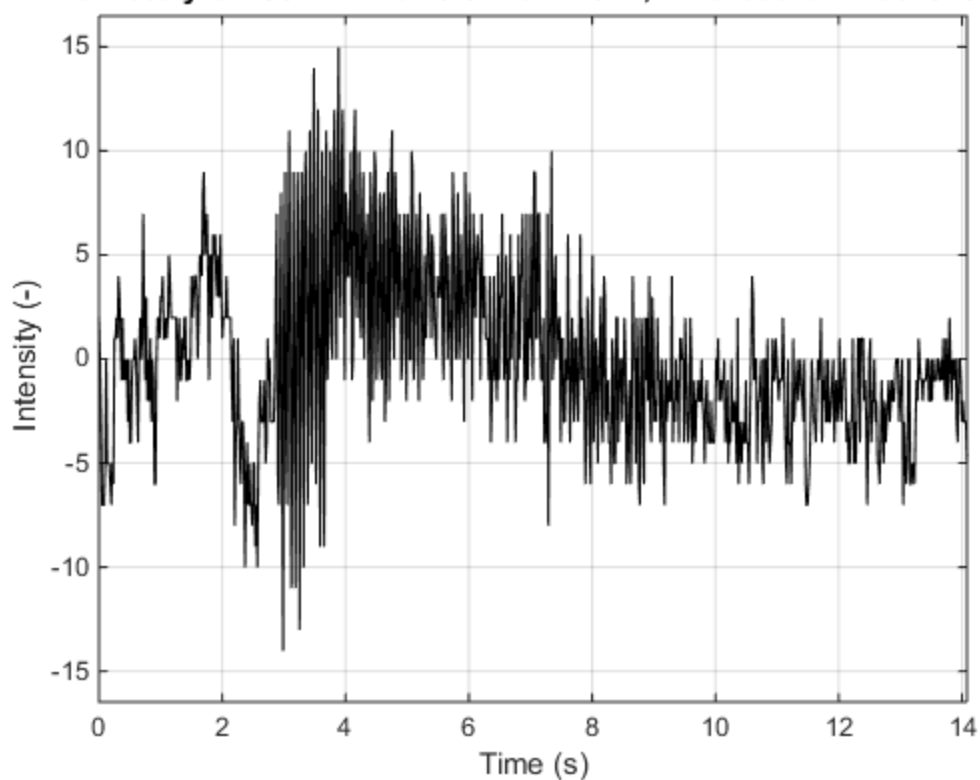
Time history of "S07T1 Feb 20 Canon.MOV", Pixel coordinates: 517 348



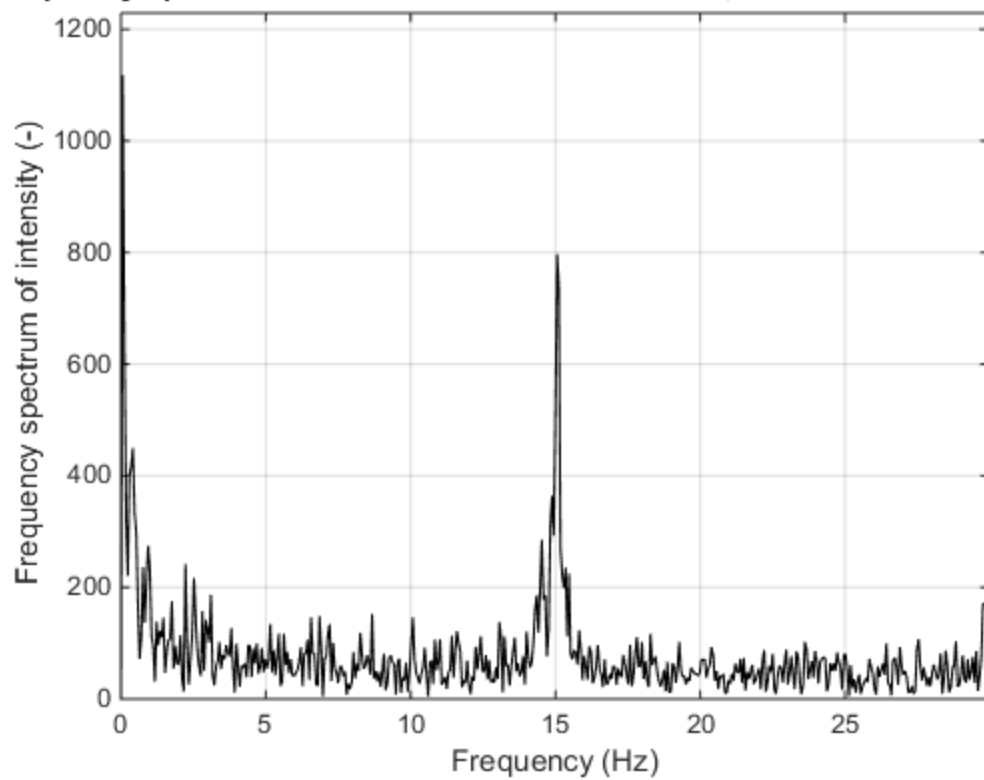
Frequency spectrum of "S07T1 Feb 20 Canon.MOV", Pixel coordinates: 517 348



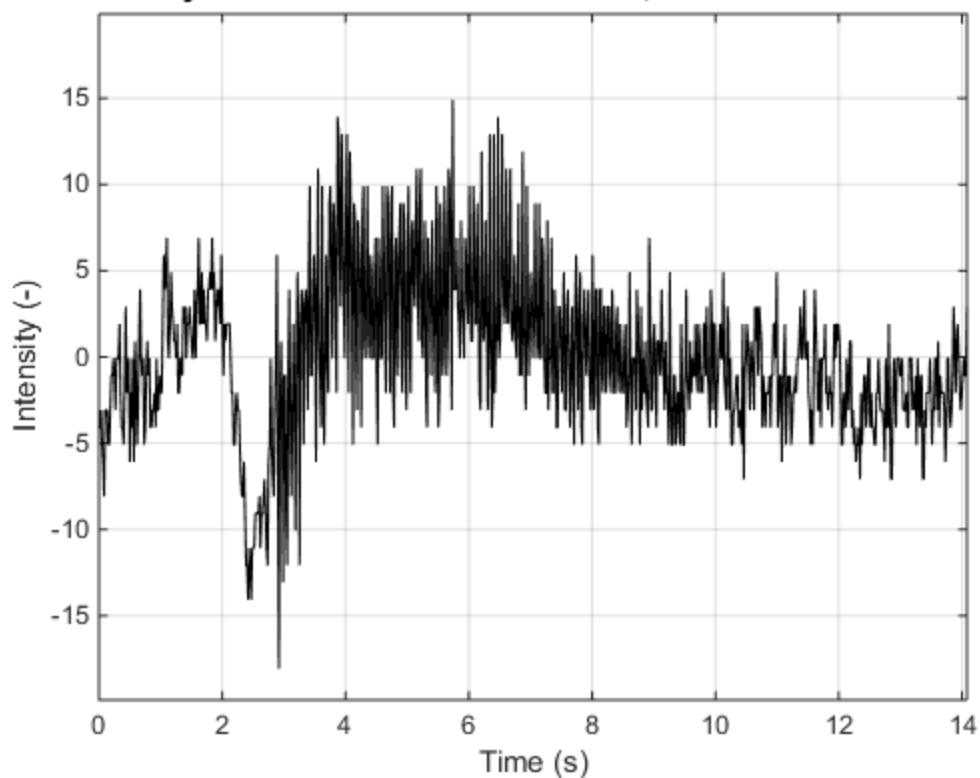
Time history of "S07T1 Feb 20 Canon.MOV", Pixel coordinates: 518 370



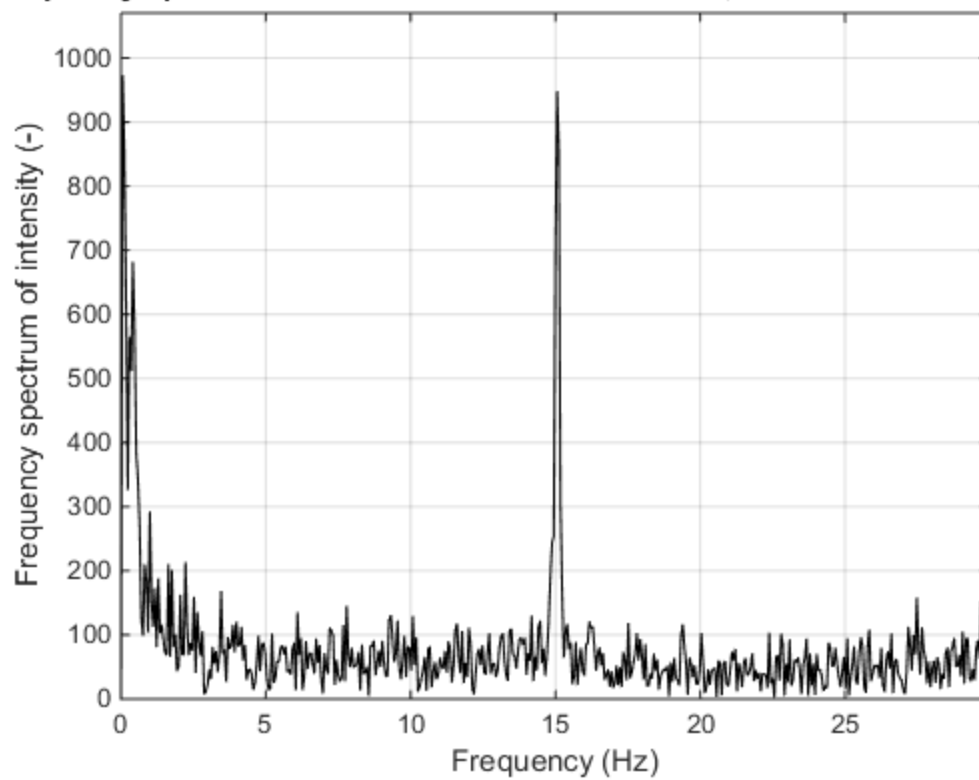
Frequency spectrum of "S07T1 Feb 20 Canon.MOV", Pixel coordinates: 518 3'



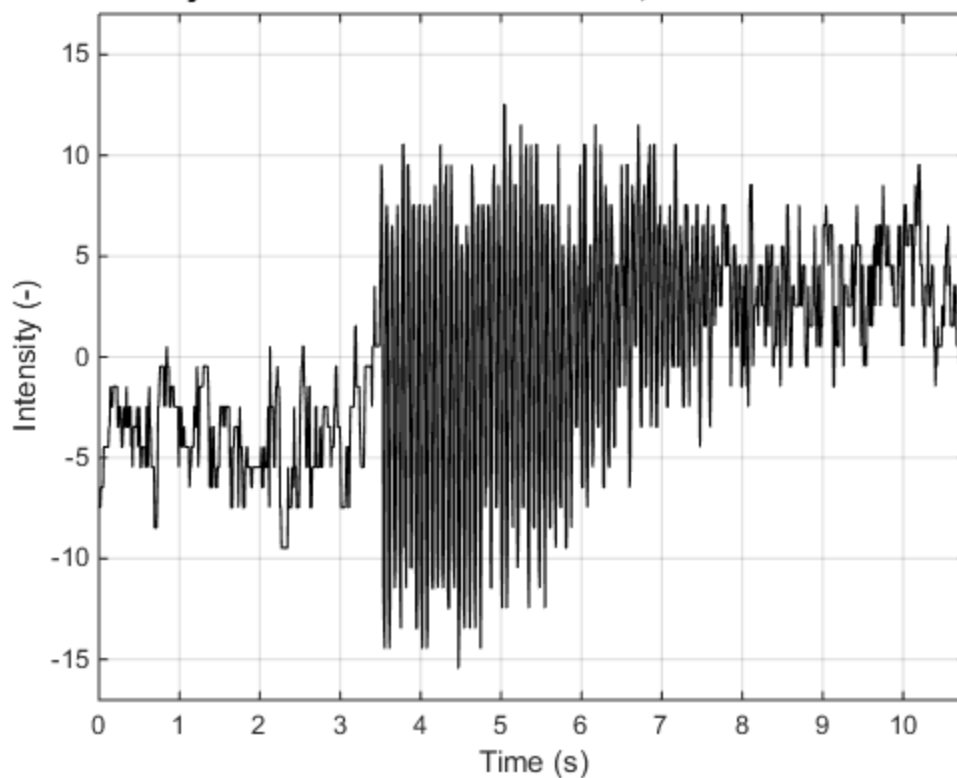
Time history of "S07T1 Feb 20 Canon.MOV", Pixel coordinates: 625 354



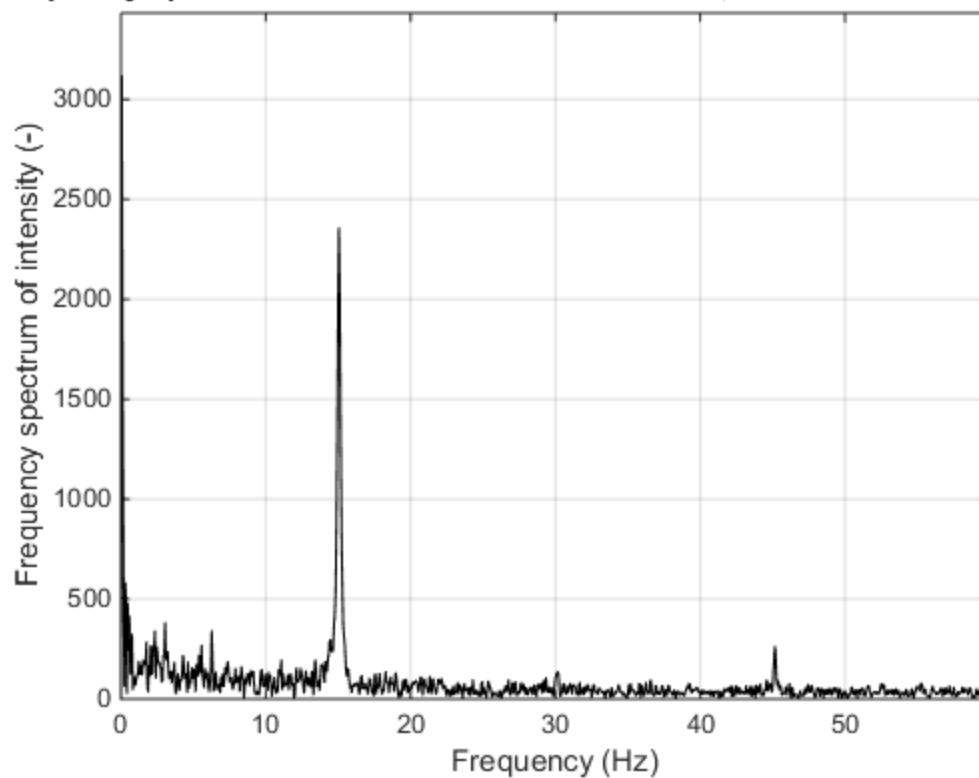
Frequency spectrum of "S07T1 Feb 20 Canon.MOV", Pixel coordinates: 625 354



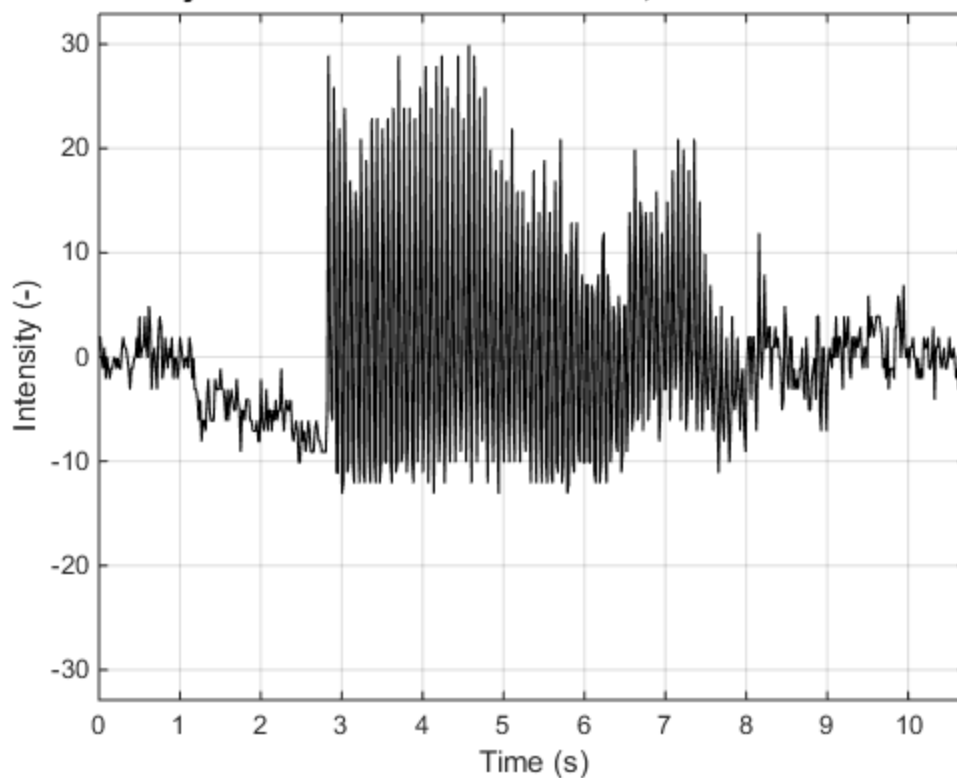
Time history of "S07T1 Feb 20 GoPro.MP4", Pixel coordinates: 738 359



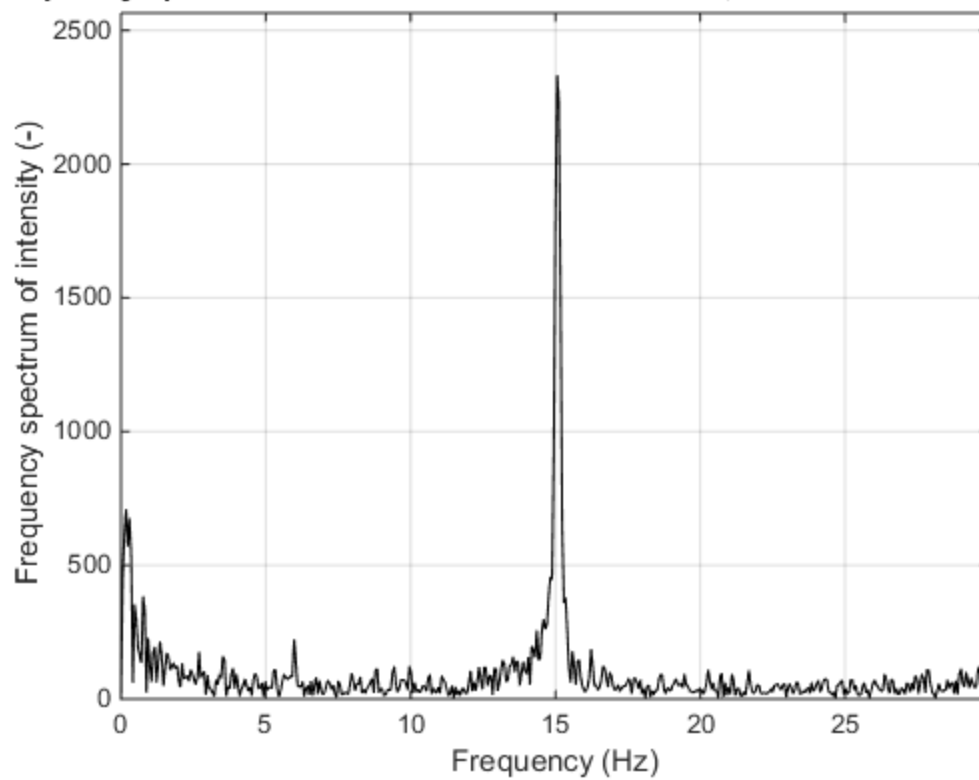
Frequency spectrum of "S07T1 Feb 20 GoPro.MP4", Pixel coordinates: 738 359



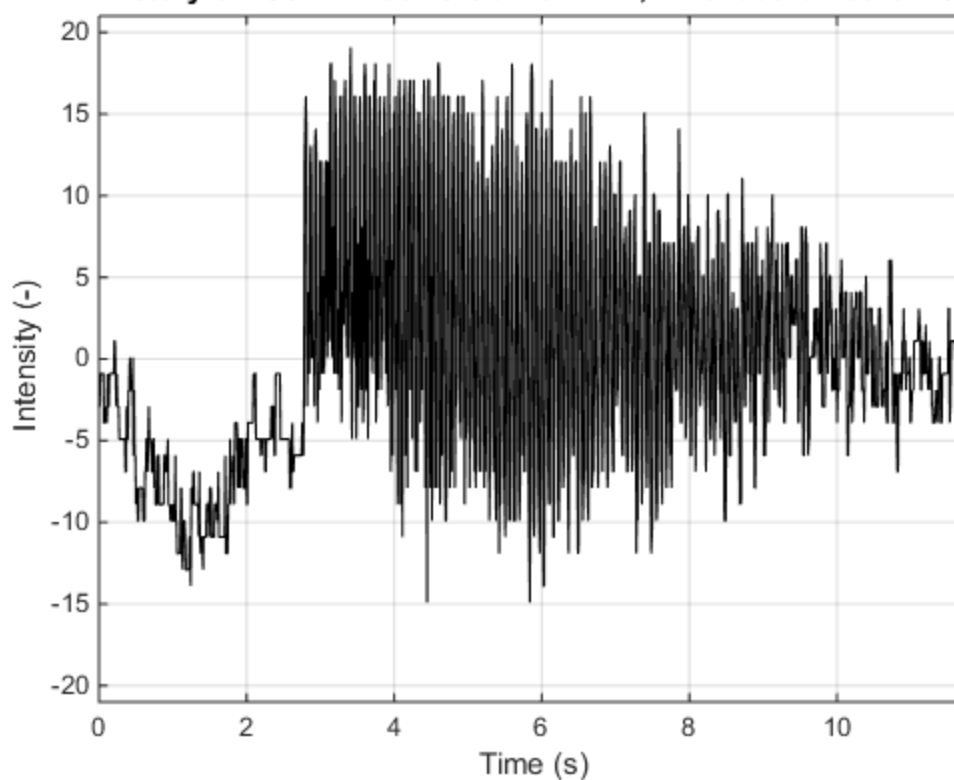
Time history of "S07T2 Feb 20 Canon.MOV", Pixel coordinates: 753 393



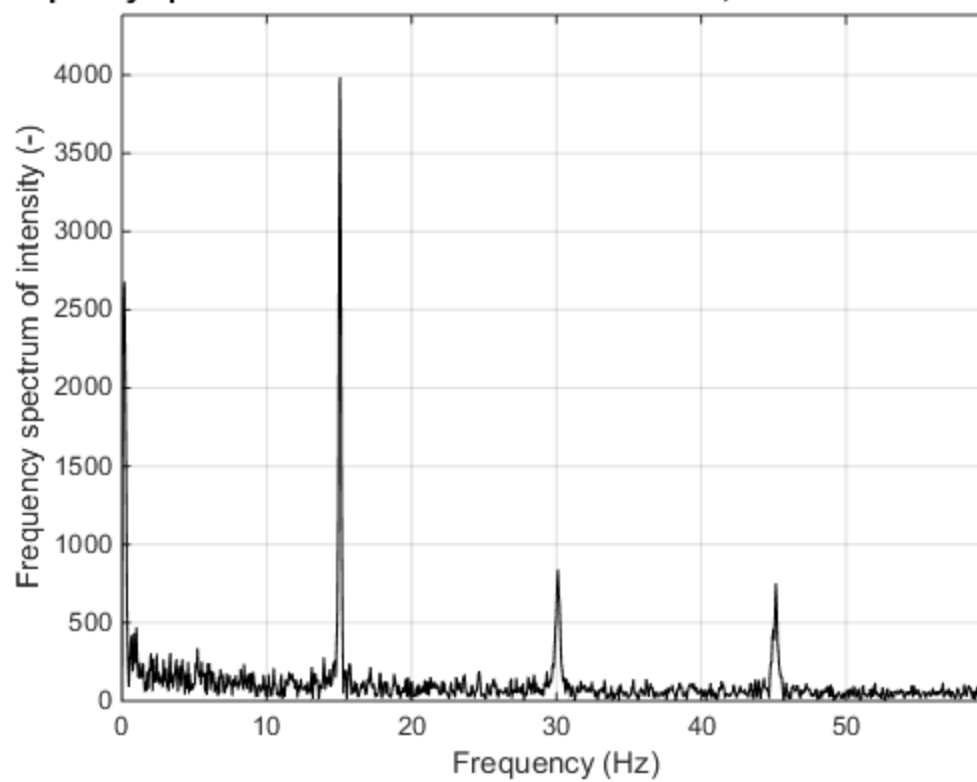
Frequency spectrum of "S07T2 Feb 20 Canon.MOV", Pixel coordinates: 753 393



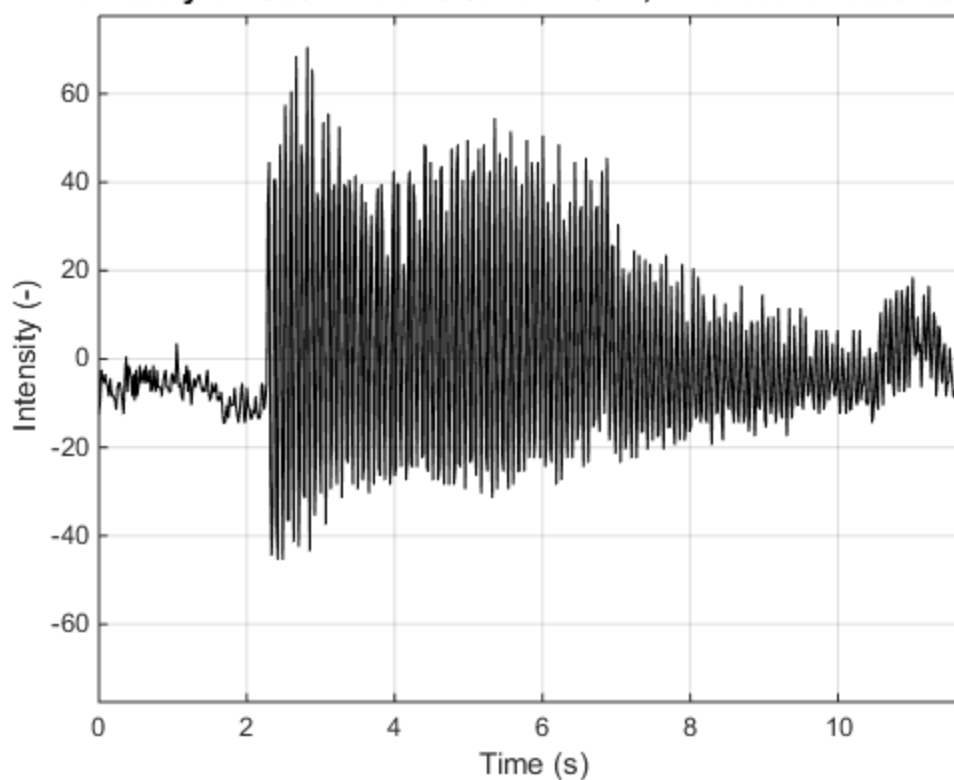
Time history of "S07T2 Feb 20 GoPro.MP4", Pixel coordinates: 763 377



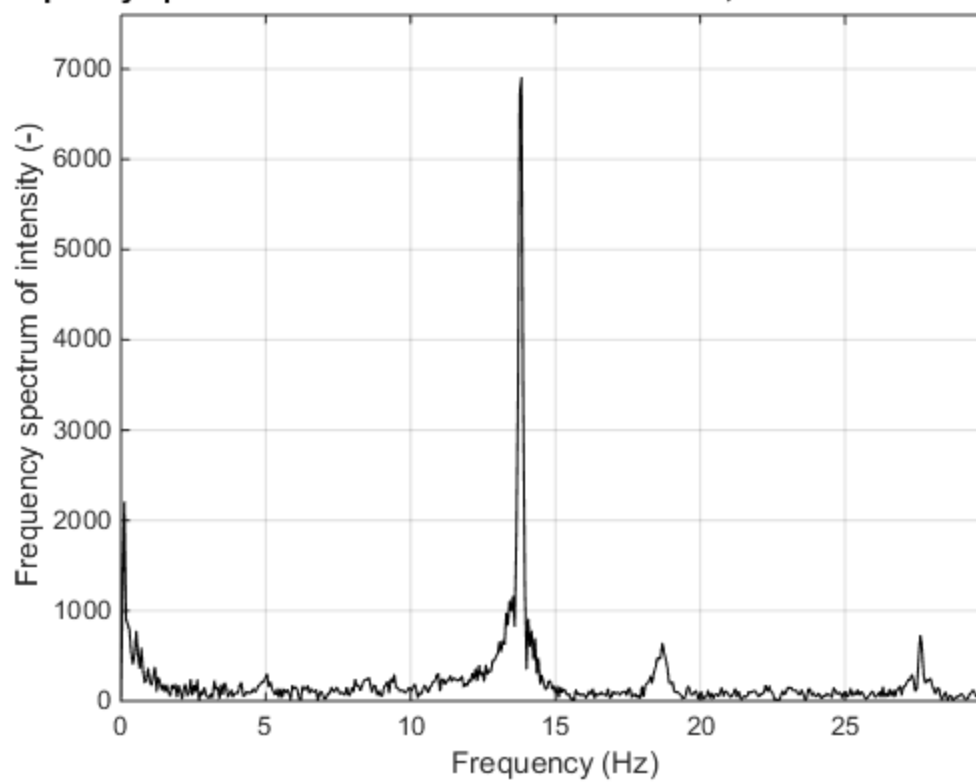
Frequency spectrum of "S07T2 Feb 20 GoPro.MP4", Pixel coordinates: 763 377



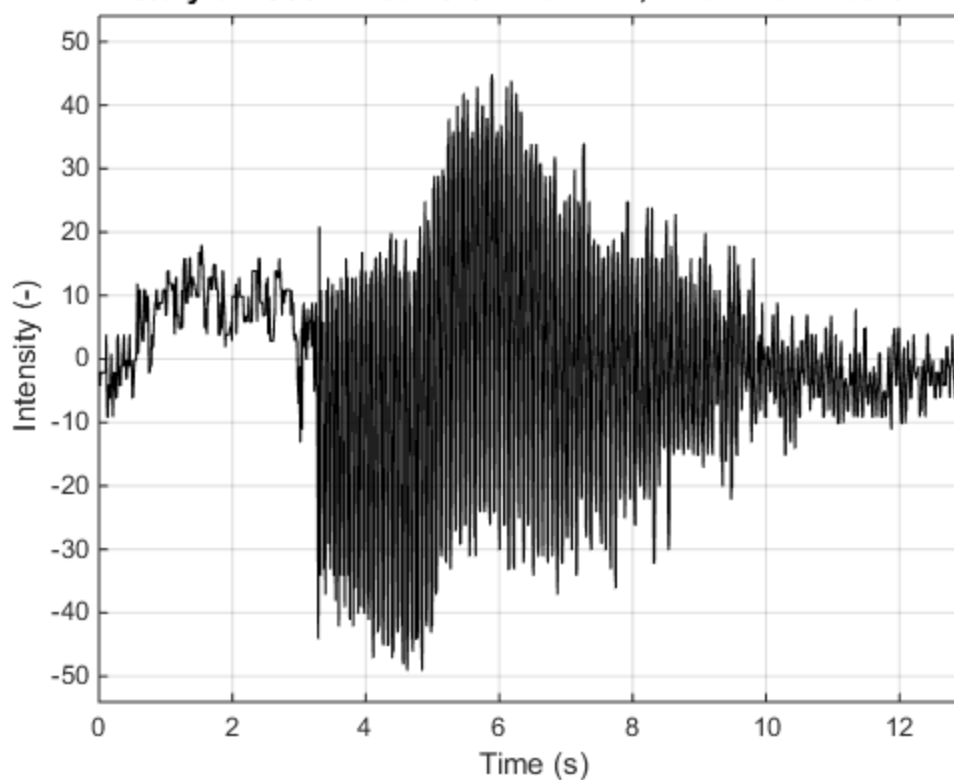
Time history of "S08T1 Feb 20 Canon.MOV", Pixel coordinates: 692 376



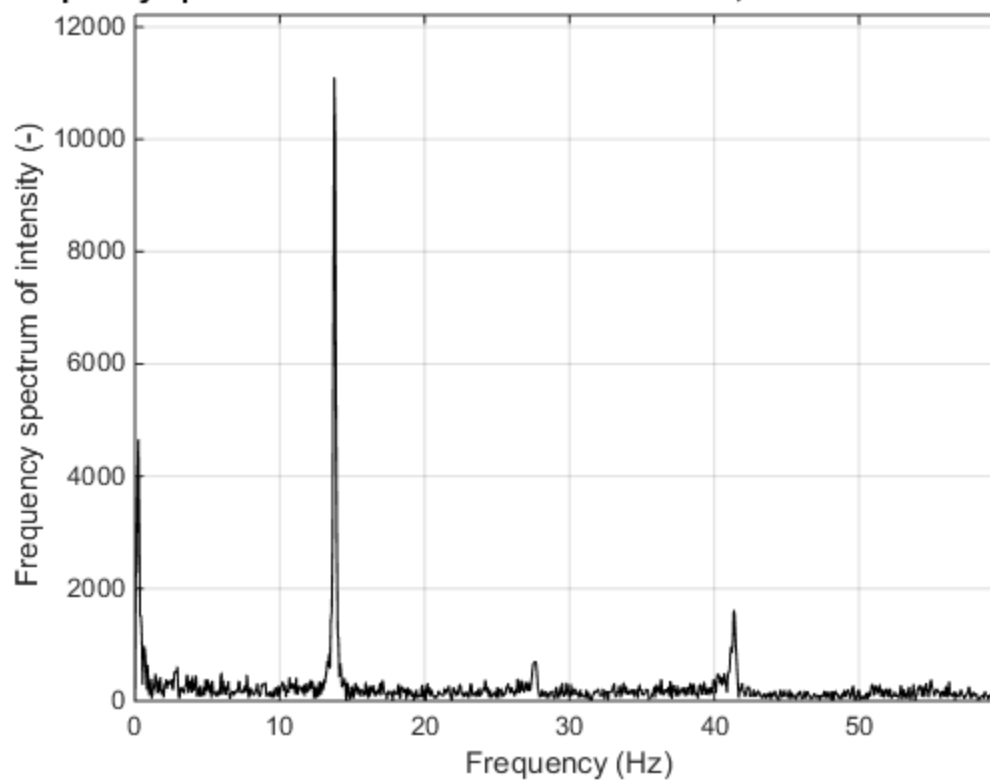
Frequency spectrum of "S08T1 Feb 20 Canon.MOV", Pixel coordinates: 692 3'



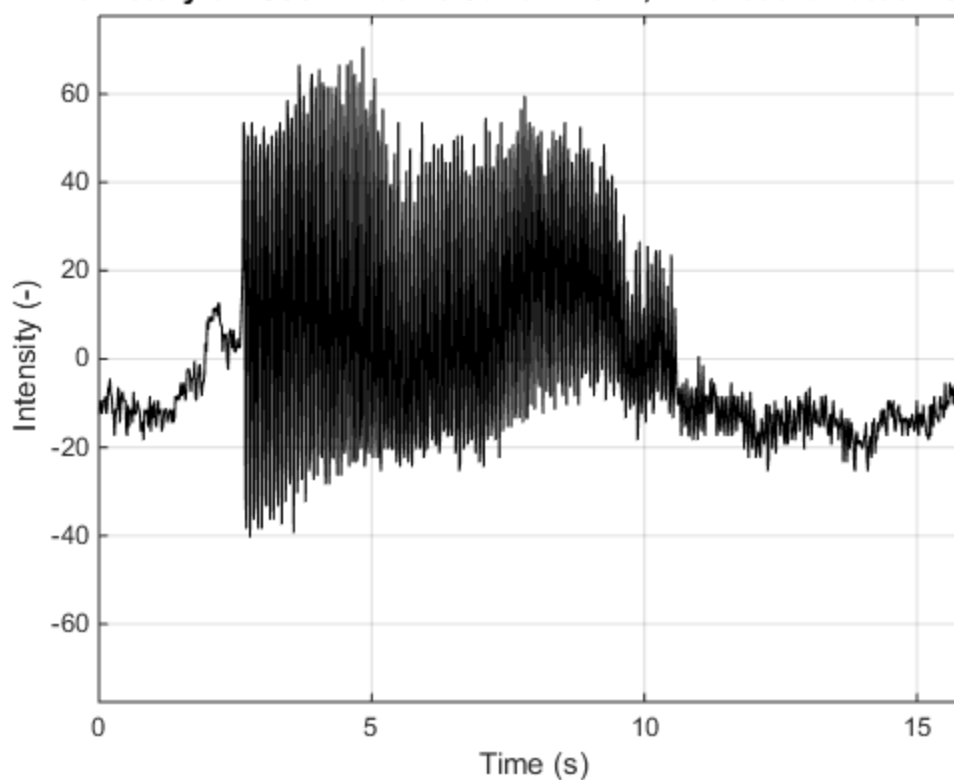
Time history of "S08T1 Feb 20 GoPro.MP4", Pixel coordinates: 441 318



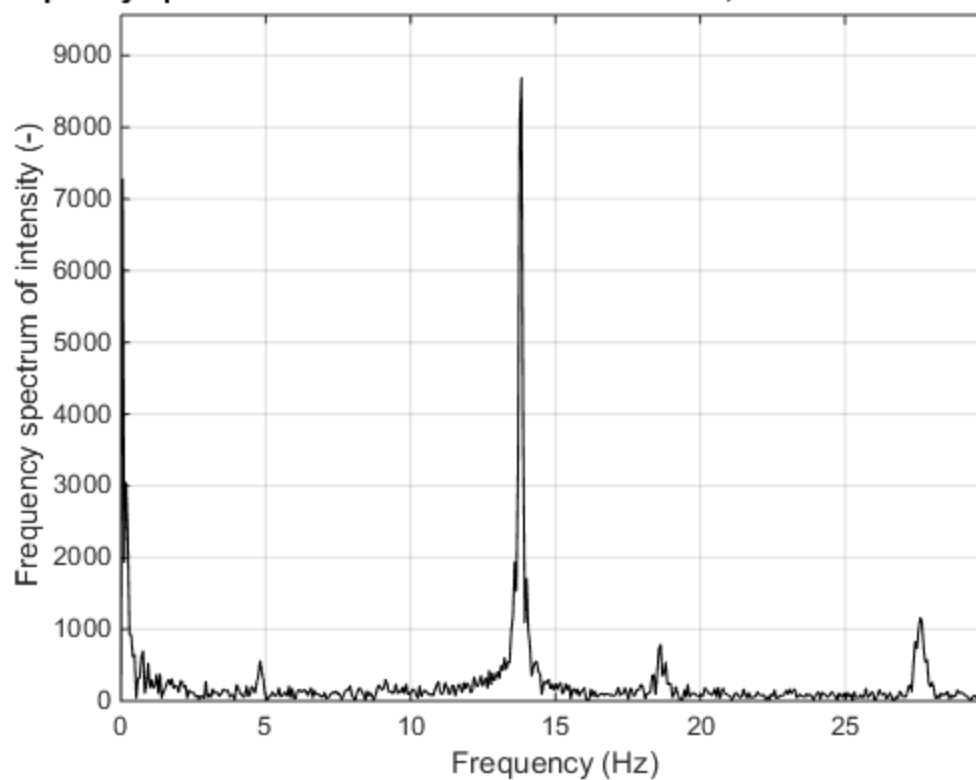
Frequency spectrum of "S08T1 Feb 20 GoPro.MP4", Pixel coordinates: 441 3'



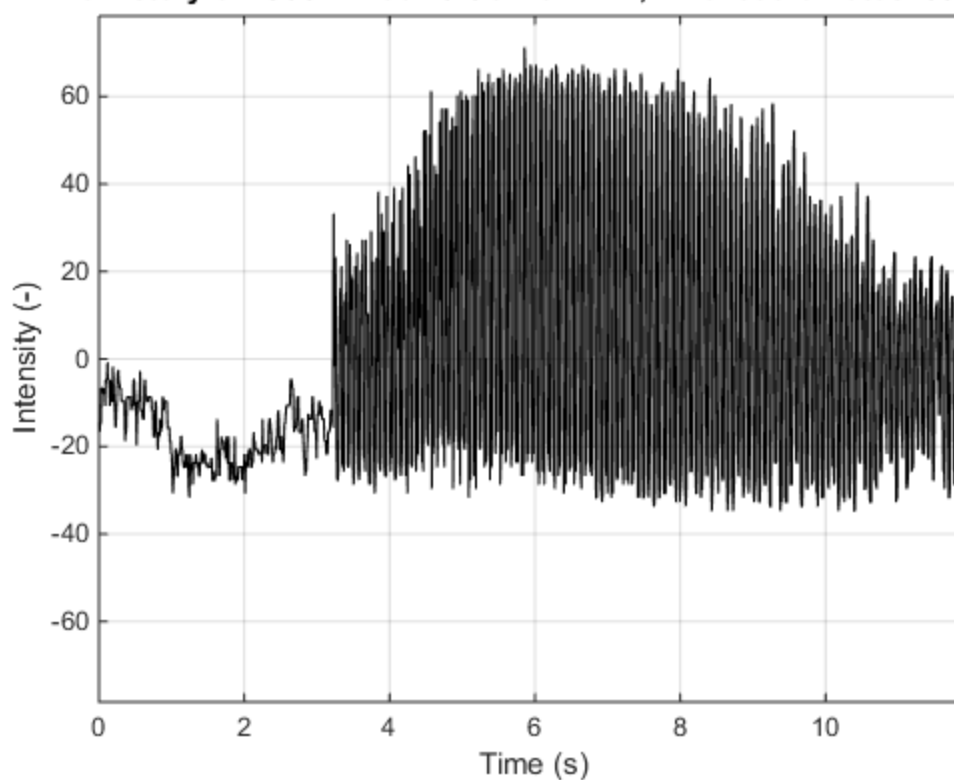
Time history of "S08T2 Feb 20 Canon.MOV", Pixel coordinates: 736 402



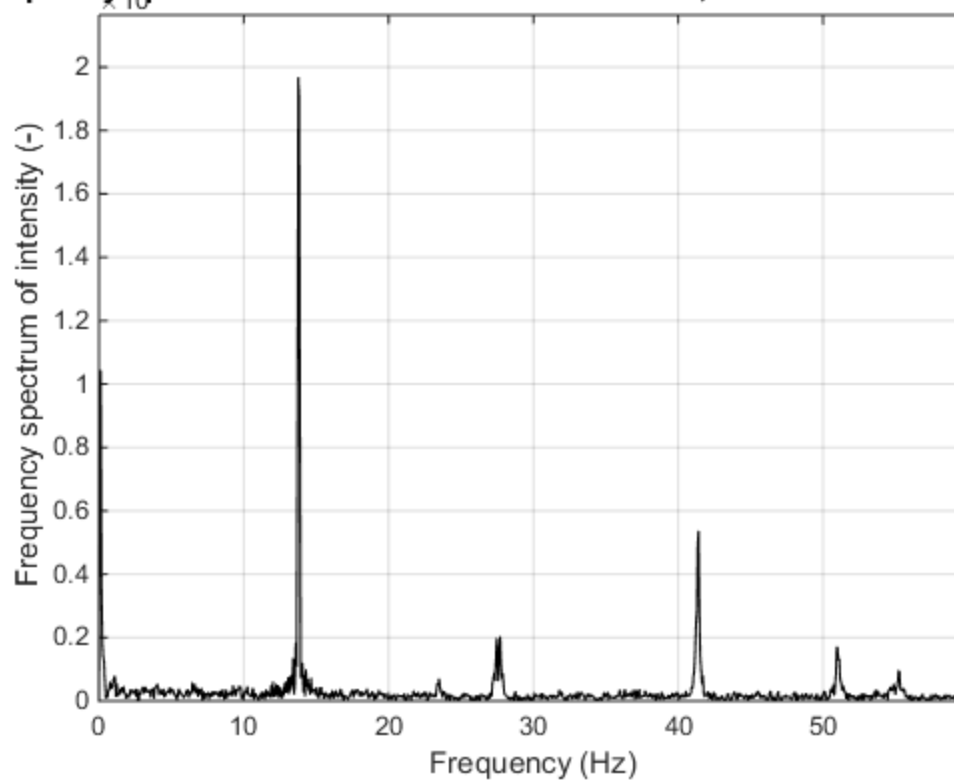
Frequency spectrum of "S08T2 Feb 20 Canon.MOV", Pixel coordinates: 736 402



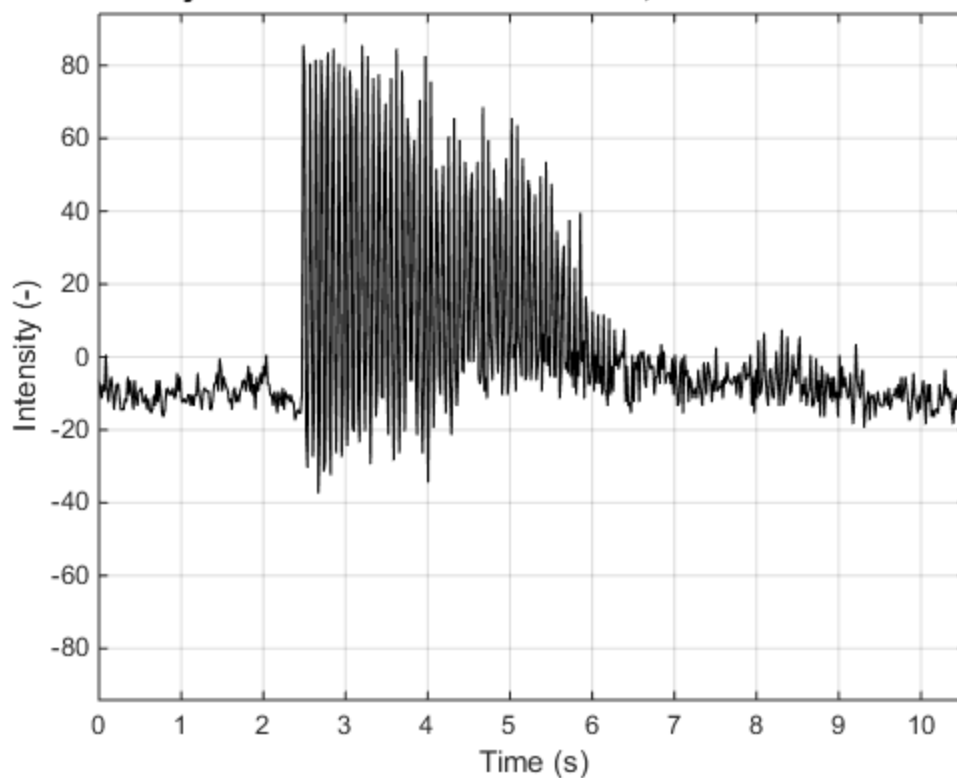
Time history of "S08T2 Feb 20 GoPro.MP4", Pixel coordinates: 380 377



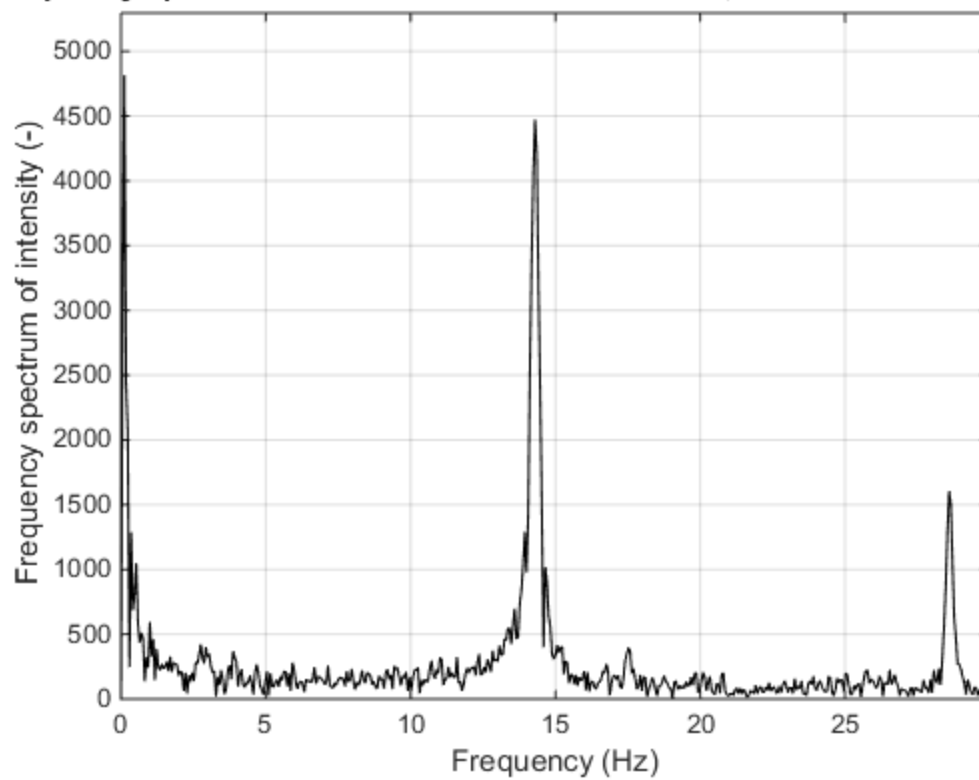
Frequency spectrum of "S08T2 Feb 20 GoPro.MP4", Pixel coordinates: 380 377



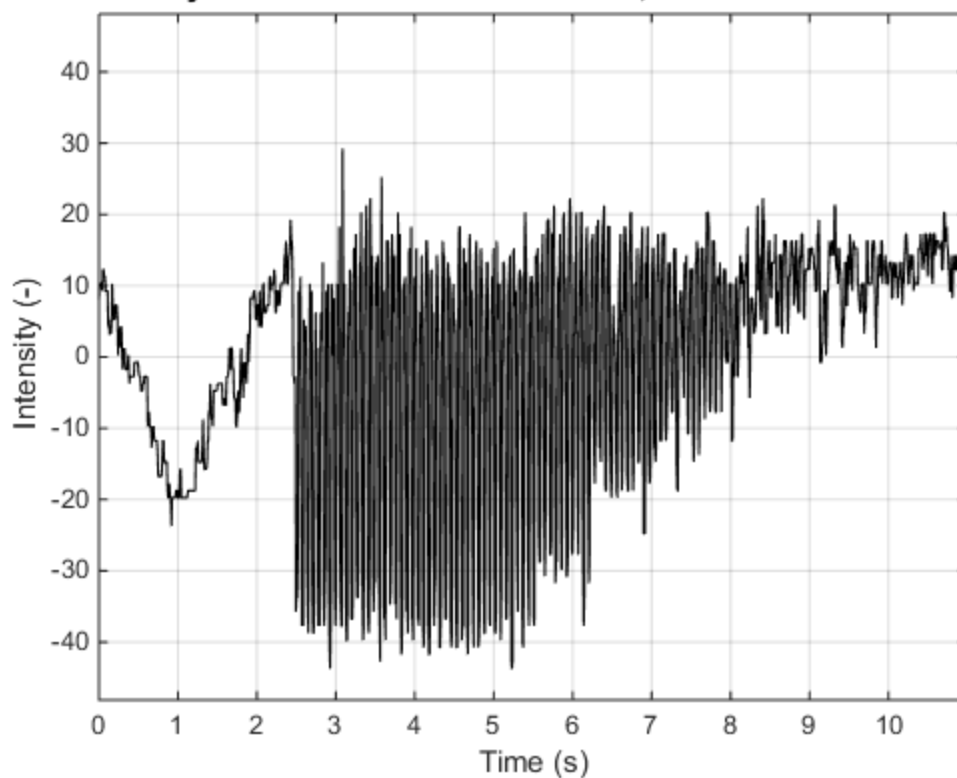
Time history of "S09T1 Feb 20 Canon.MOV", Pixel coordinates: 685 341



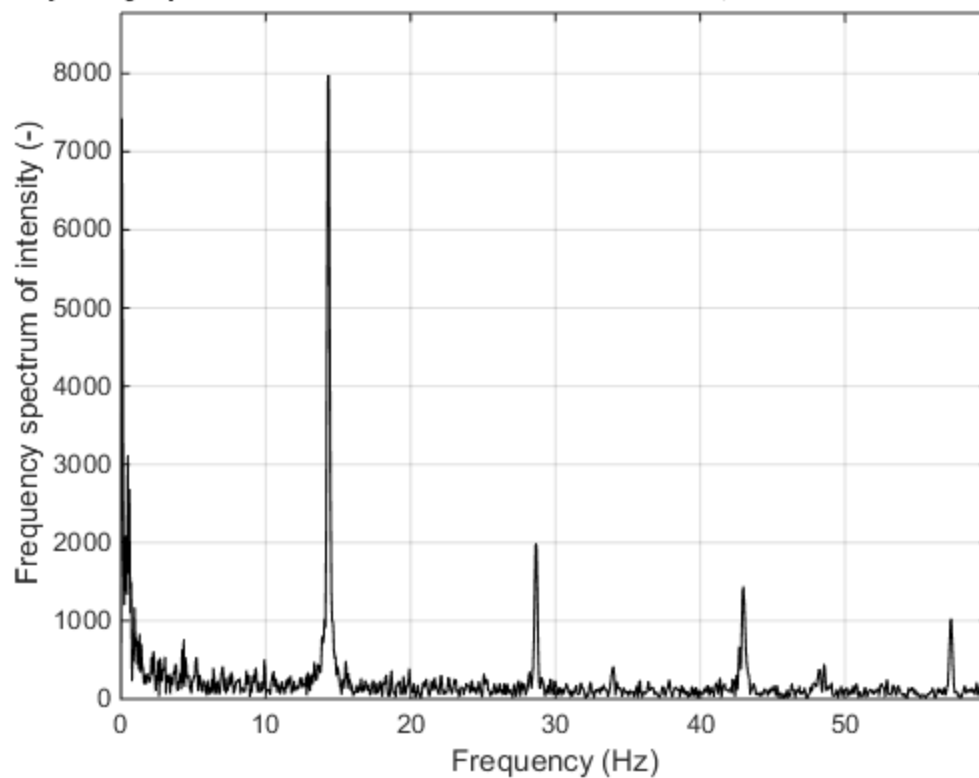
Frequency spectrum of "S09T1 Feb 20 Canon.MOV", Pixel coordinates: 685 341



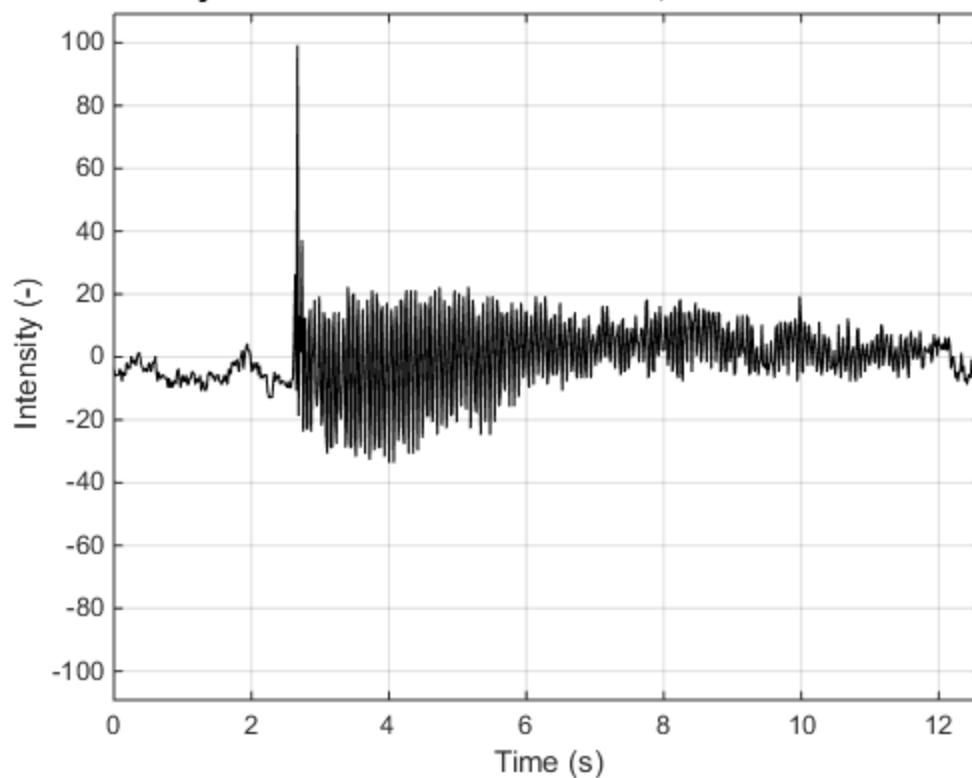
Time history of "S09T1 Feb 20 GoPro.MP4", Pixel coordinates: 692 367



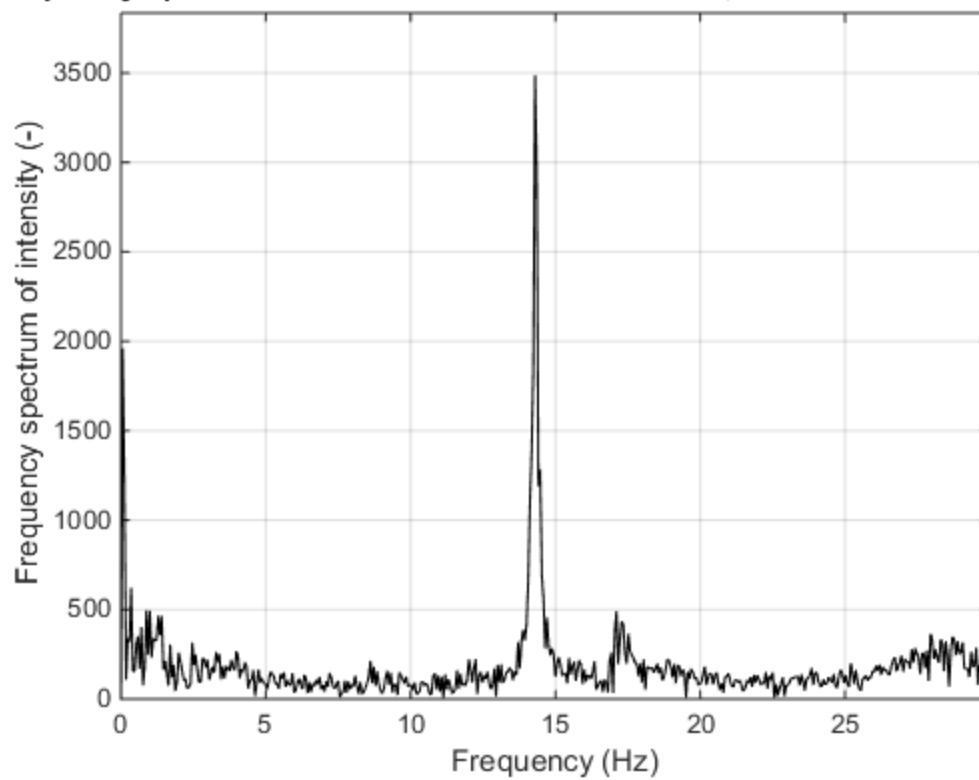
Frequency spectrum of "S09T1 Feb 20 GoPro.MP4", Pixel coordinates: 692 367



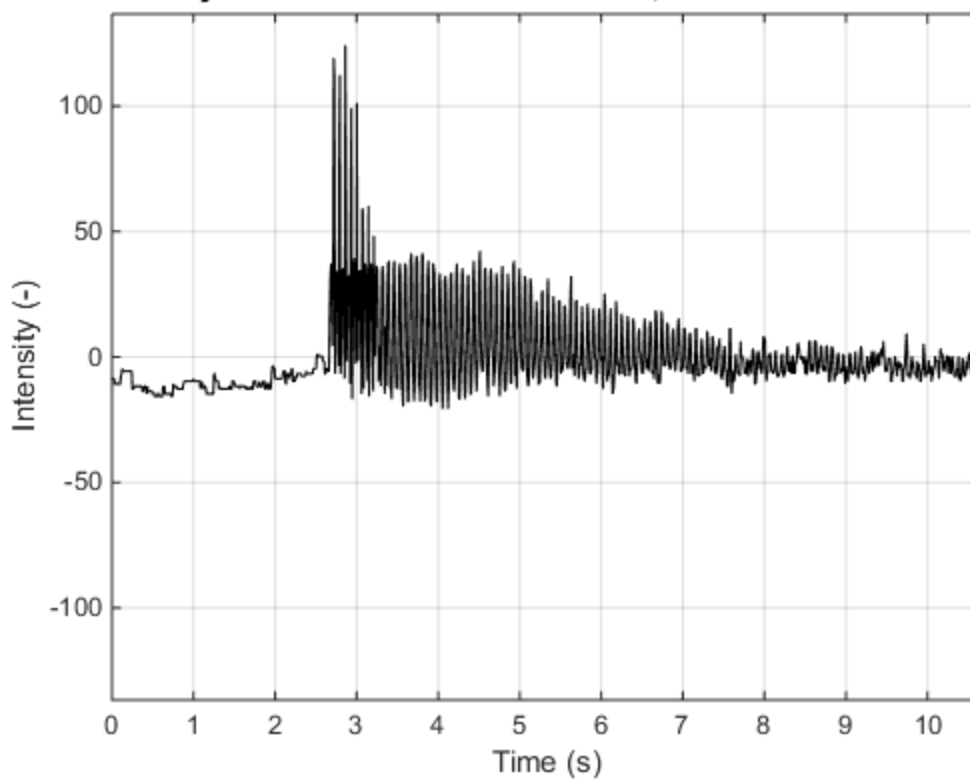
Time history of "S09T2 Feb 20 Canon.MOV", Pixel coordinates: 808 426



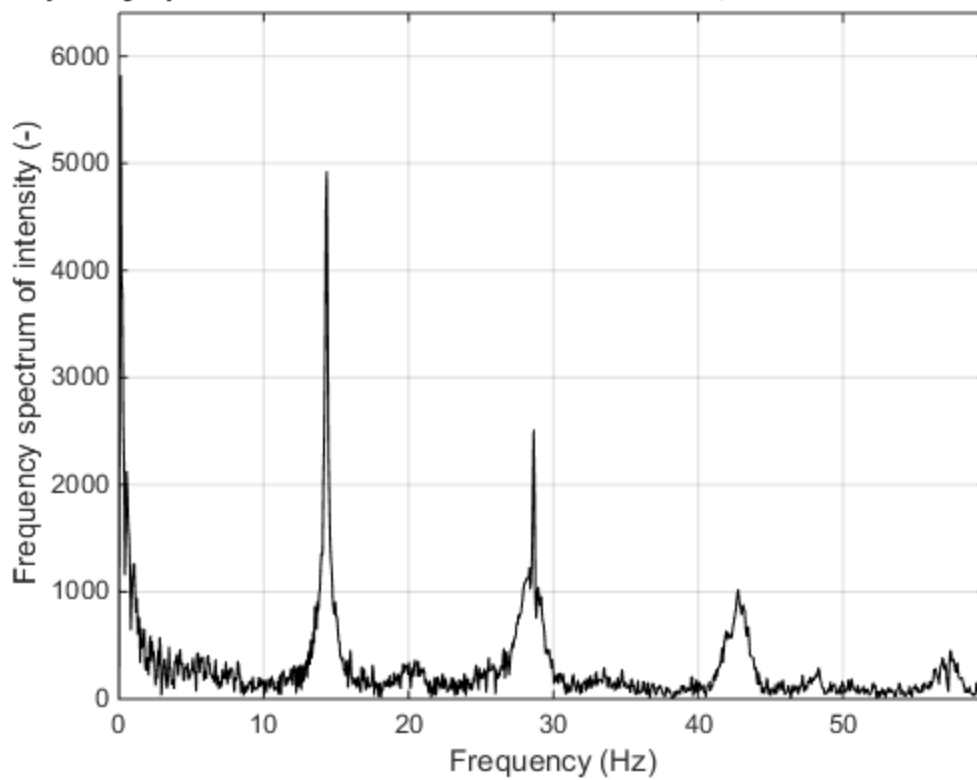
Frequency spectrum of "S09T2 Feb 20 Canon.MOV", Pixel coordinates: 808 426



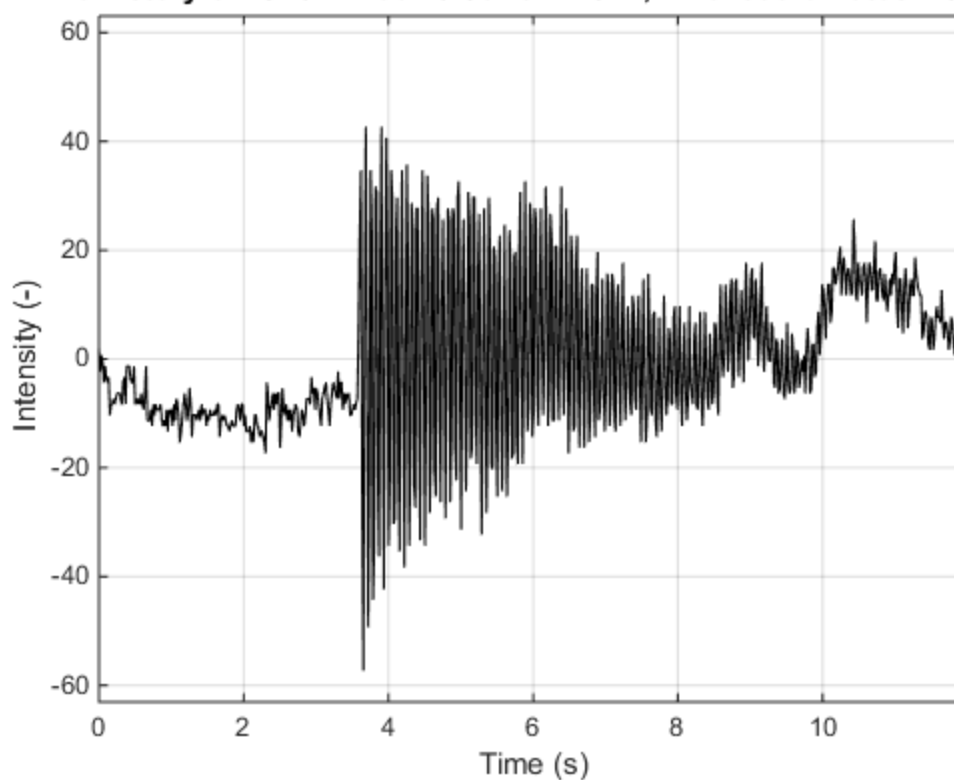
Time history of "S09T2 Feb 20 GoPro.MP4", Pixel coordinates: 579 391



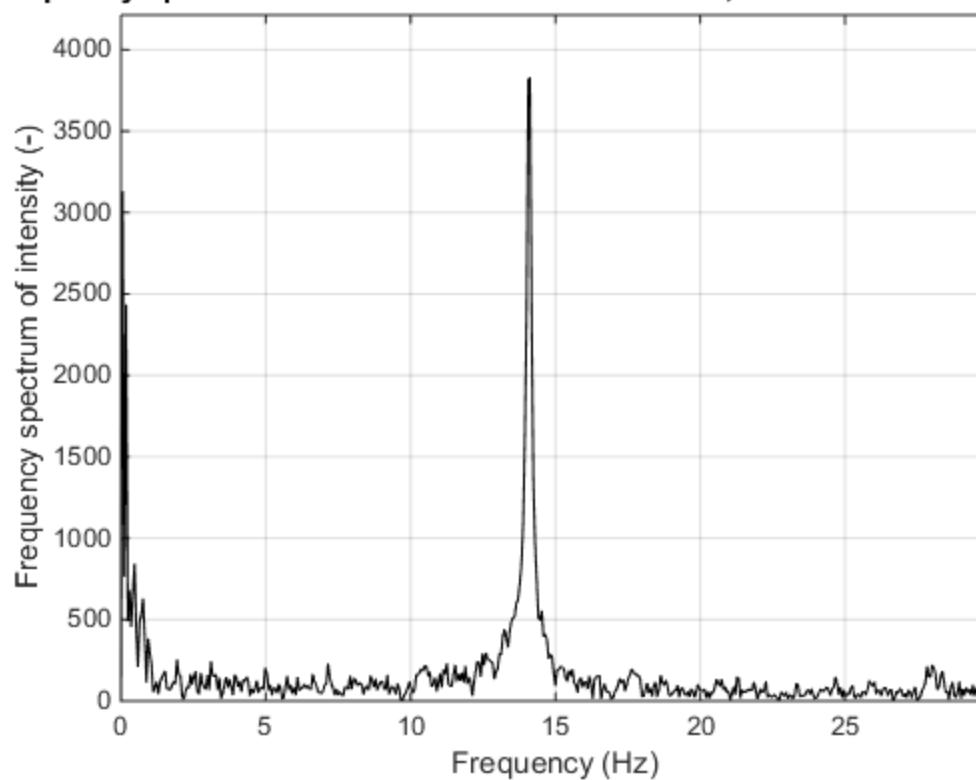
Frequency spectrum of "S09T2 Feb 20 GoPro.MP4", Pixel coordinates: 579 391



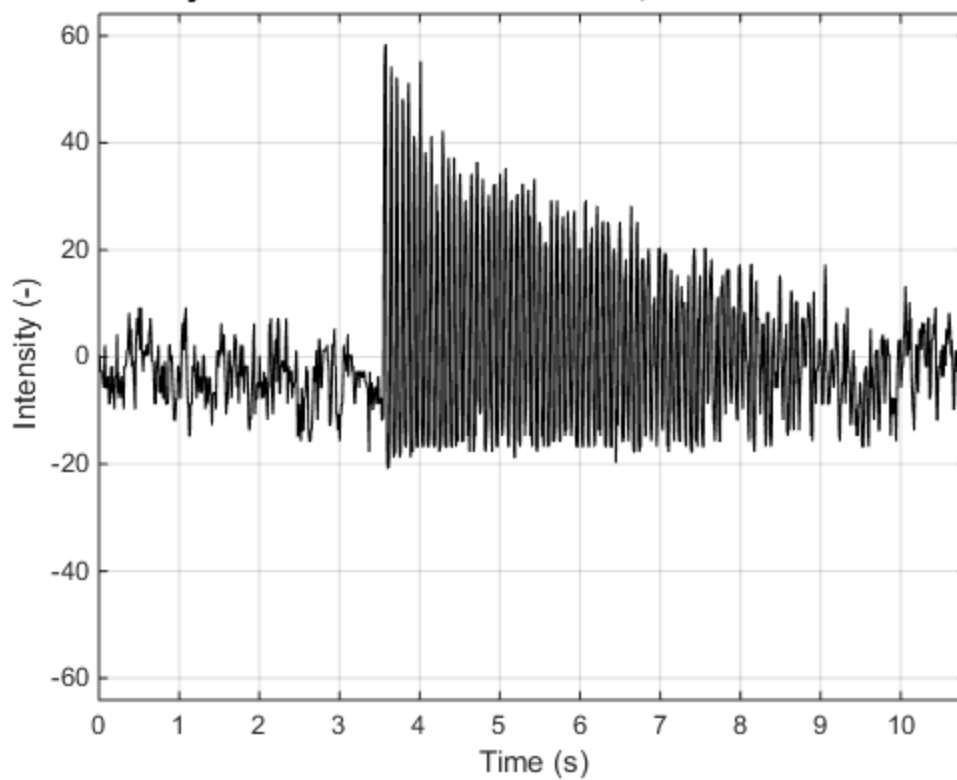
Time history of "S10T1 Feb 20 Canon.MOV", Pixel coordinates: 487 377



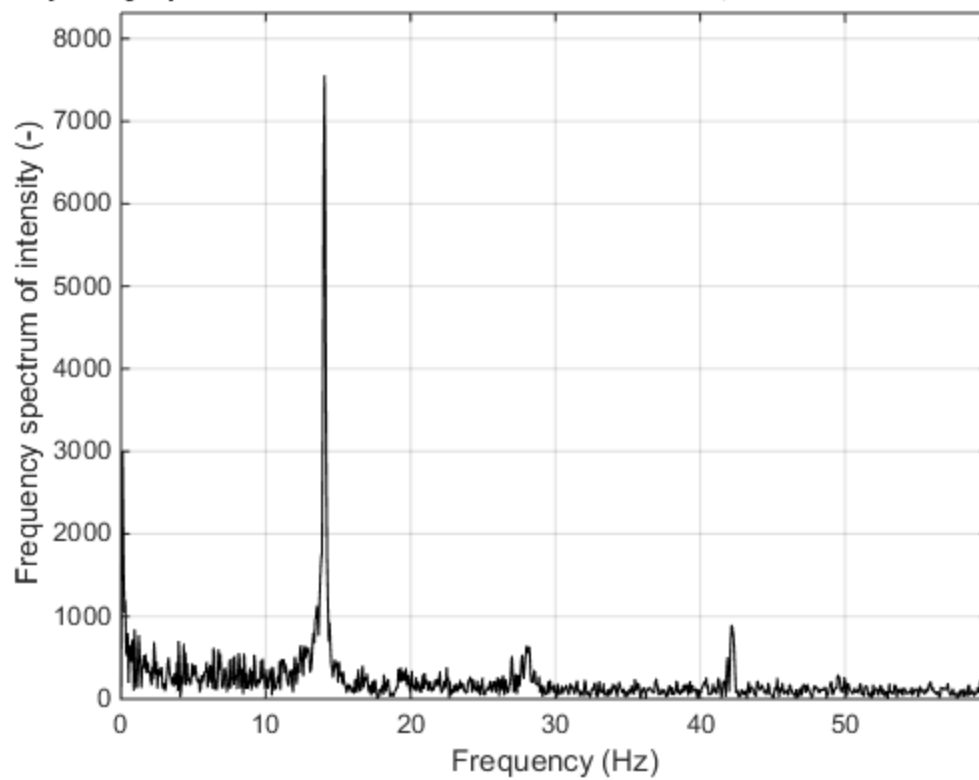
Frequency spectrum of "S10T1 Feb 20 Canon.MOV", Pixel coordinates: 487 3'



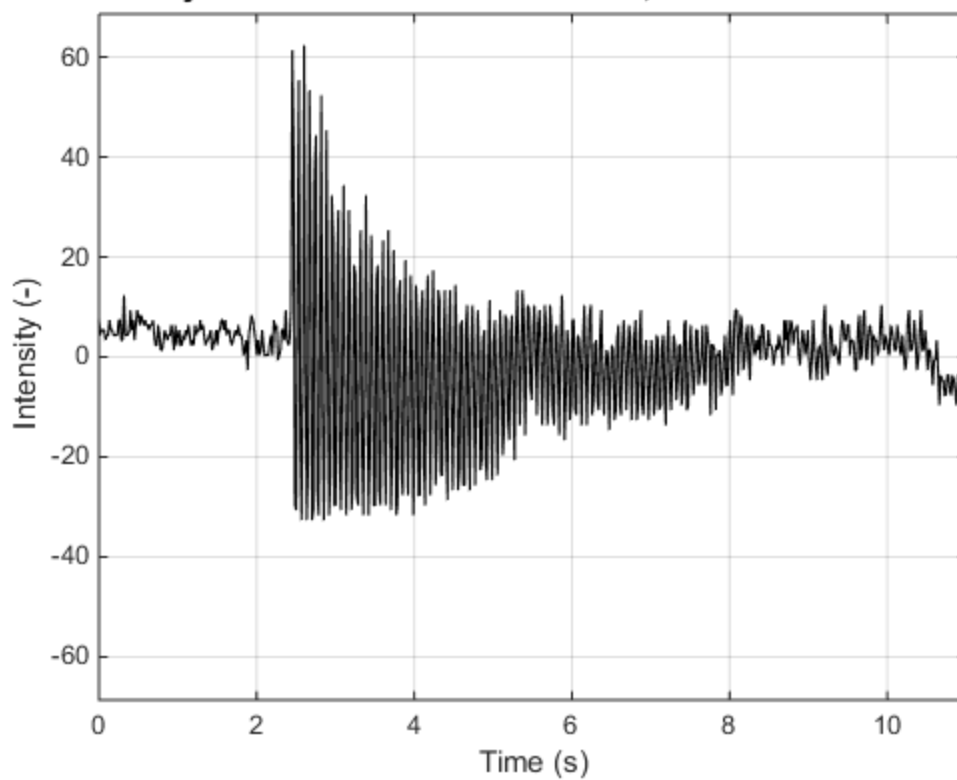
Time history of "S10T1 Feb 20 GoPro.MP4", Pixel coordinates: 467 350



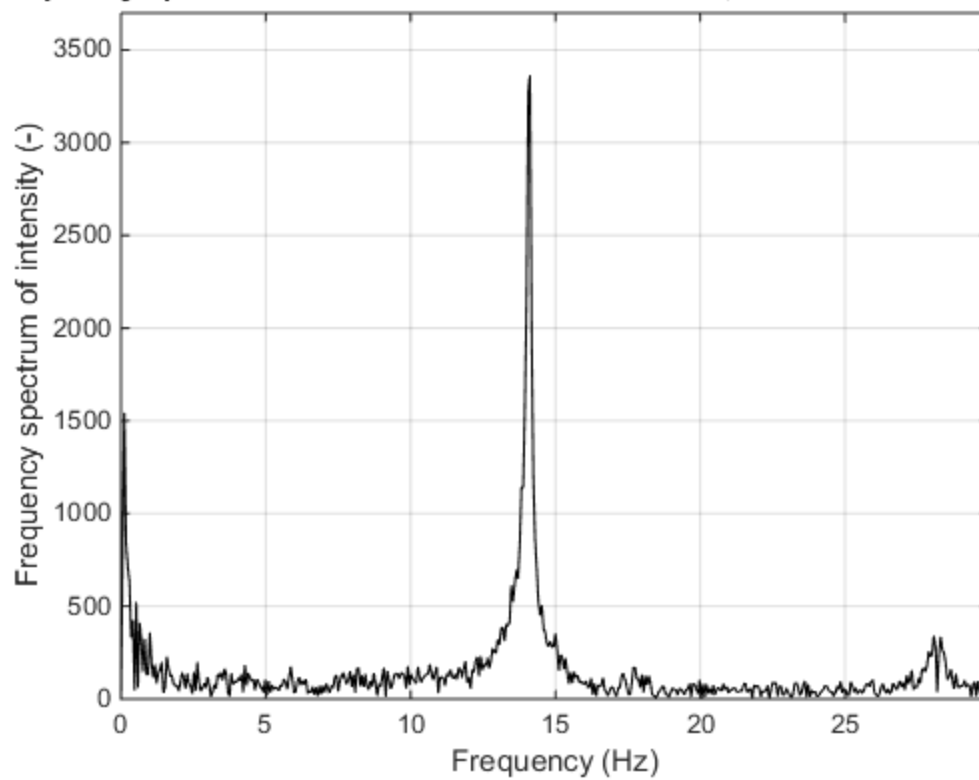
Frequency spectrum of "S10T1 Feb 20 GoPro.MP4", Pixel coordinates: 467 350



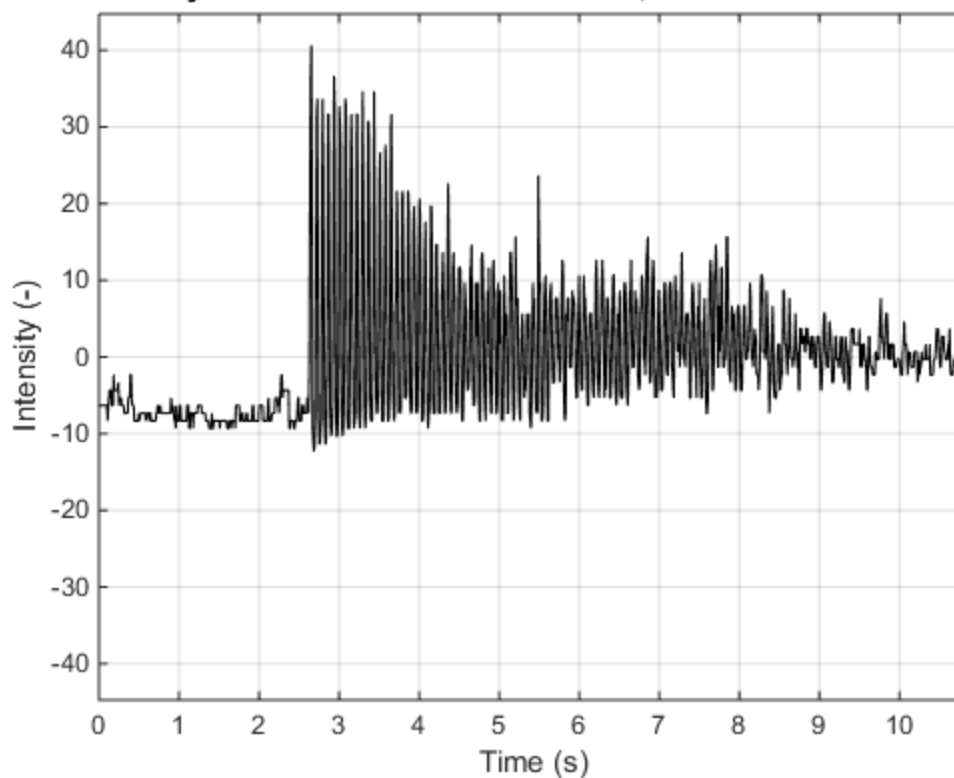
Time history of "S10T2 Feb 20 Canon.MOV", Pixel coordinates: 175 402



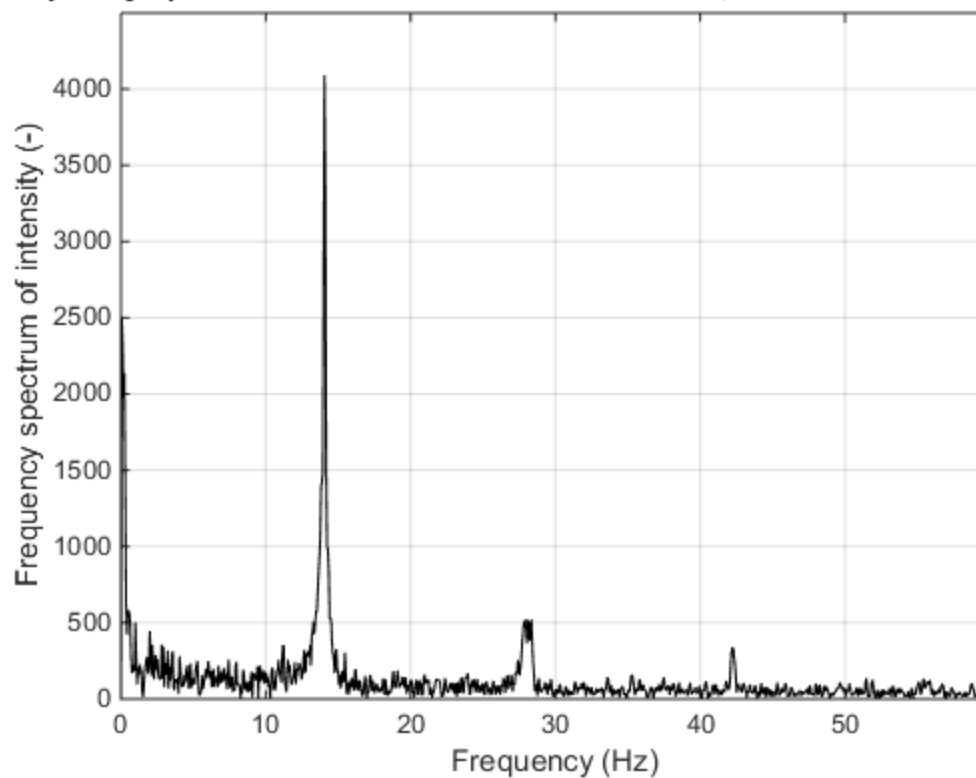
Frequency spectrum of "S10T2 Feb 20 Canon.MOV", Pixel coordinates: 175 402



Time history of "S10T2 Feb 20 GoPro.MP4", Pixel coordinates: 391 355



Frequency spectrum of "S10T2 Feb 20 GoPro.MP4", Pixel coordinates: 391 355



Appendix H – Canon VVS Figures from Simulated Damage 2x4 Experiments

- The first highlighted section contains the specimen designation followed by the test number.
 - In this example: Specimen 1, Test 1
- The second highlighted section contains the type and level of simulated damage applied
 - In this example: Planed (once)

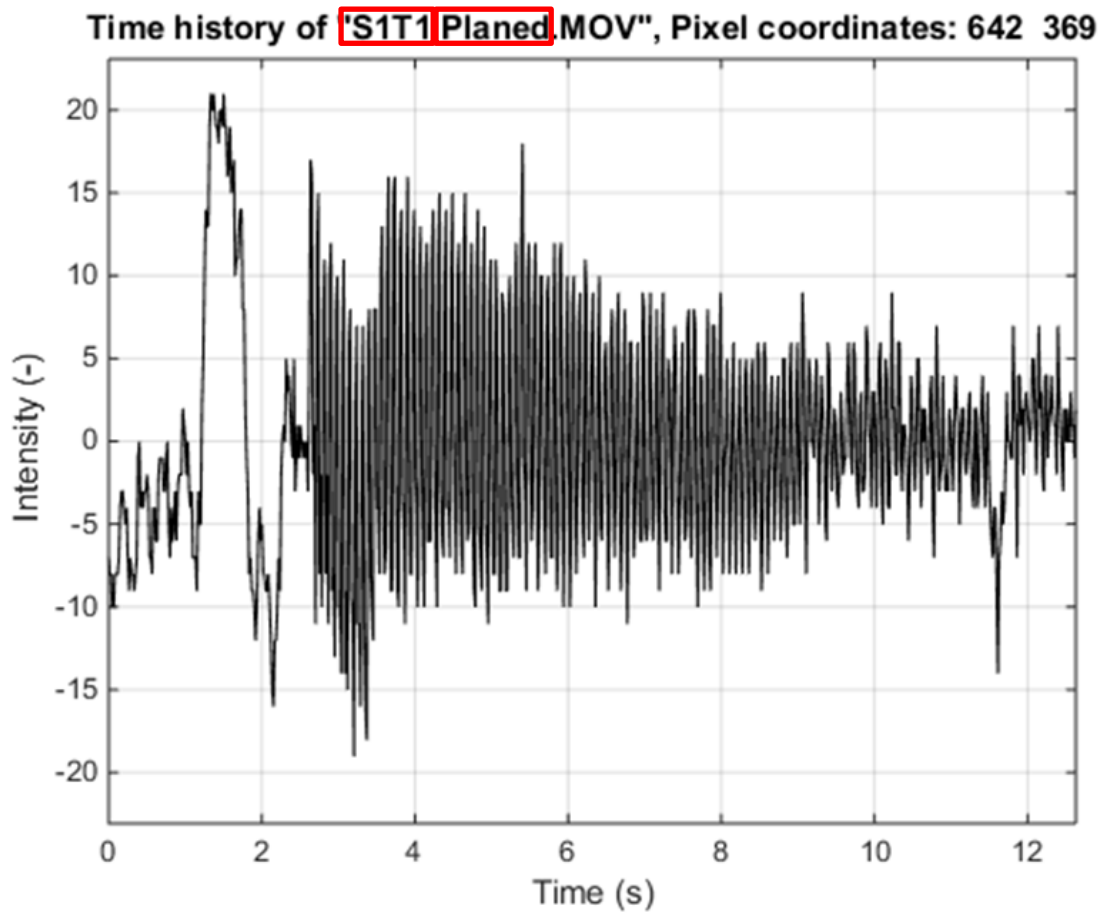
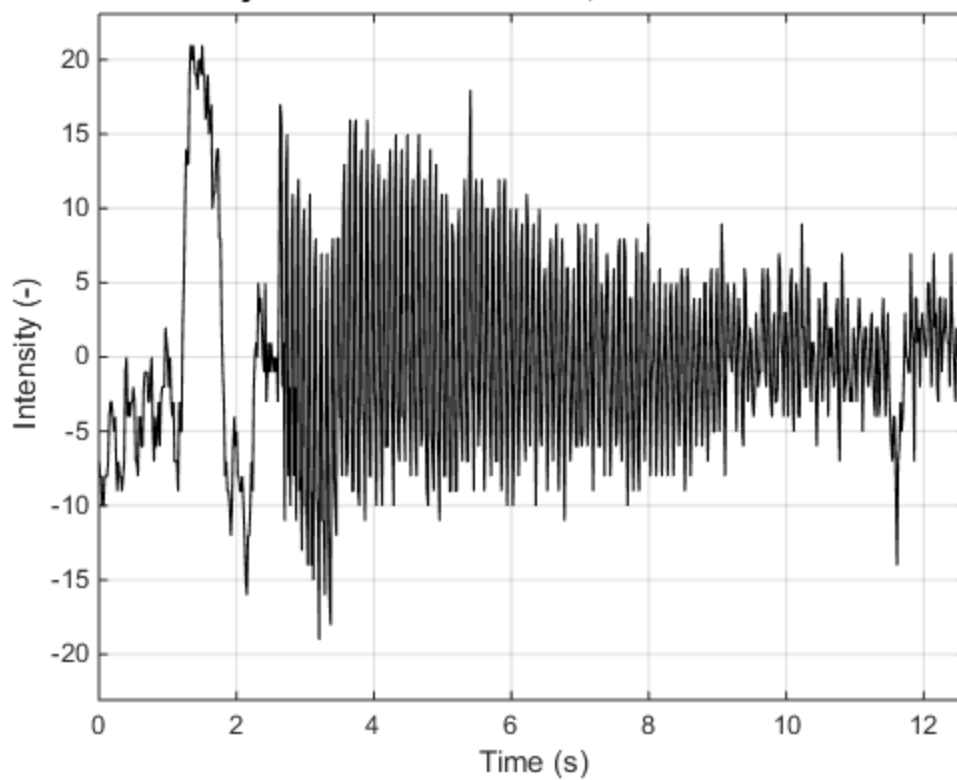
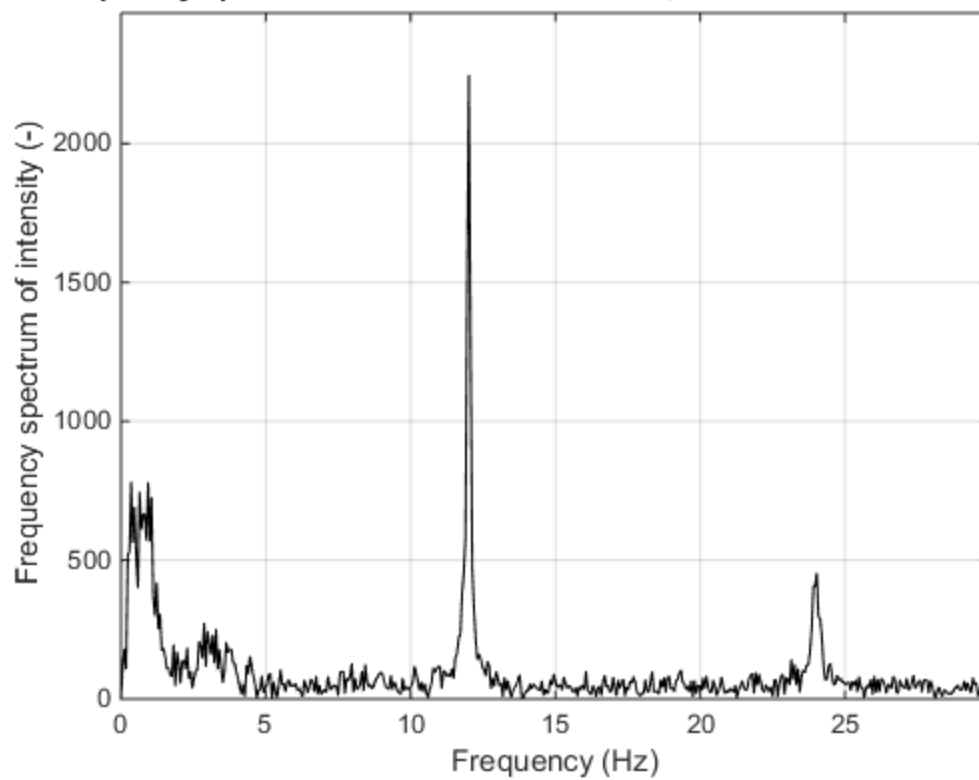


Figure G13 - Key for (Canon) 2x4 Simulated Damage Figures

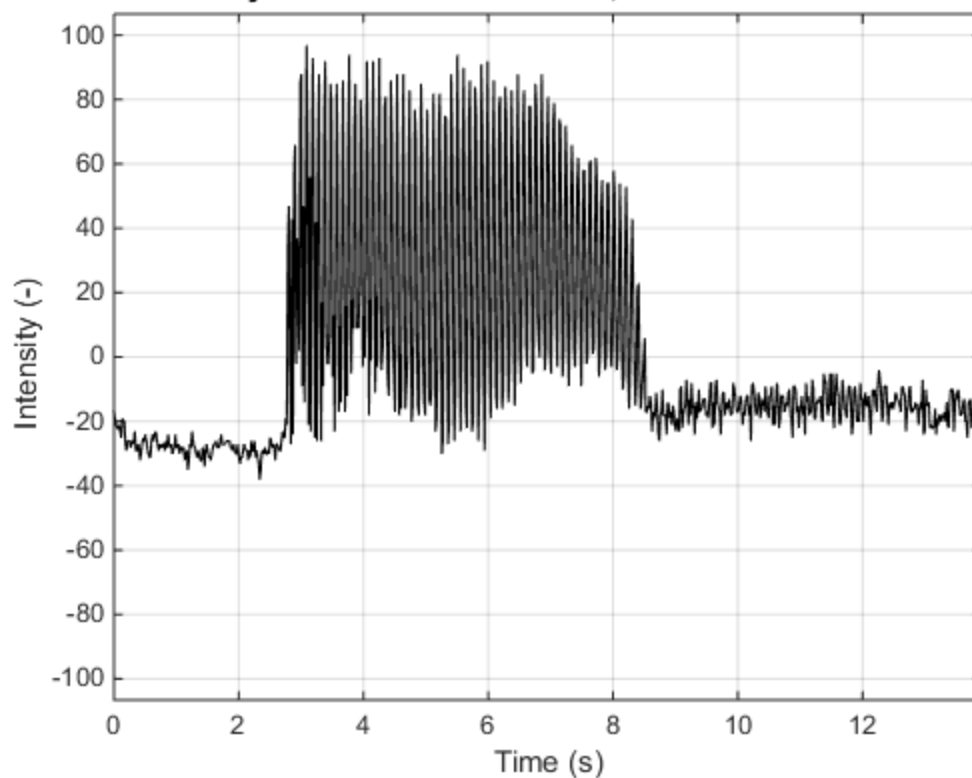
Time history of "S1T1 Planed.MOV", Pixel coordinates: 642 369



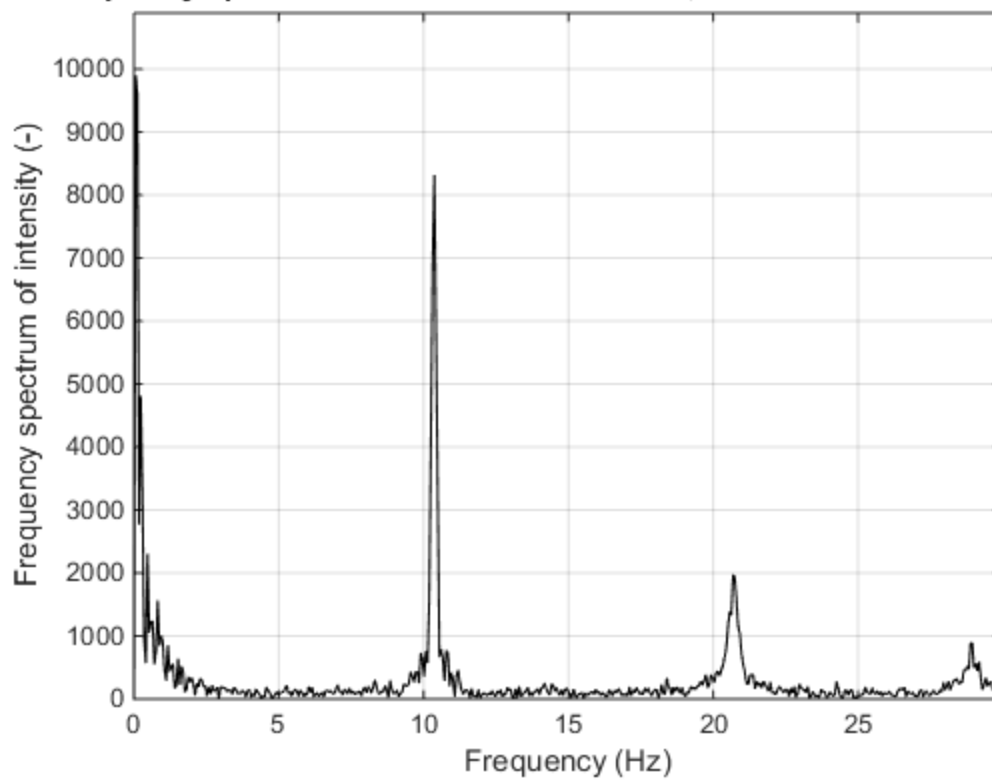
Frequency spectrum of "S1T1 Planed.MOV", Pixel coordinates: 642 369



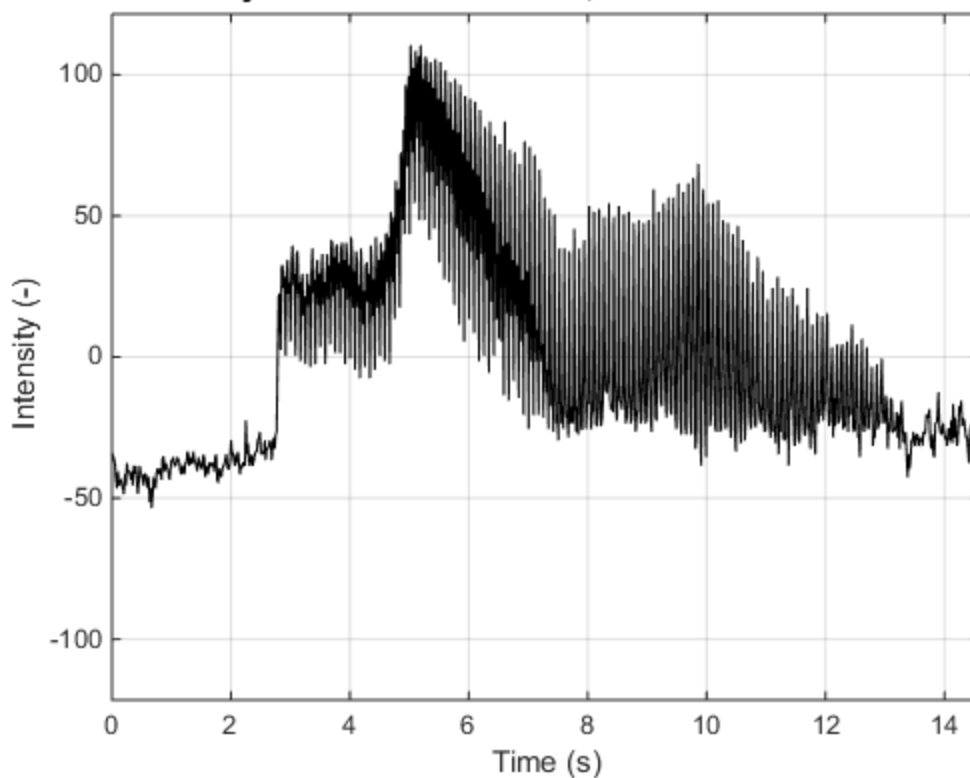
Time history of "S1T1 Planed2.MOV", Pixel coordinates: 757 397



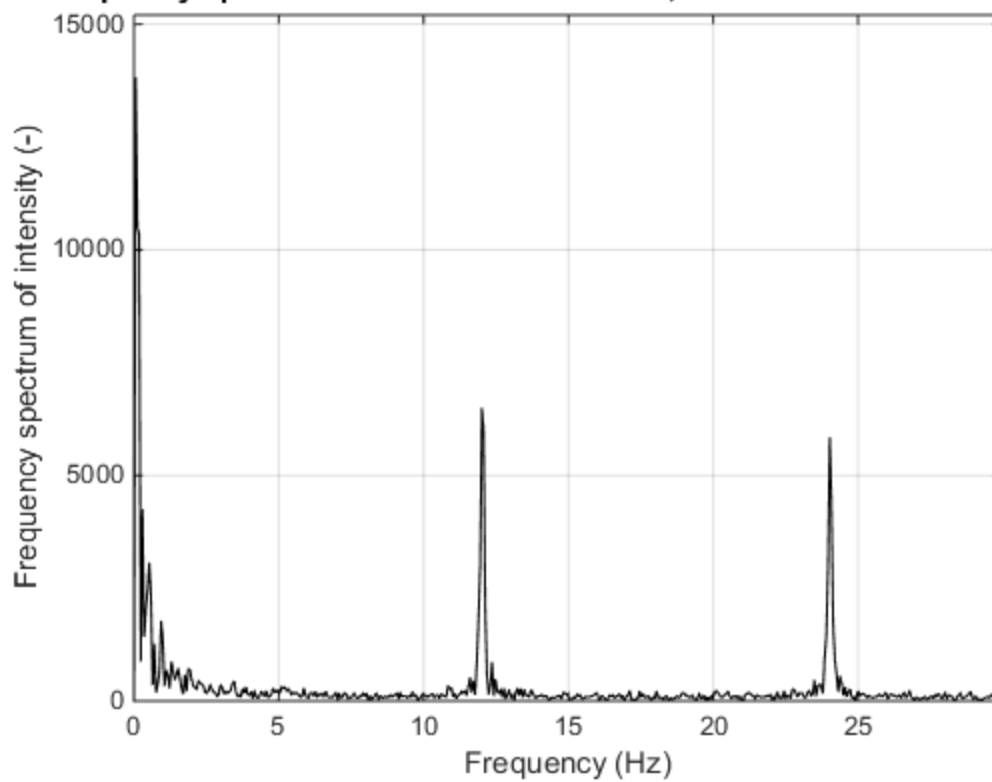
Frequency spectrum of "S1T1 Planed2.MOV", Pixel coordinates: 757 397



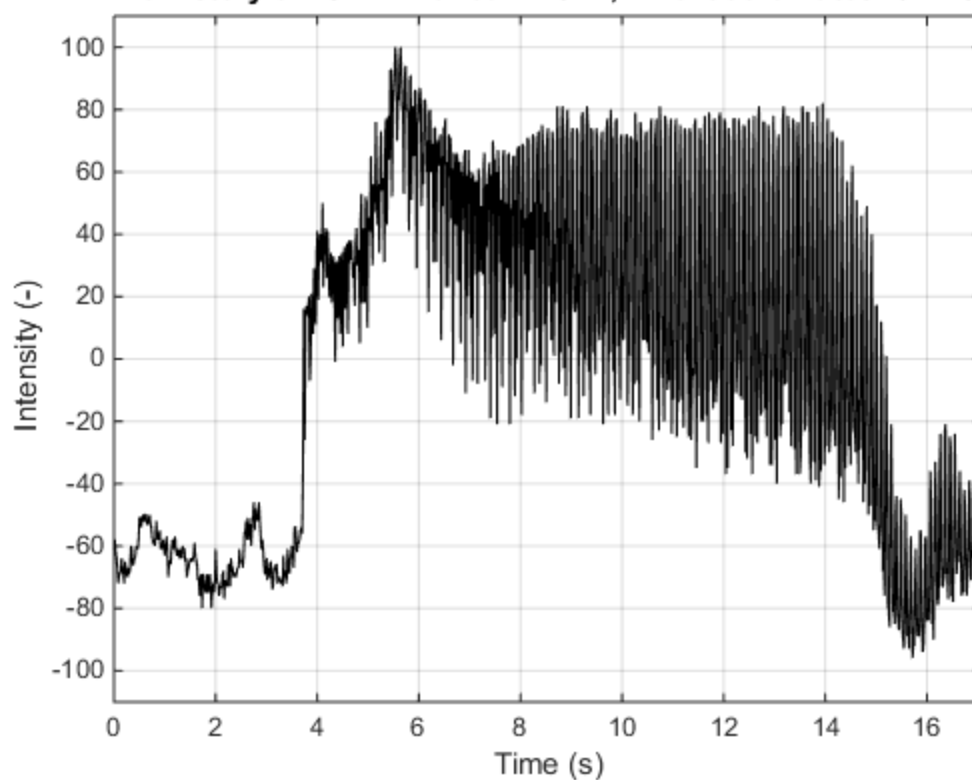
Time history of "S1T2 Planed.MOV", Pixel coordinates: 1048 387



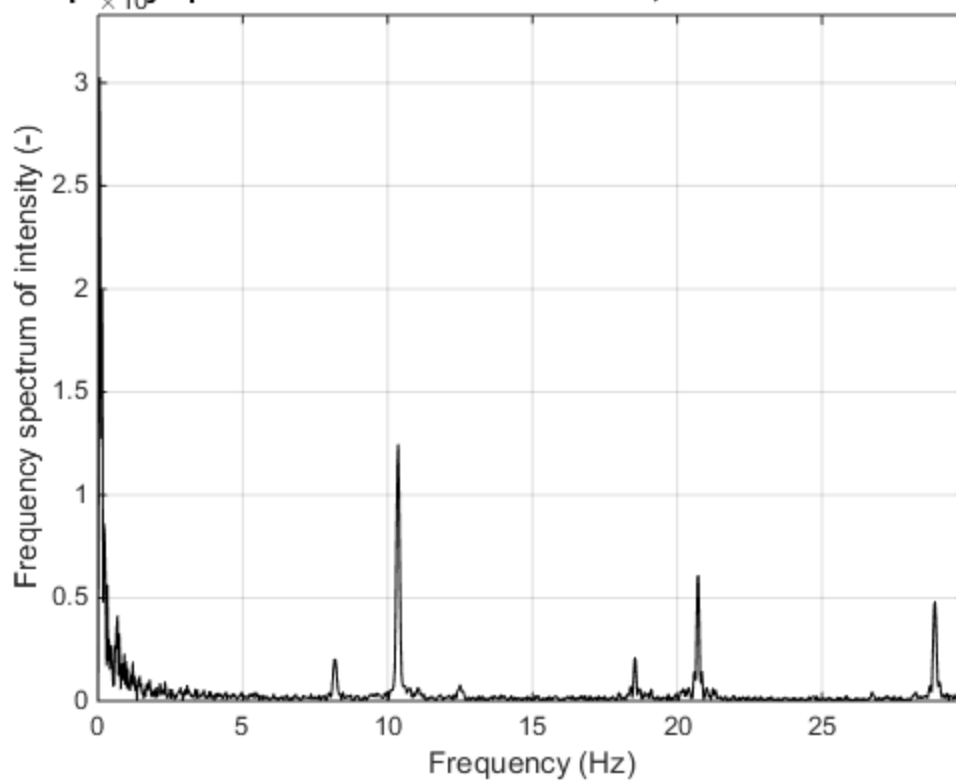
Frequency spectrum of "S1T2 Planed.MOV", Pixel coordinates: 1048 387



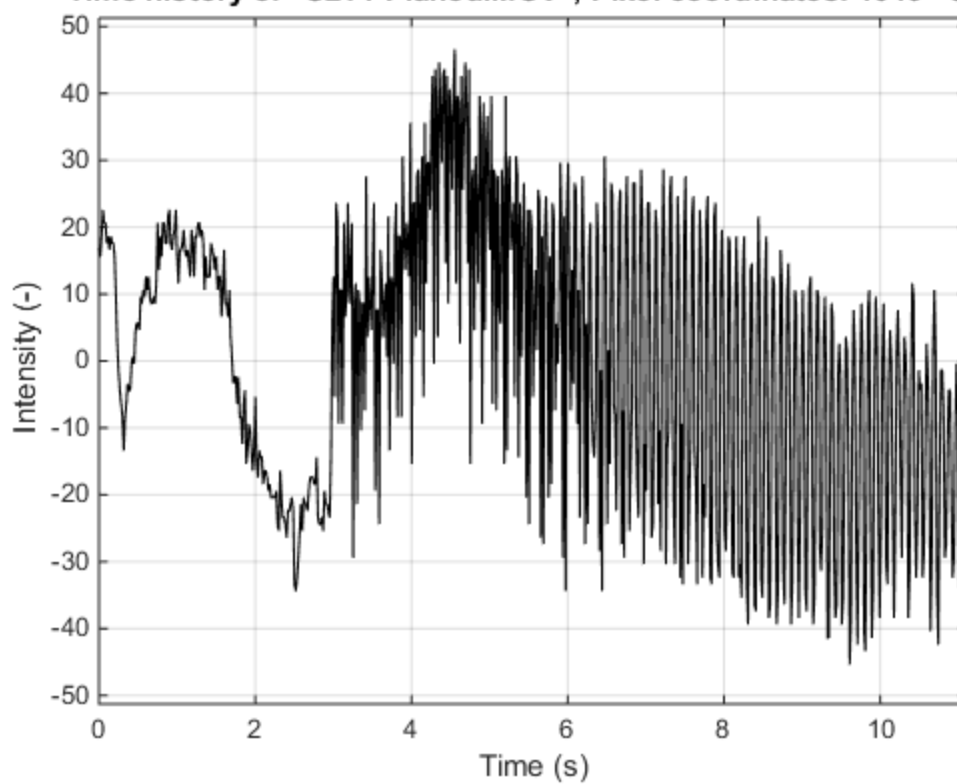
Time history of "S1T2 Planed2.MOV", Pixel coordinates: 624 368



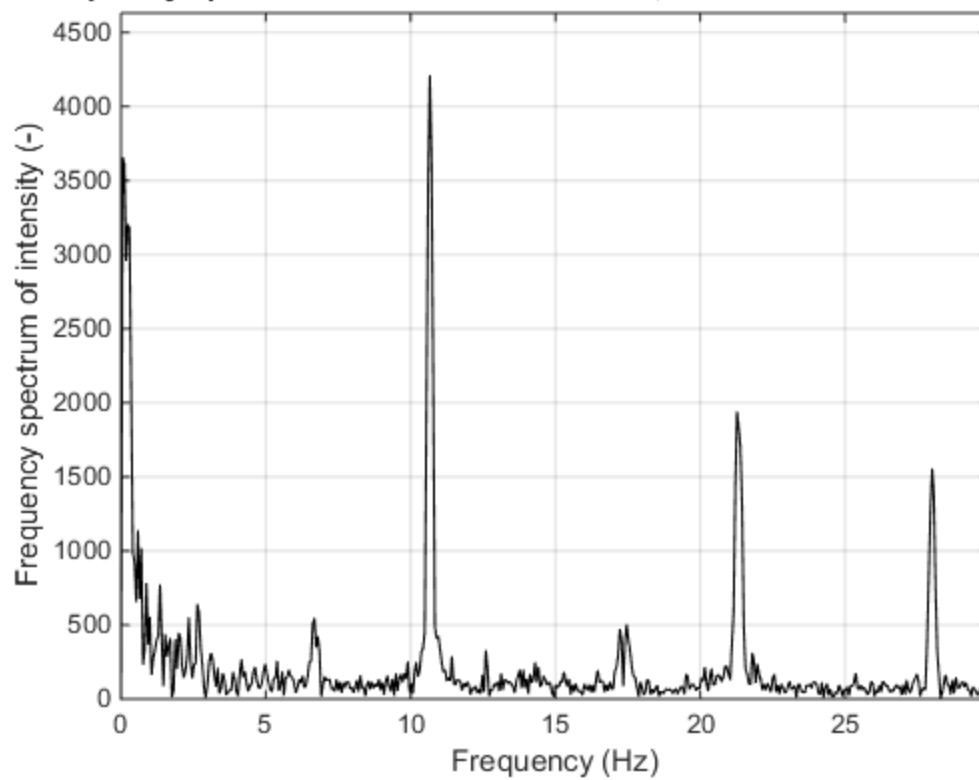
Frequency spectrum of "S1T2 Planed2.MOV", Pixel coordinates: 624 368



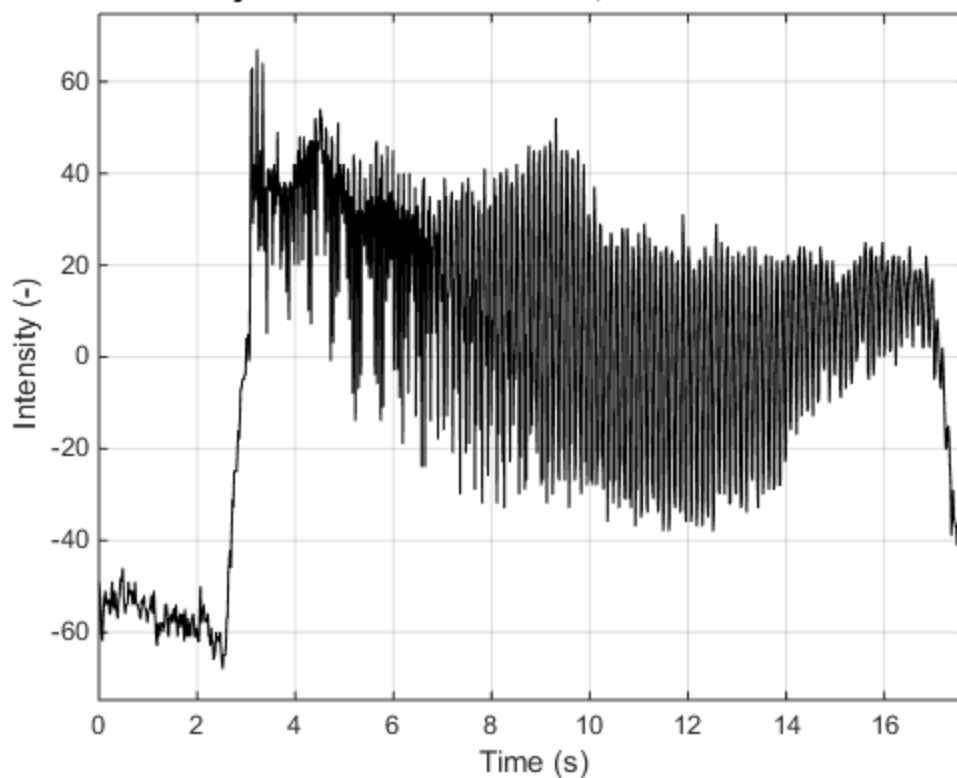
Time history of "S2T1 Planed.MOV", Pixel coordinates: 1019 320



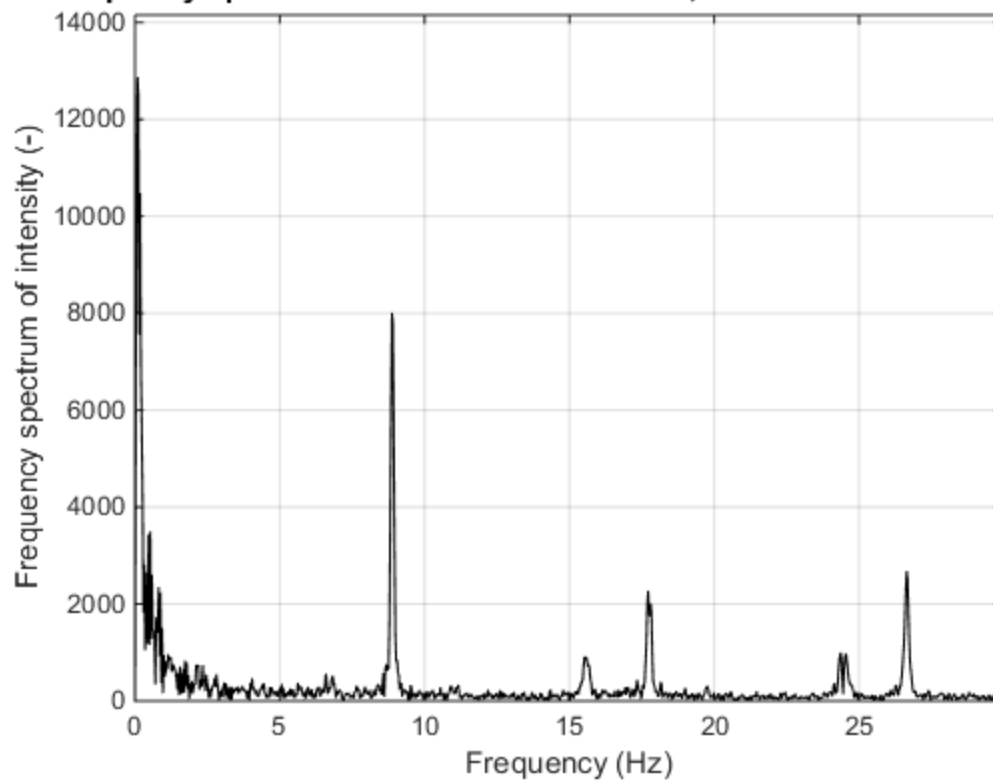
Frequency spectrum of "S2T1 Planed.MOV", Pixel coordinates: 1019 320



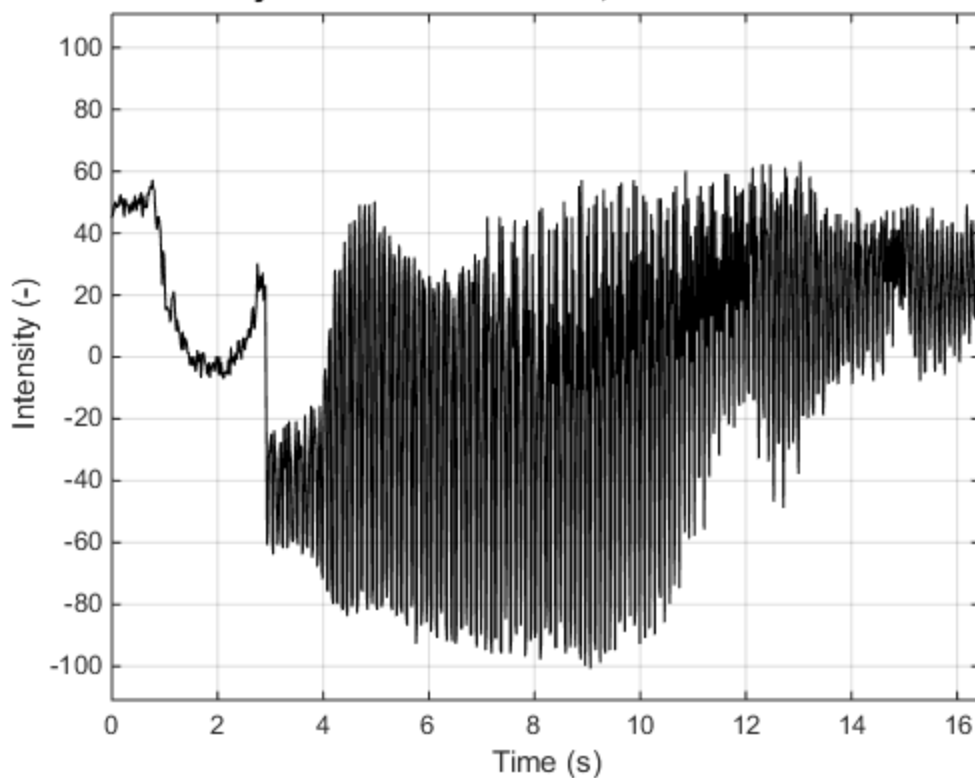
Time history of "S2T1 Planed2.MOV", Pixel coordinates: 850 368



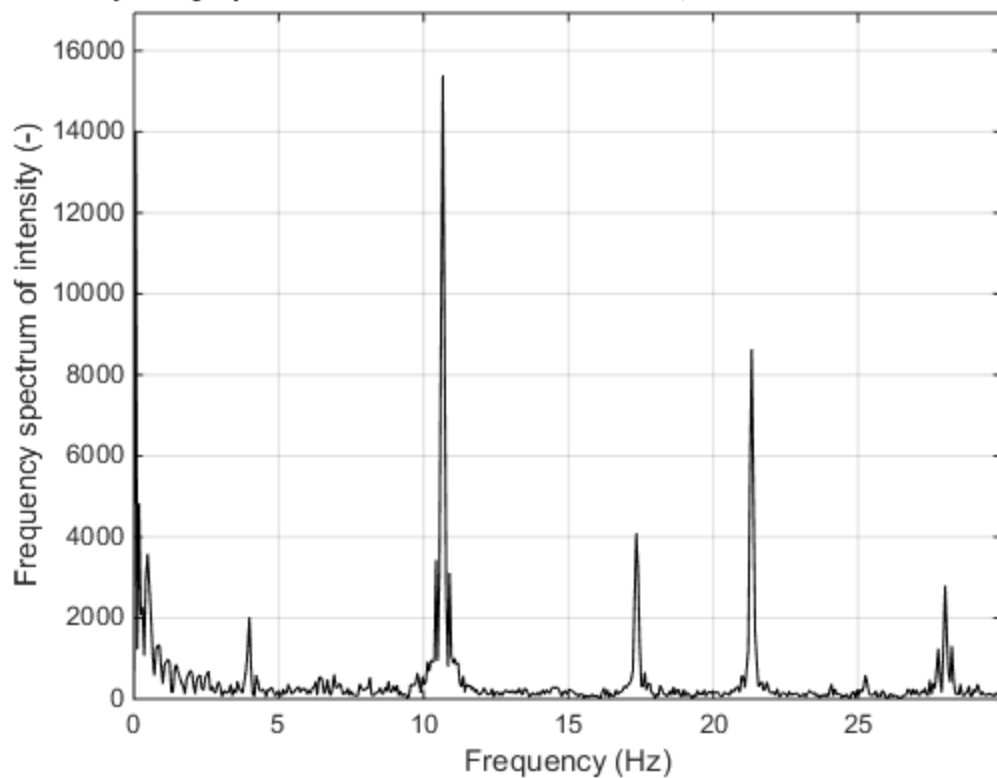
Frequency spectrum of "S2T1 Planed2.MOV", Pixel coordinates: 850 368



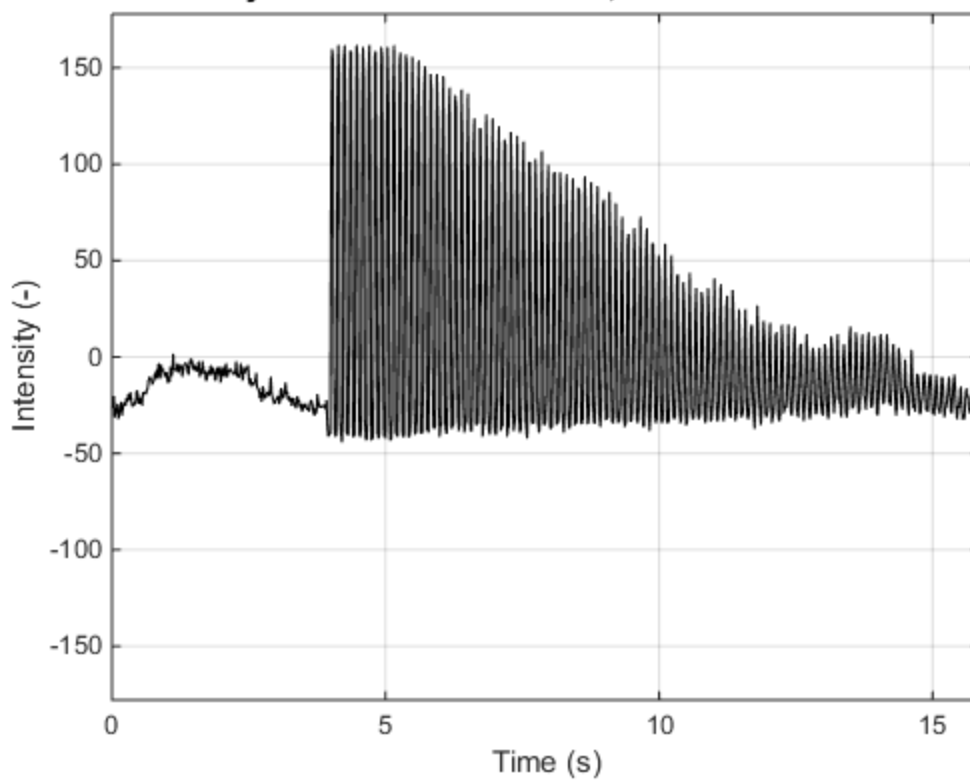
Time history of "S2T2 Planed.MOV", Pixel coordinates: 417 225



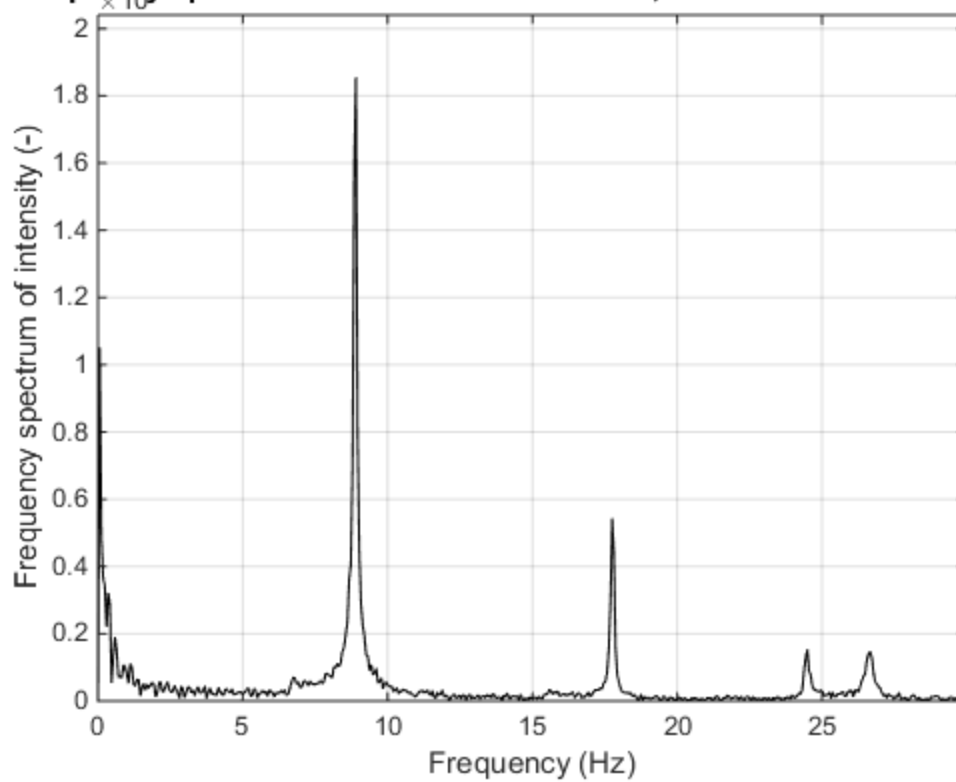
Frequency spectrum of "S2T2 Planed.MOV", Pixel coordinates: 417 225



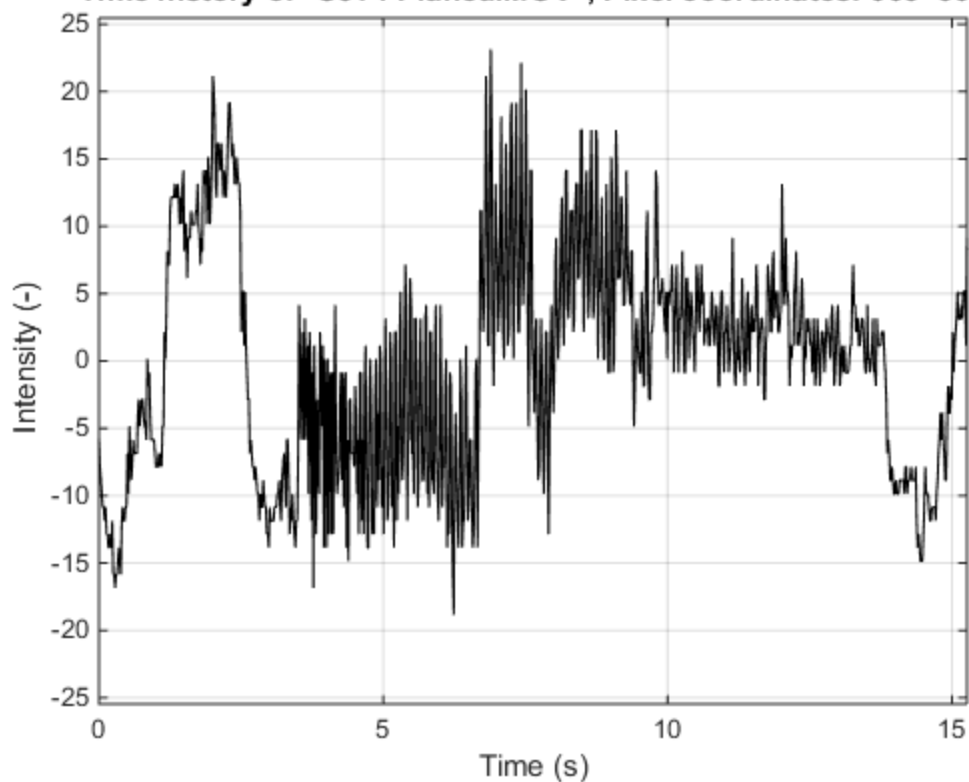
Time history of "S2T2 Planed2.MOV", Pixel coordinates: 598 337



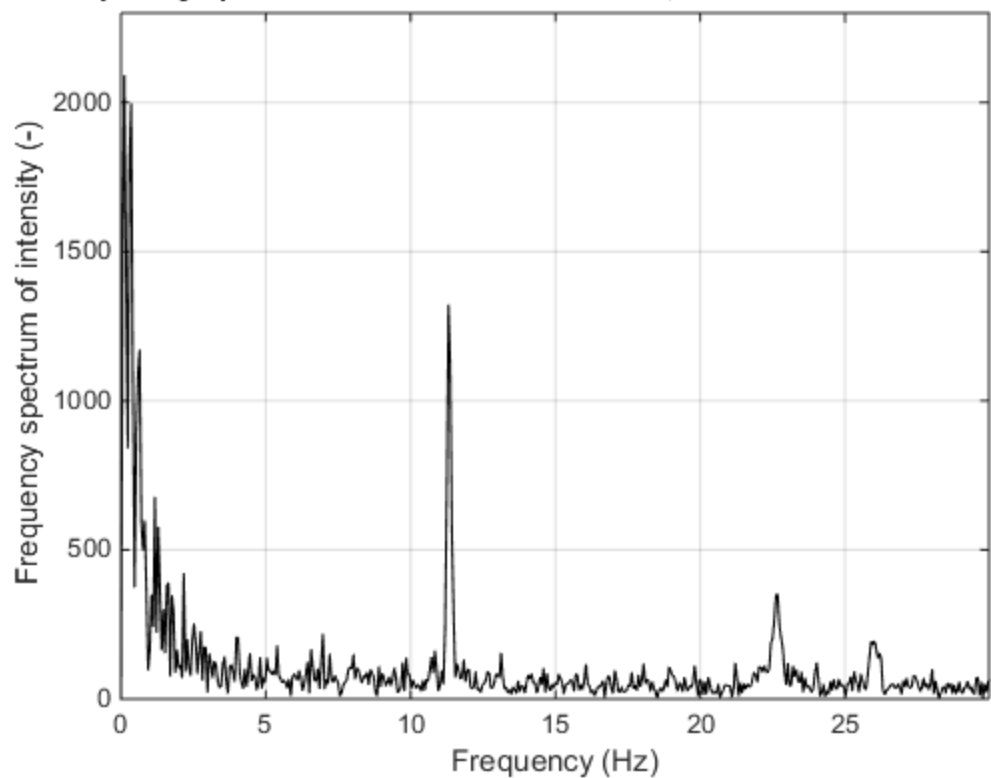
Frequency spectrum of "S2T2 Planed2.MOV", Pixel coordinates: 598 337



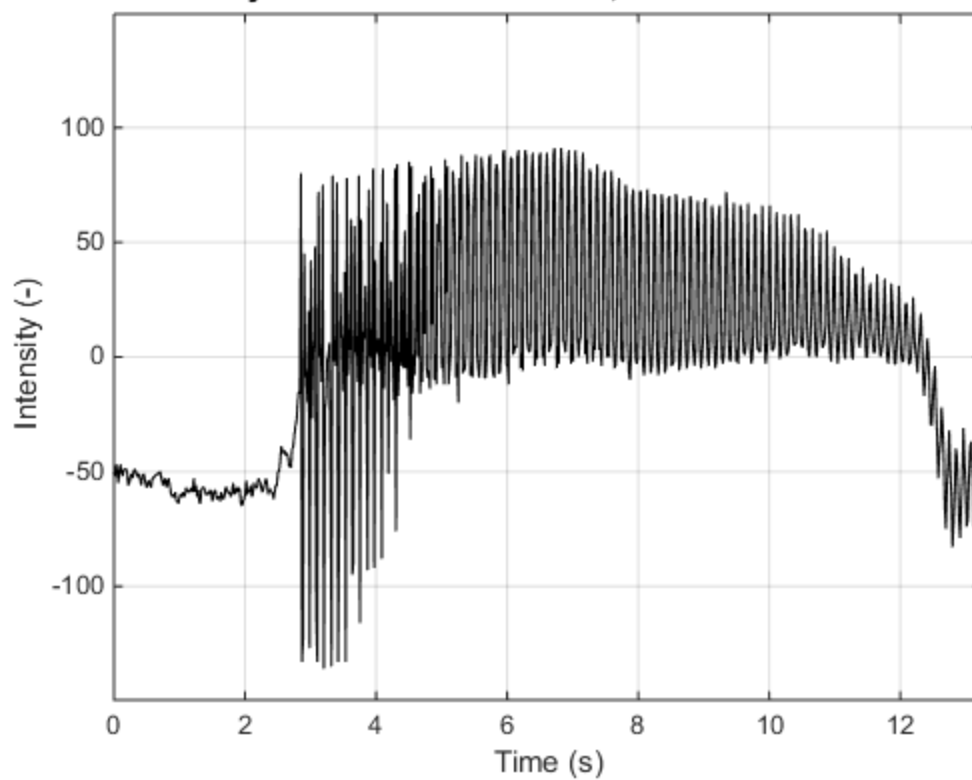
Time history of "S3T1 Planed.MOV", Pixel coordinates: 663 364



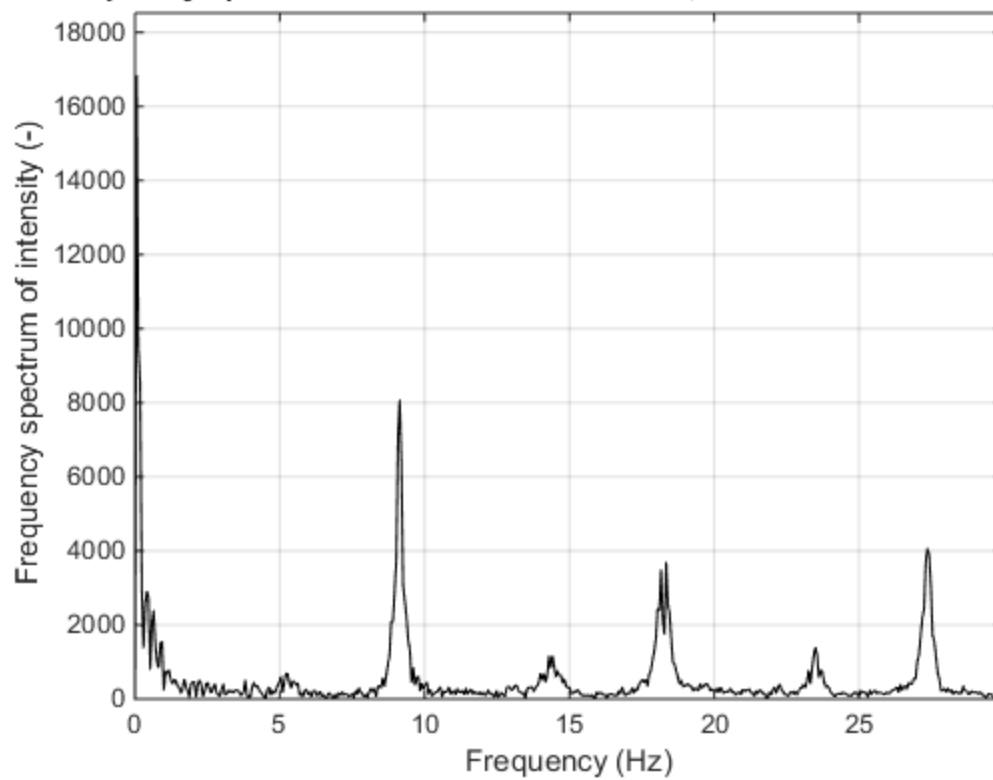
Frequency spectrum of "S3T1 Planed.MOV", Pixel coordinates: 663 364



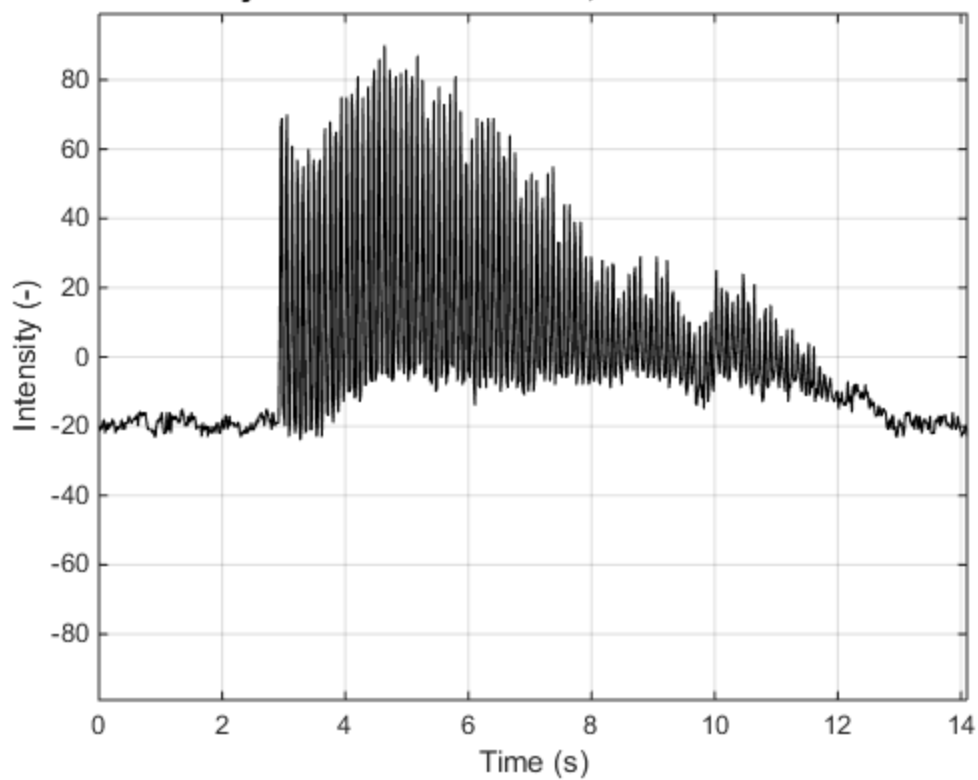
Time history of "S3T1 Planed2.MOV", Pixel coordinates: 625 353



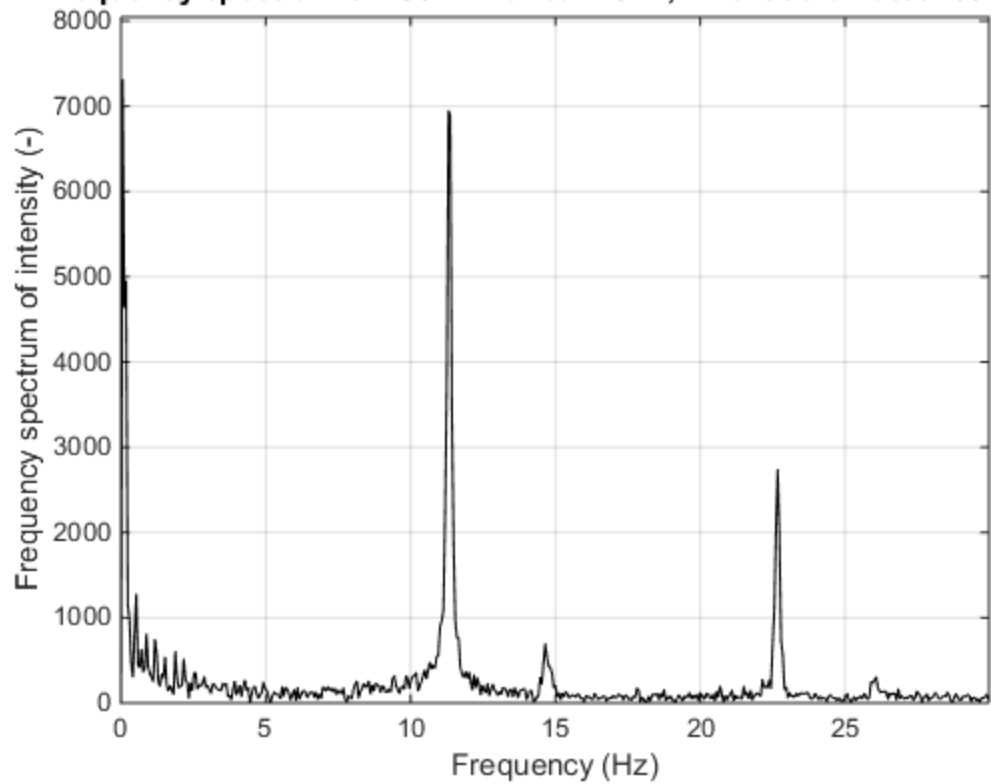
Frequency spectrum of "S3T1 Planed2.MOV", Pixel coordinates: 625 353

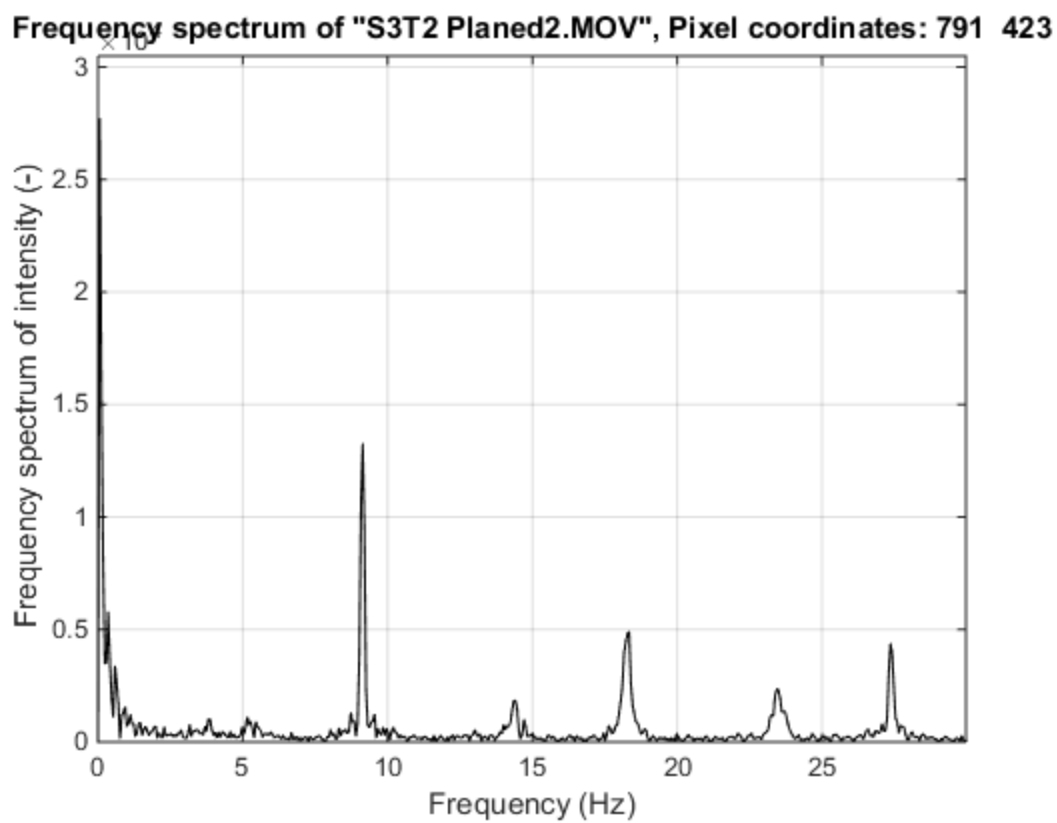
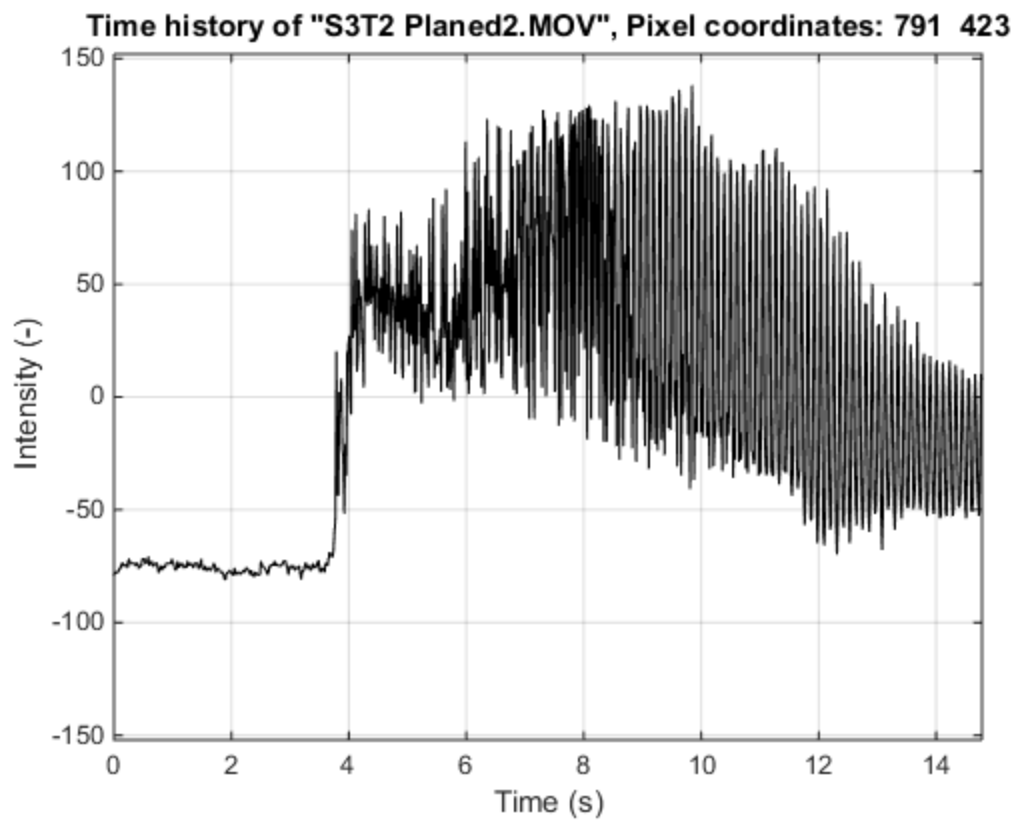


Time history of "S3T2 Planed.MOV", Pixel coordinates: 652 425

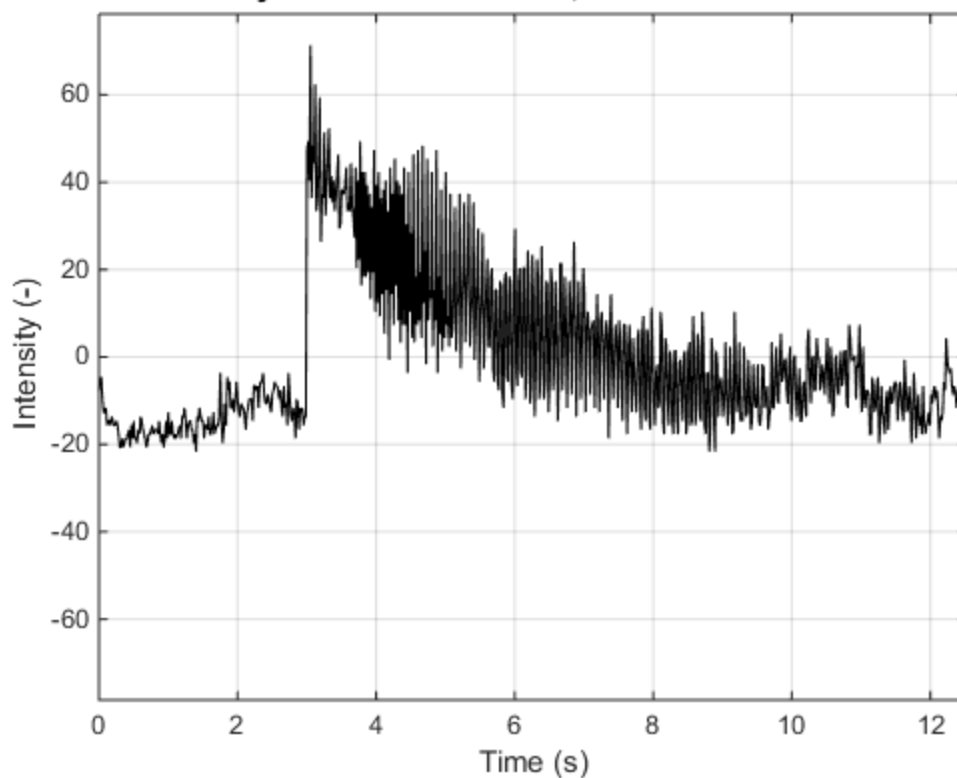


Frequency spectrum of "S3T2 Planed.MOV", Pixel coordinates: 652 425

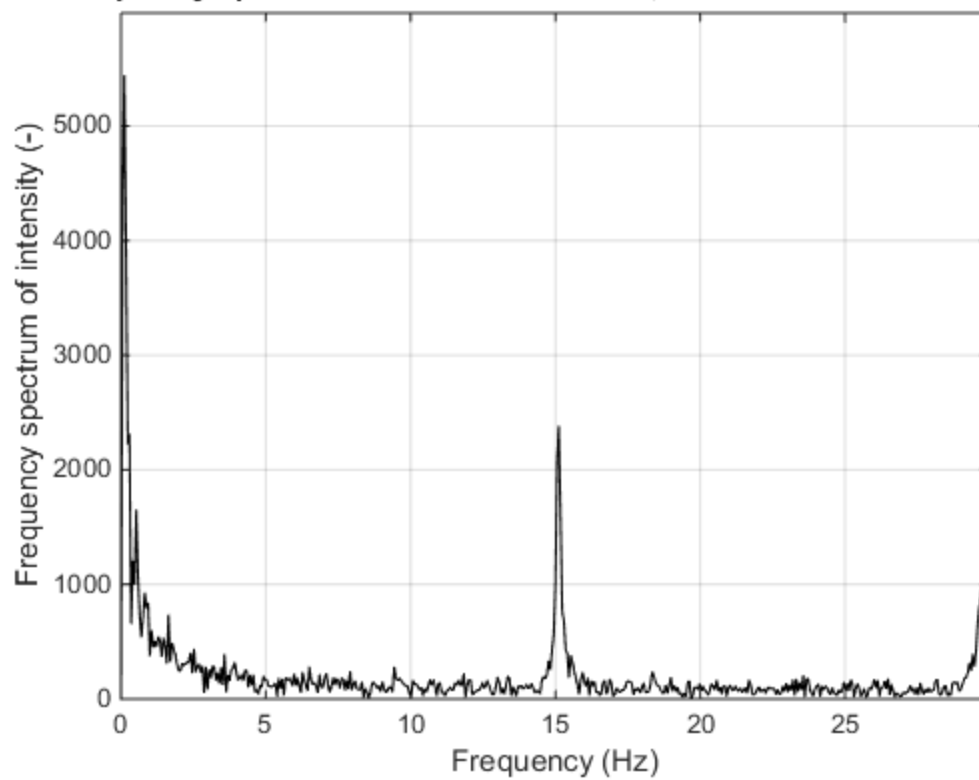




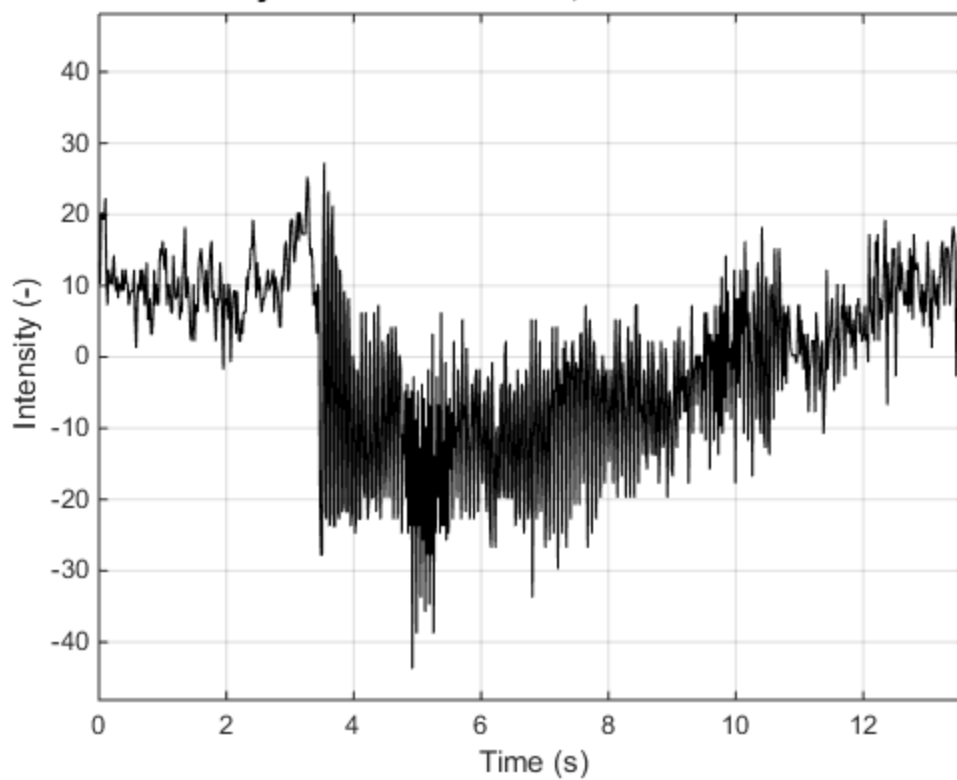
Time history of "S4T1 Knot.MOV", Pixel coordinates: 664 308



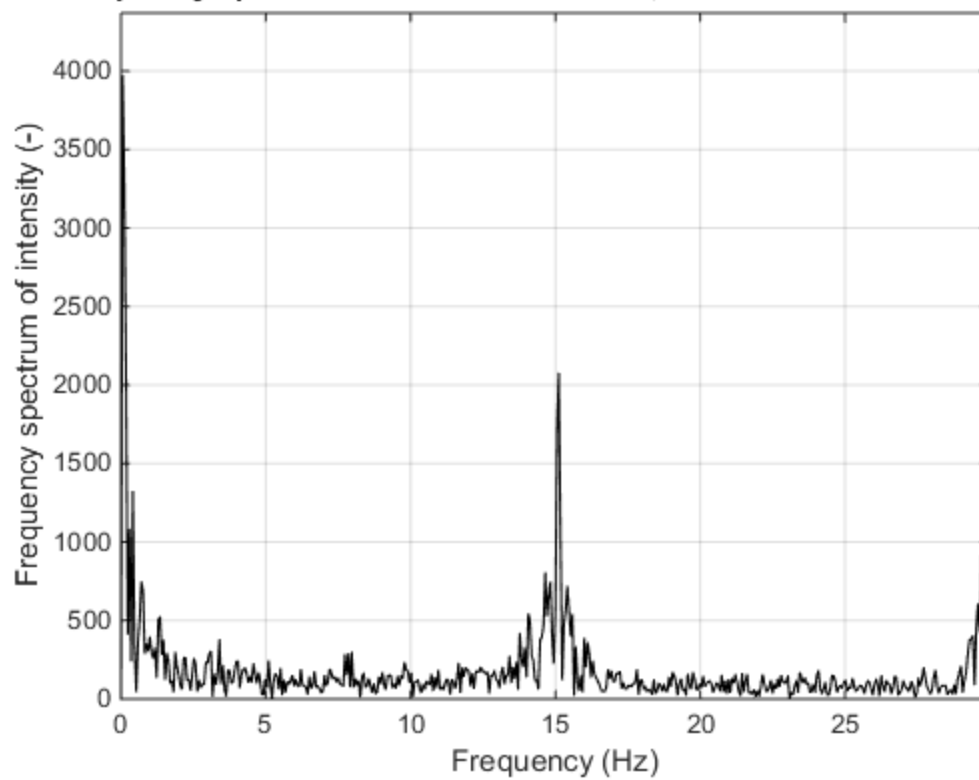
Frequency spectrum of "S4T1 Knot.MOV", Pixel coordinates: 664 308



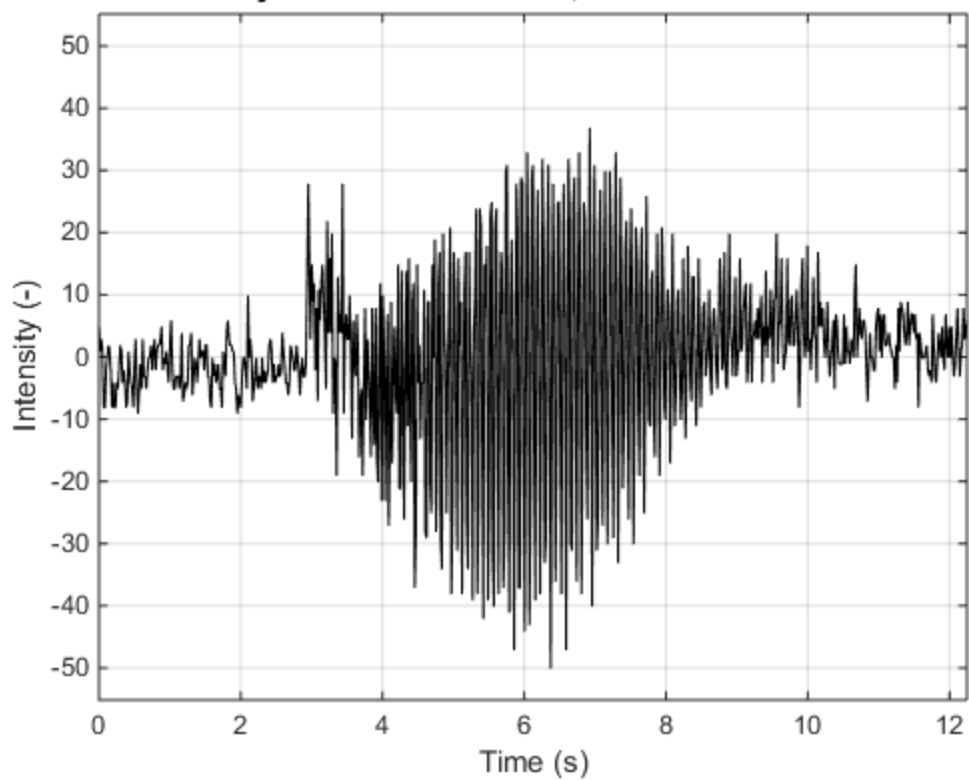
Time history of "S4T2 Knot.MOV", Pixel coordinates: 664 308



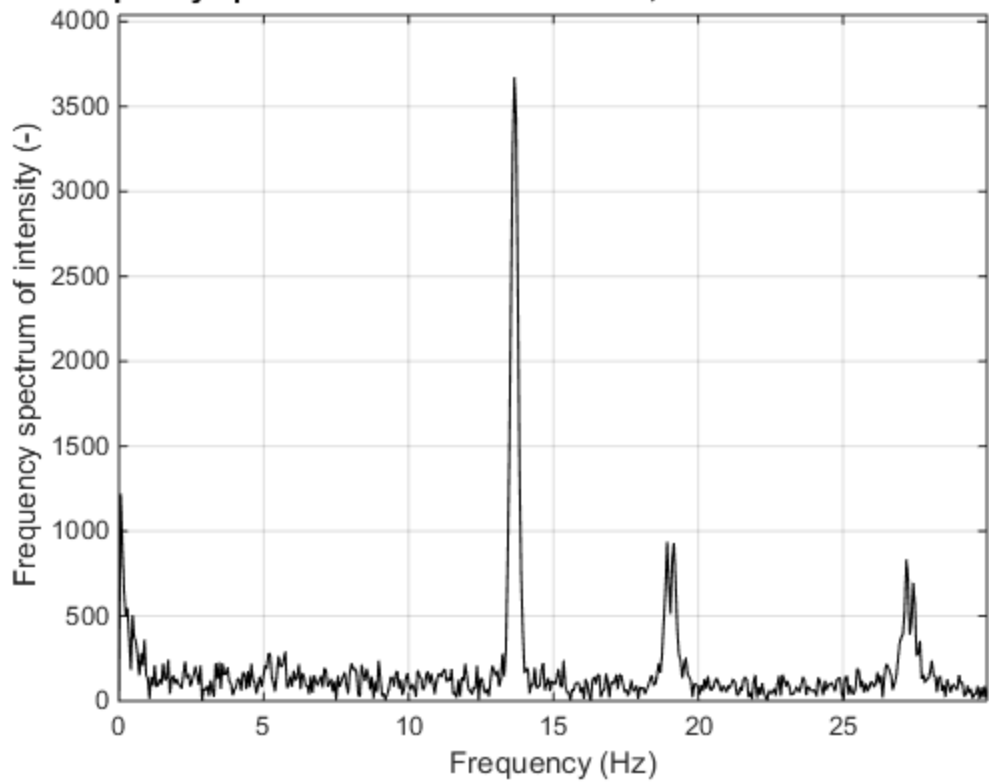
Frequency spectrum of "S4T2 Knot.MOV", Pixel coordinates: 664 308



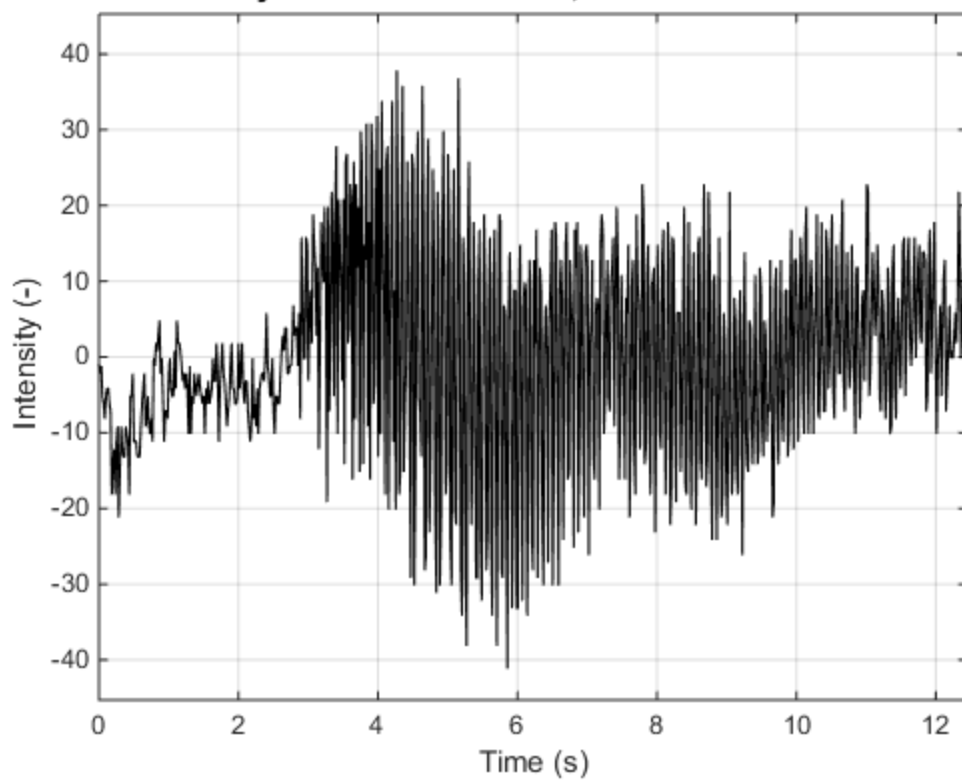
Time history of "S5T1 Knot.MOV", Pixel coordinates: 749 325



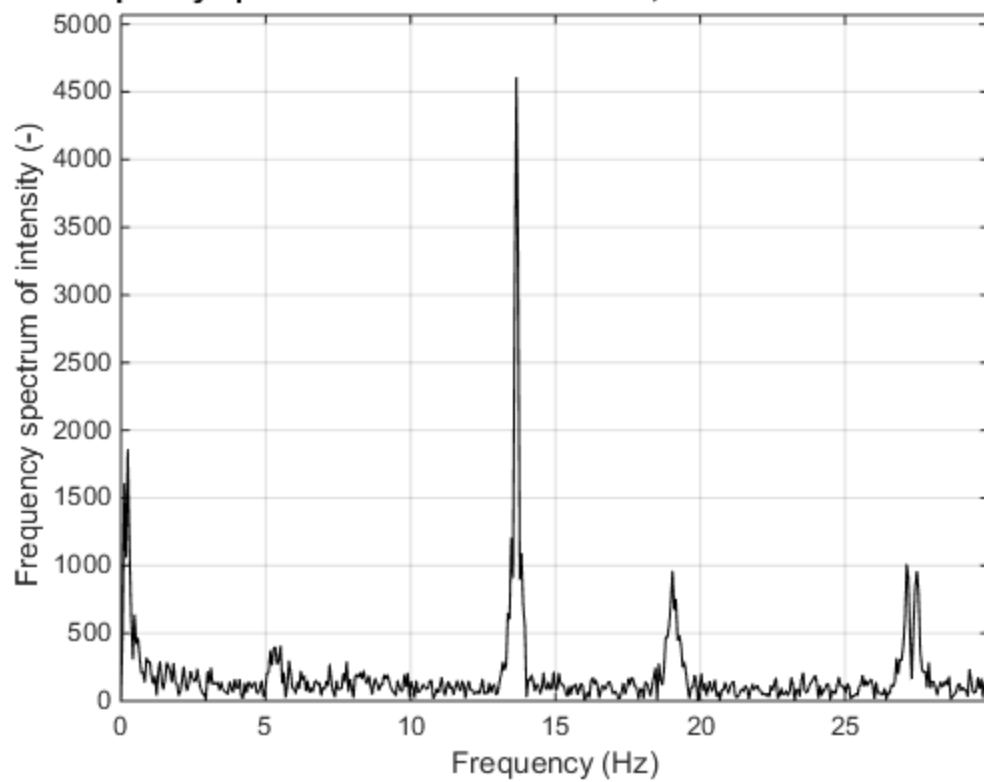
Frequency spectrum of "S5T1 Knot.MOV", Pixel coordinates: 749 325

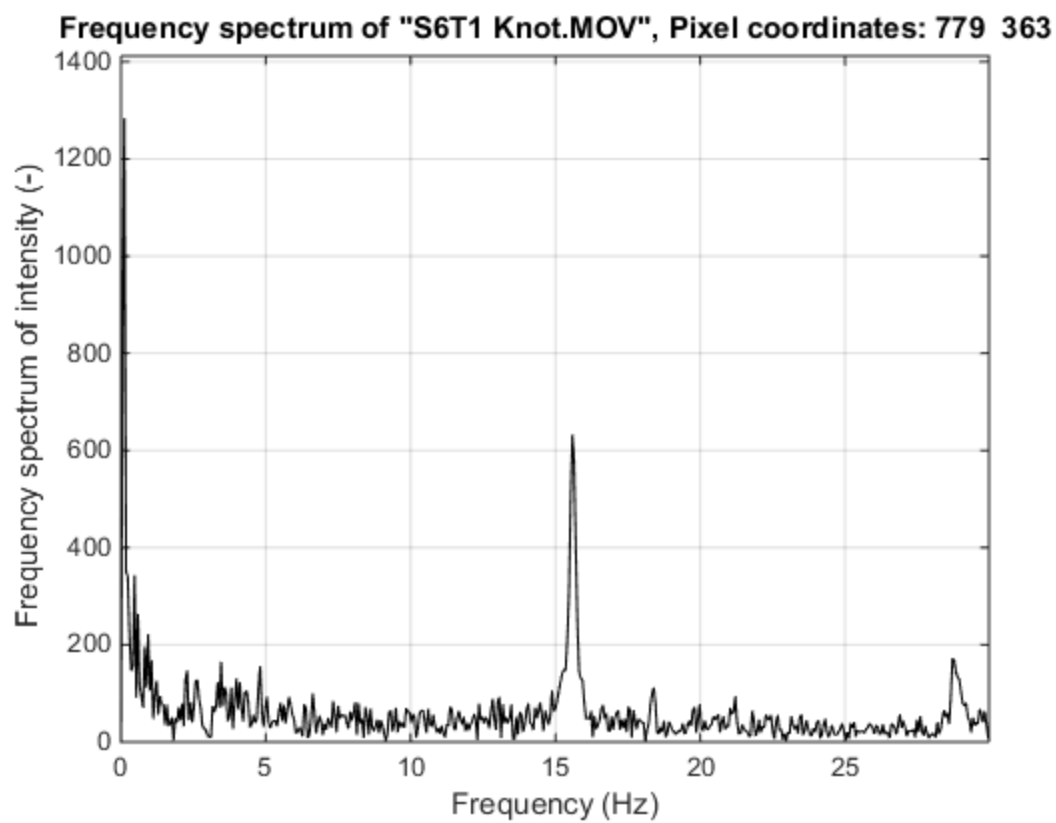
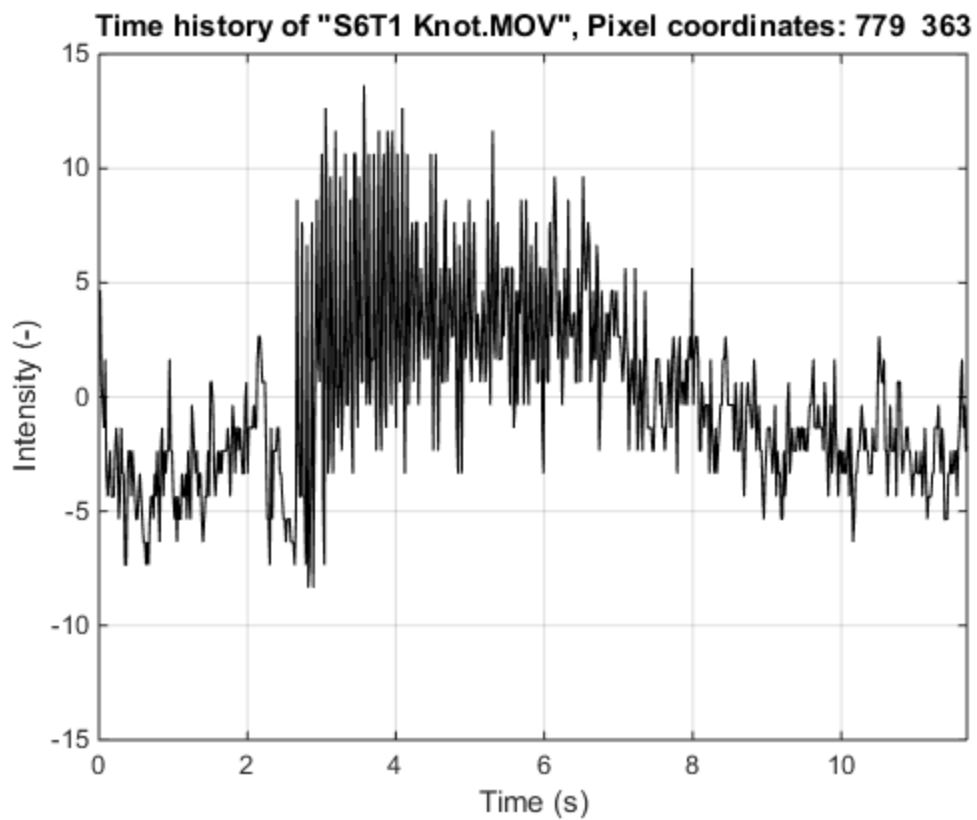


Time history of "S5T2 Knot.MOV", Pixel coordinates: 749 325

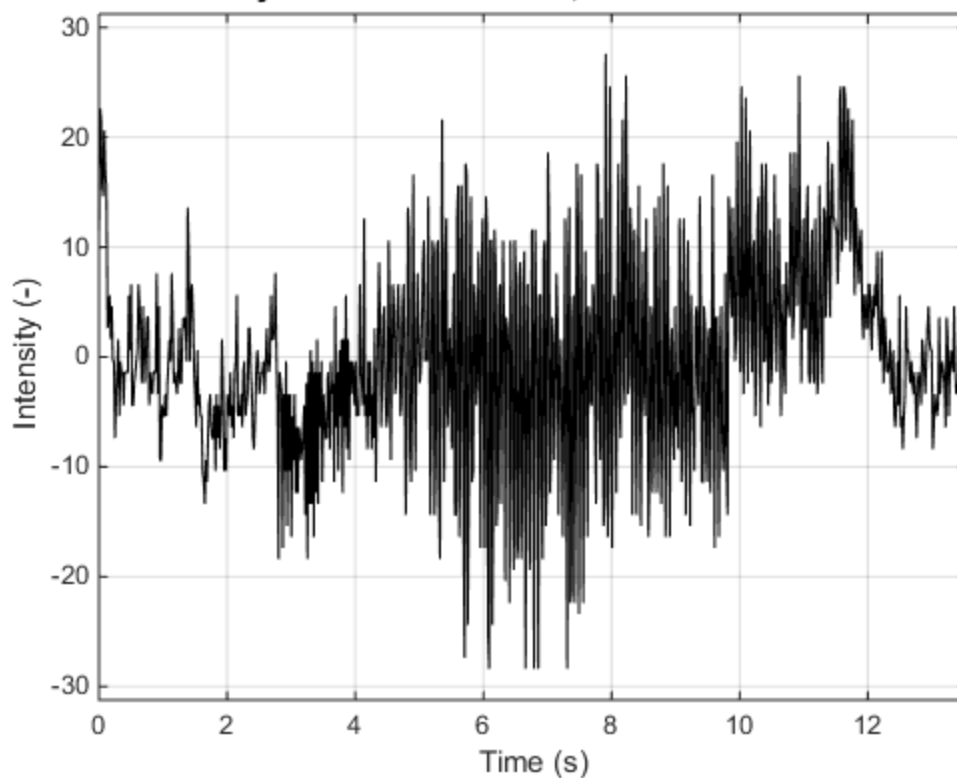


Frequency spectrum of "S5T2 Knot.MOV", Pixel coordinates: 749 325

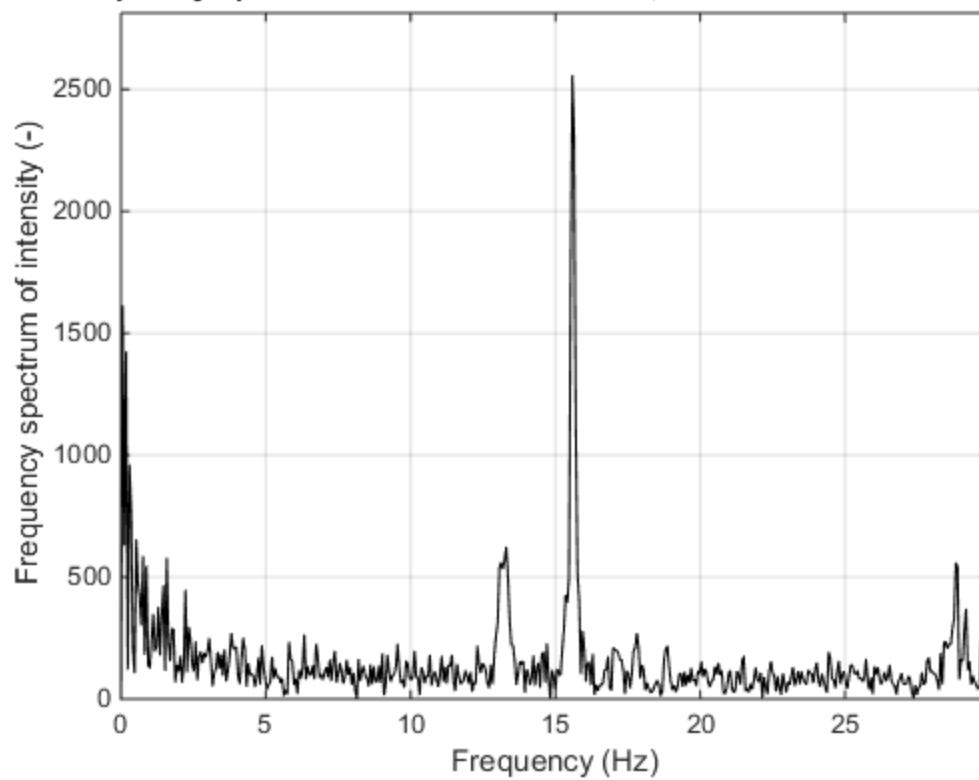




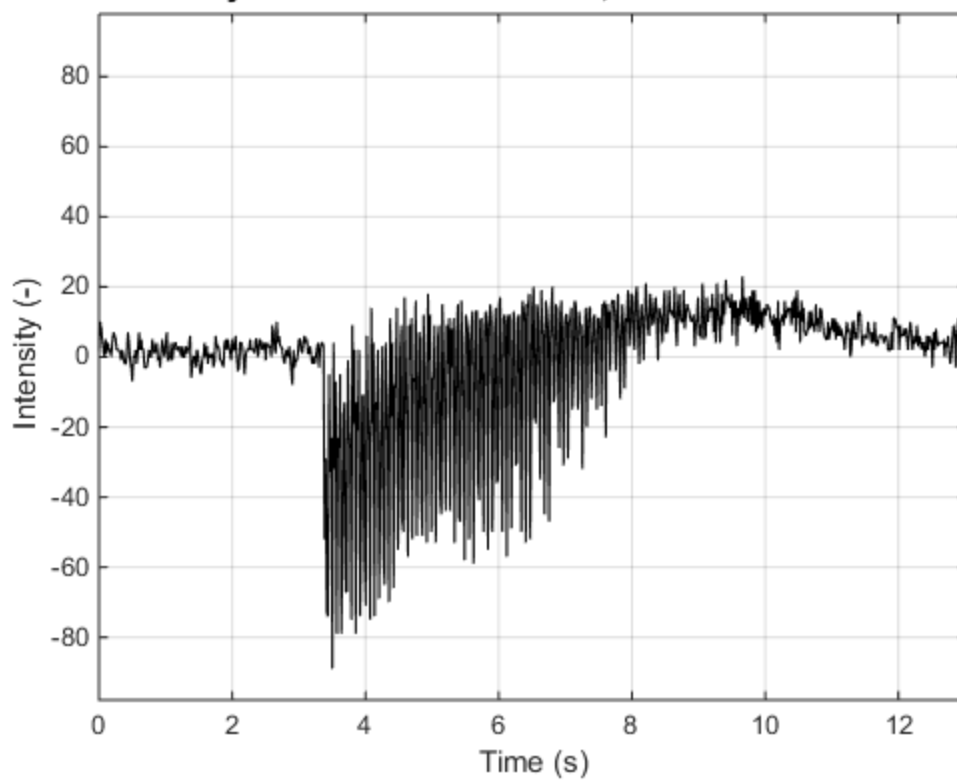
Time history of "S6T2 Knot.MOV", Pixel coordinates: 779 363



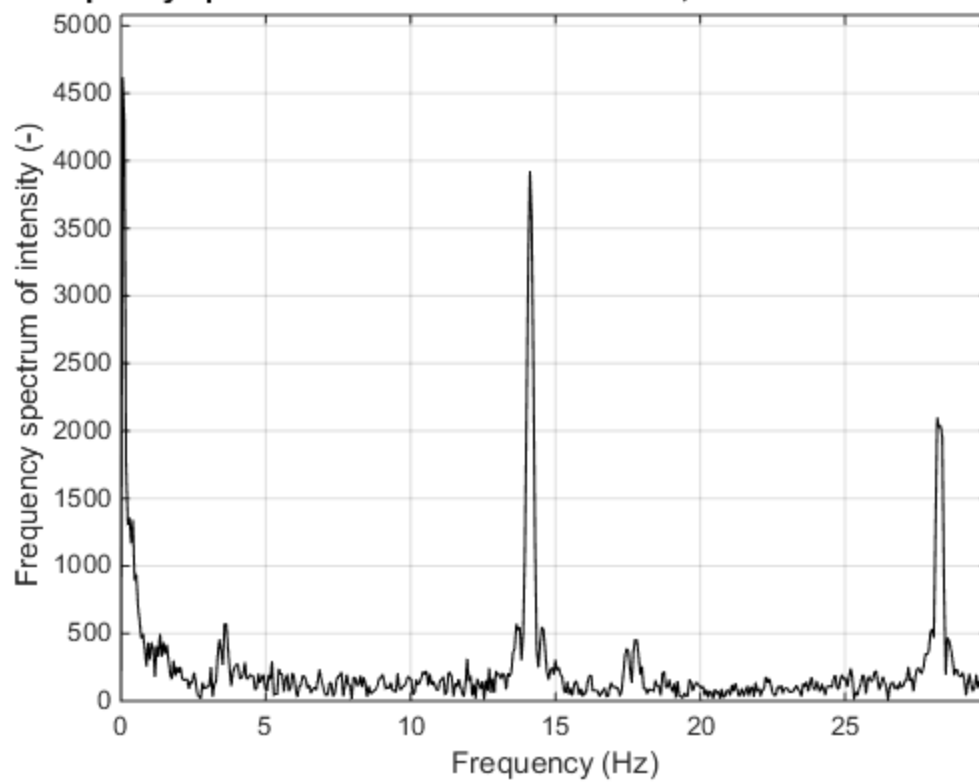
Frequency spectrum of "S6T2 Knot.MOV", Pixel coordinates: 779 363



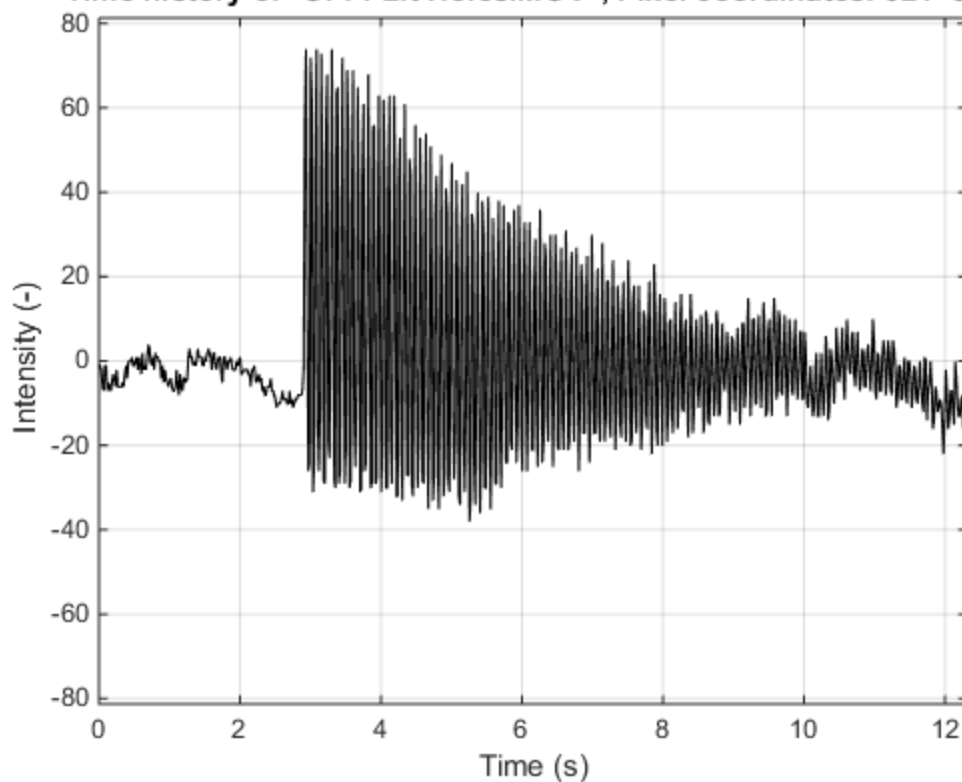
Time history of "S7T1 1ft Holes.MOV", Pixel coordinates: 562 341



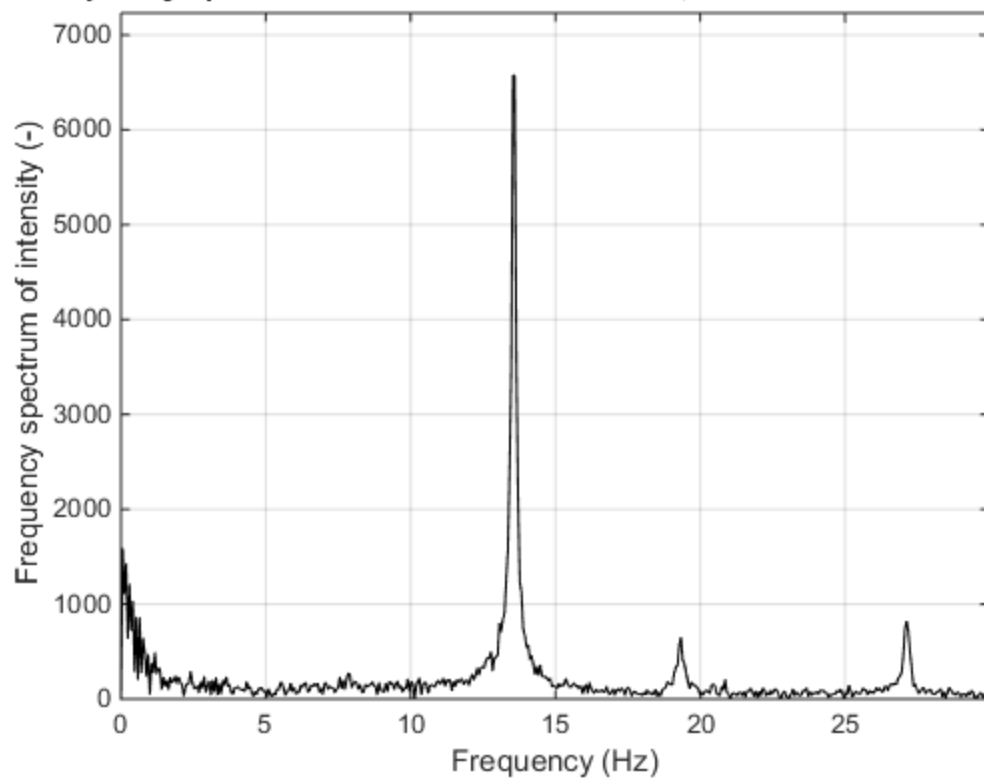
Frequency spectrum of "S7T1 1ft Holes.MOV", Pixel coordinates: 562 341



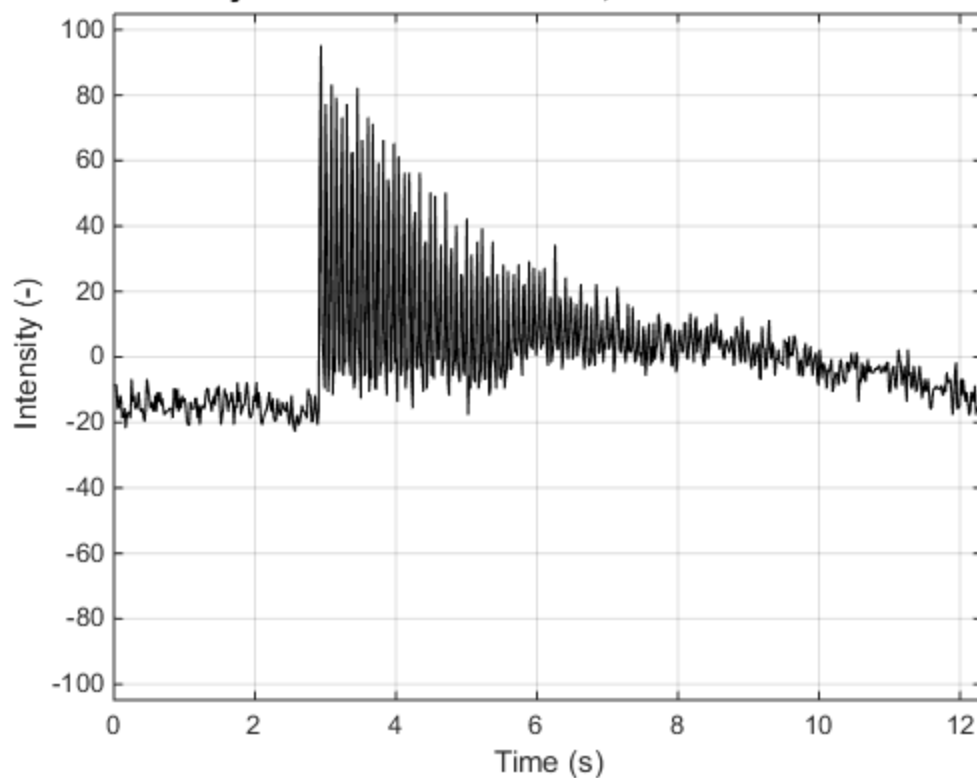
Time history of "S7T1 2ft Holes.MOV", Pixel coordinates: 621 329



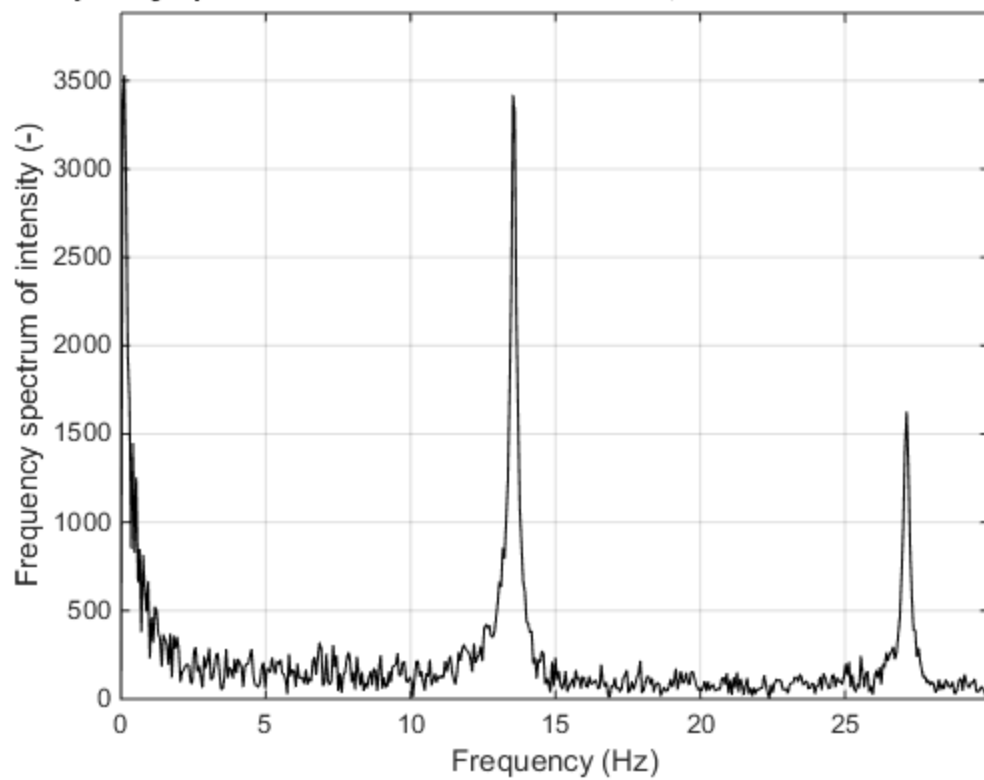
Frequency spectrum of "S7T1 2ft Holes.MOV", Pixel coordinates: 621 329



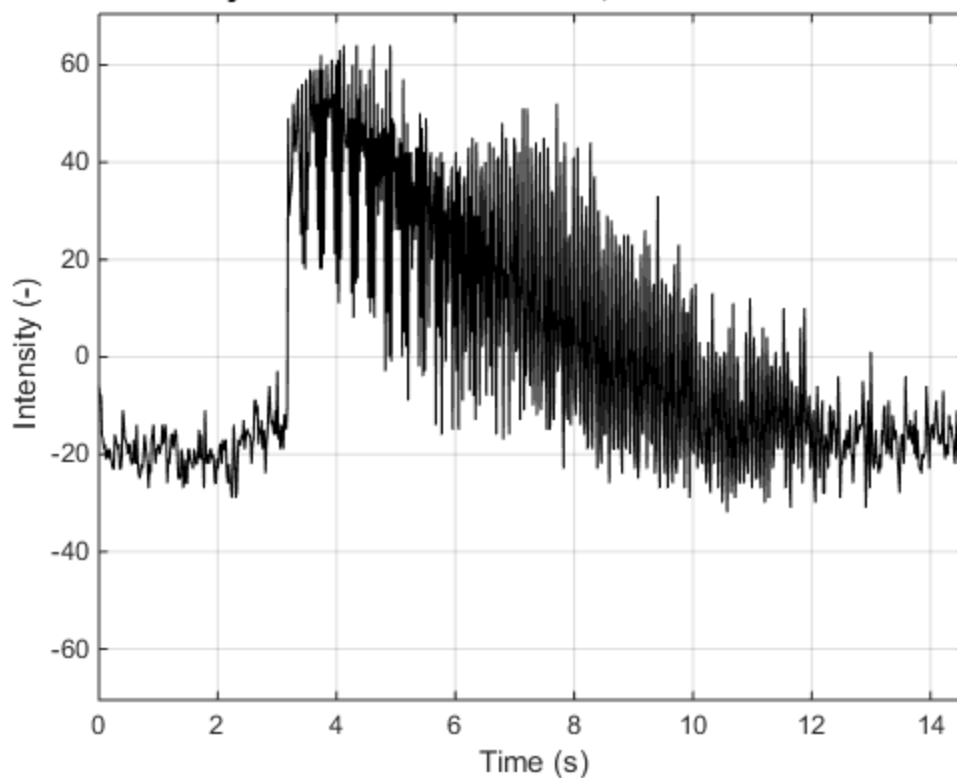
Time history of "S7T1 2ft Holes.MOV", Pixel coordinates: 1024 329



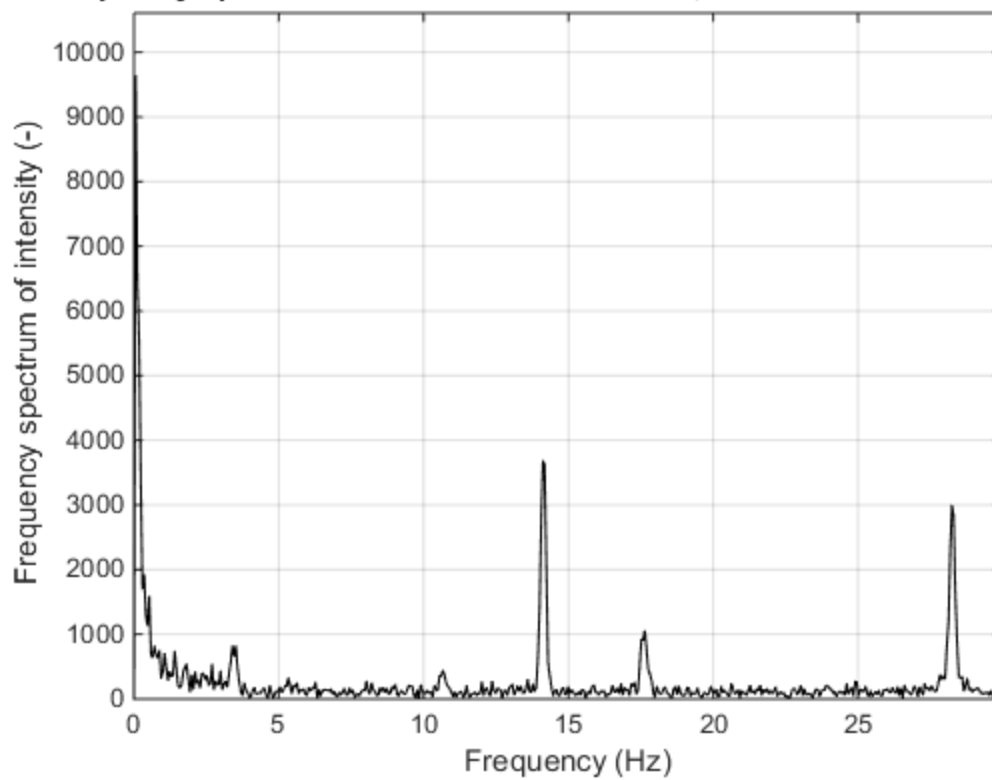
Frequency spectrum of "S7T1 2ft Holes.MOV", Pixel coordinates: 1024 329



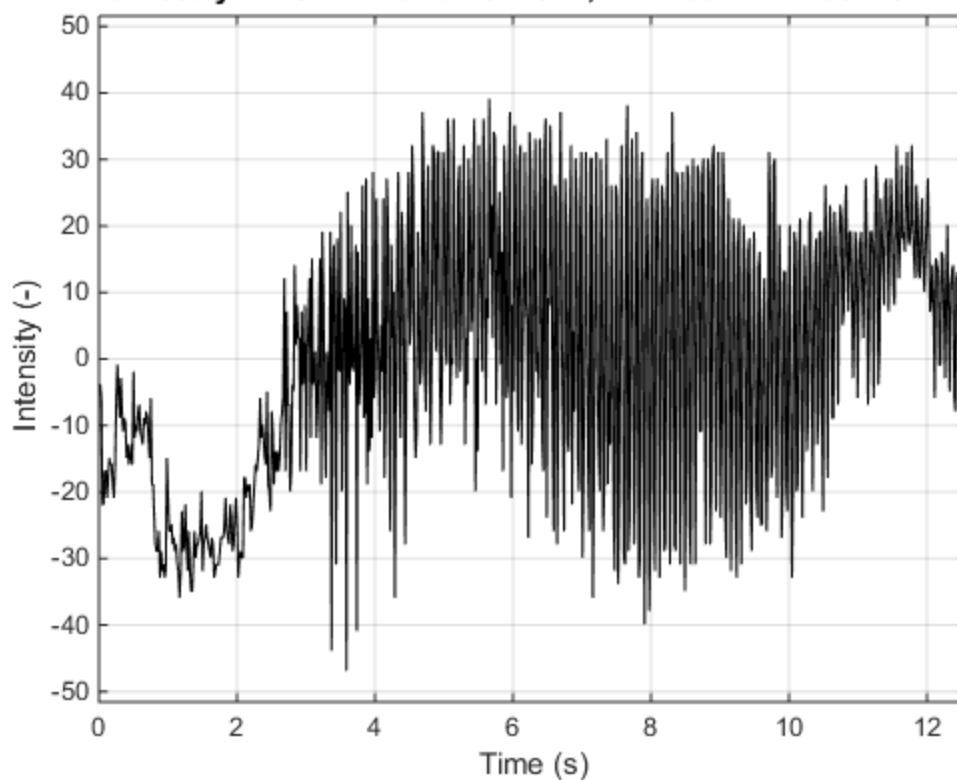
Time history of "S7T2 1ft Holes.MOV", Pixel coordinates: 860 259



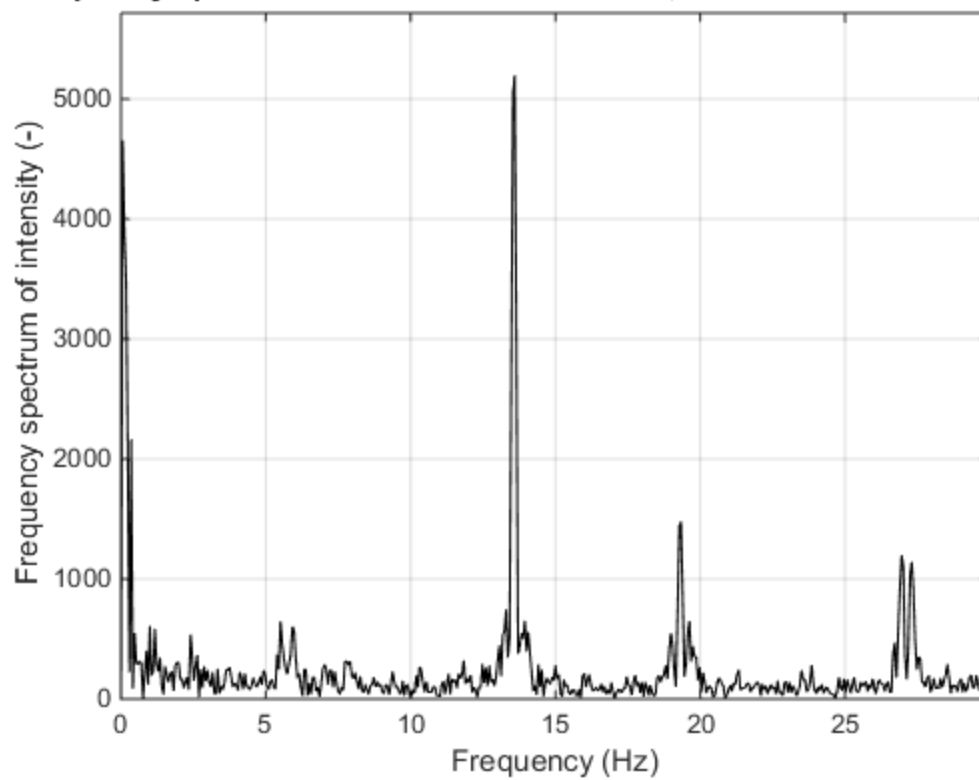
Frequency spectrum of "S7T2 1ft Holes.MOV", Pixel coordinates: 860 259



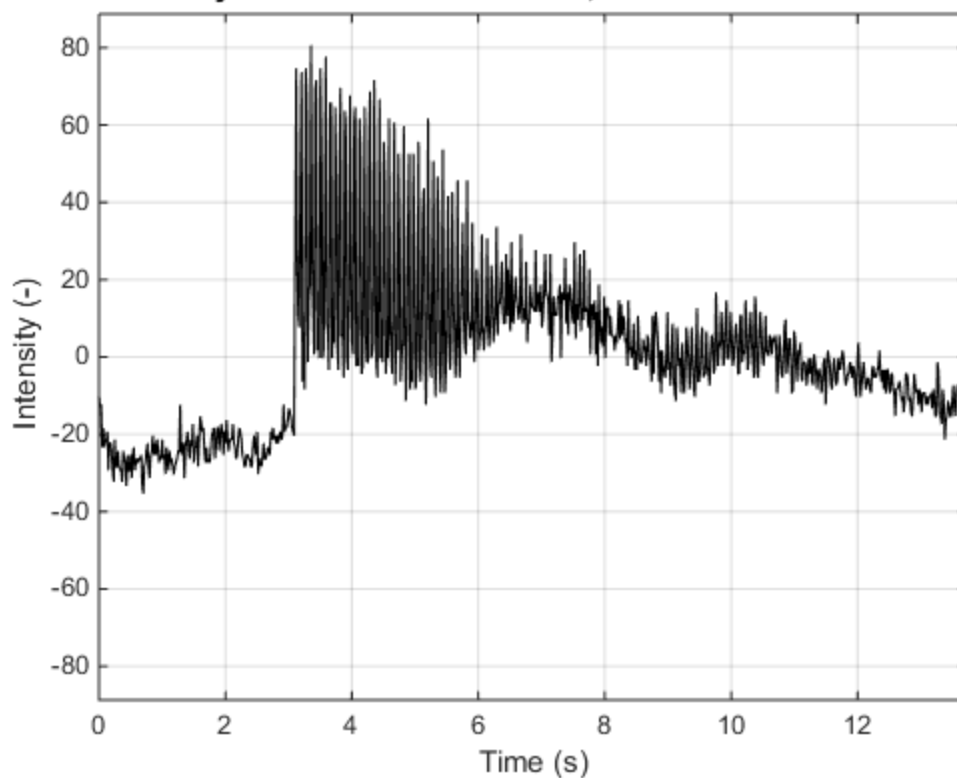
Time history of "S7T2 2ft Holes.MOV", Pixel coordinates: 1024 329



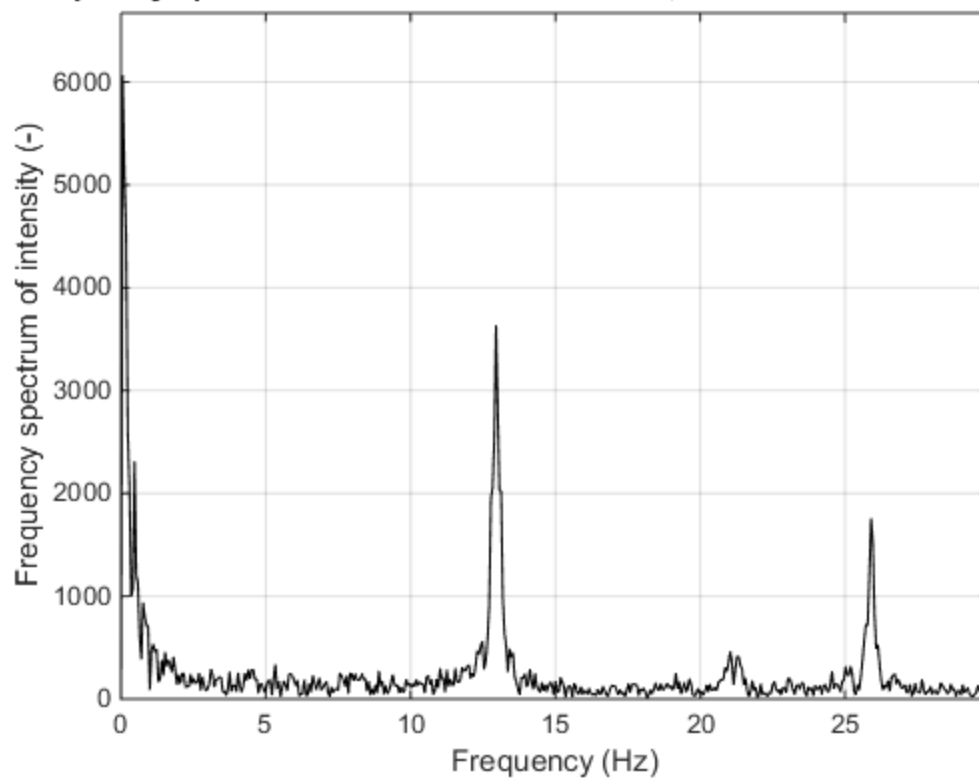
Frequency spectrum of "S7T2 2ft Holes.MOV", Pixel coordinates: 1024 329



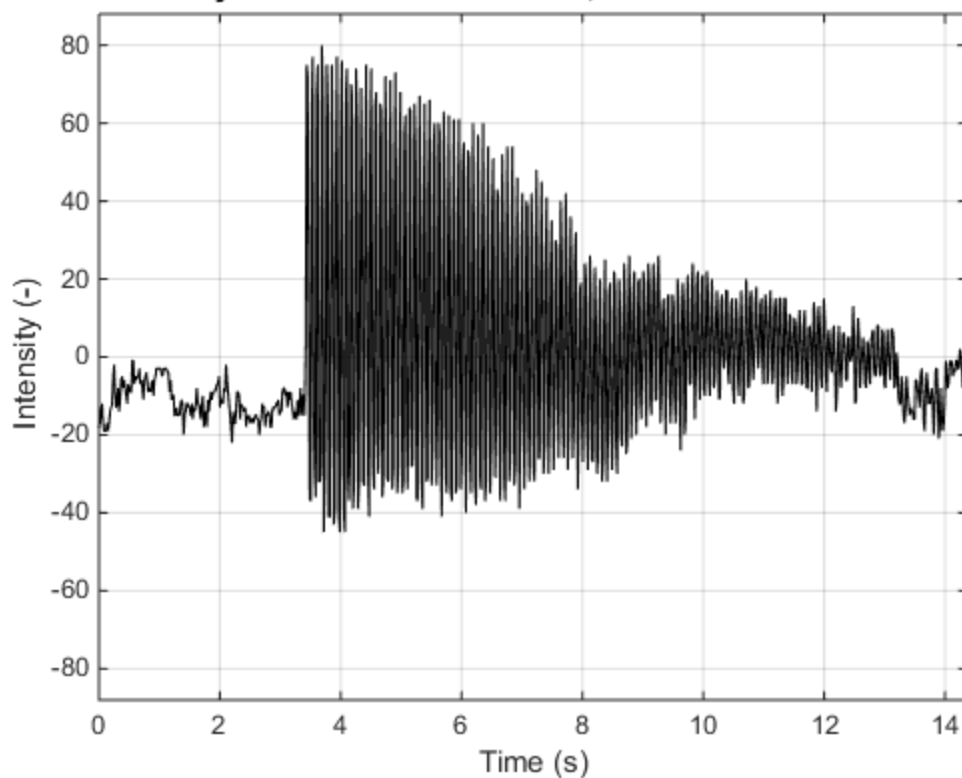
Time history of "S8T1 1ft Holes.MOV", Pixel coordinates: 1024 329



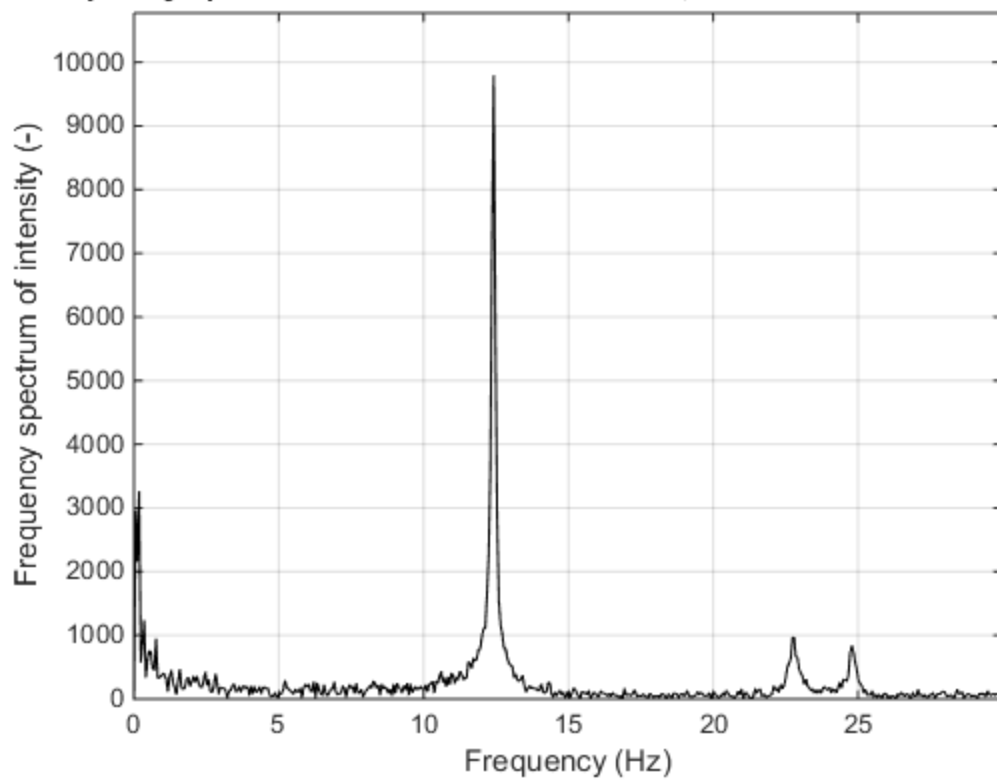
Frequency spectrum of "S8T1 1ft Holes.MOV", Pixel coordinates: 1024 329



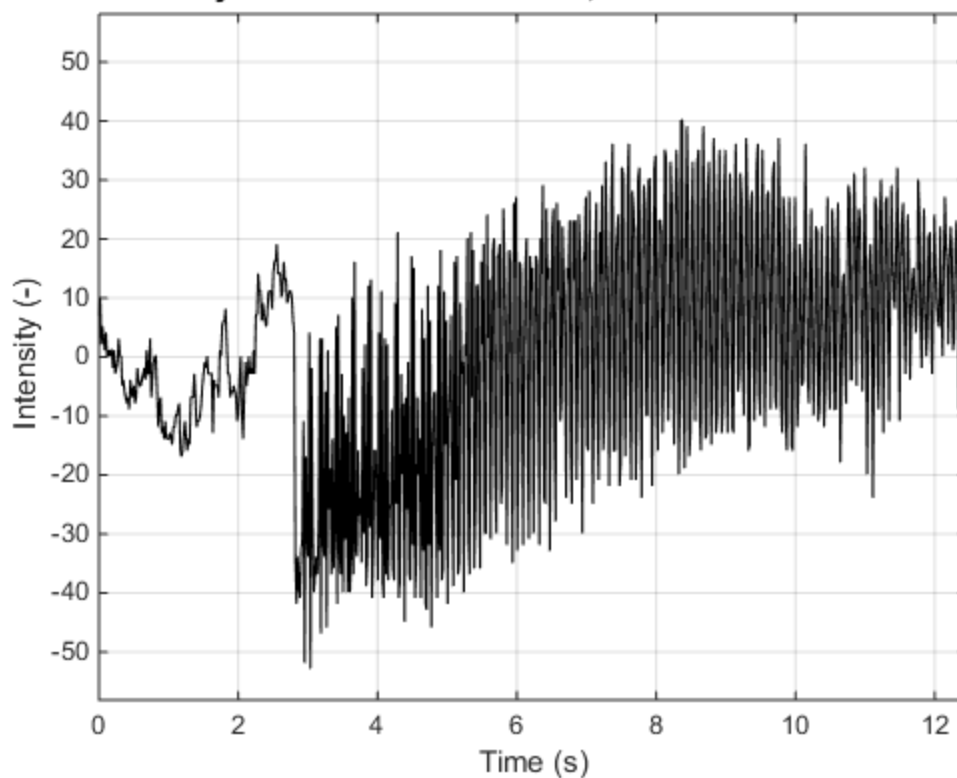
Time history of "S8T1 2ft Holes.MOV", Pixel coordinates: 1024 329



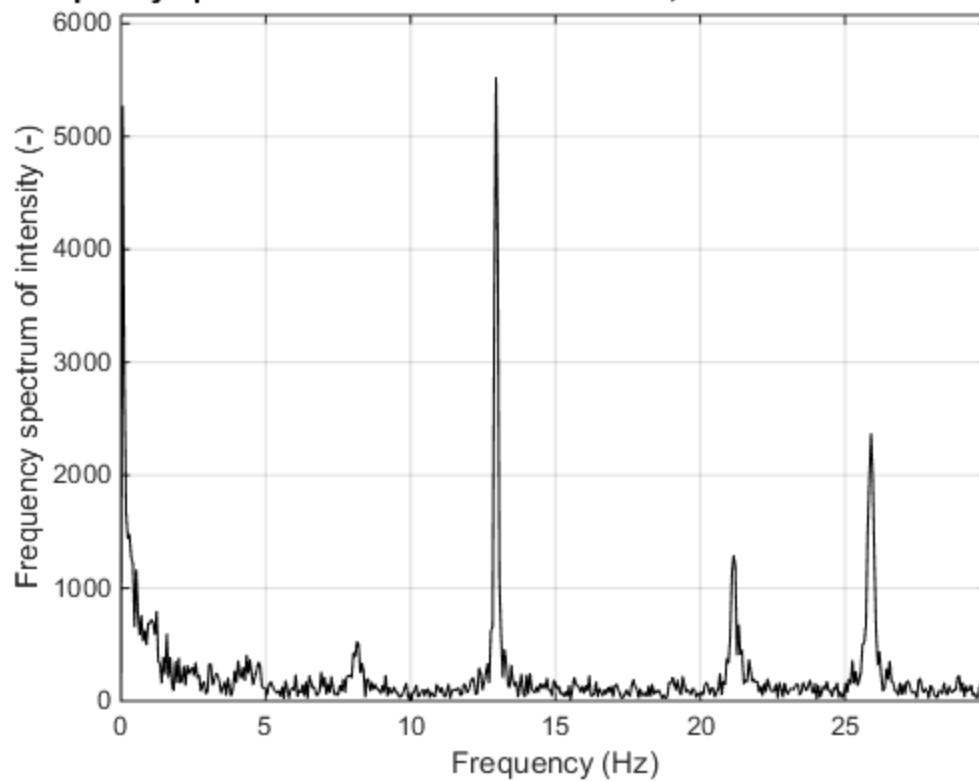
Frequency spectrum of "S8T1 2ft Holes.MOV", Pixel coordinates: 1024 329



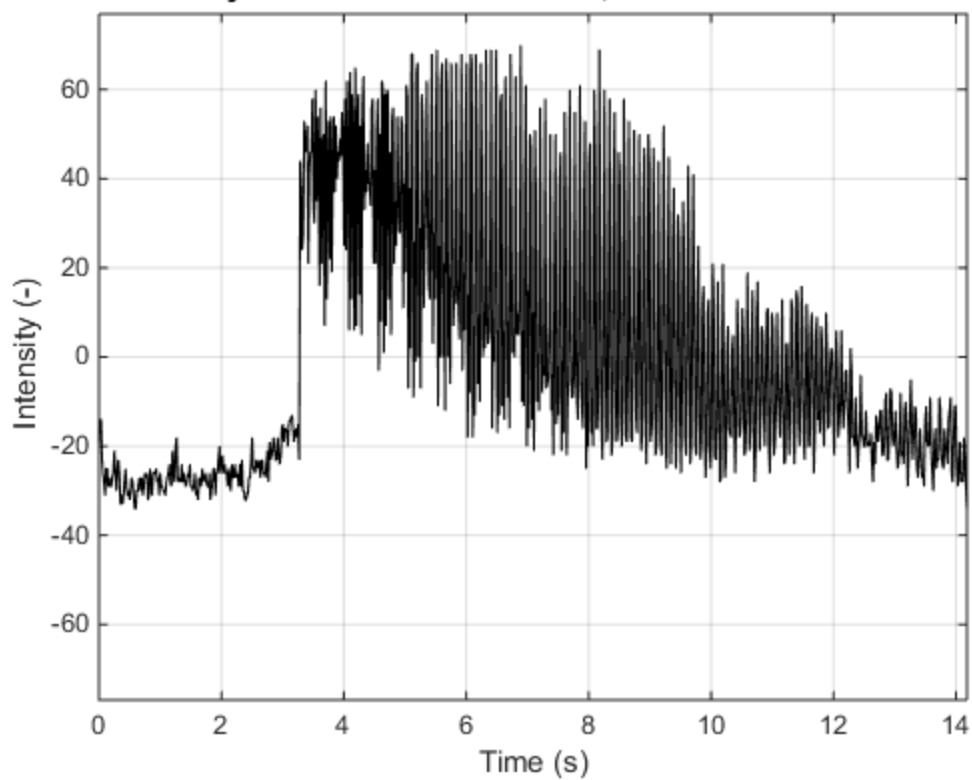
Time history of "S8T2 1ft Holes.MOV", Pixel coordinates: 1024 329



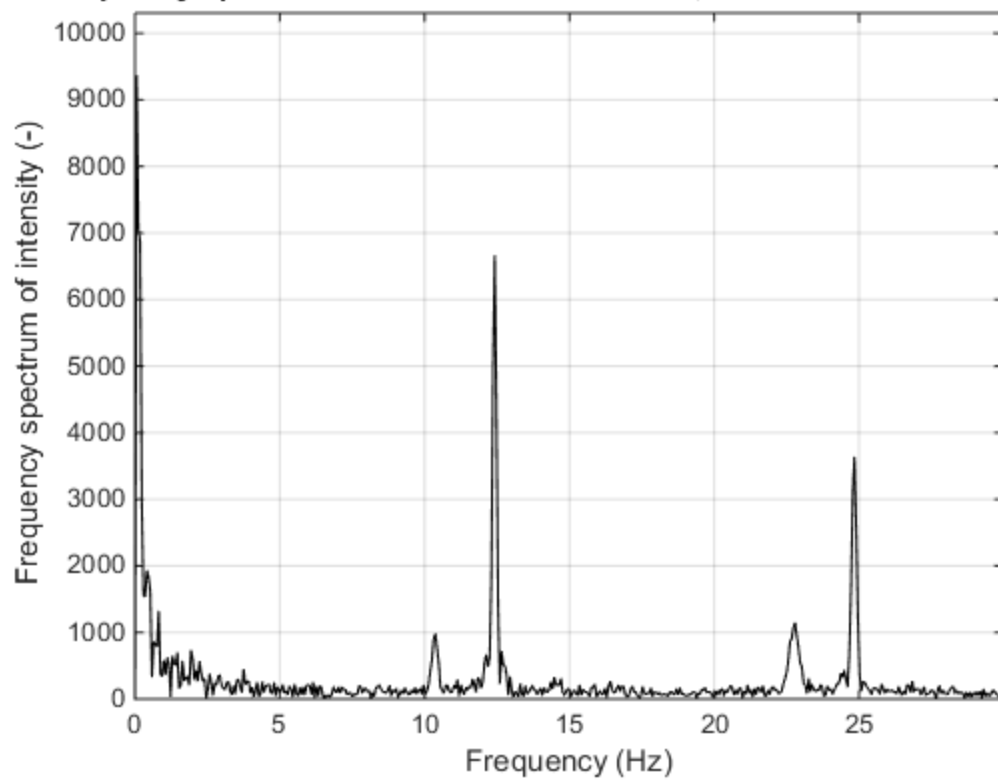
Frequency spectrum of "S8T2 1ft Holes.MOV", Pixel coordinates: 1024 329



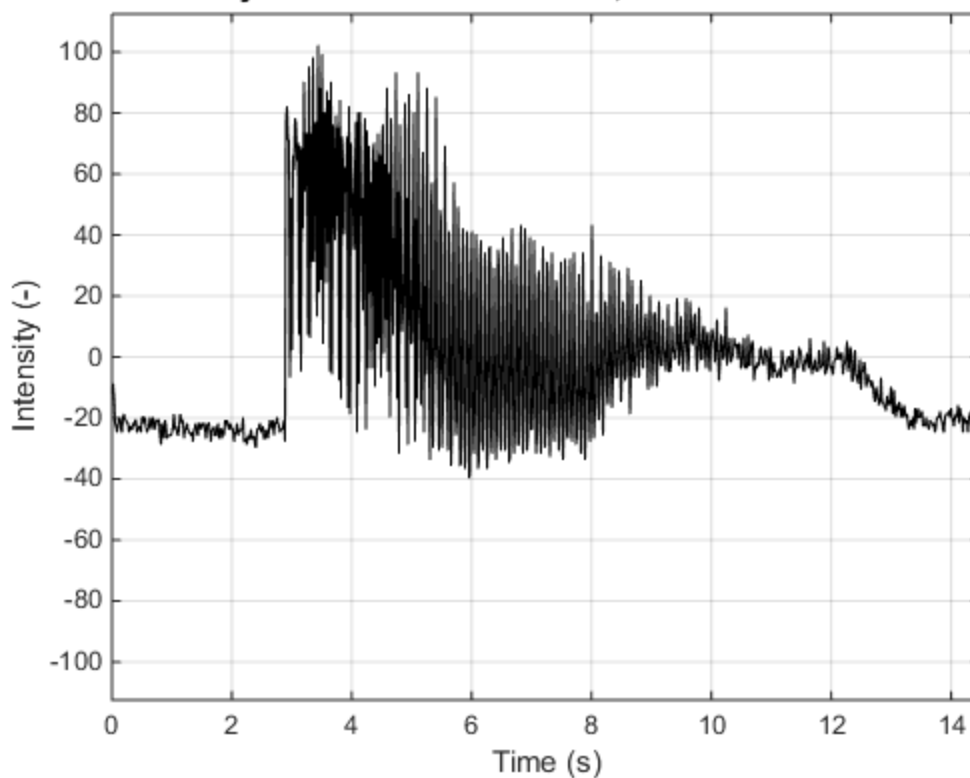
Time history of "S8T2 2ft Holes.MOV", Pixel coordinates: 567 286



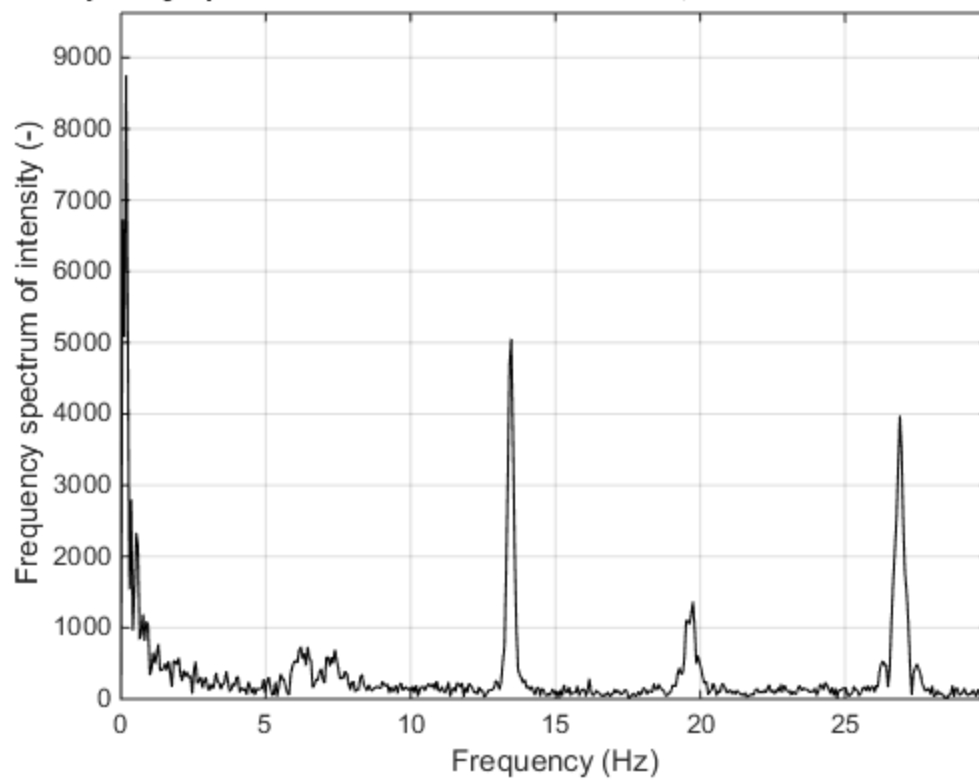
Frequency spectrum of "S8T2 2ft Holes.MOV", Pixel coordinates: 567 286



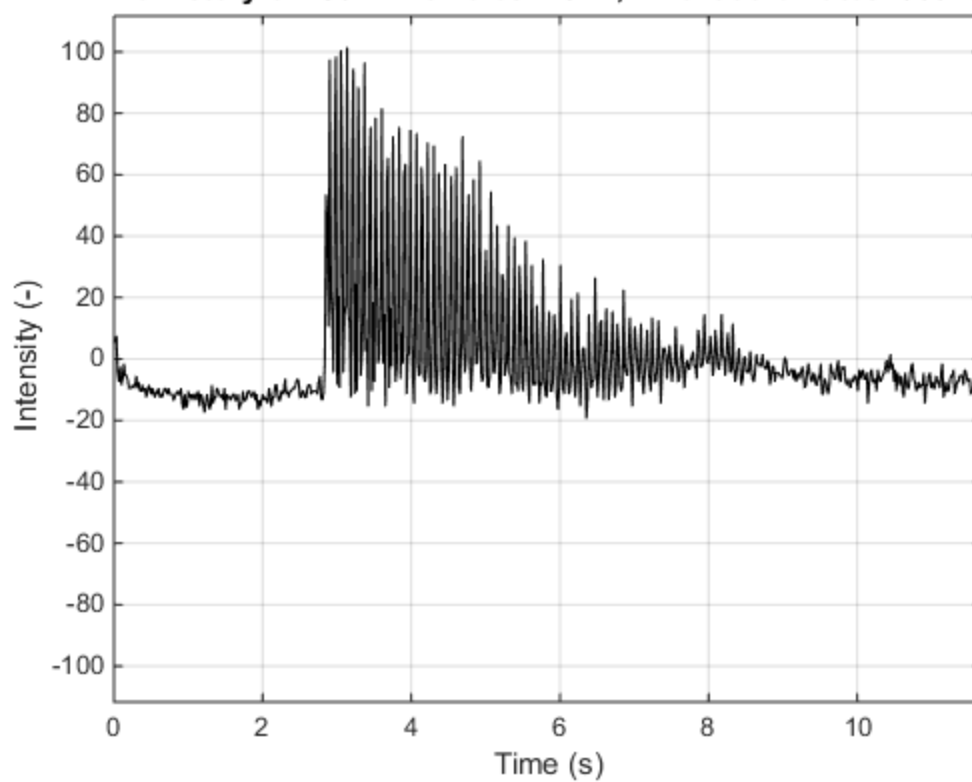
Time history of "S9T1 1ft Holes.MOV", Pixel coordinates: 677 324



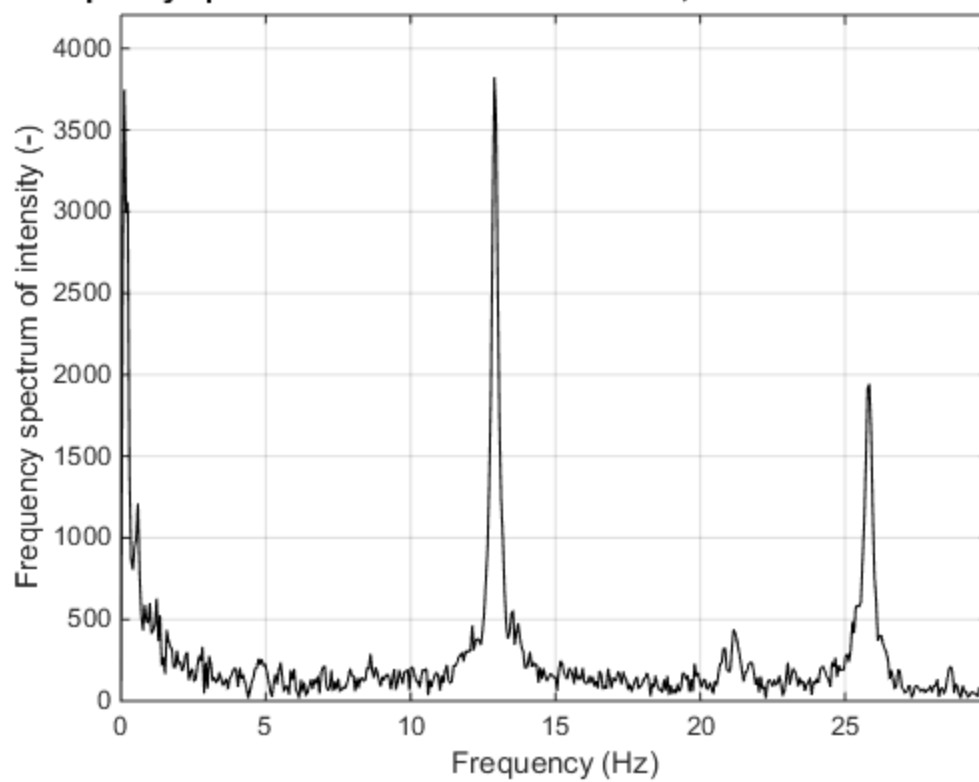
Frequency spectrum of "S9T1 1ft Holes.MOV", Pixel coordinates: 677 324



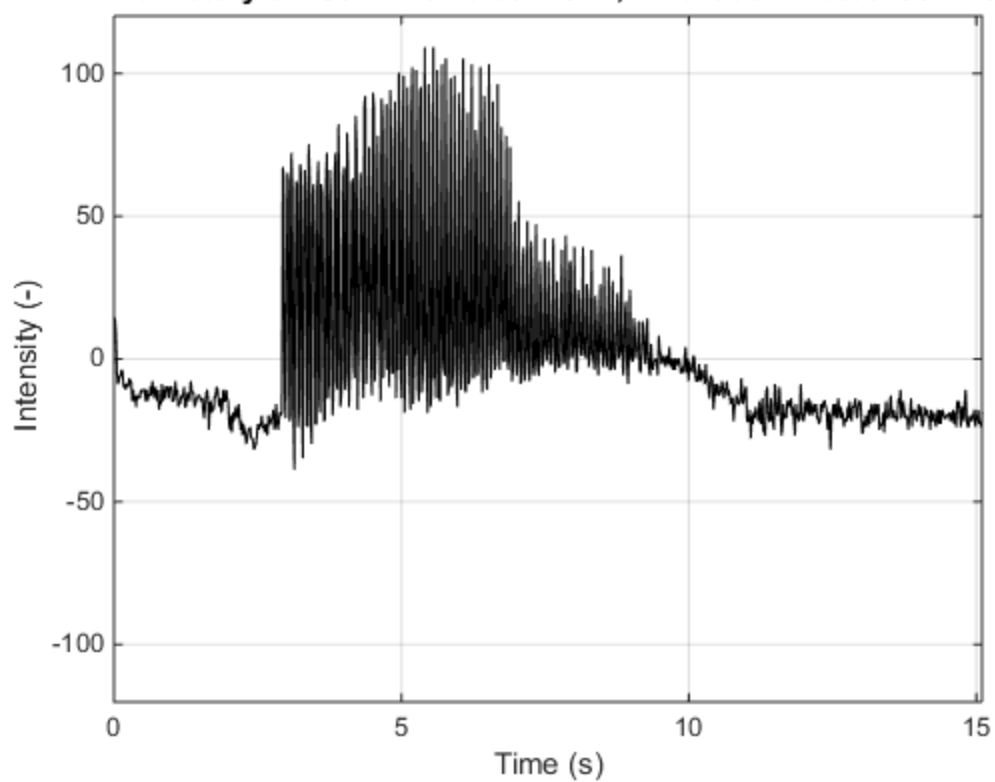
Time history of "S9T1 2ft Holes.MOV", Pixel coordinates: 600 343



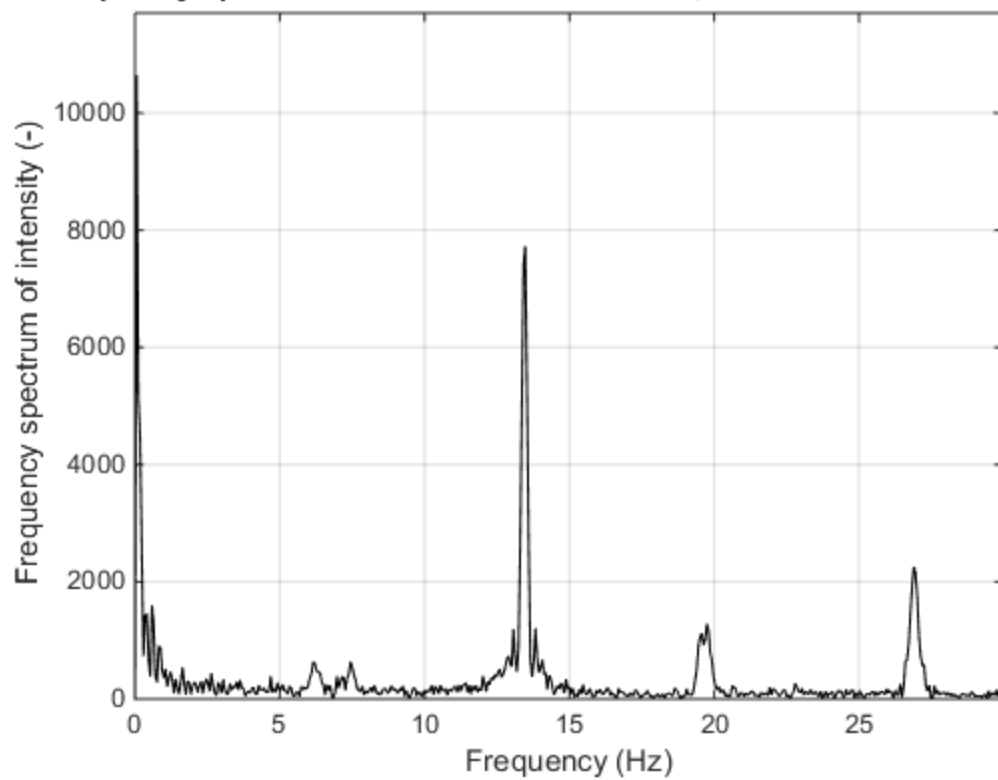
Frequency spectrum of "S9T1 2ft Holes.MOV", Pixel coordinates: 600 343



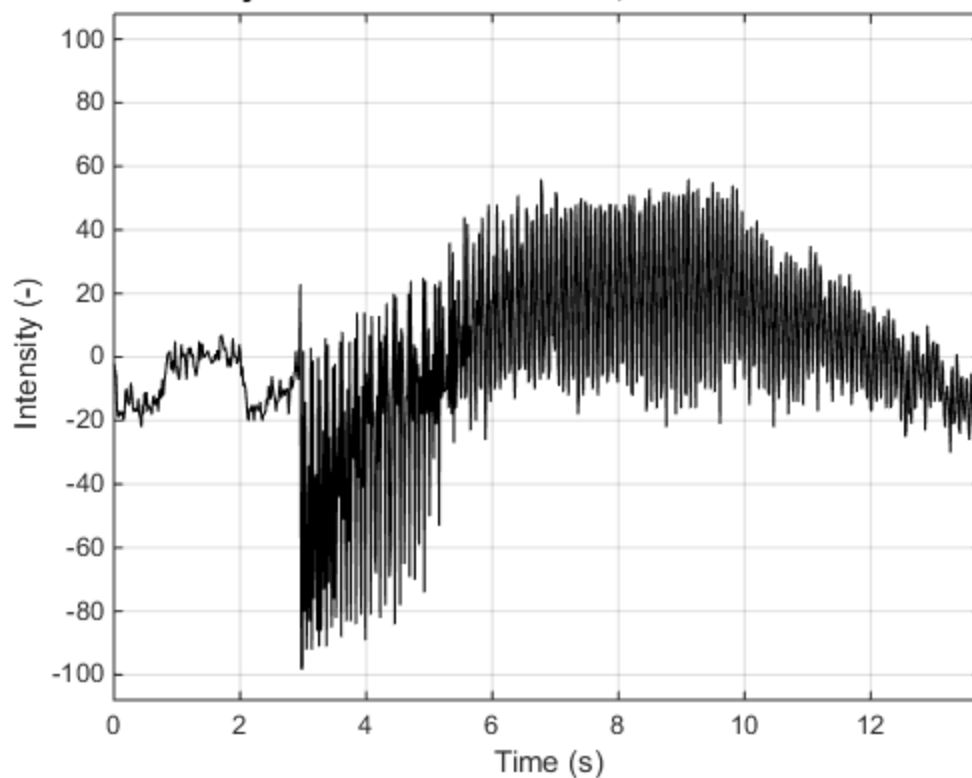
Time history of "S9T2 1ft Holes.MOV", Pixel coordinates: 807 238



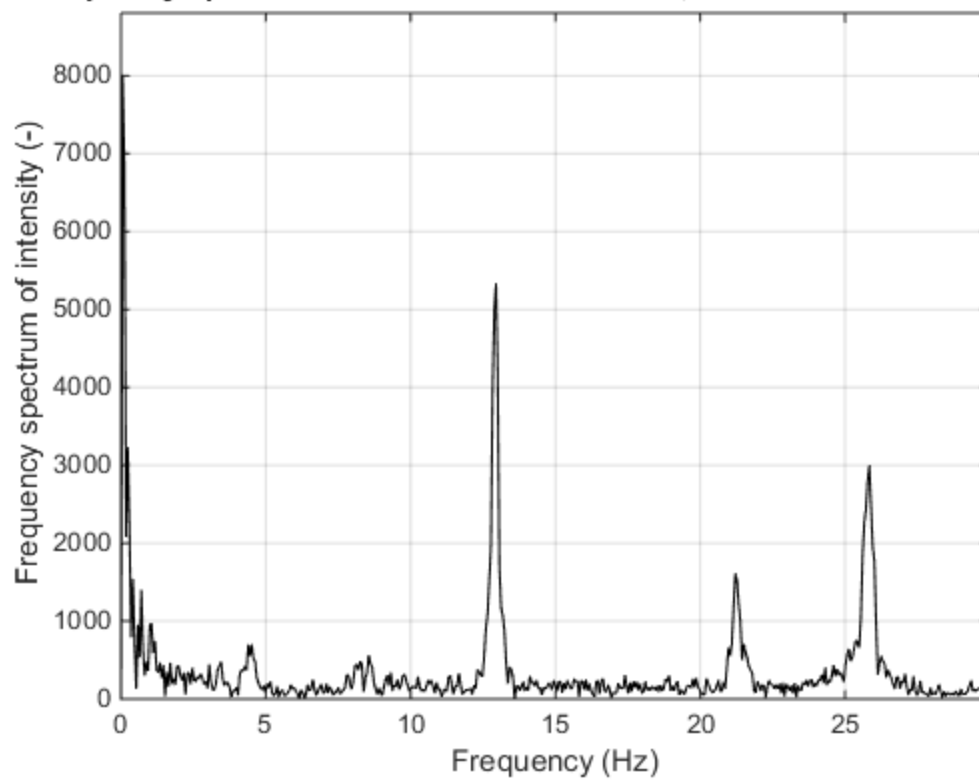
Frequency spectrum of "S9T2 1ft Holes.MOV", Pixel coordinates: 807 238



Time history of "S9T2 2ft Holes.MOV", Pixel coordinates: 740 273



Frequency spectrum of "S9T2 2ft Holes.MOV", Pixel coordinates: 740 273



Appendix I – GoPro VVS Figures from Simulated Damage 2x4 Experiments

- The first highlighted section contains the specimen designation followed by the test number.
 - In this example: Specimen 1, Test 1
- The second highlighted section contains the type and level of simulated damage applied.
 - In this example: Planed (once)

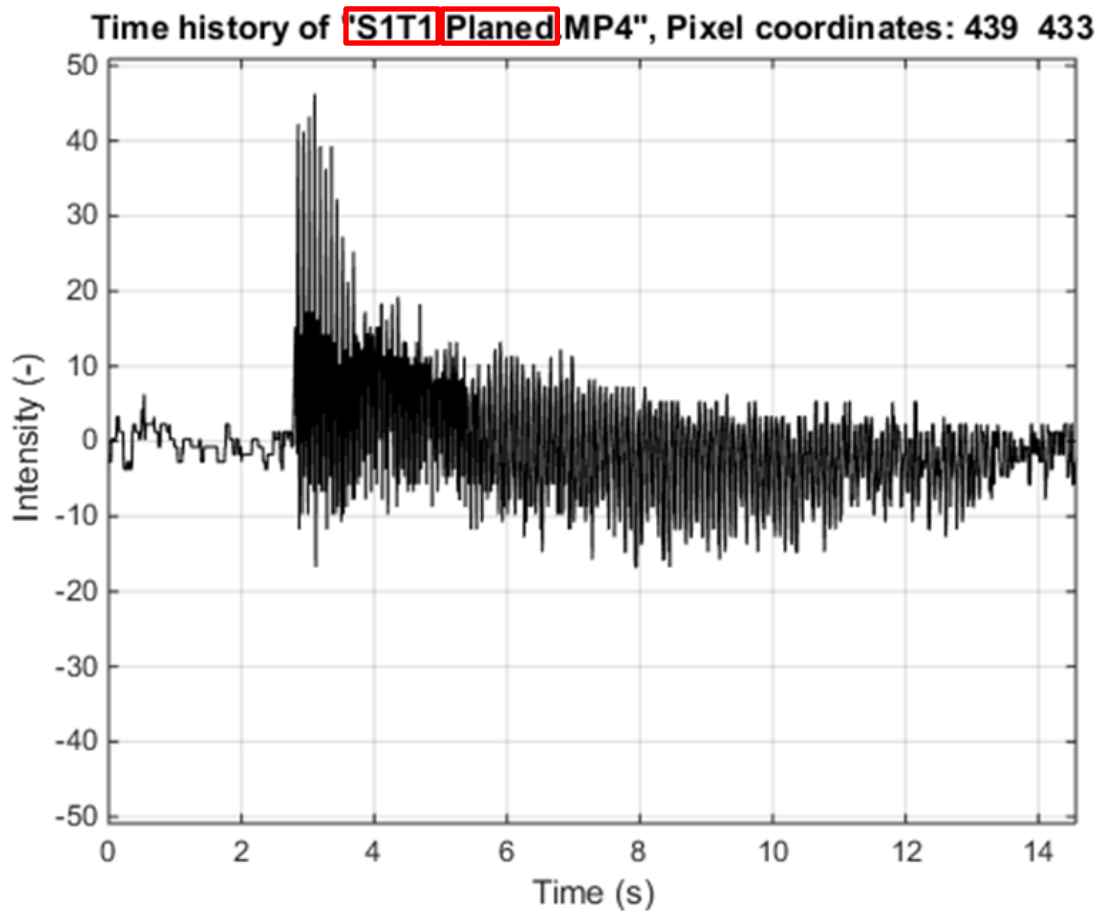
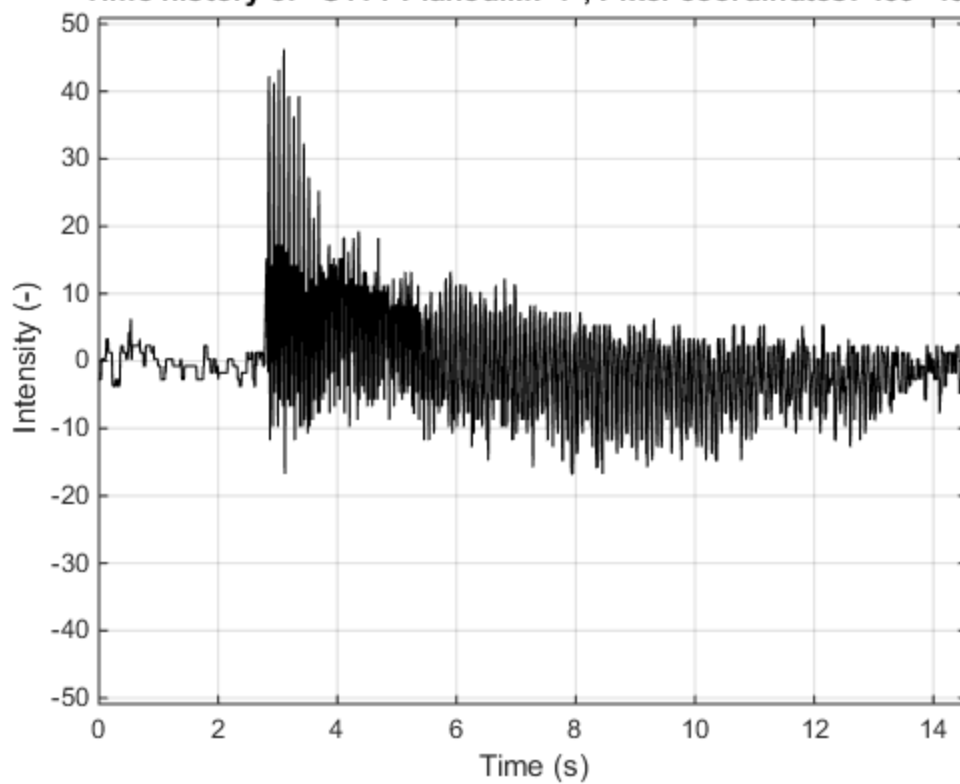
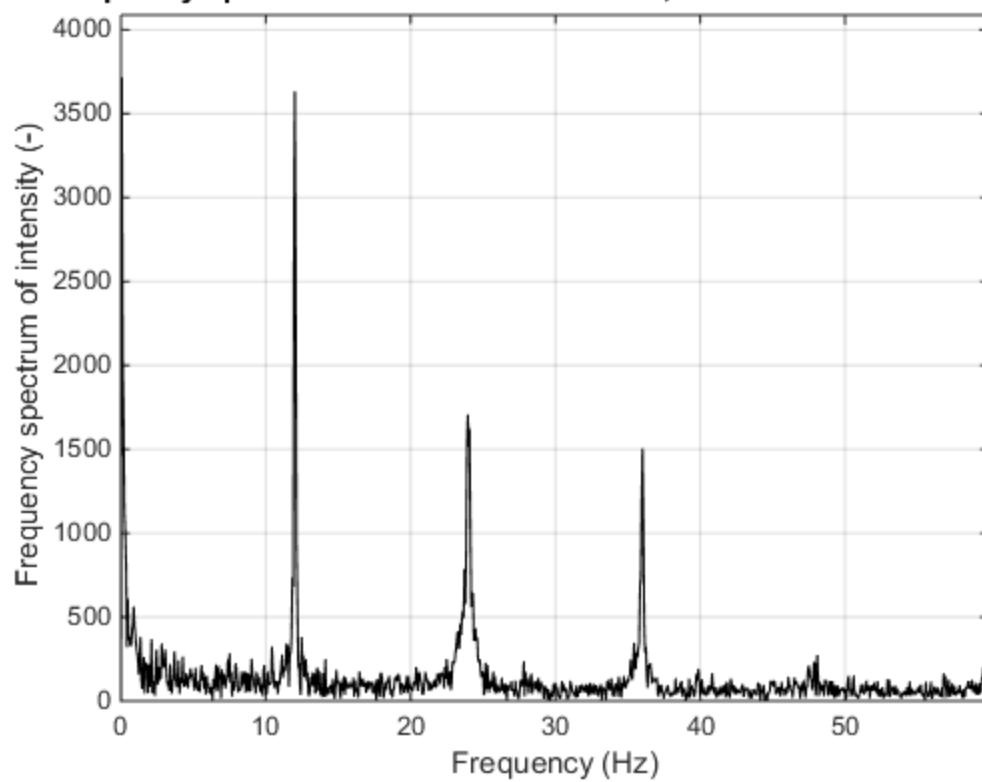


Figure H14 - Key for (GoPro) Simulated Damage Figures

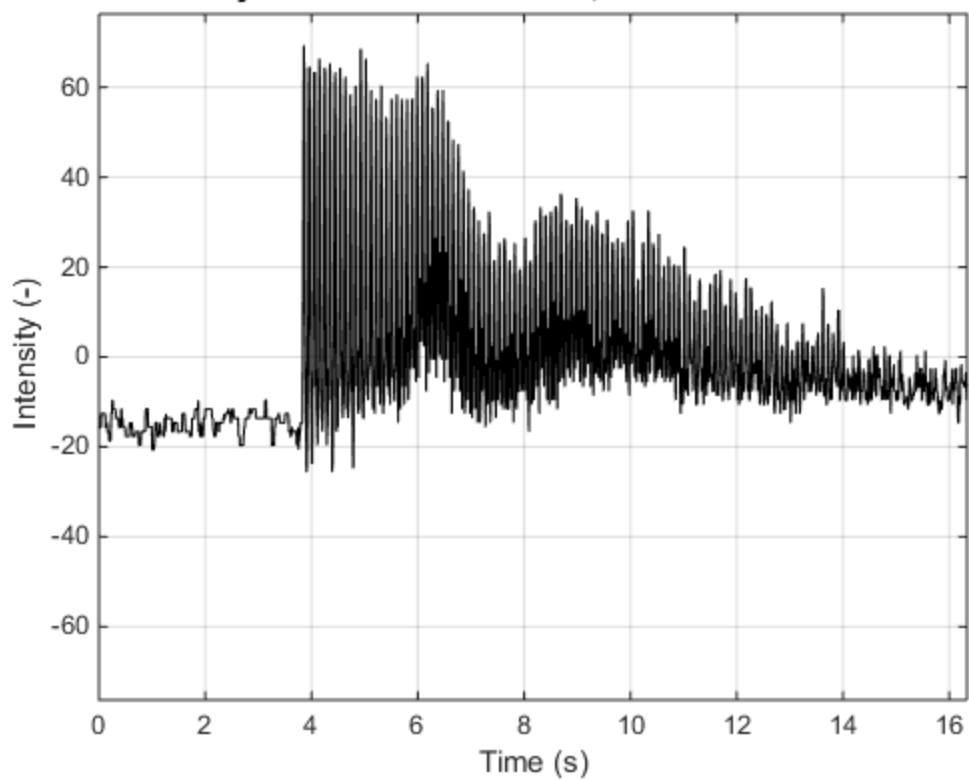
Time history of "S1T1 Planed.MP4", Pixel coordinates: 439 433



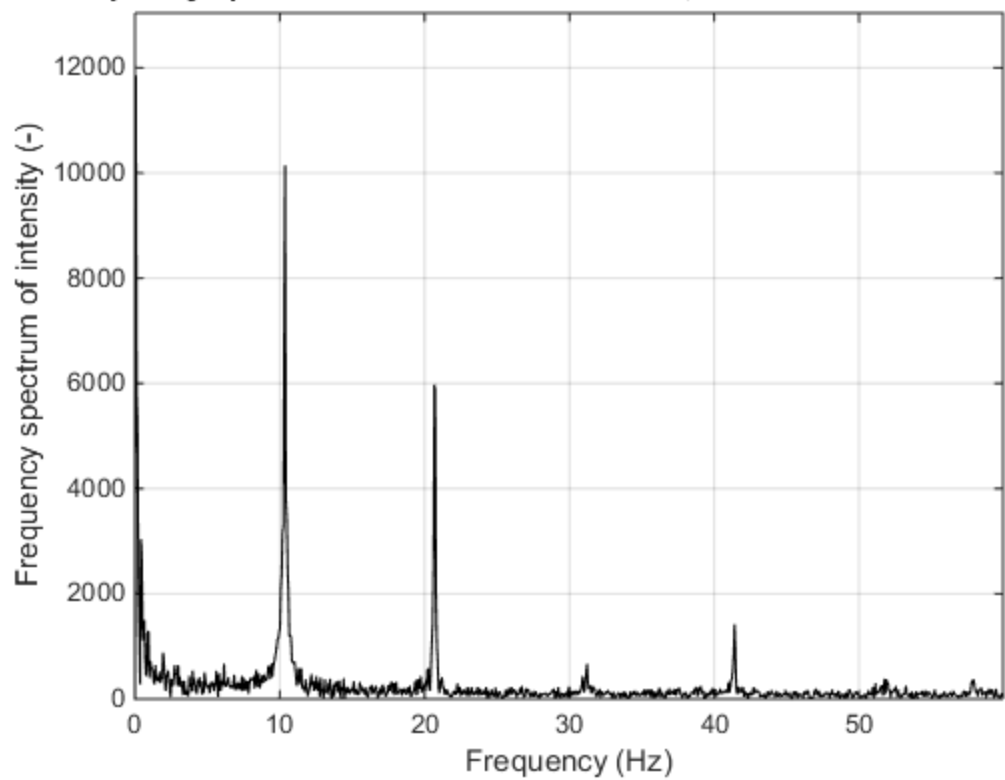
Frequency spectrum of "S1T1 Planed.MP4", Pixel coordinates: 439 433



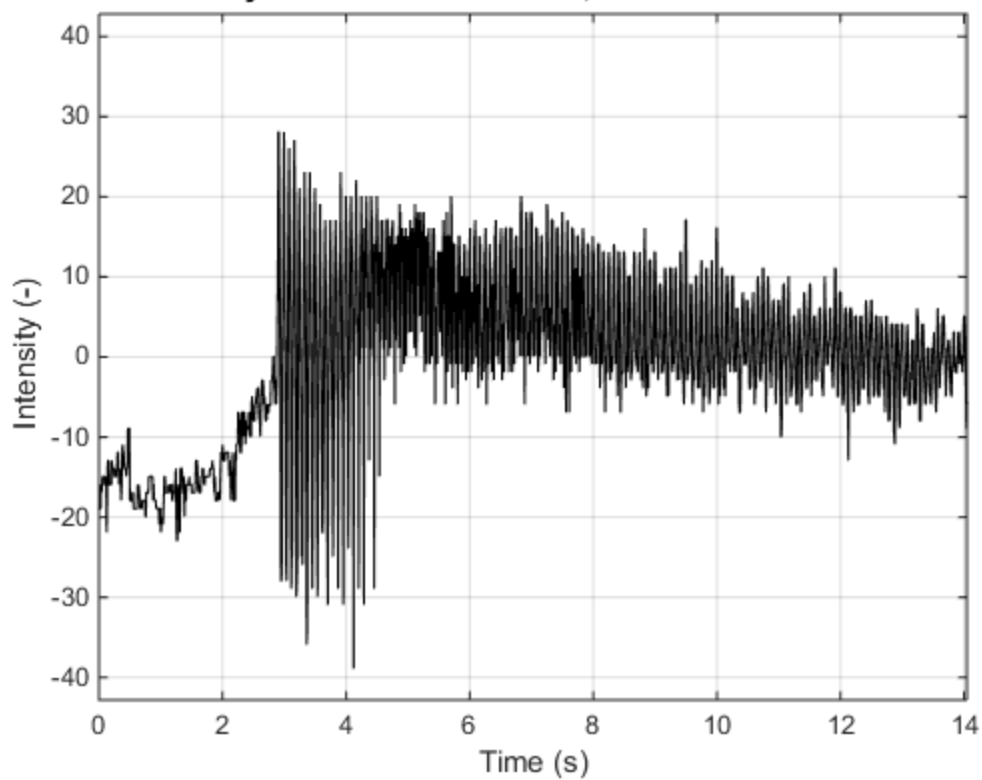
Time history of "S1T1 Planed2.MP4", Pixel coordinates: 686 418



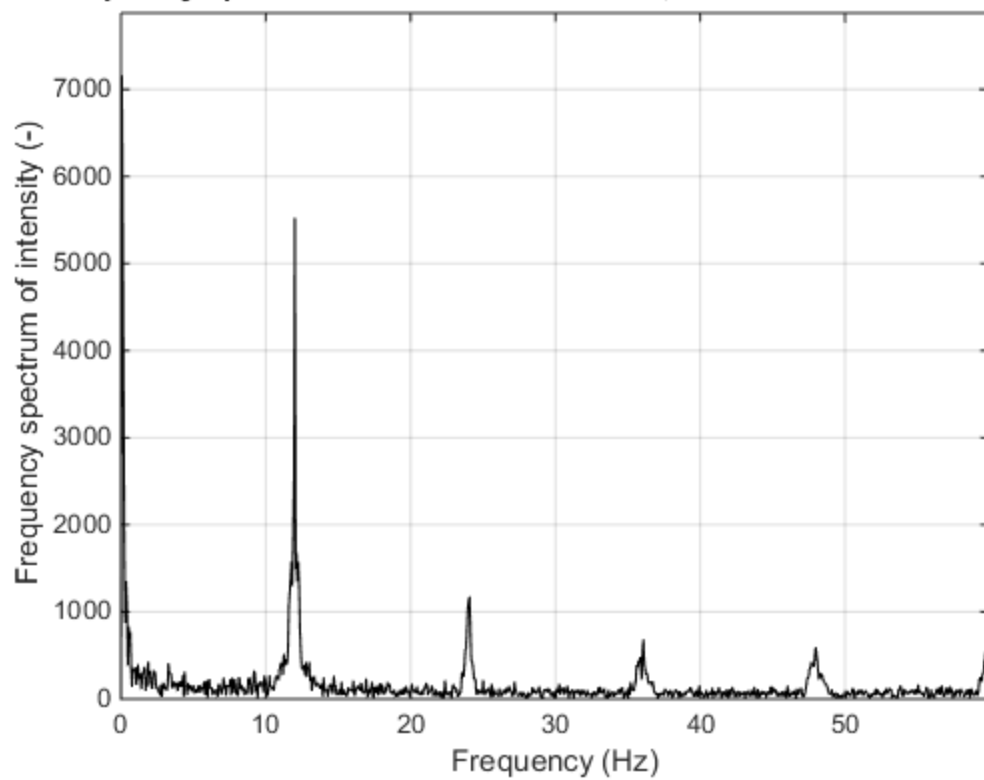
Frequency spectrum of "S1T1 Planed2.MP4", Pixel coordinates: 686 418

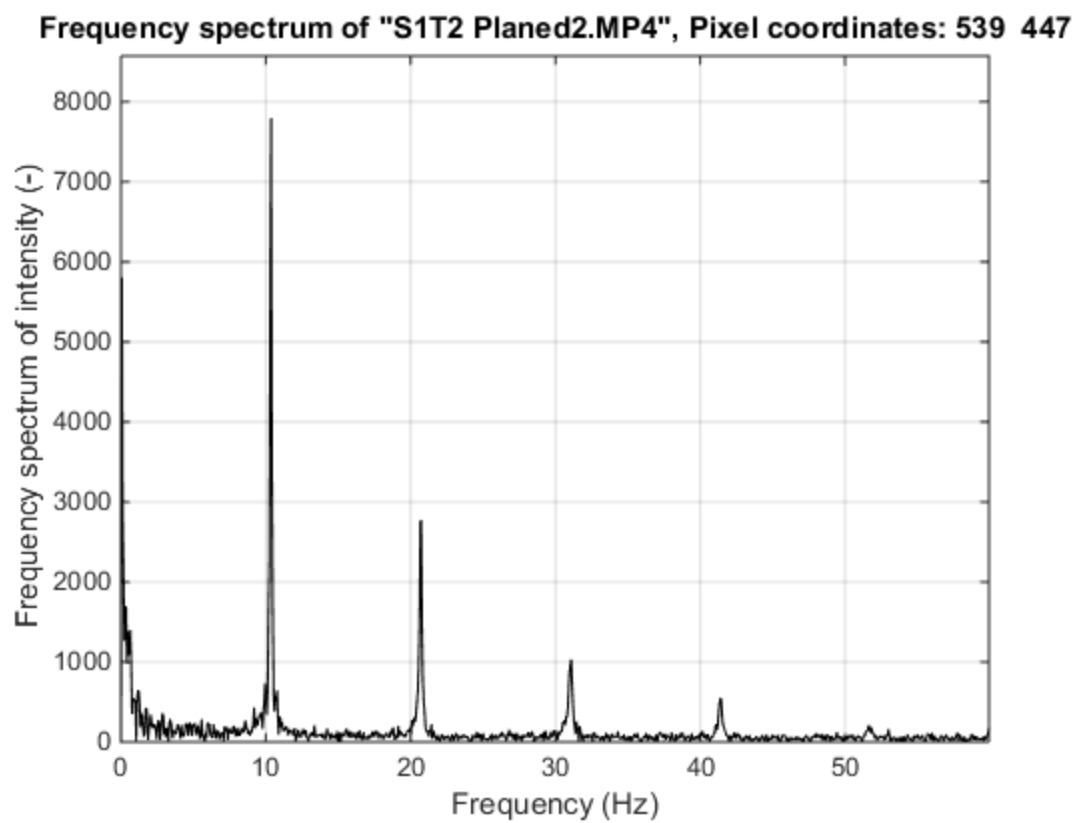
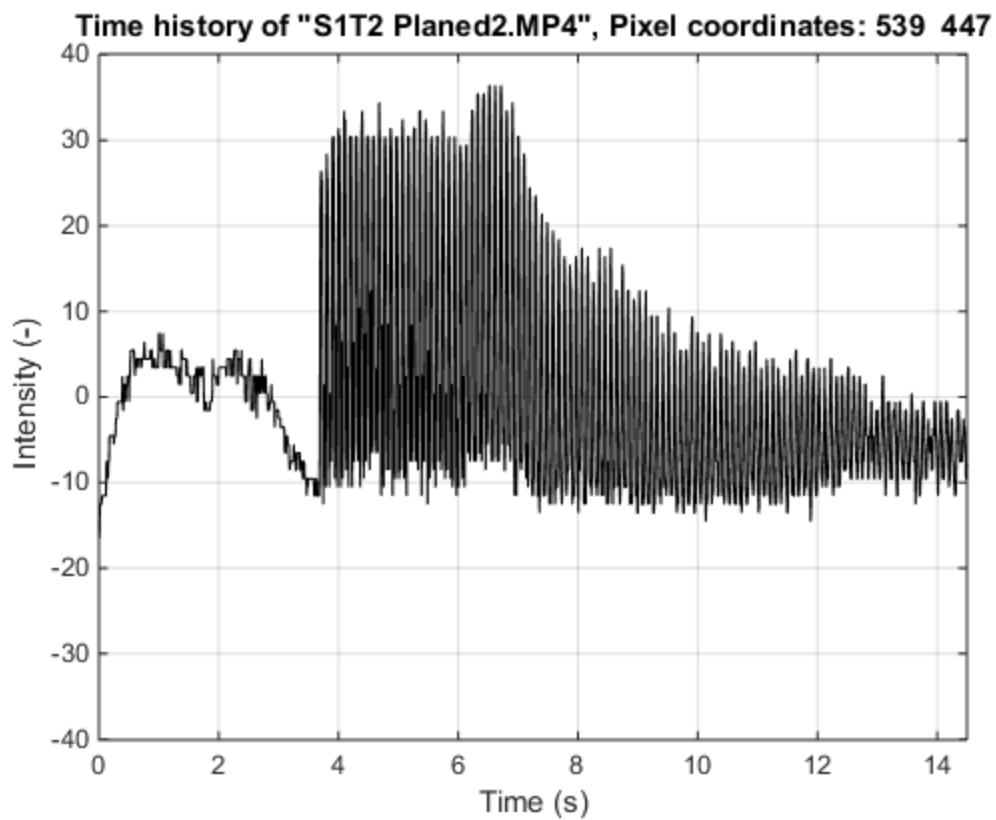


Time history of "S1T2 Planed.MP4", Pixel coordinates: 316 457

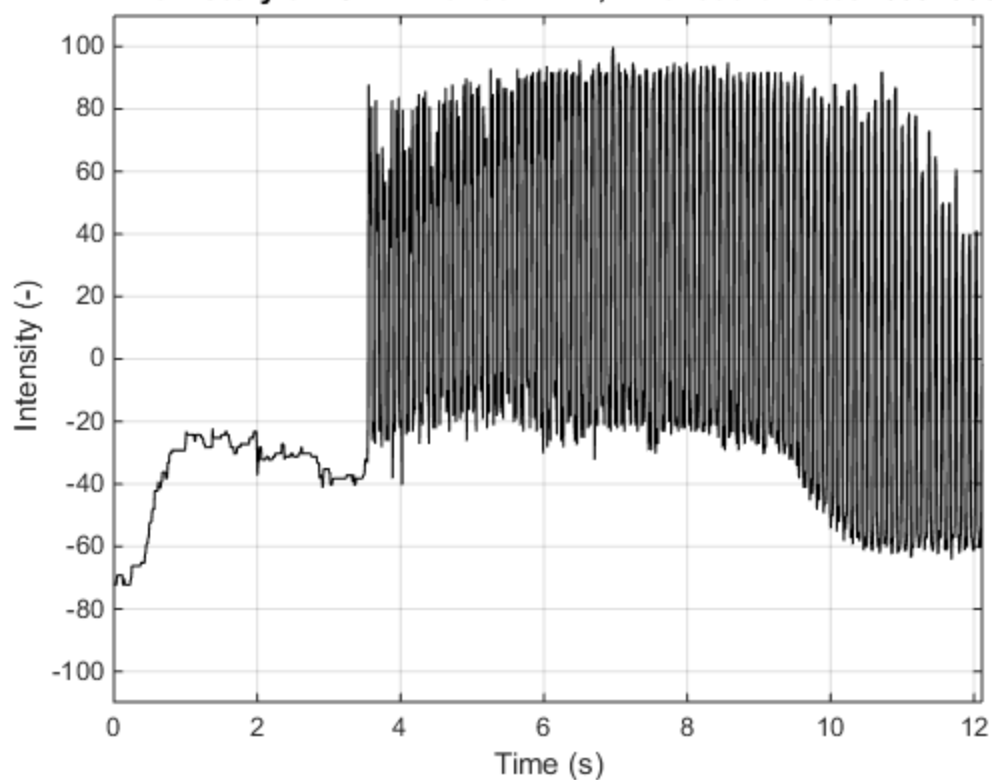


Frequency spectrum of "S1T2 Planed.MP4", Pixel coordinates: 316 457

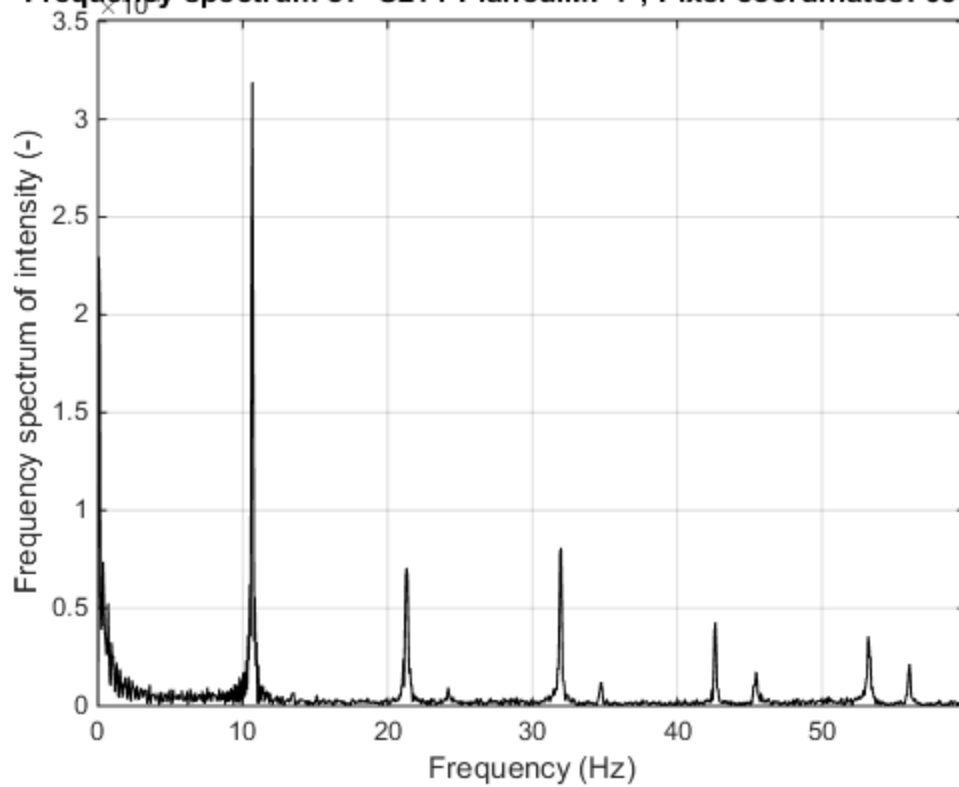


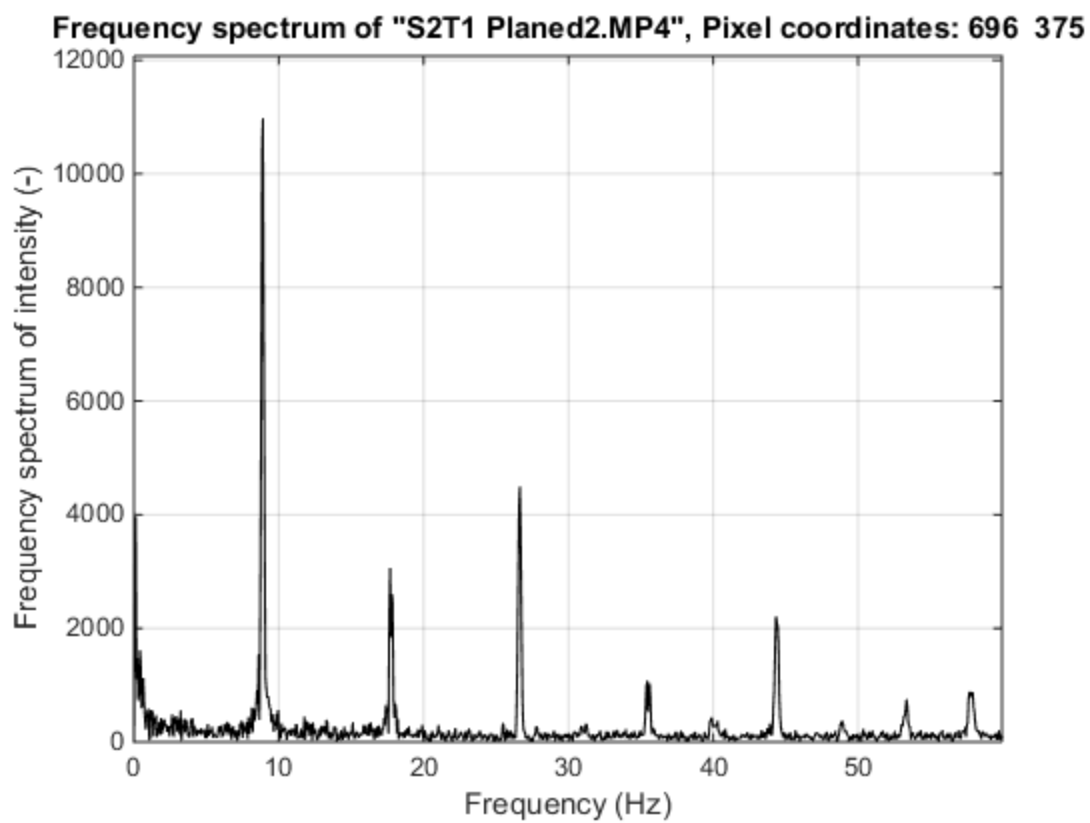
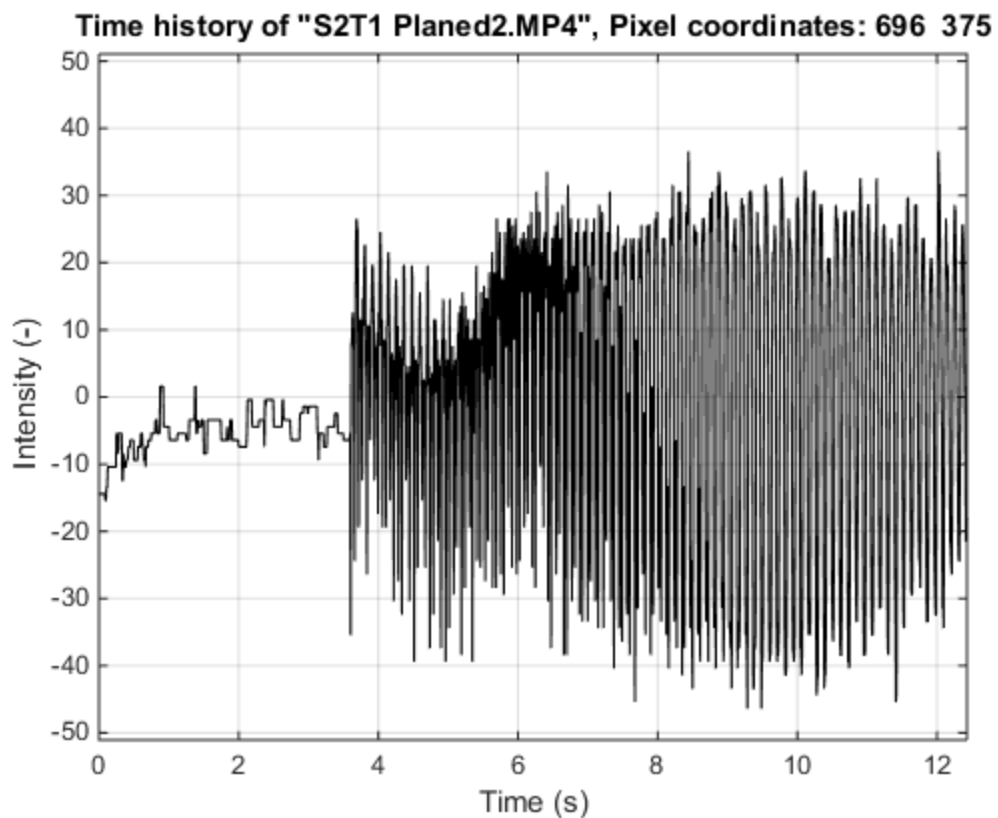


Time history of "S2T1 Planed.MP4", Pixel coordinates: 658 360

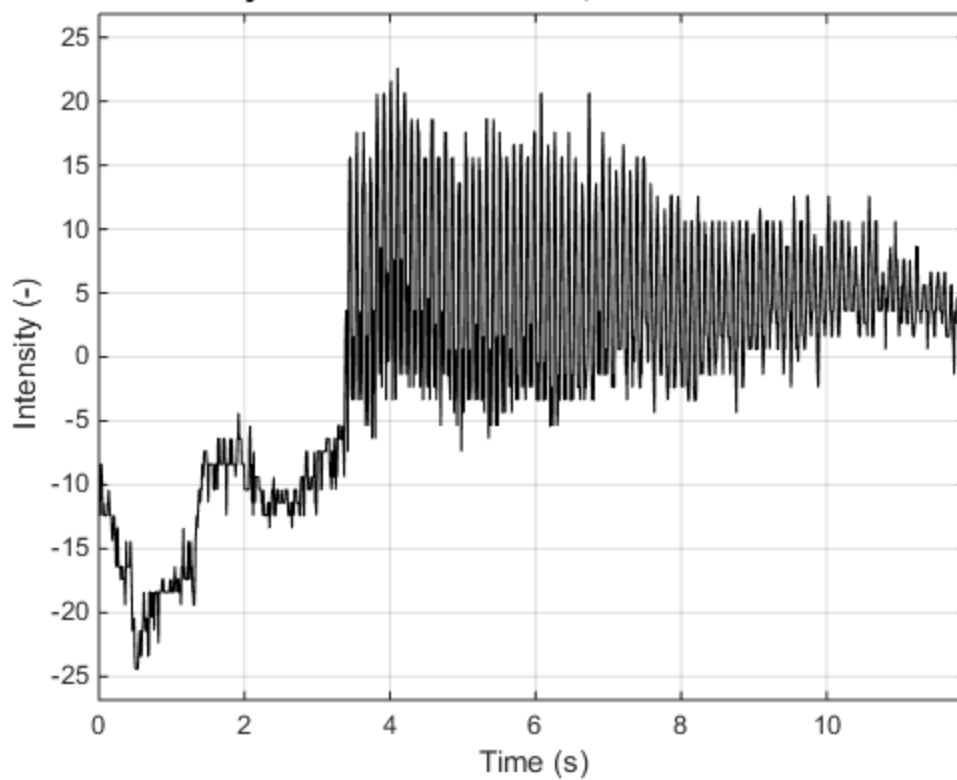


Frequency spectrum of "S2T1 Planed.MP4", Pixel coordinates: 658 360

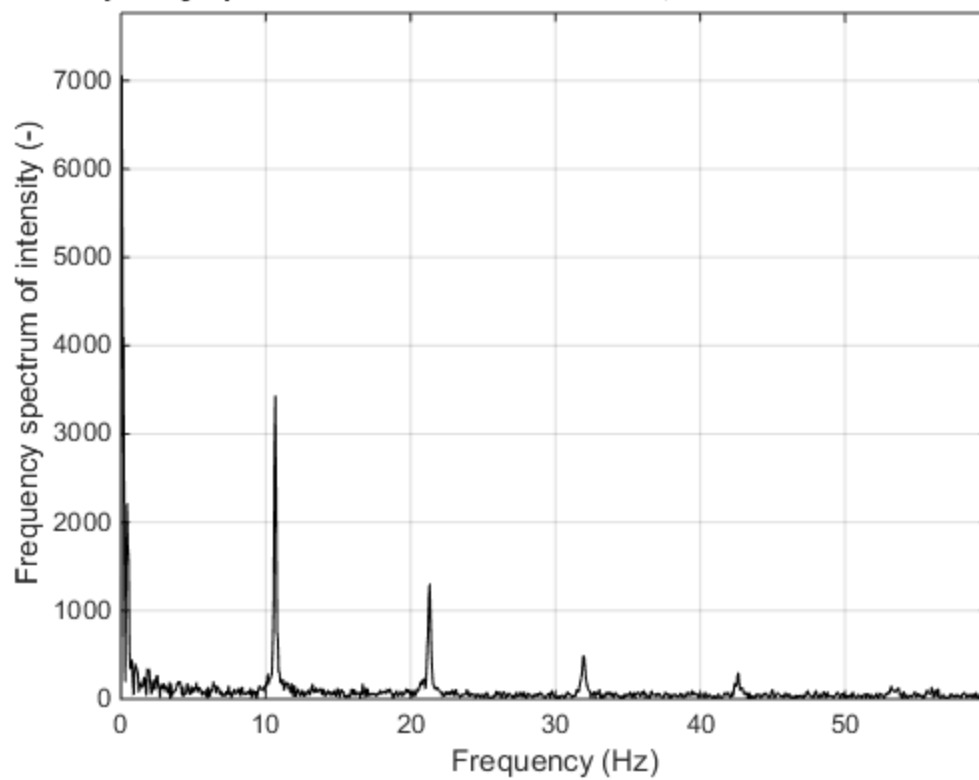


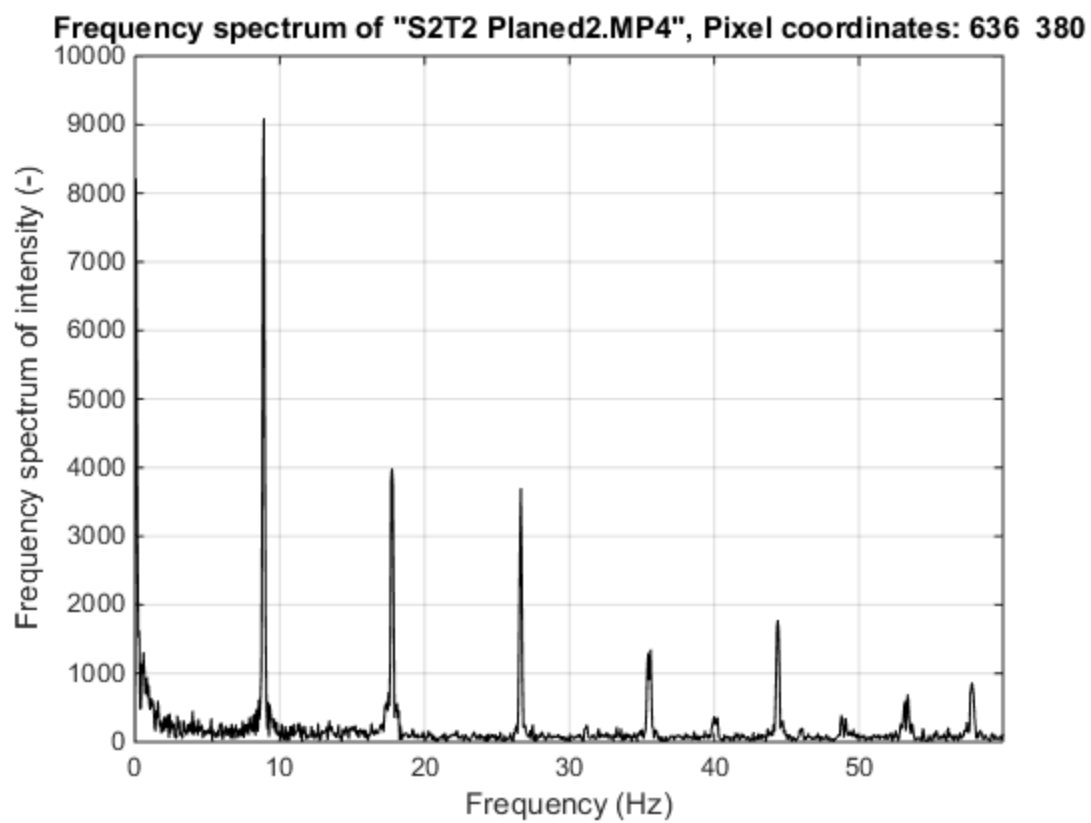
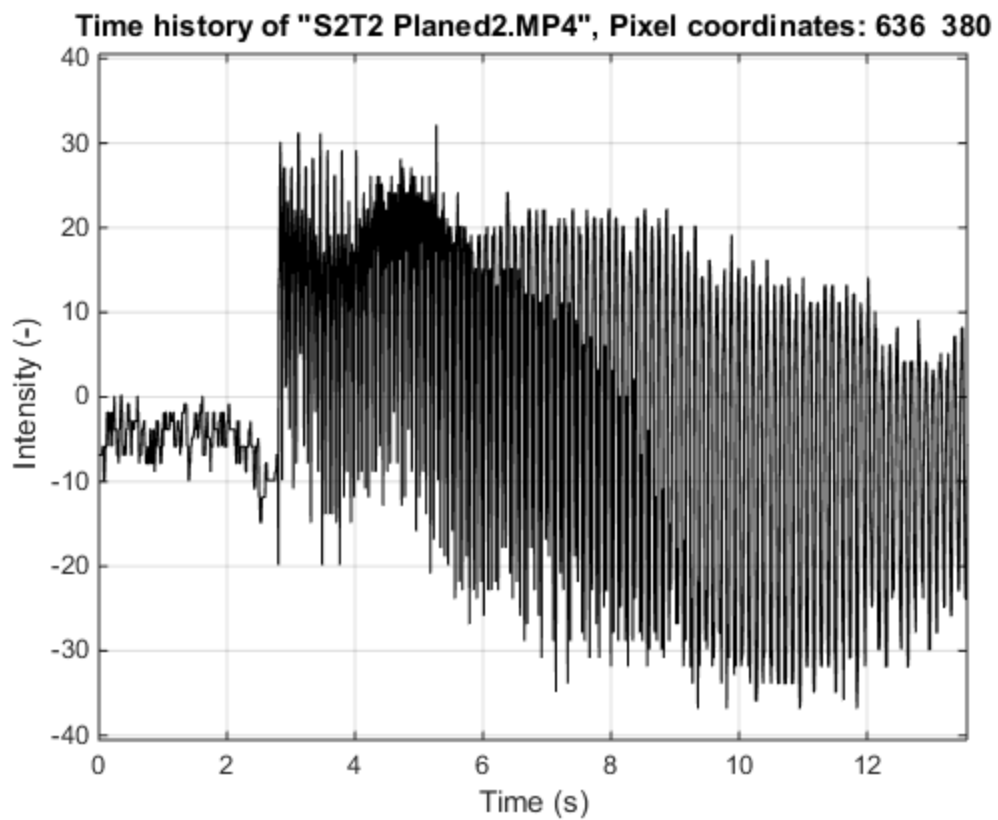


Time history of "S2T2 Planed.MP4", Pixel coordinates: 548 400

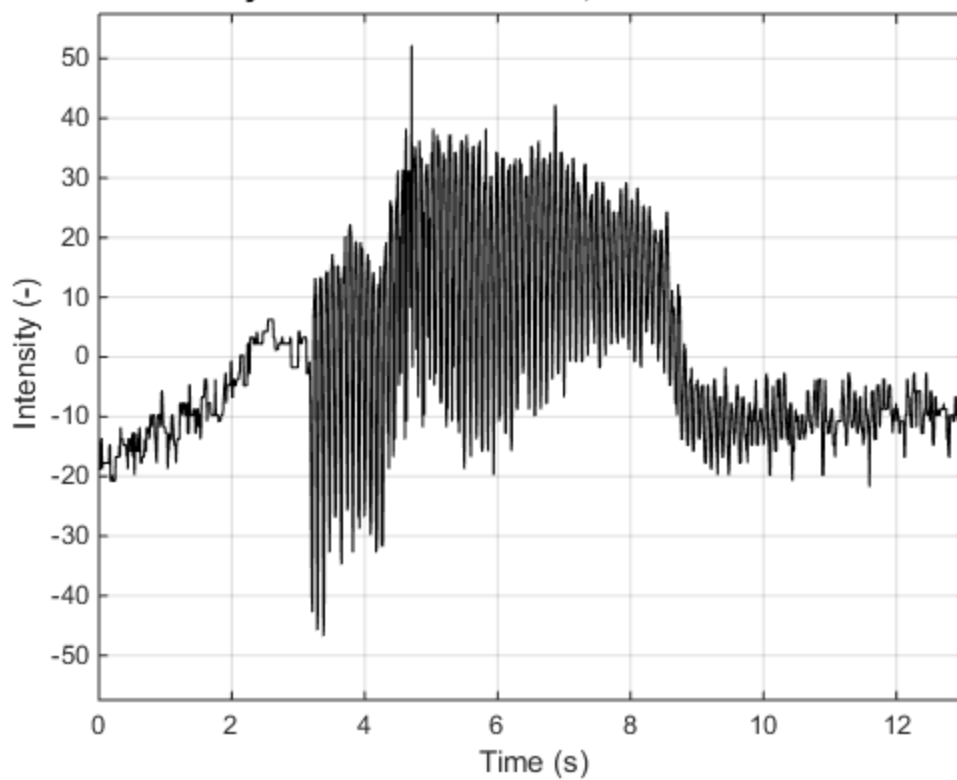


Frequency spectrum of "S2T2 Planed.MP4", Pixel coordinates: 548 400

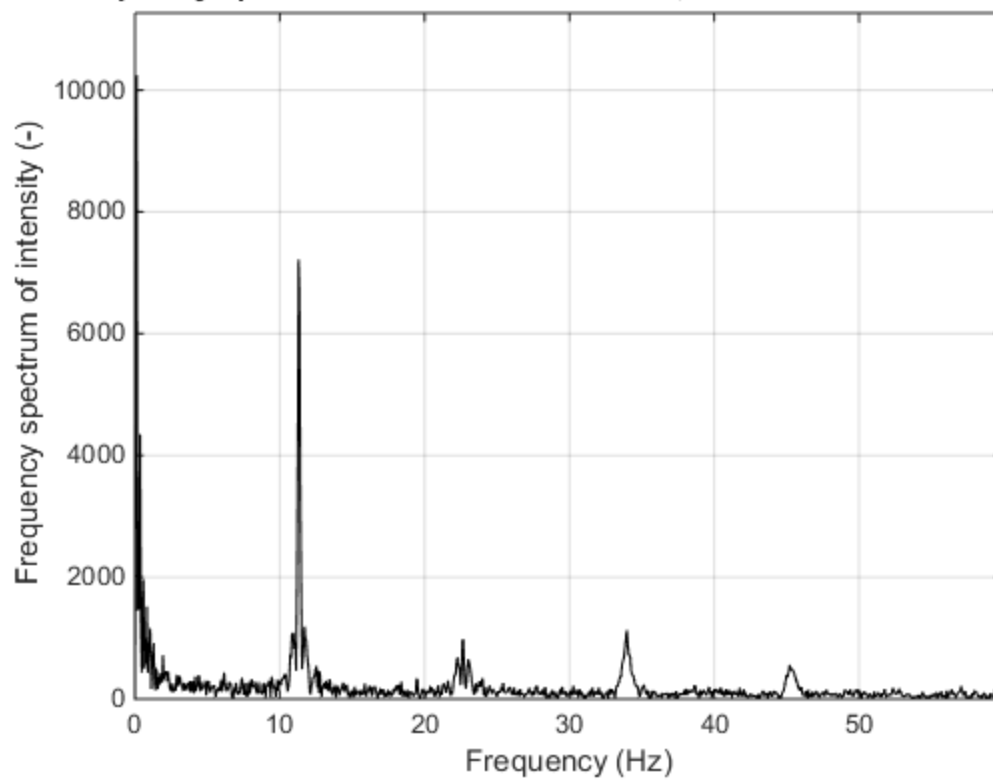




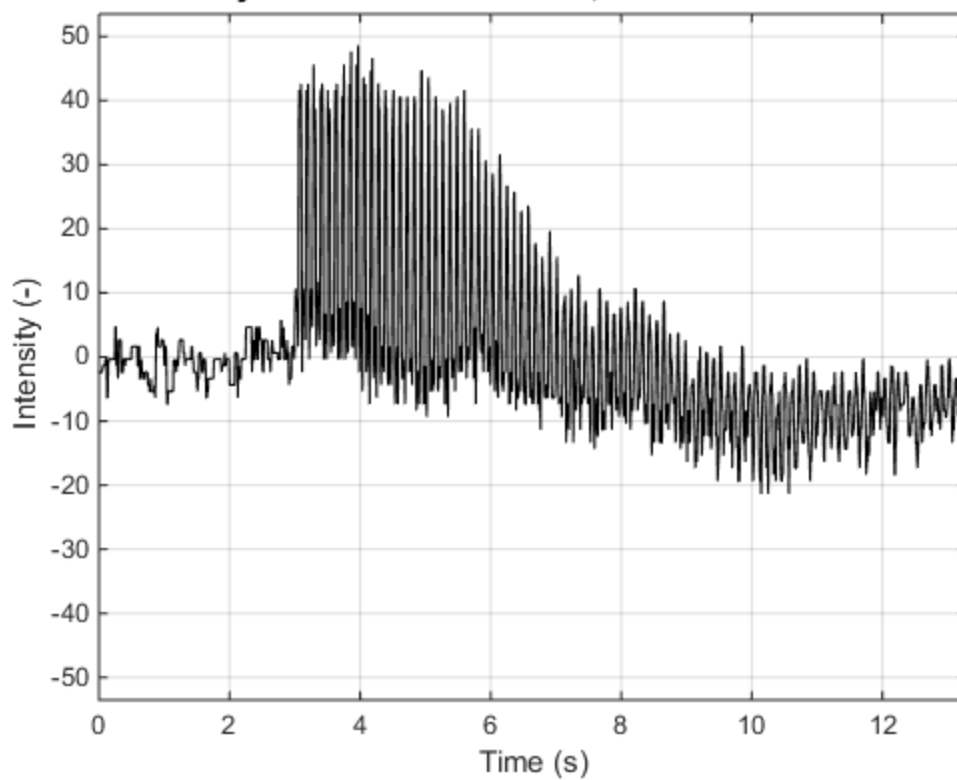
Time history of "S3T1 Planed.MP4", Pixel coordinates: 788 370



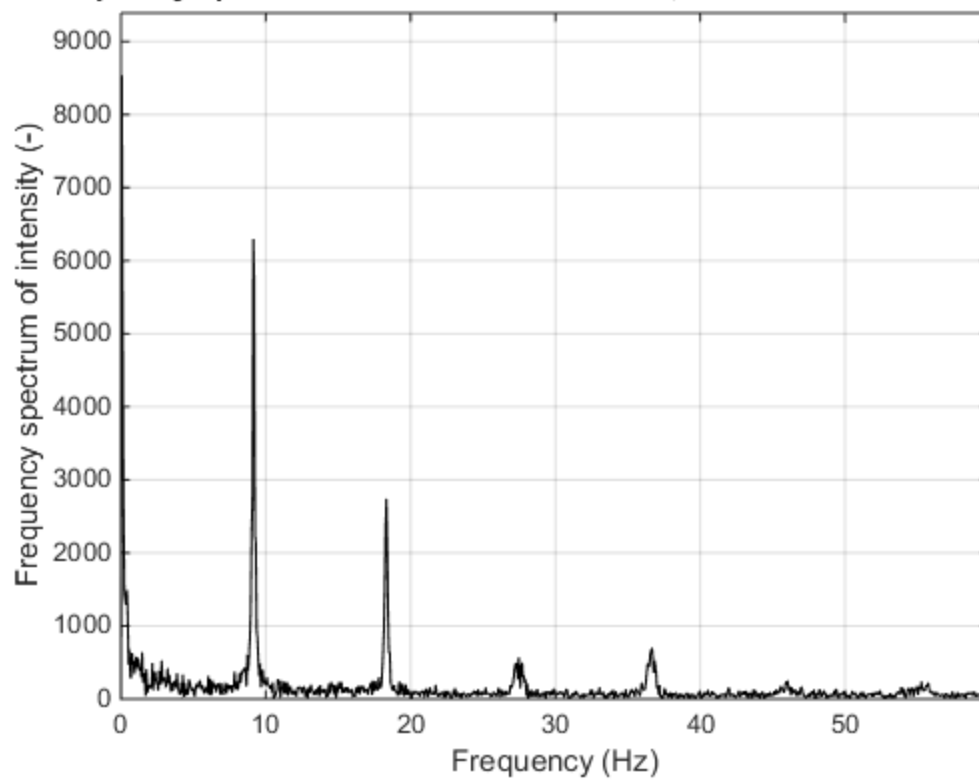
Frequency spectrum of "S3T1 Planed.MP4", Pixel coordinates: 788 370



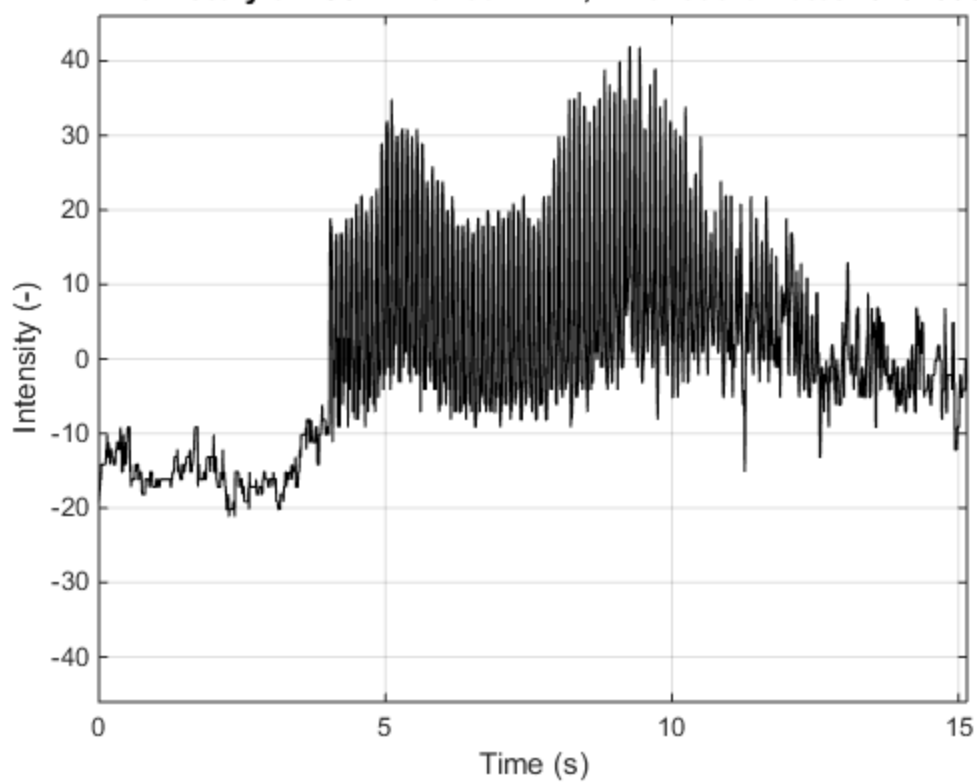
Time history of "S3T1 Planed2.MP4", Pixel coordinates: 765 412



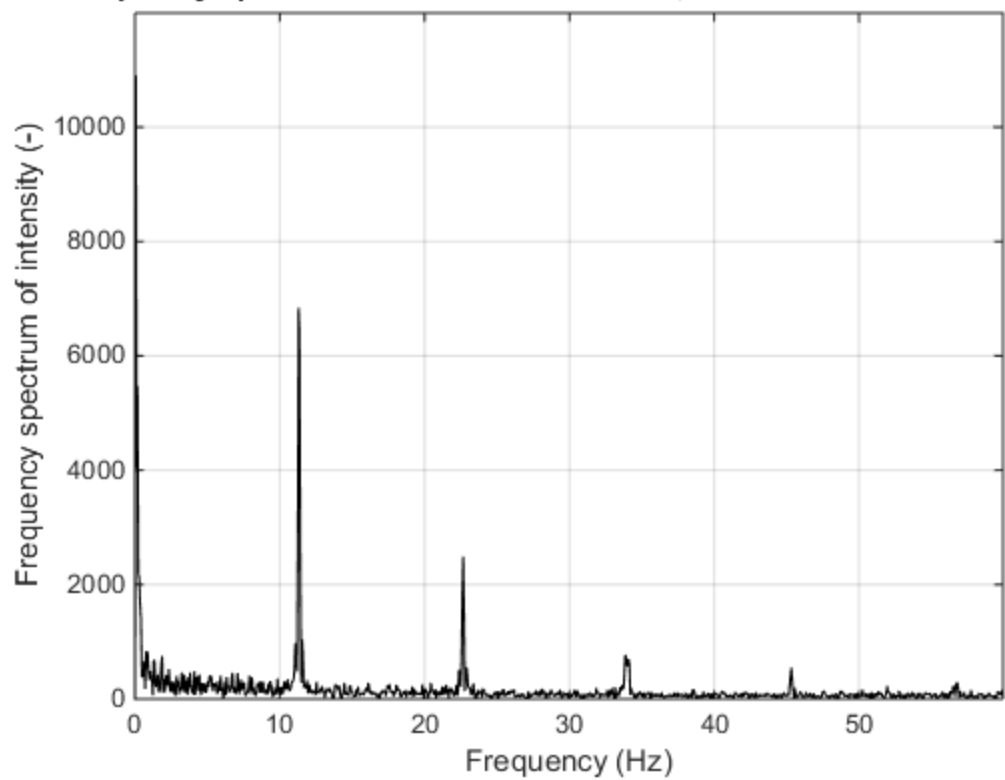
Frequency spectrum of "S3T1 Planed2.MP4", Pixel coordinates: 765 412



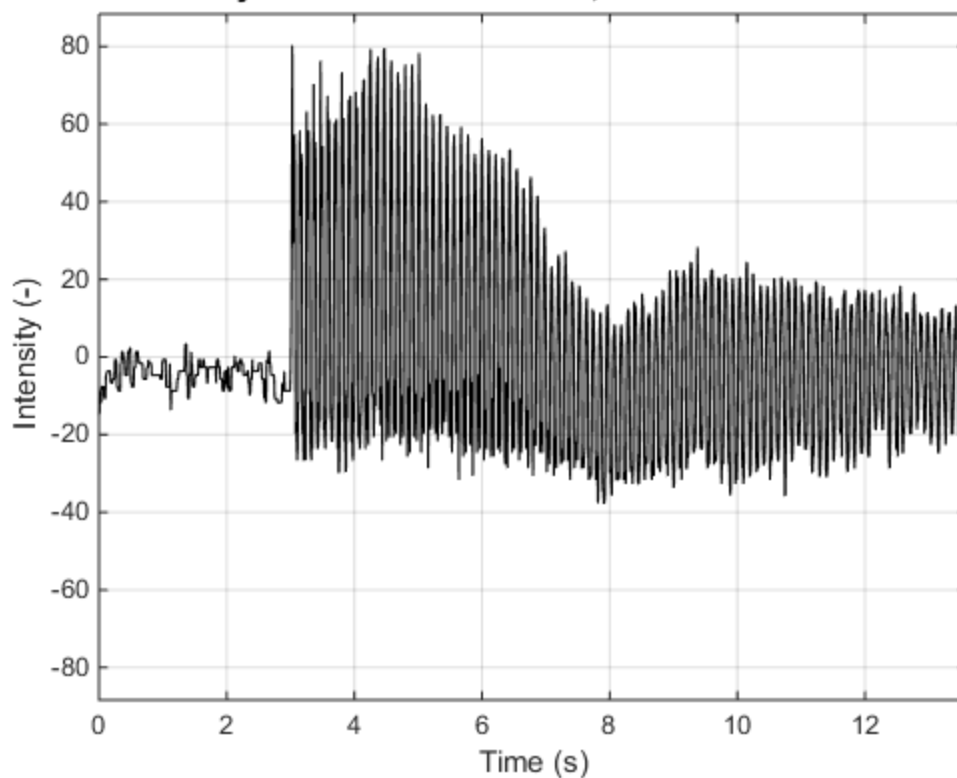
Time history of "S3T2 Planed.MP4", Pixel coordinates: 813 360



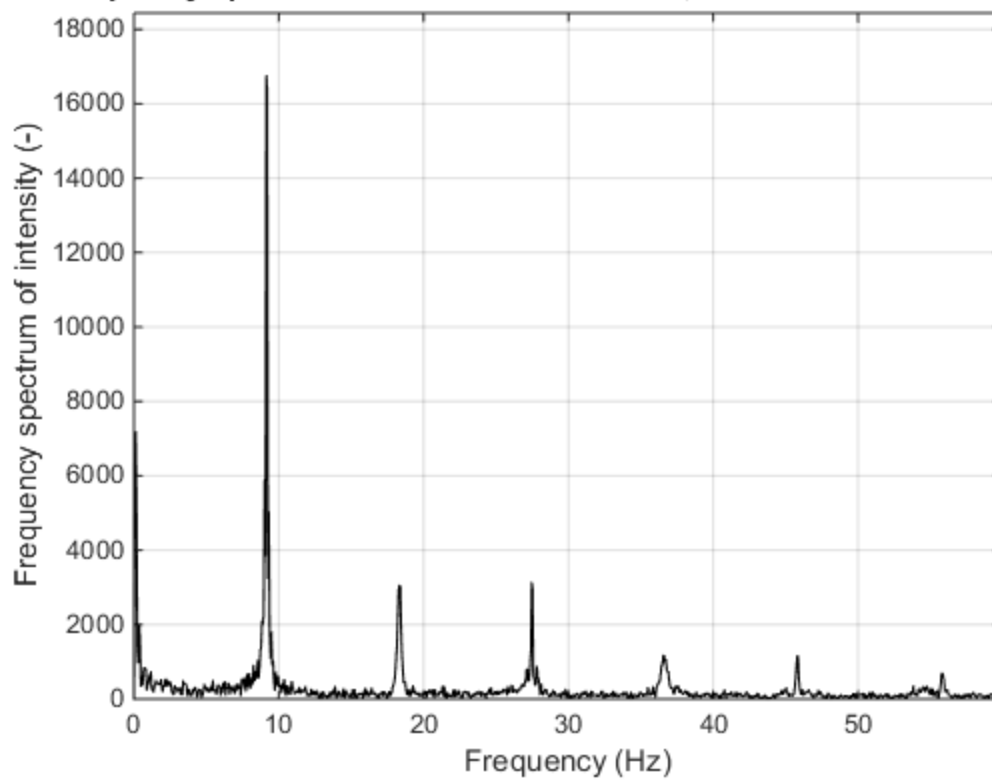
Frequency spectrum of "S3T2 Planed.MP4", Pixel coordinates: 813 360

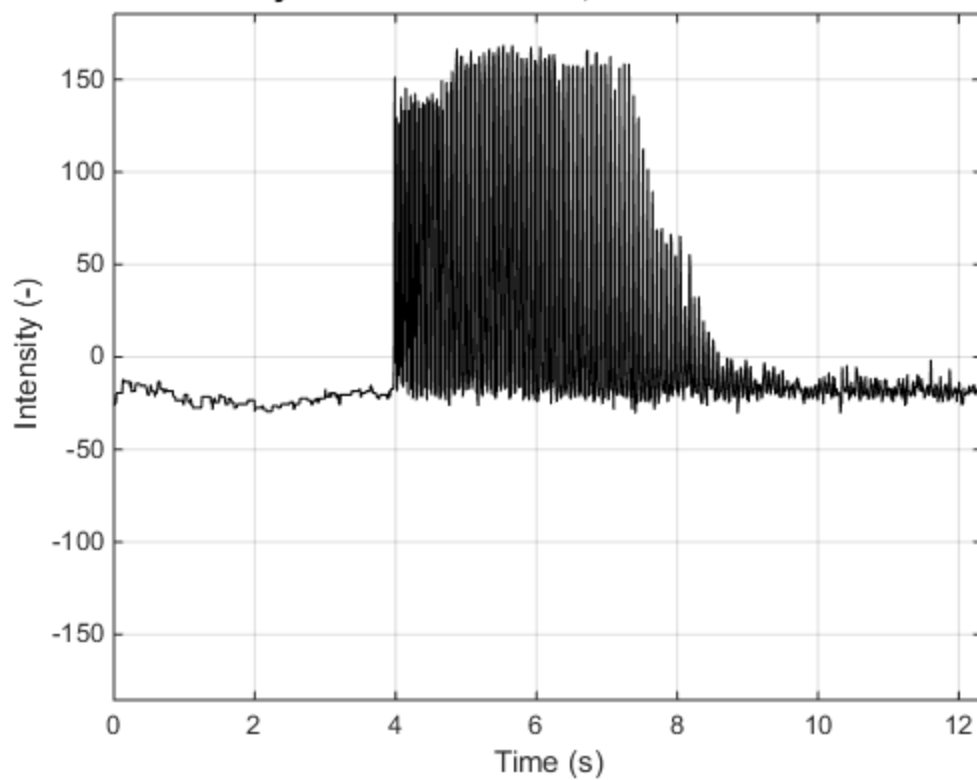
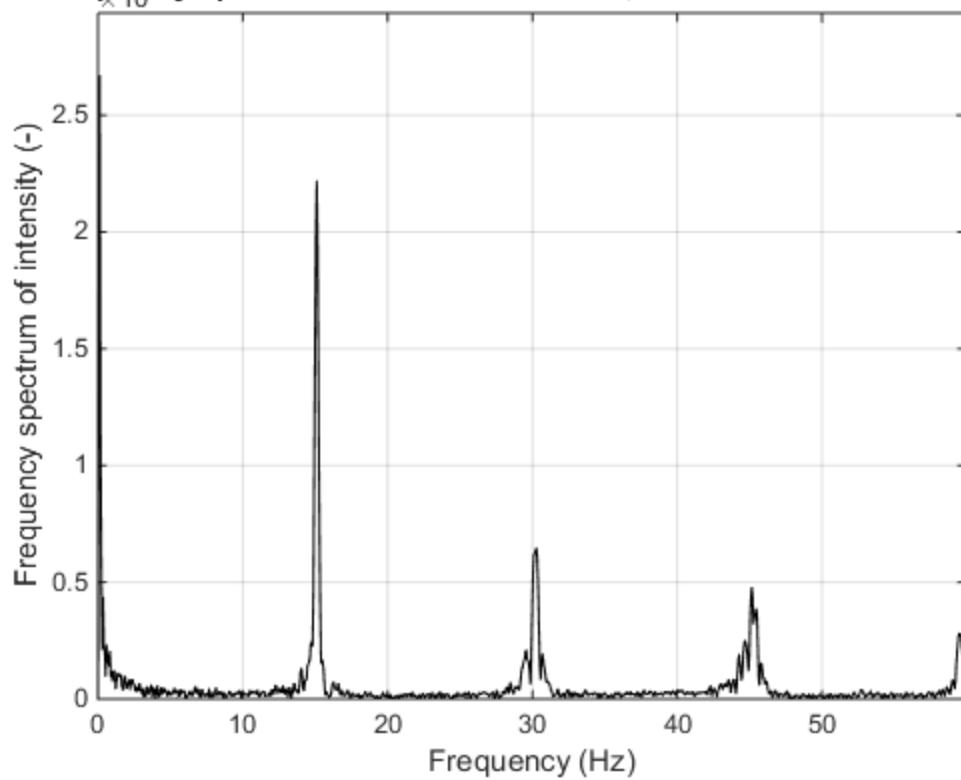


Time history of "S3T2 Planed2.MP4", Pixel coordinates: 604 417

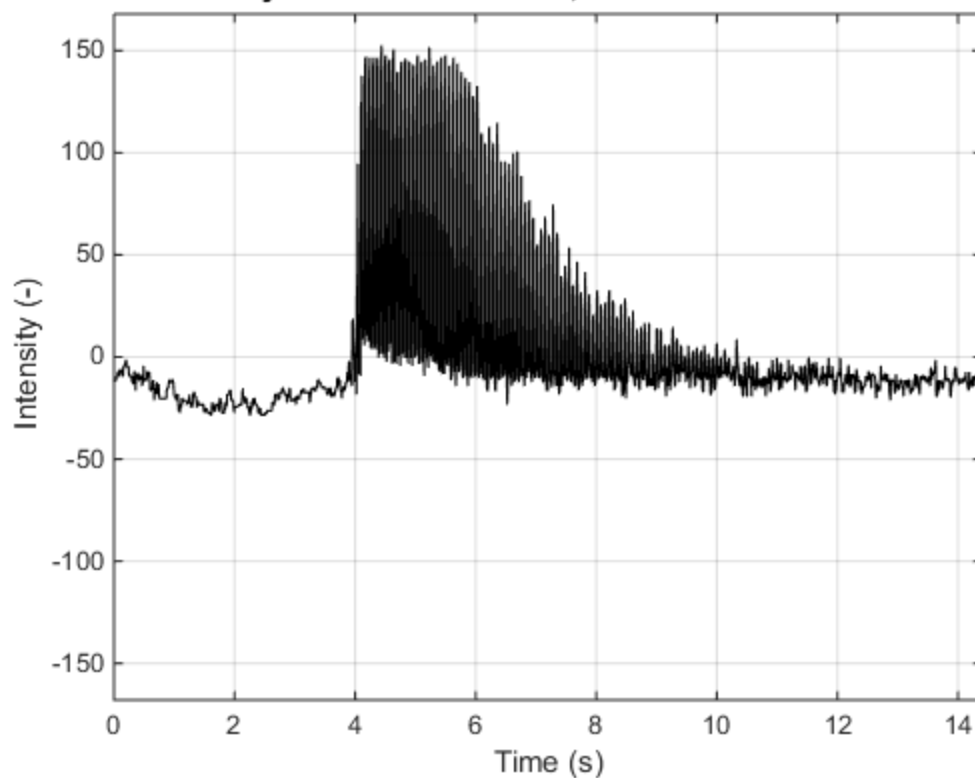


Frequency spectrum of "S3T2 Planed2.MP4", Pixel coordinates: 604 417

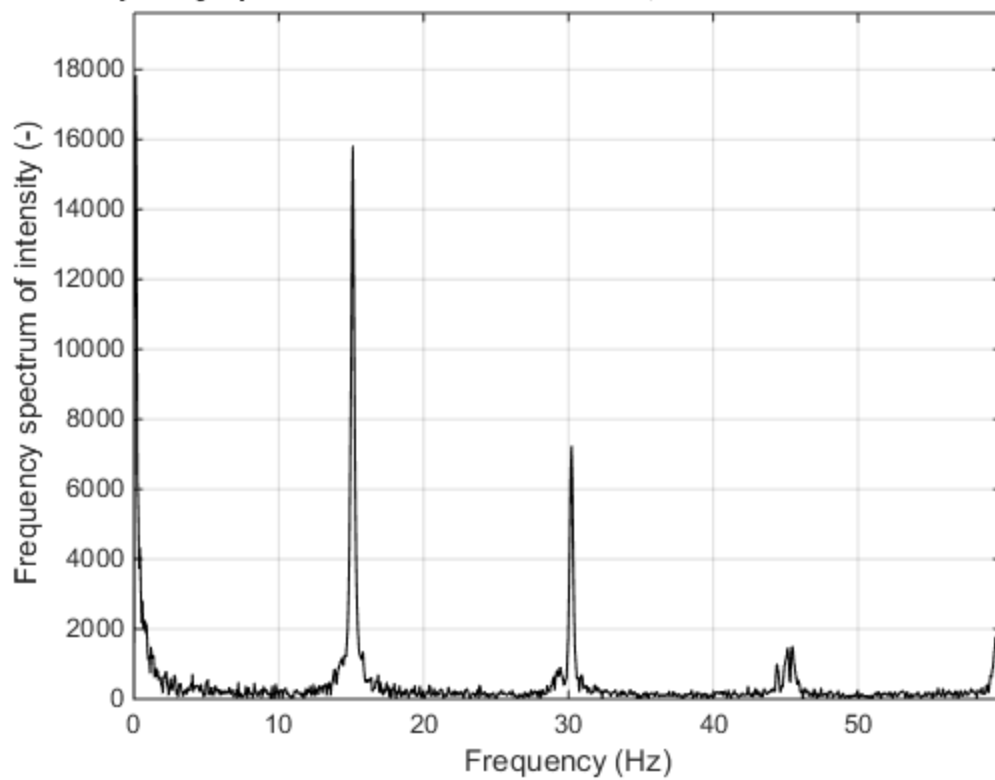


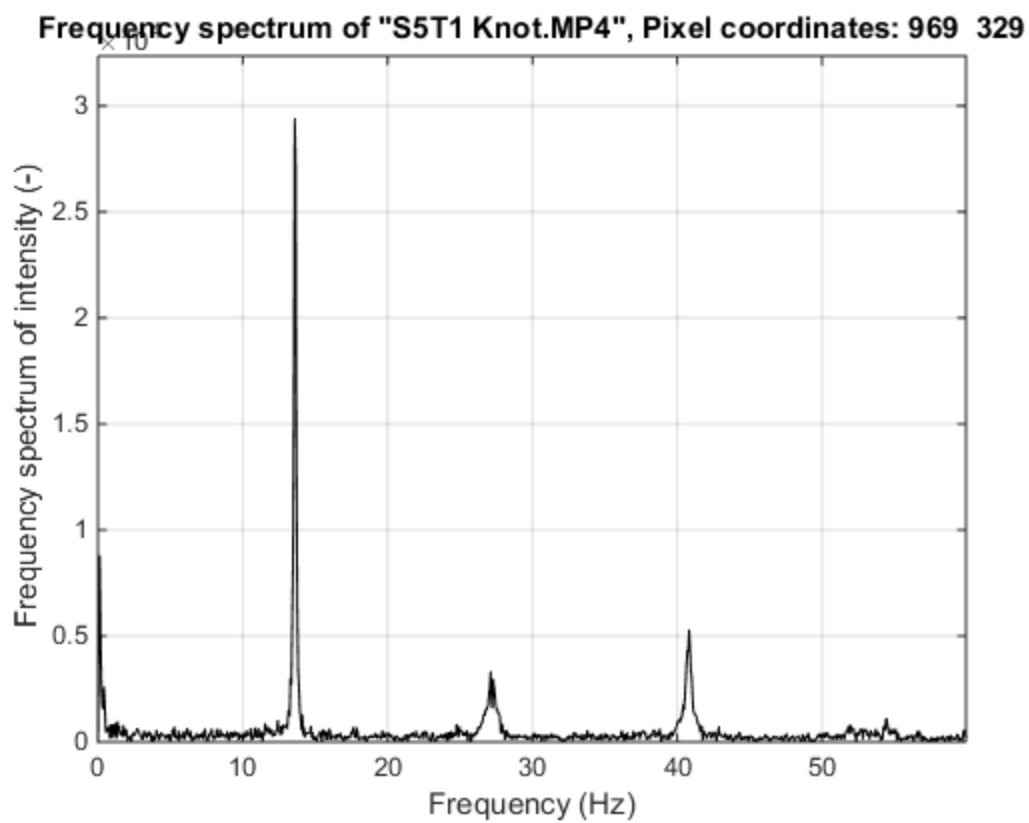
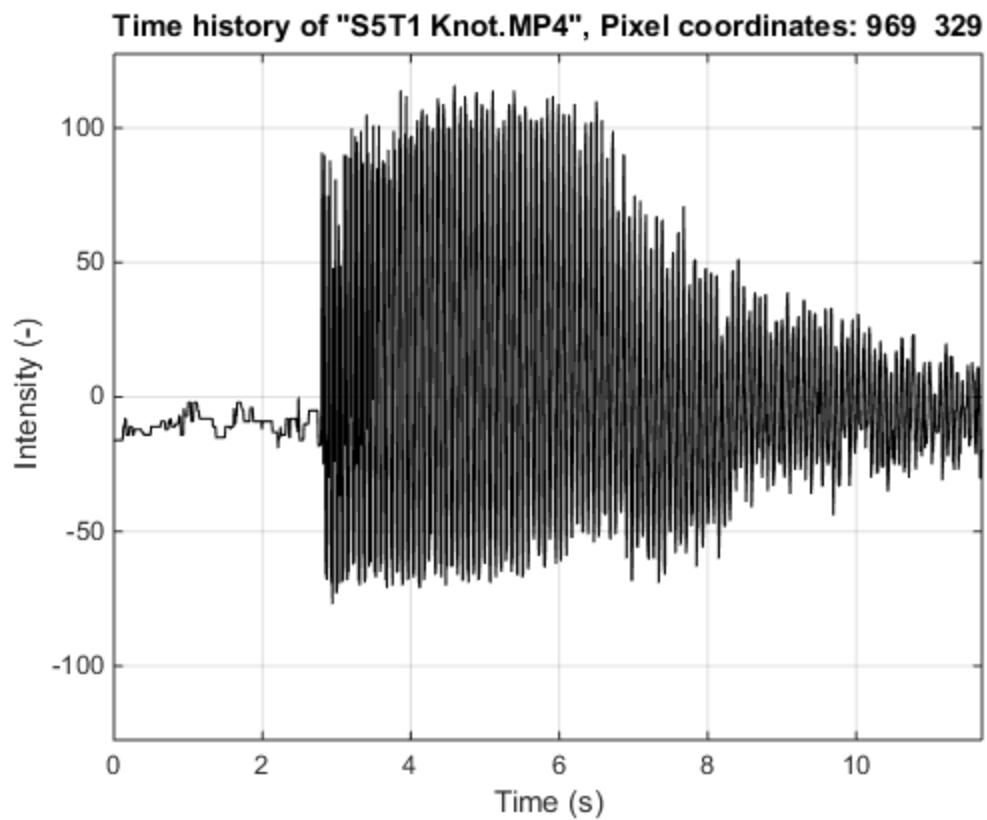
Time history of "S4T1 Knot.MP4", Pixel coordinates: 639 325**Frequency spectrum of "S4T1 Knot.MP4", Pixel coordinates: 639 325**

Time history of "S4T2 Knot.MP4", Pixel coordinates: 1120 306

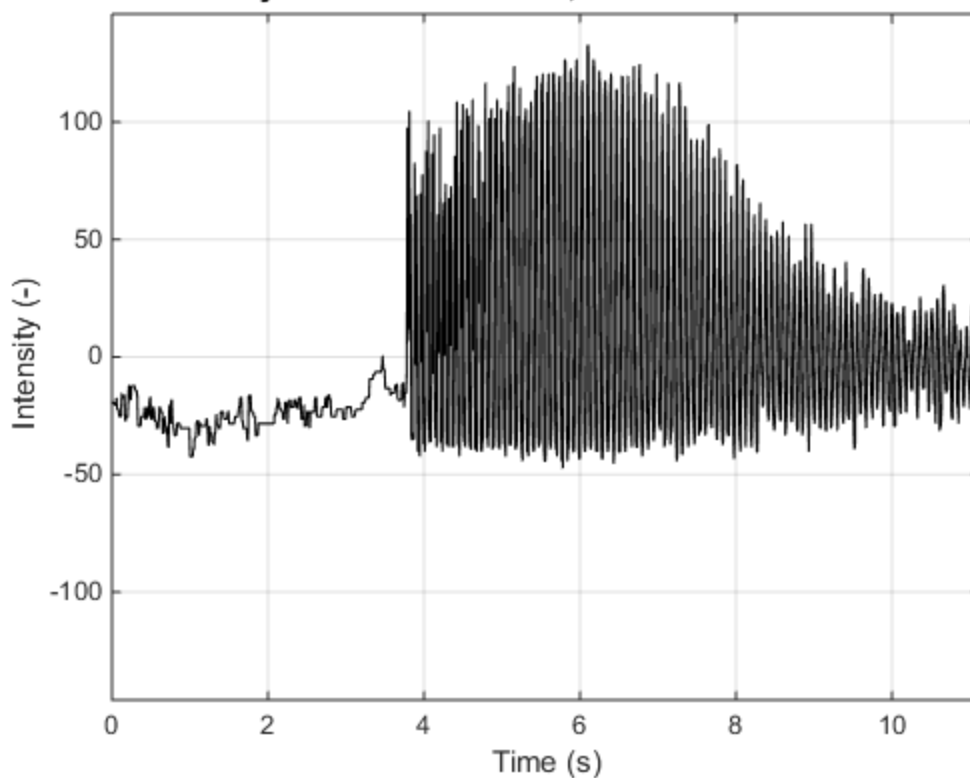


Frequency spectrum of "S4T2 Knot.MP4", Pixel coordinates: 1120 306

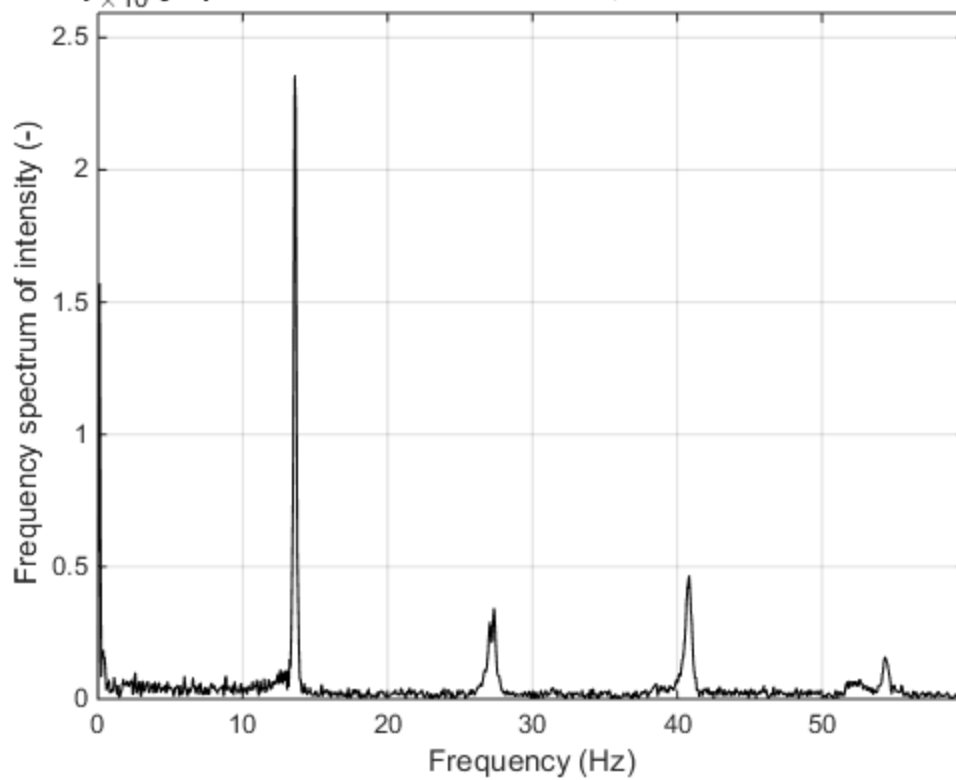


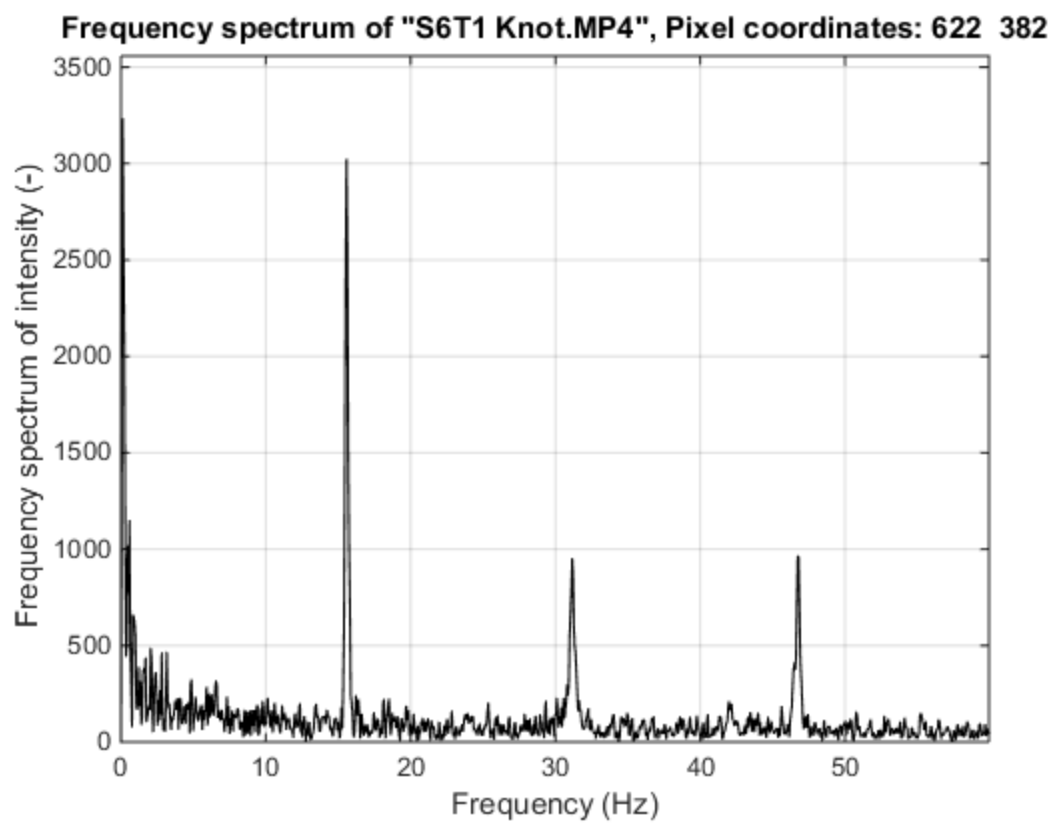
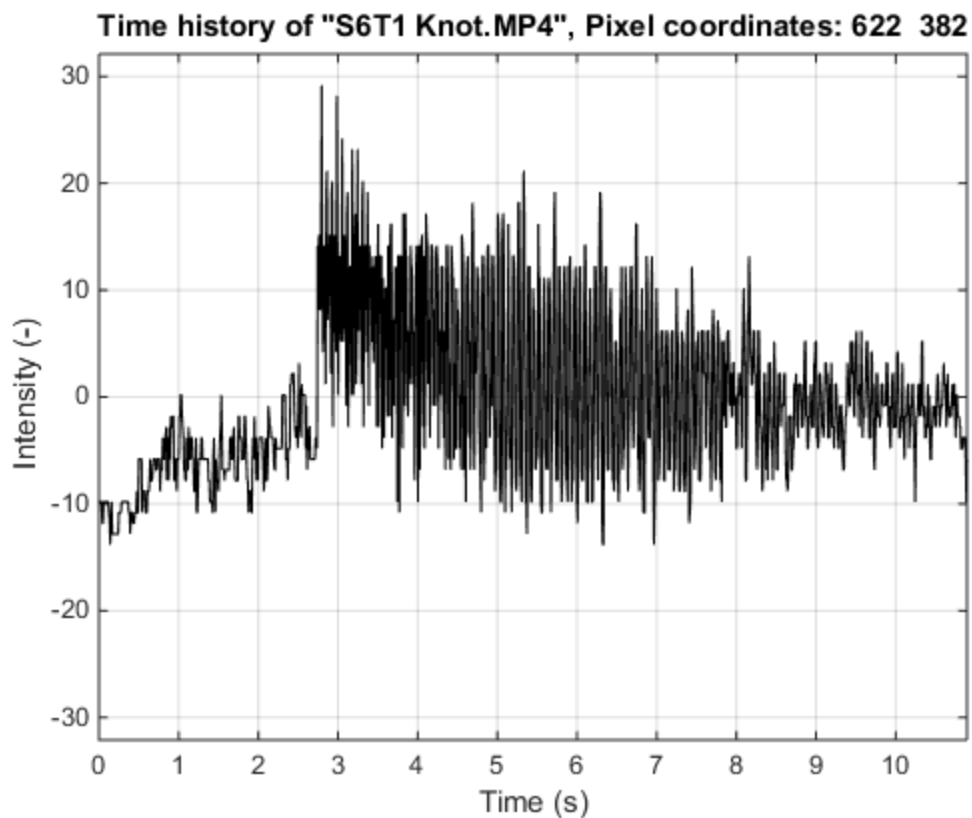


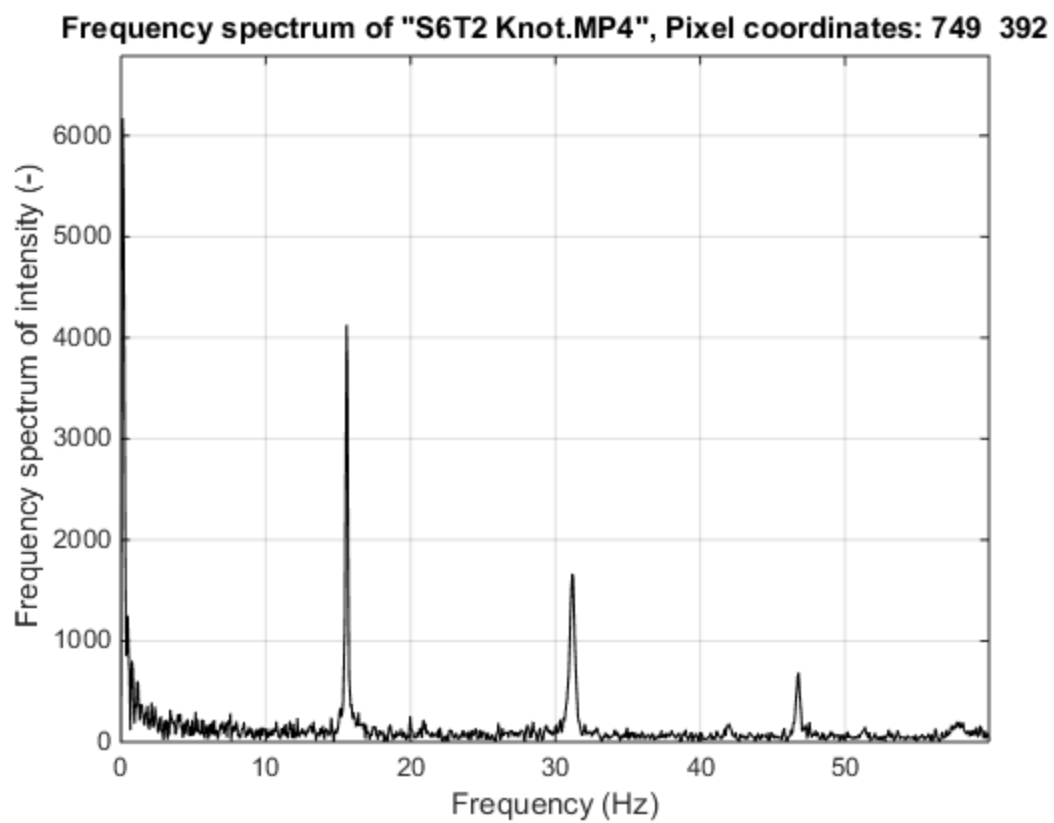
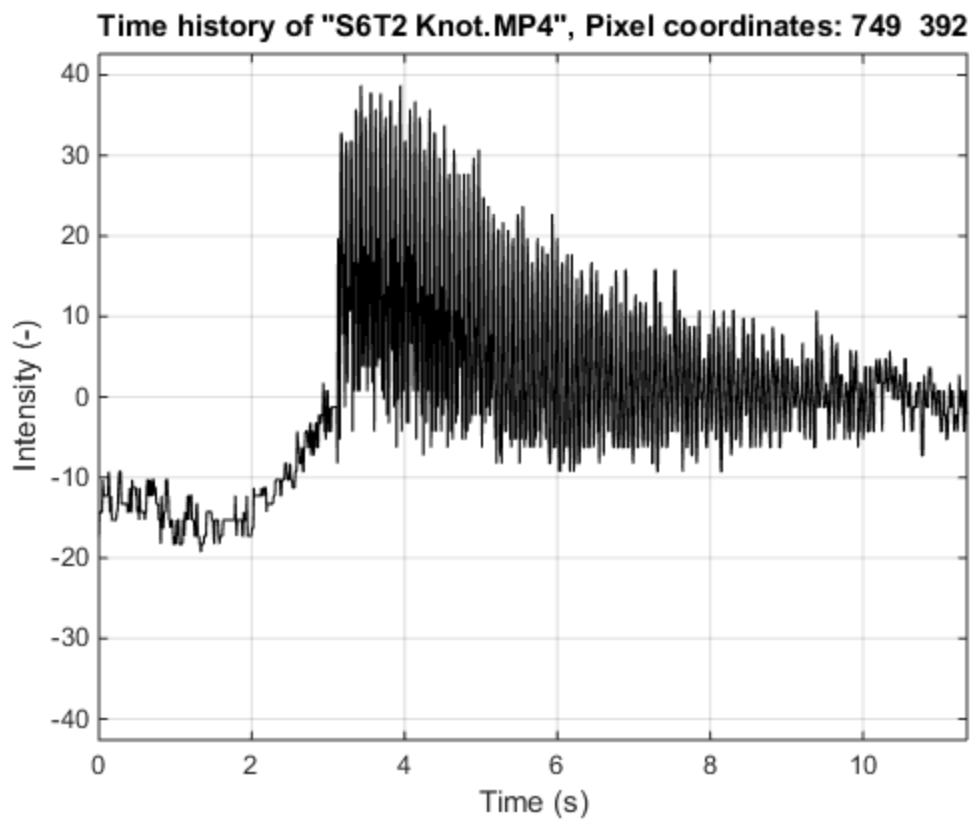
Time history of "S5T2 Knot.MP4", Pixel coordinates: 1021 318



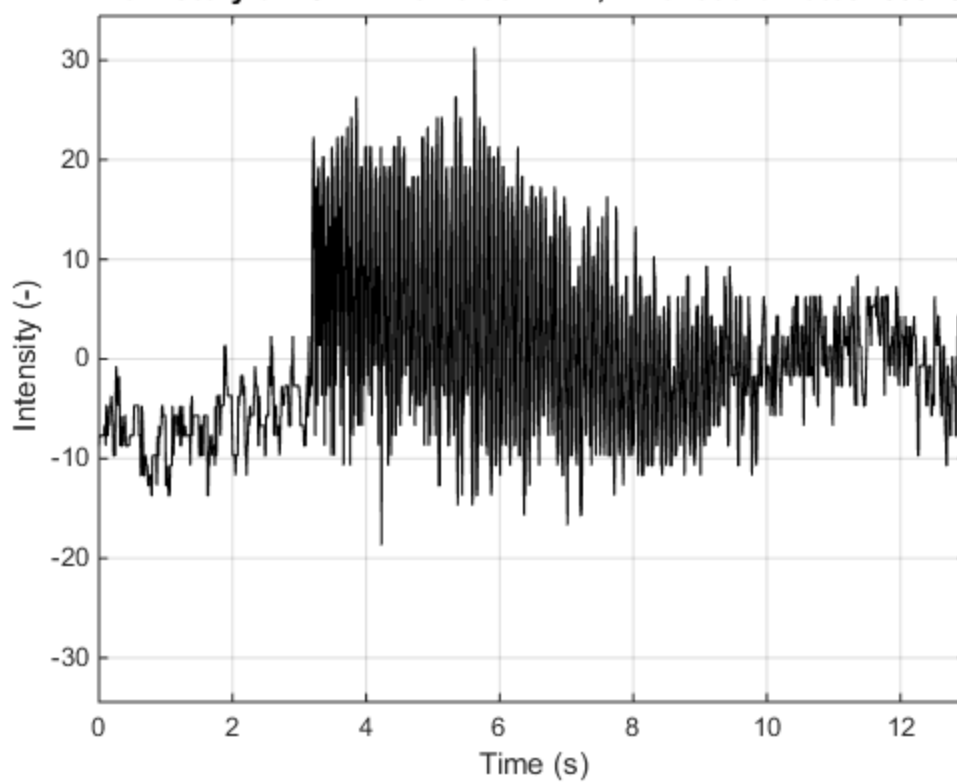
Frequency spectrum of "S5T2 Knot.MP4", Pixel coordinates: 1021 318



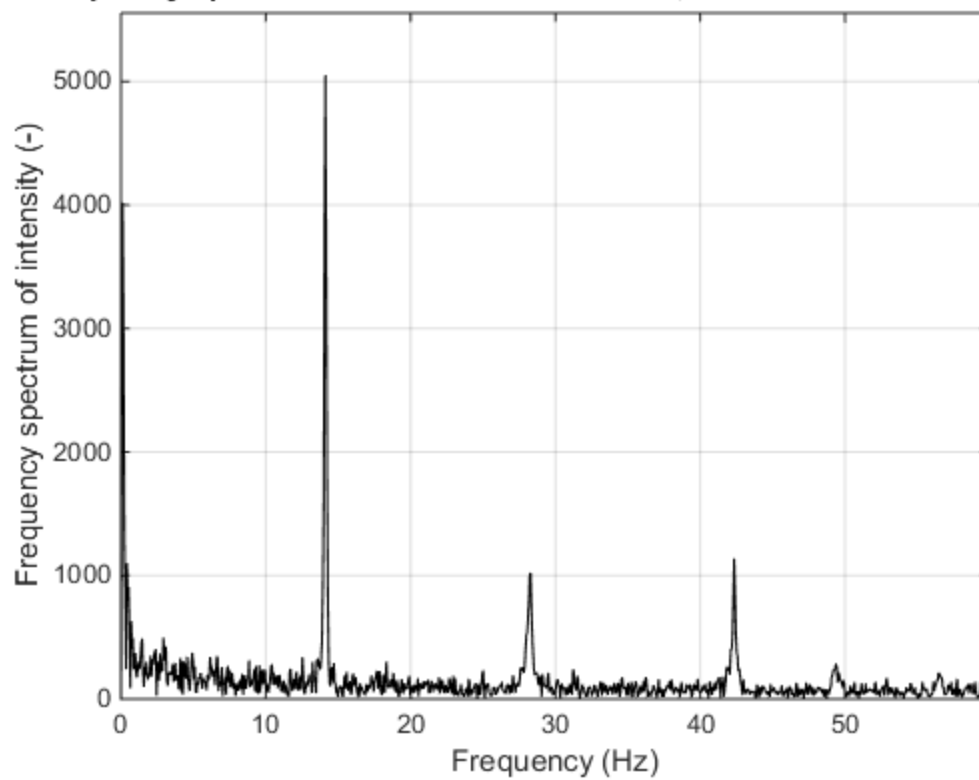




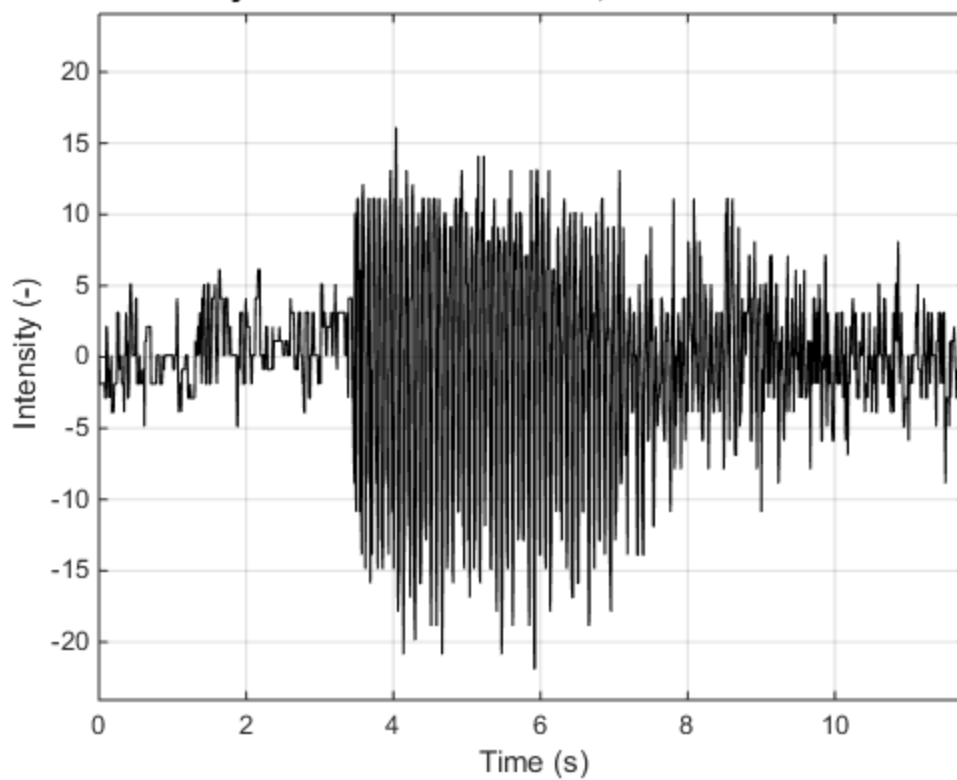
Time history of "S7T1 1ft Holes.MP4", Pixel coordinates: 500 359



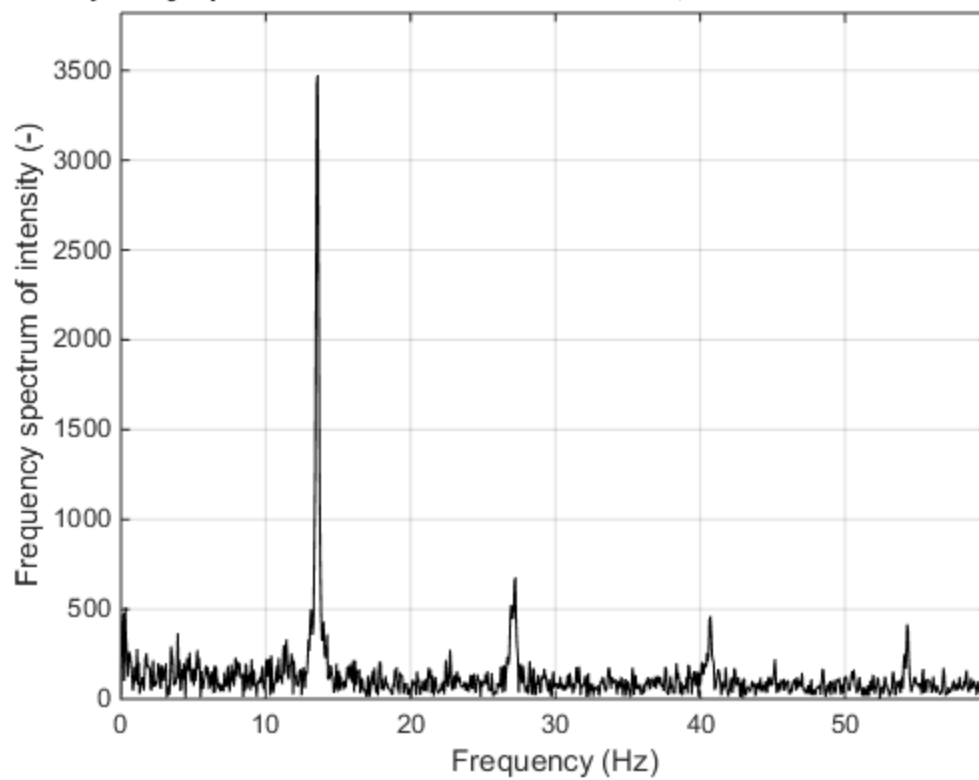
Frequency spectrum of "S7T1 1ft Holes.MP4", Pixel coordinates: 500 359



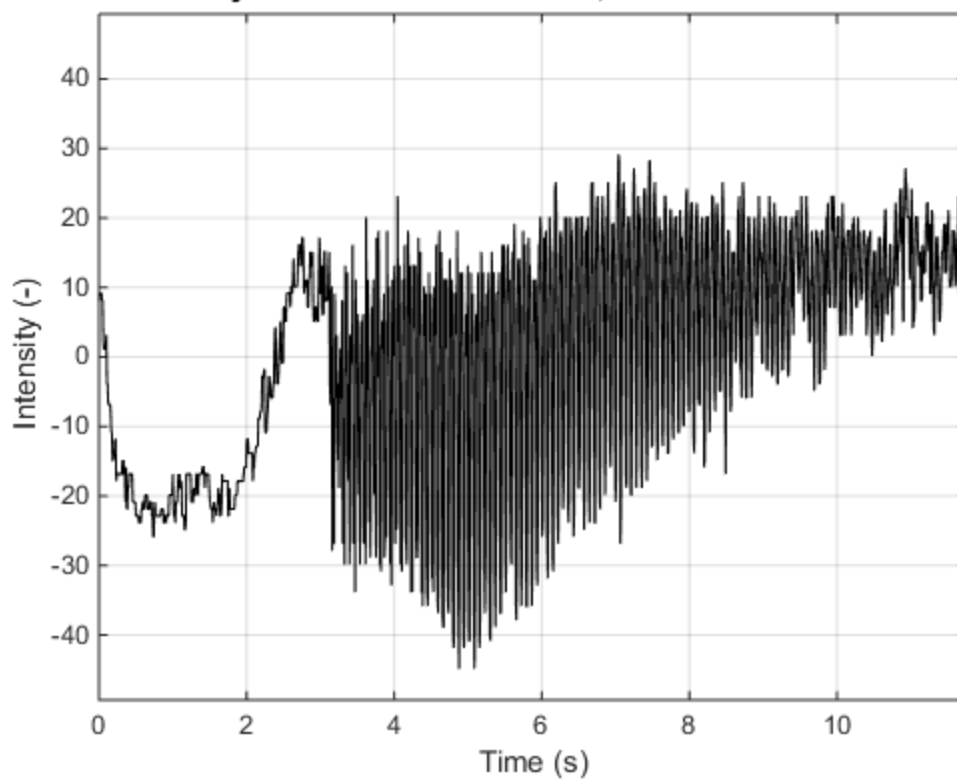
Time history of "S7T1 2ft Holes.MP4", Pixel coordinates: 461 340



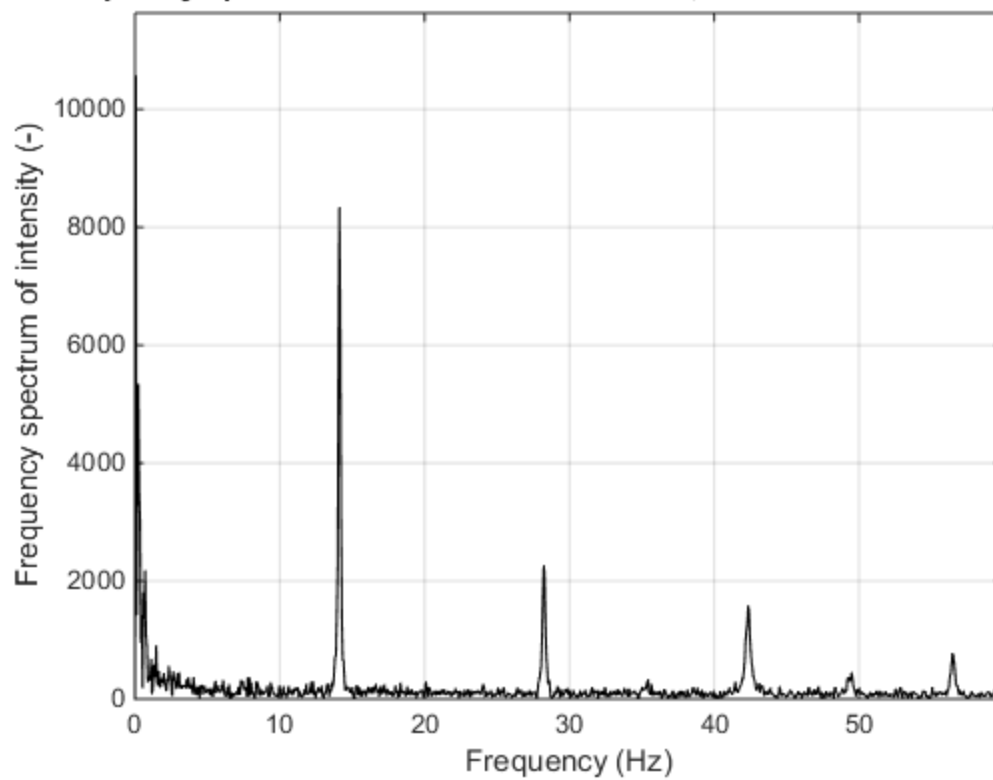
Frequency spectrum of "S7T1 2ft Holes.MP4", Pixel coordinates: 461 340



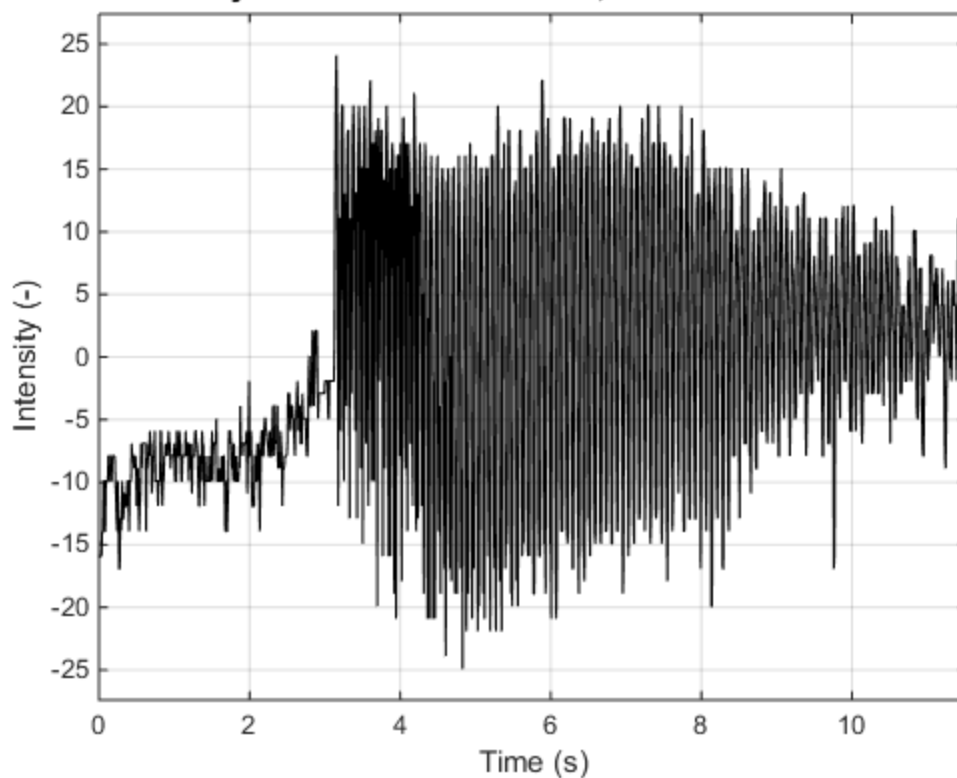
Time history of "S7T2 1ft Holes.MP4", Pixel coordinates: 680 282



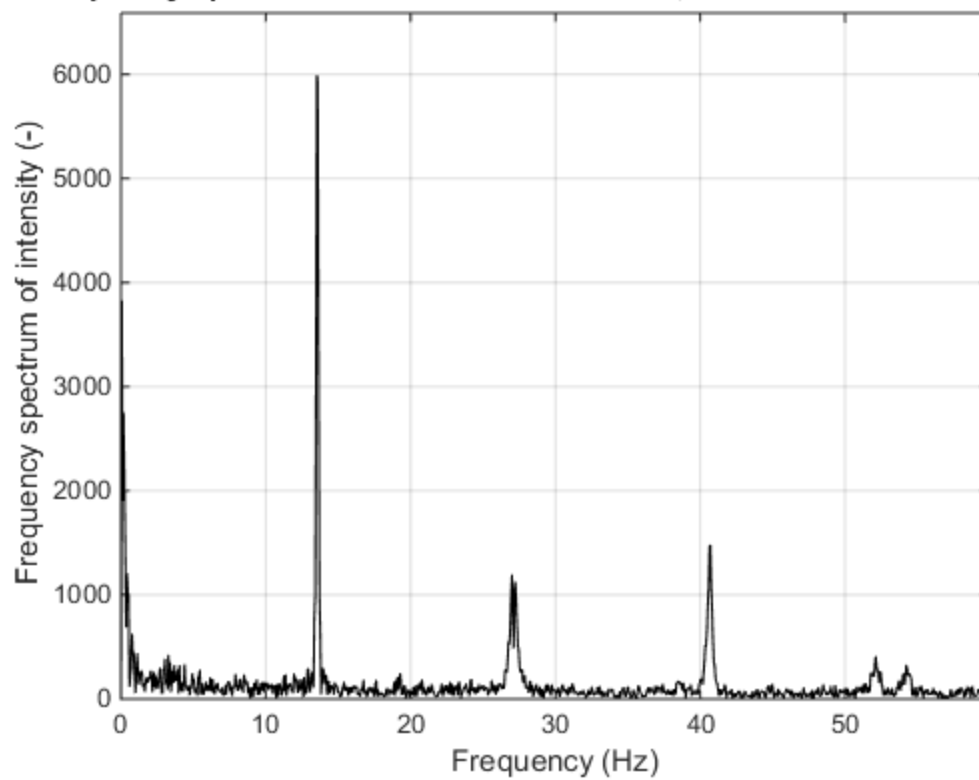
Frequency spectrum of "S7T2 1ft Holes.MP4", Pixel coordinates: 680 282



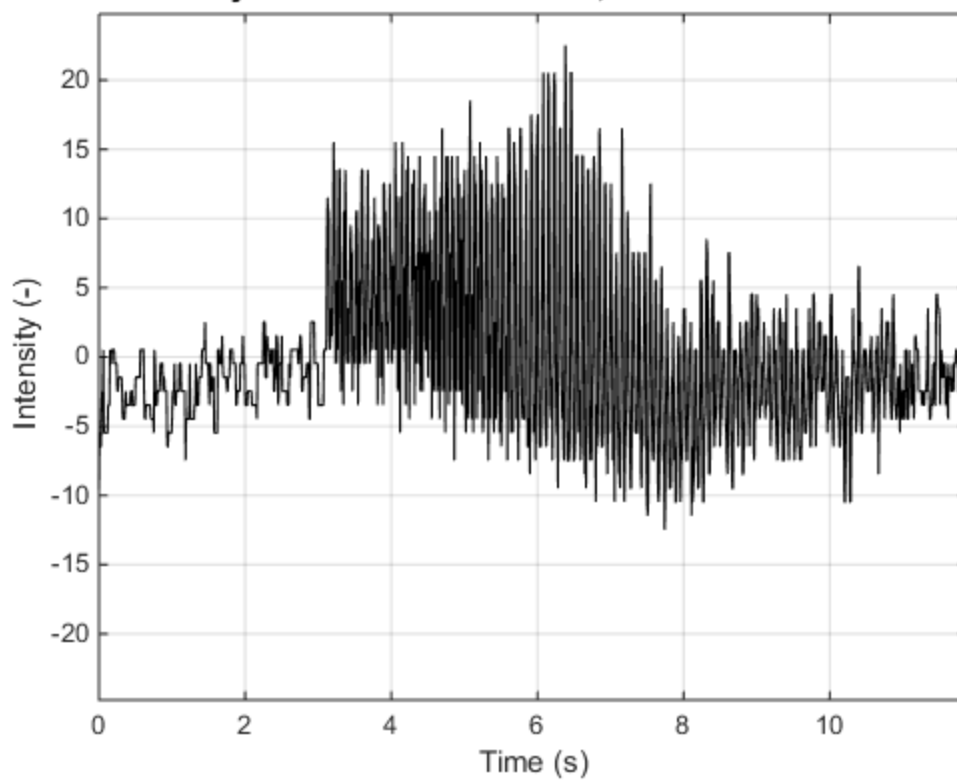
Time history of "S7T2 2ft Holes.MP4", Pixel coordinates: 482 352



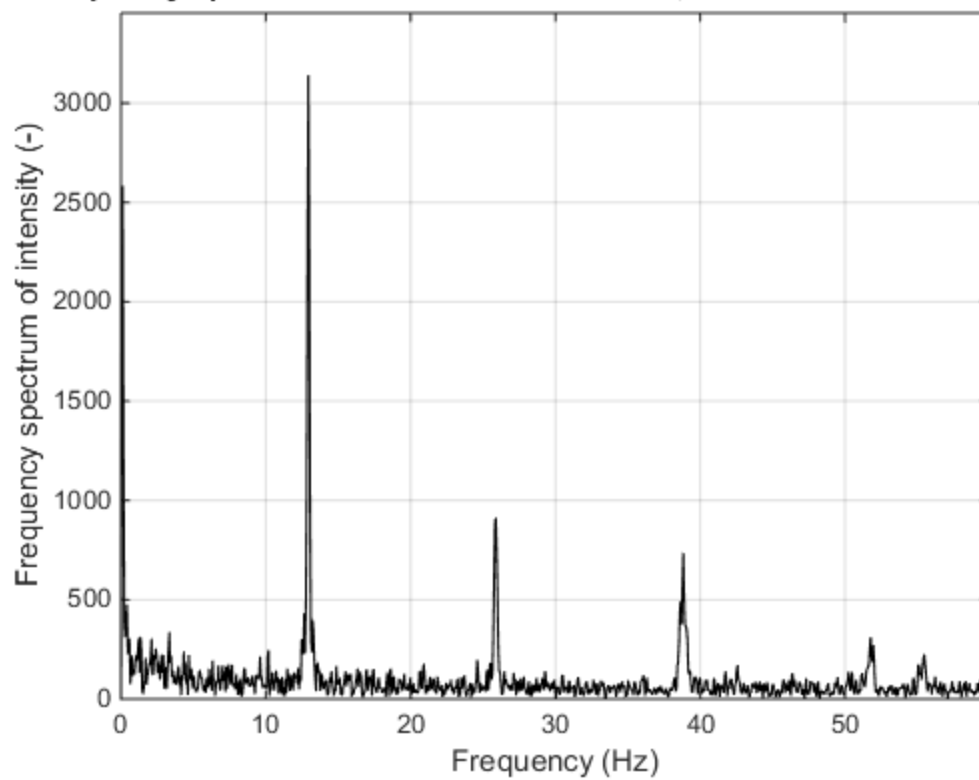
Frequency spectrum of "S7T2 2ft Holes.MP4", Pixel coordinates: 482 352



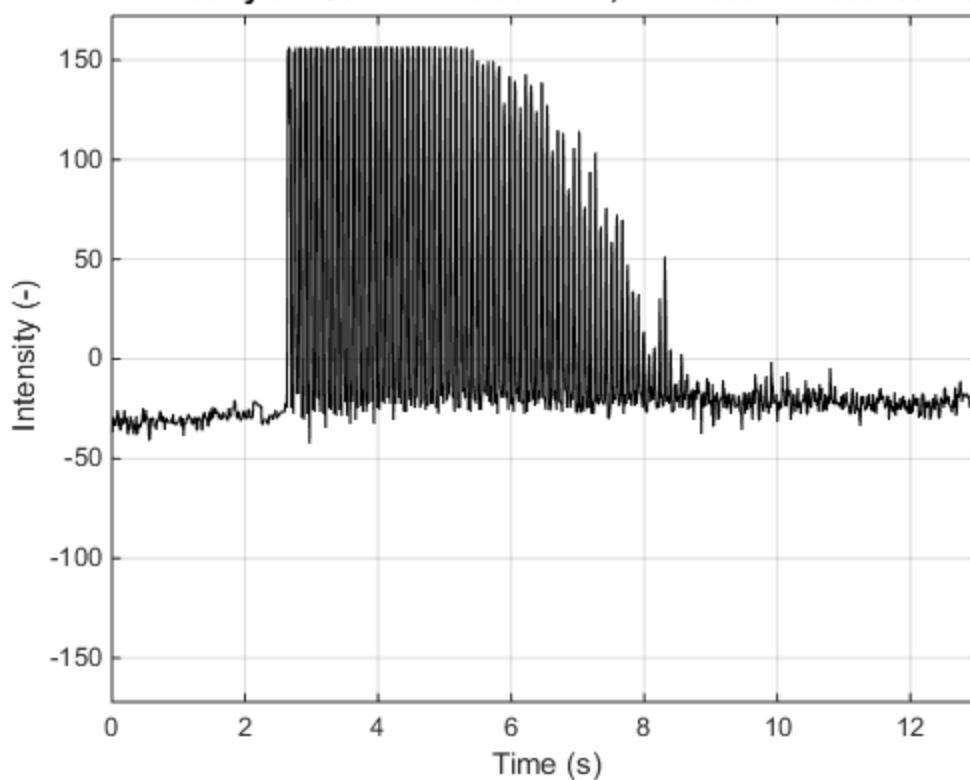
Time history of "S8T1 1ft Holes.MP4", Pixel coordinates: 482 352



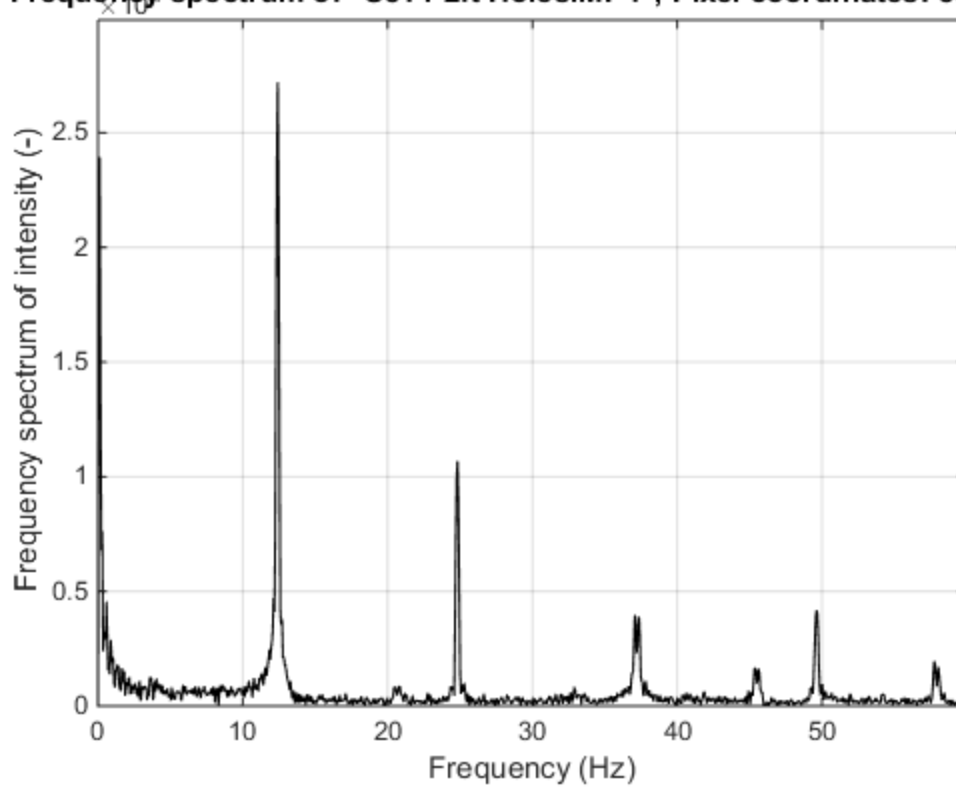
Frequency spectrum of "S8T1 1ft Holes.MP4", Pixel coordinates: 482 352



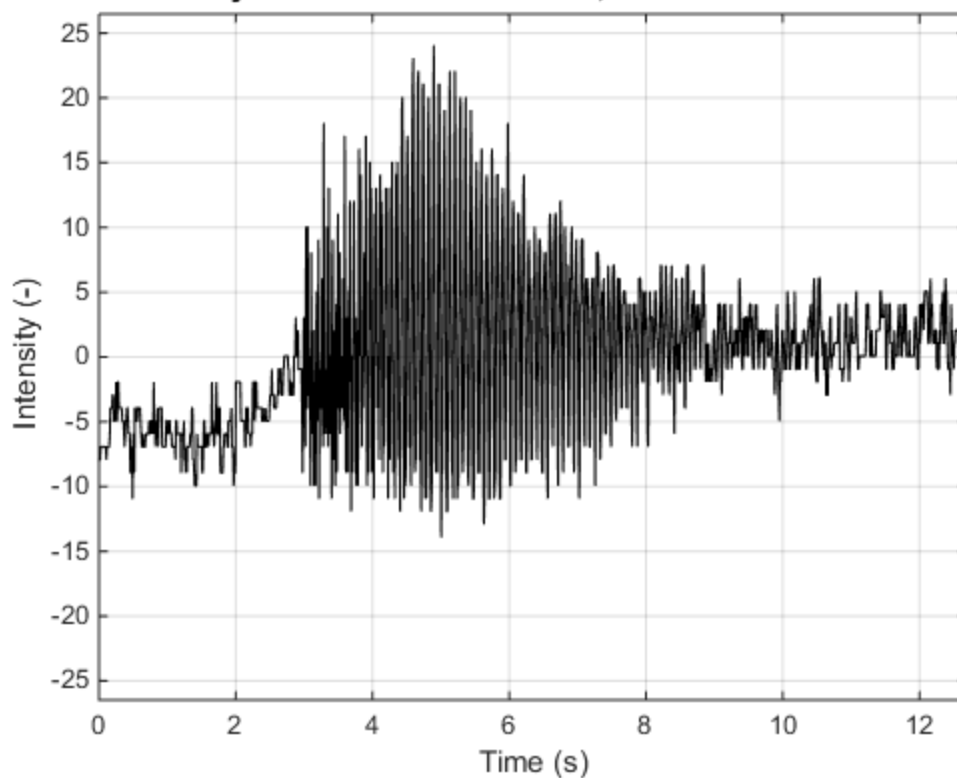
Time history of "S8T1 2ft Holes.MP4", Pixel coordinates: 804 314



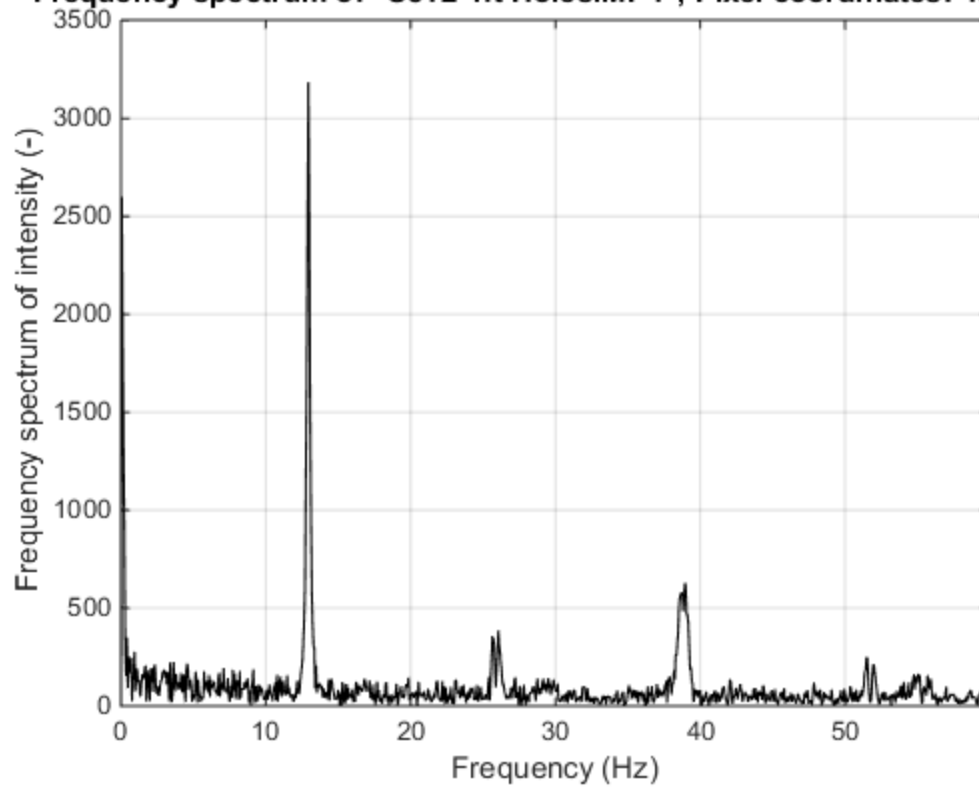
Frequency spectrum of "S8T1 2ft Holes.MP4", Pixel coordinates: 804 314



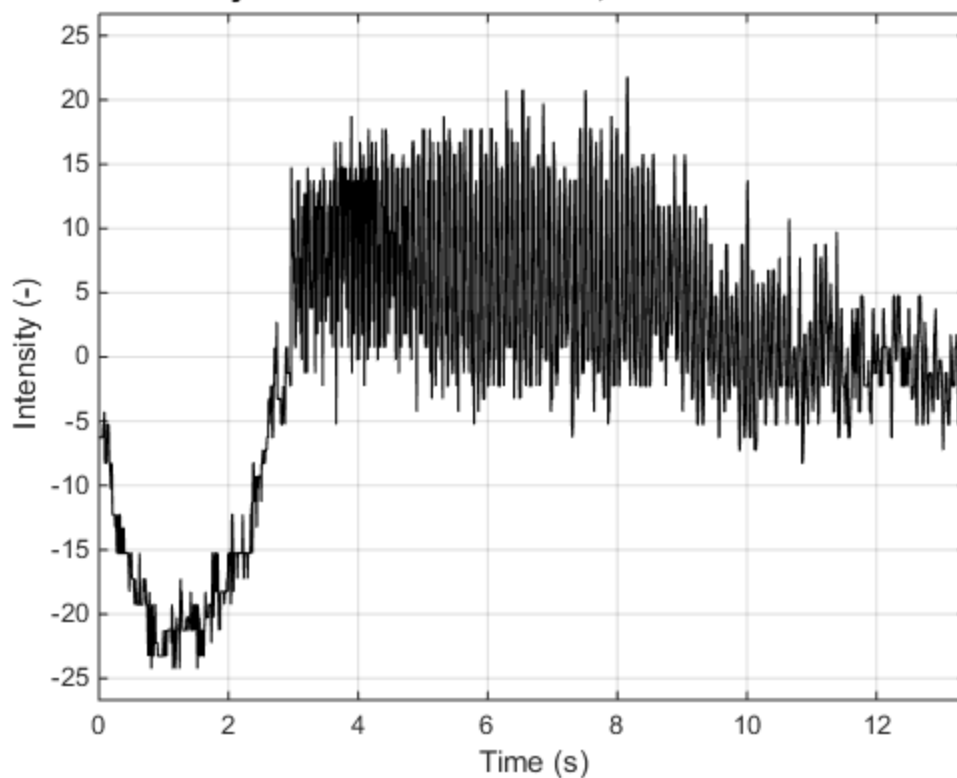
Time history of "S8T2 1ft Holes.MP4", Pixel coordinates: 482 352



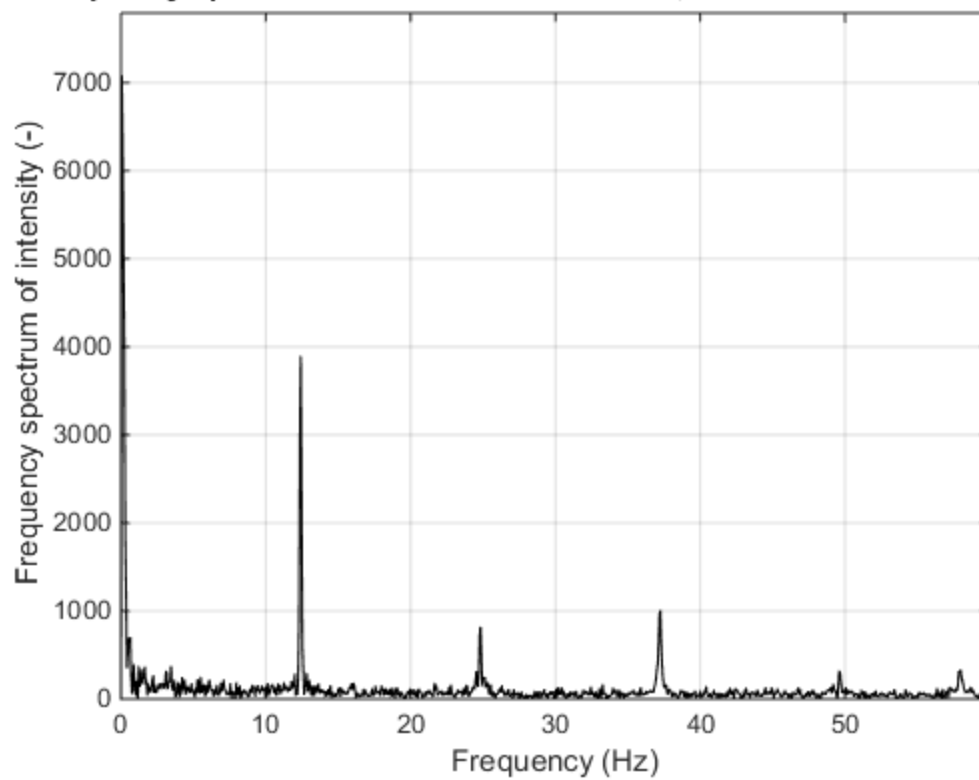
Frequency spectrum of "S8T2 1ft Holes.MP4", Pixel coordinates: 482 352



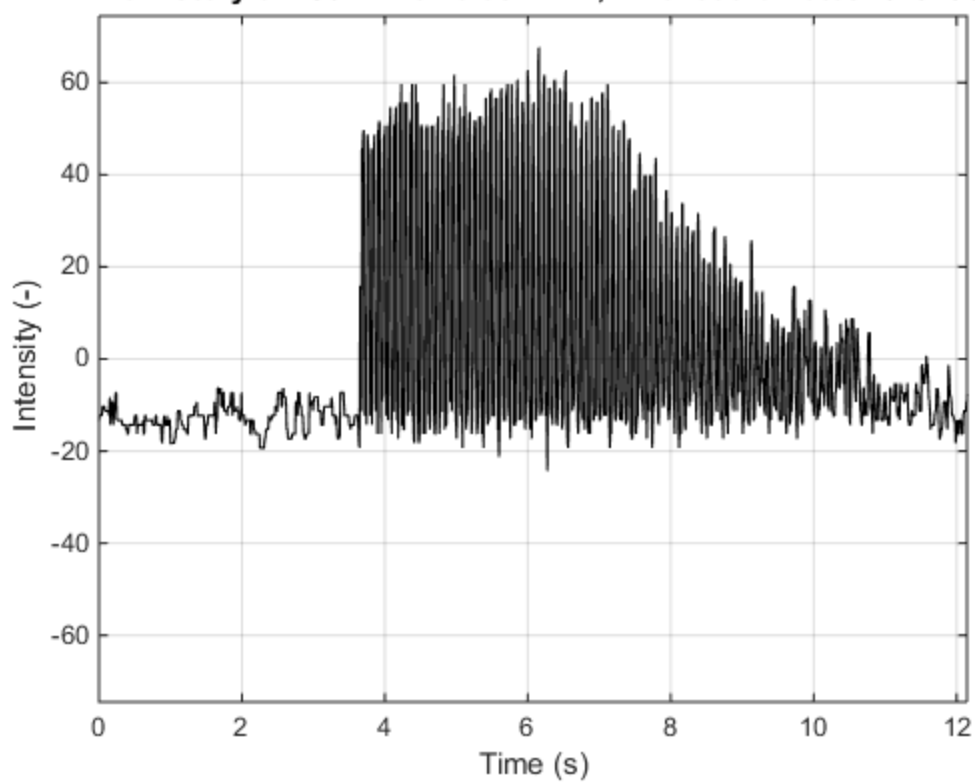
Time history of "S8T2 2ft Holes.MP4", Pixel coordinates: 804 315



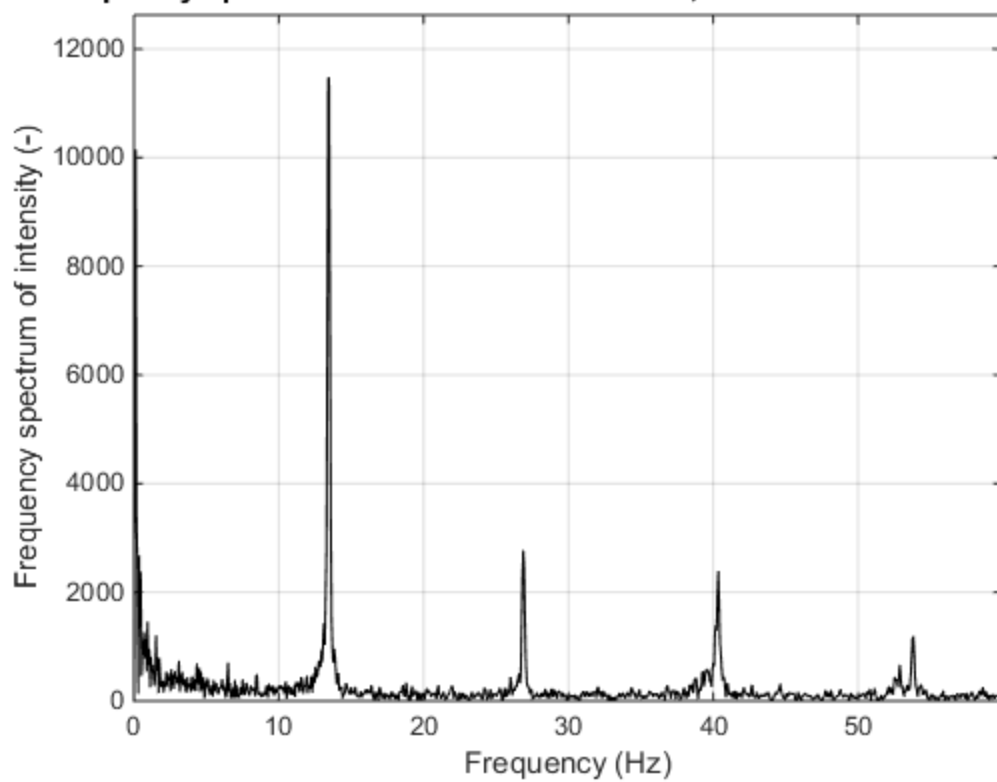
Frequency spectrum of "S8T2 2ft Holes.MP4", Pixel coordinates: 804 315



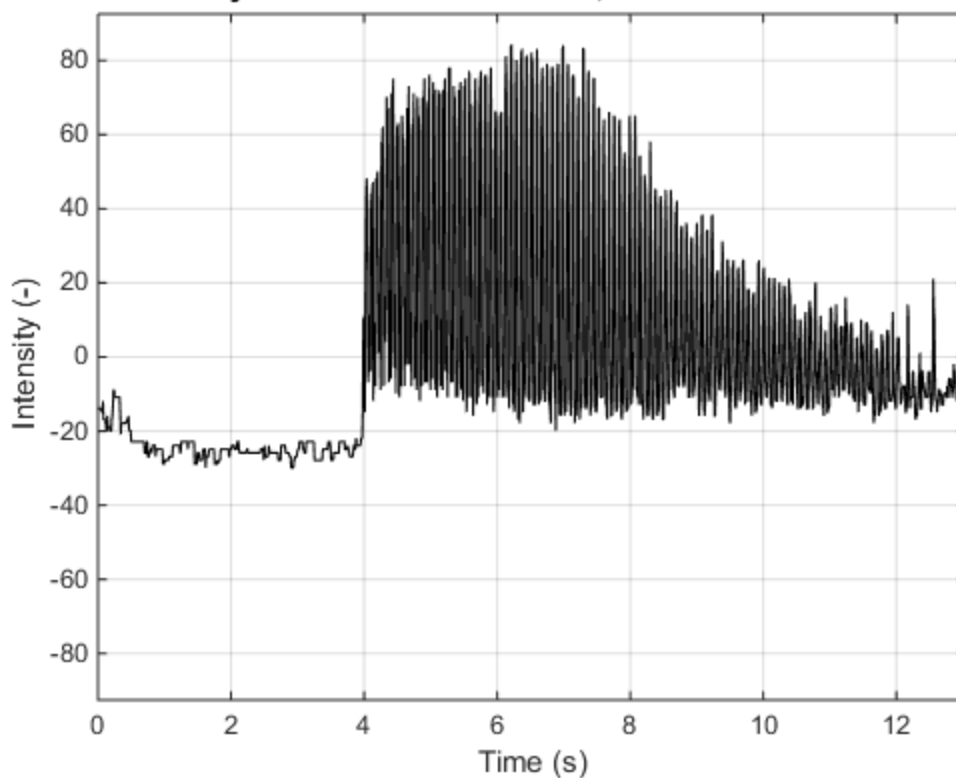
Time history of "S9T1 1ft Holes.MP4", Pixel coordinates: 625 360



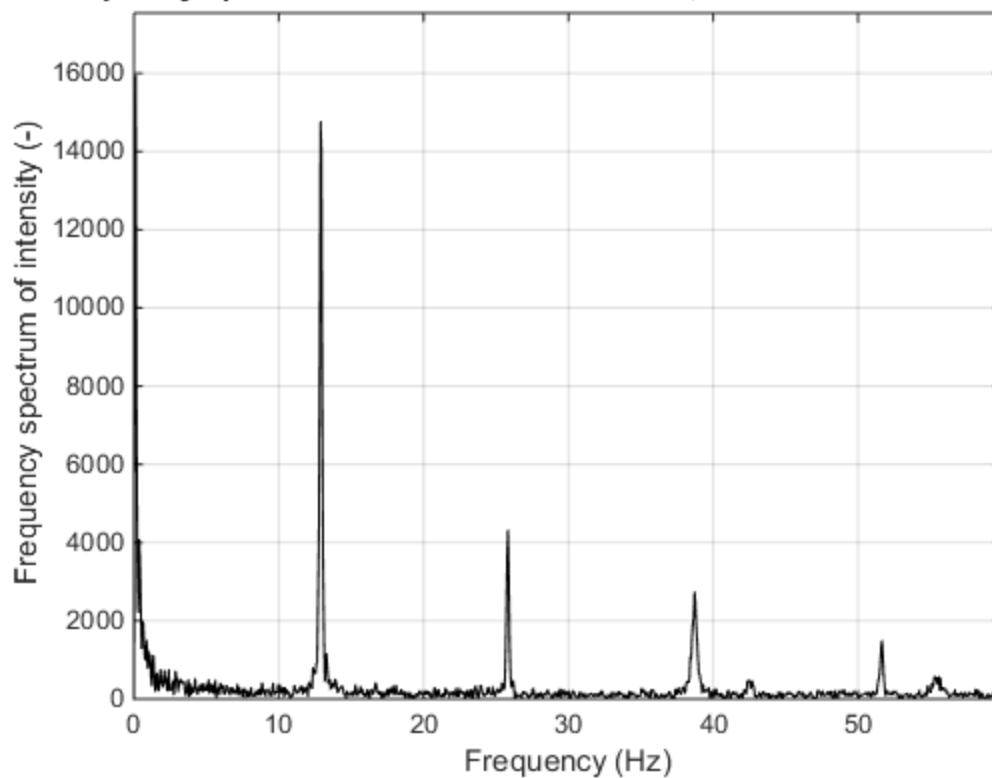
Frequency spectrum of "S9T1 1ft Holes.MP4", Pixel coordinates: 625 360



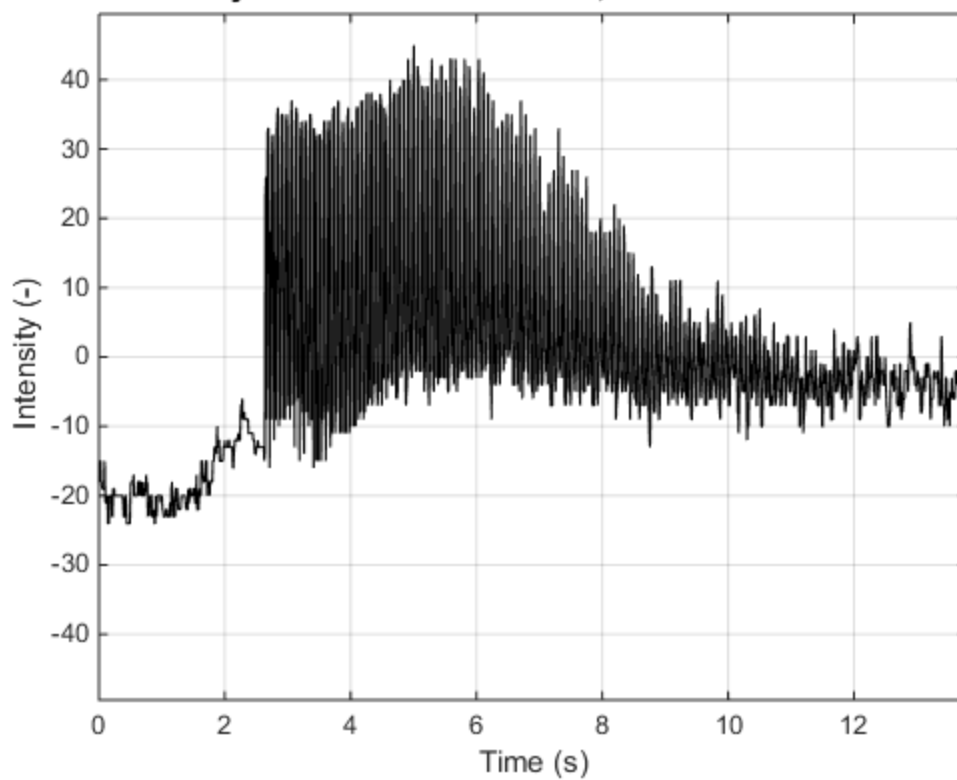
Time history of "S9T1 2ft Holes.MP4", Pixel coordinates: 929 347



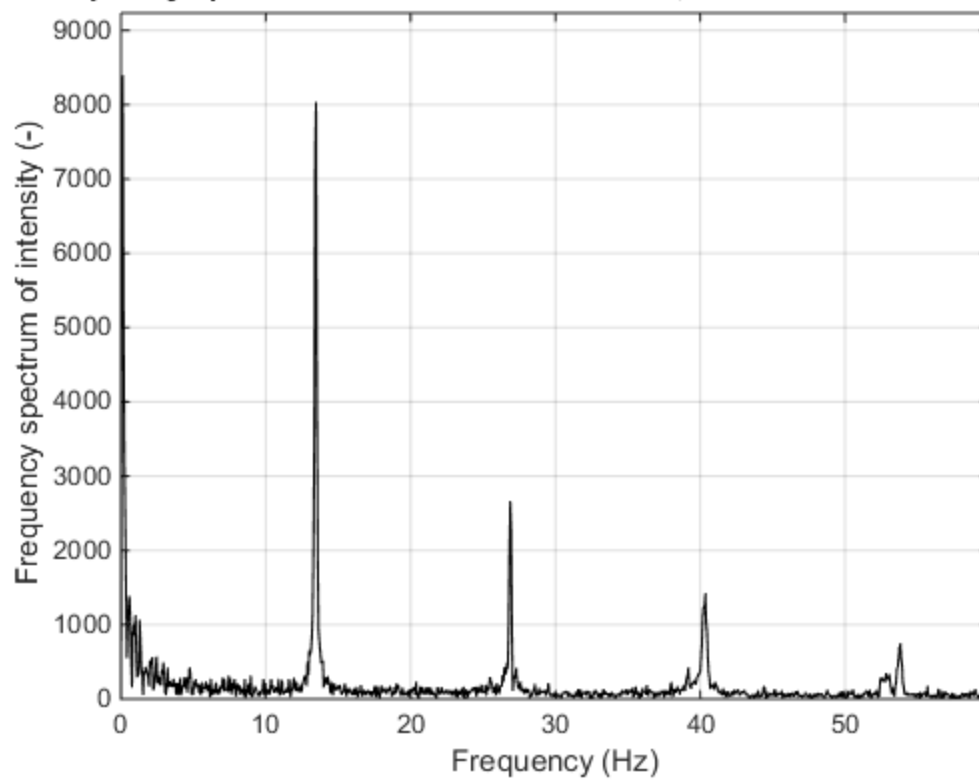
Frequency spectrum of "S9T1 2ft Holes.MP4", Pixel coordinates: 929 347



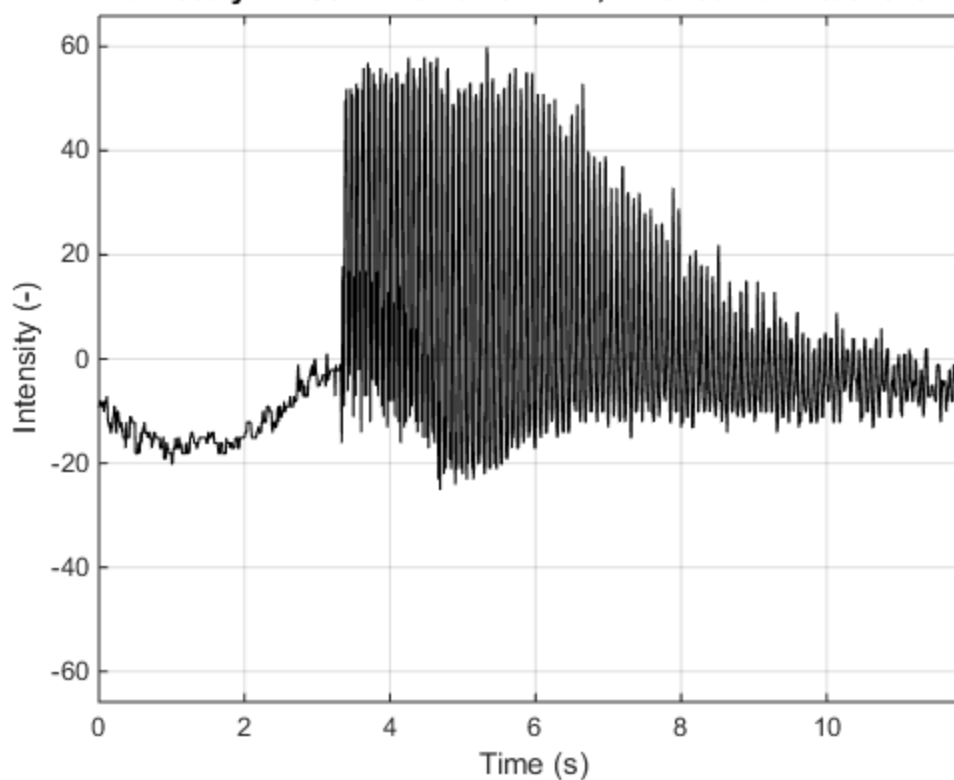
Time history of "S9T2 1ft Holes.MP4", Pixel coordinates: 625 360



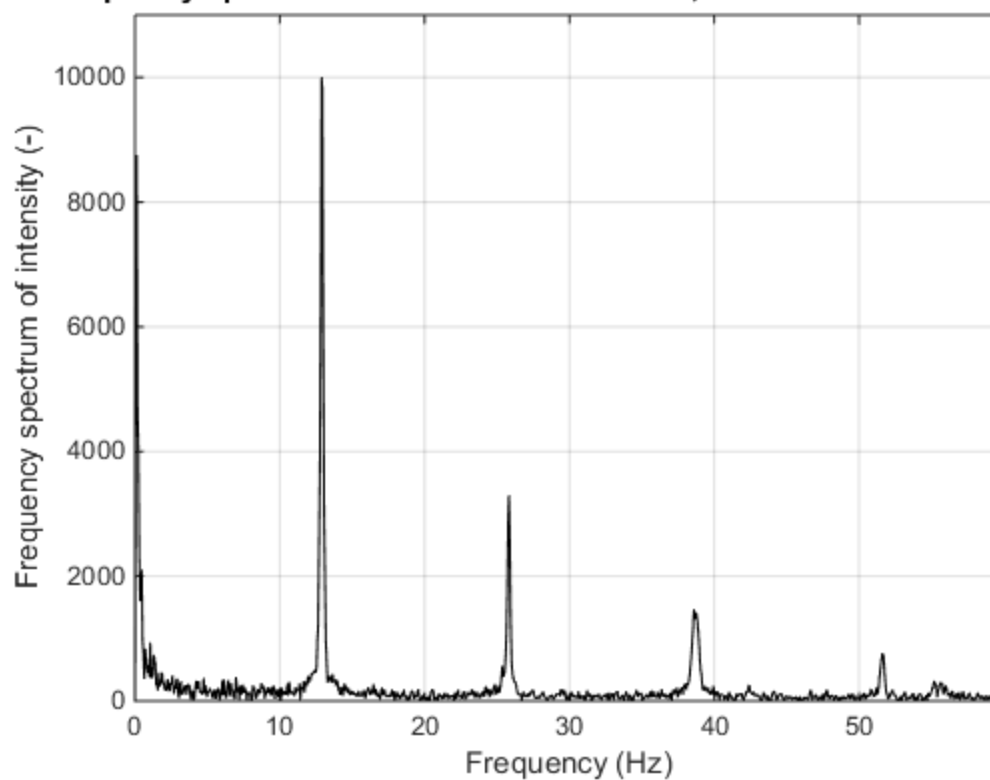
Frequency spectrum of "S9T2 1ft Holes.MP4", Pixel coordinates: 625 360



Time history of "S9T2 2ft Holes.MP4", Pixel coordinates: 929 347



Frequency spectrum of "S9T2 2ft Holes.MP4", Pixel coordinates: 929 347



Appendix J – Shake Table Accelerometer Test Results

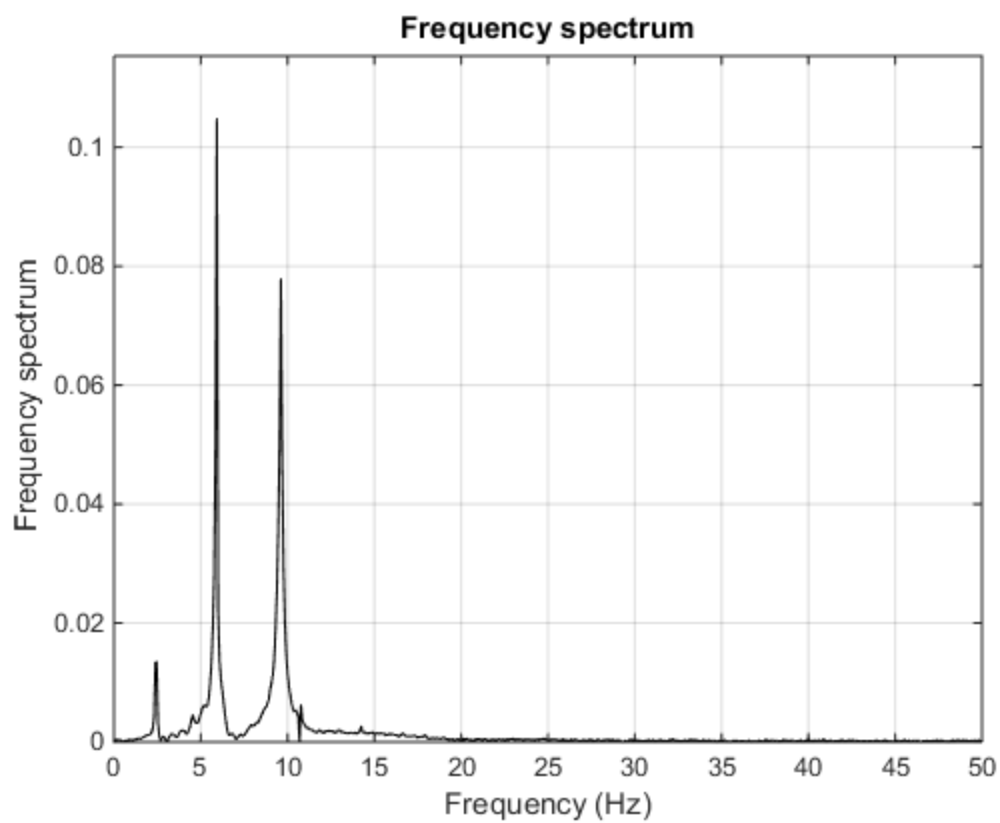
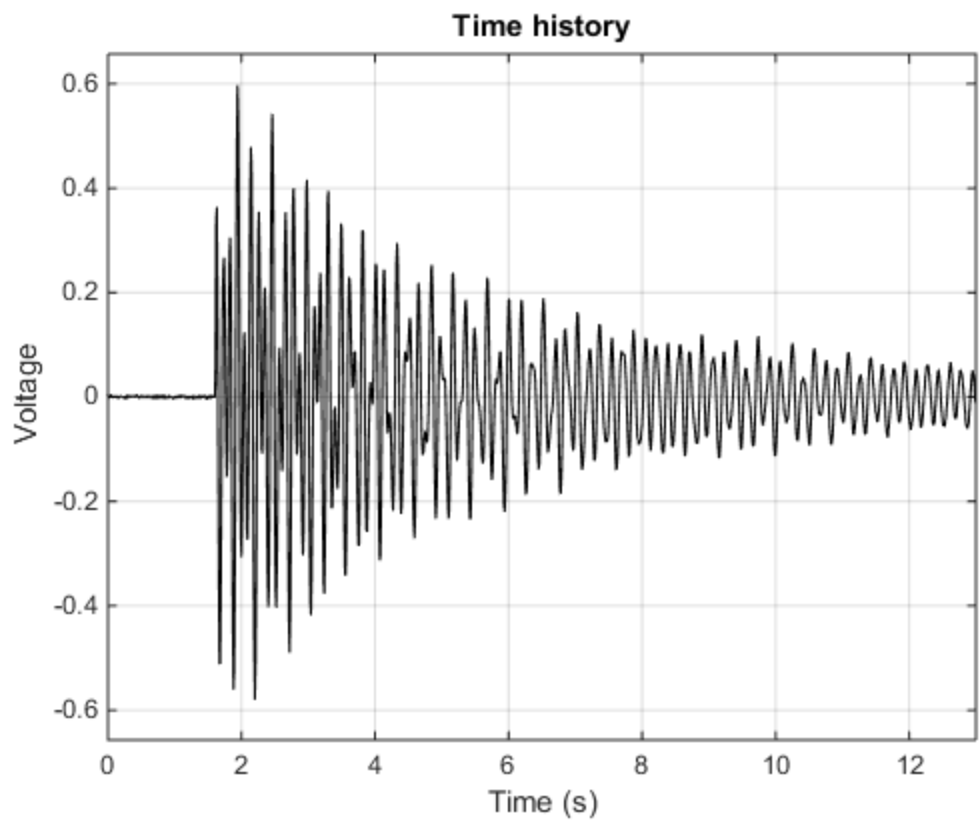
Table J1 - Shake Table Accelerometer Results (Canon)

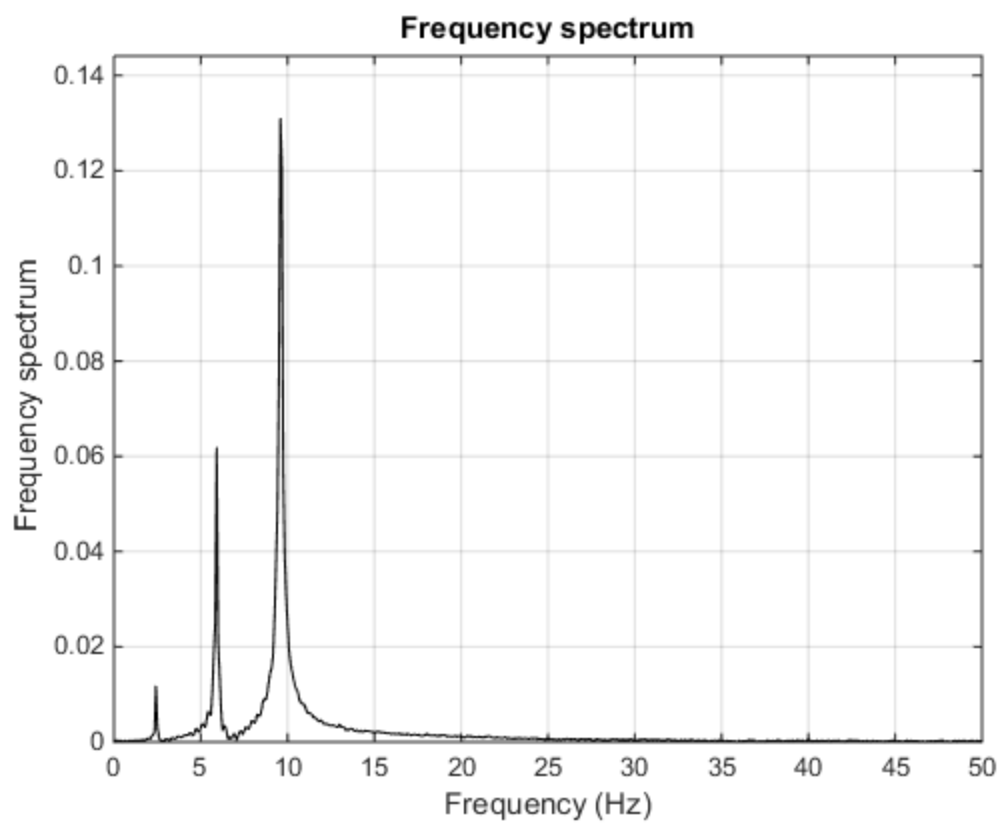
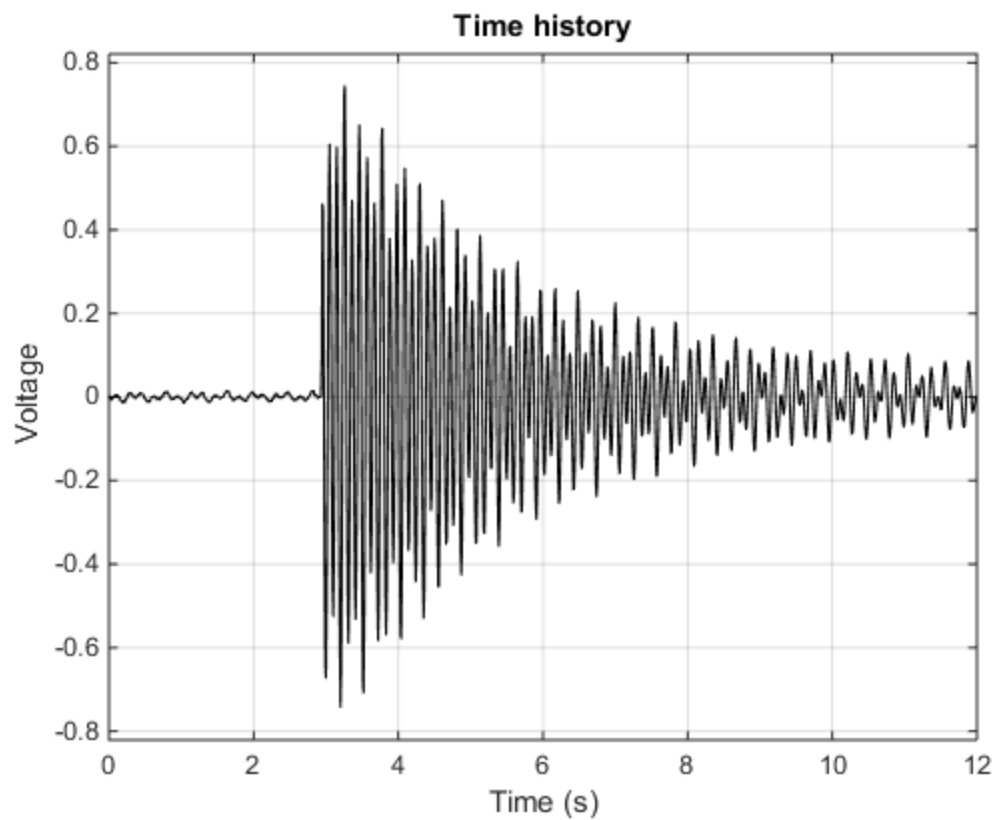
Test	Accelerometer Frequencies (Hz)			Test	Canon VVS Frequencies (Hz)		
	Mode 1	Mode 2	Mode 3		Mode 1	Mode 2	Mode 3
1	2.385	5.923	9.615	1	2.430	5.915	9.634
2	2.417	5.917	9.583	2	2.402	5.918	9.609
3	2.385	5.923	9.615	3	2.402	5.918	9.375
4	2.429	5.929	9.571	4	2.461	5.918	9.375
5	2.455	5.909	9.636	5	2.402	5.918	-
6	2.417	5.917	9.583	6	2.402	5.918	9.609
7	2.462	5.923	9.615	7	2.430	5.915	9.604
8	2.455	5.909	9.545	8	2.402	5.918	-
9	2.417	5.917	9.583	9	2.430	5.915	9.604
10	2.385	5.923	9.615	10	2.401	5.915	9.399
Average	2.421	5.919	9.596		2.416	5.917	9.526
STDEV	0.030	0.006	0.027		0.021	0.002	0.119

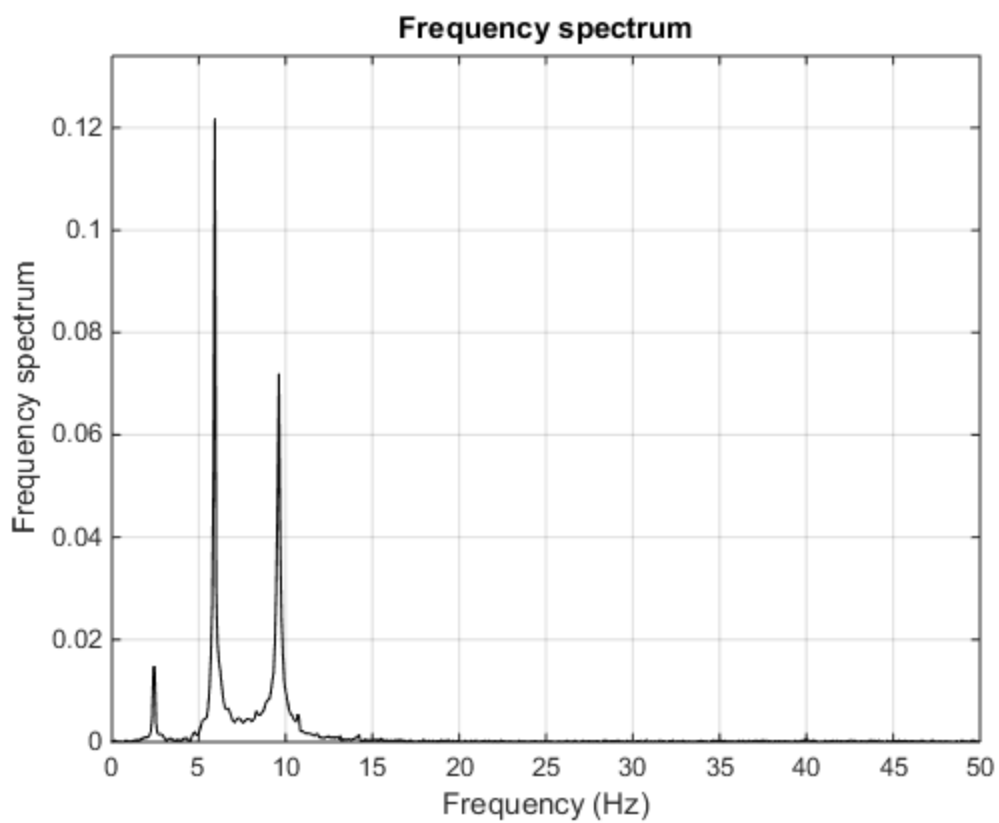
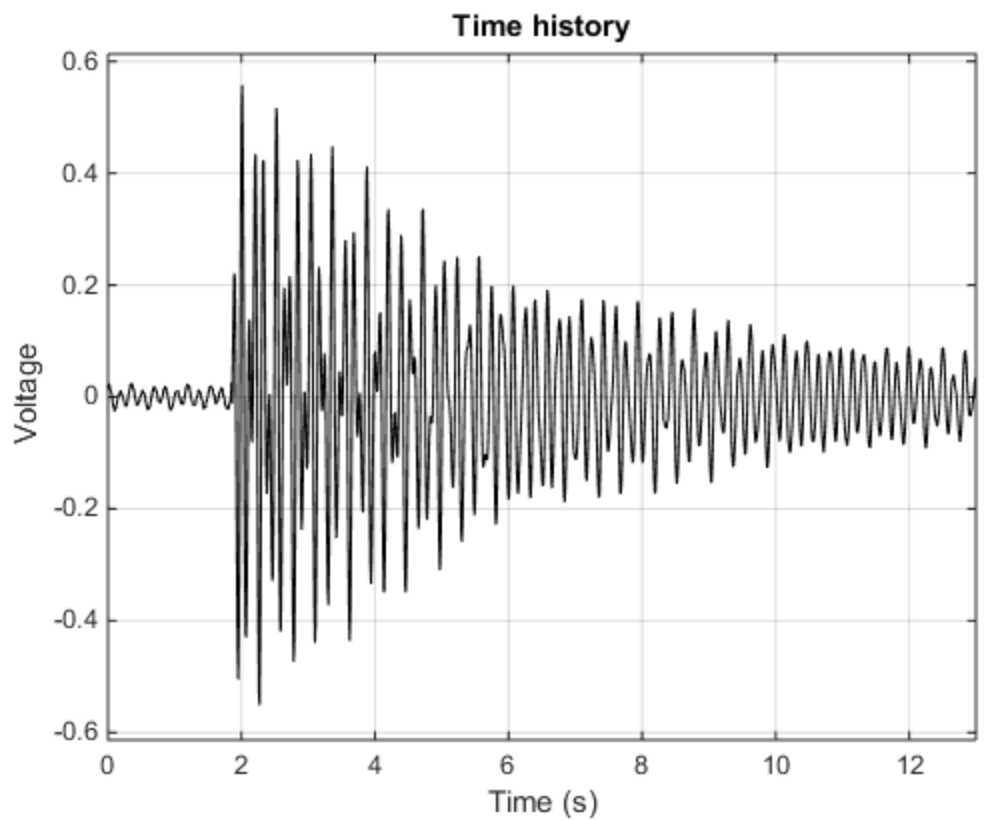
Table J2 - Shake Table Accelerometer Results (GoPro)

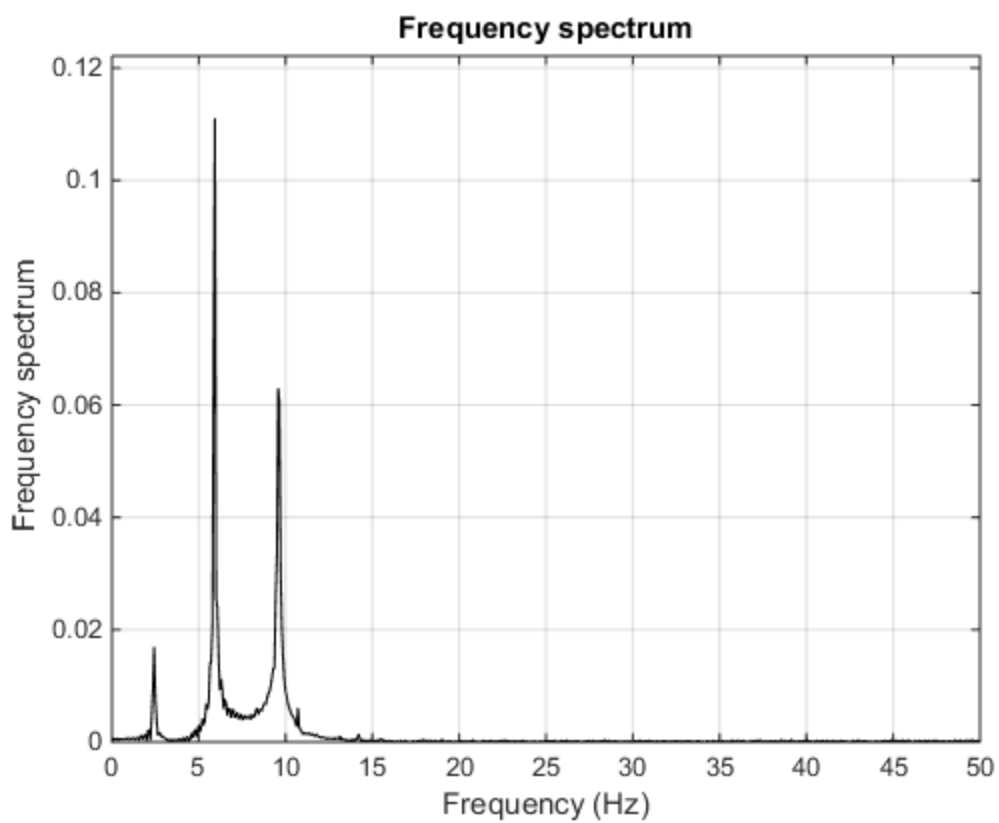
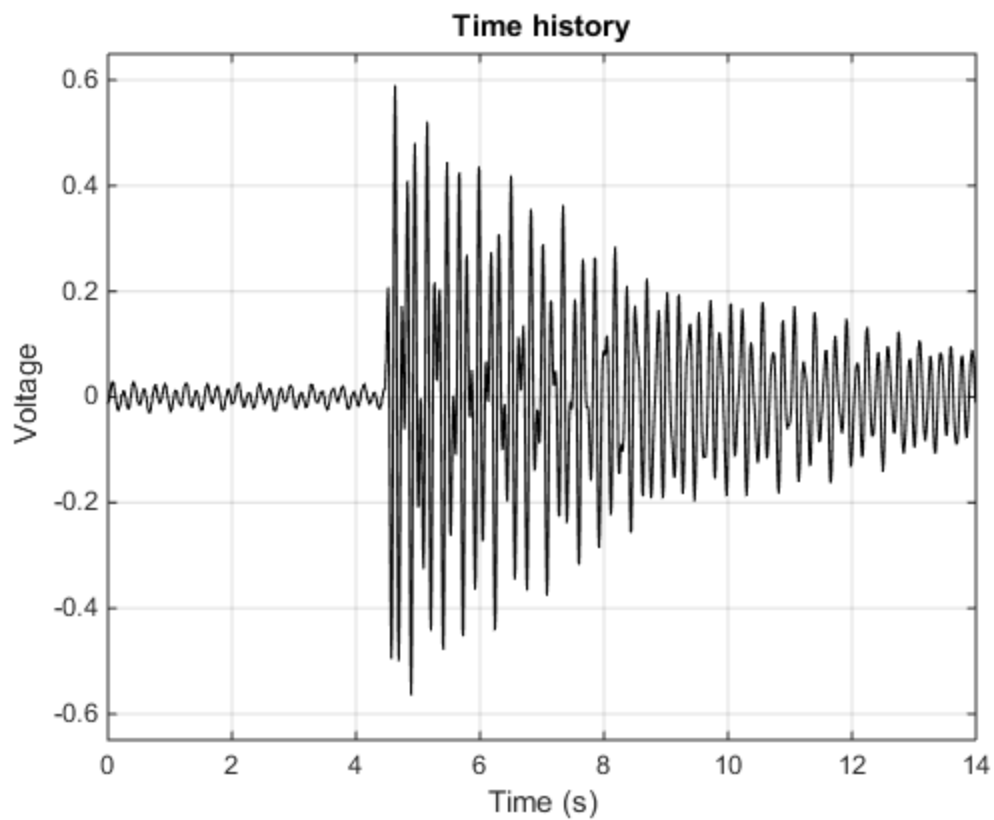
Test	Accelerometer Frequencies (Hz)			Test	GoPro VVS Frequencies (Hz)		
	Mode 1	Mode 2	Mode 3		Mode 1	Mode 2	Mode 3
1	2.444	5.889	9.611	1	2.430	5.914	-
2	2.438	5.938	9.625	2	2.430	5.914	9.69
3	2.438	5.938	9.625	3	2.430	5.914	9.602
4	2.462	5.923	9.615	4	2.401	5.914	9.631
5	2.438	5.875	9.625	5	2.430	5.914	9.368
6	2.417	5.917	9.583	6	2.460	5.915	9.605
7	2.455	5.909	9.636	7	2.401	5.915	9.605
8	2.438	5.938	9.625	8	2.459	5.914	9.631
9	2.417	5.917	9.667	9	2.460	5.915	9.605
10	2.455	5.909	9.636	10	2.460	5.915	-
Average	2.440	5.915	9.625		2.436	5.914	9.592
STDEV	0.015	0.021	0.021		0.023	0.001	0.095

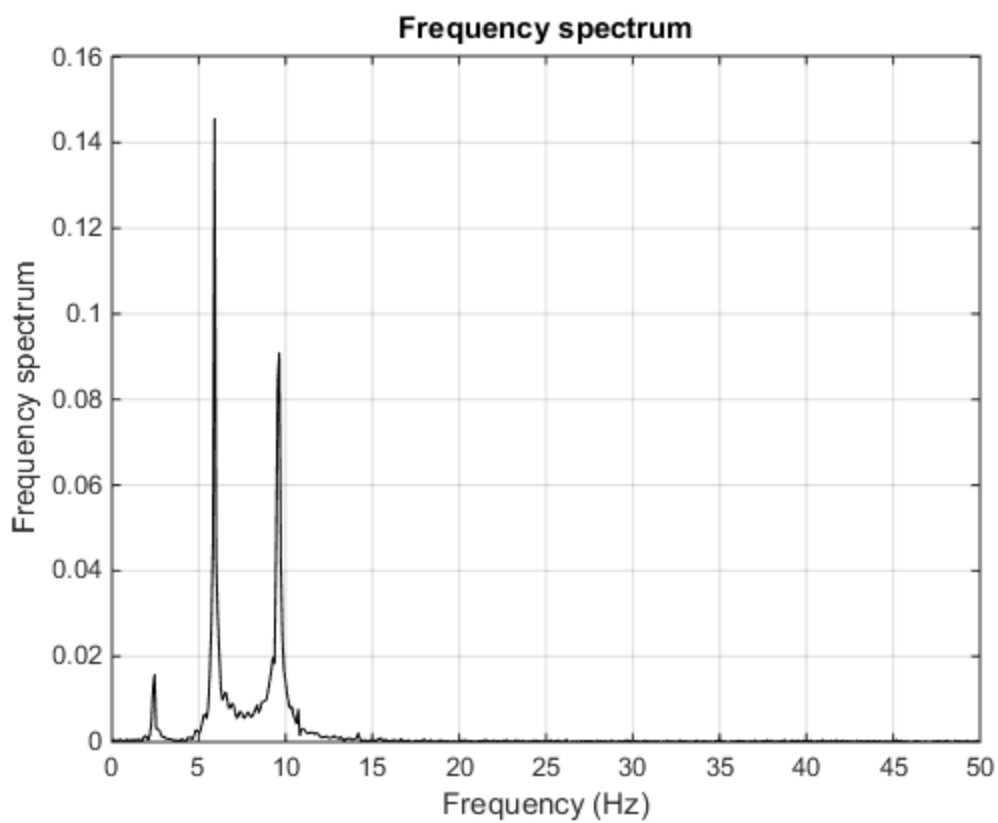
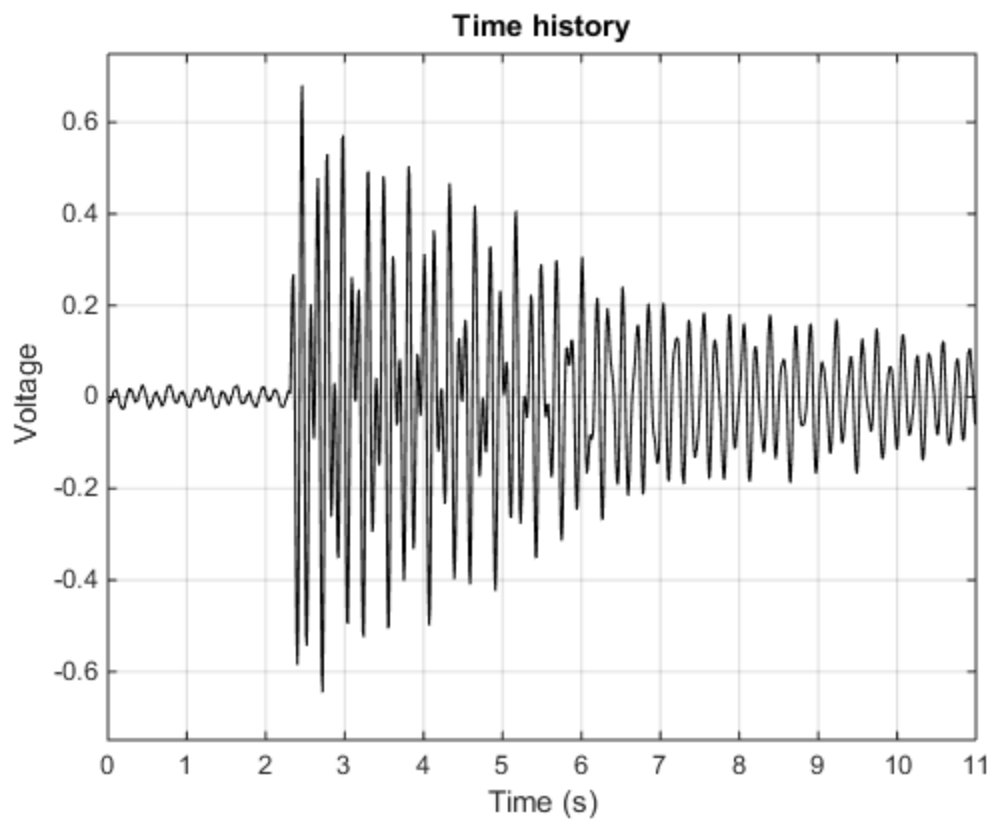
Appendix K – Shake Table Accelerometer Figures (Canon)

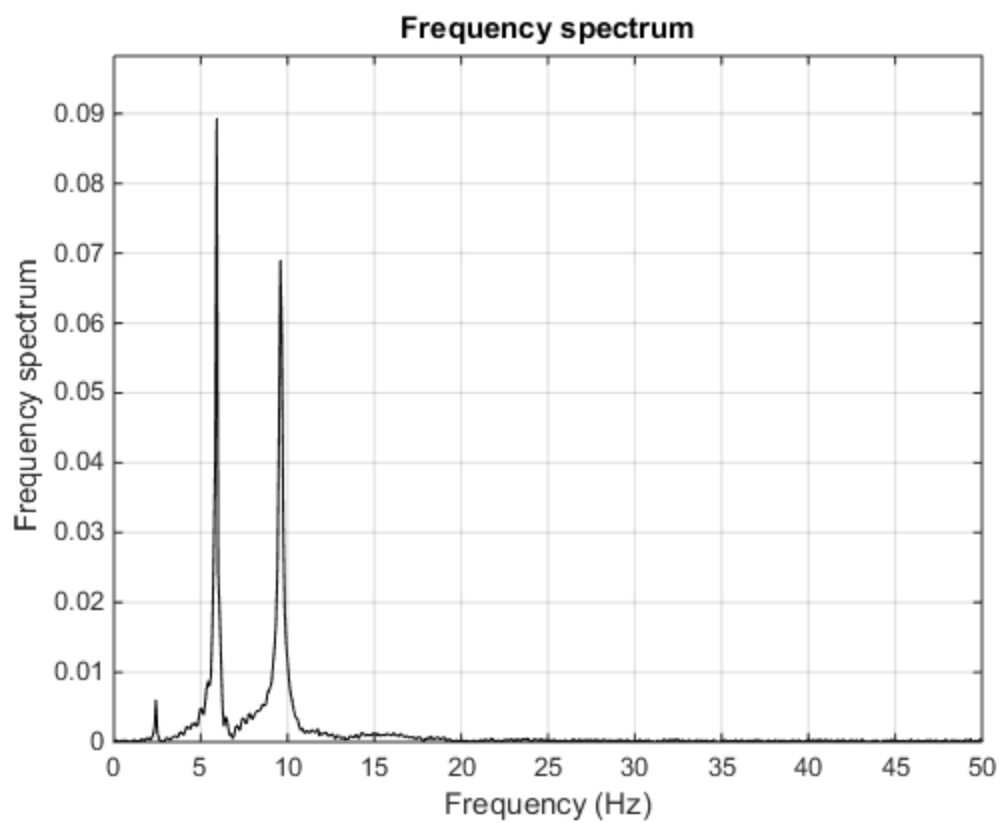
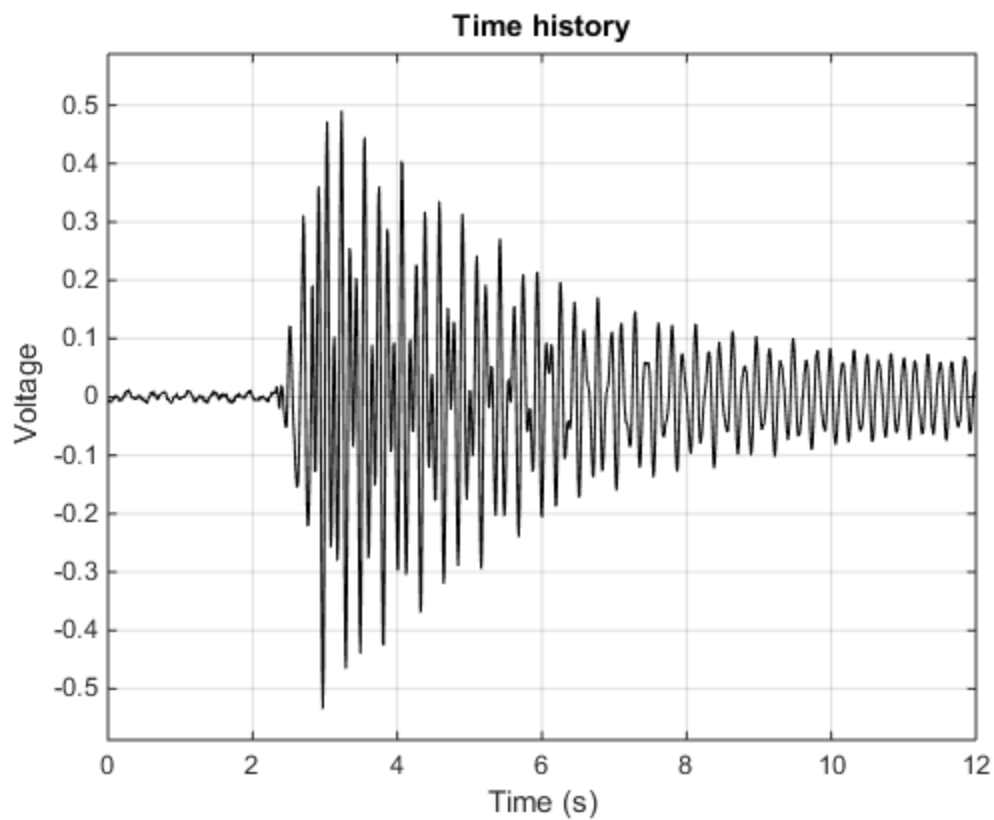


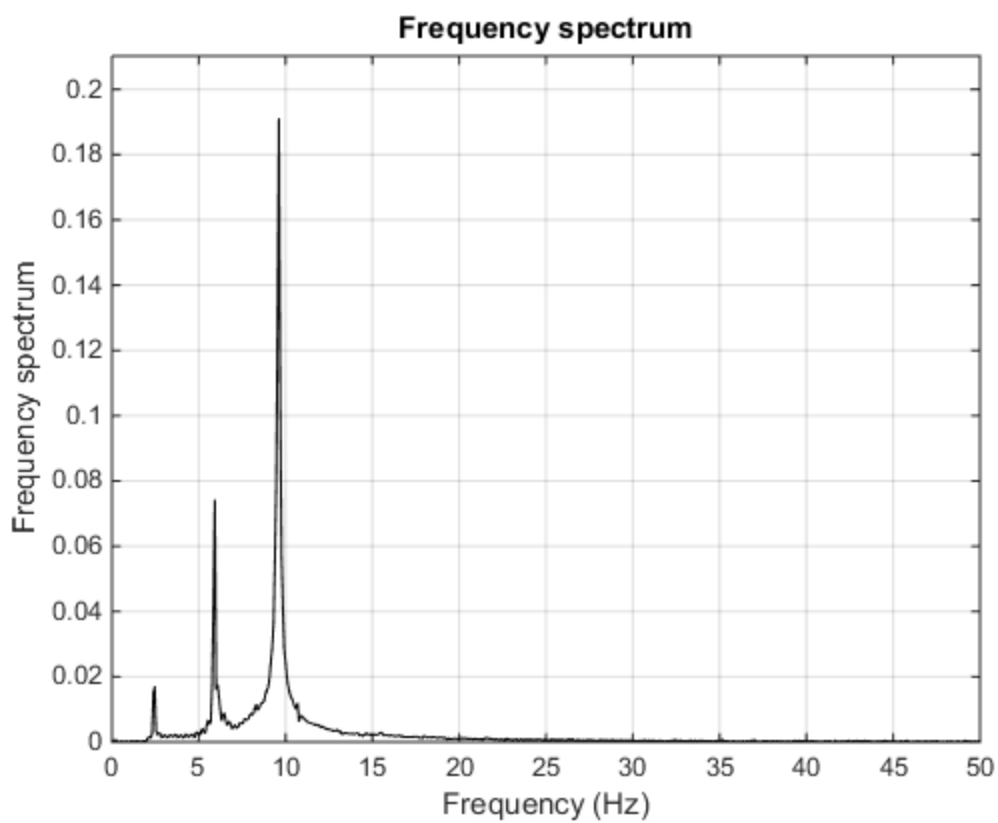
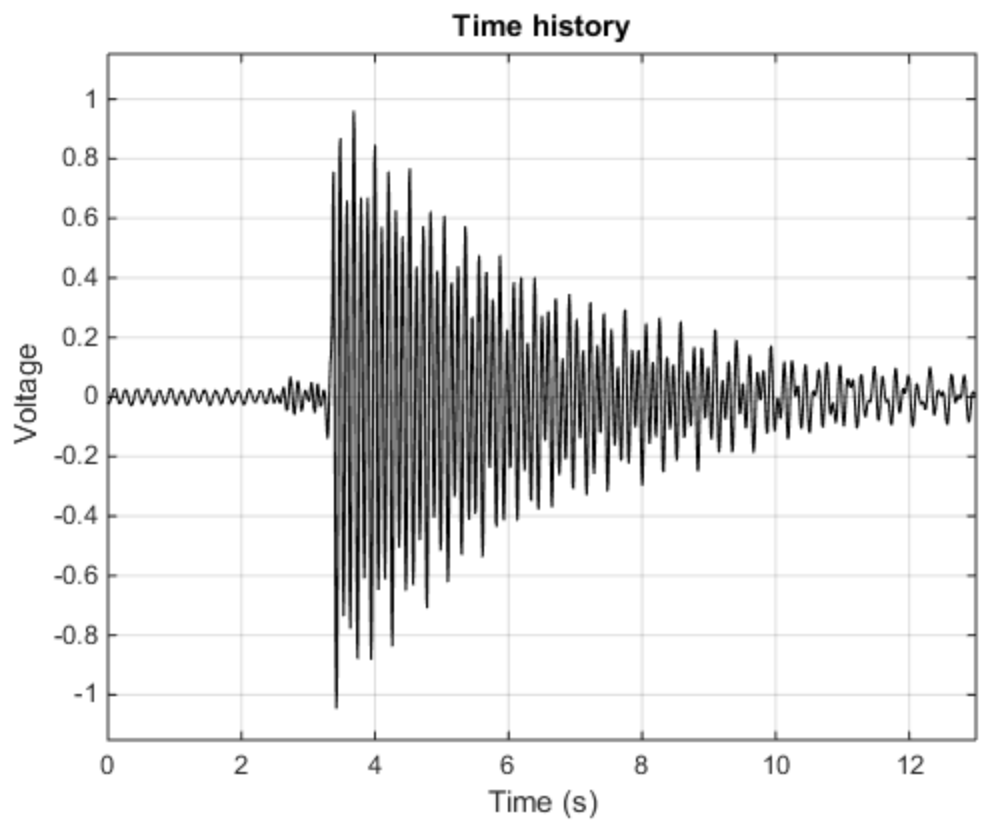


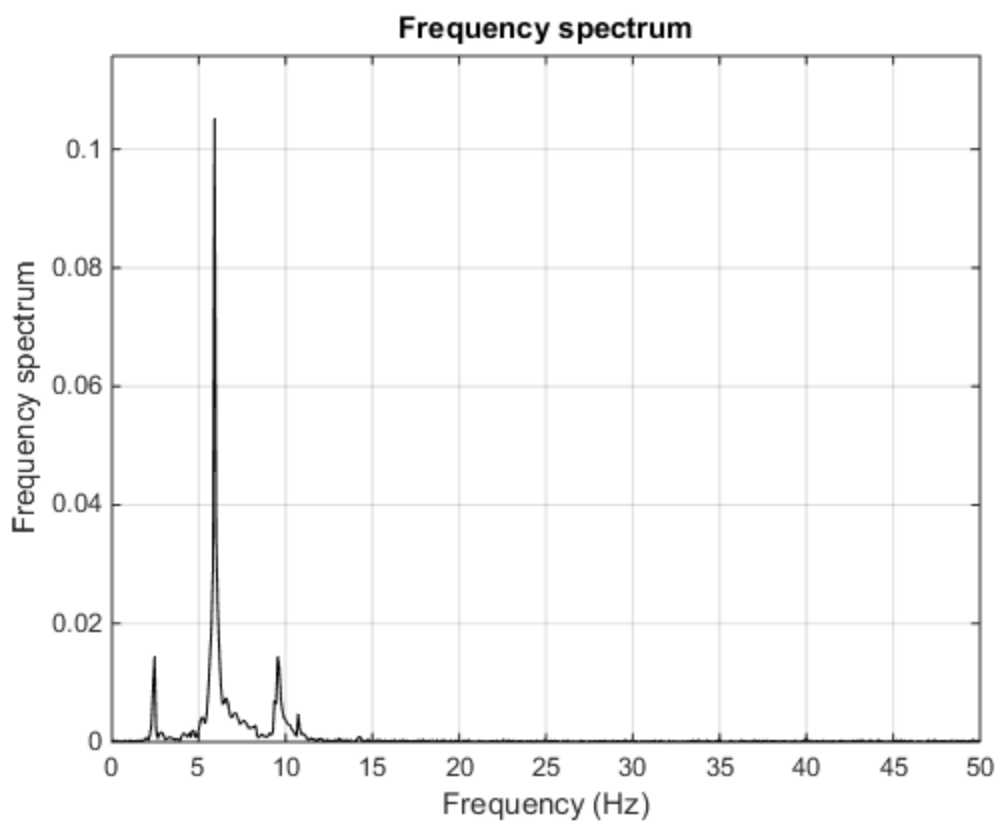
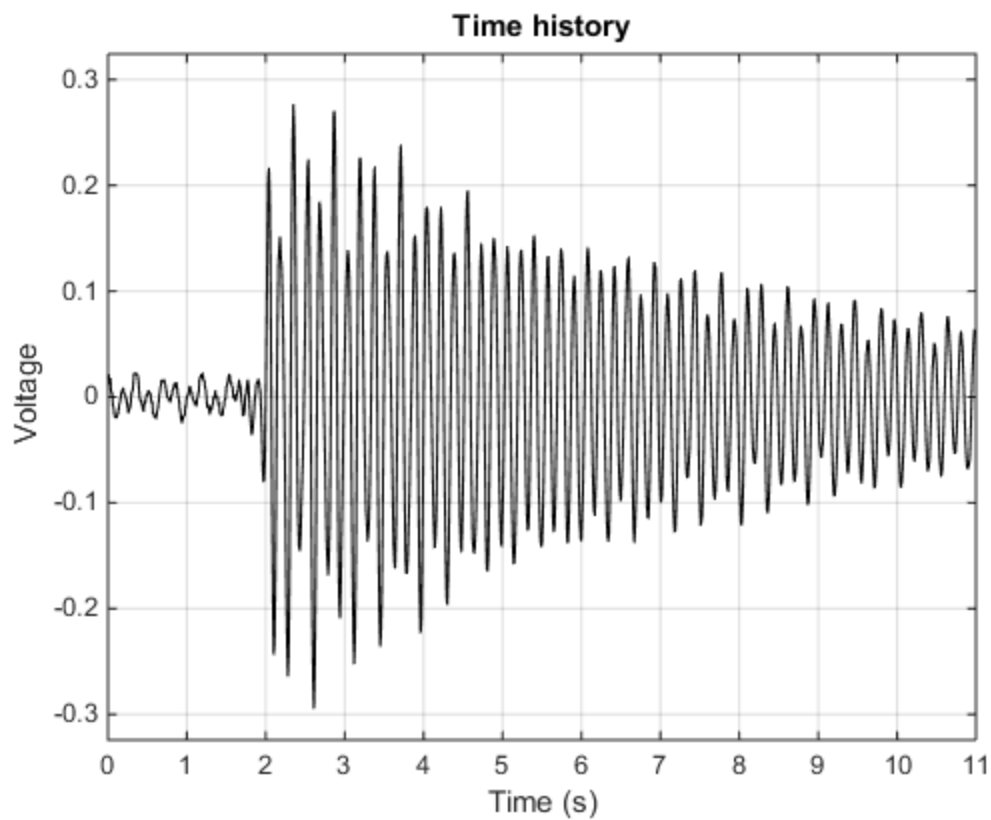


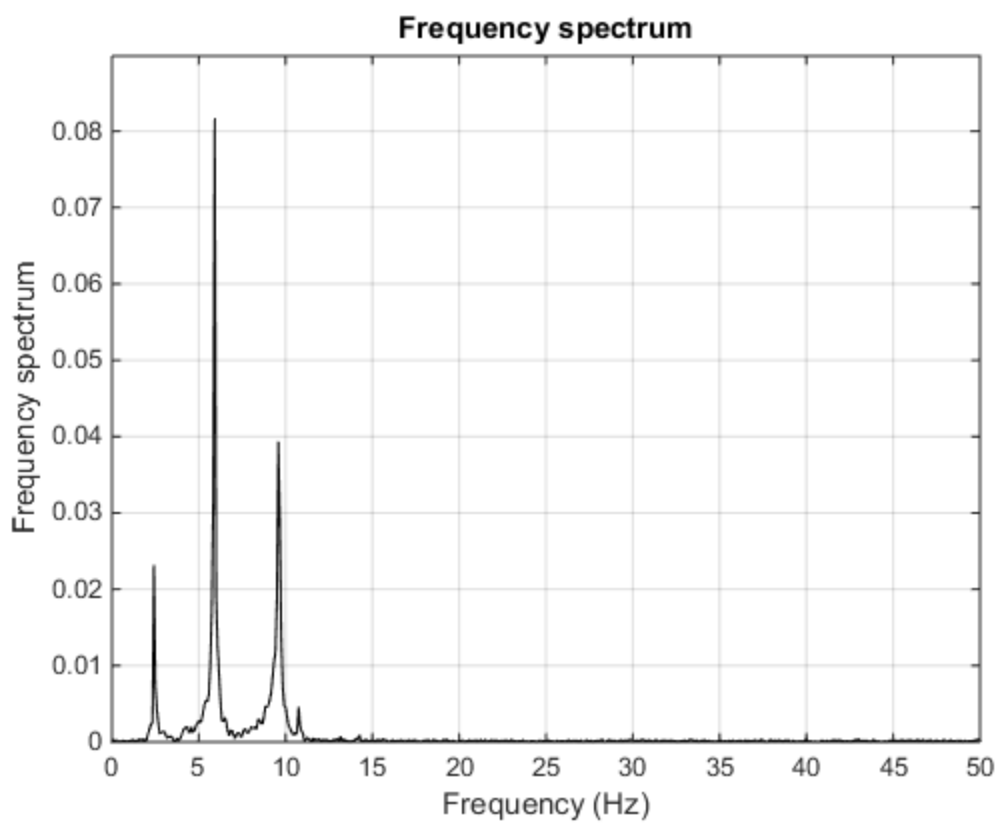
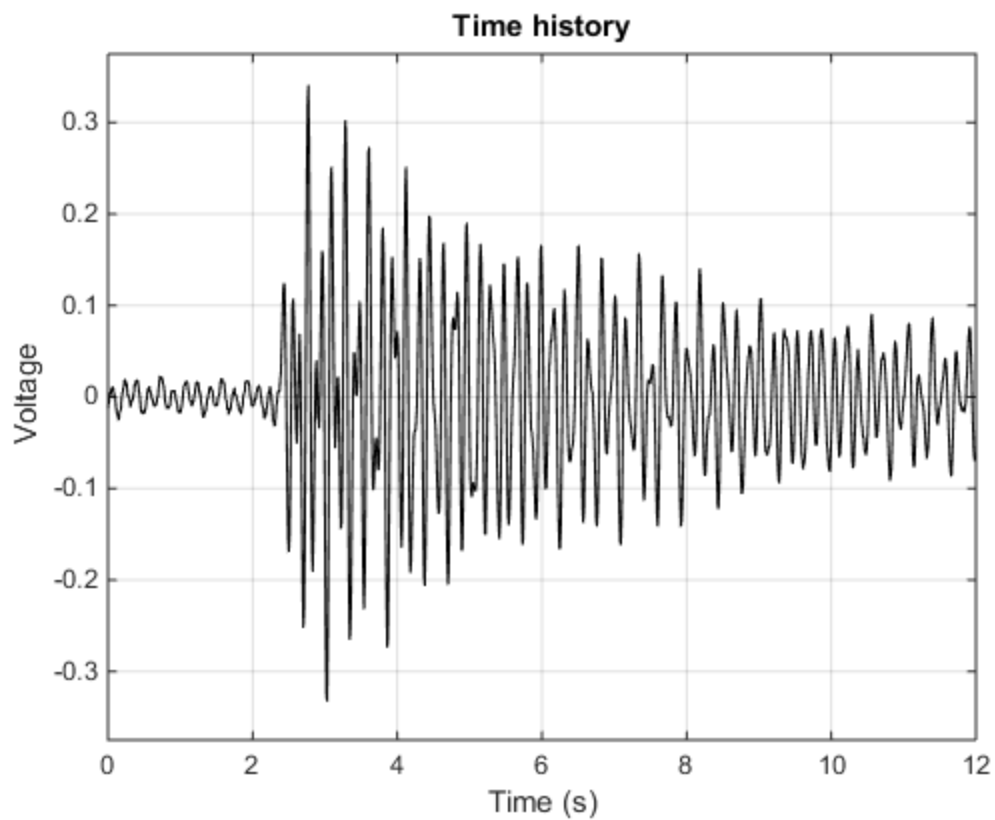


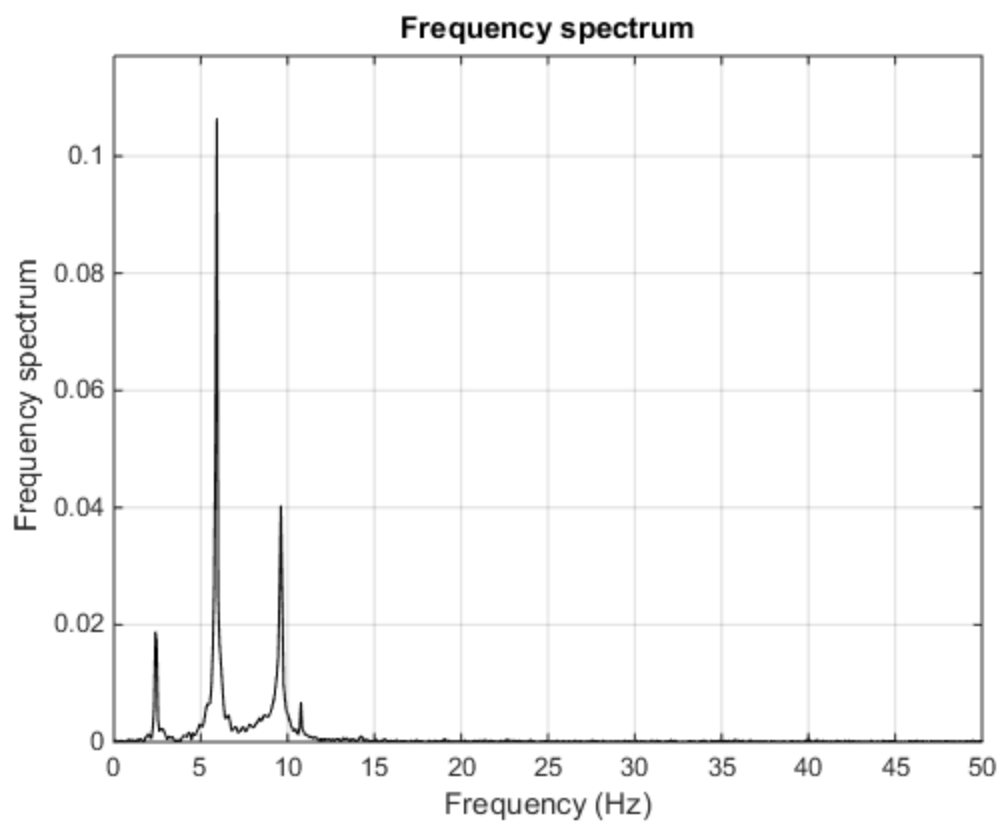
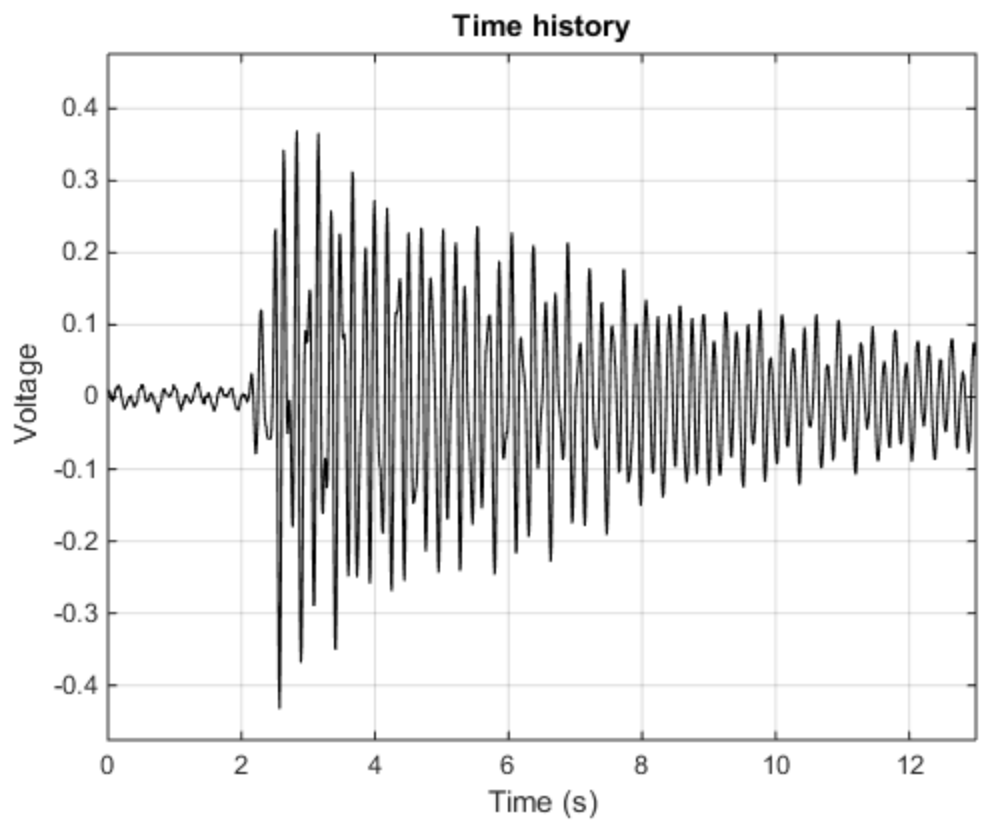






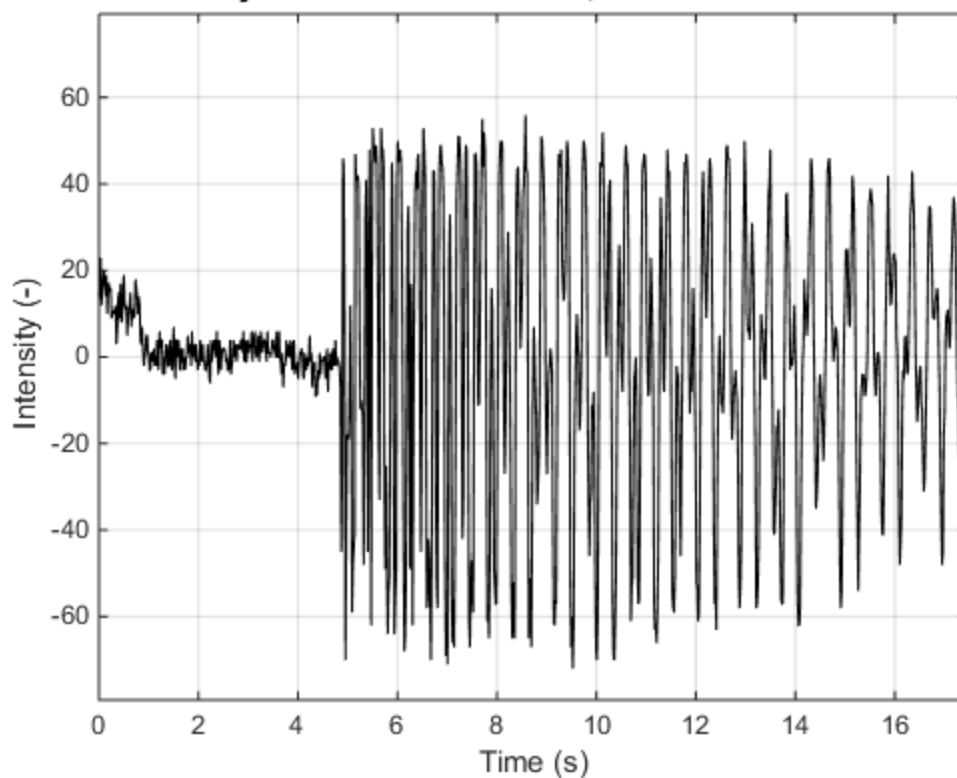




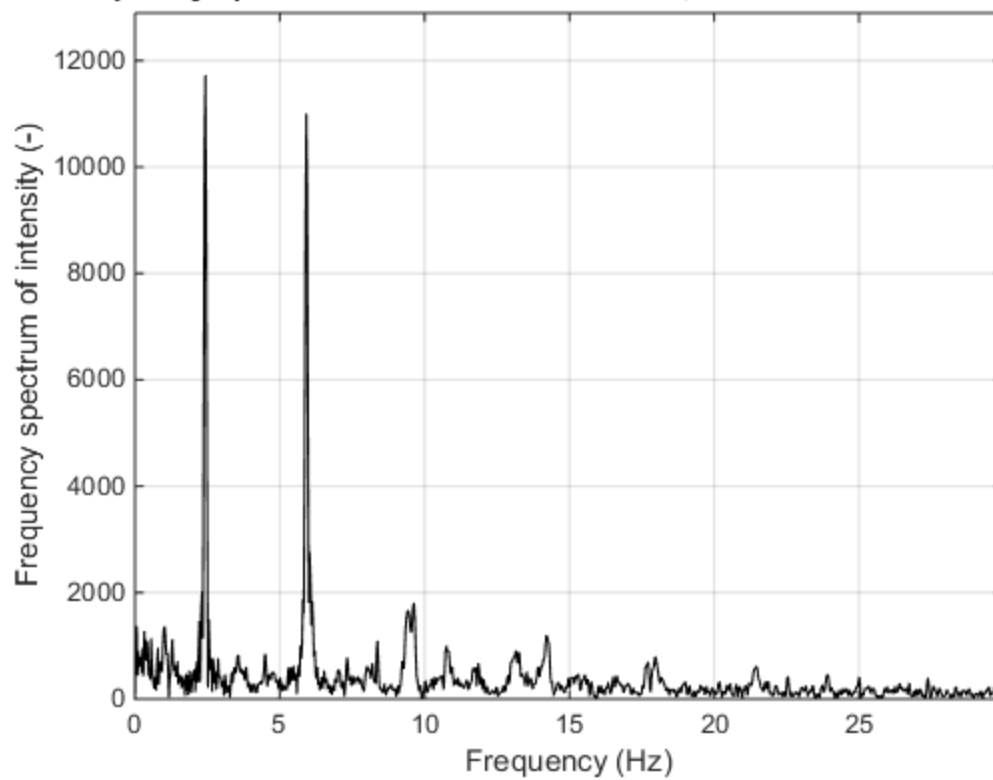


Appendix L – Shake Table VVS Figures (Canon)

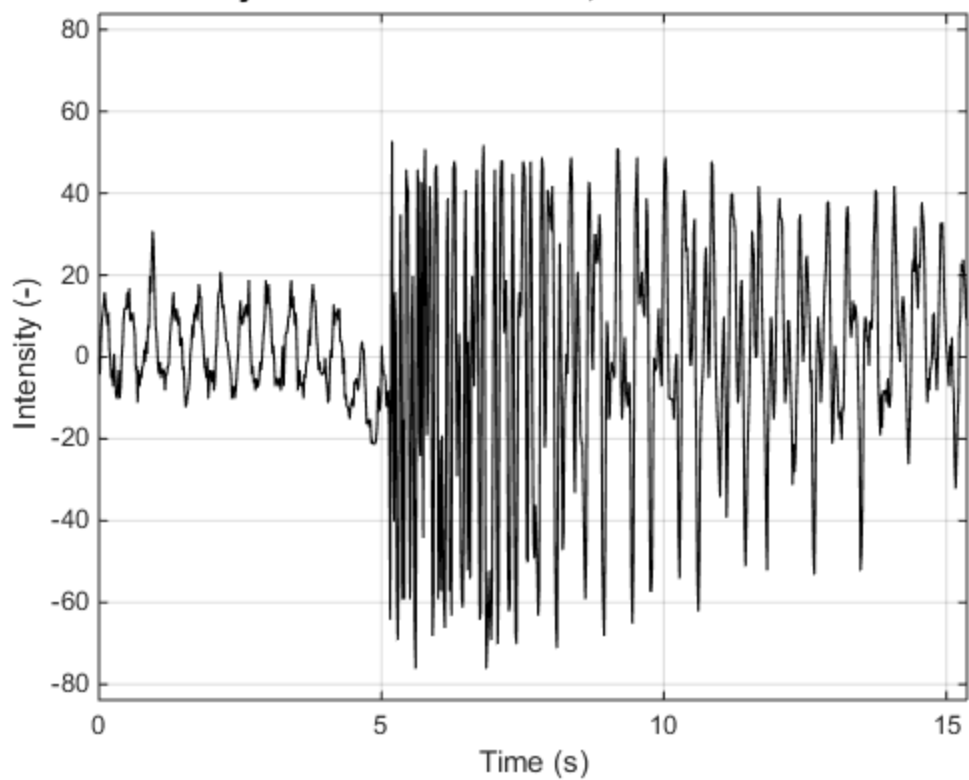
Time history of "ST Canon 01.MOV", Pixel coordinates: 522 558



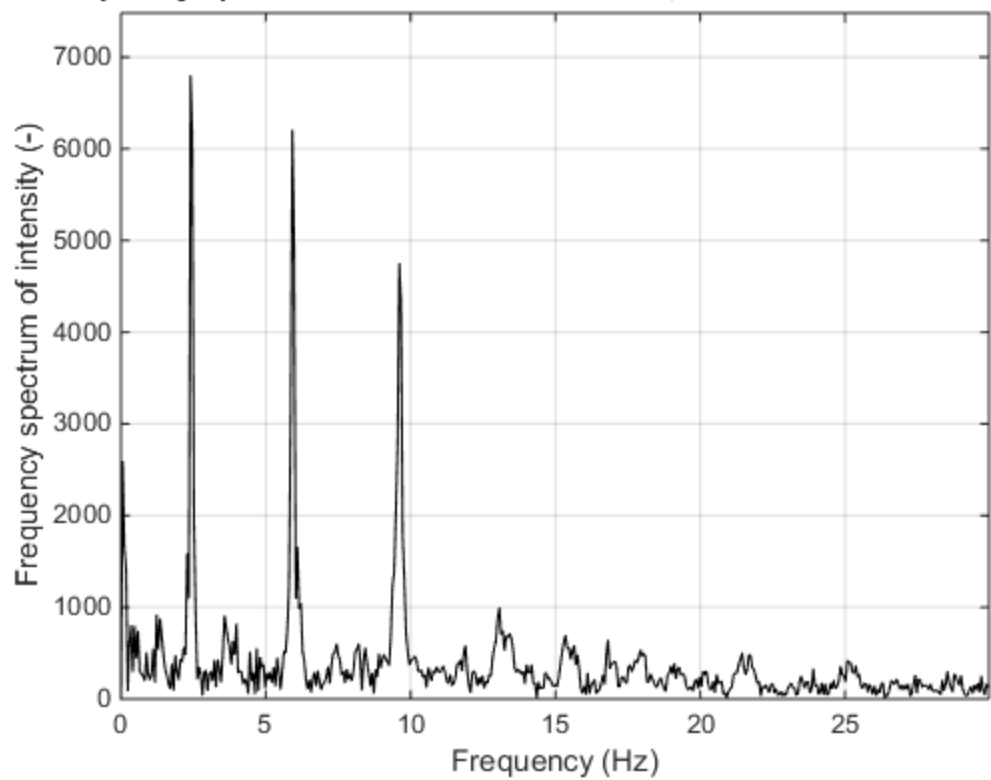
Frequency spectrum of "ST Canon 01.MOV", Pixel coordinates: 522 558

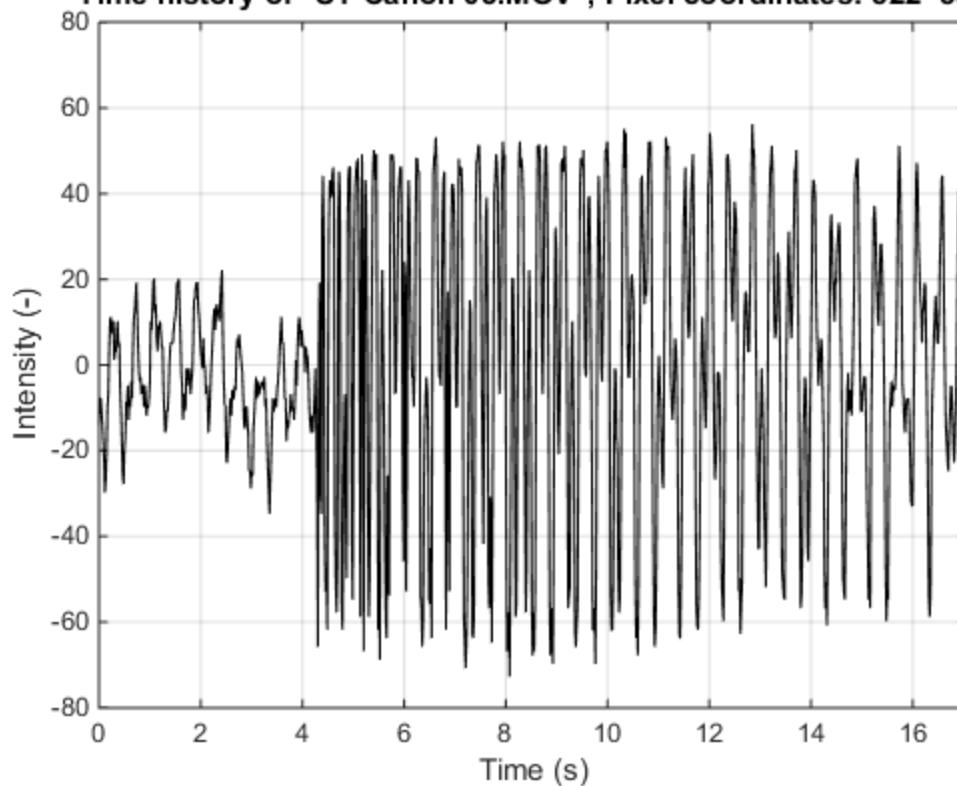
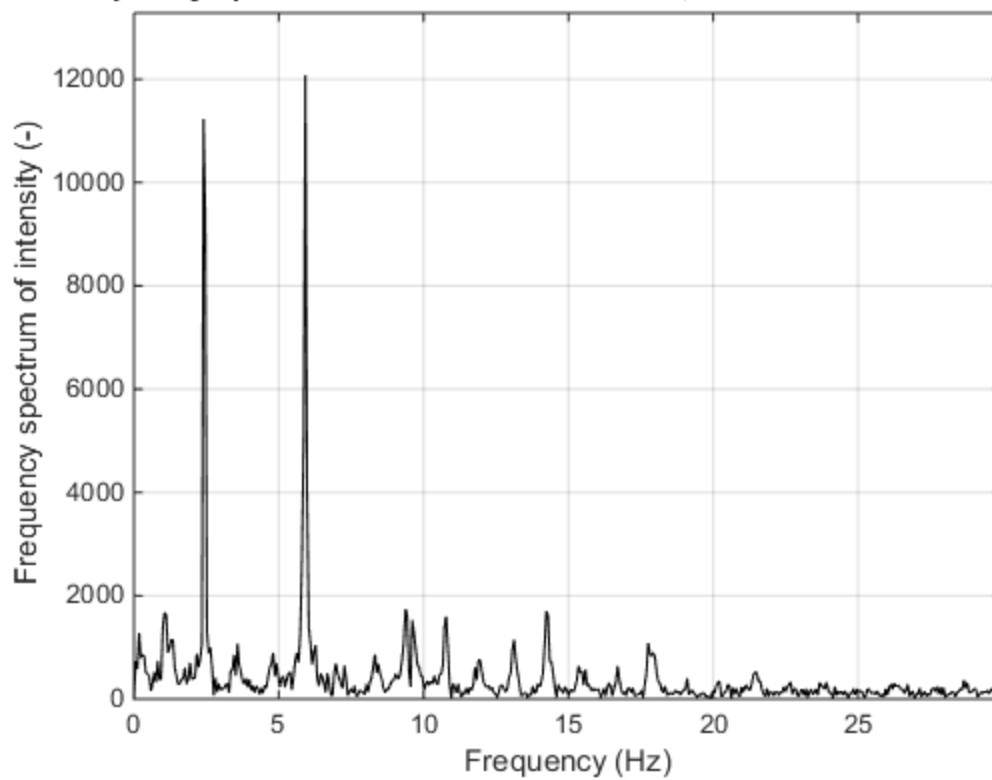


Time history of "ST Canon 02.MOV", Pixel coordinates: 522 558

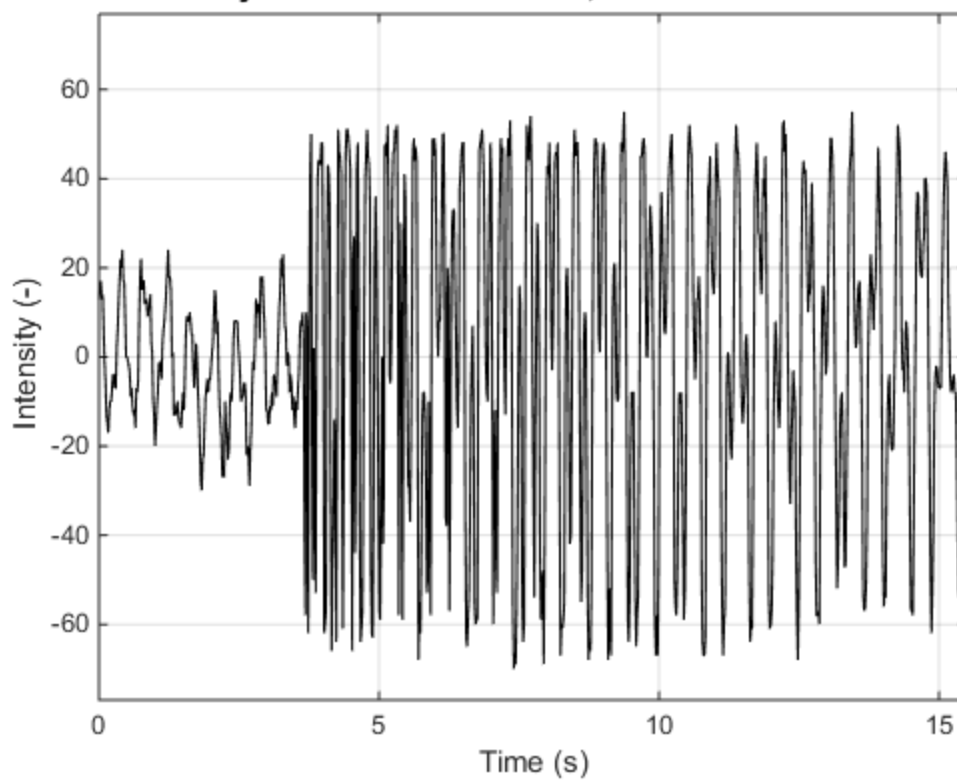


Frequency spectrum of "ST Canon 02.MOV", Pixel coordinates: 522 558

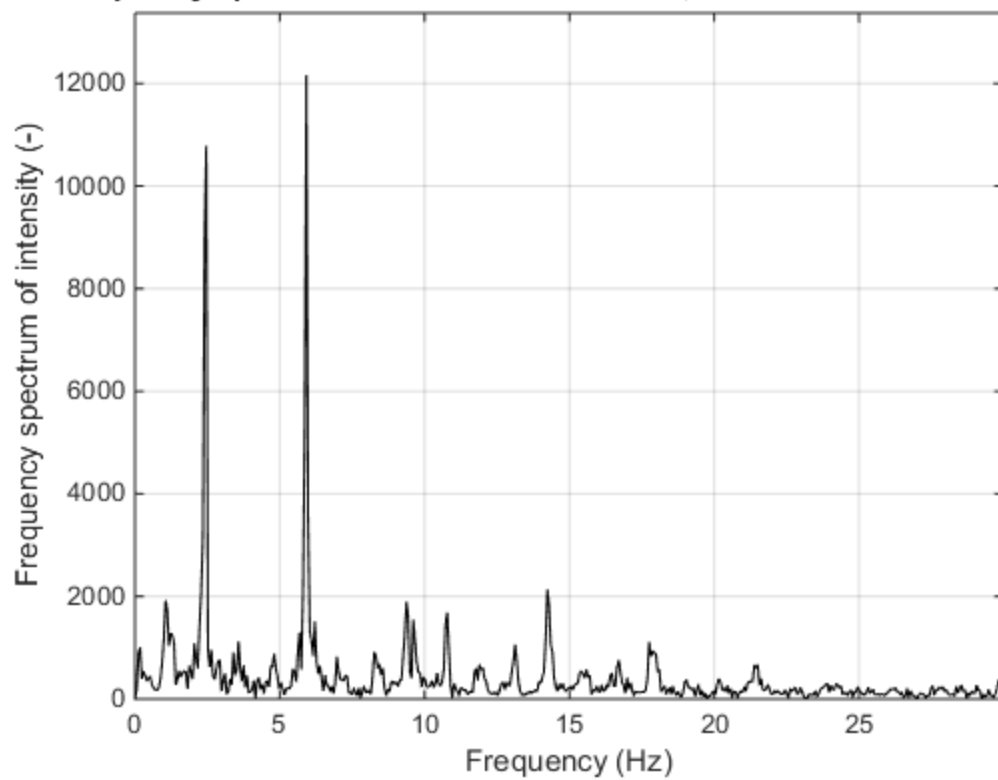


Time history of "ST Canon 03.MOV", Pixel coordinates: 522 558**Frequency spectrum of "ST Canon 03.MOV", Pixel coordinates: 522 558**

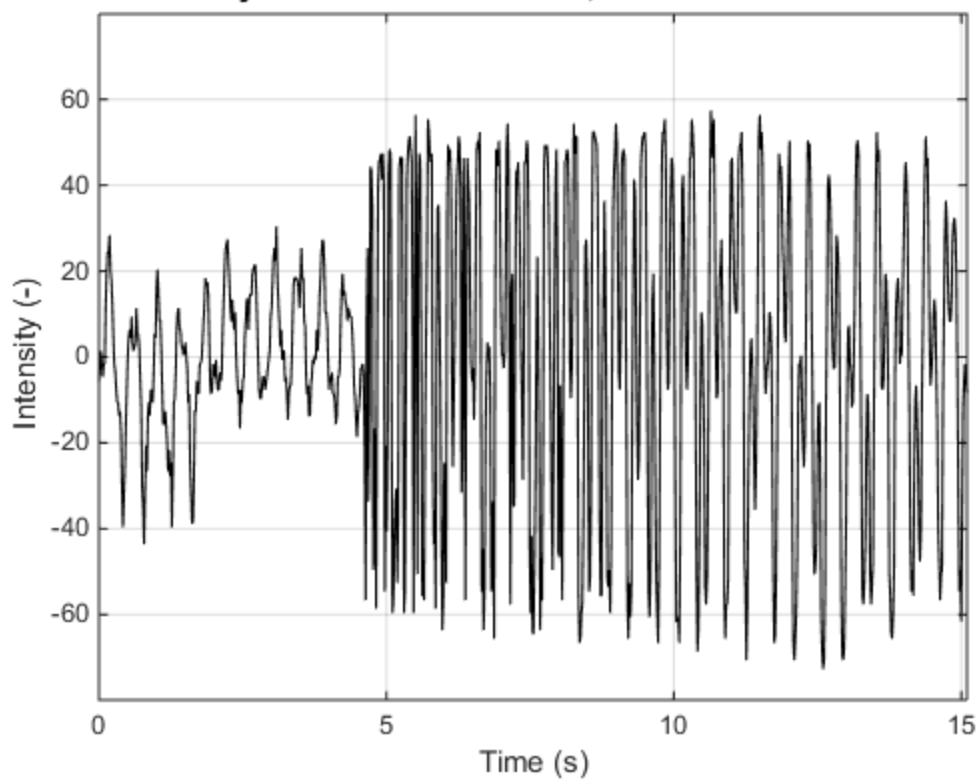
Time history of "ST Canon 04.MOV", Pixel coordinates: 522 558



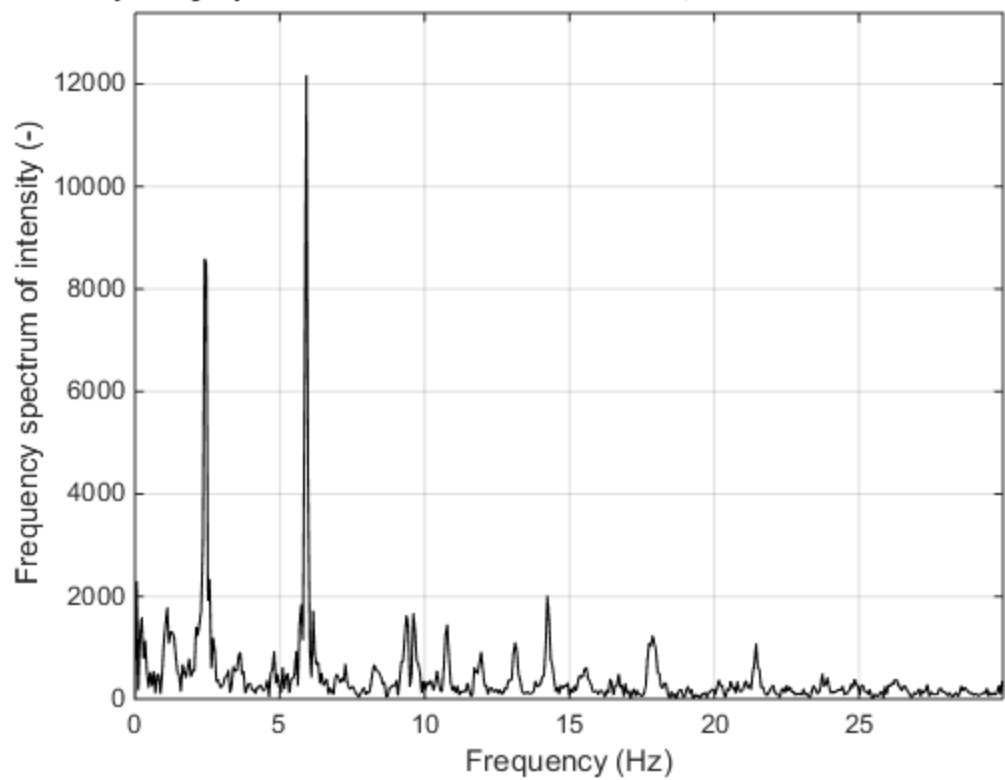
Frequency spectrum of "ST Canon 04.MOV", Pixel coordinates: 522 558



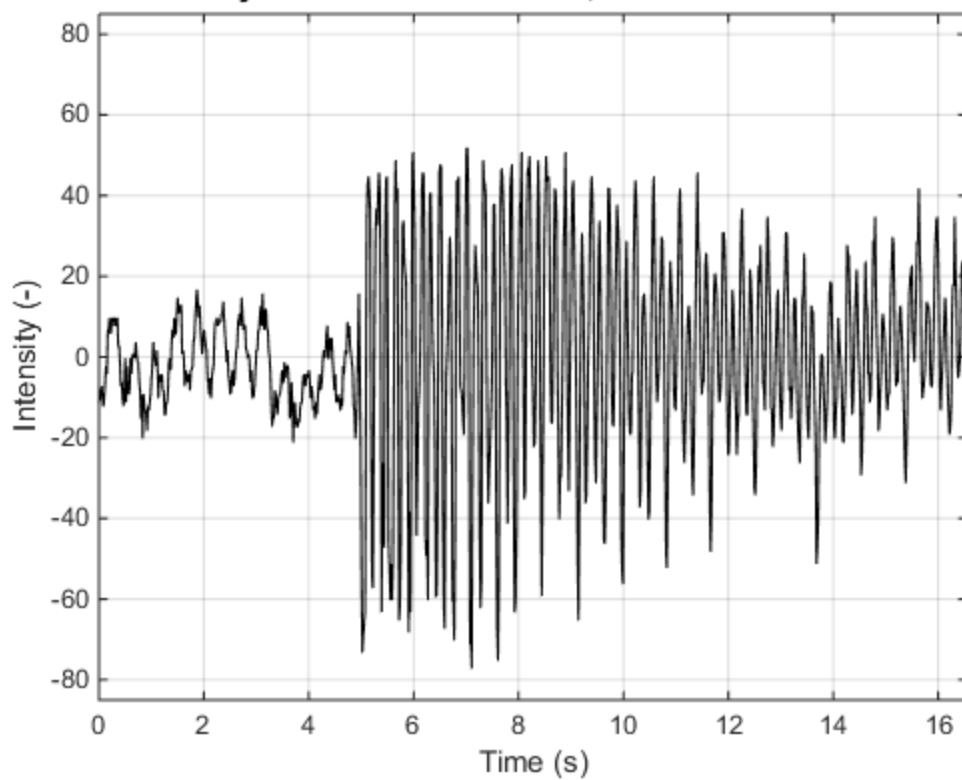
Time history of "ST Canon 05.MOV", Pixel coordinates: 522 558



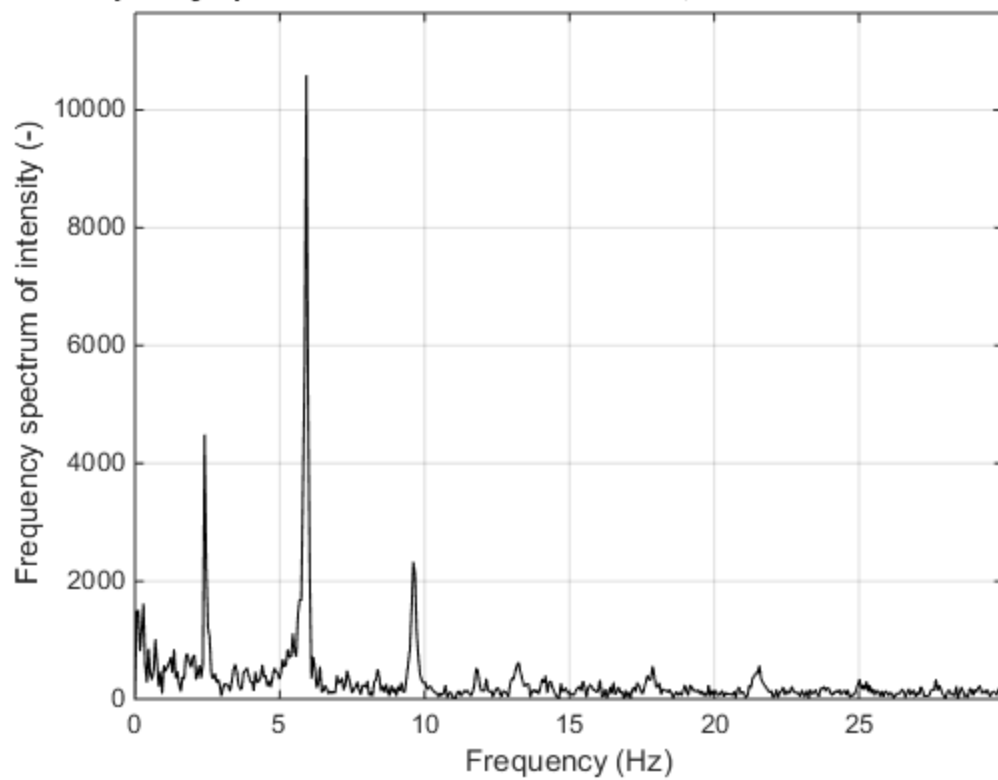
Frequency spectrum of "ST Canon 05.MOV", Pixel coordinates: 522 558



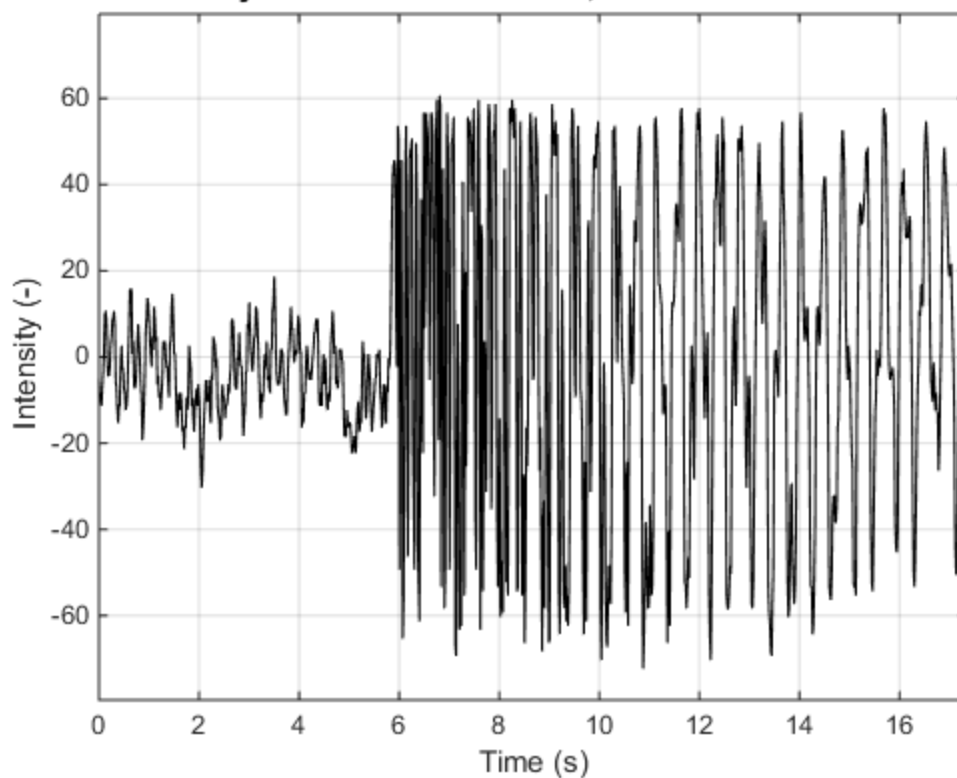
Time history of "ST Canon 06.MOV", Pixel coordinates: 522 558



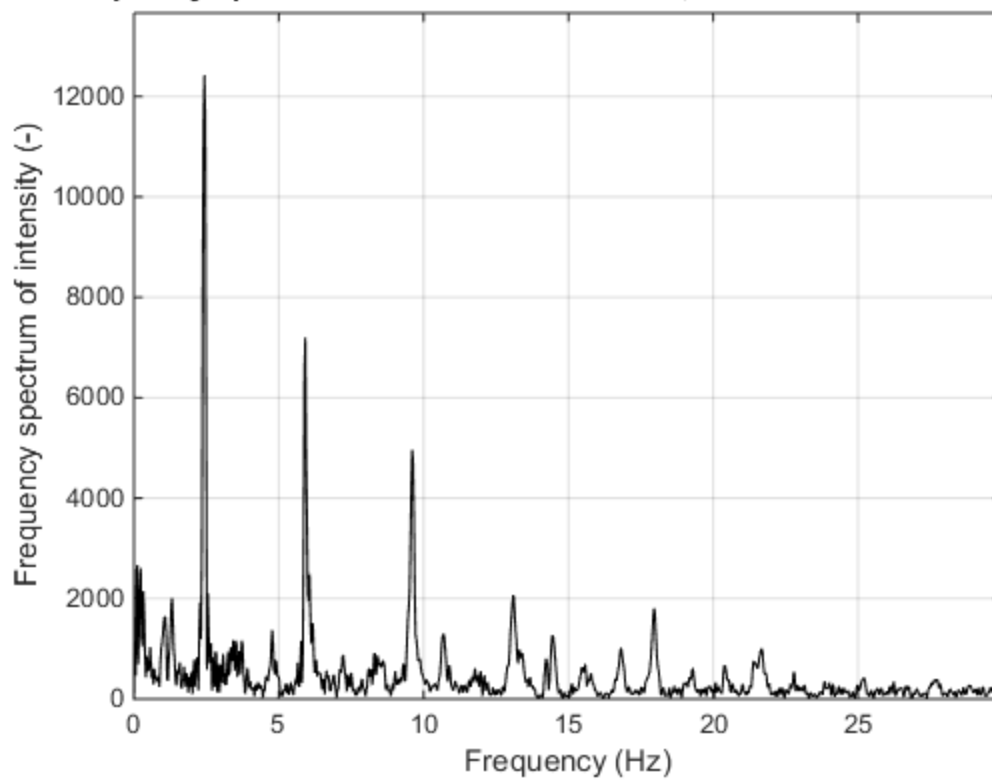
Frequency spectrum of "ST Canon 06.MOV", Pixel coordinates: 522 558



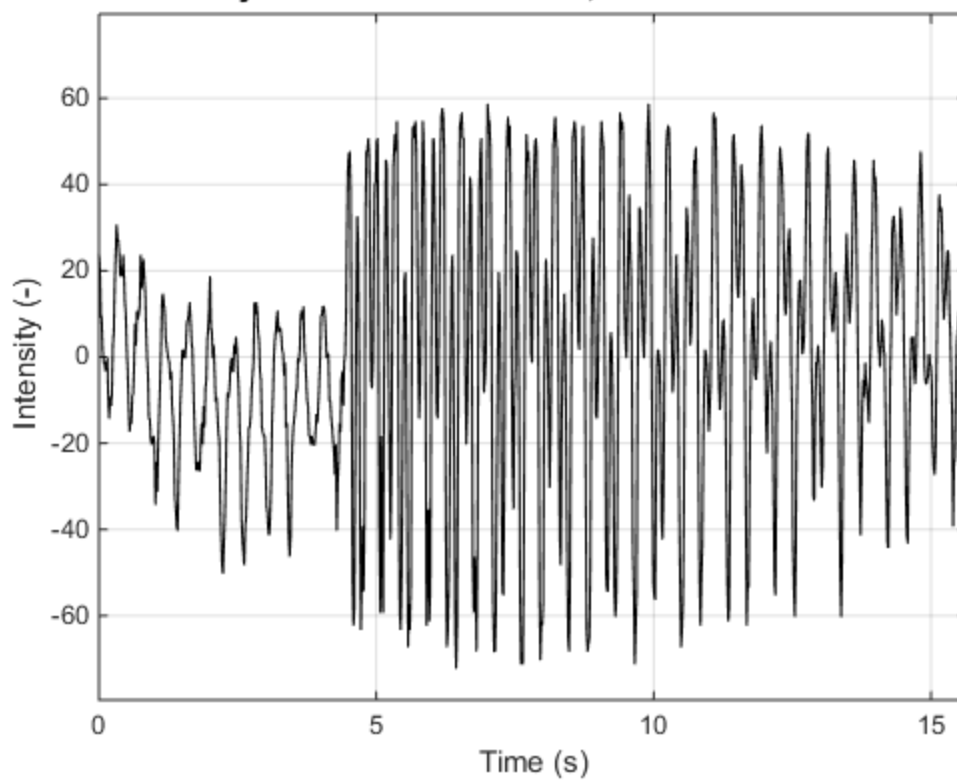
Time history of "ST Canon 07.MOV", Pixel coordinates: 522 558



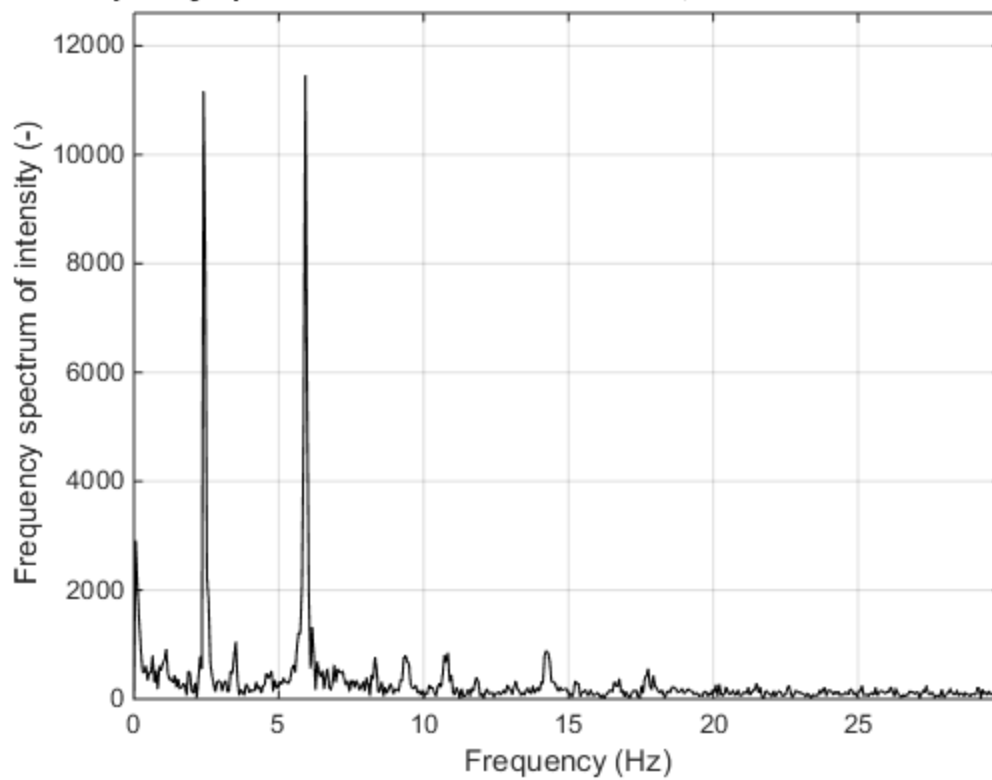
Frequency spectrum of "ST Canon 07.MOV", Pixel coordinates: 522 558

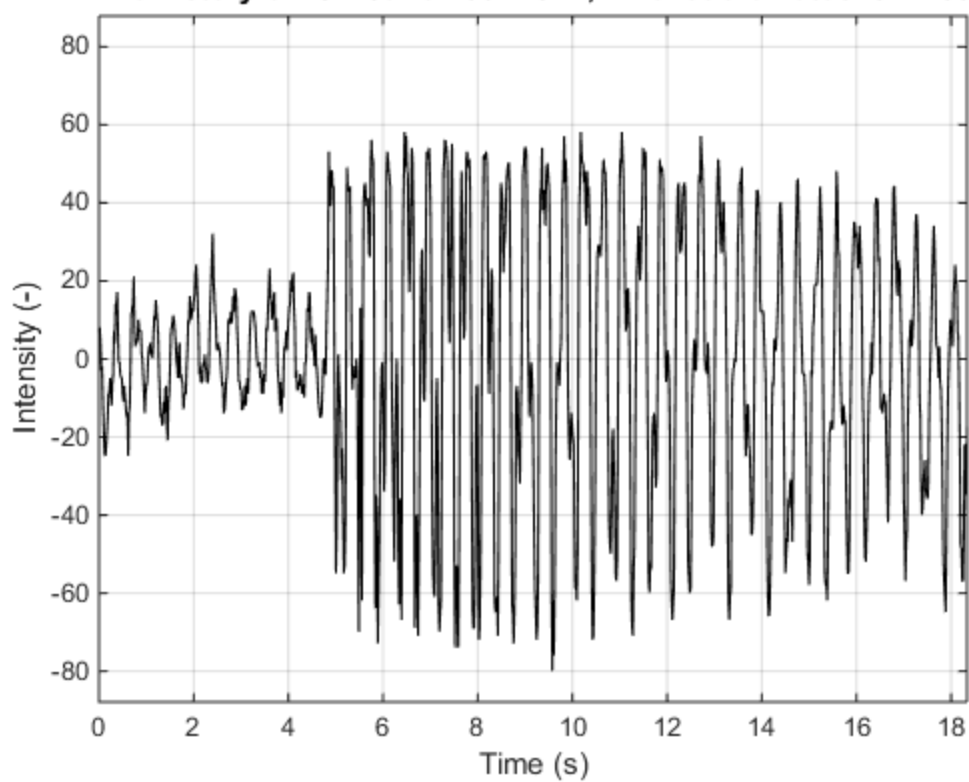
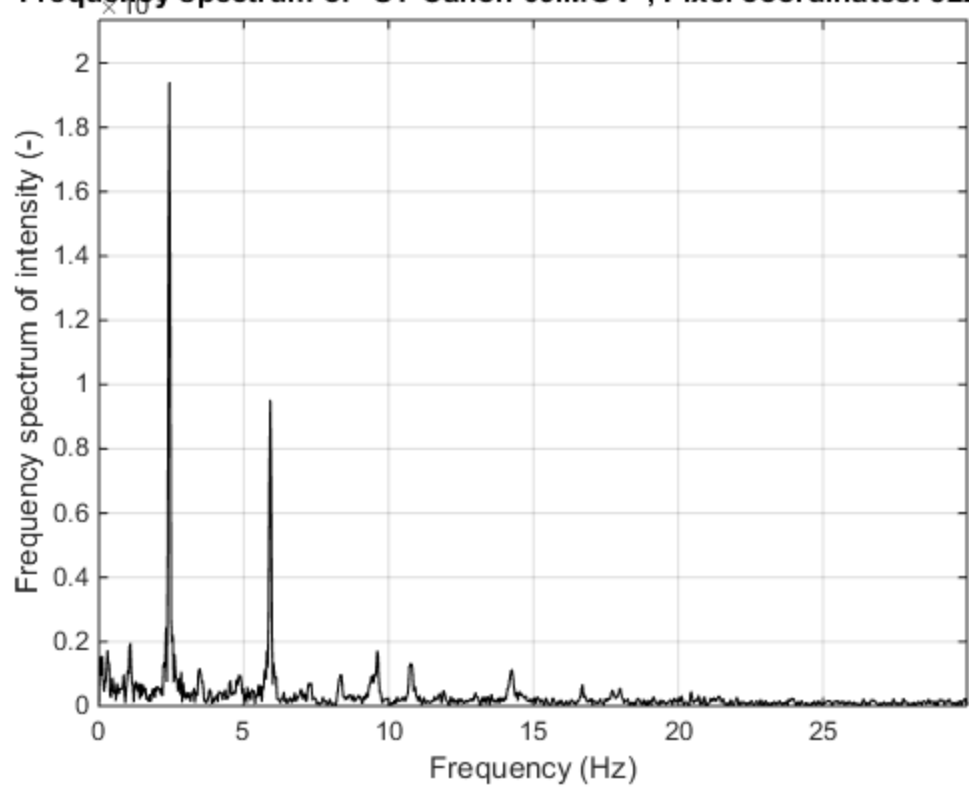


Time history of "ST Canon 08.MOV", Pixel coordinates: 522 558

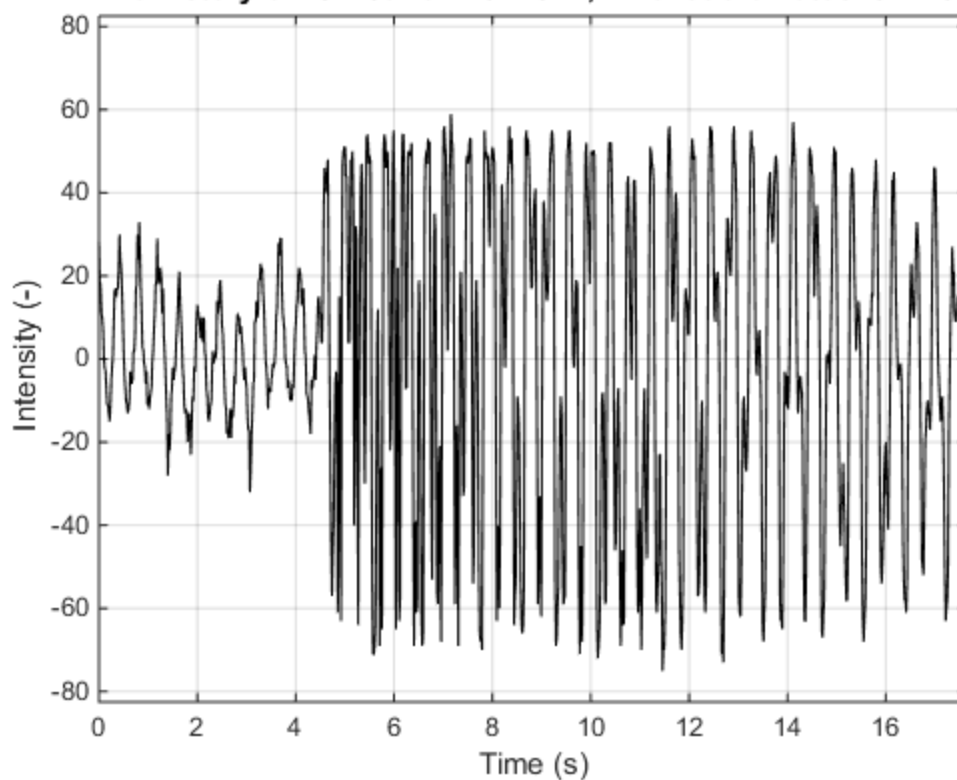


Frequency spectrum of "ST Canon 08.MOV", Pixel coordinates: 522 558

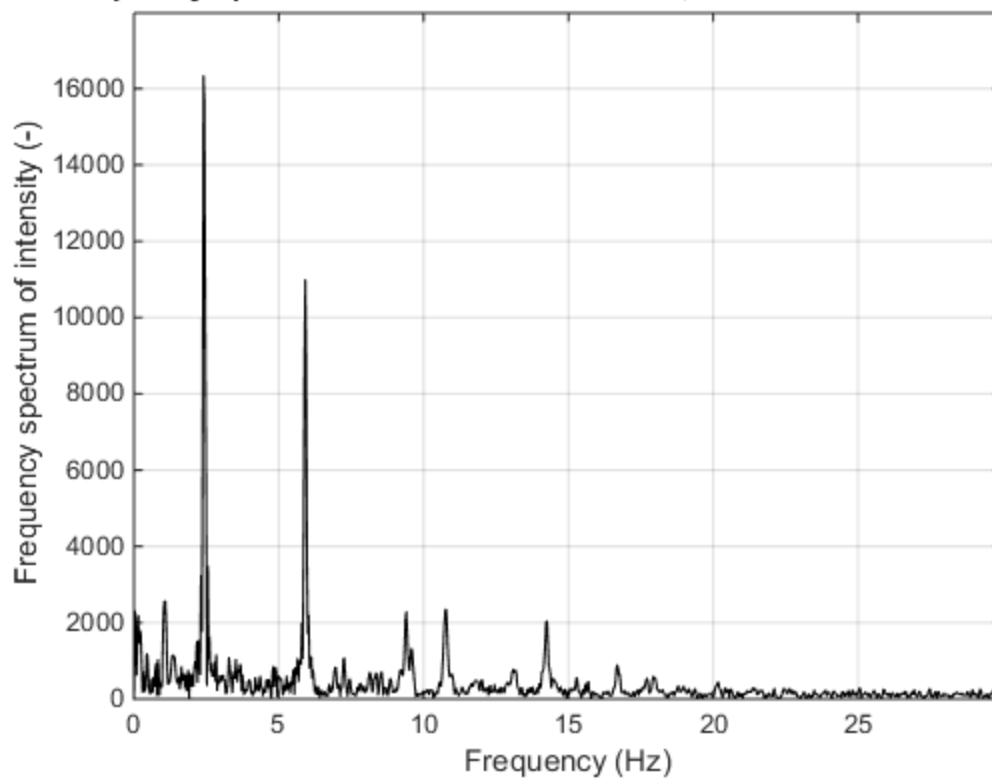


Time history of "ST Canon 09.MOV", Pixel coordinates: 522 558**Frequency spectrum of "ST Canon 09.MOV", Pixel coordinates: 522 558**

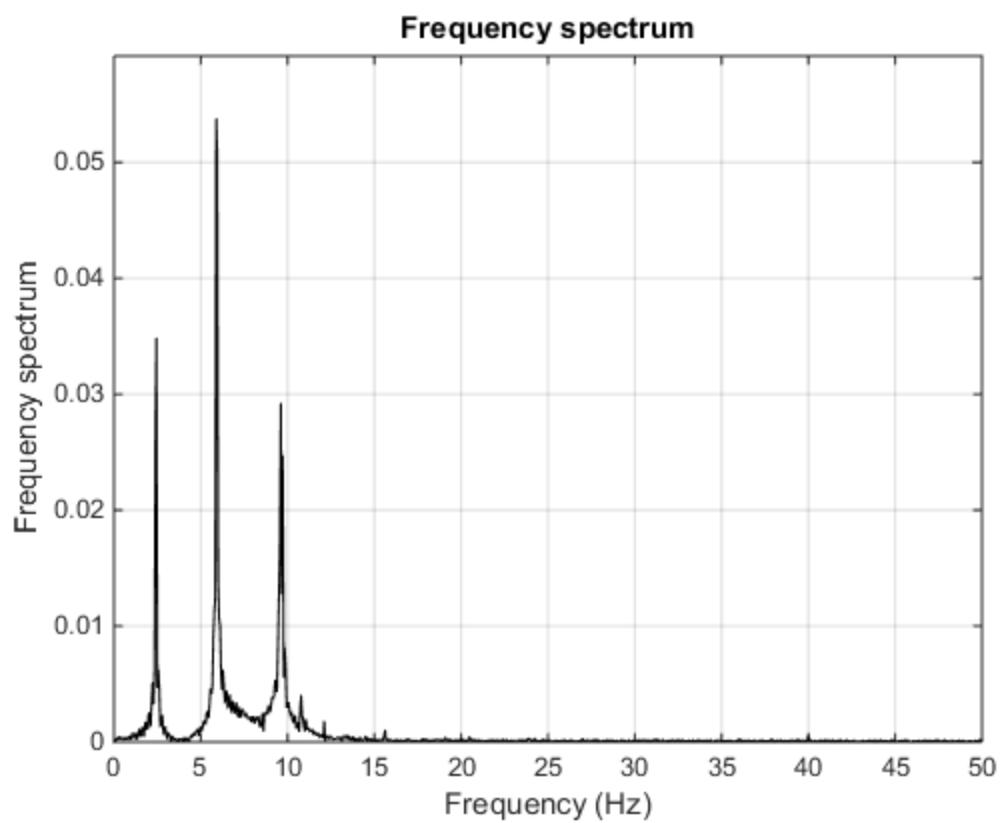
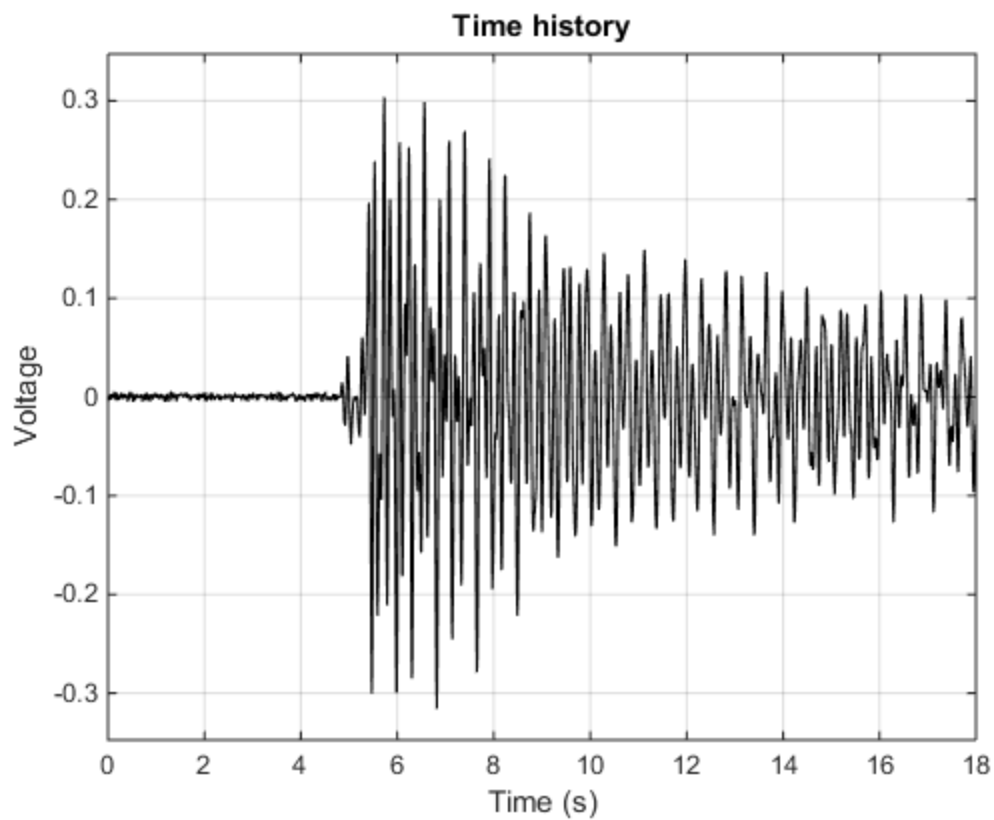
Time history of "ST Canon 10.MOV", Pixel coordinates: 522 558

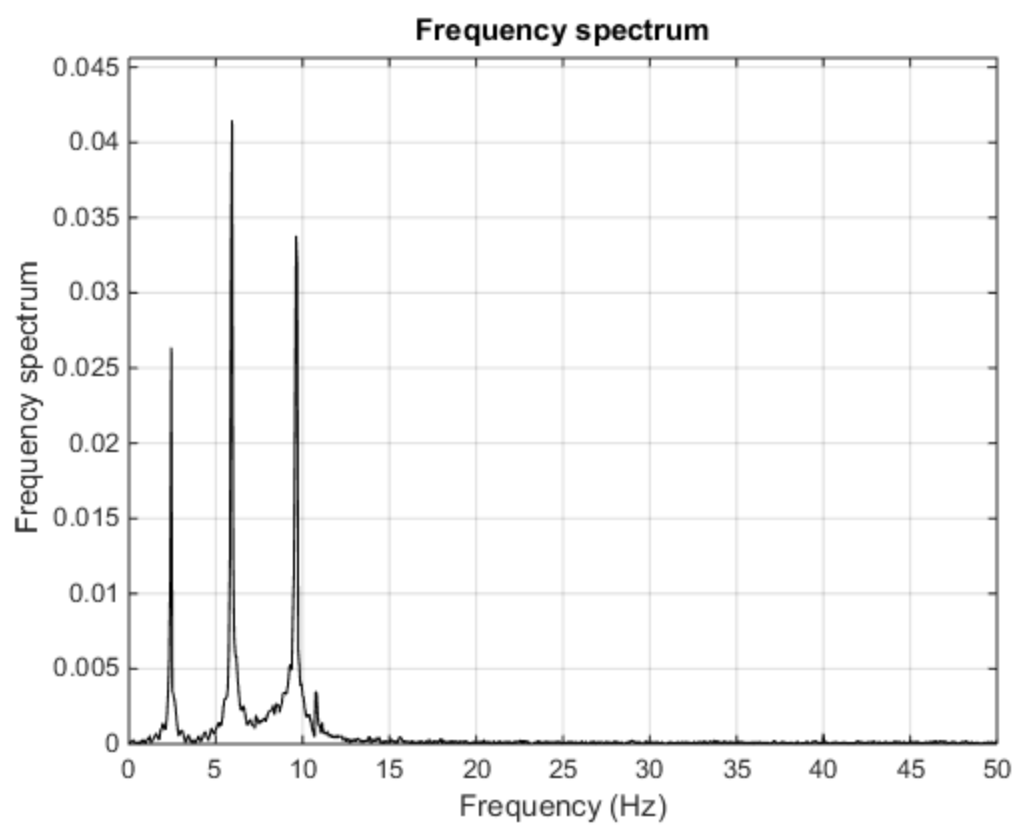
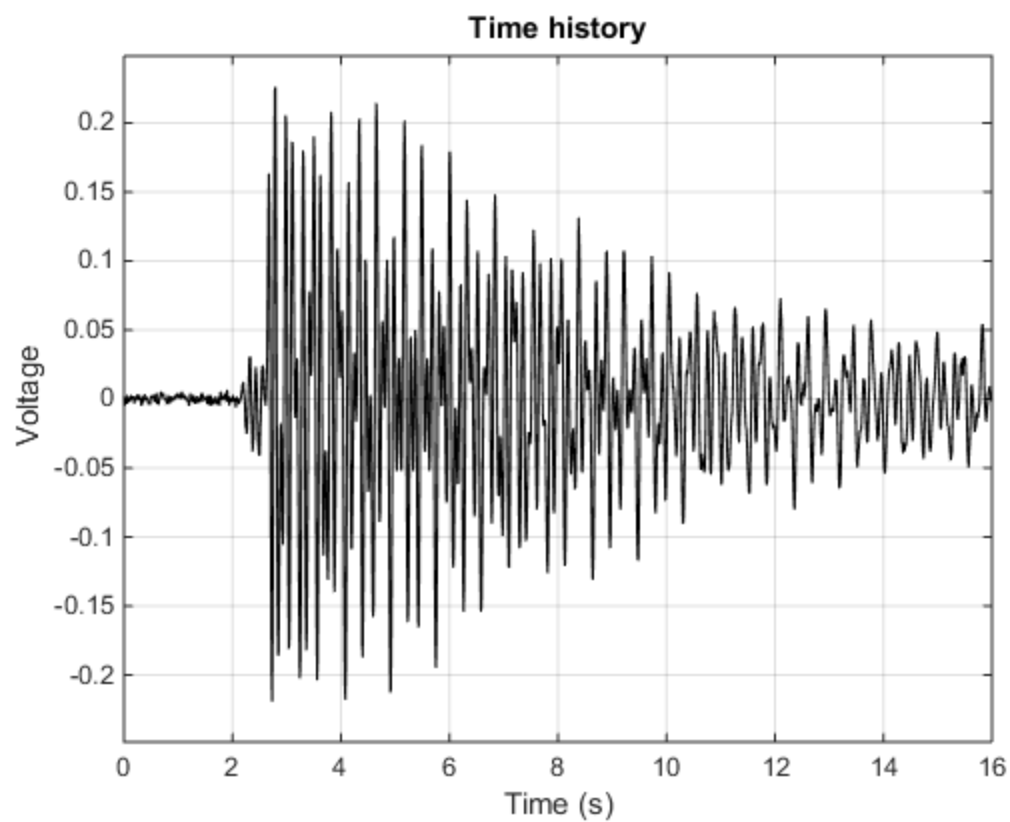


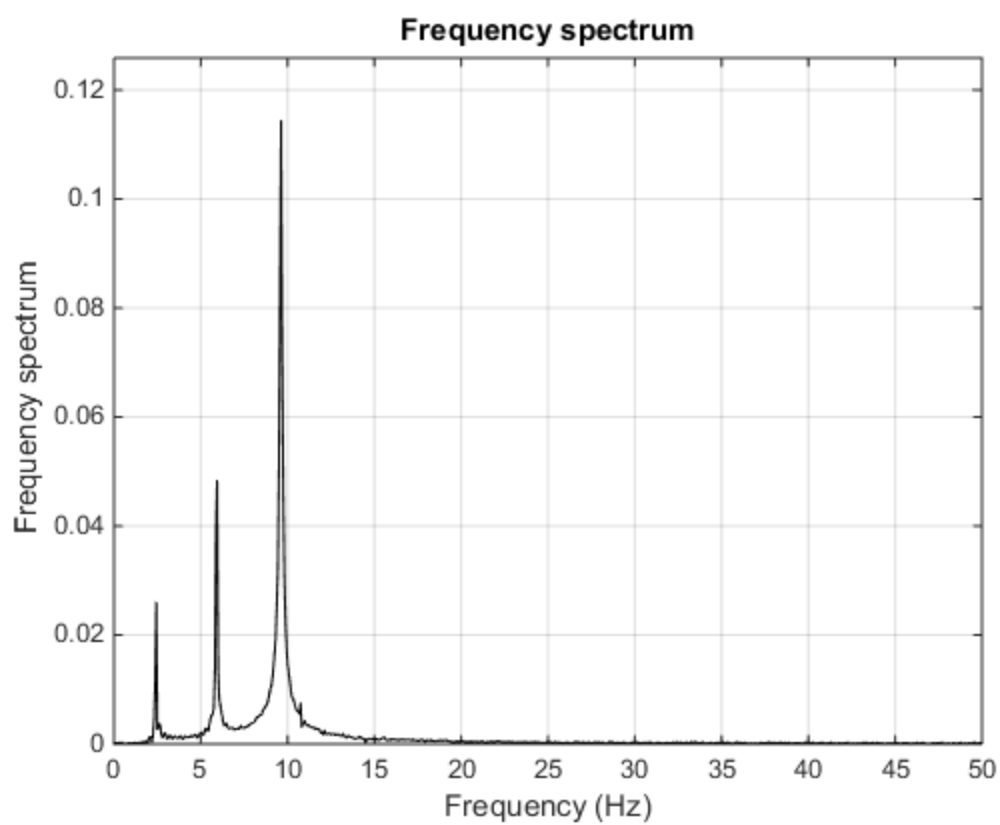
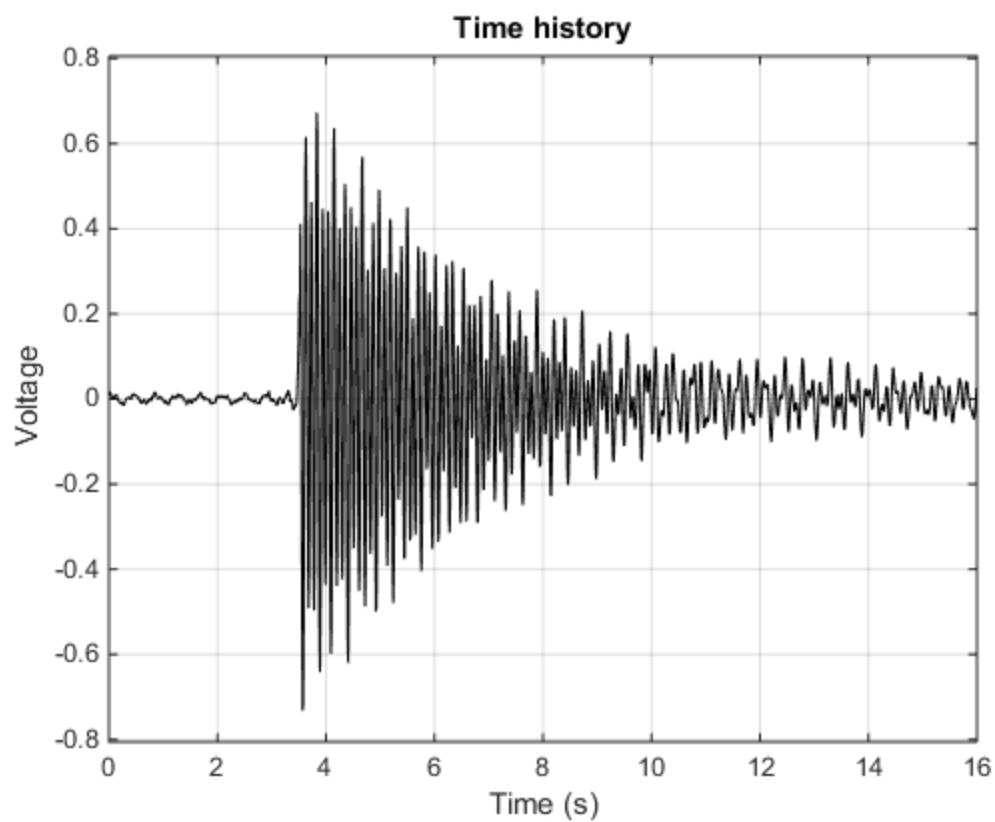
Frequency spectrum of "ST Canon 10.MOV", Pixel coordinates: 522 558

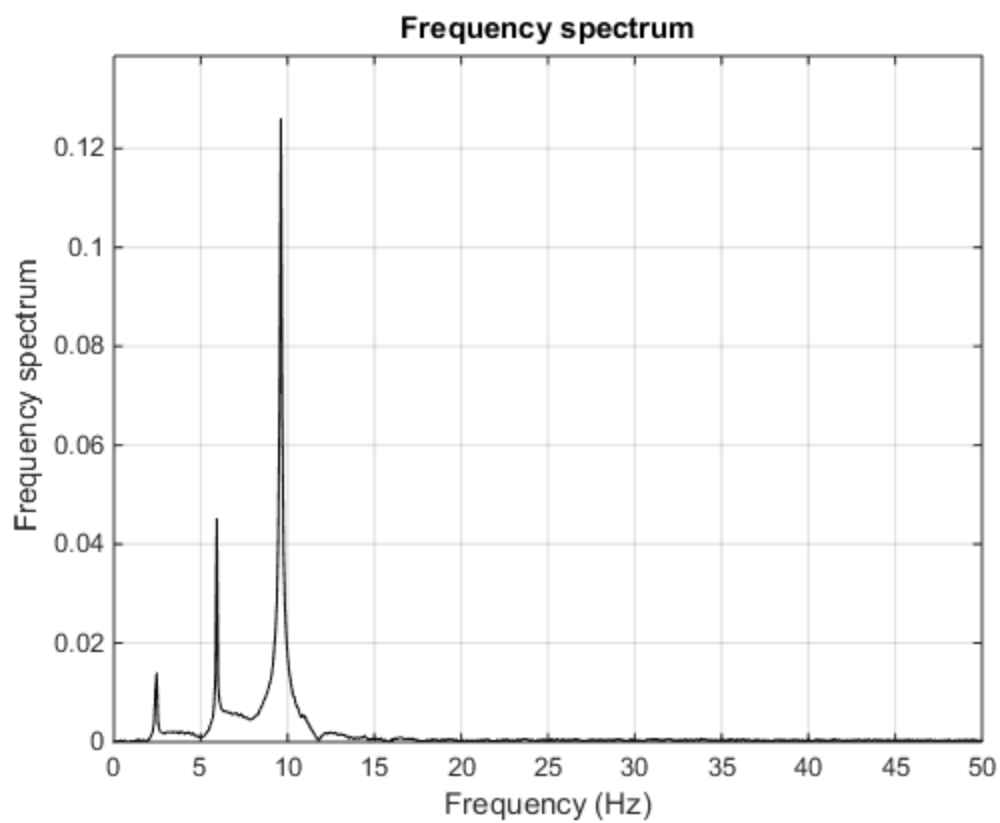
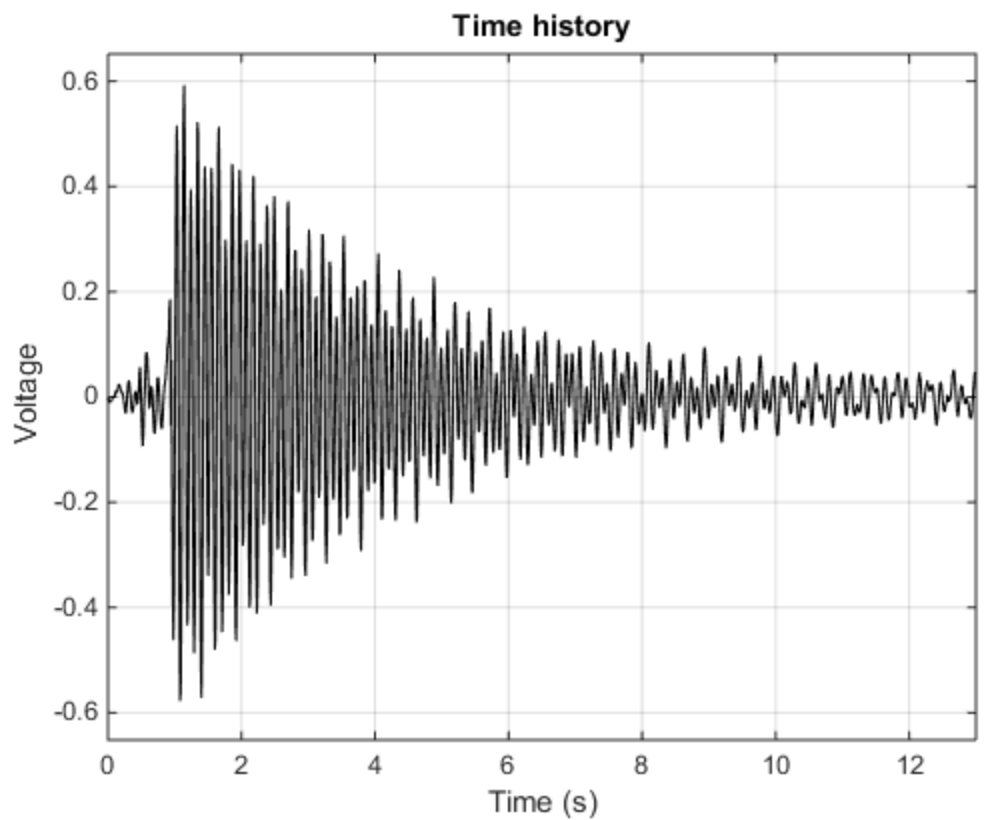


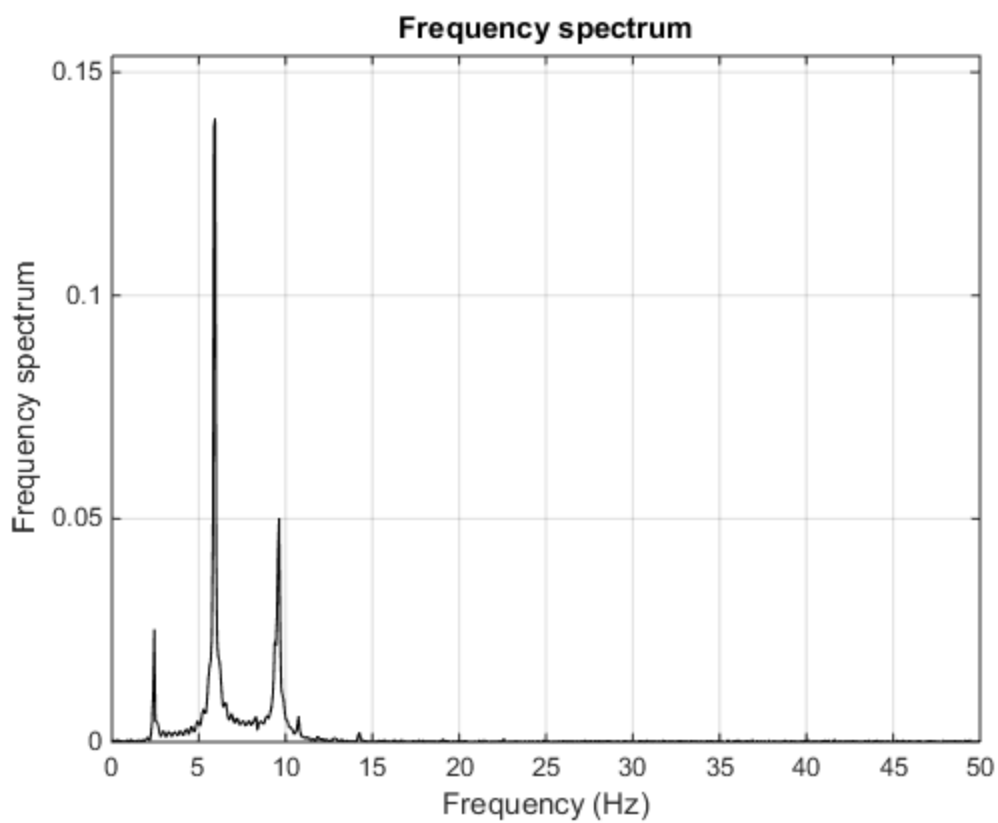
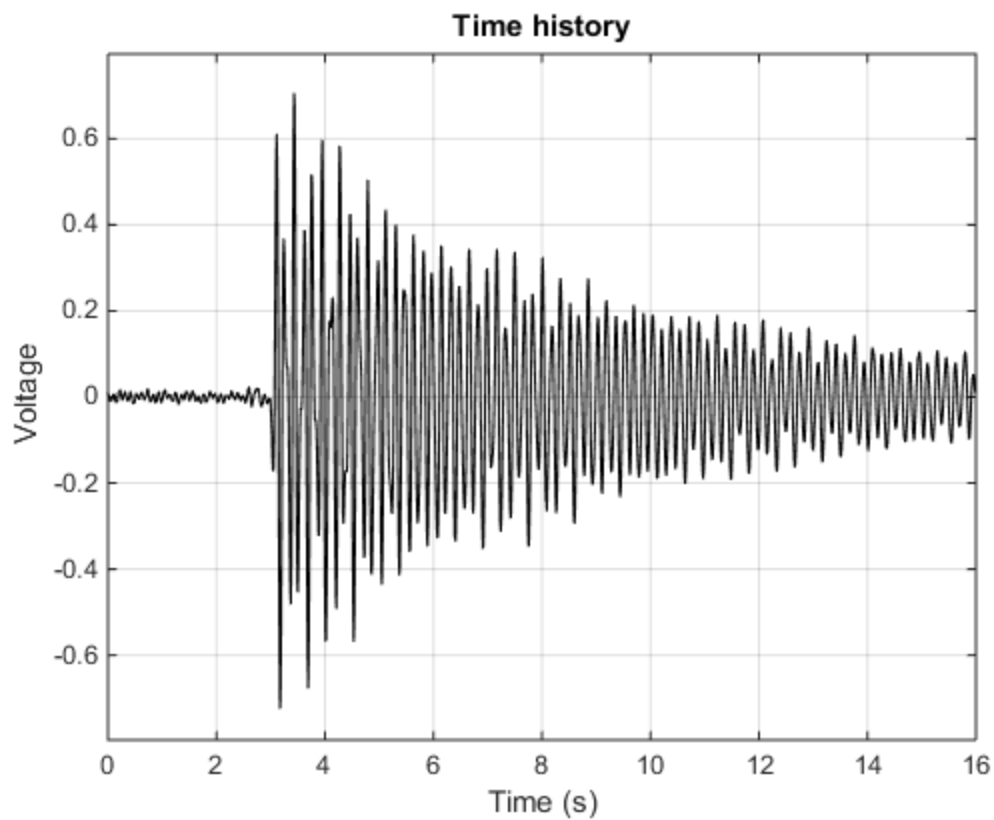
Appendix M – Shake Table Accelerometer Figures (GoPro)

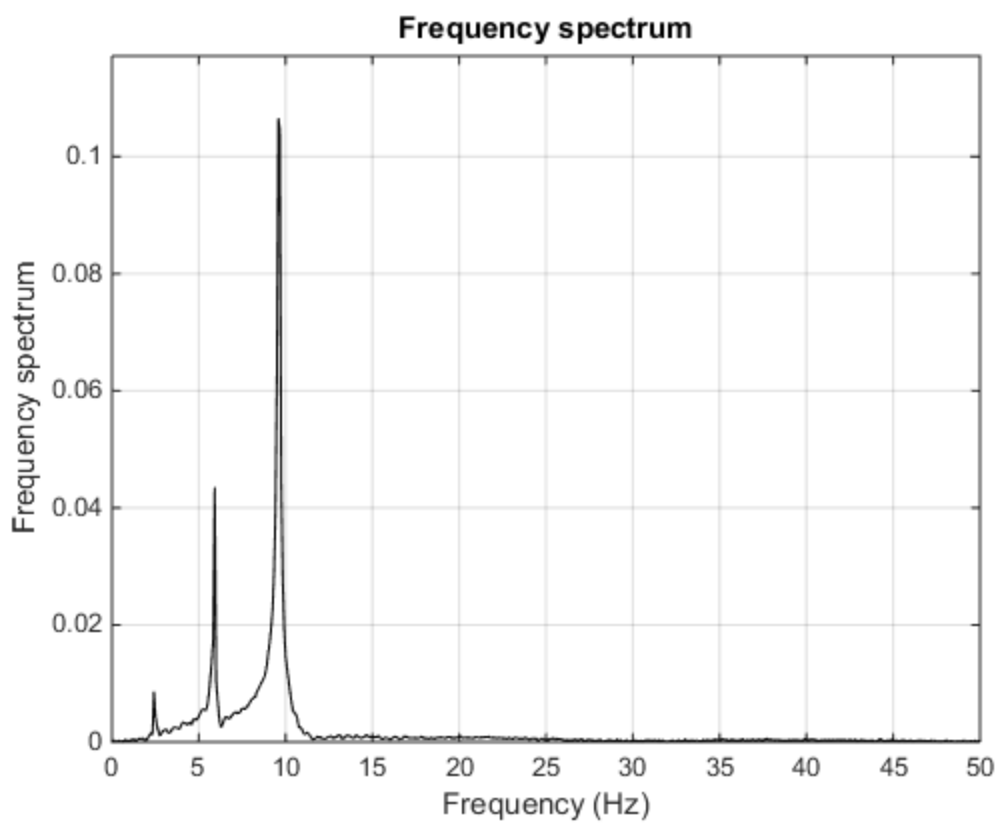
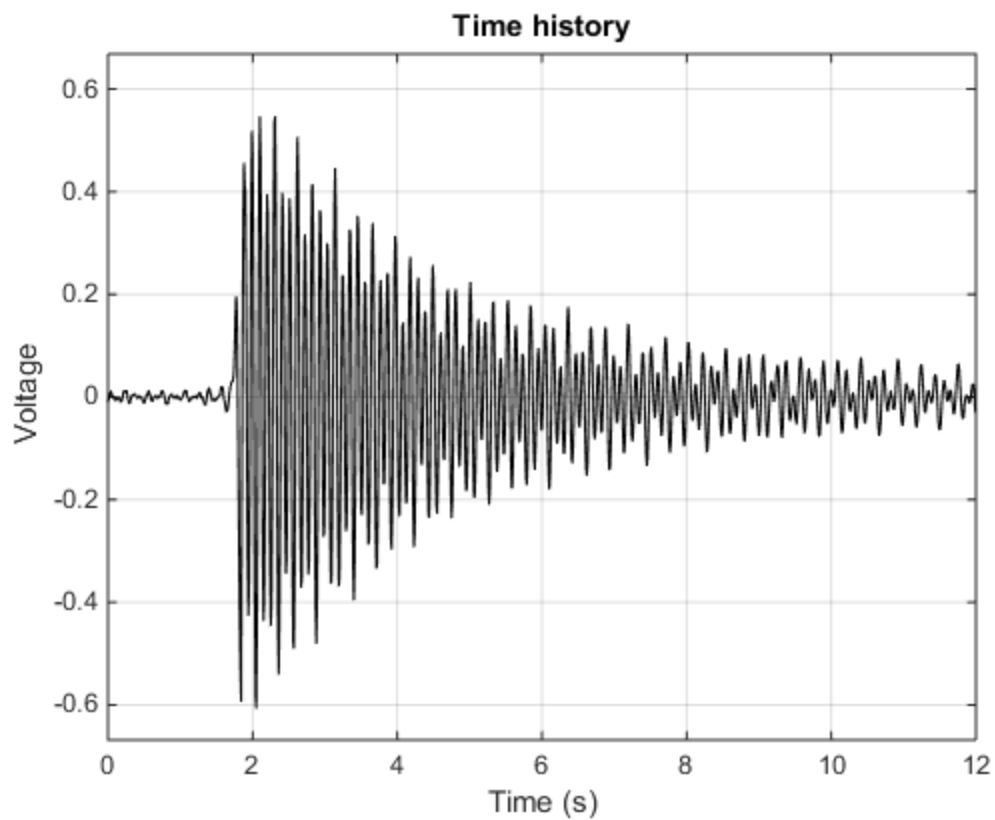


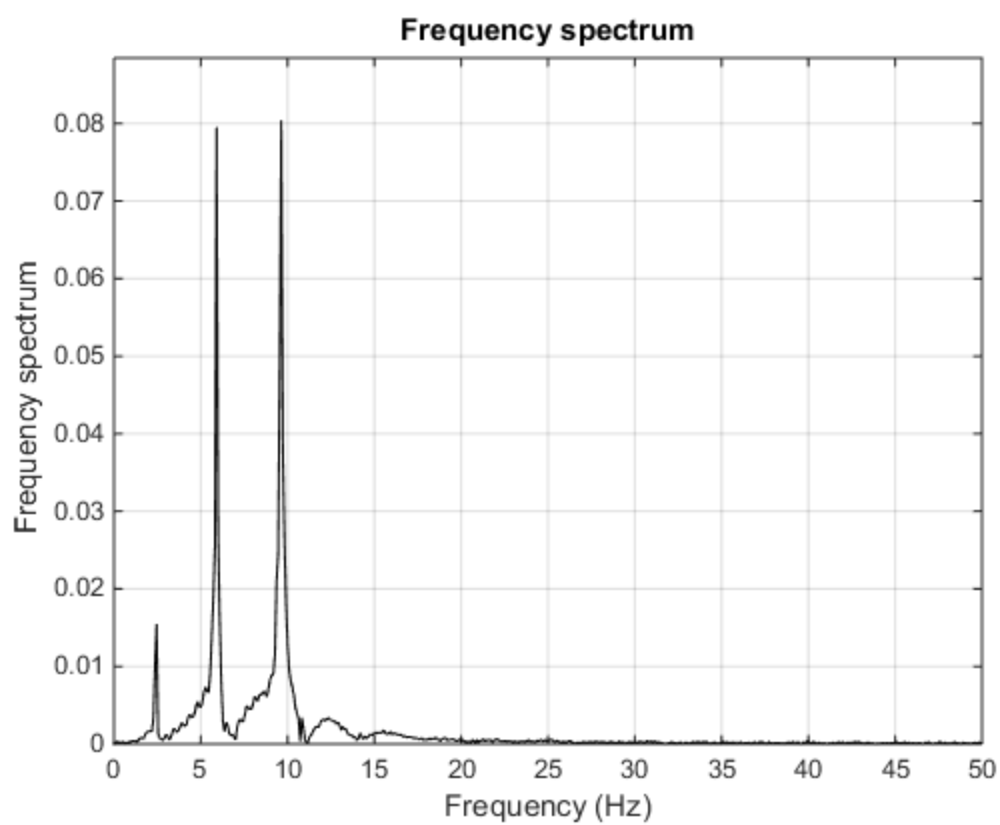
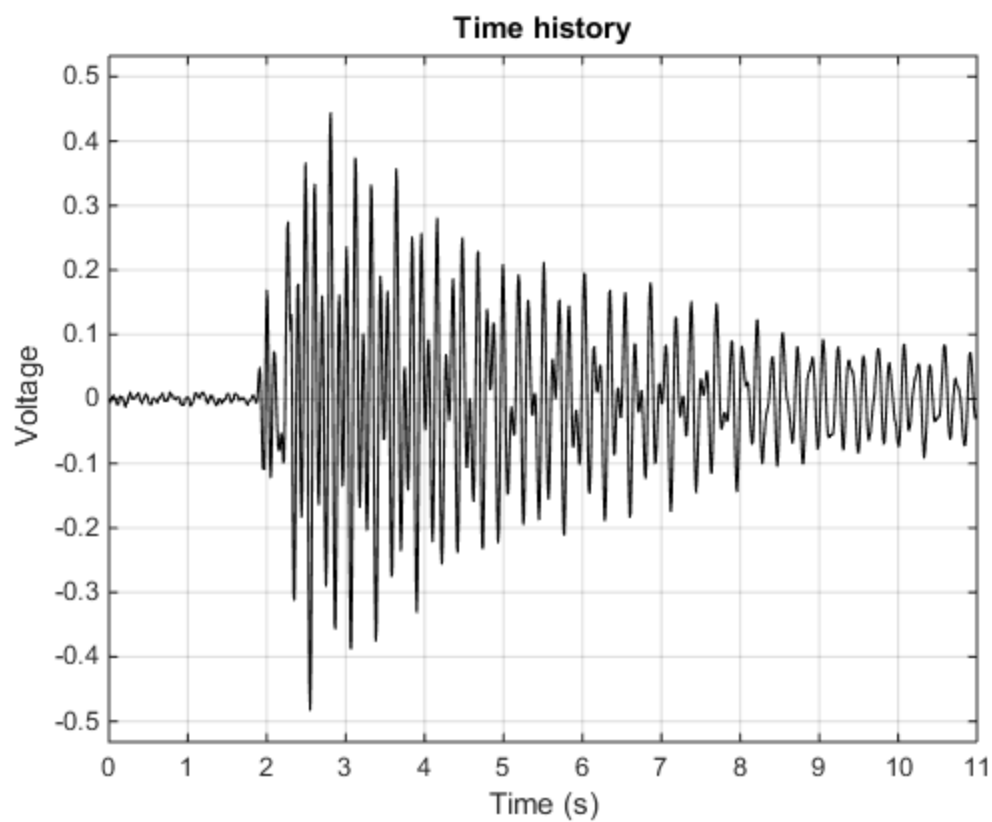


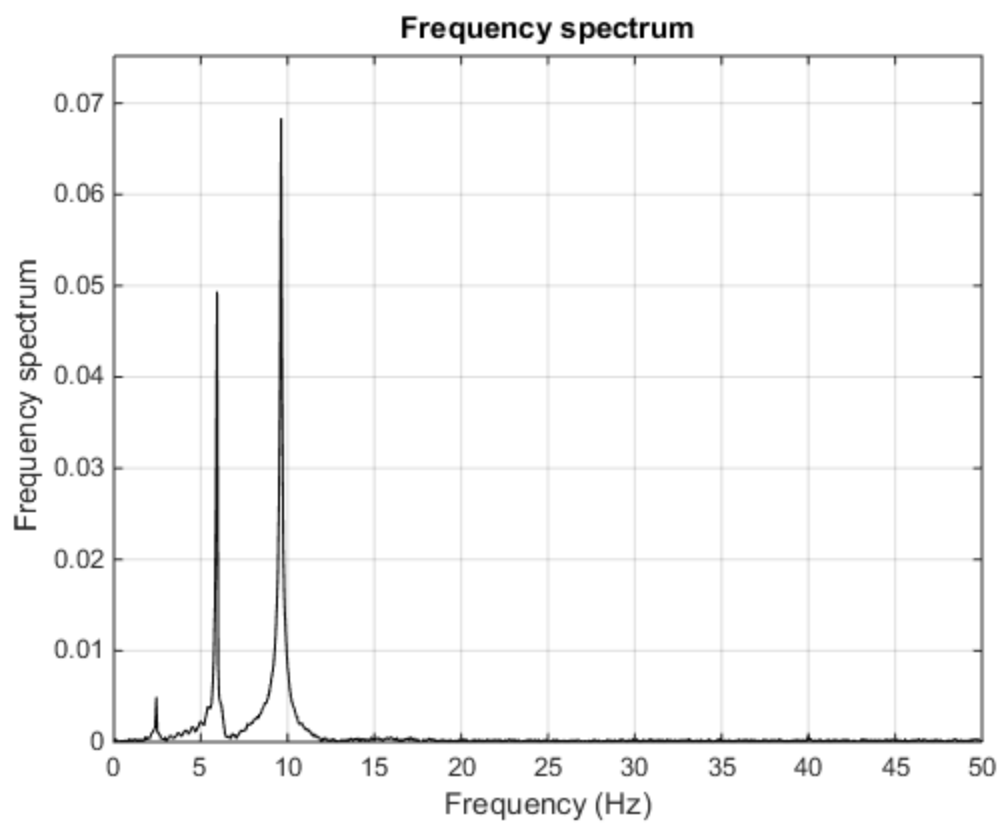
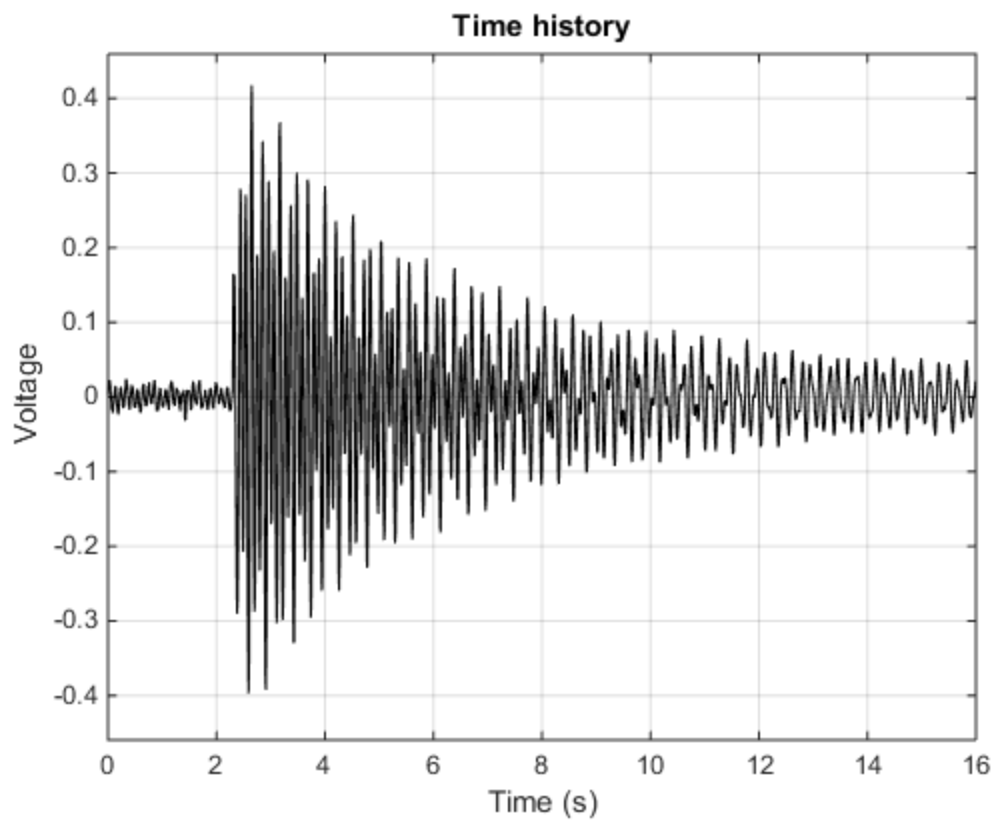


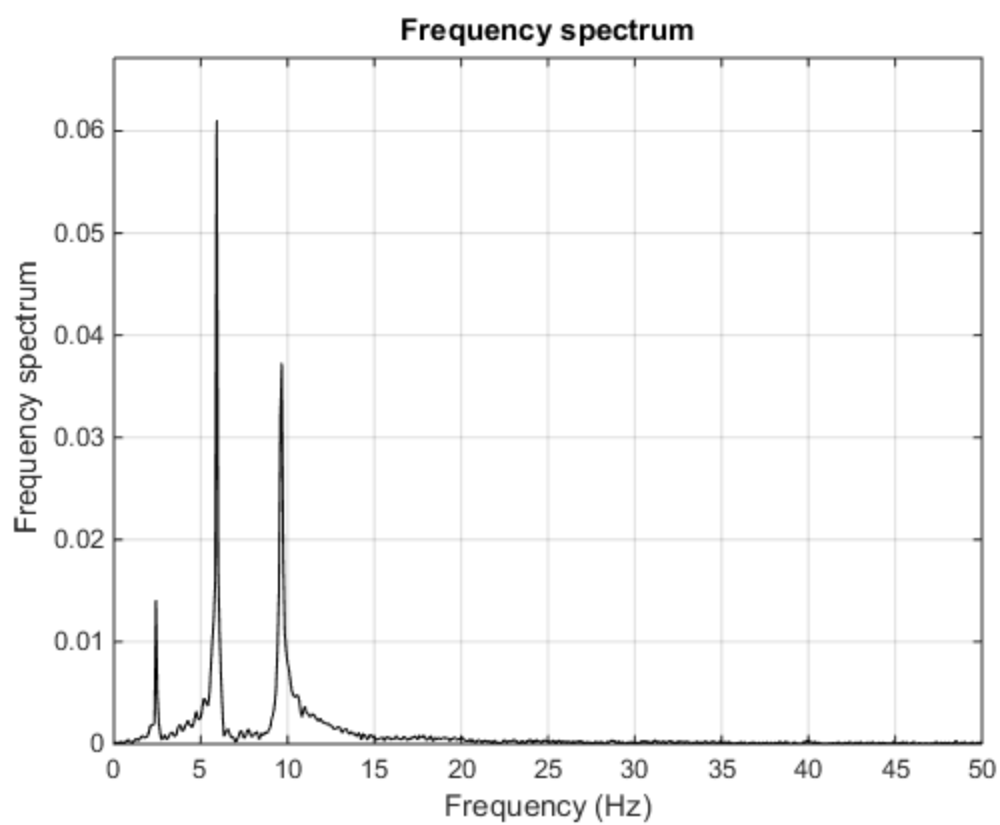
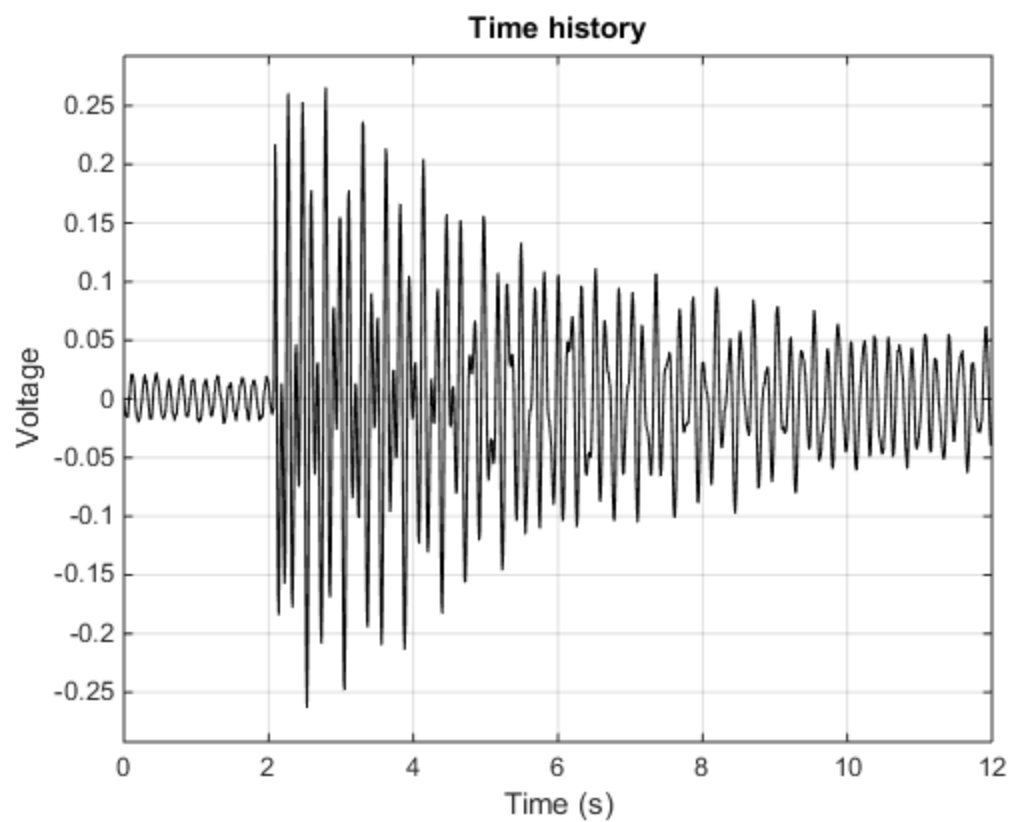


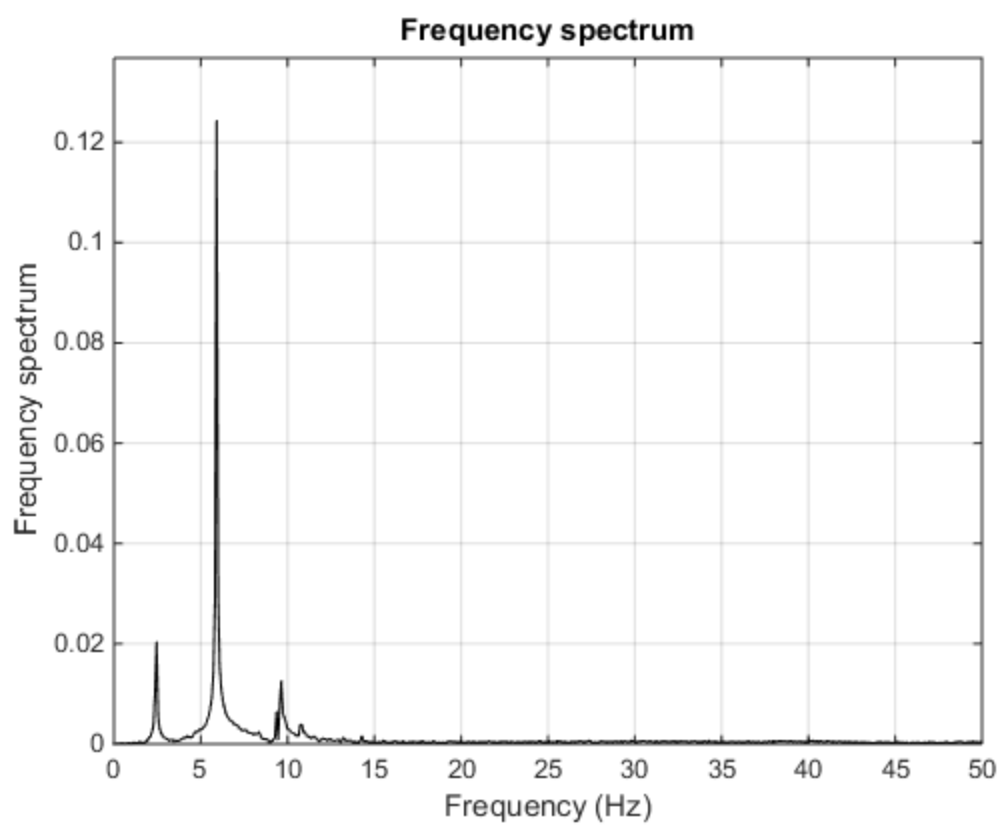
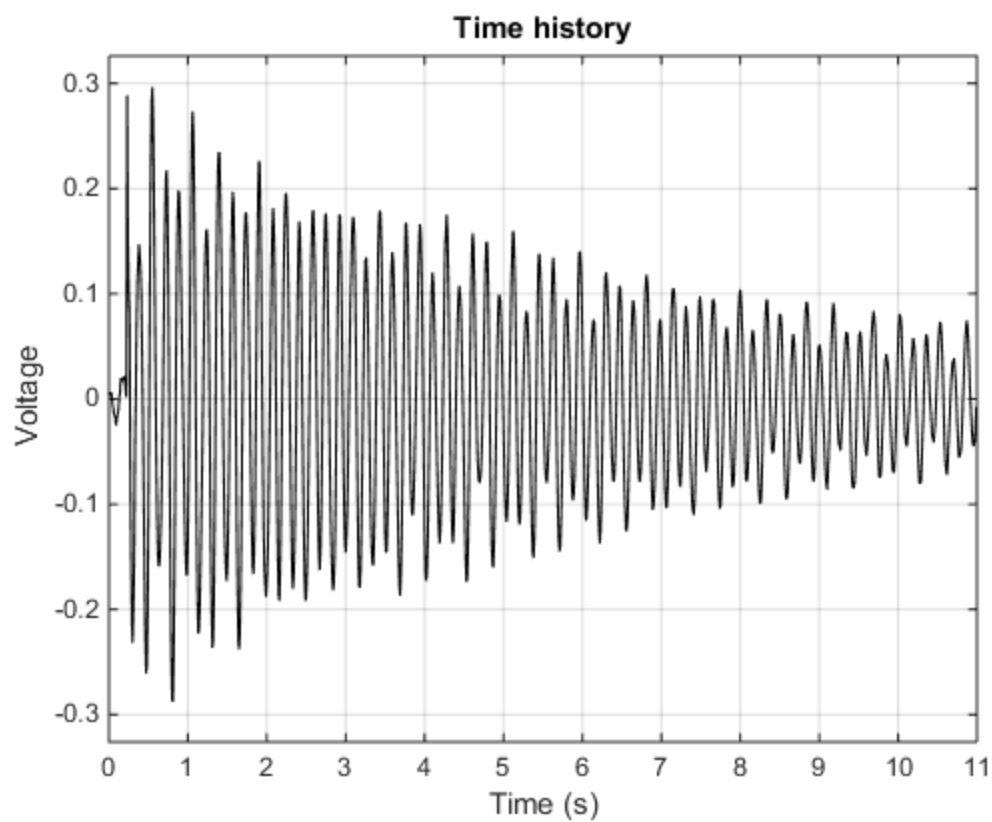






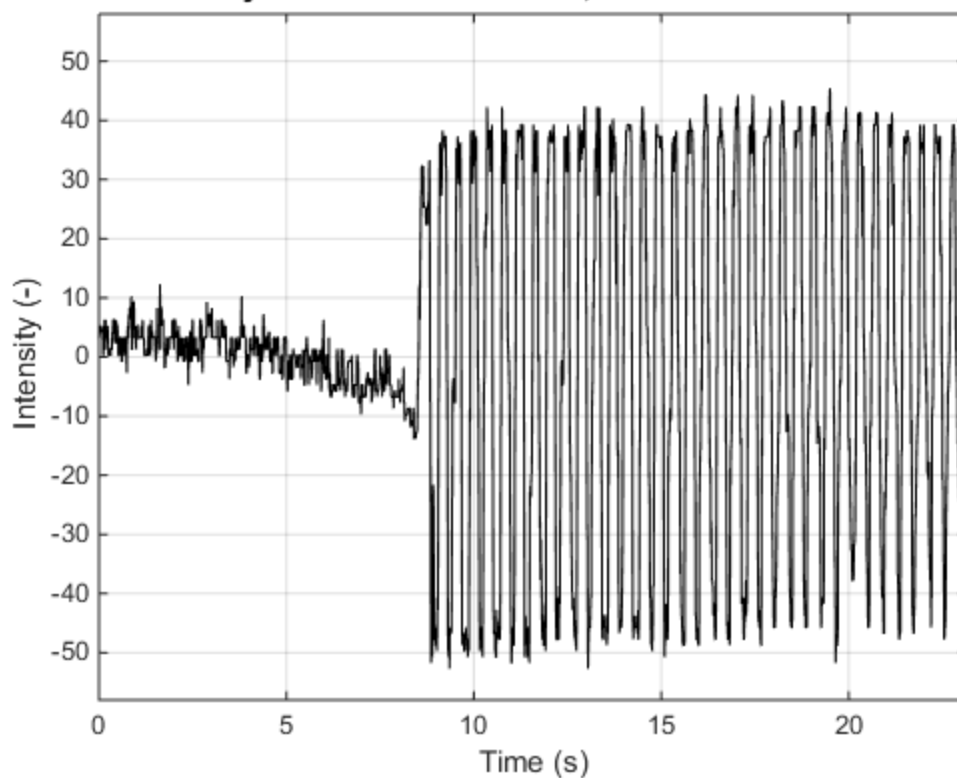




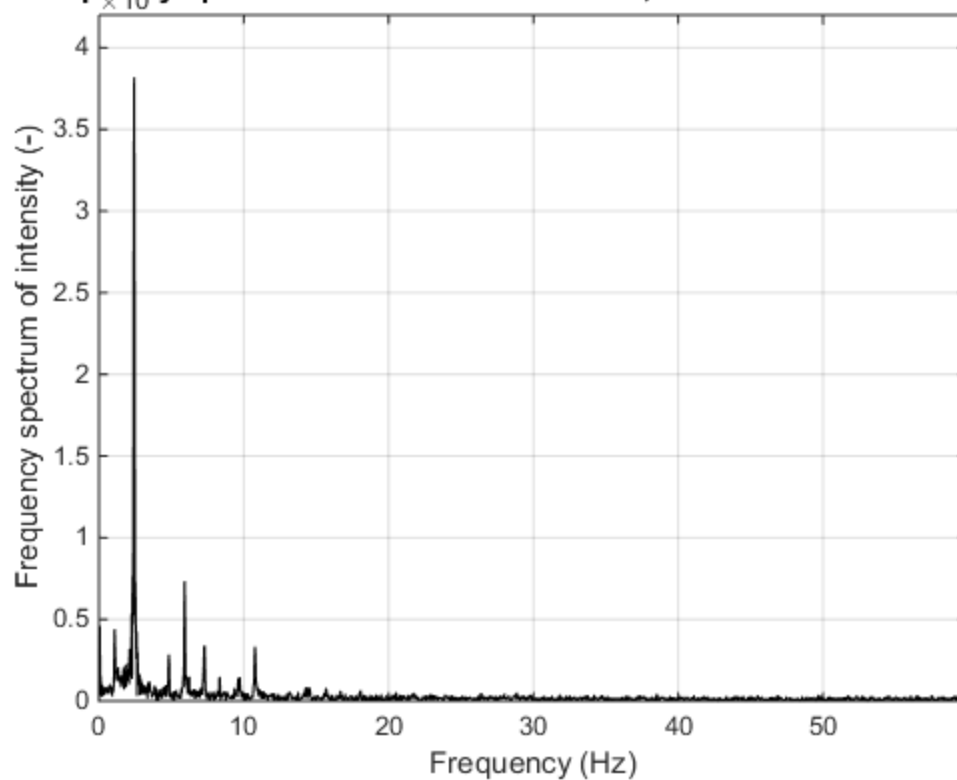


Appendix N – Shake Table VVS Figures (GoPro)

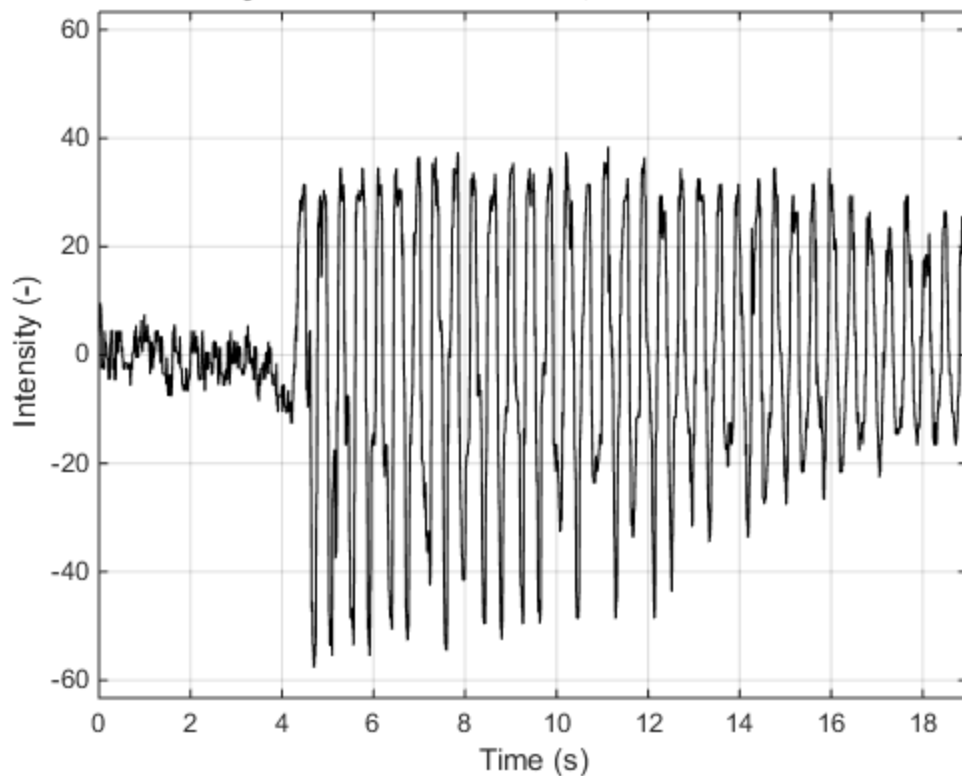
Time history of "ST GoPro 01.MP4", Pixel coordinates: 504 602



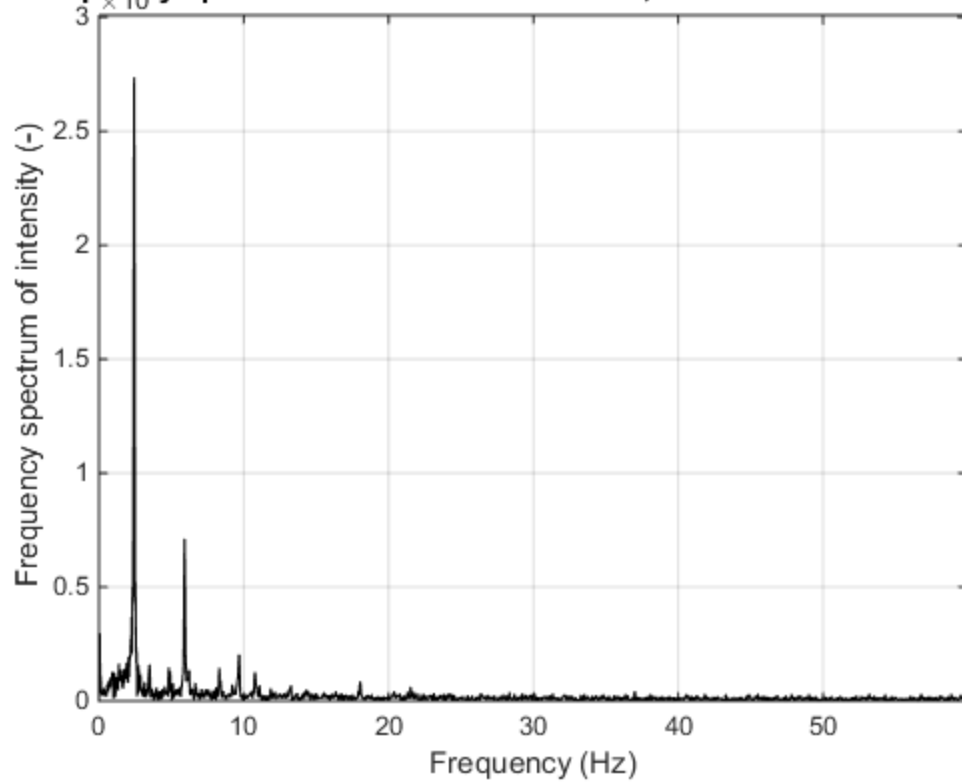
Frequency spectrum of "ST GoPro 01.MP4", Pixel coordinates: 504 602

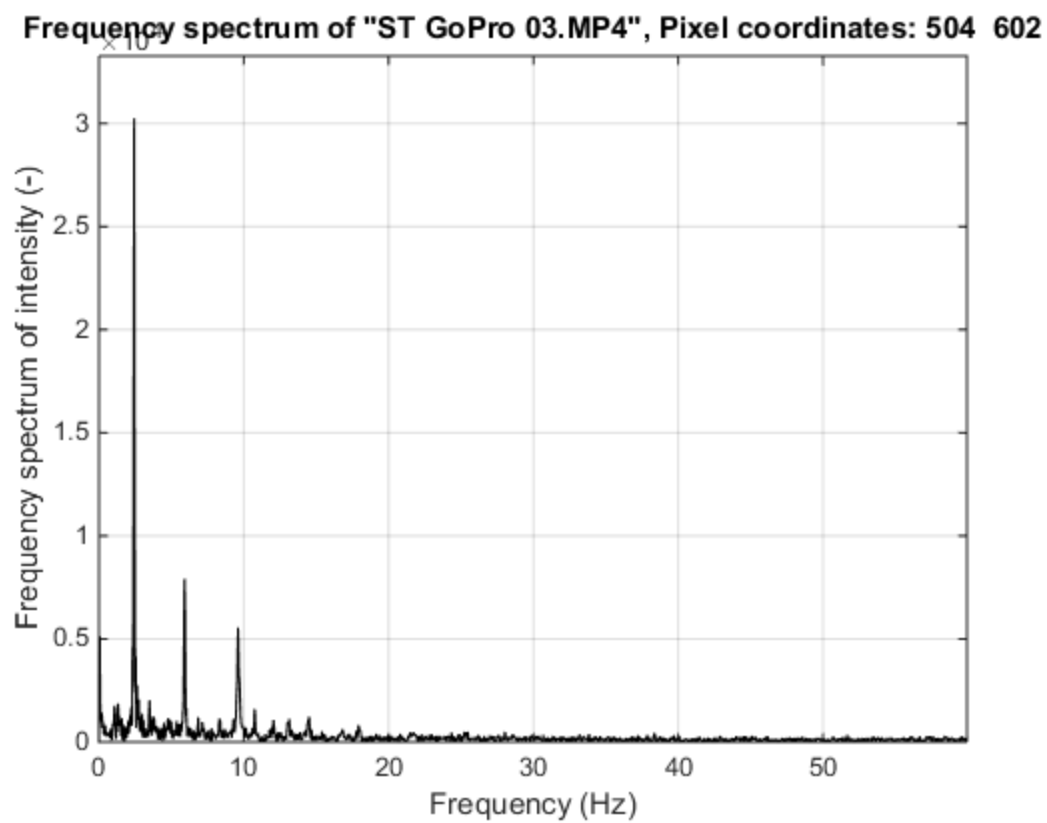
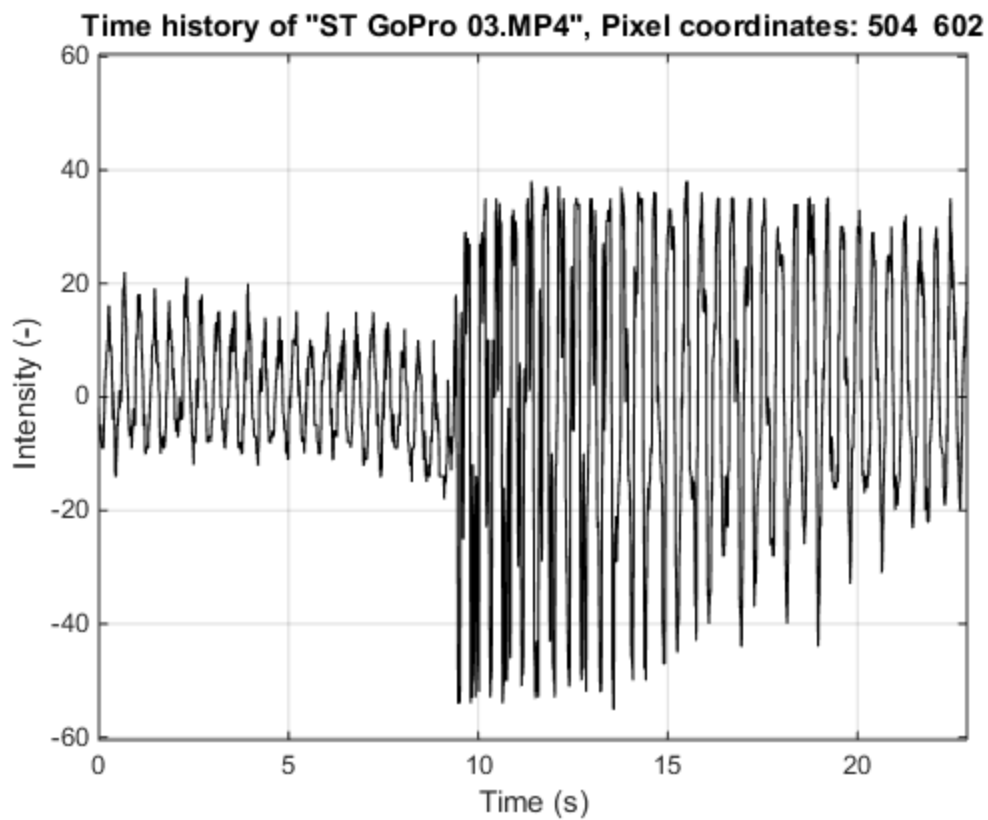


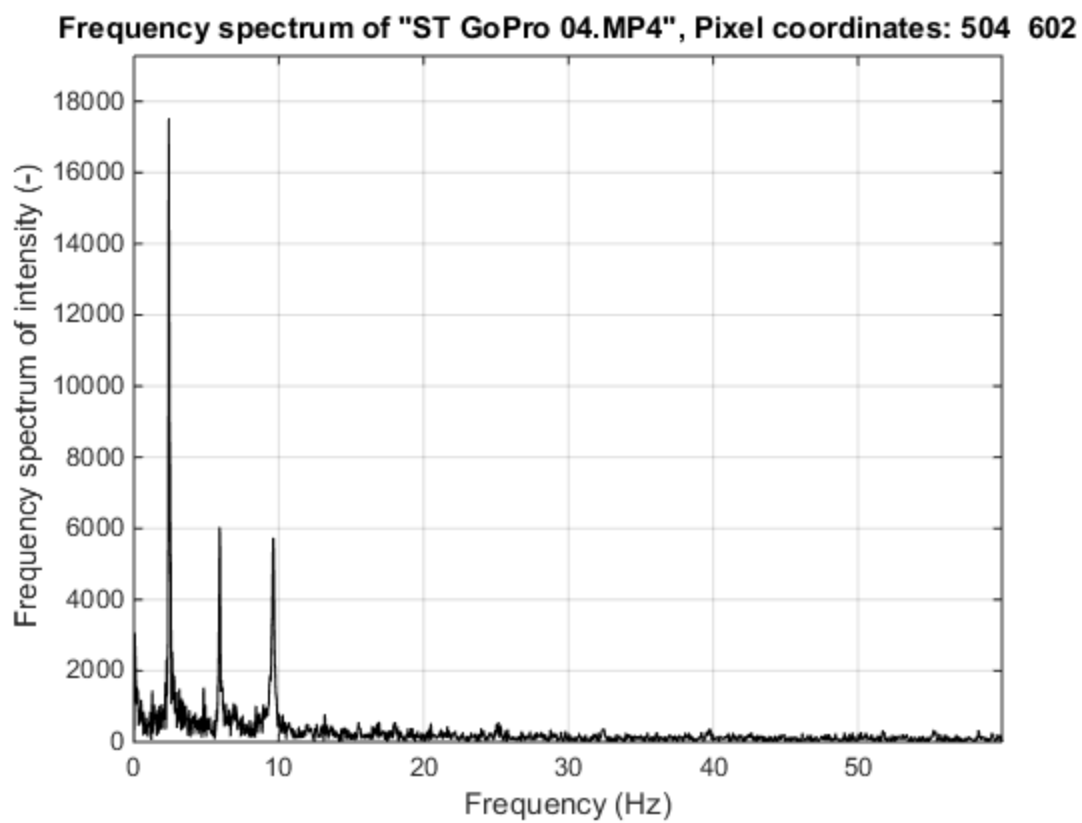
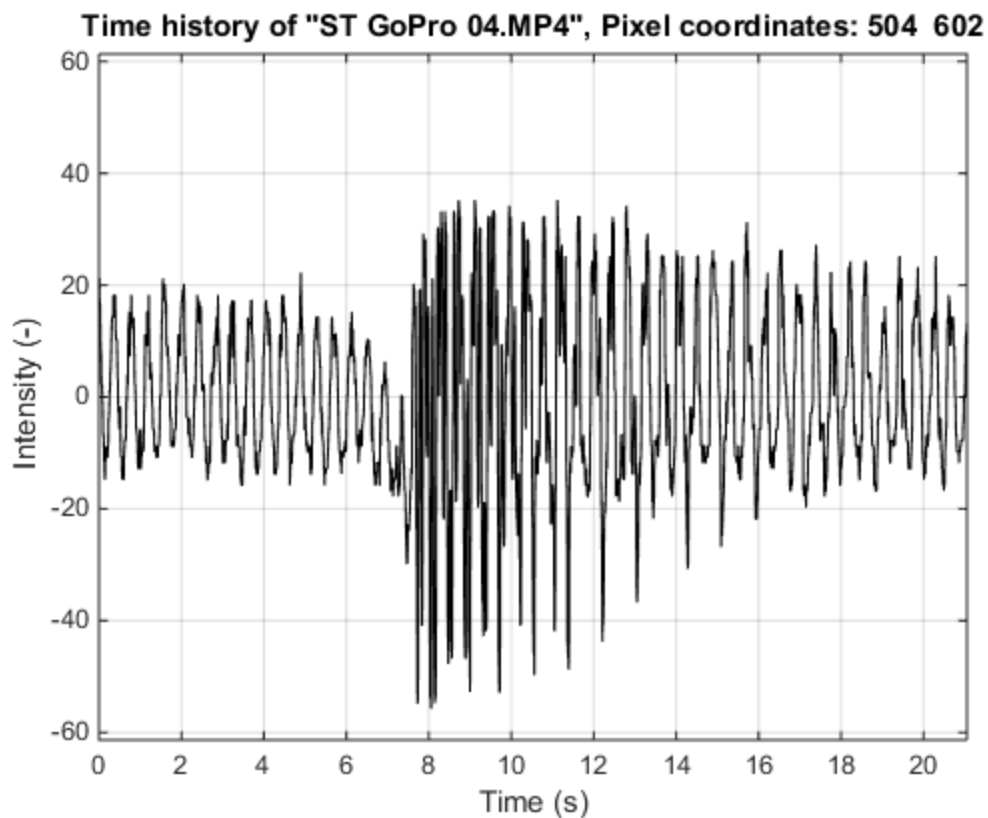
Time history of "ST GoPro 02.MP4", Pixel coordinates: 504 602

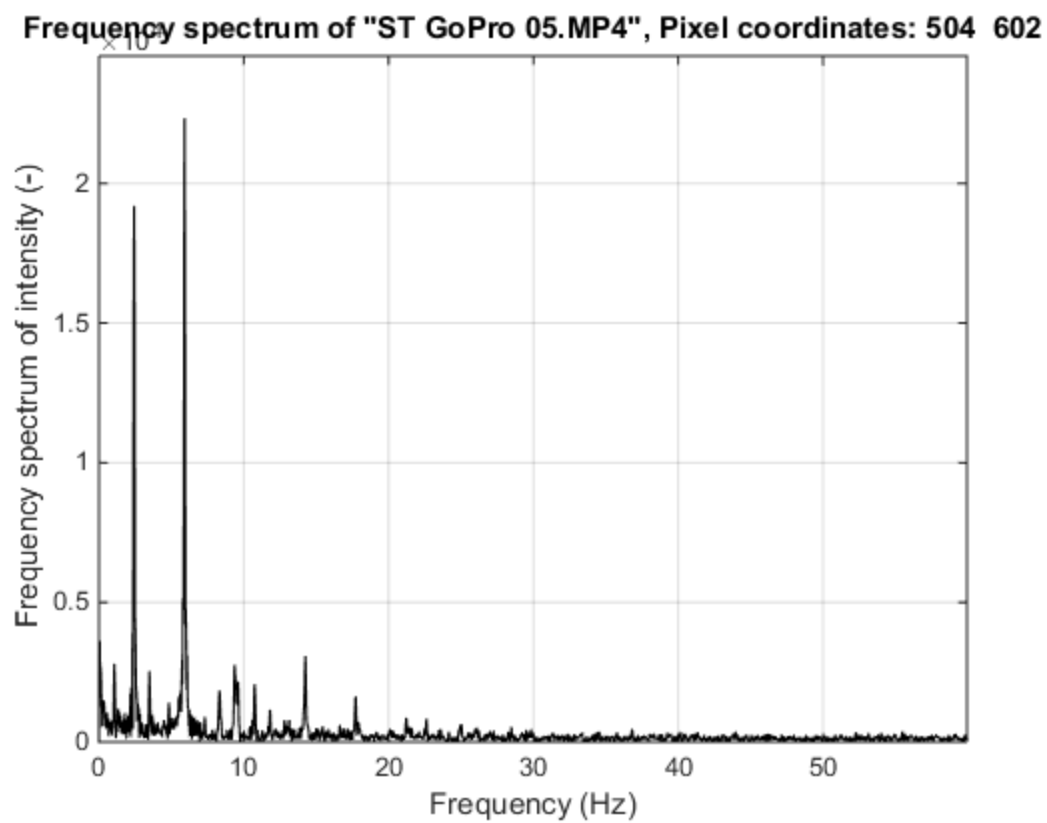
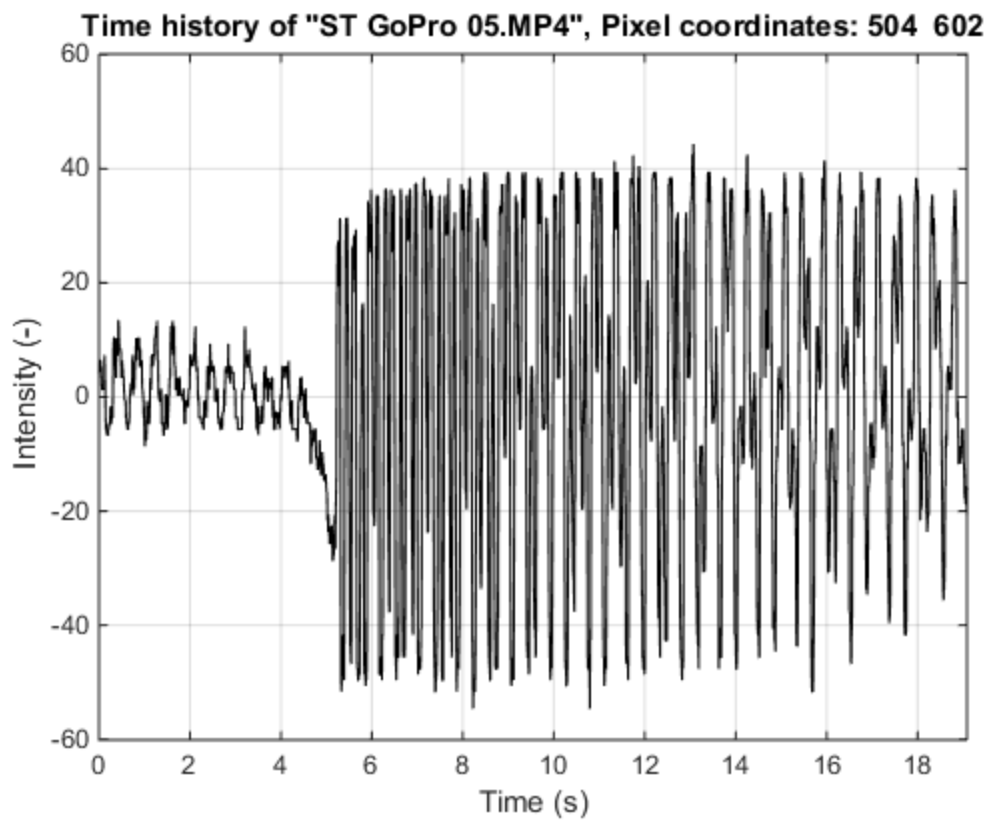


Frequency spectrum of "ST GoPro 02.MP4", Pixel coordinates: 504 602

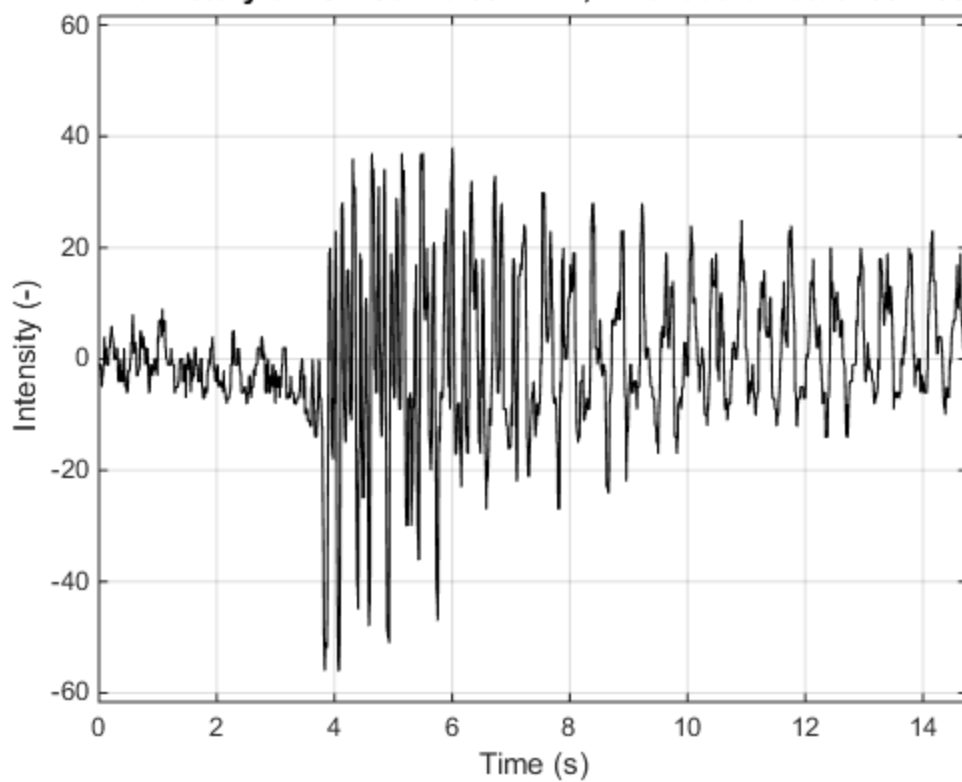




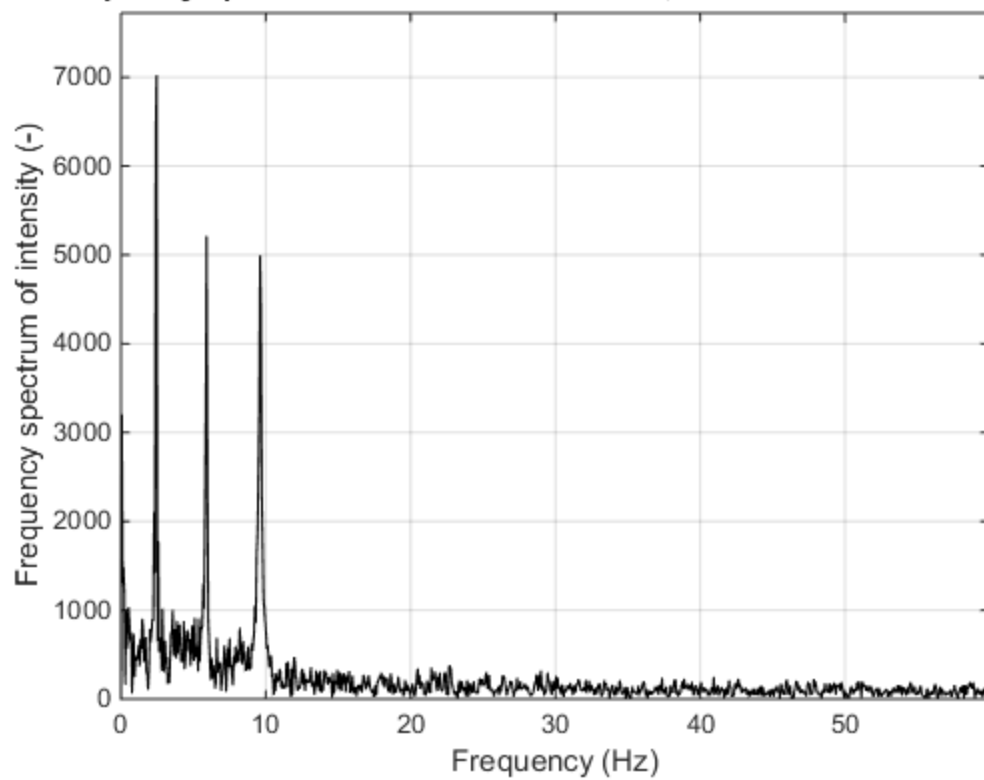




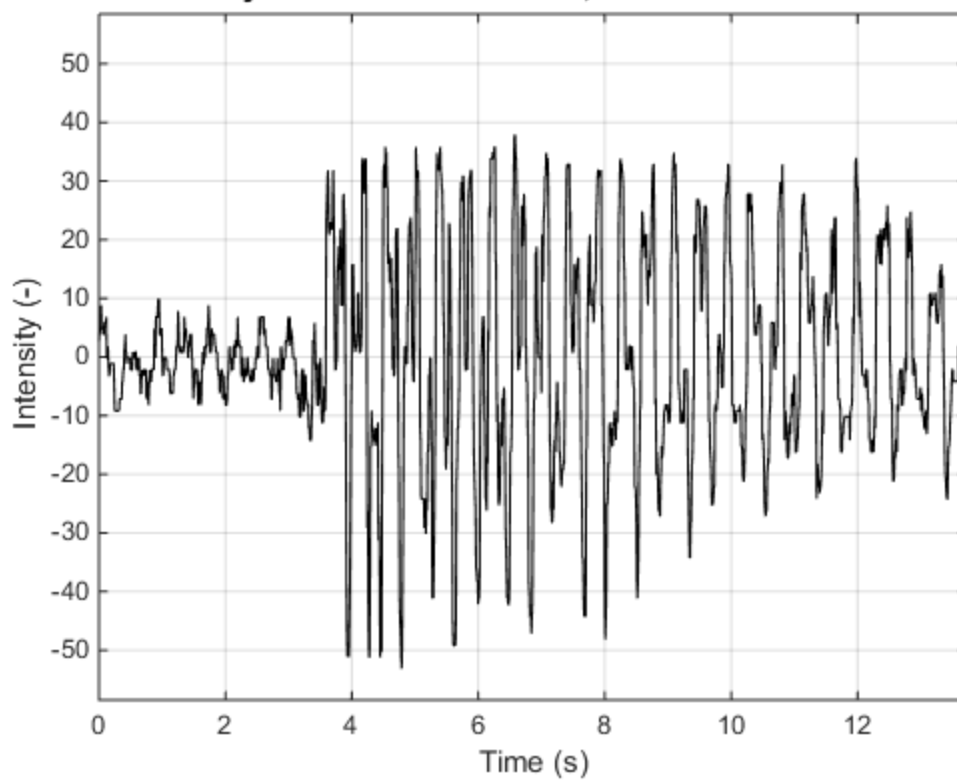
Time history of "ST GoPro 06.MP4", Pixel coordinates: 504 602



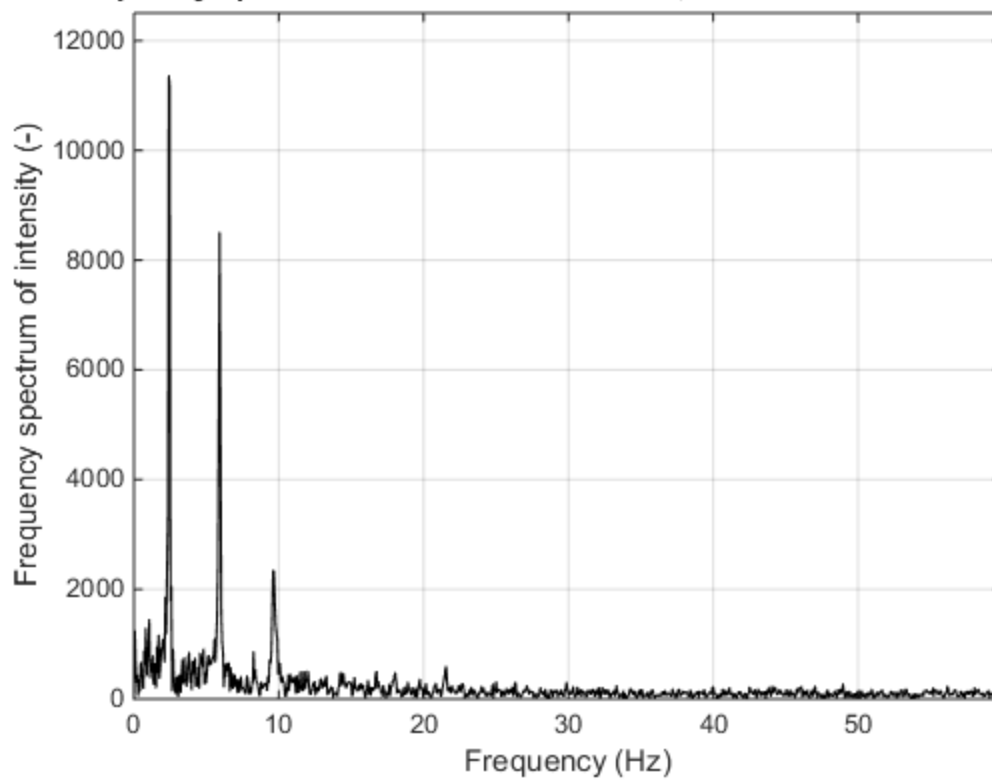
Frequency spectrum of "ST GoPro 06.MP4", Pixel coordinates: 504 602



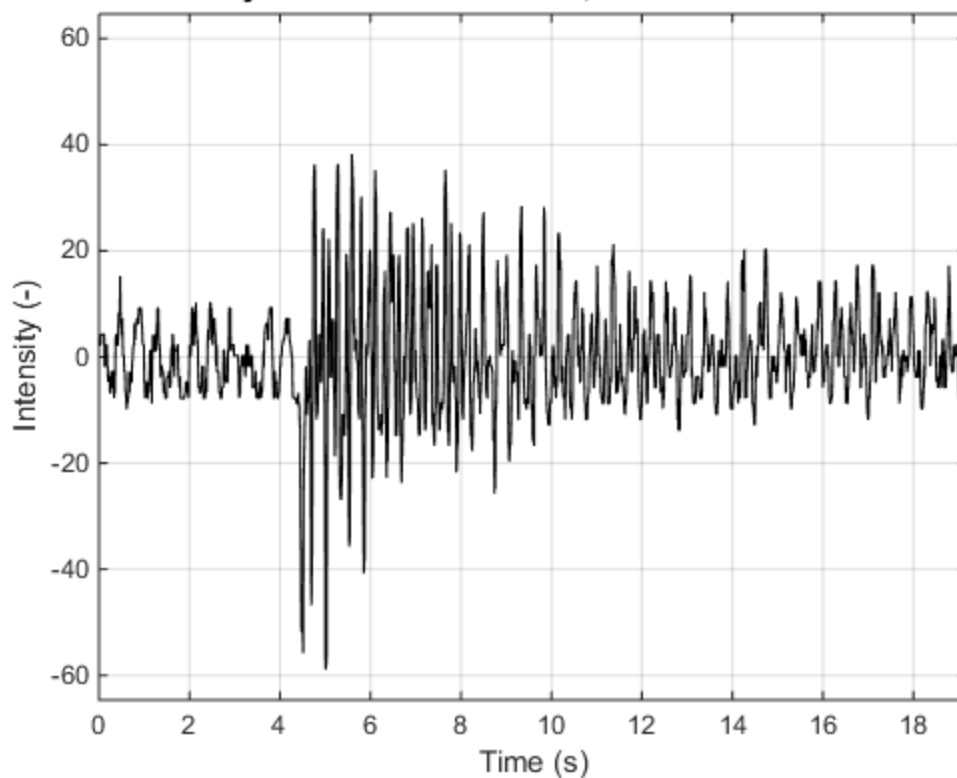
Time history of "ST GoPro 07.MP4", Pixel coordinates: 504 602



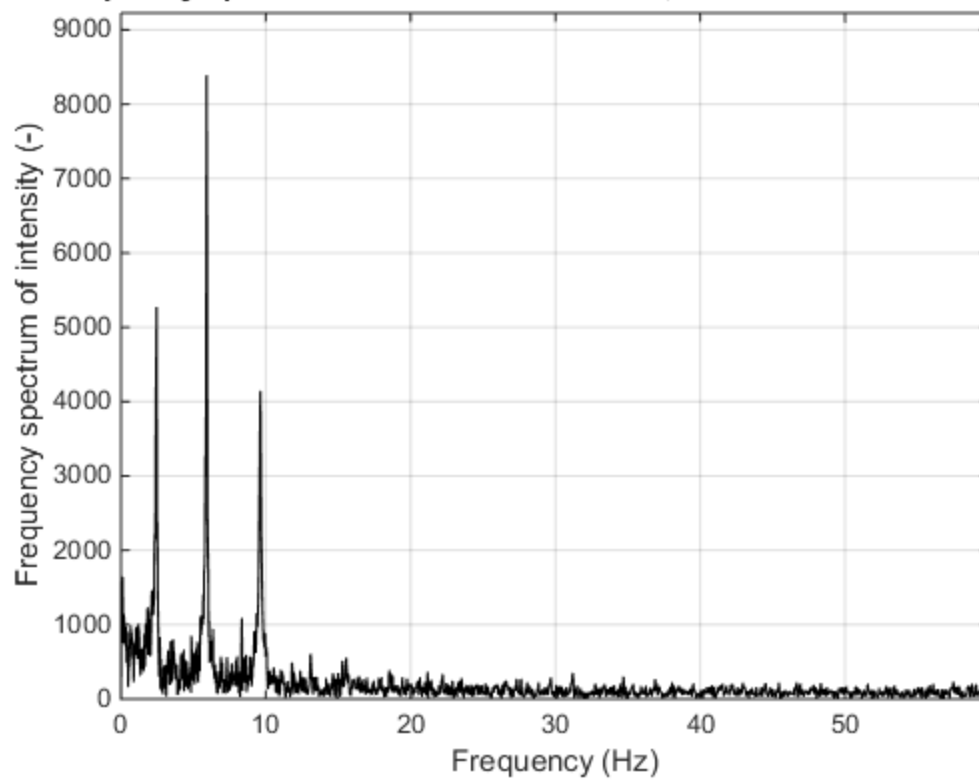
Frequency spectrum of "ST GoPro 07.MP4", Pixel coordinates: 504 602



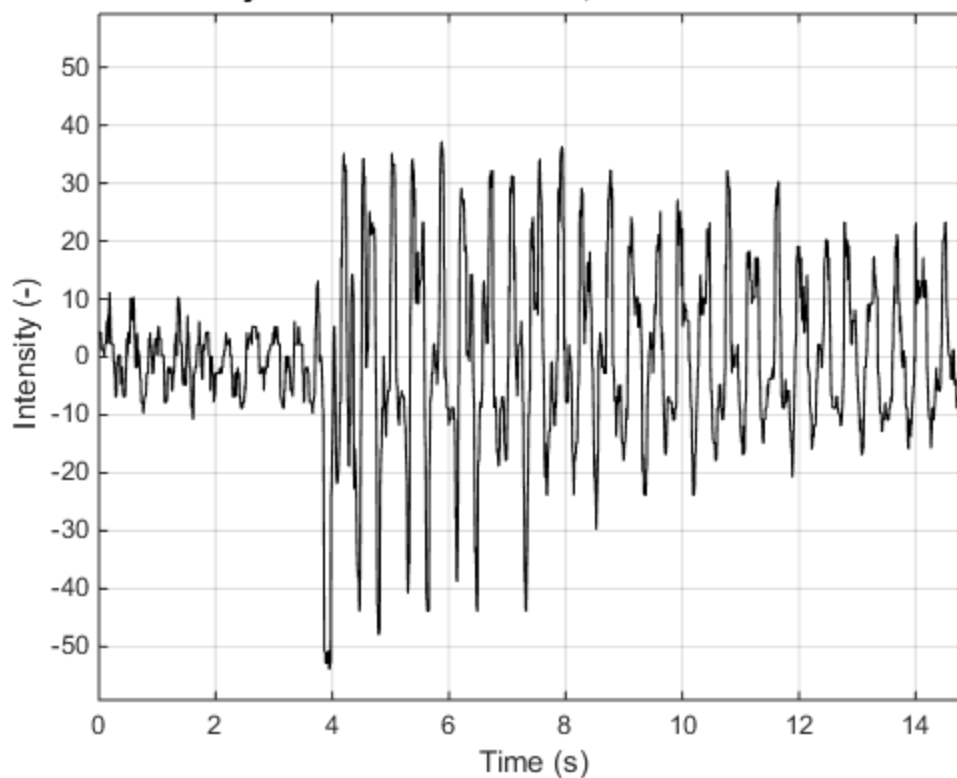
Time history of "ST GoPro 08.MP4", Pixel coordinates: 504 602



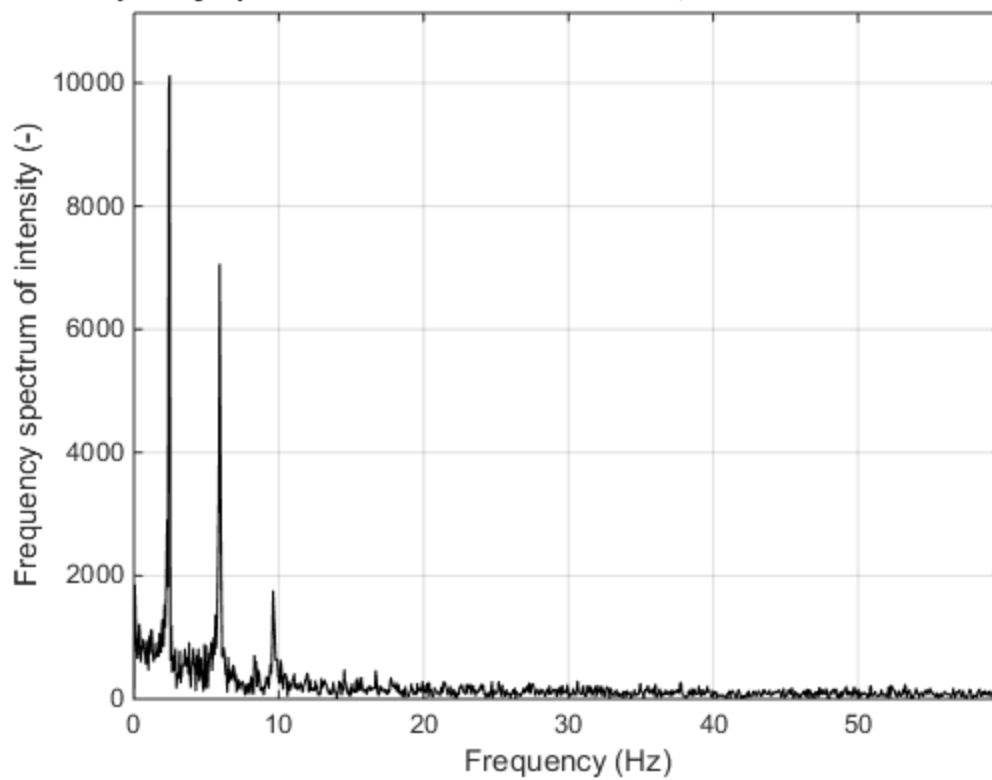
Frequency spectrum of "ST GoPro 08.MP4", Pixel coordinates: 504 602



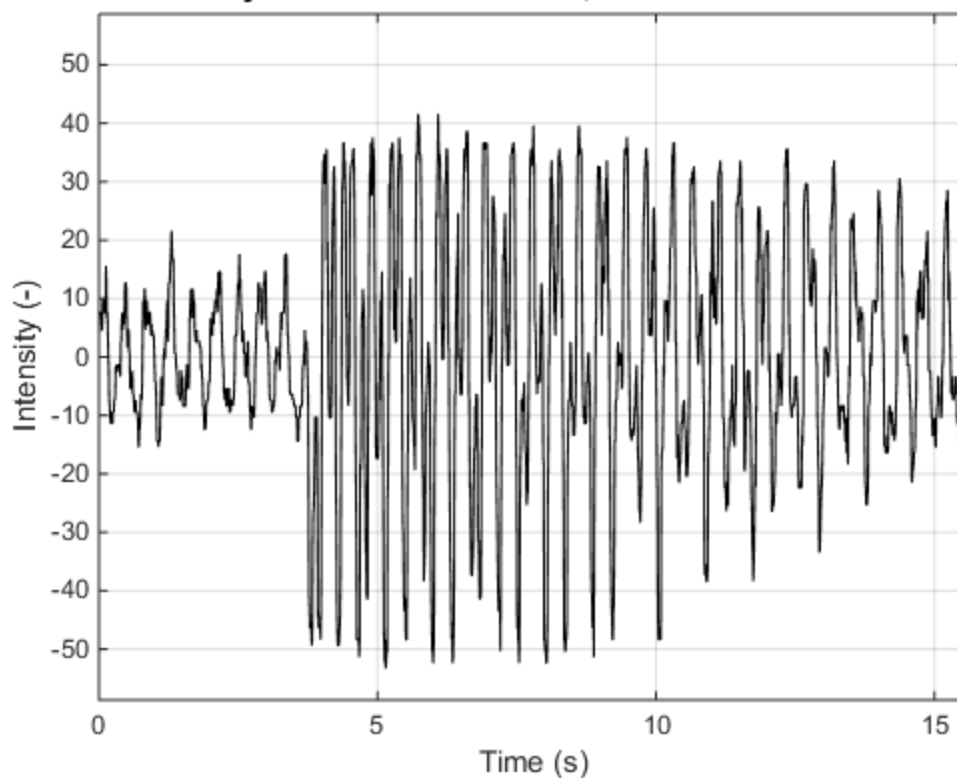
Time history of "ST GoPro 09.MP4", Pixel coordinates: 504 602



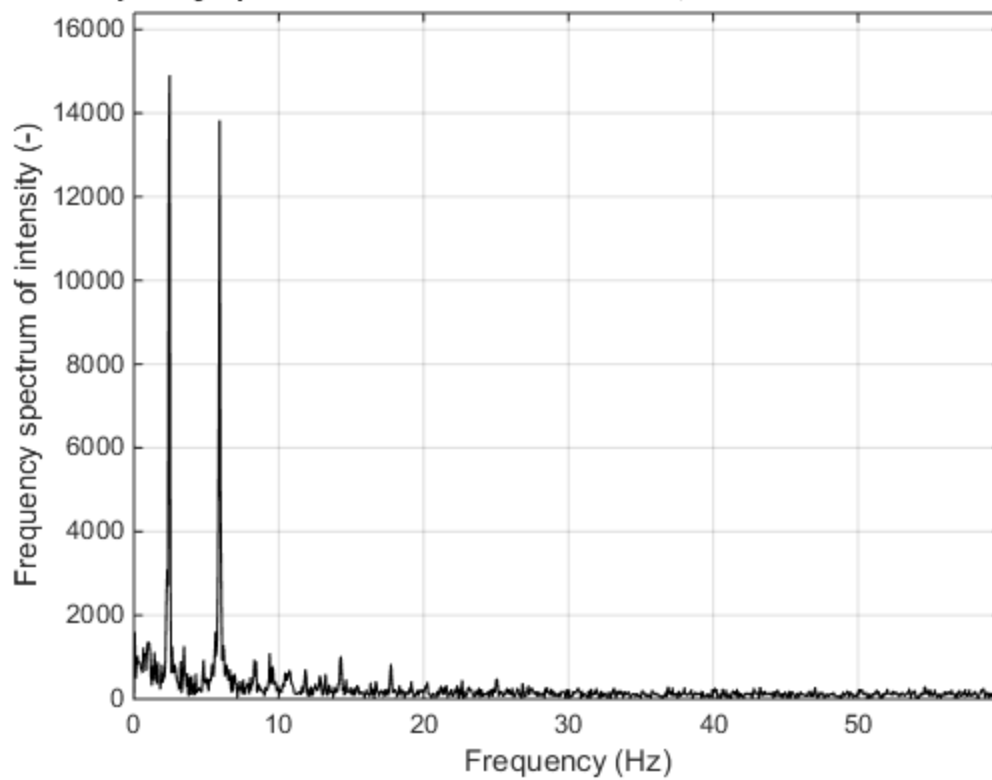
Frequency spectrum of "ST GoPro 09.MP4", Pixel coordinates: 504 602



Time history of "ST GoPro 10.MP4", Pixel coordinates: 504 602

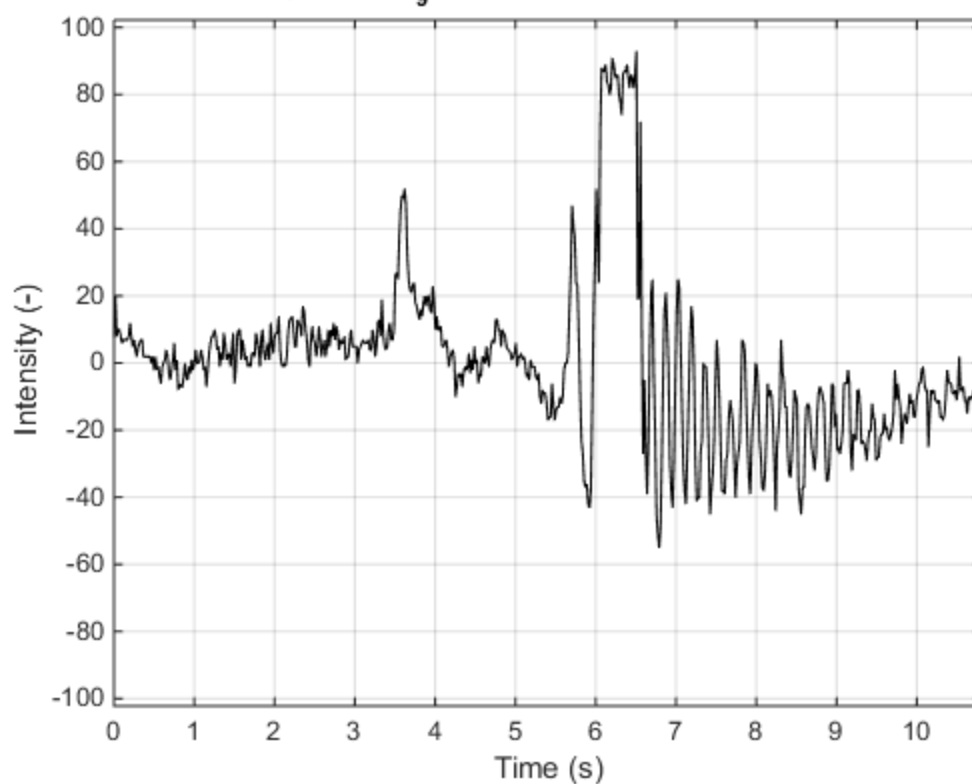


Frequency spectrum of "ST GoPro 10.MP4", Pixel coordinates: 504 602

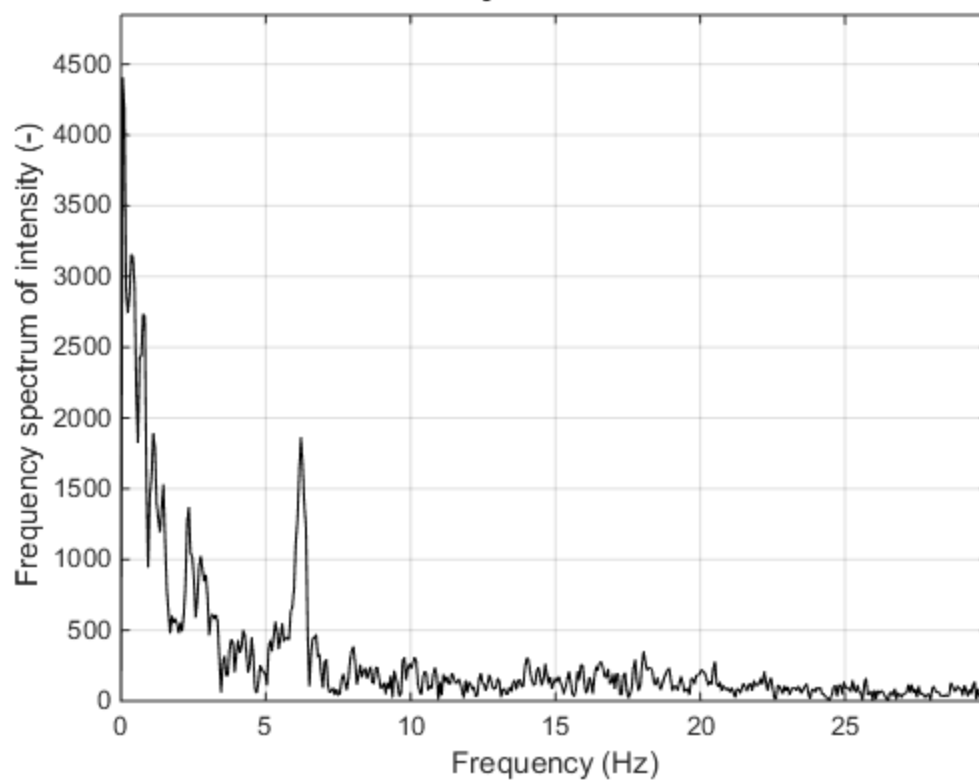


Appendix O – Forest Service Pedestrian Bridge VVS Figures (Preliminary)

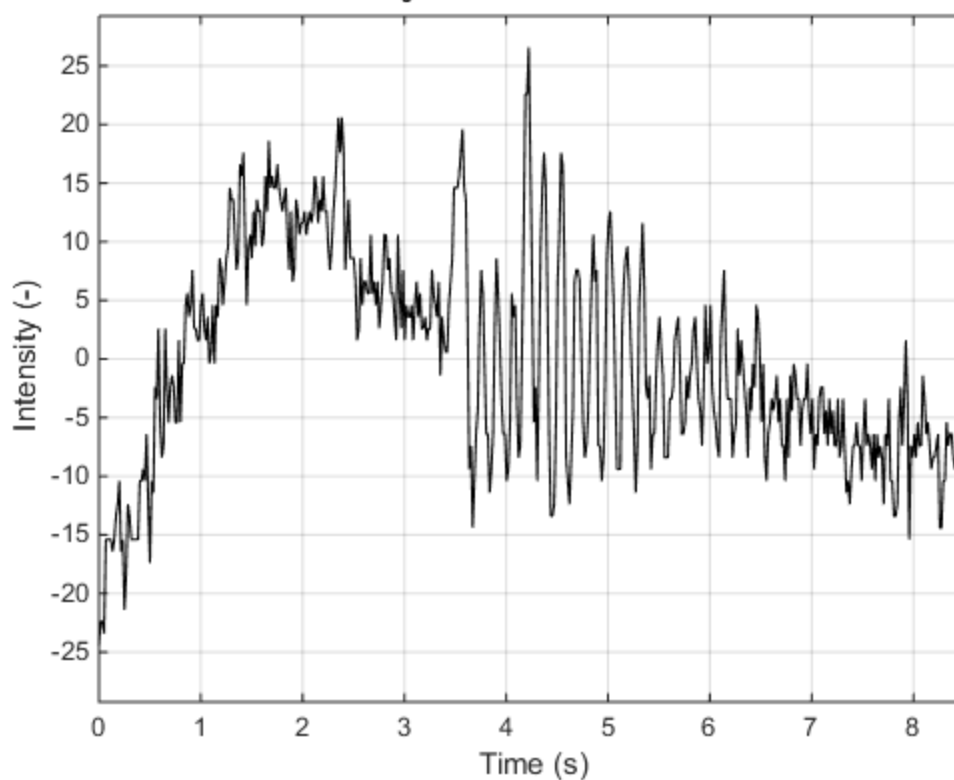
Time history of "MVI₉033.MOV", Pixel coordinates: 567 308



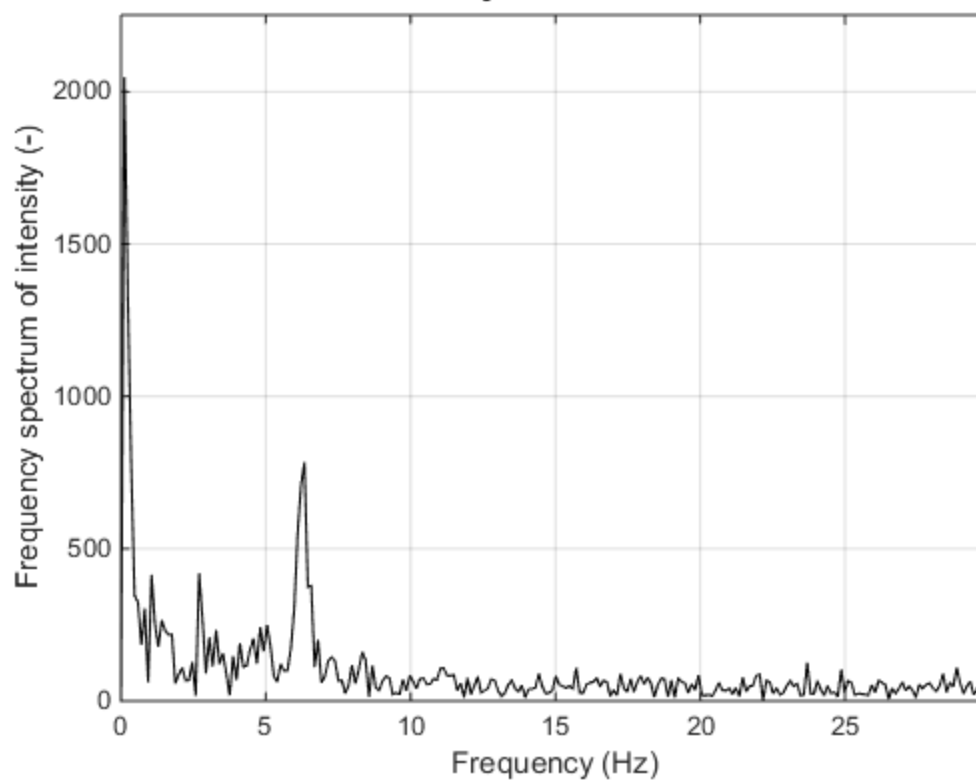
Frequency spectrum of "MVI₉033.MOV", Pixel coordinates: 567 308



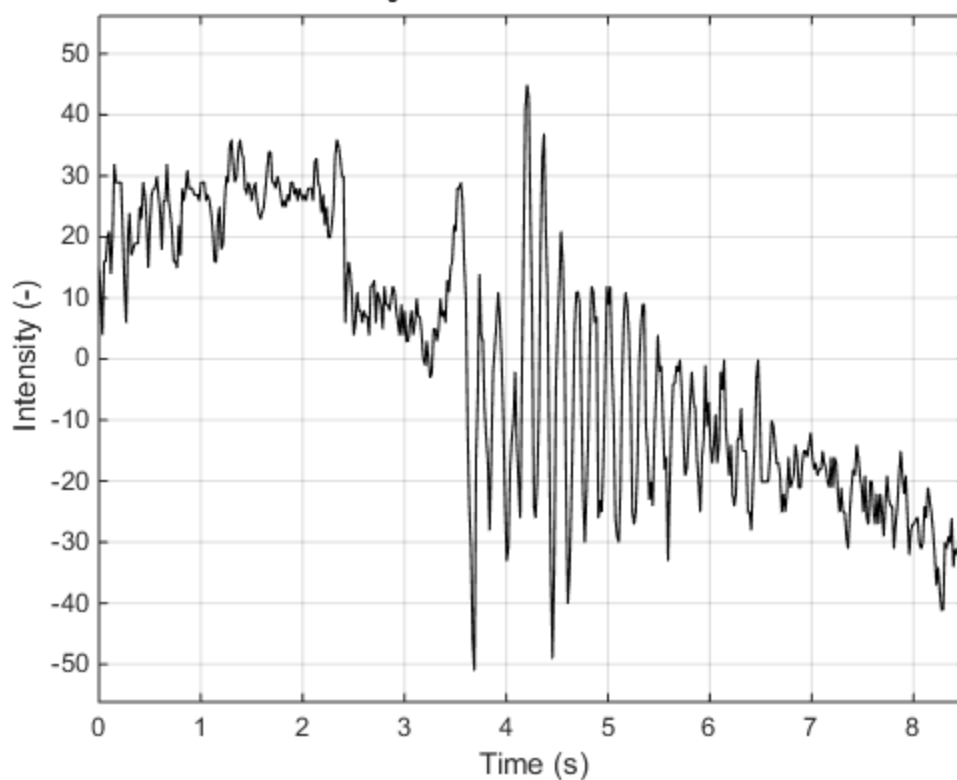
Time history of "MVI₉034.MOV", Pixel coordinates: 411 389



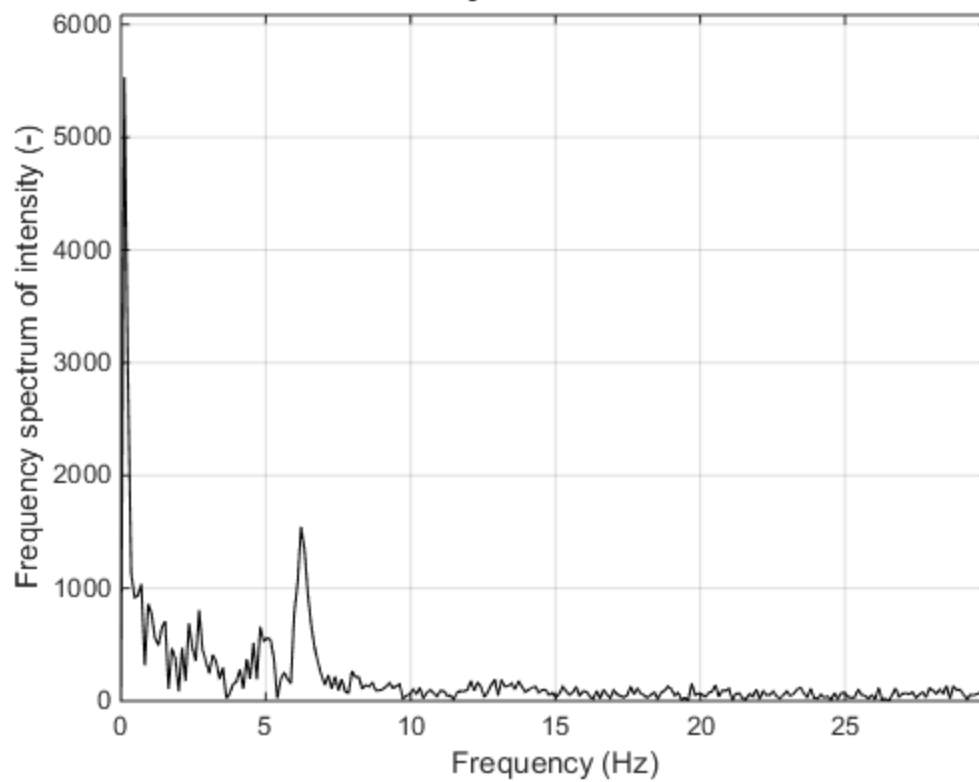
Frequency spectrum of "MVI₉034.MOV", Pixel coordinates: 411 389



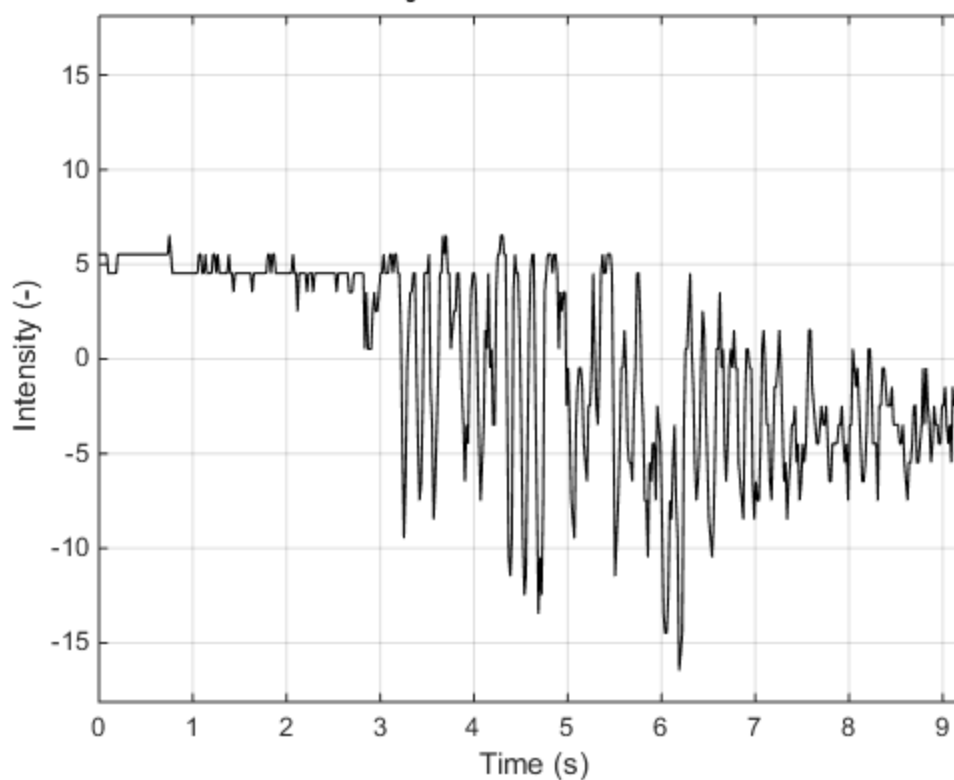
Time history of "MVI₉034.MOV", Pixel coordinates: 1107 535



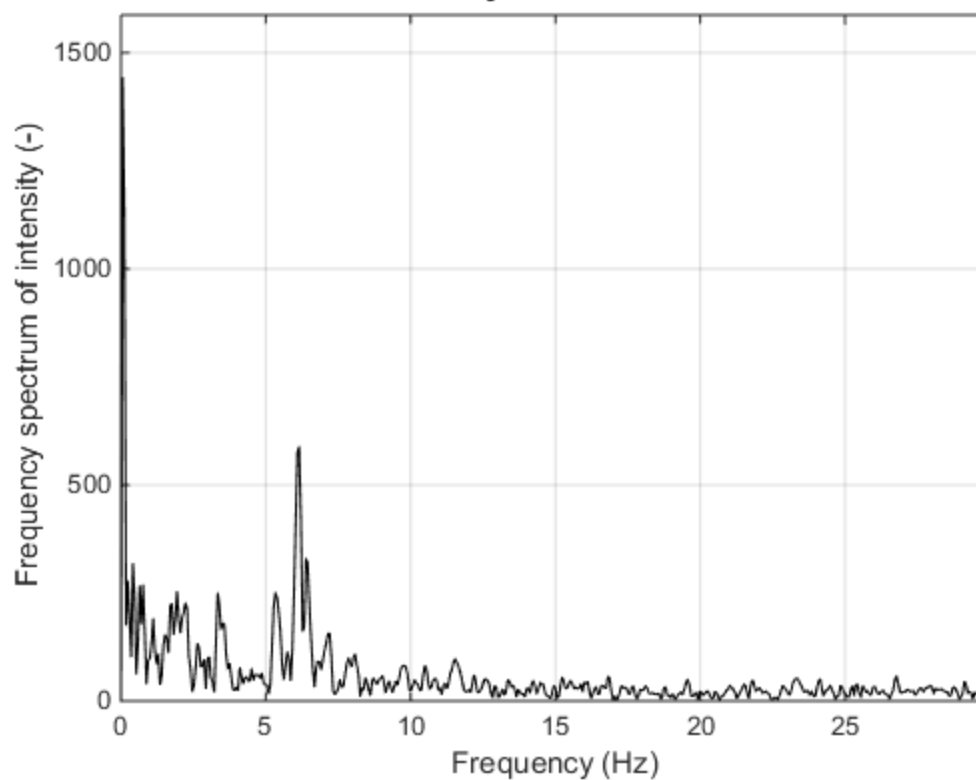
Frequency spectrum of "MVI₉034.MOV", Pixel coordinates: 1107 535



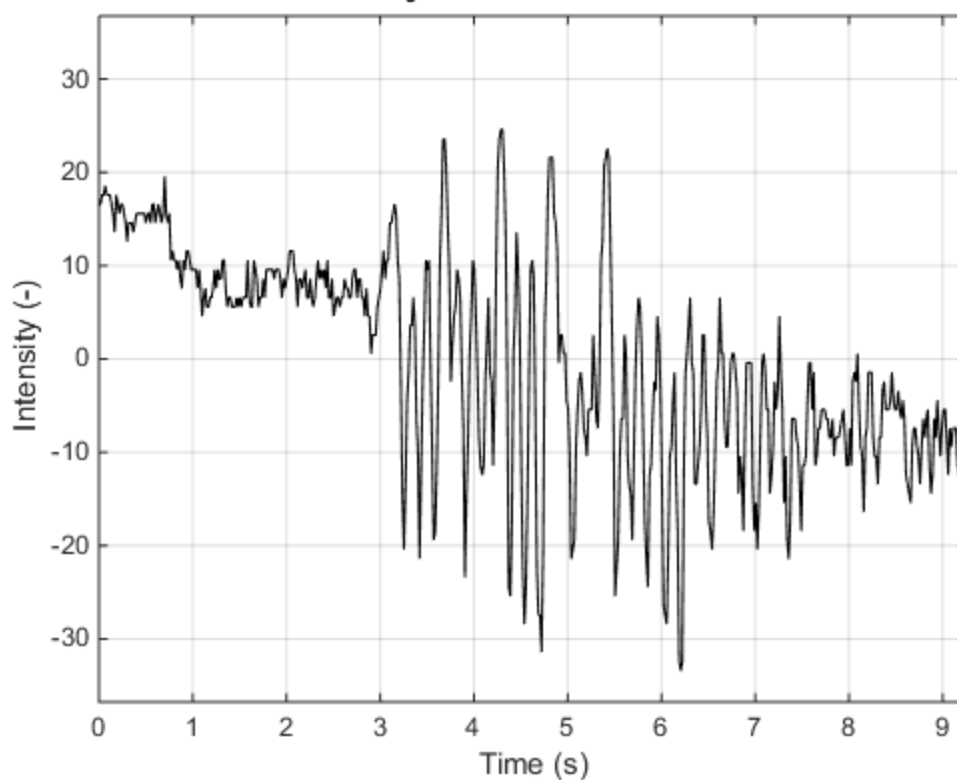
Time history of "MVI₉036.MOV", Pixel coordinates: 855 51



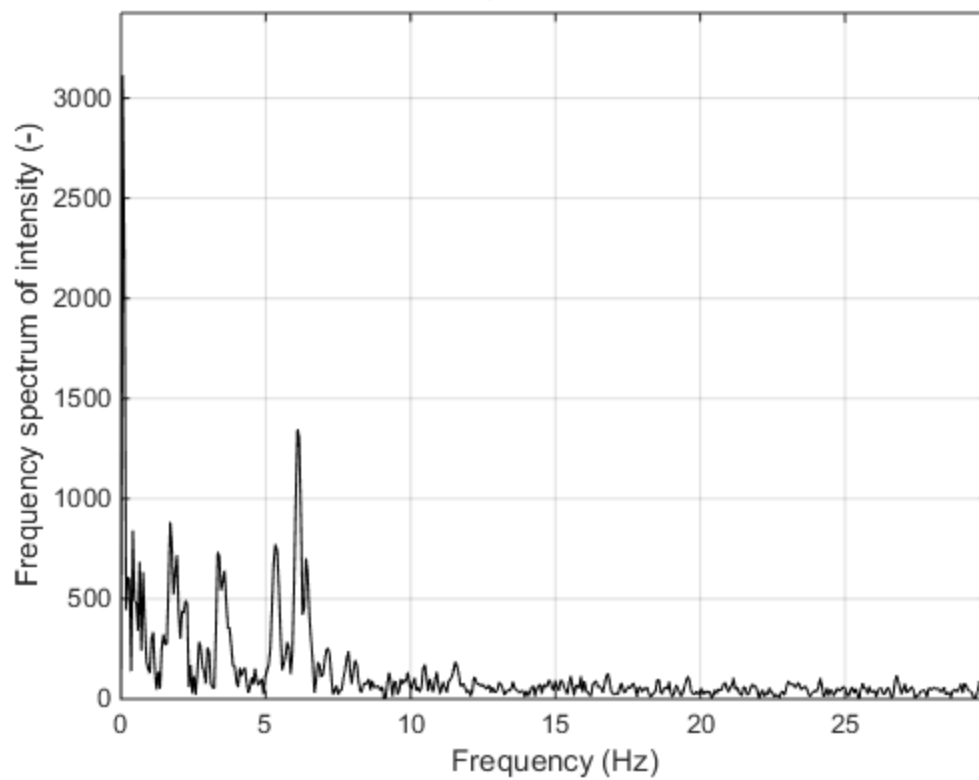
Frequency spectrum of "MVI₉036.MOV", Pixel coordinates: 855 51



Time history of "MVI₉036.MOV", Pixel coordinates: 855 52

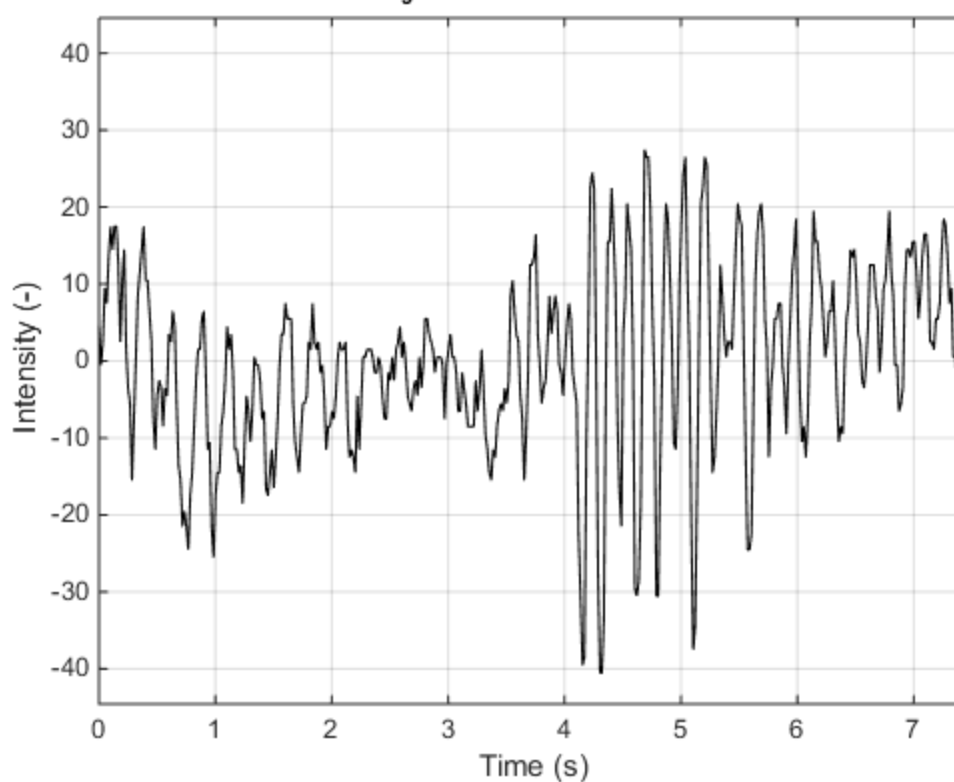


Frequency spectrum of "MVI₉036.MOV", Pixel coordinates: 855 52

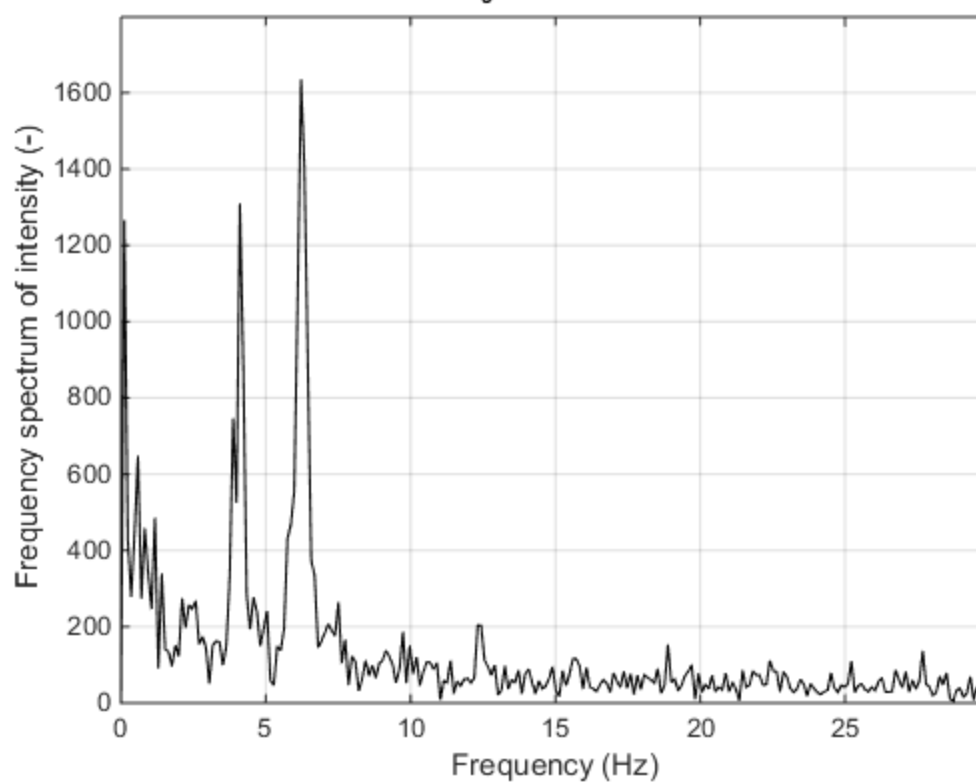


Appendix P – Forest Service Pedestrian Bridge VVS Figures (Oct 27, 2014)

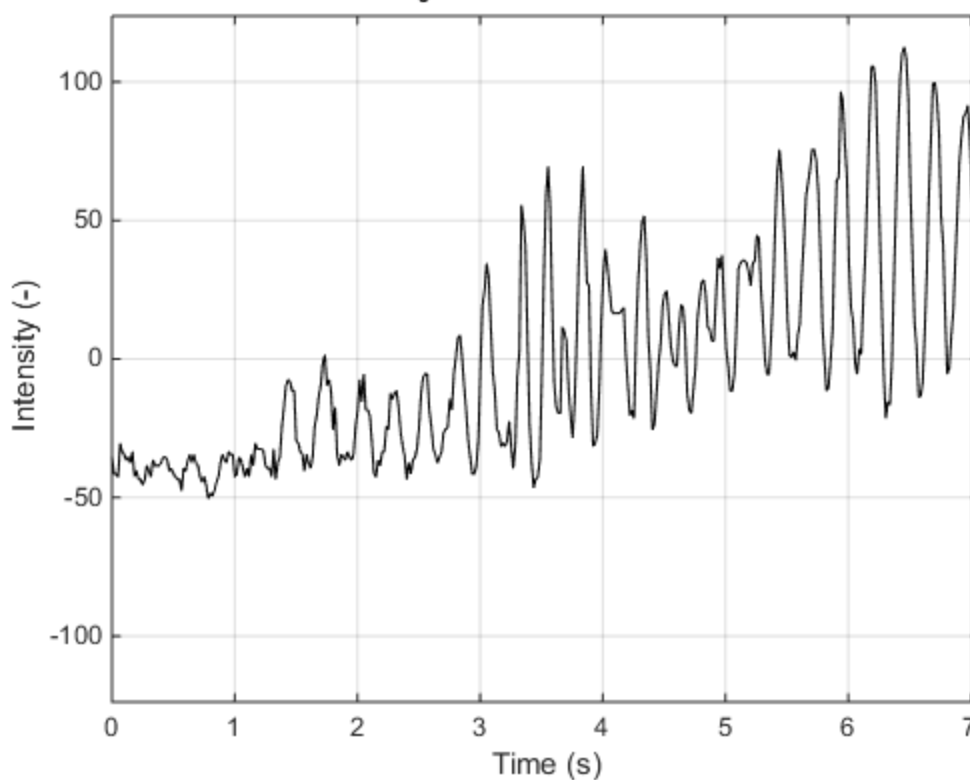
Time history of "MVI₉228.MOV", Pixel coordinates: 809 517



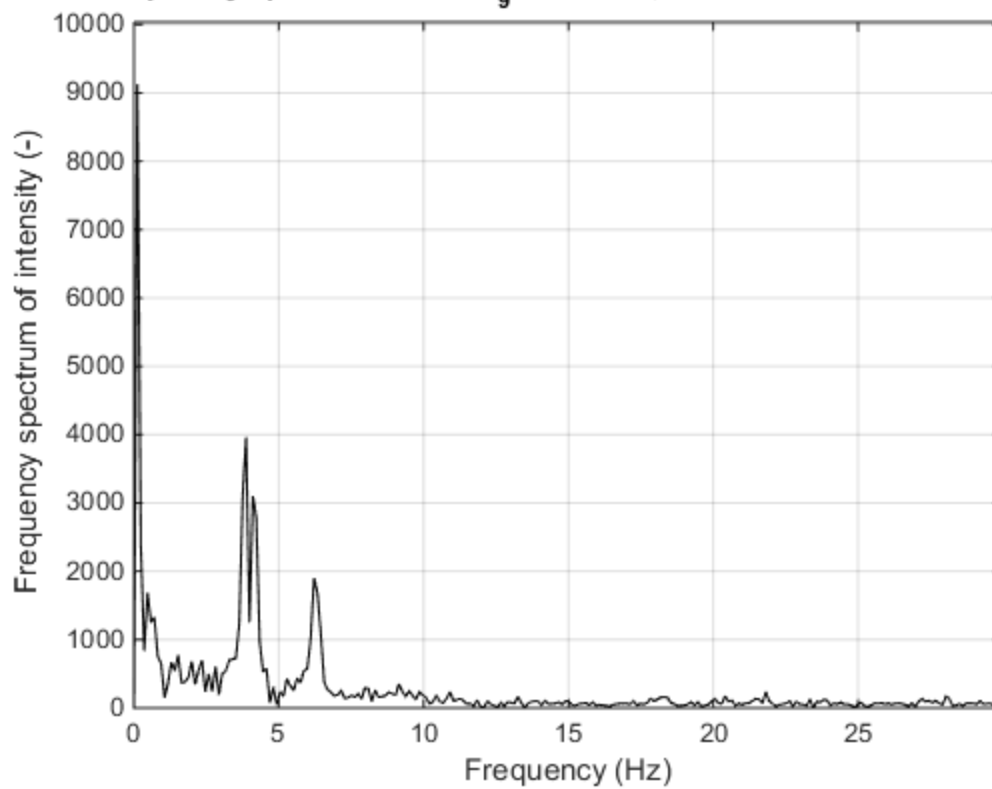
Frequency spectrum of "MVI₉228.MOV", Pixel coordinates: 809 517



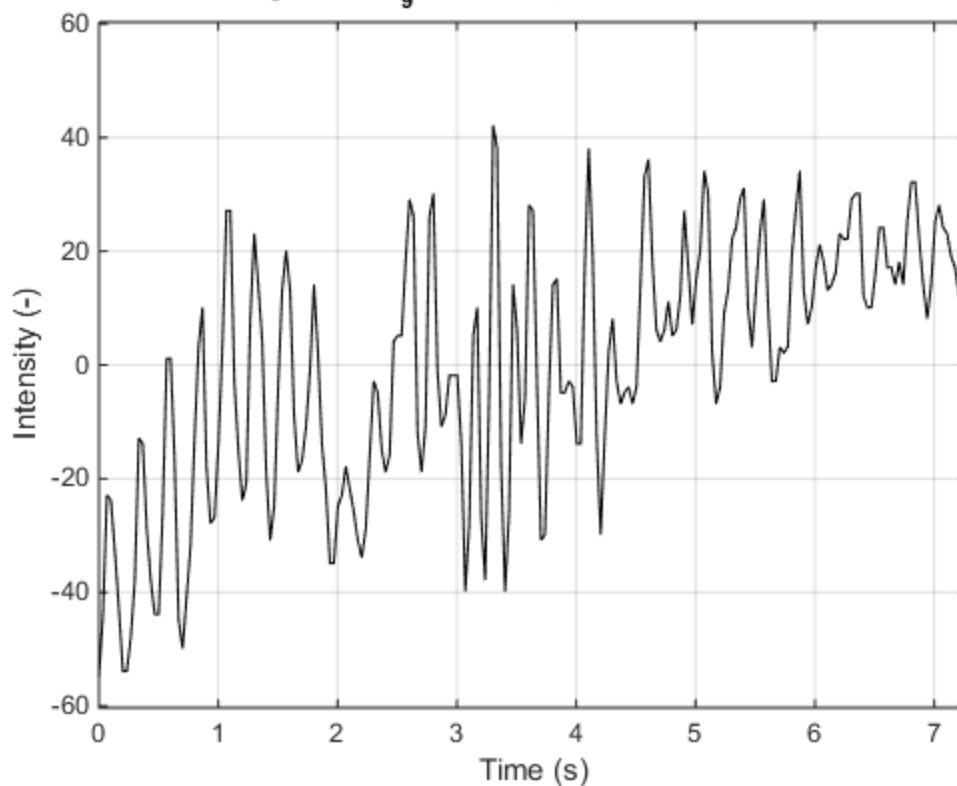
Time history of "MVI₉230.MOV", Pixel coordinates: 843 30



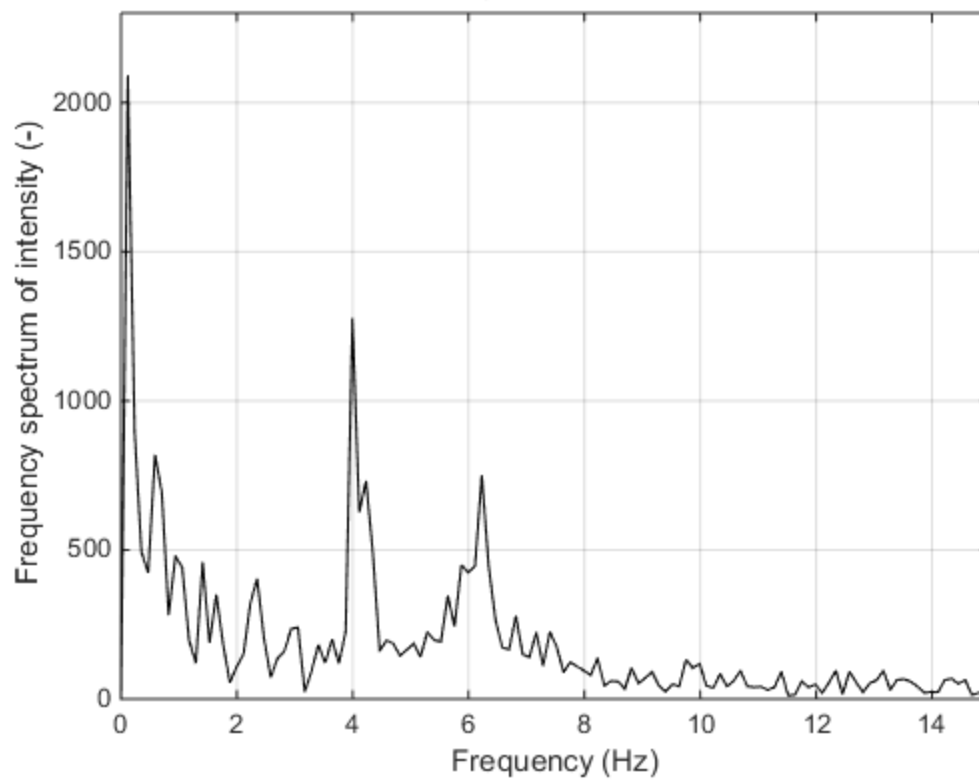
Frequency spectrum of "MVI₉230.MOV", Pixel coordinates: 843 30



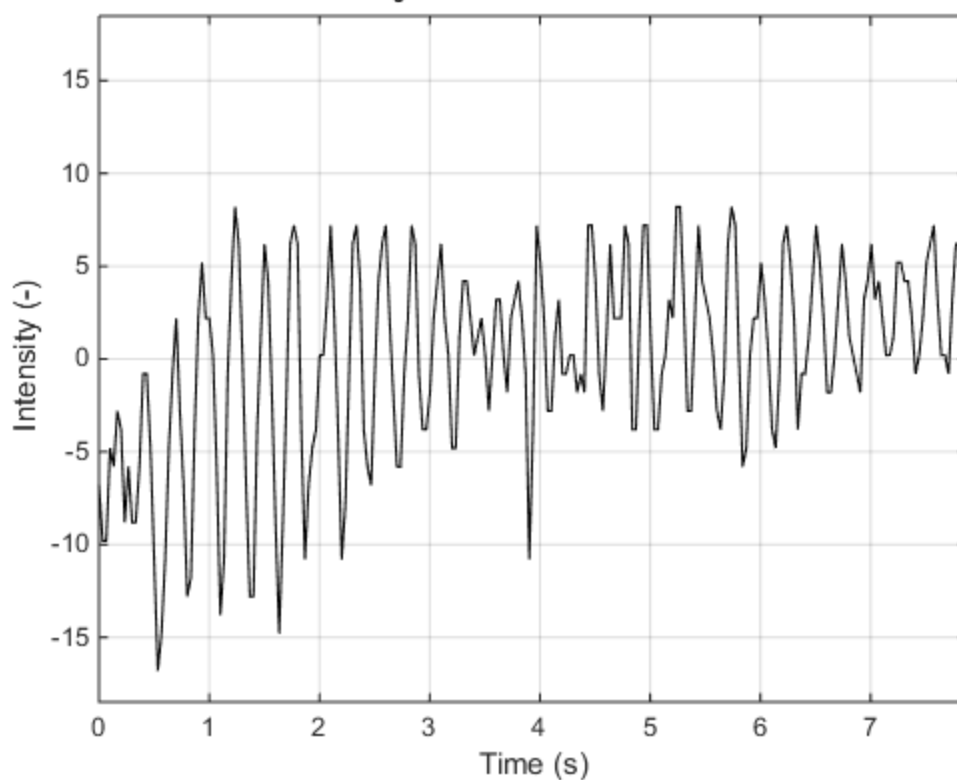
Time history of "MVI₉232.MOV", Pixel coordinates: 660 463



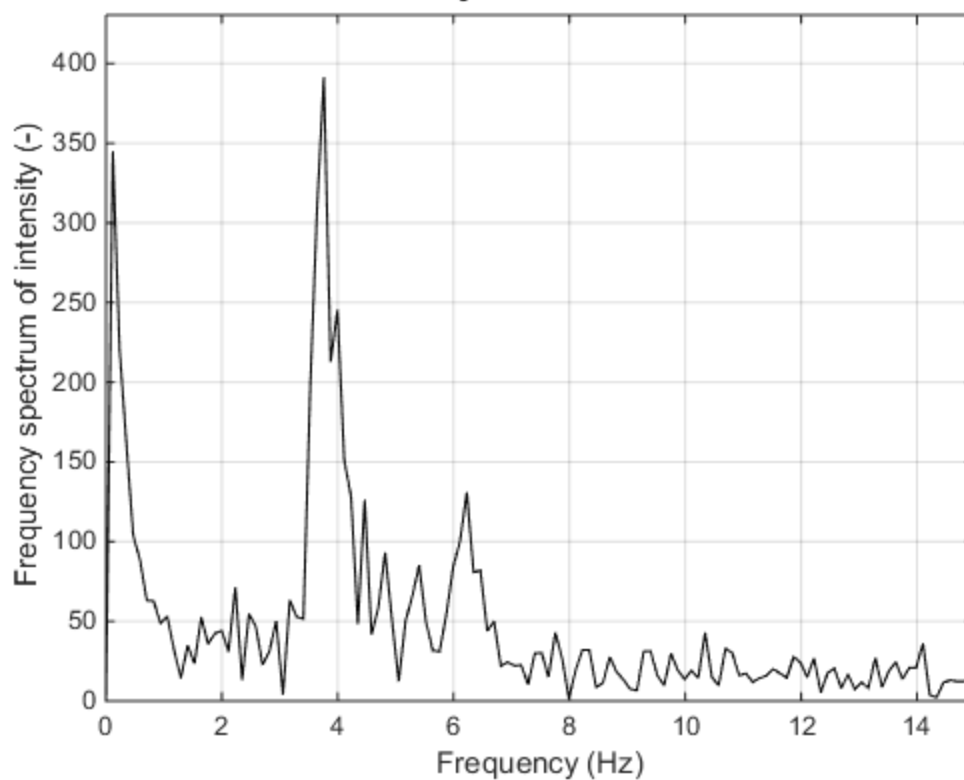
Frequency spectrum of "MVI₉232.MOV", Pixel coordinates: 660 463



Time history of "MVI₉234.MOV", Pixel coordinates: 1232 39

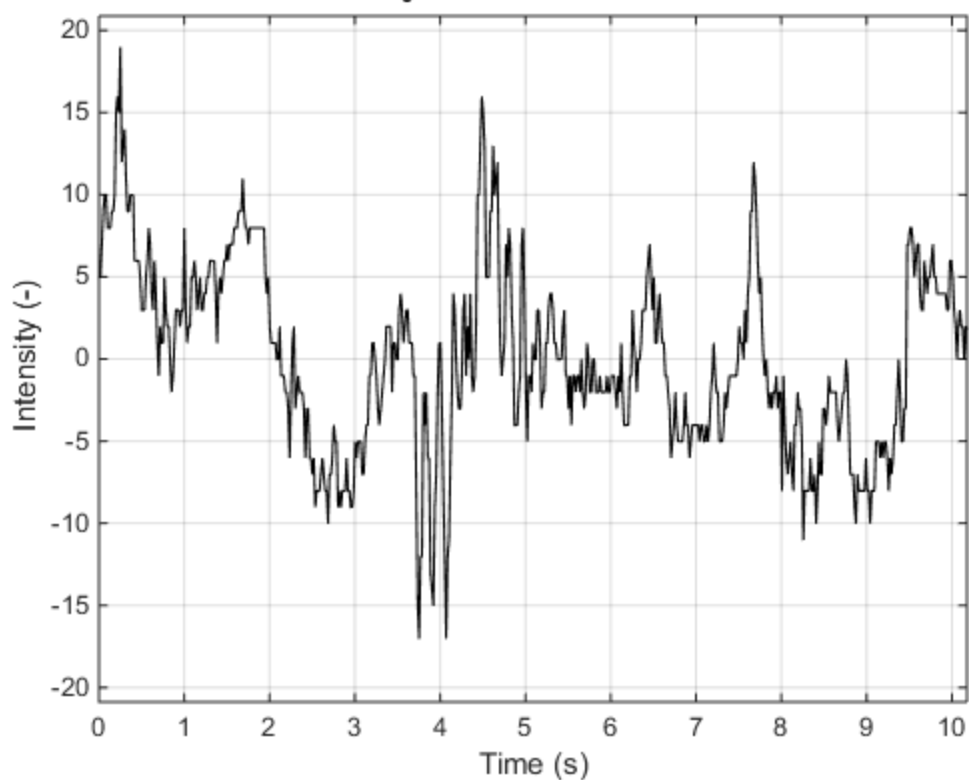


Frequency spectrum of "MVI₉234.MOV", Pixel coordinates: 1232 39

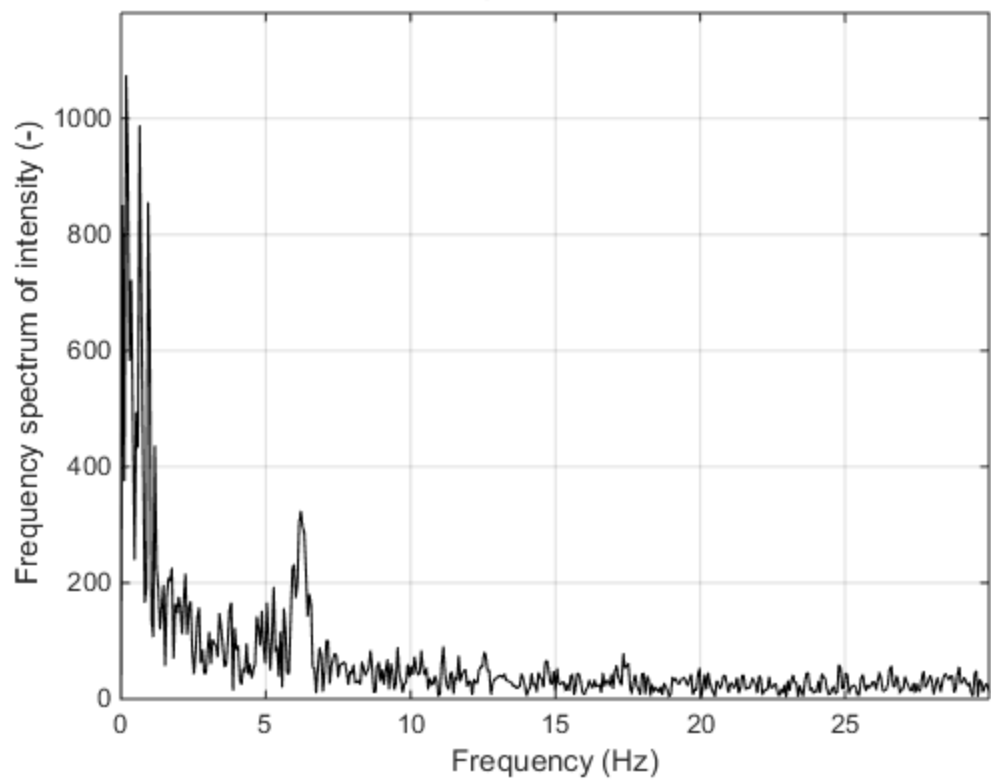


Appendix Q – Forest Service Pedestrian Bridge VVS Figures (Feb 12, 2015)

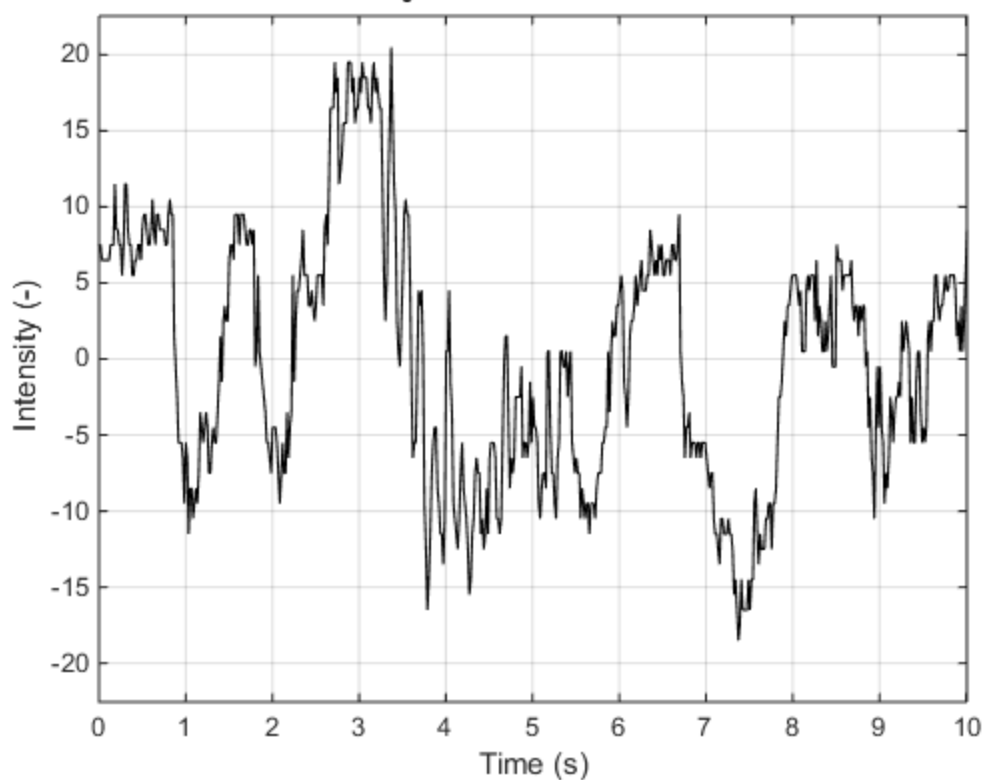
Time history of "MVI₀175.MOV", Pixel coordinates: 411 389



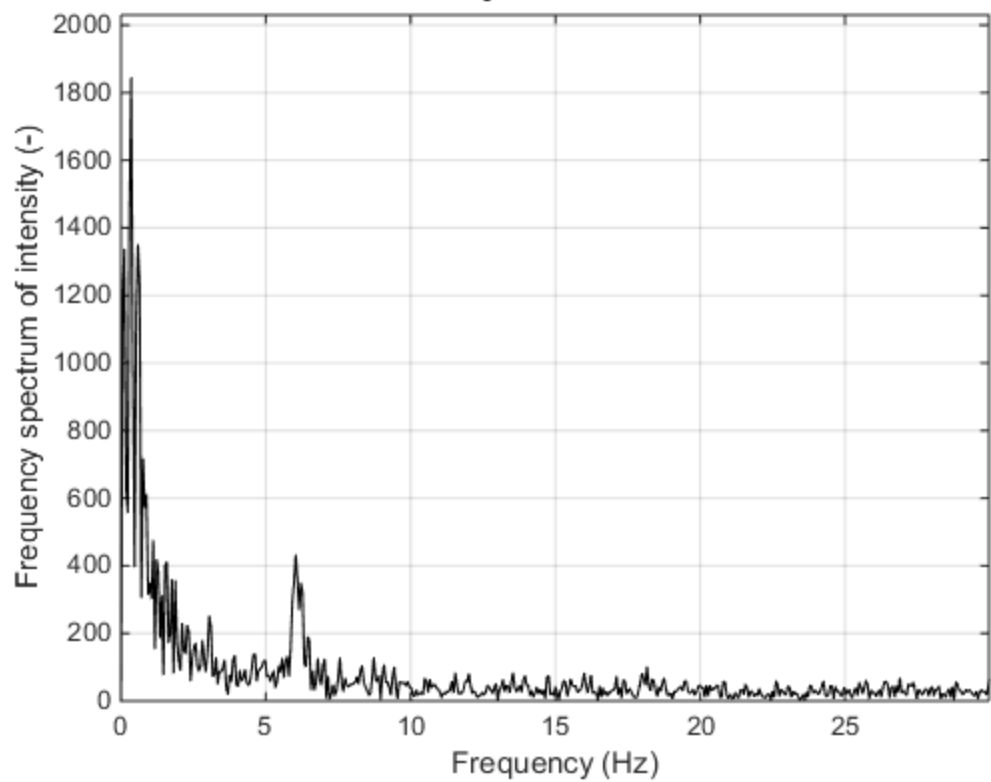
Frequency spectrum of "MVI₀175.MOV", Pixel coordinates: 411 389



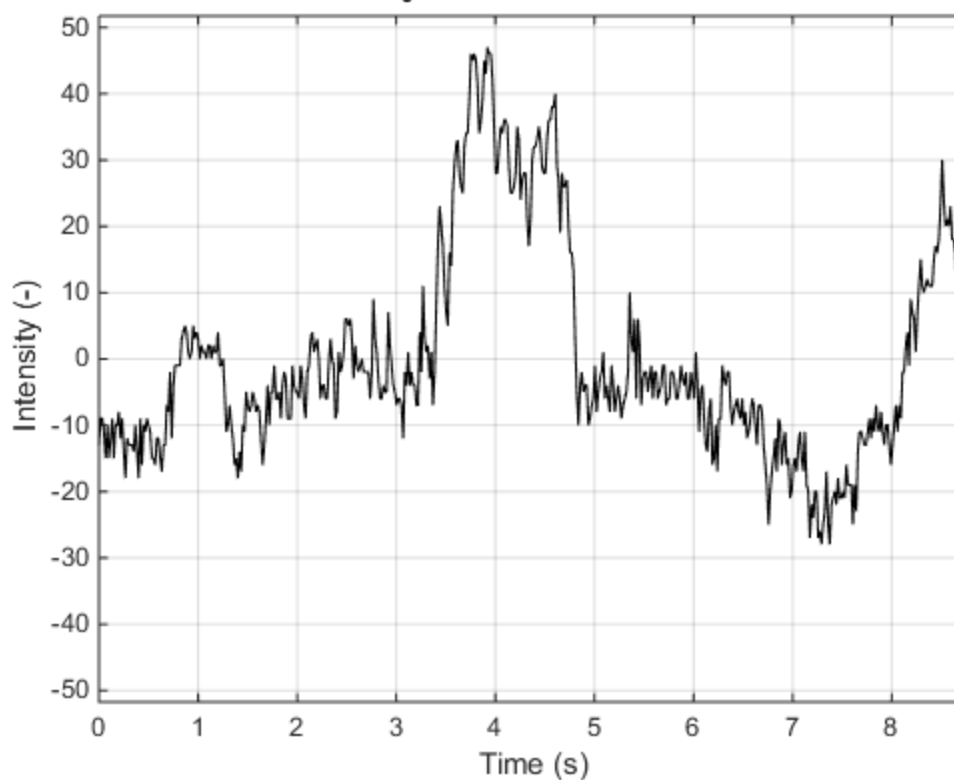
Time history of "MVI₀176.MOV", Pixel coordinates: 540 320



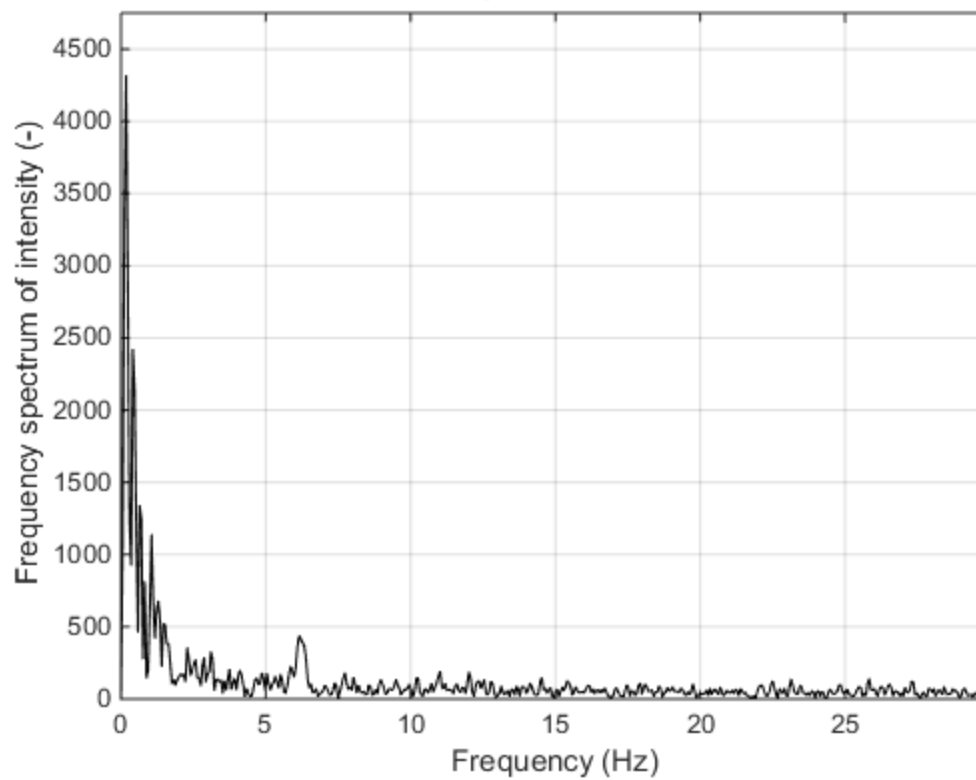
Frequency spectrum of "MVI₀176.MOV", Pixel coordinates: 540 320



Time history of "MVI₀172.MOV", Pixel coordinates: 888 380



Frequency spectrum of "MVI₀172.MOV", Pixel coordinates: 888 380



Appendix R – Results from Shake Table Statistical Analysis

Table R1 - Bootstrap Estimate of Frequency (Mode 1)

	95% Lower bound	Estimate of Mean	95% Upper bound	Est. of Standard Dev.
Accelerometer	2.4029	2.4206	2.438	0.009
Canon	2.4047	2.4162	2.4281	0.0062
Accelerometer*	2.4313	2.4401	2.4488	0.0045
GoPro*	2.4214	2.4361	2.4481	0.007

Table R2 - Bootstrap Estimate of Frequency (Mode 2)

	95% Lower bound	Estimate of Mean	95% Upper bound	Est. of Standard Dev.
Accelerometer	5.915	5.919	5.9228	0.0019
Canon	5.9159	5.9168	5.9177	0.0005
Accelerometer*	5.9026	5.9152	5.9272	0.0063
GoPro*	5.9141	5.9144	5.9147	0.0002

Table R3 - Bootstrap Estimate of Frequency (Mode 3)

	95% Lower bound	Estimate of Mean	95% Upper bound	Est. of Standard Dev.
Accelerometer	9.5800	9.5961	9.6116	0.0082
Canon	9.4449	9.5266	9.6073	0.0399
Accelerometer*	9.6118	9.6248	9.6374	0.0064
GoPro*	9.5206	9.5921	9.6416	0.0321

Table R4 - Difference in Measured Fundamental Frequencies between Methods (Mode 1)

	95% Lower bound	Est. of Mean Difference	95% Upper bound	Est. of Std. Dev.
Accelerometer - Canon	-0.0150	0.0045	0.0244	0.0102
Accelerometer* - GoPro*	-0.0164	0.0041	0.0251	0.0107

Table R5 - Difference in Measured Fundamental Frequencies between Methods (Mode 2)

	95% Lower bound	Est. of Mean Difference	95% Upper bound	Est. of Std. Dev.
Accelerometer - Canon	-0.0022	0.0022	0.0062	0.0021
Accelerometer* - GoPro*	-0.0118	0.0009	0.0125	0.0063

Table R6 - Difference in Measured Fundamental Frequencies between Methods (Mode 3)

	95% Lower bound	Est. of Mean Difference	95% Upper bound	Est. of Std. Dev.
Accelerometer - Canon	-0.0102	0.0715	0.1531	0.0405
Accelerometer* - GoPro*	-0.0196	0.0334	0.1069	0.0334

Table R7 - Difference in Measured Frequency Overall (Combining all Mode Measurements)

	95% Lower bound	Est. of Mean Difference	95% Upper bound	Est. of Std. Dev.
Accelerometer - Canon	-0.0007	0.0227	0.0511	0.0134
Accelerometer* - GoPro*	-0.0065	0.0112	0.0344	0.0106

Appendix S – Results from 2x4 Statistical Analysis

Table S1 - 2x4 T-test Results

Test	t	df	p-value
ASTM vs Hot-Dry	-2.4267	9	0.03819
ASTM vs Hot-Wet	19.304	9	1.241e-08
Hot-Dry vs Hot-Wet	5.5863	9	0.0003402
Unplaned vs Planed Once	7.606	2	0.01684
Unplaned vs Planed Twice	15.74	2	0.004012
Planed Once vs Planed Twice	12.533	2	0.006306
ASTM vs Hole Pattern 1ft	27.151	2	0.001354
ASTM vs Hole Pattern 2ft	34.993	2	0.0008157
Hole Pattern 1ft vs Hole Pattern 2ft	57	2	0.0003076
Knot Removal on Frequency	3.4644	2	0.07417

Table S2 - Bootstrap Estimate of Frequency per Moisture Treatment

	Frequency 95% lower bound	Est. Frequency	Frequency 95% upper bound	Est. Std. Deviation
Hot-Dry	14.478	14.9520	15.464	0.2525
ASTM	14.086	14.6612	15.275	0.3056
Hot-Wet	13.693	14.2716	14.886	0.3047

Table S3 - Bootstrap Estimate of difference in Frequency per Moisture Treatment

	Frequency 95% lower bound	Est. Frequency	Frequency 95% upper bound	Est. Std. Deviation
ASTM – Hot-Dry	-0.449	-0.2939	-0.042	0.1133
ASTM – Hot-Wet	0.353	0.3881	0.428	0.0190
Hot-Dry – Hot-Wet	0.422	0.6796	0.851	0.1160

Table S4 - Bootstrap Estimates of Frequency before and after Planing

	Frequency 95% lower bound	Est. Frequency	Frequency 95% upper bound	Est. Std. Deviation
ASTM – Hot-Dry	-0.449	-0.2939	-0.042	0.1133
ASTM – Hot-Wet	0.353	0.3881	0.428	0.0190
Hot-Dry – Hot-Wet	0.422	0.6796	0.851	0.1160

Table S5 - Bootstrap Estimates for Difference in Frequency due to Planing

	95% lower bound	Est. Diff. in Frequency	95% upper bound	Est. Std. Deviation
Unplaned - Planed Once	2.74	3.1973	4.04	0.3392
Unplaned - Planed Twice	4.61	5.0594	5.68	0.2613
Planed Once - Planed Twice	1.64	1.8590	2.14	0.1226

Table S6 - Bootstrap Estimates of Frequency before and after Hole Pattern

	Frequency 95% lower bound	Est. Frequency	Frequency 95% upper bound	Est. Std. Deviation
ASTM	13.78	14.3945	15.06	0.3049
Hole Pattern 1ft	12.97	13.5300	14.14	0.2748
Hole Pattern 2ft	12.41	12.9550	13.55	0.2668

Table S7 - Bootstrap Estimates for Difference in Frequency due to Hole Pattern

	95% lower bound	Est. Diff. in Frequency	95% upper bound	Est. Std. Deviation
ASTM – Hole Pattern 1ft	0.81	0.863	0.92	0.0259
ASTM – Hole Pattern 2ft	1.37	1.434	1.51	0.0339
Hole Pattern 1ft – 2ft	0.56	0.570	0.59	0.0081

Table S8 - Bootstrap Estimates of Frequency before and after Knot Removal

	95% lower bound	Est. Frequency	95% upper bound	Est. Std. Deviation
ASTM	13.81	15.2547	16.20	0.6017
Knot Removed	13.60	14.7670	15.59	0.4865

Table S9 - Bootstrap Estimates for Difference in Frequency due to Knot Removal

	95% lower bound	Est. Diff. in Frequency	95% upper bound	Est. Std. Deviation
ASTM - Knot Removed	0.21	0.4952	0.66	0.1155

Appendix T – Theoretical Estimations for Natural Frequencies

$$f = \frac{1}{2\pi} \left(\frac{n\pi}{L} \right)^2 \sqrt{\frac{EI}{\rho}}$$

2x4 Boards:

Assumptions:

1. Perfectly pinned supports
2. Uniform material properties
3. Mode 1 vibration

$$\rho = SG(\rho_{water})(A) * (1 + MC)$$

$$L = 8ft = 2.4384m$$

$$I = \frac{bh^3}{12}$$

$$A = bh$$

$$h = 1.5in = 0.0381m$$

$$b = 3.5in = 0.0889m$$

From wood handbook: Doug-fir (12% MC)

$$E = 10,400MPa$$

$$SG = 0.46$$

$$\frac{1}{2\pi} \left(\frac{\pi}{2.4384m} \right)^2 \sqrt{\frac{10,400,000,000 \text{ kg/m} \cdot \text{s}^2 \frac{0.0889m * (0.0381m)^3}{12}}{0.46(1000 \text{ kg/m}^3)(0.0381m * 0.0889m)(1 + 0.12)}} = 13.05Hz$$

$$f = \frac{1}{2\pi} \left(\frac{n\pi}{L} \right)^2 \sqrt{\frac{EI}{\rho}}$$

Forest Service Pedestrian Bridge:

Assumptions common to all estimations

1. Perfectly pinned supports
2. Uniform material properties
3. Mode 1 vibration
4. No effects from weight of person near mid-span
5. No effects from bridge camber
6. Only two main girders contribute to area moment of inertia

$$L = 69ft = 21.0312m$$

$$I = \frac{bh^3}{6}$$

$$A = bh$$

$$h = 42in = 1.0668m$$

$$b = 6.75in = 0.17145m$$

$$E(\text{specified in design}) = 1800ksi = 12,411MPa$$

Assuming mass effects from glulam girders only, wood handbook SG, and MC of 30%:

From wood handbook: Doug-fir (Green)

$$SG = 0.50$$

$$MC = 30\%$$

$$\rho = 2 * SG(\rho_{water})(A) * (1 + MC)$$

$$\frac{1}{2\pi} \left(\frac{\pi}{21.0312m} \right)^2 \sqrt{\frac{12,411,000,000 \text{ kg/m} * s^2 \frac{0.17145m * (1.0668m)^3}{6}}{2 * 0.50(1000 \text{ kg/m}^3)(0.17145m * 1.0668m)(1 + 0.30)}} = 4.78Hz$$

Assuming mass effects from glulam girders and superimposed design weight, wood handbook SG, and MC of 30%:

From wood handbook: Doug-fir (Green)

$$SG = 0.50$$

$$MC = 30\%$$

$$SDL = 40 \text{ lb/ft} = 177.93 \text{ N/m}$$

$$\rho = 2 * SG(\rho_{water})(A) * (1 + MC) + \frac{SDL}{g}$$

$$\frac{1}{2\pi} \left(\frac{\pi}{21.0312m} \right)^2 \sqrt{\frac{12,411,000,000 \text{ kg/m} * s^2 \frac{0.17145m * (1.0668m)^3}{6}}{2 * 0.50 \left(1000 \text{ kg/m}^3 \right) (0.17145m * 1.0668m)(1 + 0.30) + \frac{177.93 \text{ N/m}}{9.81 \text{ m/s}^2}}} = 4.61Hz$$

Assuming mass effects from design weight of the glulam girders only:

$$wt = 50 \text{ lb}/ft^3$$

$$density = \frac{wt}{g} = 800.65 \text{ kg}/m^3$$

$$\rho = 2(density)(A)$$

$$\frac{1}{2\pi} \left(\frac{\pi}{21.0312m} \right)^2 \sqrt{\frac{12,411,000,000 \text{ kg}/m \cdot s^2 \frac{0.17145m \cdot (1.0668m)^3}{6}}{2 * (800.65 \text{ kg}/m^3)(0.17145m * 1.0668m)}} = 4.31Hz$$

Assuming mass effects from design weight of the glulam girders and superimposed design weight of components:

$$wt = 50 \text{ lb}/ft^3$$

$$density = \frac{wt}{g} = 800.97 \text{ kg}/m^3$$

$$SDL = 40 \text{ lb}/ft = 177.93 \text{ N}/m$$

$$\rho = 2(density)(A) + \frac{SDL}{g}$$

$$\frac{1}{2\pi} \left(\frac{\pi}{21.0312m} \right)^2 \sqrt{\frac{12,411,000,000 \text{ kg}/m \cdot s^2 \frac{0.17145m \cdot (1.0668m)^3}{6}}{2 * \left(800.97 \text{ kg}/m^3 \right) (0.17145m * 1.0668m) + \frac{117.93 \text{ N}/m}{9.81 \text{ m}/s^2}}} = 4.18Hz$$

Appendix U - House Rock Camp Trail Bridge Drawings

ESTIMATE OF QUANTITIES				
ITEM NUMBER	DESCRIPTION	PAY UNIT	ESTIMATED QUANTITY	REMARKS
15101	MOBILIZATION	LUMP SUM	ALL	
20102	CLEARING AND GRUBBING	LUMP SUM	ALL	
32203	AGGREGATE BASE, GRADING D, COMPACTION METHOD F	CUBIC YARD*	1	
57102	PREFABRICATED BRIDGE SUPERSTRUCTURE, TRANSPORT AND INSTALL	LUMP SUM	ALL	INCLUDES ALL LUMBER & HARDWARE FOR BRIDGE AND STAIR STRUCTURES, EQUIPMENT TO UNLOAD BRIDGE AT PROJECT SITE, TRANSPORT OF BEAMS & MATERIALS TO BRIDGE LOCATION, INSTALLATION OF DECKING & RAILING, BEARING PADS, AND INSTALLATION OF STAIRS.

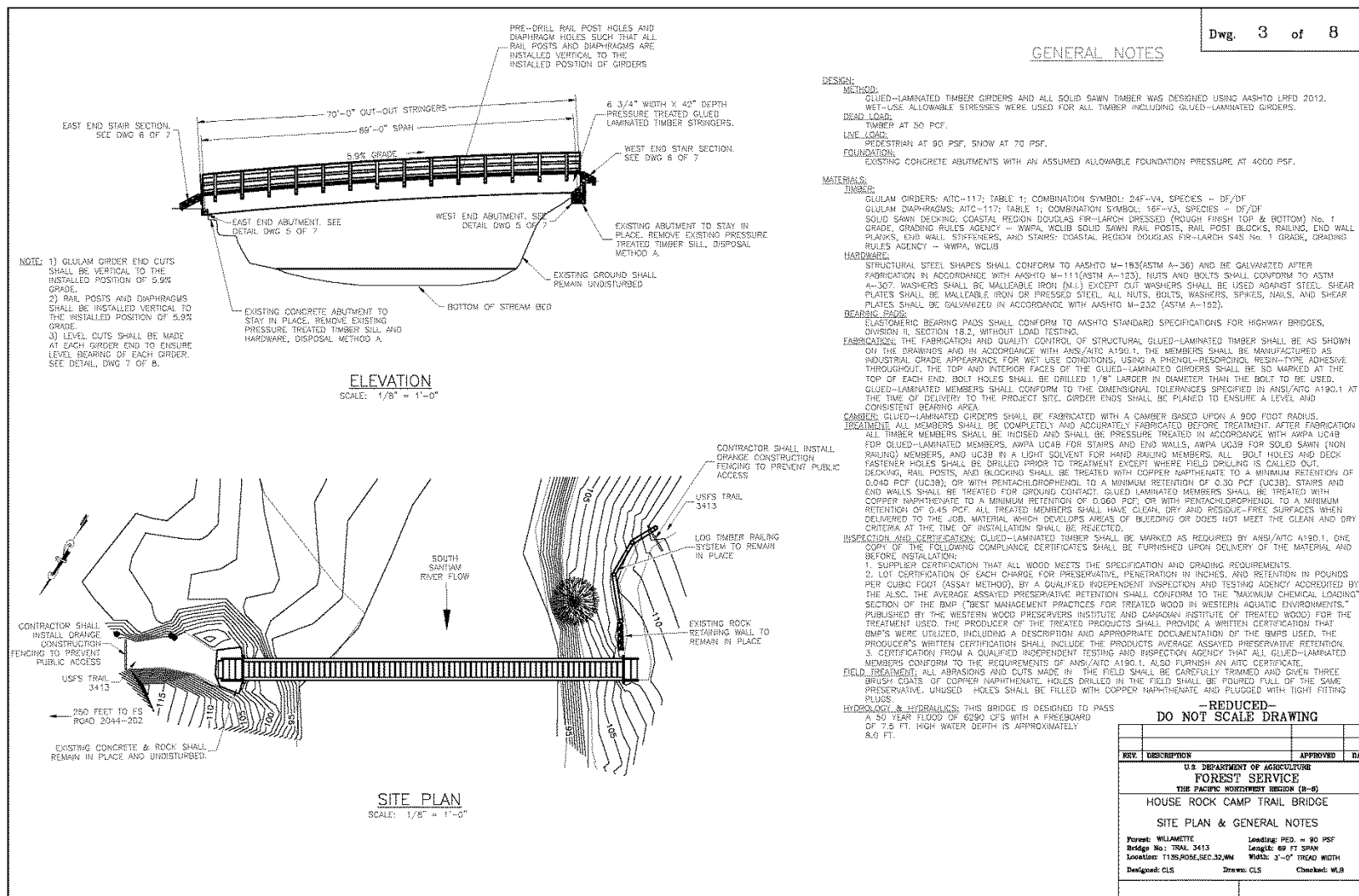
*DENOTES
CONTRACT
QUANTITY

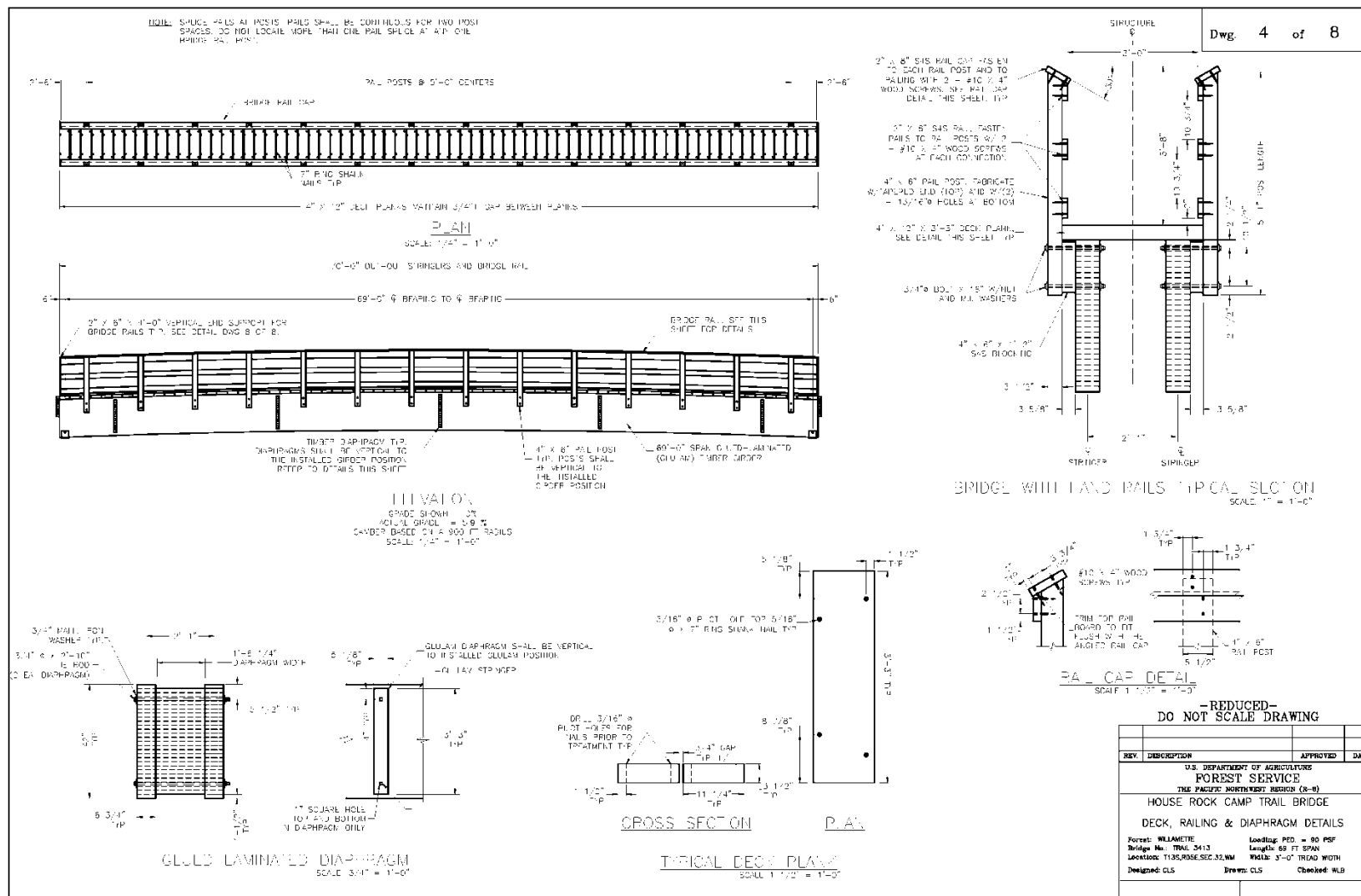
NOTES:

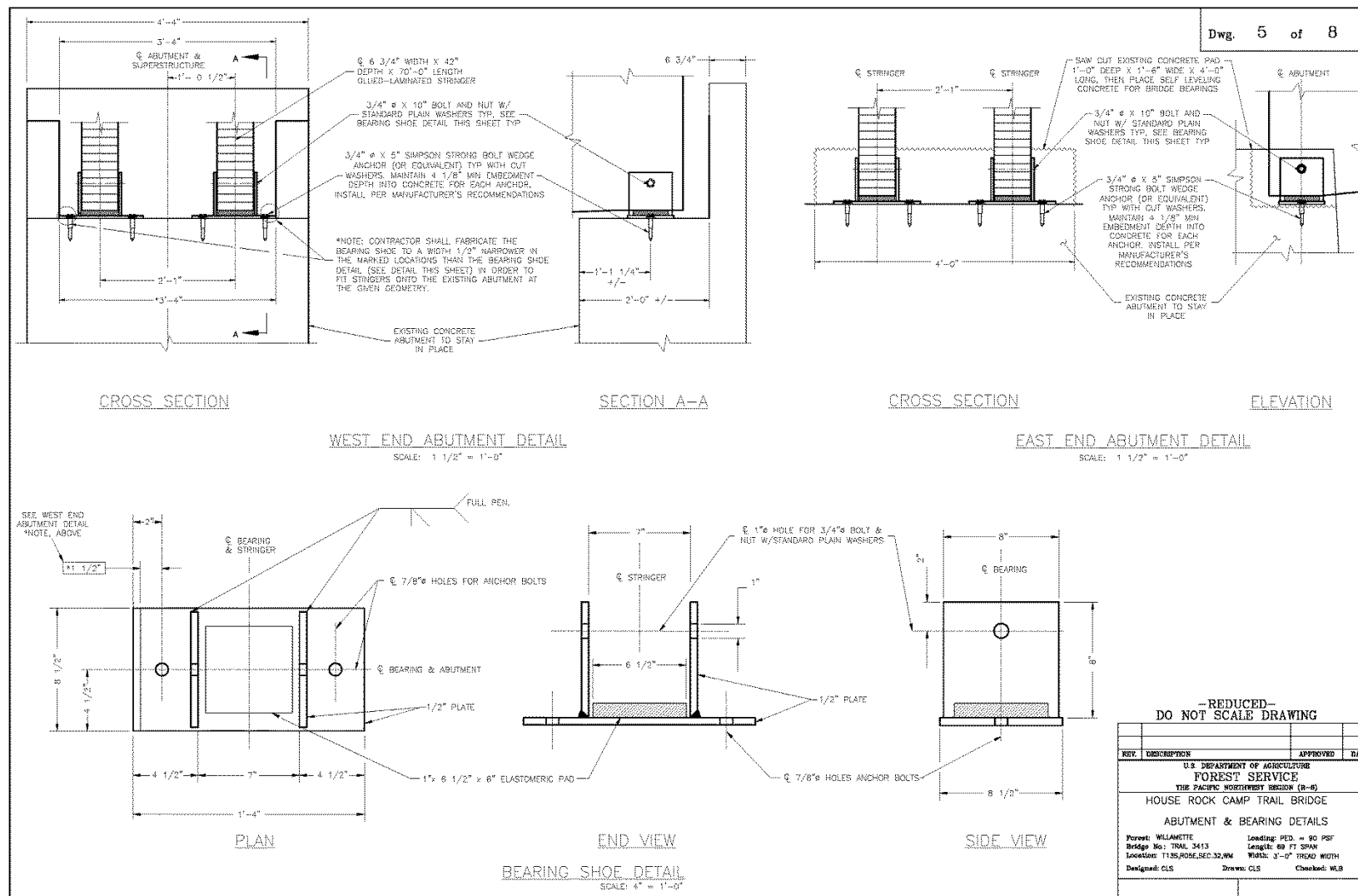
- 1) PERFORM CONSTRUCTION IN CONFORMANCE WITH THE STANDARD SPECIFICATIONS FOR CONSTRUCTION OF ROADS AND BRIDGES ON FEDERAL LANDS FP-03 US CUSTOMARY UNITS EXCEPT AS MODIFIED BY SUPPLEMENTAL SPECIFICATIONS AND CLAUSES IN THE CONTRACT DOCUMENT OR THE PLANS.
- 2) THE CONTRACTOR IS RESPONSIBLE FOR THE SAFETY OF ALL ROAD AND TRAIL USERS DURING THE LIFE OF THE CONTRACT. THE CONTRACTOR SHALL PROVIDE ORANGE CONSTRUCTION FENCING ON FS TRAIL 3413 AT EACH BRIDGE END TO PREVENT PUBLIC ACCESS.
- 3) REMOVE ALL CONSTRUCTION RELATED REFUSE FROM FEDERAL LAND PRIOR TO FINAL ACCEPTANCE.
- 4) REPAIR ANY DAMAGE TO THE EXISTING ROAD AND TRAIL SYSTEM DUE TO CONTRACTOR'S OPERATIONS AT THE CONTRACTOR'S EXPENSE, PRIOR TO FINAL ACCEPTANCE.
- 5) CONFINE CONSTRUCTION EQUIPMENT TO THE ROADWAY, UNLESS OTHERWISE SHOWN ON THE PLANS OR APPROVED BY THE CONTRACTING OFFICER IN WRITING.
- 6) STORING OF ALL EQUIPMENT ON GOVERNMENT LANDS WILL BE AT THE CONTRACTOR'S RISK AND AT A LOCATION APPROVED BY THE CONTRACTING OFFICER IN WRITING.

-REDUCED-
DO NOT SCALE DRAWING

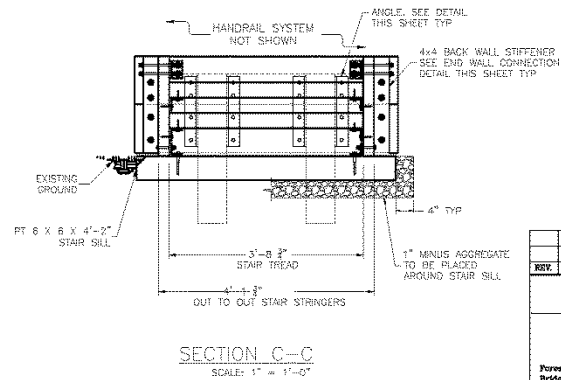
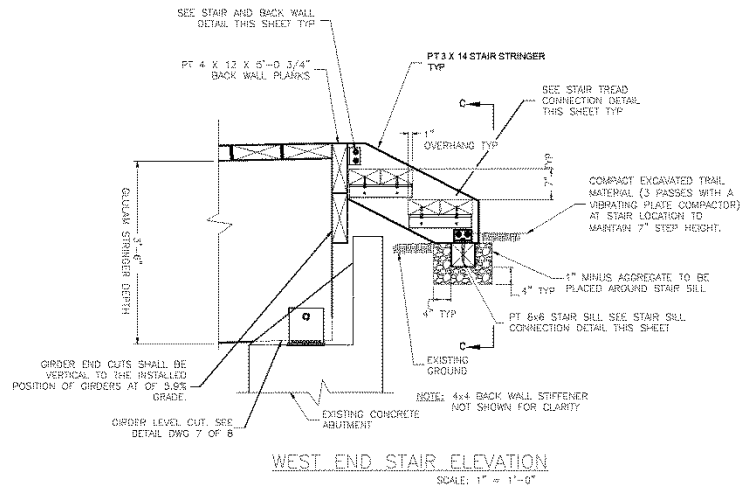
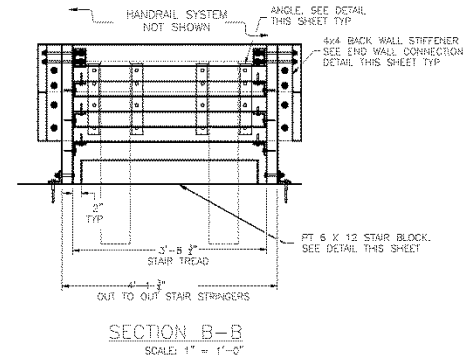
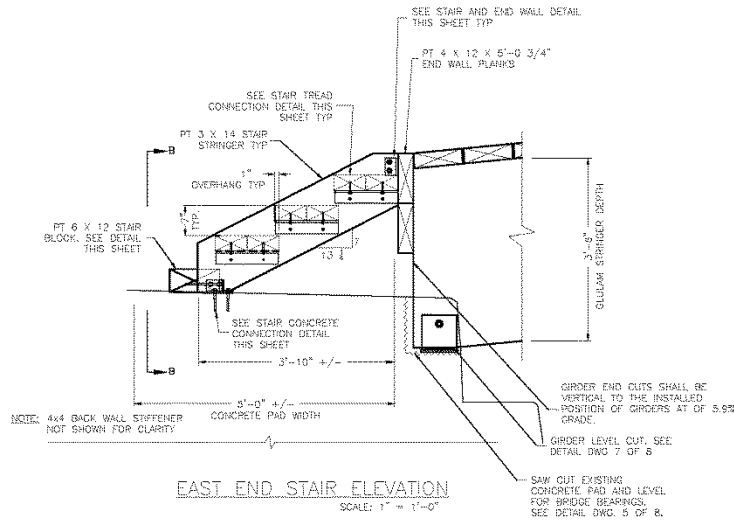
REV.	DESCRIPTION	APPROVED	DATE
U.S. DEPARTMENT OF AGRICULTURE FOREST SERVICE THE PACIFIC NORTHWEST REGION (2-8)			
HOUSE ROCK CAMP TRAIL BRIDGE			
ESTIMATE OF QUANTITIES			
Forest: WELAMETTE		Loading: PED. = 80 PSF	
Bridge No.: TRNL 3413		Length: 99 FT SPAN	
Location: 1135,HOUSE,SEC.32,NM		Width: 3'-0" TREAD WIDTH	
Designed: CLS		Drawn: CLS	
		Checked: WLB	







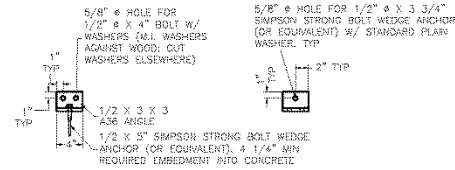
Dwg. 6 of 8



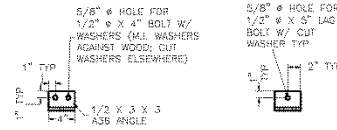
**-REDUCED-
DO NOT SCALE DRAWING**

REV.	DESCRIPTION	APPROVED	DATE
<p style="text-align: center;">U.S. DEPARTMENT OF AGRICULTURE FOREST SERVICE THE PACIFIC NORTHWEST REGION (B-5) HOUSE ROCK CAMP TRAIL BRIDGE</p> <p style="text-align: center;">STAIR DETAILS</p> <p> Forestry: WILANETTE Loading: PED. = 90 PSF Bridge No: TRAL 3413 Length: 89 FT SPAN Location: T135,POB,SEC.32,NW Width: 3'-0" TREAD WIDTH Designed: CLS Drawn: CLS Checked: WLS </p>			

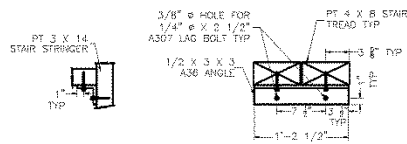
Dwg. 7 of 8



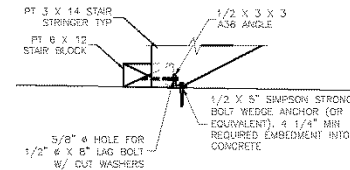
ELEVATION VIEW PLAN VIEW
STAIR CONCRETE CONNECTION DETAIL
SCALE: 1 1/2" = 1'-0"



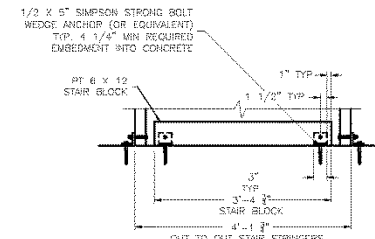
ELEVATION VIEW PLAN VIEW
STAIR SILL CONNECTION DETAIL
SCALE: 1 1/2" = 1'-0"



ELEVATION VIEW PLAN VIEW
STAIR TREAD CONNECTION DETAIL
SCALE: 1 1/2" = 1'-0"

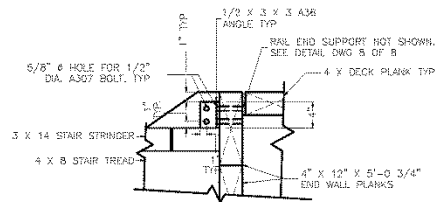


ELEVATION



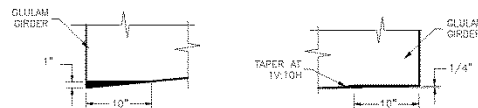
CROSS SECTION

STAIR BLOCK
SCALE: 1" = 1'-0"



NOTE: 4x4 BACK WALL STIFFENER NOT SHOWN FOR CLARITY. SEE END WALL CONNECTION DETAIL THIS SHEET TYP

STAIR & END WALL DETAIL
SCALE: 1 1/2" = 1'-0"



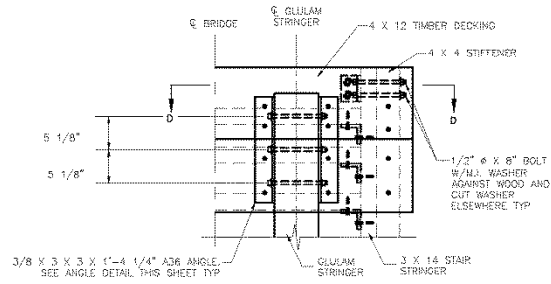
EAST END ABUTMENT WEST END ABUTMENT

GIRDER LEVEL CUT DETAIL
SCALE: 1 1/2" = 1'-0"

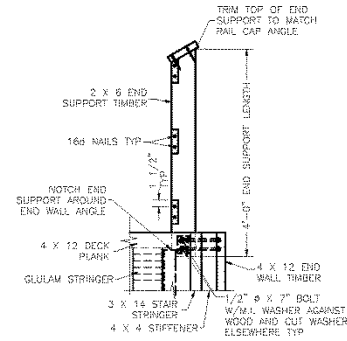
-REDUCED-
DO NOT SCALE DRAWING

REV.	DESCRIPTION	APPROVED	DATE
U.S. DEPARTMENT OF AGRICULTURE FOREST SERVICE THE PACIFIC NORTHWEST REGION (2-2)			
HOUSE ROCK CAMP TRAIL BRIDGE STRINGER END NOTCH, STAIR BLOCK & STAIR CONNECTION DETAILS			
Forest: WILLAMETTE		Loading: FEM = 80 PSF	
Bridge No.: TRAIL 3413		Length: 50 FT SPAN	
Location: 7135/ROSE/SEC-32/WM		Width: 5'-0" TREAD WIDTH	
Designed: CLS		Drawn: CLS	
		Checked: WLS	

Dwg. 8 of 8

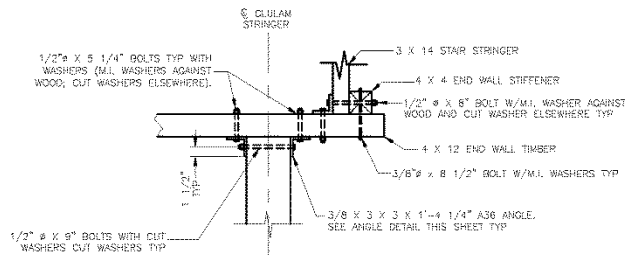


END WALL CONNECTION DETAIL
SCALE: 1 1/2" = 1'-0"

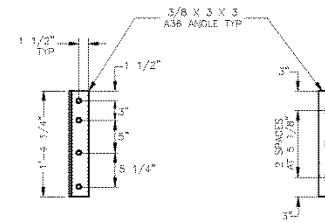


RAIL END SUPPORT DETAIL
SCALE: 1" = 1'-0"

NOTE: 4x4 BACK WALL STIFFENER NOT SHOWN FOR CLARITY. SEE END WALL CONNECTION DETAIL THIS SHEET TYP



SECTION D-D
SCALE: 1 1/2" = 1'-0"



NOTE: SLOT HOLES IN LEG OF 3"x3" ANGLE WHERE ATTACHED TO GLULAM.

ANGLE DETAIL
SCALE: 1 1/2" = 1'-0"

—REDUCED—
DO NOT SCALE DRAWING

REV.	DESCRIPTION	APPROVED	DATE
U.S. DEPARTMENT OF AGRICULTURE FOREST SERVICE THE PACIFIC NORTHWEST REGION (2-8) HOUSE ROCK CAMP TRAIL BRIDGE END WALL & RAIL END SUPPORT DETAILS			
Forest: WELAMETTE Bridge No: TRNL 3413 Location: T135,HOUSE,SEC.32,WM		Loading: PED. = 80 PSF Length: 69 FT SPAN Width: 5'-0" TREAD WIDTH	
Designed: CLS		Drawn: CLS	Checked: WLB

Appendix V - MATLAB Code Used for Analysis

6/6/15 7:08 PM D:\Documents\Kris\Research\FreqAnalysis.m 1 of 2

```
% Frequency Analysis of Digital Videos using Eulerian Coordinates
% This script can be used to plot and compute the frequency spectrum
% of one Eulerian coordinate in a digital video.
%
% Author: Ali Shariati, University of Delaware, Newark, DE 19716

% Load video

clear all;
clc

Vid = VideoReader('MVI_9234.MOV');    % Read video file (USER INPUT)
NF = Vid.NumberofFrames;              % Read number of frames

St = 1;                               % Start time reading
En = NF;                              % End time reading
I = read(Vid, [St En]);               % Read intensity

Duration = En-St+1;
image = I(:, :, :, Duration-1);

% Enter pixel coordinate to be analyzed

figure(1), imshow(image)             % Show one frame of video to help with pixel selection

X = 1232; Y = 39;                    % X and Y coordinate of the pixel to be analyzed (USER INPUT)

% Track intensity

int2GR = 0.2989*I(Y,X,1,:)+0.5870*I(Y,X,2,:)+0.1140*I(Y,X,3,:); % Compute gray value for RGB
int2GR = reshape(int2GR,1,length(int2GR)); % Reshape data
int2GR = double(int2GR); % Convert to double
int2GR = int2GR-mean(int2GR); % Subtract the DC part (= mean) of the signal

ZPI = 2^nextpow2(length(int2GR)); % Zero padding for FFT
int2GR(length(int2GR)+1:ZPI) = 0;
t = 0:1/Vid.FrameRate:(ZPI-1)/Vid.FrameRate; % Create time vector

% Plot time history

figure(2);
plot(t,int2GR,'black');
grid on; hold on;
xlabel('Time (s)');
ylabel('Intensity (-)');
```

6/6/15 7:08 PM D:\Documents\Kris\Research\FreqAnalysis.m 2 of 2

```

title(['Time history of "' Vid.Name '"', Pixel coordinates: ' num2str([X Y])]);
axis([0 t(Duration) -1.1*max(abs(int2GR)) 1.1*max(abs(int2GR))]);
%saveas(figure(2),['Pixel ' num2str([X Y]) 'time'],'fig'); % Save figure
hold off;
% save(['Pixel ' num2str(P) ' Time'],'int2R'); % Save time history data

% Compute FFT and plot frequency spectrum

freq = (0:(ZPI-1))/t(end);
intGRF = fft(int2GR);

%Peaks = findpeaks(intGRF);

figure(3);
plot(freq,abs(intGRF),'black');
hold on; grid on;
xlabel('Frequency (Hz)');
ylabel('Frequency spectrum of intensity (-)');
title(['Frequency spectrum of "' Vid.Name '"', Pixel coordinates: ' num2str([X Y])]);
axis([0 Vid.FrameRate/2 0 1.1*max(abs(intGRF))]);
%saveas(figure(3),['Pixel ' num2str([X Y]) 'freq'],'fig');
hold off;
% save(['Pixel ' num2str(P) ' Freq'],'FF'); %Save Freq Data

%Create table for export
%T1 = table(freq);
%T2 = table(abs(intGRF));

%File to export TO
filename = 'ThisWasMoreEffortThanItsWorth.xlsx';
%writetable(T1,filename,'Sheet',1,'Range','A1')
%writetable(T2,filename,'Sheet',1,'Range','A3')

```

Appendix W – Analysis Step-by-Step Guide

1. Camera set up and recording

a. Position

- i. Place the camera to be used in a plane as perpendicular to the expected plane of motion as possible.

1. For example, a simply supported board is expected to deflect in a vertical manner when excited by a gravity load. In this case the camera should be set somewhat level to the beam. For observation of a structure such as a house, place the camera perpendicular to the expected direction of motion. This allows for greater amplitudes of motion to be observed. Other perspectives can work, such as looking at the corner of a building at a 45° angle, but a closer perspective could be required to see the relatively lower amplitude of vibration.
2. Be sure to use a tripod support and remote activation of the camera if possible. This reduces extraneous camera motion which could cause difficulty in video analysis or the introduction of additional noise to the analysis step.

b. Target

- i. Once the position of the camera is determined, the camera should be focused on the structure.
 1. Try to aim the video camera at a location on the structure where vibration amplitude is expected to be greatest.

2. Choose an area with a variety of color gradients available within the camera focus. The changes in color allow for the camera to easily detect the changes in motion which will help in the analysis.
 - a. Any edge on a structure perpendicular to the direction of motion can be used for the analysis process and an edge should be included in the video focus if possible.
 - b. Naturally occurring color gradients, or transitions from one color to another, can be useful.
 - i. Larger color gradients are beneficial in that they can be used to observe a wider range of vibration amplitudes.
 - ii. In wood structures, knots, stains, heartwood-to-sapwood transitions, and growth rings can all be potentially useful color gradients.
 - iii. Other targets found to be useful were rounded features such as semi-spherical bolt heads and edges shadows on the structure from outcropping features.
 - c. Zoom
 - i. After selecting a target the level of zoom must be determined for recording. Vibrational motion can be relatively small in amplitude so in most cases a closer perspective or zoom is beneficial. It can be difficult to predict the

amount of motion that will be displayed and the usefulness of color gradients so it is recommended to record video at multiple zoom levels.

1. Optical zoom is recommended as no experimentation was done with digital zoom.
2. If vibration amplitudes are large a closer perspective might not be the most beneficial.

d. Video pixel density

- i. Video pixel density is directly related to the level of zoom.
 1. As video pixel density increases the size of individual pixels in relation to the recorded image decreases. Smaller pixel sizes create more sensitive virtual visual sensors.
 2. A high pixel density is best, but for most digital video cameras the recording framerate capability will decrease at higher pixel densities. Because of this, the selected pixel density must be balanced with the selected recording framerate.

e. Video recording framerate

- i. Theoretically, successful Fourier transform can be done as long as the recording framerate is at least twice that of the frequency of vibration observed; however, this low of a recording rate can be a source of significant error.

1. Higher recording framerates are recommended because of the reduction to the amount of noise in an analysis and increase in precision.
2. Oversampling is possible. For example in the study conducted the difference between the 60 fps of the Canon and the 120 fps of the GoPro was largely negligible. For this study the highest frequency of vibration observed was about 16 Hz.

f. Video recording length

- i. Record several complete cycles of the vibrational period. In this study, videos were generally recorded for about 10 seconds.
 1. If the structure has several modes of vibration, higher modes may be missed in shorter videos.
 2. More vibrational periods observed lead to greater accuracy in the Fourier transform when determining the frequency of vibration.

2. Video Analysis

a. Use of MATLAB script

- i. There are two user input fields in the MATLAB script: the video file name and the video pixel coordinate to be analyzed.

- ii. Running the script will output three figures: a sample frame from the video, the time-intensity diagram for the selected pixel coordinate, and the Fourier transform of this signal.

1. The sample video frame is a tool to help in pixel coordinate selection.

- a. Use of MATLAB's data cursor will return the pixel coordinate of selected locations on the video frame.

b. Coordinate Selection

- i. Pixel coordinate selection relates back to the color gradients used as targets for video recording. Select a pixel coordinate located along the length of the color gradient.

1. It is recommended to start near the edge of the color gradient and move one pixel at a time towards the center of the gradient.

c. Interpretation of results

- i. There are two things to look at when considering the results of the analysis:

1. Clarity of time-intensity diagram

- a. The time-intensity diagram looks similar to and is proportional to a position-time diagram. If this is not the case, then the Fourier transform is likely to be inconclusive or unclear.
 - b. The time-intensity diagram can also give clues as to the behavior of the structure.

- i. For example, in one of the experiments done in this study there was no successful observation of vibration but when looking at the time-intensity diagram there was a clear change in pixel intensity (proportional to a deflection) at the exact moment a truck went over the bridge. This gave some indication of the structure deflecting under load, even without successful observation of vibrational frequency.

2. Clarity of Fourier transform

- a. A successful Fourier transform should include distinct peaks in the diagram which indicate observed vibrational frequencies.

- i. The signal will almost always have a peak at 0 Hz.
- ii. Several peaks can occur if the structure is vibrating with multiple modes or if the external loading is not identical to the natural frequency of the structure.
- iii. There could also be additional peaks resulting from a poorly chosen color gradient or one that is too small. Further analysis with different pixel coordinates will help in determining when these effects occur.

Appendix X – R Software Bootstrap Analysis Code


```

# Sort bootstrap means, from smallest to largest
sbsm <- sort(bsm)

# Determine which ordered bootstrap out of n corresponds
# to the 2.5th and 97.5th (or ci-th) percentile
high <- floor((1-(1-ci)/2)*n)
low <- floor((1-ci)/2*n)

# The estimate of the mean is the mean of the
# bootstrap means, and the variance of the distribution
# is the variance of the bootstrap means. (Note, this
# variance isn't particularly useful if the distribution
# isn't normal or T, anyways!
est <- mean(sbsm)
vest <- var(sbsm)

# Create a plot using GGPlot2
p <- qplot( x = sbsm, binwidth = diff(range(sbsm))/30) +
  geom_vline(xintercept = c(sbsm[low], sbsm[high])) +
  labs(x = label, y = "Count")

# If plot is toggled T, display the plot.
if(plot == T)
{
  # Uncomment the following if you would like text reports
  # of what the confidence intervals are, in addition to plots.

  # message(paste("95% CI: (",round(sbsm[low],4),
  #               ",",round(sbsm[high],4),")"))
  # message(paste("Estimate of Frequency: ", est))
  # message(paste("Standard Deviation: ", sqrt(vest)))
  print(p)
}

# Return the 95% lower bound, estimate,
# 95% upper bound, and standard deviation.
return(c(sbsm[low],est,sbsm[high], sqrt(vest)))
}

```